

Inductors and Transformers for Power Electronics

Inductors and Transformers for Power Electronics

Alex Van den Bossche

*Ghent University
Gent, Belgium*

Vencislav Cekov Valchev

*Ghent University
Gent, Belgium*



Taylor & Francis
Taylor & Francis Group

Boca Raton London New York Singapore

A CRC title, part of the Taylor & Francis imprint, a member of the
Taylor & Francis Group, the academic division of T&F Informa plc.

The authors try to be accurate and clear, but they cannot guarantee the results or possible interpretations, which might cause direct or indirect injuries, equipment damage, or economic damage by the use of the contents of the book.

Published in 2005 by
CRC Press
Taylor & Francis Group
6000 Broken Sound Parkway NW, Suite 300
Boca Raton, FL 33487-2742

© 2005 by Taylor & Francis Group, LLC
CRC Press is an imprint of Taylor & Francis Group

No claim to original U.S. Government works
Printed in the United States of America on acid-free paper
10 9 8 7 6 5 4 3 2 1

International Standard Book Number-10: 1-57444-679-7 (Hardcover)
International Standard Book Number-13: 978-1-57444-679-1 (Hardcover)
Library of Congress Card Number 2004061860

This book contains information obtained from authentic and highly regarded sources. Reprinted material is quoted with permission, and sources are indicated. A wide variety of references are listed. Reasonable efforts have been made to publish reliable data and information, but the author and the publisher cannot assume responsibility for the validity of all materials or for the consequences of their use.

No part of this book may be reprinted, reproduced, transmitted, or utilized in any form by any electronic, mechanical, or other means, now known or hereafter invented, including photocopying, microfilming, and recording, or in any information storage or retrieval system, without written permission from the publishers.

For permission to photocopy or use material electronically from this work, please access www.copyright.com (<http://www.copyright.com/>) or contact the Copyright Clearance Center, Inc. (CCC) 222 Rosewood Drive, Danvers, MA 01923, 978-750-8400. CCC is a not-for-profit organization that provides licenses and registration for a variety of users. For organizations that have been granted a photocopy license by the CCC, a separate system of payment has been arranged.

Trademark Notice: Product or corporate names may be trademarks or registered trademarks, and are used only for identification and explanation without intent to infringe.

Library of Congress Cataloging-in-Publication Data

Bossche, Alex van den.

Inductors and transformers for power electronics / Alex van den

Bossche, Vencislav Valchev.

p. cm.

Includes bibliographical references and index.

ISBN 1-57444-679-7

1. Electric inductors. 2. Electric transformers. 3. Power electronics—Equipment and supplies. I. Valchev, Vencislav. II. Title.

TK7872.I63B67 2004

621.31'7--dc22

2004061860

T&F informa

Taylor & Francis Group
is the Academic Division of T&F Informa plc.

Visit the Taylor & Francis Web site at
<http://www.taylorandfrancis.com>

and the CRC Press Web site at
<http://www.crcpress.com>

To our children

Maxime, Nathan and Laura

Coetelina and Iasen

Preface

This book is mainly intended for designers and users of magnetic components in power electronics. It can also be used for didactical purposes. Magnetic components such as inductors and transformers constitute together with the control and the semiconductor components, the main parts in the design of power electronic converters. Some experience teaches that the design of the magnetic parts is still often done by trial and error. This can be explained by a (too) long working-in time for designing inductors and transformers. The design has many aspects, such as the magnetic core and winding, eddy currents, insulation, thermal design, parasitic effects, and measurements. A lot of literature exists concerning those subjects, but the information is spread over many articles and methods. This book is mainly focused on classical methods and uses numerical tools such as finite element methods in the background.

We try to give some overview of the basics and technological aspects of the design. In the different chapters we also describe analytical approximations based on known analytical solutions, but tuned by finite elements. In most of the cases, a sufficient accuracy can be obtained and the results are obtained almost instantaneously, even for graphics using many calculation points. A fast approximation method is useful as a first step in the design stage, whereas numerical tools such as finite elements are good in analysis. Specific books on finite elements exist and the description will not be repeated here.

Some basic introduction on magnetic principles and materials are given in Chapter 1.

Today power electronics use quite a high switching frequency. Simple rules of thumb such as that “the eddy copper current losses are always negligible when the diameter of the wire is smaller than the penetration depth” are not true. However, it is clear that the main cause of the eddy current losses is caused by the presence of high frequency transverse magnetic field components. This is the base of the fast design method in Chapter 2. The method is further improved using some corrections for other effects and is embedded in a decision flow chart of a design procedure. More insight and better accuracy is provided in the other chapters. We invite the readers to let them guide by the contents of the book to their specific subjects of interest.

The chapters in the book are organized in a quite independent way with respective local appendices and references. The general appendices at the end provide information that is not linked to a specific chapter and can be used independently.

This work can be seen as complementary information to books on power electronic circuits. Different levels of complexity are proposed depending on the available time, the desired accuracy, and the mathematical level of the designer.

Acknowledgments

We want to thank several institutions, that permitted the research and the achievement of this book: DWTC and FWO – Belgium; NATO Research Program; BOF in Ghent University; Fellowships of scientific exchange between Belgium and Bulgaria; E.E.C. Tempus and Socrates exchange programs.

The authors are also grateful to the department heads Prof. Dr. ir Jan Melkebeek of the Ghent University Electrical Energy Laboratory and Prof. Dr. Eng. Dimitar Yudov, who supported us.

We want also to acknowledge the companies such as Philips, Tyco, Inverto, Barco, Fabricom in Belgium and Struna in Bulgaria. The opportunity to design for them induced industrial realism.

Many collaborators did a wonderful job while reading and giving suggestions of improvements and encouragements to the fulfillment of this book.

About the Authors

Alex P. M. Van den Bossche received the M.S. and the Ph.D. degrees from the University of Ghent, Belgium in 1980 and 1990 respectively. He has worked there at the Electrical Energy Laboratory Department, EESA. He has been engaged in research and published articles in the field of electrical drives and power electronics concerning various converter types, drives and various aspects of magnetic components and materials. His interests are also in renewable energy conversion. Since 1993, he has been a full professor at the same university. He is a senior member of the IEEE (M'99S'03).

Vencislav V. Valchev received the M.Sc. and Ph.D. degrees in electrical engineering from the Technical University of Varna, Bulgaria in 1987 and 2000, respectively. Since 1988 he has been with the Department of Electronics, Technical University of Varna, where he has been a lecturer. His research interests include power electronics, soft switching converters, resonant converters, and magnetic components for power electronics, renewable energy conversion.

Dr. Valchev had a cumulated common research period of about four years in the Electric Energy Laboratory research group in Ghent University, Belgium.

Nomenclature

The symbols do mainly follow the standard ISO 31-11

Concerning upper and lower cases we try to keep the following conventions:

Voltage and current:

Time dependent values of voltage and current are denoted by low cases (v , i)

RMS values are capitals without index for sinusoidal waveforms.

The index_{rms} is mentioned explicitly for RMS values of non-sinusoidal waveforms.

Field quantities such as H and B are always written in capital case, the context shows what it is e.g. $B_p = \hat{B}$ is the peak value of the induction $B(t)$ is the value depending on time.

Matrices and vectors are written in bold.

Variables are written in italic.

Functions, operators, universal constants are non-italic.

Complex variables are underlined if confusion is possible.

Blanks are used as multiplication.

We did split the nomenclature in variables, subscripts, superscripts, constants and frequently used abbreviations. The specific combination of variables with subscripts is defined in the respective chapters at their first appearance.

Variables

A	area	[m ²]
a	geometrical dimension	[m]
B	magnetic induction = magnetic flux density	[T]
b	width of the window area, geometrical dimension	[m]
C	coefficient	[W/(m ² K)]
c	geometrical dimension	[m]
D	duty ratio	[]
d	diameter	[m]
E	electric field	[V/m]
e	dimension	[m]
F	function, factor	—
f	frequency	[Hz] = [periods/s]
G	function	—
g	dimension	[m]
H	magnetic field	[A/m]

i	instantaneous current	[A]
I	RMS current (sine wave)	[A]
k	coefficient	—
k	thermal conductivity	[W/m °C]
L	Inductance	[H]
L	characteristic distance, Chapter 6	[m]
l	length	[m]
M	total numbers of layers	—
N	number of wires	—
m	layer number	—
n	conductor number in a layer	—
P	power	[W]
p	primary	
p	pressure, Chapter 6	[Pa]
q	tuning parameter; heat transfer rate	[W]; —
R	resistance; (with index θ : thermal)	[Ω]; [K/W] = [°C; W]
r	radius	[m]
S	surface	[m ²]
s	secondary; distance (with index)	—; [m]
s	Laplace operator	—; [m]
T	period; absolute temperature (with index)	[s]; [K]
t	time; thickness (with index)	[s]; [m]
V	voltage	[V]
v	instantaneous value of the voltage	[V]
V	RMS value of the voltage (sine wave)	[V]
W	area; energy	[m ²]; [J]
w	winding width	[m]
X	reactance	[Ω]
x	horizontal distance to origin	[m]
Y	admittance	[Ω^{-1}] = [S]
y	vertical distance to origin	[m]
z	complex distance to origin	[m]
Z	Impedance	[Ω]
α	(Alpha) frequency exponent; angle (with index)	—; [rad]
β	(Beta) induction exponent	—
γ	(Gamma) exponent	—
δ	(Delta) penetration depth	[m]
ε	(Epsilon) function;	—
ε	relative number of turns (Chapter 10)	—
ε	emissivity (Chapter 6)	—
ζ	(Zeta) parameter	—
η	(Eta) horizontal filling factor	—
θ	(Theta) angle; temperature	[rad][°C]
κ	(Kappa) parameter for the field factor	—
λ	(Lambda) vertical filling factor	—
μ	(Mu) permeability	—

ν	(Nu) kinematic viscosity	[m ² /s]
ξ	(Xi) relative height	—
ρ	(Rho) resistivity	[Ω m]
σ	(Sigma) conductivity	[Ω^{-1} m ⁻¹] = [S/m]
τ	(Tau) time constant	[s]
Φ	(Phi) main flux	[Wb] = [Tm ⁻²]
φ	(Phi) angle	[rad]
χ	(Chi) function (influence of penetration depth on dipole effect)	—
Ψ	(Psi) flux linkage	[V s] = [T m ⁻²]
ψ	(Psi) angle	[rad]
ω	(Omega)= $2\pi f$	[Hz] = [rad/s]

Subscripts

1 2 3	number or harmonic
<i>A</i>	around (= local)
<i>a</i>	ambient
<i>av</i>	average
<i>bot</i>	bottom (of conductor)
<i>c</i>	core; curie (temperature),
<i>c</i>	wide frequency (combined low-high), for coefficients
<i>c</i>	conductor (for length)
<i>cd</i>	conduction heat transfer
<i>cv</i>	convection heat transfer
<i>cu</i>	copper
<i>d</i>	differential
<i>D</i>	Dowell
<i>cu</i>	copper
<i>e</i>	effective
<i>F</i>	from field pattern
<i>f</i>	finished (area)
<i>ff</i>	filling factor
<i>fe</i>	iron, ferrite
<i>g</i>	gap, graph
<i>h</i>	thermal
<i>h</i>	horizontal
<i>hf</i>	high frequency
<i>hy</i>	hyperbolic (field type)
<i>hs</i>	hot spot
<i>i,j,k,l,m,n</i>	elements of a vector
<i>i</i>	induced
<i>in</i>	internal
<i>LF</i>	low frequency
<i>m</i>	middle

<i>max</i>	maximum
<i>min</i>	minimum
<i>N</i>	nominal
<i>o</i>	no-load; outer (diameter)
<i>own</i>	own (of the conductor itself)
<i>p</i>	practical, pressure, parallel
<i>R</i>	radiation heat transfer
<i>r</i>	relative
<i>rad</i>	radiation
<i>ref</i>	reference
<i>s</i>	saturation (inductance), series
<i>sf</i>	stacking factor
<i>sin</i>	sine wave
<i>T</i>	transverse, temperature
<i>t</i>	thickness
<i>top</i>	top (top of conductor)
<i>tip</i>	tip (top or bottom of foil)
<i>tr</i>	transverse (field type)
<i>tri</i>	triangular wave
<i>v</i>	vertical
<i>w</i>	wall, surface, winding
<i>WFM</i>	wide frequency method
<i>x</i>	in the x-direction
<i>y</i>	in the y-direction
<i>0</i>	absolute (permeability), characteristic (impedance)
θ	thermal
Σ	Sum
σ	leakage

Superscripts

\wedge	peak
*	complex conjugate

Constants

$e = 2.71828$	—
$\epsilon_0 = 8.842 \times 10^{-12}$	[F/m]
$\mu_0 = 4\pi 10^{-7}$, absolute permeability	[H/m]
$\pi = 3.14159$	—
$j = \sqrt{-1}$, imaginary constant	—

Frequently Used Abbreviations

<i>EMC</i>	Electro Magnetic Compatibility
<i>EMF</i>	Electro Motive Force
<i>RMS</i>	Root Mean Square
<i>MLT</i>	Mean Length of Turn

Table of Contents

1 Fundamentals of Magnetic Theory

- 1.1 Basic Laws of Magnetic Theory
 - 1.1.1 Ampere's Law and Magnetomotive Force
 - 1.1.2 Faraday's Law and EMF
 - 1.1.3 Lenz's Law and Gauss's Law for Magnetic Circuits
- 1.2 Magnetic Materials.
 - 1.2.1 Ferromagnetic Materials
 - 1.2.2 Magnetization Processes
 - 1.2.3 Hysteresis Loop
 - 1.2.4 Permeability
 - 1.2.4.1 Complex Permeability
 - 1.2.4.2 Hysteresis Material Constant
- 1.3 Magnetic Circuits
 - 1.3.1 Basic Laws for Magnetic Circuits
 - 1.3.2 Inductance
 - 1.3.2.1 Flux Linkage
 - 1.3.2.2 Inductance: Definitions
 - 1.3.2.3 Inductance: Additional Considerations
 - 1.3.2.4 Self-inductance and Mutual Inductance
 - 1.3.3 Transformer Models
 - 1.3.3.1 Ideal Transformer
 - 1.3.3.2 Practical Transformer
 - 1.3.4 Magnetic and Electrical Analogy
- References

2 Fast Design Approach Including Eddy Current Losses

- 2.1 Fast Design Approach
 - 2.1.1 Non-Saturated Thermal Limited Design
 - Step 1) Choose a Core Material and Size
 - Step 2) Calculate the Heat Dissipation Capability P_h
 - Step 3) Copper Loss/Core Loss Ratio
 - Step 4) Calculate the Specific Core Losses $P_{fe,sp}$
 - Step 5) Find the Peak Induction $B_{p,g}$ from Graphical Data
 - Step 6) Check if the Peak Induction B_p is Higher Than the Saturation Value B_{sat}
 - Symmetrical Waveforms
 - Asymmetrical Waveforms
 - Step 7) Calculate the Winding Turns N_i

- Step 8) Distribute Allowed Total Copper Losses $P_{h, cu}$ Among the Windings
- Step 9) Determine Wire Diameter d_i
- Step 10) Calculate the Actual Copper Losses P_{cu}
 - I) Ohmic Copper Losses
 - II) Low-Frequency Transverse Field Eddy Current Losses.
 - III) Wide Frequency Eddy Current Losses
 - IV) Total Copper Losses
- Step 11) Check if the Copper Losses P_{cu} are Lower Than the Allowed Copper Dissipation $P_{h, cu}$
- Step 12) Is Improvement Possible?
- Step 12a) Optimize the Diameter and Winding Arrangement
 - I) Transformers
 - II) Inductors
- Step 13) Check the Copper Filling Factor
- Step 13a) Choose a Larger Core
- Step 14) Check if the Chosen Core Size in Step 1) is not Too High
- Step 14a) Choose a Smaller Core
- Step 15) Calculate the Total Air Gap Length Σl_g

2.1.2

- Saturated Thermally Limited Design
- Step 1') Find the Peak-to-Peak Induction B_{pp}
- Step 2') Choose a Core, Material, and Size
- Step 3') Find the Core Losses P_{fe} from Graphical Data
- Step 4') Find the Heat Dissipation Capability P_h of the Component
- Step 5') Check the Ratio P_{fe}/P_h
- Step 6') Estimate the Allowed Copper Dissipation Capability

2.1.3 Signal Quality Limited Design

2.2 Examples

2.2.1 Non-Saturated Thermally Limited Design Example

- 2.2.1.1 Design Steps
- Conclusions:
- 2.2.1.2 Improvements of the Design
- 2.2.1.3 Measuring and Validation of the Design

2.2.2 Saturated Thermal Limited Design Example

- 2.2.2.1 Design Procedure
 - Equation Approach
- 2.2.2.2 Measurements and Validation of the Eddy Current Losses

2.3 Conclusions

- Appendix 2.A.1 Core Size Scale Law for Ferrites
in Non-Saturated Thermal Limited Design
- Appendix 2.A.2 Eddy Current Losses for Wide Frequency
 - 2.A.2.1 Approximation of k_c
 - 2.A.2.2 Transformers
 - 2.A.2.2.1 Direct Calculations
 - 2.A.2.2.2 Graphical Transformer Method
 - 2.A.2.3 Inductors
 - 2.A.2.3.1 Direct Calculations
 - 2.A.2.3.2 Graphical Inductor Method
- Appendix 2.A.3 Mathcad Example Files
- References

3 Soft Magnetic Materials

- 3.1 Magnetic Core Materials
 - 3.1.1 Iron-Based Soft Magnetic Materials
 - 3.1.1.1 Laminated Cores
 - 3.1.1.2 Powdered Iron and Carbonyl Iron Cores
 - Powdered Iron
 - Carbonyl Iron
 - 3.1.1.3 Amorphous Alloys
 - Production Process and
Microstructure Characteristics
 - Magnetic Properties
 - Applications
 - Shapes
 - 3.1.1.4 Nanocrystalline Magnetic Materials
 - Production Process and
Microstructure Characteristics
 - Magnetic Properties
 - Temperature Behavior
 - Shapes
 - Applications
 - 3.1.2 Ferrites
 - Production Process and
Microstructure Characteristics
 - Magnetic Properties
 - Low Induction Level (Signal Level)
Parameters
 - High Induction Level (Power Level)
Parameters
 - Shapes
- 3.2 Comparison and Applications of the Core Materials
in Power Electronics
- 3.3 Losses in Soft Magnetic Materials
 - 3.3.1 Simplified Approach for Laminated Steel Cores

- 3.3.2 Hysteresis Losses
- 3.3.3 Eddy-Current Losses
 - 3.3.3.1 Eddy Current Losses in Laminated Cores
 - Low Frequency Approximation of Eddy Current Losses in Laminated Cores
 - 3.3.3.2 Eddy Current Losses in Laminated Cores at Arbitrary Frequencies
- 3.3.4 Anomalous (Residual, Excess) Losses
- 3.4 Ferrite Core Losses with Non-Sinusoidal Voltage Waveforms
 - 3.4.1 Identification of the Steinmetz Equation
 - 3.4.2 Natural Steinmetz Extension for Ferrite Core Losses with Non-Sinusoidal Voltage Waveforms
- 3.5 Wide Frequency Model of Magnetic Sheets Including Hysteresis Effects
 - 3.5.1 Constant Loss Angle Impedance
 - 3.5.2 Transmission Line Approach with Constant Loss Angle Material
 - 3.5.3 Wide Frequency Complex Permeability Function
 - 3.5.4 Real, Reactive, and Apparent Power
 - 3.5.5 Dependence on Saturation Level
 - 3.5.6 Wide Frequency Model Curves of Typical Materials
 - 3.5.6.1 Silicon Steel
 - 3.5.6.2 Nanocrystalline Material
 - 3.5.6.3 Wide Frequency Model for Ferrites
- Appendix 3.A Power and Impedance of Magnetic Sheets
- References

4 Coil Winding and Electrical Insulation

- 4.1 Filling Factor
 - 4.1.1 Round Wires
 - 4.1.1.1 Square Fitting
 - 4.1.1.2 Hexagonal Fitting
 - 4.1.1.3 Practical Case
 - 4.1.2 Foil Windings
 - 4.1.3 Wires with Rectangular Cross Section
 - 4.1.4 Litz Wires
- 4.2 Wire Length
 - 4.2.1 Circular Coil Formers
 - 4.2.2 Rectangular Coil Formers
- 4.3 Physical Aspects of Breakdown
 - 4.3.1 Breakdown Voltage in Air
 - 4.3.2 Breakdown Voltage in Solid Insulation Material
 - 4.3.3 Corona Discharge

- 4.4 Insulation Requirements and Standards
 - 4.4.1 Basic, Supplementary, and Reinforced Insulation
 - 4.4.2 Standard Insulation Distances
 - 4.4.2.1 Clearance
 - 4.4.2.2 Creepage Distance
 - 4.4.3 Electric Strength Tests
 - 4.4.4 Leakage Currents
- 4.5 Thermal Requirements and Standards
 - 4.5.1 Thermal Evaluation of Insulation Materials and Systems
 - 4.5.2 Requirements and Standards for Inductive (Magnetic) Modules
 - 4.5.3 Standards for Wires
 - Bare Material Diameter
 - Enamel Thickness
 - Resistance Per Meter
 - Thermal Classes of Magnet Wires
- 4.6 Magnetic Component Manufacturing Sheet
 - Coupling
 - Air Gaps
 - Impregnating
 - Partially Filled Layer

References

5 Eddy Currents in Conductors

- 5.1 Introduction
 - Current Power Electronics Needs
 - Skin Effect
 - Proximity Effect
 - Air Gap Effects
 - Eddy Current Losses in Conductors
- 5.2 Basic Approximations
 - 5.2.1 Low Frequency Approximation
 - 5.2.2 High Frequency Approximation
 - 5.2.3 Superposition of Losses
 - 5.2.4 Wide Frequency Approximation
- 5.3 Losses in Rectangular Conductors
 - 5.3.1 Exact Solution For a Current Carrying Rectangular Conductor in a Transverse Field
 - 5.3.2 Low Frequency Approximation
 - 5.3.2.1 Current Carrying Conductor Without Transverse Field
 - 5.3.2.2 Conductor Without Current in a Transverse Field
 - 5.3.3 High Frequency Approximation
 - 5.3.3.1 Ideal Case

- 5.3.4 Spaced Conductors
 - 5.3.4.1 Classical Approach
 - 5.3.4.2 Low Filling Factor and High Frequency
- 5.4 Quadrature of the Circle Method for Round Conductors
 - 5.4.1 Equivalent Rectangle Principle
 - 5.4.2 Adapted Equations
 - 5.4.3 Low Frequency Approximation
 - Accuracy of Dowell Method
 - 5.4.4 Improved Quadrature of the Circle Method
 - 5.4.5 Discussion of Quadrature of the Circle Methods
 - Conclusions for Classical Dowell Method
 - Conclusions for IQOC Method
- 5.5 Losses of a Current Carrying Round Conductor in 2-D Approach
 - 5.5.1 Exact Solution
 - 5.5.2 Low and High Frequency Approximation
 - 5.5.3 Wide Frequency Approximation
- 5.6 Losses of a Round Conductor in a Uniform Transverse AC Field
 - 5.6.1 Exact Solution
 - 5.6.2 Low Frequency Approximation
 - 5.6.3 High Frequency Approximation
 - 5.6.4 Wide Frequency Approximation
 - 5.6.5 Discussion
- 5.7 Low Frequency 2-D Approximation Method for Round Conductors
 - 5.7.1 Direct Integration Method for Round Wires
 - 5.7.2 Three-Field Approximation
 - 5.7.3 Solution in a Magnetic Window Using Mirroring
 - 5.7.4 Suppression of the First Infinite Sum
- 5.8 Wide Frequency Method for Calculating Eddy Current Losses in Windings
 - 5.8.1 High Frequency Effect of Other Wires, Using Dipoles
 - 5.8.2 Wide Frequency Method, Tuning with Finite Element Solutions
 - 5.8.2.1 A Wire in a Transverse Field
 - 5.8.2.2 A Wire in a Half Layer
 - Conclusions of the Comparisons
 - 5.8.2.3 Losses in the General Case of a Transformer Winding
 - 5.8.2.4 Losses in an Inductor Winding
 - 5.8.3 High Frequency, High Filling Factor Relations
 - 5.8.4 Summary of the Wide Frequency Method
 - 5.8.5 Comparison of Analytically Based Methods

- 5.8.5.1 Low Frequency Methods
- 5.8.5.2 Wide Frequency Method and Quadrature of Circle Methods
- 5.9 Losses in Foil Windings
 - 5.9.1 Homogenous Field Parallel to the Foil
 - 5.9.2 Induced Losses by Air Gaps
 - 5.9.2.1 Analytical Modeling
 - 5.9.3 Tip Currents in Foil Conductors
 - Foil Inductors
 - Foil Transformers
 - Conclusions Concerning Tip Currents
 - 5.9.4 Conclusions for Foil Windings
- 5.10 Losses in Planar Windings
 - Advantages of the Planar Cores
 - Losses in Planar Magnetic Components
 - Specifics
- Appendix 5.A.1 Eddy Current 1-D Model for Rectangular Conductors
 - 5.A.1.1 Basic Derivations
 - 5.A.1.2 Single Conductor in a Slot
 - 5.A.1.3 Superimposed Rectangular Conductors in a Slot
 - 5.A.1.4 Taylor Expansion and Low Frequency Approximation for Superimposed Rectangular Conductors in a Slot
 - 5.A.1.5 Approximation for Rectangular Conductors with Air
 - 5.A.1.5.1 Classical Approach
- Appendix 5.A.2 Low Frequency 2-D Models for Eddy Current Losses in Round Wires
 - 5.A.2.1 Low Frequency Approach
 - 5.A.2.2 Defining a 2-D Winding Arrangement
 - 5.A.2.3 Eddy Current Losses by The Direct Integration Method
 - 5.A.2.4 The Proposed Three Orthogonal Fields Method
 - 5.A.2.4.1 The Field of the Conductor
 - 5.A.2.4.2 The Transverse Field
 - 5.A.2.4.3 The Hyperbolic Field
 - 5.A.2.4.4 Residual Field
 - 5.A.2.4.5 Eddy Current Losses by the Three Orthogonal Fields
 - 5.A.2.5 Validation of the Proposed 3-Field Approximation
 - 5.A.2.6 Extension of the Obtained Solution
- Appendix 5.A.3 Field Factor For Inductors
 - 5.A.3.1 2-D Analytical Approximation of the Field Factor k_F

5.A.3.2 Simplified Approach

5.A.3.3 Parallel and Perpendicular Components of k_F

References.

6 Thermal Aspects

6.1 Fast Thermal Design Approach (Level 0 Thermal Design)

6.1.1 Specific Dissipation p for Ferrites

6.1.2 Conclusion About Level 0 Thermal Design

6.2 Single Thermal Resistance Design Approach
(Level 1 Thermal Design)

6.3 Classic Heat Transfer Mechanisms

6.3.1 Conduction Heat Transfer

6.3.2 Convection Heat Transfer

6.3.2.1 Natural and Forced Convection

6.3.2.2 Convection Heat Transfer Coefficient h_c

6.3.3 Radiation Heat Transfer

6.4 Thermal Design Utilizing a Resistance Network
Level 2 Thermal Design

6.4.1 Thermal Resistances

6.4.2 Finding Temperature Rise.

6.5 Contribution to Heat Transfer Theory of Magnetic Components

6.5.1 Practical Experience

6.5.2 Precise Expression of the Natural Convection
Coefficient h_c

6.5.2.1 Derivation of Convection Coefficient h_c

6.5.2.2 Dependencies of h_c on the Parameter L and
on the Position and Shape

6.5.3 Forced Convection

6.5.3.1 Classical Approach

6.5.3.2 Adapted Approach

6.5.4 Relationship with Thermal Resistance Networks

6.6 Transient Heat Transfer

6.6.1 Thermal Capacitances in Magnetic Components

6.6.2 Transient Heating

6.6.3 Adiabatic Loading Conditions

6.7 Summary

Appendix 6.A Accurate Natural Convection Modeling
for Magnetic Components.

6.A.1 Experimental Set Up

6.A.2 Thermal Measurements with the Box-Type Model

6.A.3 Thermal Measurements with the EE Transformer
Type Model

6.A.3.1 Thermal Measurements at an Ambient
Temperature of 25°C

6.A.3.2 Thermal Measurements at an Ambient
Temperature of 60°C

- 6.A.4 Derivation of an Accurate Presentation of the Convection Coefficient h_c
- 6.A.5 Comparison of the Experimental Results and Proposed Thermal Modeling

References

7 Parasitic Capacitances in Magnetic Components

- 7.1 Capacitance Between Windings: Inter Capacitance
 - 7.1.1 Effects of the Inter Capacitance
 - 7.1.2 Calculating Inter Capacitances and the Equivalent Voltage .
 - 7.1.3 Measuring Inter Capacitances
- 7.2 Self-Capacitance of a Winding: Intra Capacitance
 - 7.2.1 Effects of Intra Capacitance
 - 7.2.2 Calculating Intra Capacitances of a Winding
 - 7.2.3 Measuring Intra Capacitances of Windings
 - 7.2.3.1 Single Parasitic Capacitance Model
 - 7.2.3.2 Model with a Parasitic Capacitance for Each Winding
- 7.3 Capacitance Between the Windings and the Magnetic Material
- 7.4 Practical Approaches for Decreasing the Effects of Parasitic Capacitances
 - 7.4.1 Low Intra-Capacitance Windings
 - 7.4.2 Decreasing the Effects of the Inter Capacitance
 - 7.4.3 Screening

References

8 Inductor Design

- 8.1 Air Coils and Related Shapes
 - 8.1.1 Air Coils
 - 8.1.2 Solenoids
 - 8.1.3 Toroidal Coils
 - 8.1.4 Coils with Rectangular Cross Sections
 - 8.1.4.1 General Case
 - 8.1.4.2 'Four Square' Cylindrical Air Coil
- 8.2 Inductor Shapes
- 8.3 Typical Ferrite Inductor Shapes
- 8.4 Fringing in Wire-Wound Inductors with Magnetic Cores
 - 8.4.1 Center Gapped, Spacer and Side Gapped Inductors
 - 8.4.2 Simplified Approach to the Center Gapped Inductors
 - 8.4.3 Improved Approximation for Fringing Permeances of Gapped Inductors
 - 8.4.3.1 Fringing Coefficients
 - 8.4.3.2 Equivalent Surface
 - 8.4.3.3 Single and Multiple Air Gap Cases

- 8.5 Eddy Currents in Inductor Windings
 - 8.5.1 Referring to Described Methods
 - 8.5.2 Multiple Air Gap Inductors
 - 8.5.3 Avoiding Winding Close to the Air Gap
- 8.6 Foil Wound Inductors
 - 8.6.1 Foil Inductor—Ideal Case
 - 8.6.2 Single and Multiple Air Gap Design in Foil Inductors
 - 8.6.3 Eddy Current Losses in Foil Windings of Gapped Inductors
 - 8.6.4 Planar Inductors
- 8.7 Inductor Types Depending on Application
 - 8.7.1 DC Inductors
 - 8.7.2 HF Inductors
 - 8.7.3 Combined DC-HF Inductor
 - 8.7.3.1 Classical Solutions
 - 8.7.3.2 Special, Combined Design: Litz Wire—Full Wire Inductor Winding
 - 8.7.3.3 Analytical Modeling of the Combined Full-Wire—Litz-Wire Inductor
- 8.8 Design Examples of Different Types of Inductors
 - 8.8.1 Boost Converter Inductor Design
 - 8.8.2 Coupled Inductor Design
 - 8.8.3 Flyback Transformer Design
- 8.A.1 Fringing Coefficients For Gapped-Wire-Wound Inductors
 - 8.A.1.1 Basic Cases
 - 8.A.1.1.1 Basic Case 1
 - 8.A.1.1.2 Basic Case 2
 - 8.A.1.1.3 Basic Case 3
 - 8.A.1.1.4 Basic Case 4
 - 8.A.1.2 Symmetrical Cases
 - 8.A.1.2.1 Case 1s
 - 8.A.1.2.2 Case 2s
 - 8.A.1.2.3 Case 3s
 - 8.A.1.2.4 Case 4s
 - 8.A.1.3 Application to Gapped Rectangular Cores
 - 8.A.1.4 Application to Center Gapped Rectangular Cores
 - 8.A.1.5 Application to Center Gapped Round Cores
- 8.A.2 Analytical Modeling of Combined Litz-Wire—Full-Wire Inductors
 - 8.A.2.1 Example of a Combined Litz-Wire—Full-Wire Inductor
 - 8.A.2.2 Experimental Results
 - 8.A.2.3 Conclusion

References

9 Transformer Design

- 9.1 Transformer Design in Power Electronics
 - 9.2 Magnetizing Inductance
 - 9.2.1 Basics
 - 9.2.2 Design
 - 9.3 Leakage Inductance
 - 9.3.1 Leakage Inductance of Concentric Windings
 - 9.3.2 Leakage Inductance of Windings in Separate Rooms
 - 9.3.2.1 General Case
 - 9.3.2.2 Axis-Symmetrical Case
 - 9.3.3 Leakage Inductance in T, L and M Models of Transformers
 - 9.3.3.1 *T* Transformer Model
 - 9.3.3.2 *L* Transformer Model
 - 9.3.3.3 *M* Transformer Model
 - 9.4 Using Parallel Wires and Litz Wires
 - 9.4.1 Parallel Wires
 - 9.4.1.1 Low Frequency Case: $d < 1.6\delta$
 - 9.4.1.2 High Frequency Case: $d > 2.7\delta$
 - 9.4.2 Parallel Windings Using Symmetry in the Magnetic Path
 - 9.4.3 Using Litz Wire
 - 9.4.3.1 Example in the Low-Frequency Approximation
 - 9.4.4 Half Turns
 - 9.5 Interleaved Windings
 - 9.6 Superimposing Frequency Components
 - 9.6.1 Magnetic Materials
 - 9.6.2 Eddy Currents in Conductors
 - 9.6.2.1 General Solution
 - 9.7 Superimposing Modes
- References

10 Optimal Copper/Core Loss Ratio in Magnetic Components

- 10.1 Simplified Approach
 - 10.1.1 Transformer
 - 10.1.2 Inductor
- 10.2 Loss Minimization in the General Case
- 10.3 Loss Minimization Without Eddy Current Losses
 - 10.3.1 Constant Copper Volume
 - 10.3.2 Constant Wire Cross Section
 - 10.3.3 Equal Core and Copper Surface Temperatures
- 10.4 Loss Minimization Including Low-Frequency Eddy Current Losses

- 10.4.1 Constant Copper Wire Cross Section
- 10.4.2 Constant Copper Wire Volume
- 10.4.3 Variable Wire Cross Section and Number of Turns
- 10.4.4 More General Problems with Eddy Currents
- 10.5 Summary
- 10.6 Examples
- References

11 Measurements

- 11.1 Introduction
- 11.2 Temperature Measurements
 - 11.2.1 Thermocouple Measurement
 - 11.2.2 PT100 Thermistor Temperature Measurement
 - 11.2.3 NTC Thermistor Temperature Measurement
 - 11.2.4 Glass Fiber Optic Temperature Measurement
 - 11.2.5 Infrared Surface Temperature Measurement
 - 11.2.6 Thermal Paint and Strips
 - 11.2.7 Winding Resistance Measurement Method
- 11.3 Power Losses Measurements
 - 11.3.1 Circuit Wattmeter Measurement
 - 11.3.2 Oscilloscope Measurements
 - 11.3.1.1 Example of the Accuracy Problem in Oscilloscope Measurement
 - 11.3.2 Impedance Analyzers and RLC Meters
 - 11.3.2.1 Impedance Analyzers
 - 11.3.2.2 RLC Meters
 - 11.3.3 Q-factor Test of LC Networks
 - 11.3.4 Power Loss Estimation by Thermal Resistance
 - 11.3.5 Calorimetric Power Loss Measurement
 - 11.3.5.1 Inertia Calorimeter
 - 11.3.5.2 Flow Calorimeter
 - 11.3.5.2.1 Principle of Operation
 - 11.3.5.2.2 Accuracy of Flow Calorimeters
 - 11.3.5.2.3 Practical Flow Calorimeter
 - 11.3.5.2.4 Conclusions
- 11.4 Measurement of Inductances
 - 11.4.1 Measurement of the Inductance of an Inductor
 - 11.4.2 No Load Test of Transformers
 - 11.4.3 Short Circuit Test
 - 11.4.4 Measurement of the Inductances in Transformers
 - 11.4.5 Measurement of Low Inductances
- 11.5 Core Loss Measurements
 - 11.5.1 Classical Four-Wire Method
 - 11.5.2 Two-Wire Method
 - 11.5.2.1 Oscilloscope Based Measurement
 - 11.5.2.2 Wide Band Current Probe

- 11.5.2.3 Corresponding Voltage Probe
- 11.5.2.4 Flux Measurement Probe
- 11.5.3 Practical Ferrite Power Loss Measurement Set Up
- 11.6 Measurement of Parasitic Capacitances
 - 11.6.1 Measurement of Capacitance Between Windings
 - 11.6.2 Measurement of the Equivalent Parallel Capacitance of a Winding
- 11.7 Combined Measuring Instruments
- References

Appendix A RMS Values of Waveforms

A.1 Definitions

- Physical Meaning of the RMS Value
- RMS Value in the Frequency Domain
- RMS Value in the Time Domain

A.2 RMS Values of Some Basic Waveforms

- A.2.1 Discontinuous Waveforms
- A.2.2 Repeating Line Waveforms
- A.2.3 Waveforms Consisting of Different Repeating Line Parts

A.3 RMS Values of Common Waveforms

- A.3.1 Sawtooth Wave, Fig. A.4.
- A.3.2 Clipped Sawtooth, Fig. A.5
- A.3.3 Triangular Waveform, No DC Component, Fig. A.6.
- A.3.4 Triangular Waveform with DC Component, Fig. A.7
- A.3.5 Clipped Triangular Waveform, Fig. A.8.
- A.3.6 Square Wave, Fig. A.9
- A.3.7 Rectangular Pulse Wave, Fig. A.10
- A.3.8 Sine Wave, Fig. A.11.
- A.3.9 Clipped Sinusoid, Full Wave, Fig. A.12.
- A.3.10 Clipped Sinusoid, Half Wave, Fig. A.13
- A.3.11 Trapezoidal Pulse Wave, Fig. A.14

Appendix B Magnetic Core Data

- B.1 ETD Core Data (Economic Transformer Design Core)
- B.2 EE Core Data
- B.3 Planar EE Core Data
- B.4 ER Core Data
- B.5 UU Core Data
- B.6 Ring Core Data (Toroid Core)
- B.7 P Core Data (Pot Core)
- B.8 PQ Core Data
- B.9 RM Core Data
- B.10 Other Information

Appendix C Copper Wires Data

C.1 Round Wire Data

C.2 American Wire Gauge Data

C.3 Litz Wire Data

Appendix D Mathematical Functions

References

1

Fundamentals of Magnetic Theory

This chapter gives a brief review of the basic laws, quantities, and units of magnetic theory. Magnetic circuits are included together with some examples. The analogy between electric and magnetic circuits and quantities is presented. Hysteresis and basic properties of ferromagnetic materials are also discussed. The models of the ideal transformers and inductors are shown.

1.1 Basic Laws of Magnetic Theory

The experimental laws of electromagnetic theory are summed up by the Maxwell equations. In 1865, after becoming acquainted with the experimental results of his fellow Englishman Faraday, Maxwell gave the electromagnetic theory a complete mathematical form. We will present specific parts of the Maxwell equations: Ampere's law, Faraday's law, and Gauss's law, which together with Lenz's law are the basis of magnetic circuit analysis. These are the laws that are useful in the design of magnetic components for power electronics.

1.1.1 Ampere's Law and Magnetomotive Force

When an electrical conductor carries current, a magnetic field is induced around the conductor, as shown in Fig. 1.1. The induced magnetic field is characterized by its *magnetic field intensity* H . The direction of the magnetic field intensity can be found by the so-called *thumb rule*, according to which, if the conductor is held with the right hand and the thumb indicates the current, the fingers indicate the direction of the magnetic field.

The magnetic field intensity H is defined by *Ampere's law*. According to Ampere's law the integral of H [A/m] around a closed path is equal to the total current passing through the interior of the path (note that a line above a quantity denotes that it is a vector):

$$\oint_l H \cdot dl = \int_s J \cdot dS \quad (1.1)$$

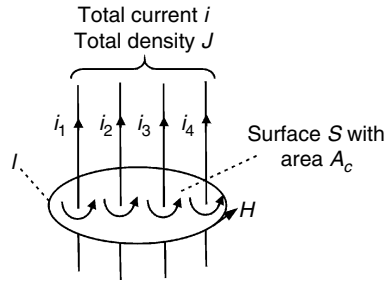


FIGURE 1.1

Illustration of Ampere's law. The MMF around a closed loop is equal to the sum of the positive and negative currents passing through the interior of the loop.

where

H is the field intensity vector [A/m]

$d\mathbf{l}$ is a vector length element pointing in the direction of the path l [m]

J is the electrical current density vector [A/m²]

dS is a vector area having direction normal to the surface [m²]

l is the length of the circumference of the contour [m]

S is the surface of the contour [m²]

If the currents are carried by wires in a coil with N turns, then

$$\oint_l \mathbf{H} \cdot d\mathbf{l} = \int_S \mathbf{J} \cdot d\mathbf{S} = Ni \quad (1.2)$$

where

i is the current in the coil

N is the number of the turns

The terms $\int \bar{H} \cdot d\bar{l}$ and Ni in Equation (1.2) are equivalent to a source called *magnetomotive force* (MMF), which is usually denoted by the symbol F [A · turns]. Note that the number of turns N does not have dimension, but the value Ni is an actual MMF and not a current. According to Equation (1.1) the net MMF around a closed loop with length l_c is equal to the total current enclosed by the loop. Applying Ampere's law to Fig. 1.1 we obtain

$$\oint_l \mathbf{H} \cdot d\mathbf{l} = \sum_1^n i = i_1 + i_2 + i_3 + i_4 \quad (1.3)$$

In Fig. 1.1 the reference directions of the current and the H field vector are shown. The magnetic field intensity H leads to a resulting *magnetic flux density* B given by

$$\mathbf{B} = \mu_0 \mu_r \mathbf{H} = \mu \mathbf{H} \quad (1.4)$$

where:

μ is a specific characteristic of the magnetic material termed *permeability*
 μ_0 is the *permeability of free space*, a constant equal to $4\pi \times 10^{-7}$ H/m
 μ_r is the *relative permeability* of the magnetic material

The value of μ_r for air and electrical conductors (e.g., copper, aluminum) is 1. For ferromagnetic materials such as iron, nickel, and cobalt the value of μ_r is much higher and varies from several hundred to tens of thousands.

The magnetic flux density B is also called *magnetic induction* and, for simplicity, in this book we will use the term *induction* for this magnetic quantity. The vector B is the surface density of the magnetic flux. The scalar value of the total *magnetic flux* Φ passing through a surface S is given by

$$\Phi = \int_S B \cdot dS \quad (1.5)$$

If the induction B is uniform and perpendicular to the whole surface area A_c , then the expression in Equation (1.5) results in

$$\Phi = BA_c \quad (1.6)$$

We have to mention that the expression given by Equation (1.1) is not complete; there is a term missing in the right-hand side. The missing term, which is a current in fact, is called *displacement current* and was added to the expression by Maxwell in 1865. The full form of the law is

$$\oint_l H \cdot dl = \int_S J \cdot dS + \frac{\partial}{\partial t} \int_S \epsilon E \cdot dS \quad (1.7)$$

where

ϵ is the permittivity of the medium
 E is the electric field

Maxwell's correction to Ampere's law is important mainly for high-frequency applications with low current density. In magnetic components for power electronics the expected current density is of the order of at least $J = 10^6$ A/m². In all normal applications the second term on the right-hand side of Equation (1.7) (the Maxwell's correction) is almost surely not more than 10 A/m², and can be neglected. Exceptions are the currents in capacitors, currents caused by so-called parasitic capacitances, and currents in transmission lines. This conclusion allows us to use the simplified expression in Equation (1.1) in power electronics magnetic circuit analysis, an approach called the quasi-static approach.

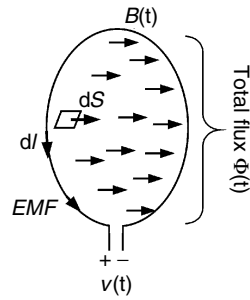


FIGURE 1.2
 Illustration of Faraday's law. The voltage $v(t)$ induced in a closed loop by a time-changing flux $\Phi(t)$ passing the loop (generator convention).

1.1.2 Faraday's Law and EMF

A time-changing flux $\Phi(t)$ passing through a closed loop (a winding) generates voltage in the loop. The relationship between the generated voltage $v(t)$ and the magnetic flux $\Phi(t)$ is given by *Faraday's law*. According to Faraday's law the generated voltage $v(t)$ is

$$v(t) = \frac{d\Phi(t)}{dt} \quad (1.8)$$

If we denote the intensity of the electric field as E , then Faraday's law is

$$\oint_l E \cdot dI = -\frac{d}{dt} \int_s B \cdot dS \quad (1.9)$$

Equation (1.9) is valid for the generator convention. For the consumer convention there is no minus sign in it. In this book we use the consumer convention. The positive senses of B , dI , dS , and the generated *electromotive force (EMF)* are shown by arrows in [Fig. 1.2](#).

Faraday's law is valid in two cases:

- A fixed circuit linked by a time-changing magnetic flux, such as a transformer
- A moving circuit related to a time-stationary magnetic flux in a way that produces a time-changing flux passing through the interior of the circuit.

Rotating electrical machines generate EMF by the latter mechanism.

1.1.3 Lenz's Law and Gauss's Law for Magnetic Circuits

Lenz's law states that the voltage $v(t)$ generated by a fast time-changing magnetic flux $\Phi(t)$ has the direction to drive a current in the closed loop, which induces a flux that tends to oppose the changes in the applied flux $\Phi(t)$. [Figure 1.3](#) shows an example of Lenz's law.

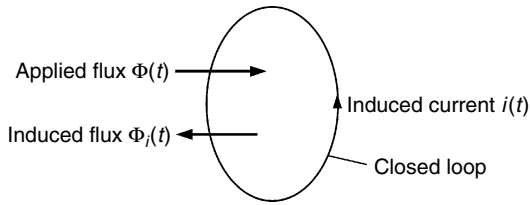


FIGURE 1.3

Illustration of Lenz's law in a closed winding. The applied flux $\Phi(t)$ induces current $i(t)$, which generates induced flux $\Phi_i(t)$ that opposes the changes in $\Phi(t)$.

Lenz's law is useful for understanding the eddy current effects in magnetic cores as well in the coil conductors. The eddy currents are one of the major phenomena causing losses in magnetic cores and in coil conductors.

Gauss's law for magnetic circuits states that for any closed surface S with arbitrary form the total flux entering the volume defined by S is exactly equal to the total flux coming out of the volume. This means that the total resulting flux through the surface is zero:

$$\oint_S \mathbf{B} \cdot d\mathbf{S} = 0 \quad (1.10)$$

Gauss's law for magnetic circuits is analogous to Kirchoff's current density law for electrical circuits.

1.2 Magnetic Materials

Magnetic materials can be classified in three general groups according to their magnetic properties:

- Diamagnetic materials
- Paramagnetic materials
- Ferromagnetic materials

The relative permeability μ_r of diamagnetic and paramagnetic materials is close to unity. The values of B and H are linearly related for both materials. *Diamagnetic materials* have a value of μ_r less than unity, which means that they tend to slightly exclude magnetic field, that is, a magnetic field intensity is generally smaller in a diamagnetic material than it would be in a paramagnetic material under the same conditions. The atoms of diamagnetic materials

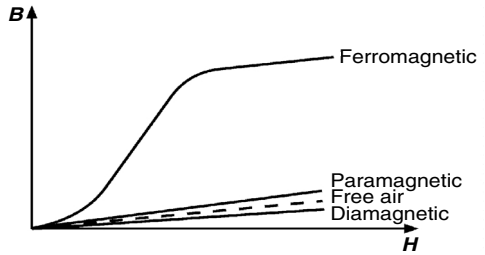


FIGURE 1.4
Magnetization curves for different types of magnetic materials. The scale of the magnetization curve of ferromagnetic materials is much higher.

do not have permanent magnetic moments. *Superconductors* are a specific class of diamagnetic materials. In these materials there are macrocurrents circulating in the structure. These currents oppose the applied field and as a result the material excludes all exterior fields. *Paramagnetic materials* have a value of μ_r greater than unity, and they are slightly magnetized by an applied magnetic field. *Ferromagnetic materials* are characterized by values of μ_r much higher than unity (10–100,000) [1]. For the design of magnetic components for power electronics, the third type of materials, the ferromagnetic materials, are of real importance, especially ferromagnetic ceramics and metals. Comparison of B - H relation of different types of magnetic materials is shown in Fig. 1.4.

1.2.1 Ferromagnetic Materials

To understand ferromagnetic materials we will start with the magnetic moments of atoms and the structure of metals. Each electron possesses an electrical charge and its own magnetic (spin) moment. Besides the spin, each electron of the atom has another magnetic moment, a so-called orbital moment, caused by its rotation around the nucleus. In the atoms of many elements the electrons are arranged in such a way that the net atomic moment is almost zero. Nevertheless, the atoms of more than one-third of the known elements possess a magnetic moment. Thus, every single atom of these elements has a definite magnetic moment as a result of the contributions of all of its electrons. This magnetic moment can be associated with an atomic magnet.

In metals there is an interaction between the atoms, which defines the magnetic properties of the total structure. In most cases the atomic moments in the crystal are inter-coupled by coupling forces. If the atomic moments are arranged in parallel with crystal lattice sites, then the moments of the individual atoms are summed up resulting in the *ferromagnetic effect*. The coupling forces in the ferromagnetic materials of technical interest are strong and at room temperature almost all atomic magnets are parallel-aligned. The alignment of the atomic magnets does not occur in the entire structure, but only within certain regions. These regions of alignment of the atomic magnets are called *ferromagnetic domains* or *Weiss domains*. In polycrystalline

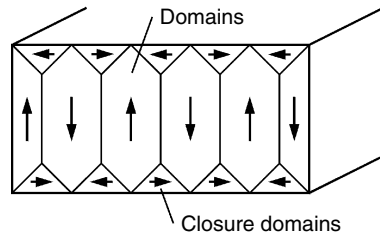


FIGURE 1.5
Orientation of domain magnetic moments in the structure of unmagnetized iron.

materials they usually have a laminar pattern. The size of the domains varies considerably, from 0.001 mm^3 to 1 mm^3 . Each domain contains many atoms and is characterized by an overall magnetic moment, as a result of the summing of the atomic magnets. The directions of the domain magnetic moments in an unmagnetized crystal are not completely random among all available directions. The domain magnetic moments are oriented so as to minimize the total external field, and in that way to keep the energy content as low as possible. To follow this rule, adjacent domains have opposite magnetic moments, as shown in Fig. 1.5. The net external field is reduced additionally by so-called *closure domains*, shown in Fig. 1.5.

In every crystal the domains are divided from each other by boundaries, so-called *domain walls* or *Bloch walls*. Across the domain walls the atomic magnetic moments reverse their direction, as shown in Fig. 1.6

The described mechanism of summing the atomic magnetic moments, resulting in spontaneous magnetization of the domains in ferromagnetic materials, is valid until a specific temperature, called the *Curie temperature* T_C . The value of T_C is clearly defined for every material. If the temperature of the material is increased above that value the thermal oscillations of the atomic magnets increase significantly and overcome the coupling forces that maintain the alignment of the atomic magnets in the domains. The final effect disturbs the alignment of magnetic moments of adjacent atoms. When a ferromagnetic material is heated above its Curie temperature T_C , its magnetic properties are completely changed and it behaves like a paramagnetic material. The permeability of the material drops suddenly to $\mu_r \approx 1$, and both coercivity and remanence become zero (the terms coercivity and remanence will be discussed in the next section). When the material is cooled, the alignment of the atomic magnets in the domains will recover, but the magnetic moments of the domains will be orientated randomly to each other.

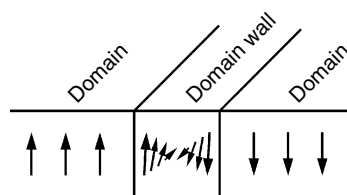


FIGURE 1.6
Domain (Bloch) walls.

TABLE 1.1

Curie Temperatures of Various Ferromagnetic Elements and Materials

Material	Curie temperature, T_C [°C]
Iron	770
Cobalt	1130
Nickel	358
Gadolinium	16
Terfenol	380–430
Alnico	850
Hard ferrites	400–700
Soft ferrites	125–450
Amorphous materials	350–400

Thus, the total external field in the structure will be zero. This means that heating a ferromagnetic material above T_C demagnetizes it completely. The Curie temperatures of various ferromagnetic elements and materials are shown in Table 1.1.

1.2.2 Magnetization Processes

Each crystal of a ferromagnetic material contains many domains. The shape, size, and magnetic orientation of these domains depend on the level and direction of the applied external field.

Let us start with an unmagnetized sample of a ferromagnetic material (Fig. 1.7, a). Suppose an external magnetic field H_{ext} in a direction parallel of the domain magnetic moments. With increasing intensity of the applied field the domain walls begin to move (*wall displacement*), first slowly, then quickly, and at the end, in jumps. In the presence of an external field the atomic magnets are subjected to a torque, which tends to align them with the direction of the applied field. The magnetic moments that are in the direction of H_{ext} do not experience a resulting torque. The magnetic moments that are not aligned with H_{ext} are subjected to a torque tending to rotate them in the direction of H_{ext} . As a result, the overall domain wall structure becomes mobile and the domains that are in the direction of the applied external field H_{ext} increase in size by the movement of the domain walls into the domains with direction opposite to H_{ext} (Fig. 1.7b). There will be a net magnetic flux in the sample. The *magnetization*, which is the average value per unit volume of all atomic magnets, is increased.

When the applied external field H_{ext} is small, the described domain wall displacements are reversible. When H_{ext} is strong, nonelastic wall displacements occur, which cause hysteresis in the B - H relation. Above a certain level of the applied external field, *Barkhausen jumps* of the domain walls occur (Fig. 1.7c). By these jumps, a domain having the direction of the applied field absorbs an adjacent domain with a direction opposite to the applied field.

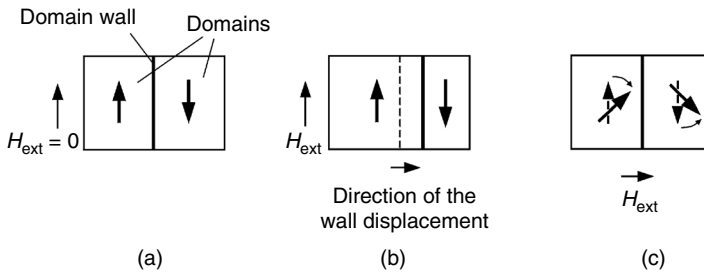


FIGURE 1.7

Magnetization of a ferromagnetic sample: (a) without applied external field; (b) with applied external field H_{ext} —movement of the domain walls; (c) with applied external field H_{ext} —rotation of the domain magnetic moments.

When the strength of the applied external field H_{ext} is increased further, the process of *domain rotation* occurs. The domain magnetic moments rotate in order to align themselves to the direction of H_{ext} , thus increasing the magnetization. The process tends to align the domains more to the direction of the applied external field in spite of their initial direction along the crystal axes.

The total magnetization process includes domain wall displacements and jumps and domain rotations. In the case of ferromagnetic metals, at the start the process is realized mainly by means of the wall displacements and jumps, and the rotations of the whole domains take place at the end of the process, doing the final alignment in the preferred directions, defined by the external field.

For further reading, the magnetization processes are described in detail in standard texts [1,2].

1.2.3 Hysteresis Loop

Let us suppose a magnetic core with a coil, as shown in Fig. 1.8. At the beginning, the net magnetic flux B in the core, the current i in the coil, and the magnetic field intensity H are zero. Increasing the current in the coil results in applying the field with intensity H according to the Ampere's law

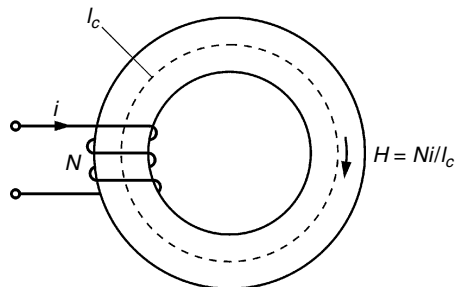


FIGURE 1.8

Magnetic core with a coil.

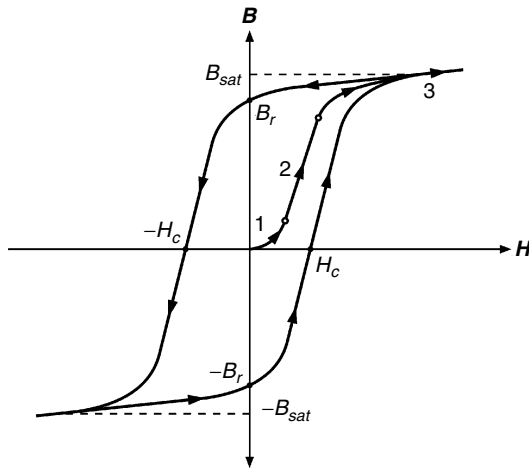


FIGURE 1.9
Hysteresis loop and magnetization curve of a ferromagnetic material.

($Hl_c = Ni$, assuming that H is uniform in the core). The first, slowly rising initial section of the magnetization curve, Fig. 1.9, corresponds to reversible domain walls displacements. In the second section of the curve, the induction B increases much more quickly with the increase of H and the curve is steep. The significant increase of B in the second section is explained with the Barkhausen jumps of the domain walls, which occur when the applied external field intensity reaches a necessary level. At the end of this section the structure of the ferromagnetic material contains mainly domains, which are almost aligned along the crystal axes nearest to the direction of the applied external field. The increase of the magnetic flux in the material is not any more possible by domain wall motion. Further increase in H to larger values results in non-significant increase in B . and the third section of the magnetization curve is flat. Because the level of H is already much greater than in section 1 and 2, it is enough to initiate the domain rotation process. The contribution of this process to the total magnetic flux is relatively small and gradually decreases. The material reaches saturation and further increase in H results in very small increase in B . The maximum value of B : the *saturation induction value* B_{sat} , is practically reached. All the atomic magnets are aligned along the direction of the applied external field H .

Let us observe the process of decreasing H , which means decreasing the excitation current i in the coil. The first reaction of reducing H is the rotation of the domains back to their preferred initial directions in parallel with the crystal axes. Further, some domain walls move back in their initial positions, but most of the domain walls remain in the positions reached in the wall displacement process. Thus, the flux B does not return along the same curve, along which it rises with increasing H . The new curve, observed with reducing H , lags behind the initial magnetization curve. When H reaches zero,

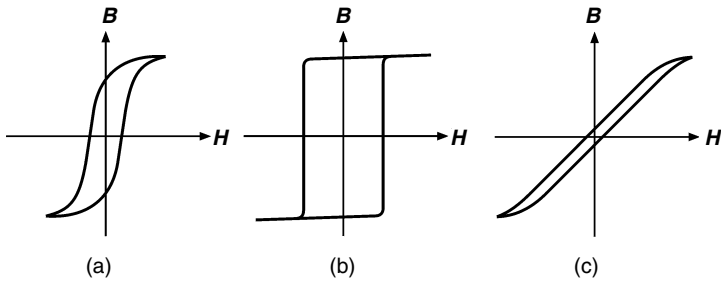


FIGURE 1.10

Typical hysteresis loop shapes: (a) round loop, R-type; (b) rectangular loop, Z-type; (c) flat loop, F-type.

residual flux density or remanence, B_r , remains mainly due to non-elastic wall displacement process. To reduce this residual flux density B_r to zero, a negative (reversed) field H is necessary to be applied. That field should be sufficient to restore the initial positions of the domain walls. The negative value of H at which B is reduced to zero is called coercive force or coercivity of the material H_c . A further increase of H in the opposite direction results in a process of magnetization as the one described above and B reaches saturation level $-B_{sat}$ ($| -B_{sat} | = B_{sat}$). If the current of the excitation coil is repeatedly cycling between the two opposite extreme values, corresponding to the two opposite maximum values of H , the hysteresis loop is traced out, as shown in Fig. 1.9.

The hysteresis loop gives the relation between the induction B and the flux intensity H for a closed reversal cycle of magnetization of a ferromagnetic material. The shape of the hysteresis loop is material dependent. Other factors that influence the shape are the excitation frequency and the conditions of the treatment of the material. Some typical hysteresis loops are shown in Fig. 1.10.

The surface of the loop in the B - H plane is the energy loss per volume for one cycle.

According to their coercive force H_c the ferromagnetic materials are subdivided in two general classes:

- Soft magnetic materials
- Hard magnetic materials

Soft magnetic materials are characterized by an ease of change of magnetic alignment in their structure. This fact results in low coercive force H_c and a narrow hysteresis loop as shown in Fig. 1.11. Soft magnetic materials are of main importance for modern electrical engineering and electronics and are indispensable for many devices and applications. In power electronics most of the magnetic components use cores made from soft magnetic materials.

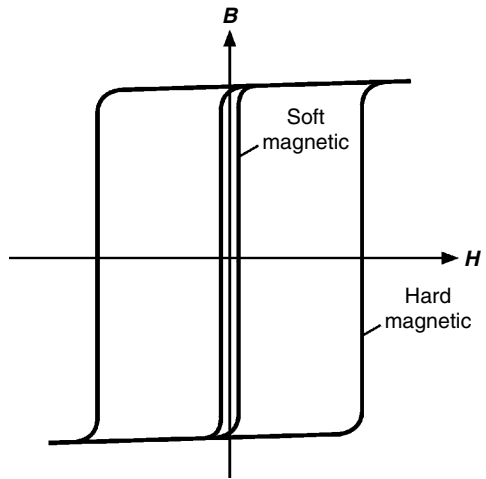


FIGURE 1.11

Typical hysteresis loops: (a) a soft magnetic material, narrow loop, low H_c ; (b) a hard magnetic material, square loop, high H_c and B_r .

Hard magnetic materials are also called permanent magnets. The initial alignment of the magnetic moments in hard magnetic materials strongly resists any influence of an external magnetic field and the coercive force H_c is much higher than that of soft magnetic materials. Another important property of permanent magnets is their high value of the remanence induction B_r . A typical hysteresis loop of a permanent magnet is shown in Fig. 1.11. The permanent magnets produce flux even without any external field. The typical applications of permanent magnets are in electrical motors, generators, sensing devices, and mechanical holding.

The following ranges can be used as approximate criteria for classifying a material as a soft or hard magnetic material [2]:

$H_c < 1000 \text{ A/m}$ soft magnetic material

$H_c > 10\,000 \text{ A/m}$ hard magnetic material

Usually, the values of H_c of most of the used in practice materials are $H_c < 400 \text{ A/m}$ for soft materials and $H_c > 100,000 \text{ A/m}$ for hard magnetic materials.

1.2.4 Permeability

Permeability is an important property of magnetic materials and therefore we will discuss it in detail. The relative permeability μ_r , introduced in Section 1.1 has several different interpretations depending on the specific conditions of defining and measuring it. The index r is omitted and only the corresponding index is used in denoting the different versions: amplitude permeability μ_a , initial permeability μ_i , effective permeability μ_e , incremental permeability μ_{in} , reversible permeability μ_{rev} , and complex permeability $\underline{\mu}$.

Amplitude permeability μ_a is the relative permeability under alternating external field H , which gives the relation between the peak value of the induction B and the magnetic field H . Its general definition is

$$\mu_a = \frac{1}{\mu_0} \frac{\hat{B}}{\hat{H}} \tag{1.11}$$

where

\hat{B} is the amplitude induction value averaged out over the core cross-section
 \hat{H} is the amplitude field parallel to the surface of the core

The initial permeability μ_i is the relative permeability of the magnetic material when the applied magnetic field H is very low:

$$\mu_i = \frac{1}{\mu_0} \frac{\Delta B}{\Delta H} (\Delta H \rightarrow 0) \tag{1.12}$$

For practical purposes the value obtained at a small field H is standardized [2], e.g., as the permeability at $H = 0.4 \text{ A/m}$ (see Fig. 1.12).

If there is an air gap in a closed magnetic circuit, the apparent total permeability of the circuit is called effective permeability μ_e , which is much lower than the permeability of the same core without an air gap. The effective permeability depends on the initial permeability μ_i of the magnetic material and the dimensions of the core and the air gap. For cores with relatively small (short) air gaps the effective permeability is given by

$$\mu_e = \frac{\mu_i}{1 + \frac{A_g \mu_i}{l_c}} \tag{1.13}$$

where

A_g is the cross-sectional area of the air gap
 l_c is the effective length of the magnetic path

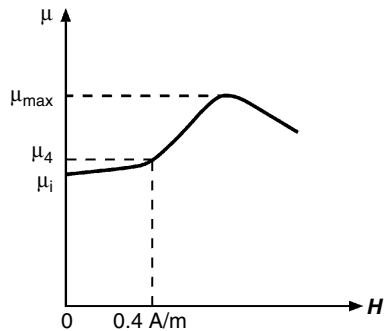


FIGURE 1.12
 Definition of μ_i , μ_4 , and μ_{Δ} dependent on the field H .

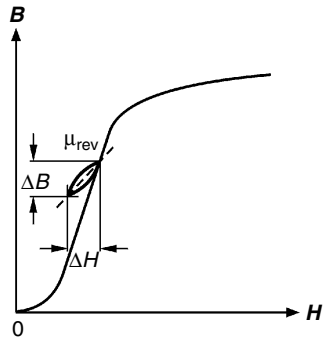


FIGURE 1.13
Definition of the reversible permeability μ_{rev} .

If the air gap is long, some part of the flux passes outside the air gap and this additional flux results in an increased value of the effective permeability in comparison with Equation (1.13). Therefore Equation (1.13) is valid only when fringing permeability is neglected. The effective permeability is also known as the permeability of an equivalent homogeneous toroidal core.

Incremental permeability μ_{Δ} is defined when an alternating magnetic field H_{AC} is superimposed on a static magnetic field H_{DC} . The hysteresis loop follows a minor loop path. The incremental permeability is

$$\mu_{\Delta} = \left(\frac{1}{\mu_0} \frac{\Delta B}{\Delta H} \right)_{H_{\text{DC}}} \quad (1.14)$$

The limiting value of the incremental permeability μ_{in} , when the amplitude of the alternating field excitation H_{AC} is very small, is termed *reversible permeability* μ_{rev} (see Fig. 1.13):

$$\mu_{\text{rev}} = \frac{1}{\mu_0} \frac{\Delta B}{\Delta H}, \quad \Delta H \rightarrow 0 \quad (1.15)$$

1.2.4.1 Complex Permeability

In practice, we never have an ideal inductance when the core is made from a magnetic material. Under sinusoidal excitation there is a phase shift between the fundamental components of the induction B and the magnetic field H . By using a complex quantity for the relative permeability, consisting of a real part and an imaginary part, these effects are easily presented. The imaginary part of the *complex permeability* $\underline{\mu}$ is associated with the losses in the material. There are two different forms of the complex permeability $\underline{\mu}$.

- Series representation, according to the series equivalent circuit of magnetic component shown in Fig. 1.14a:

$$\underline{\mu} = \mu'_s - j\mu''_s \quad (1.16)$$

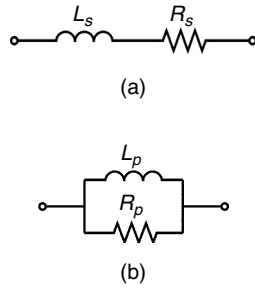


FIGURE 1.14
Series and parallel equivalent circuits.

where

μ'_s and μ''_s are the real and imaginary parts of the complex permeability

- Parallel representation, according to the parallel equivalent circuit shown in Fig. 1.14b):

$$\frac{1}{\underline{\mu}} = \frac{1}{\mu'_p} + j \frac{1}{\mu''_p} \tag{1.17}$$

where

μ'_p and μ''_p are the real and imaginary parts of the complex permeability

In Fig. 1.15 the complex permeability is represented by the series terms in the frequency domain. These values are often given in the data to describe the behavior of the material at very low induction levels (signal applications). The graphs of the real and imaginary parts versus frequency are often shown to describe the frequency behavior of the material. The values of the real and imaginary parts of the complex permeability in the series presentation for a given frequency can be calculated from the measured inductance L_s and resistance R_s of the coil of its series equivalent circuit.

The parallel representation has the advantage that the loss associated part μ''_p does not change when an air gap is added in the magnetic circuit. Usually in applications the induction B is known, which allows the calculation of the losses directly by using μ''_p . The parallel representation is more often used in power applications.

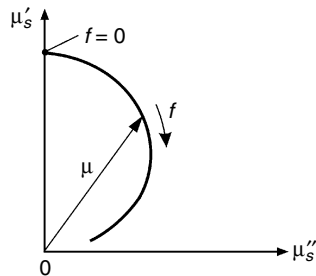


FIGURE 1.15
Complex permeability presented by the series terms in the frequency domain.

Depending on the application and purpose, the series or parallel presentation may be used. The following expressions give the relation between the series and parallel presentation parts of the complex permeability:

$$\mu'_p = \mu'_s(1 + \tan^2 \delta) \quad (1.18)$$

$$\mu''_p = \mu''_s \left(1 + \frac{1}{\tan^2 \delta} \right) \quad (1.19)$$

In Equations (1.18) (1.19) δ is the *loss angle*, which is also the phase lag of the induction B with respect to the applied magnetic field H . The tangent of the loss angle δ is given by the expression

$$\tan \delta = \frac{\mu''_s}{\mu'_s} = \frac{\mu'_p}{\mu''_p} \quad (1.20)$$

The quantity $\tan \delta$ is also the ratio of the equivalent series resistance of a coil (neglecting copper resistance) to its reactance, which is the reciprocal value of quality factor of the inductance:

$$\tan \delta = \frac{R}{\omega L} = \frac{1}{Q} \quad (1.21)$$

The complex permeability is mainly used in signal electronics and for low induction levels and is less often used in power electronics. In power electronics the magnetic materials have a nonlinear frequency behavior. We would like to warn the reader that if the ferrite losses at high induction levels are estimated by μ' and μ'' values, which are relevant at low induction levels, then the losses can be severely underestimated. The reason is that the losses in the ferrites increase more than the square of the induction B .

1.2.4.2 Hysteresis Material Constant

The losses of some ferrite grades are described using the hysteresis constant η_B , which is defined at low induction levels. The hysteresis constant η_B is defined by the following expression [7]:

$$\Delta \tan \delta_h = \mu_e \eta_B \Delta \hat{B} \quad (1.22)$$

where

$\Delta \hat{B}$ is the amplitude of the induction B

μ_e is the effective permeability

The hysteresis losses increase when the induction in a core increases. The contribution of the hysteresis losses to the total losses can be estimated by

means of the results of two measurements, usually at the induction levels 1.5 mT and 3 mT [4]. By these measurements the hysteresis constant η_B is found from

$$\eta_B = \frac{\Delta \tan \delta}{\mu_c \Delta \hat{B}} \quad (1.23)$$

and then it is used to find δ_i by Equation (1.22).

The consequence of this behavior is that at low B values the losses tend to increase with B^2 , whereas at large B values the dependence is close to B^3 .

1.3 Magnetic Circuits

1.3.1 Basic Laws for Magnetic Circuits

According to Ampere's law, the sum of the MMF around a closed magnetic loop is zero:

$$\sum MMF_{\text{loop}} = 0, \quad \sum MMF_{\text{source}} = \sum MMF_{\text{drop}} \quad (1.24)$$

This requirement is analogous to the Kirchoff's voltage law. The MMF_{drop} for an element of a magnetic circuit is

$$MMF_{\text{drop}} = Hl \text{ [A} \cdot \text{turns]} \quad (1.25)$$

Substituting $H = B/\mu$ and $B = \Phi/A_c$ results in the following expressions:

$$\int MMF_{\text{drop}} = \Phi \frac{l}{\mu A_c} = \Phi \mathfrak{R} = \frac{\Phi}{\Lambda} \quad (1.26)$$

$$Hl = \Phi \mathfrak{R} \Rightarrow F = \Phi \mathfrak{R} \quad (1.27)$$

In Equation (1.26) the magnetic flux Φ is analogous to current I , and the quantity $\mathfrak{R} = l/\mu A_c$ is analogous to resistance R . The quantity $\mathfrak{R} = l/\mu A_c$ [A · turns/Wb] is called *reluctance* and we will use the symbol \mathfrak{R} for it. The quantity $1/\mathfrak{R}$ [Wb/A · turns] is called *permeance* Λ of the magnetic path (in soft ferrites data this value is often denoted as A_L value).

For a magnetic circuit with an air gap (Fig. 1.16), by splitting the left side into two terms and assuming that H is almost uniform in both mediums, the Ampere's law can be written as

$$H_c l_c + H_g l_g = NI \quad (1.28)$$

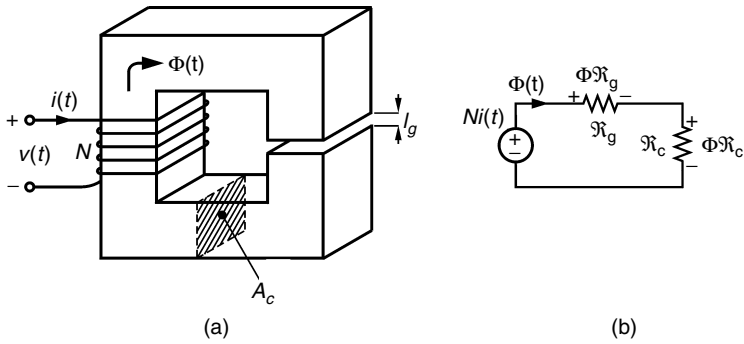


FIGURE 1.16 Magnetic circuit with an air gap: (a) physical geometry; (b) equivalent circuit scheme.

where

- H_c and H_g are the field intensity in the core and in the air gap, respectively
- l_c is the magnetic path length in core
- l_g is the length of air gap

Considering Fig. 1.16, the application of Gauss's law for a closed surface crossing the core and the air gap and including the total transition surface between them, gives the expression

$$\int \mathbf{B}_c \cdot d\mathbf{S} + \int \mathbf{B}_g \cdot d\mathbf{S} = 0 \quad (1.29)$$

which yields

$$\Phi_c = \Phi_g = \Phi \quad (1.30)$$

Equation (1.28) can be rewritten as

$$\Phi_c \mathfrak{R}_c + \Phi_g \mathfrak{R}_g = \Phi(\mathfrak{R}_c + \mathfrak{R}_g) = NI \quad (1.31)$$

where

- Φ_c is the magnetic flux in the core
- Φ_g is the magnetic flux in the air
- \mathfrak{R}_c is the reluctance of core path
- \mathfrak{R}_g is the reluctance of the air gap

Equations (1.29) and (1.30) are valid only for small air gaps. At larger air gaps, the flux tends to the outside. In contrast to electrical circuits true "insulation" is not present, as the relative permeability of air equals 1, which is nonzero.

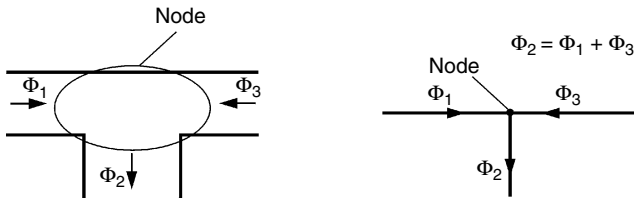


FIGURE 1.17
Application of Gauss's law to a node of a magnetic circuit.

The application of Gauss's law for a node of a magnetic circuit gives the result that the algebraic sum of fluxes coming out of the node is equal to zero, as it is shown in Fig. 1.17:

$$\oint_S \mathbf{B} \cdot d\mathbf{s} = 0 \Rightarrow \sum_{i=1}^n \Phi_i = 0 \quad (1.32)$$

Equation (1.32) is analogous to Kirchoff's current law.

For further reading, magnetic circuits and components are presented in a suitable way for the needs and the applications of power electronics in textbooks on power electronics [3,4,5]. Electromagnetic concepts and applications are described in detail in Marshall et al. [6].

1.3.2 Inductance

1.3.2.1 Flux Linkage

First, we will define the term *flux linkage*, Ψ (flux linked to all turns). The instantaneous voltage across a coil can be presented as

$$v(t) = Ri(t) + \frac{d\Psi(t)}{dt} = Ri(t) + e(t) \quad (1.33)$$

where R is the ohmic resistance of the coil, $i(t)$ is the coil current and $e(t)$ is the electromotive force.

From that expression we define the term $\Psi(t)$:

$$\Psi(t) = \int e(t) dt = \int (v(t) - Ri(t)) dt \quad (1.34)$$

with dimension [Weber] or $[V \cdot s]$.

We prefer $[V \cdot s]$, as it reminds that the quantity is a flux linkage and not a physical flux.

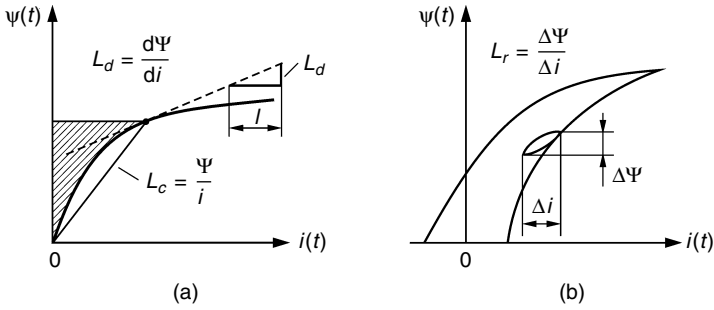


FIGURE 1.18

Flux linkage Ψ as a function of current i and definitions of L_c , L_d , and L_r .

1.3.2.2 Inductance: Definitions

The term *inductance* can be defined in different ways with respect to the nonlinearity of the B - H dependence. For simplicity, we do *not consider core losses* in this section. Here we explain the different definitions and presentations of the term *inductance*.

Chord Inductance or Amplitude Inductance

The slope of the chord in the curve $\Psi = \Psi(i)$ is called *chord inductance* or *amplitude inductance* (see Fig. 1.18a), and is denoted L_c , L_a , or simply L :

$$L_c = \frac{\Psi}{i} \text{ [H] (Henry) or } [\Omega \cdot \text{s}] \quad (1.35)$$

Differential Inductance

The (derivative) of the flux linkage $\Psi = \Psi(i)$ is the *differential inductance* L_d . This inductance is observed when small signals are superimposed to the coil current i .

$$L_d = \frac{d\Psi}{di} \quad (1.36)$$

Note that with material having hysteresis losses, see Fig. 1.18b, a minor loop is observed resulting in a lower small signal inductance, called *reversible inductance*:

$$L_r = \frac{\Delta\Psi}{\Delta i} \quad (1.37)$$

Neglecting the losses, the differential inductance equals to the reversible:
 $L_d = L_r$.

Energetic Inductance

The shaded area in Fig. 1.18a represents the stored inductive energy. Therefore an *energetic* inductance L_w can be defined as

$$L_w = \frac{2 \int_0^\Psi i d\Psi}{i^2} \quad (1.38)$$

The relation between the different definitions of inductance for a normal saturating curve (without hysteresis and with a negative second derivation) is $L_d < L_w < L_c$. This energetic definition is useful in converters, such as inverting choppers, fly-back converters, and Cúk converters, which first store energy in an inductive component and then deliver it to the load.

Inductance in a Classical “No-load” Test with Sinusoidal Voltage

In a classical “no-load” test an almost sinusoidal voltage or EMF is used. The resulting measured inductance is

$$L_v = \frac{V_{rms}}{\omega I_{rms}} \quad \omega = 2\pi f \quad (1.39)$$

where V_{rms} and I_{rms} are the measured RMS values. The current is non-sinusoidal.

Inductance in a Classical “No-load” Test with Sinusoidal Current

The same measurement can be done feeding with a sinusoidal current. The voltage is non-sinusoidal. Then the measured inductance is

$$L_i = \frac{V_{rms}}{\omega I_{rms}} \quad (1.40)$$

Close to saturation level of a core, one can expect the following relations:
 $L_d < L_v < L_i < L_c$.

1.3.2.3 Inductance: Additional Considerations

The *average flux* Φ for one turn is obtained by dividing the flux linkage Ψ by the number of turns N :

$$\Phi = \frac{\Psi}{N} \text{ [Weber/turn]} \quad (1.41)$$

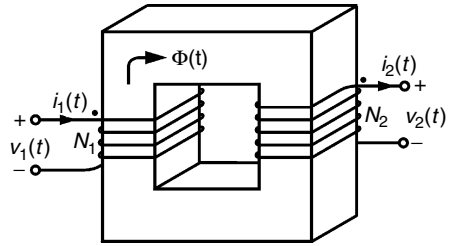


FIGURE 1.19

A two-winding transformer, physical geometry.

The average flux is equal to the physical flux of the core only when the leakage flux is neglected.

- 1) The average flux of one turn can be compared to the total *MMF*: $MMF = Ni$ [$A \cdot \text{turns}$]. That flux can be presented in a diagram, similar to Fig 1.19. Then the slope of the chord is called *permeance* Λ . It has also different possible definitions as the inductance (given above). In ferrite data sheets the permeance is called the *inductance factor*, A_L . The unit is [H/turn^2], which has the dimension Henry [H]. Using the term A_L , the inductance L can be expressed as

$$L = A_L N^2, \quad A_L = \Lambda \tag{1.42}$$

The quantity A_L^{-1} represents the total reluctance [turn^2/H] of the magnetic circuit. It can be presented as the sum of the reluctances of the total magnetic path (core reluctances and air gap reluctances).

- 2) Depending on the application, the so-called *linearity limit* or *saturation point* can be defined. Such a practical limit in power electronics is the point at which the differential inductance L_d is reduced to a half of its maximum value due to saturation. For example, in a design of an L - C low-pass filter at that point the voltage ripples at the output are doubled and so does an open-loop gain! In AC sinusoidal voltage excitation the current waveform is quite deviating from a sine wave when the peak current reaches the saturation point (it gets closer to a triangle).

1.3.2.4 Self-inductance and Mutual Inductance

The *self-inductance* L relates the flux linkage produced by a coil to the current in that coil:

$$L = \frac{\Psi}{i} = \frac{N \Phi}{i} = \frac{N^2}{\mathfrak{R}} = N^2 \Lambda \tag{1.43}$$

where

Ψ is the *effective flux linkage*

Φ is the physical magnetic flux linking the coil

\mathfrak{R} is the reluctance of the magnetic circuit

Λ is the permeance of the magnetic circuit

The magnetic coupling between the windings of a magnetic device is expressed by *mutual inductance* M . The mutual inductance is defined by the following relation:

$$M = \frac{N_1 \Phi_{12}}{i_2} = \frac{N_2 \Phi_{21}}{i_1} \quad (1.44)$$

where

N_1 is the turn number of the primary winding

i_1 is the primary winding current

Φ_{12} is the magnetic flux linking the primary winding as a result of the current in the secondary winding

N_2 is the turn number of the secondary winding

i_2 is the secondary winding current

Φ_{21} is the magnetic flux linking the secondary winding as a result of the current in the primary winding

1.3.3 Transformer Models

Consider the two-winding transformer shown in Fig. 1.19. The core reluctance is

$$\mathfrak{R} = l_e / \mu A_e \quad (1.45)$$

where

l_e is the mean effective magnetic path length

A_e is the effective core cross sectional area

μ is the permeability of the core material

There are two windings in the transformer, and applying the Ampere's law yields

$$MMF = N_1 i_1 + N_2 i_2 \quad (1.46)$$

Substituting $MMF = \Phi \mathfrak{R}$ we obtain

$$\Phi \mathfrak{R} = N_1 i_1 + N_2 i_2 \quad (1.47)$$

1.3.3.1 Ideal Transformer

In the ideal transformer the core reluctance is zero $\mathfrak{R} = 0$ and the resistances of the windings are neglected. Thus, the core *MMF* is also zero and Equation (1.47) becomes

$$0 = N_1 i_1 + N_2 i_2 \quad (1.48)$$

Applying the Faraday's law to an ideal transformer, we obtain

$$v_1 = N_1 \frac{d\Phi_c}{dt}, \quad v_2 = N_2 \frac{d\Phi_c}{dt}, \quad v_1 = e_1, \quad v_2 = e_2 \quad (1.49)$$

where Φ_c is the core flux. Eliminating Φ_c yields:

$$\frac{e_1}{N_1} = \frac{e_2}{N_2} \quad (1.50)$$

For the ideal transformer shown in Fig. 1.20, Equations (1.47) and (1.49) can be rewritten as

$$\frac{e_1}{e_2} = \frac{N_1}{N_2}, \quad \frac{i_1}{i_2} = -\frac{N_2}{N_1} \quad (1.51)$$

Thus, the ideal transformer is a lossless zero-reluctance device that acts as a voltage ratio changer. The power toward a transformer is set positive, which explains the convention in Fig. 1.20. There are three classifications of transformer, depending on the relative voltage at which power is received and delivered:

1. When a transformer receives power at a low-voltage winding and delivers power to a high-voltage winding, the transformer is called *step-up transformer*.
2. When a transformer receives power at a high-voltage winding and delivers power to a low-voltage winding, the transformer is called *step-down transformer*.
3. When the turn number of the windings is the same, the transformer is called *one-to-one transformer*.

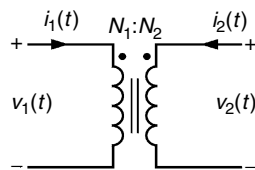


FIGURE 1.20
An ideal transformer, equivalent scheme.

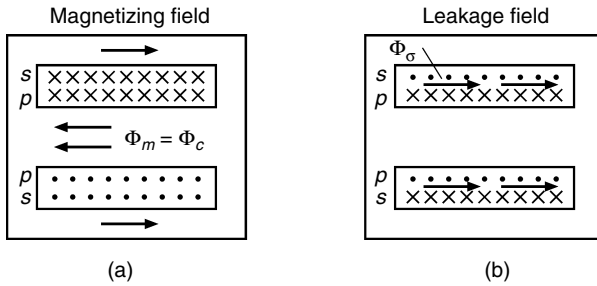


FIGURE 1.21 Magnetizing and leakage fields in a transformer, p : primary winding, s : secondary winding.

1.3.3.2 Practical Transformer

In a practical transformer the core reluctance is nonzero. Then we can write

$$\Phi_c = \frac{N_1 i_1 + N_2 i_2}{\mathfrak{R}_c} \quad (1.52)$$

and substituting this expression for Φ in $e_1 = N_1 \frac{d\Phi_c}{dt}$, we have:

$$e_1 = \frac{N_1^2}{\mathfrak{R}_c} \frac{d\left(i_1 + i_2 \frac{N_2}{N_1}\right)}{dt} \quad (1.53)$$

In Equation (1.53) we can distinguish two terms. The term $L_m = \frac{N_1^2}{\mathfrak{R}_c}$ that is equivalent to inductance is called *magnetizing inductance*, referred to the primary winding. The term $i_m = i_1 + i_2 \frac{N_2}{N_1}$ is called *magnetizing current*, also referred to the primary winding.

In a real transformer there is always some flux that links only one winding, but not the other winding and it is called *leakage flux* (see Fig. 1.21). Let us denote by $\Phi_{\sigma 1}$ the leakage flux for the primary winding and by $\Phi_{\sigma 2}$ the leakage flux for the secondary winding. The leakage flux usually leaks through the air. This flux leads to so called *leakage inductances* $L_{\sigma 1}$ and $L_{\sigma 2}$. Hence:

$$L_{\sigma 1} = \frac{N_1 \Phi_{\sigma 1}}{i_1}, \quad L_{\sigma 2} = \frac{N_2 \Phi_{\sigma 2}}{i_2} \quad (1.54)$$

where

$L_{\sigma 1}$ is the primary leakage inductance

$L_{\sigma 2}$ is the secondary leakage inductance

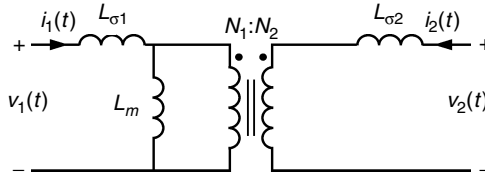


FIGURE 1.22

A two-winding transformer model including magnetizing inductance L_m and primary and secondary leakage inductances $L_{\sigma 1}$ and $L_{\sigma 2}$.

The leakage inductances are in series with the windings. In Fig. 1.22 we show the transformer model including magnetizing inductance L_m and primary and secondary leakage inductances $L_{\sigma 1}$ and $L_{\sigma 2}$. We can write

$$L_1 = L_{\sigma 1} + L_{m1} = L_{\sigma 1} + M \frac{N_1}{N_2} \quad (1.55)$$

$$L_2 = L_{\sigma 2} + L_{m2} = L_{\sigma 2} + M \frac{N_2}{N_1} \quad (1.56)$$

where

L_1 is the primary *self-inductance* inductance

L_2 is the secondary *self-inductance* inductance

L_{m1} is the magnetizing inductance placed in the primary side

L_{m2} is the magnetizing inductance placed in the secondary side

The quantities L_1 and L_2 are called the primary and secondary *self-inductances* of the transformer.

Another equivalent transformer scheme is shown in Fig. 1.23, where Λ_m is the magnetizing permeance. We can write

$$M = \Lambda_m N_1 N_2 \quad (1.57)$$

$$L_{m1} = \Lambda_m N_1^2 \quad (1.58)$$

$$L_{m2} = \Lambda_m N_2^2 \quad (1.59)$$

The following expressions relate the magnetizing and mutual inductances in a transformer:

$$M = \frac{L_{m1} N_2}{N_1} = \frac{L_{m2} N_1}{N_2} \quad (1.60)$$

$$L_{m2} = L_{m1} \left(\frac{N_2}{N_1} \right)^2 \quad (1.61)$$

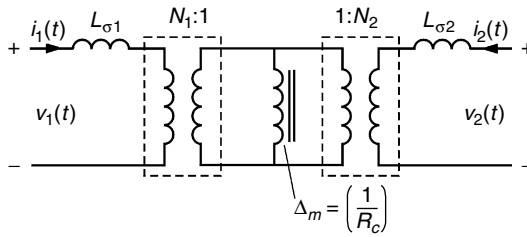


FIGURE 1.23
T-scheme transformer model with magnetizing permeance.

Using the self- and mutual inductances, the equations for the primary and secondary winding voltages are

$$v_1 = L_1 \frac{di_1}{dt} + M \frac{di_2}{dt} \quad (1.62)$$

$$v_2 = M \frac{di_1}{dt} + L_2 \frac{di_2}{dt} \quad (1.63)$$

Note that L_1, L_2, L_{m1}, L_{m2} , and Λ_m are always positive. The terms N_1 and N_2 can be positive or negative depending on the winding direction. The mutual inductance M can be also negative or positive in that aspect.

We can also define the *coupling* coefficient k :

$$k = \frac{M}{\sqrt{L_1 L_2}} \quad (1.64)$$

The coupling coefficient k is in the range $-1 \leq k \leq 1$ and it represents the degree of magnetic coupling between the primary and the secondary windings. If a transformer is perfectly coupled, then the leakage inductances $L_{\sigma 1}$ and $L_{\sigma 2}$ are zero. Then the coupling coefficient is zero. Usually the low-voltage transformer constructions can obtain a coupling coefficient of 0.99. In power electronics not always a high value of k is the target of the design. Note that k decreases when the core saturates. In many converter circuits the leakage inductances are used to obtain the desired voltage and current waveforms, especially in the resonant circuits.

The inductance L_1 can be measured in a no-load condition test, fed at the primary. The inductance $L_{\sigma 1} + L_{\sigma 2}(N_1/N_2)^2$ can be measured in a short-circuit test at the primary.

More information can be found in [Chapter 11](#).

1.3.4 Magnetic and Electrical Analogy

The already mentioned analogy between magnetic and DC electrical quantities and circuits is summarized in [Table 1.2](#).

TABLE 1.2

Analogy between Magnetic and Electrical Quantities and Laws

Magnetic Quantities and Laws	Electric Quantities and Laws
Flux, Φ [Wb]	Current, I [A]
Flux linkage, Ψ [V · s]	No equivalent
Flux density (induction), B [T]	Current density, J [A/m]
Magnetomotive force, F [A · turns]	Voltage, V [V]
Magnetic field intensity, H [A/m]	Electrical field intensity, E [V/m]
Reluctance, $\mathfrak{R} = l/\mu A_c$ [A · turns/Wb]	Resistance, $R = l/\sigma S$ [Ω]
Permeability, μ [H/m]	Conductivity, σ [m/ Ω]
Permeance, $\Delta = 1/\mathfrak{R}$ [Wb/A · turns]	Conductance, $G = 1/R$ [Ω^{-1}]
Inductance, L [H]	No equivalent
Mutual inductance, M [H]	No equivalent
Leakage inductance L_σ [H]	No equivalent
Magnetizing inductance L_μ [H]	No equivalent
Gauss's law, $\sum \Phi_{\text{node}} = 0$	Kirchoff's current law, $\sum i_{\text{node}} = 0$
$\sum \text{MMF}_{\text{node}} = 0$	Kirchoff's voltage law, $\sum v_{\text{node}} = 0$
$\Phi = \text{MMF}/\mathfrak{R}$	Ohm's law, $I = V/R$

The analogy between the magnetic and electrical quantities and circuits is of course, not complete. There are a few differences:

- The relationship between B and H in soft magnetic materials, which is usually non-linear.
- In the magnetic circuits with air gaps there is fringing flux changing the total reluctance of the circuit, but in electrical circuits there is no such effect (exception is the electrostatic equivalent). The electrical isolation conductivity is on the order of 10^{20} times lower than the conductivity of metals and all current flows in wires. The air permeance μ_0 is only about 10^3 times less than the permeance of the magnetic materials. Thus, leakage flux does not have an analogue in electrical circuits.
- Mutual inductance and mutual coupling also do not have an analogue in electrical circuits.
- In wires carrying current there is I^2R loss, but no $\Phi^2\mathfrak{R}$ loss exists in magnetic circuits.

References

- [1] Bertotti, G., *Hysteresis in Magnetism*, Academic Press, San Diego, CA, 1998, pp. 225–429.
- [2] Boll, R., Soft magnetic materials, in *The Vacuumschmelze Handbook*, Heyden & Son Ltd., London, 1979, pp. 20–36.
- [3] Erickson, R.W., *Fundamentals of Power Electronics*, KAP, Norwell, MA, 2001, pp. 491–531.

- [4] Mohan, N., Undeland, T.M., and Robbins, W.P., *Power Electronics*, 2nd ed., John Wiley & Sons, New York, 1995, pp. 744–792.
- [5] Krein, P.T., *Elements of Power Electronics*, Oxford University Press, New York, 1998, pp. 409–450.
- [6] Marshall, S.V., DuBoff, R.E., and Skitek, G.G., *Electromagnetic Concepts and Applications*, Prentice Hall, Upper Saddle River, NJ, 1996, pp. 101–446.
- [7] Soft ferrites, in *Phillips Data Handbook*, Phillips, Eindhoven, The Netherlands, 1996, pp. 8–10.

2

Fast Design Approach Including Eddy Current Losses

In today's power electronics, the active switches can withstand high switching frequencies. This means that the major part of the magnetic component of power electronics is subjected to eddy current losses. In this chapter we propose a fast design method that includes eddy current losses—neglecting eddy currents may result in significant errors. The word fast means that a decision tree is given to guide the designer and that no time-consuming mathematical tools are used. The fast design uses methods that do not achieve the highest accuracy, e.g., the proposed thermal approach. However, the provided accuracy is sufficient for most power electronics applications. Moreover, the same design flowchart can also be used with more precise methods (e.g., a more accurate thermal model or a transverse field computation by finite elements).

The fast design approach is applicable to both transformers and inductors for a wide range of designs using round wires. The approach simplifies the design, makes it more systematic, and categorizes it into two major cases: saturated thermally limited design and non-saturated thermally limited design. The design procedure is illustrated with two fully calculated design examples and several other examples that concern specific parts of the design.

2.1 Fast Design Approach

The method includes simplified assumptions and omits certain details in the design, but the accuracy is usually sufficient for first experiments or as a fast calculation before a more precise approach.

In the fast design approach presented here the following simplifications are made:

- the leakage inductance of transformers is neglected for the flux calculation
- the field pattern is only approximated

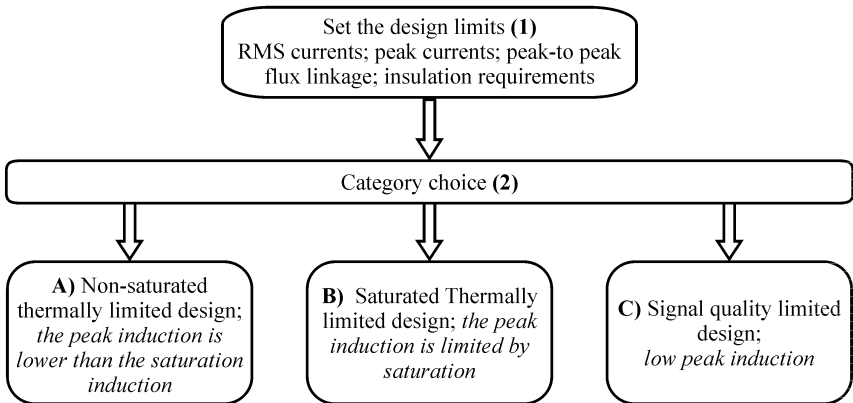


FIGURE 2.1
General flowchart of the fast design approach.

- the method is limited to round wires
- the method loses accuracy when partially filled layers are used
- for inductors, only gaps in the center leg are considered
- the insulation distances and clearances are considered but not in details

For more details and limits concerning coil windings, refer to [Chapter 4](#) and to standards, e.g., IEC950. The standards are not very restrictive, but the limits, such as creepage distances, can greatly influence the size of the transformers and, thus, the total design procedure.

The design is done step by step and begins with finding the design limits and defining the design category, as shown in Fig. 2.1.

1. Design limits

For the circuit in which the component is used, a number of parameters and requirements can usually be calculated:

- RMS current of the windings
- Peak current of the windings
- Peak to peak flux linkage
- Peak flux linkage
- Insulation requirements (clearance, creepage distance) (for detailed information concerning these insulation distances, refer to Chapter 4)

2. Category choice

The second step is choosing one of the three possible general cases (approaches).

- (A) Saturated thermally limited design
- (B) Non-saturated thermally limited design
- (C) Signal quality limited design

As no design results are known up to this point, the category choice is made on experience using the input design parameters. If the initial choice is not the right one, it will be noticed in the next design steps and then the right choice will be made.

Here we give some practical examples and recommendations on how to choose the design category:

- Magnetic components for high frequency AC applications correspond to case (A).
- Magnetic components for applications with a high DC component or low frequency applications correspond to case (B). Examples: Pulse applications, DC-chokes, applications with small duty cycles.
- Signal quality limited design includes components used in audio, telephone, or radio frequency applications, for measuring in power electronics systems (voltage and current transformers), of accurate inductors, and for applications with a high Q-factor.

2.1.1 Non-Saturated Thermal Limited Design

A compromise between core losses and copper losses has to be considered for the total heat dissipation. To realize this, we present a design procedure consisting of several steps. The flowchart of the design is shown in Fig. 2.2.

Step 1) Choose a Core Material and Size

To choose the core size we use a simple scaling law based on natural convection in air, which compares the total volt-amp rating of the component and a core characteristic size parameter a_{ch} :

$$S_{tot} = \sum_{all\ windings} V_{rms} I_{rms} = A a_{ch}^{\gamma} \Rightarrow a_{ch} = \left(\frac{S_{tot}}{A} \right)^{1/\gamma} \quad (2.1)$$

where

A is a coefficient; for ferrites, $A = (5-25) \times 10^6$ if a_{ch} is in [m] (A is in the range $A = 5-25$ if a_{ch} is in [cm]), see the remarks below

a_{ch} is the largest dimension of the component, used as a *scaling parameter*

γ is an exponent, characterizing the material and shape of the core, $\gamma = 3$

S_{tot} is the total volt-amp rating of the component

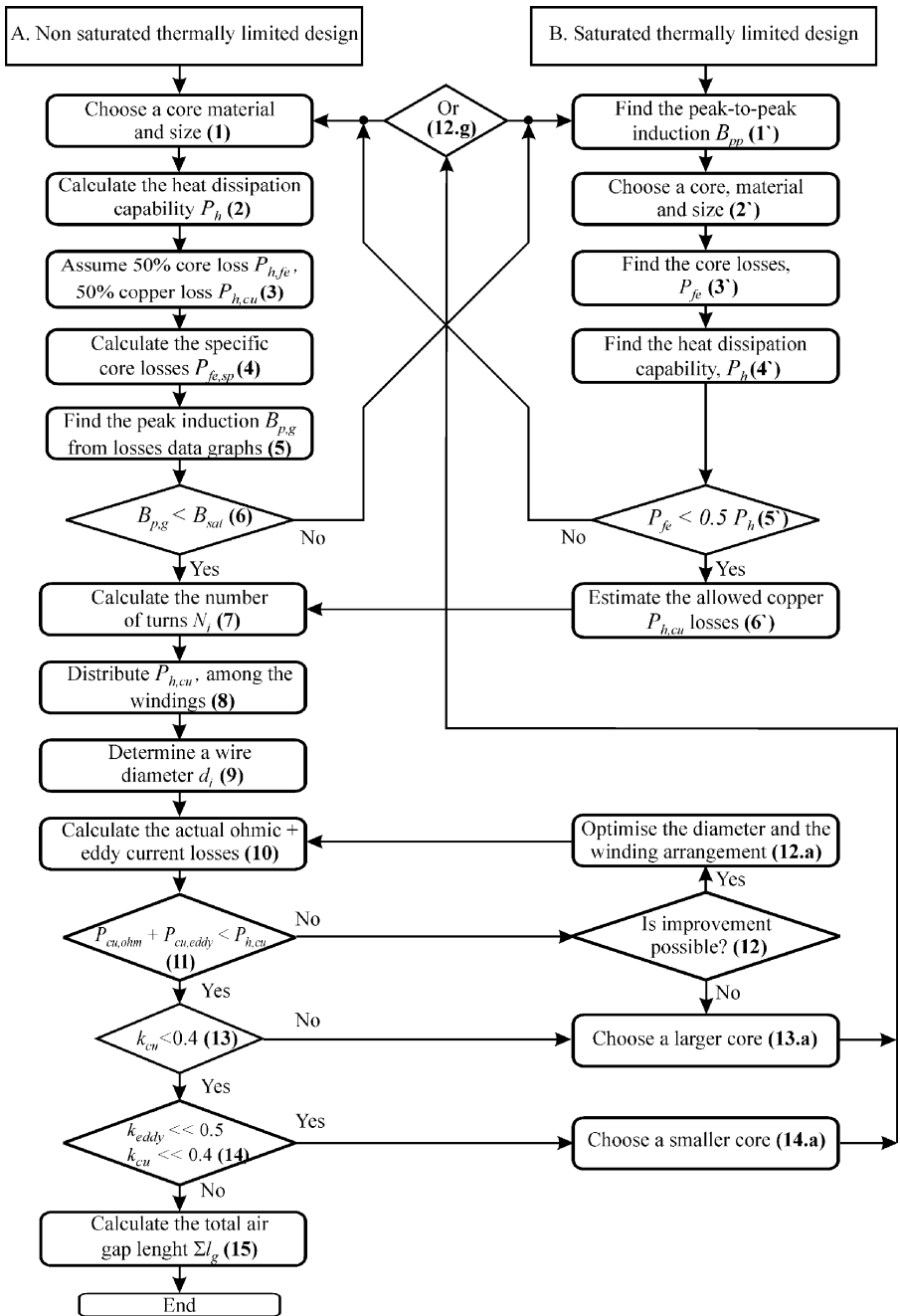


FIGURE 2.2
Flowchart of the fast magnetic component design procedure.

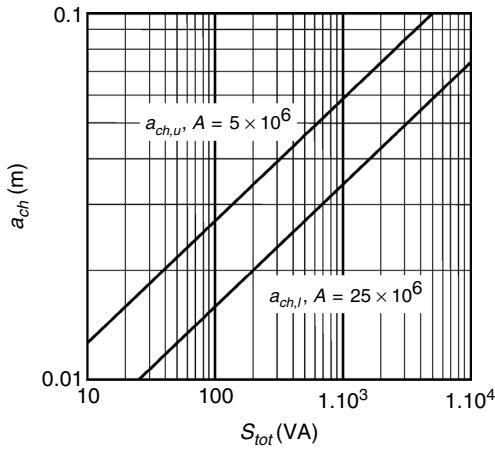


FIGURE 2.3

Core size estimation for a non-saturated thermally limited ferrite core design: upper $a_{ch,u}$ ($A = 5 \times 10^6$) and low $a_{ch,l}$ ($A = 25 \times 10^6$) values of the scaling parameter a_{ch} as a function of the total V-A rating S_{tot} of the component.

Equation (2.1) is used to compare the ability of the different core sizes of one shape to meet the allowed volt-amp rating of the component. From Equation (2.1) we find a_{ch} . As a component characteristic size parameter (scaling parameter) a_{ch} we use the largest dimension of a ferrite core (for instance, for an EE42 core, $a_{ch} = 0.042$ m) or the diameter of a ring core.

In Fig. 2.3 we show the possible ranges of the scaling parameter a_{ch} , upper value $a_{ch,u}$ ($A = 5 \times 10^6$) and lower value $a_{ch,l}$ ($A = 25 \times 10^6$), as a function of the total V-A rating S of the component. Figure 2.3 can be used as a fast approach for obtaining the value of a_{ch} .

Depending on the core material and on induction B , the coefficient γ varies approximately in the range $2.8 < \gamma < 3.2$. The derivation of the value of γ is presented in detail in Appendix A.2.1 at the end of this chapter. For simplicity, we use the value $\gamma = 3$.

REMARKS CONCERNING THE EQUATION (2.1)

1. An incorrect choice in step 1 is detected later in the next steps. This may lead to a smaller or a larger core size.
2. The low values of A are applicable for low-frequency design (20–30 kHz) and low-frequency materials or presence of high DC current components. The high values $A = (20 - 25) \times 10^6$ are applicable for high-frequency design (100–500 kHz) and high-frequency materials in applications with good thermal conditions.
3. Insulation requirements tend to decrease the coefficient A .
4. The coefficient A is lower for high-current applications because of eddy current effects.

- The final accuracy of the design is achieved in the next steps of the design procedure.
- For $A = 10 \times 10^6$, an easy order of magnitude to remember is the following: 1 cm of a_{ch} corresponds to 10 W. The line for $A = 10 \times 10^6$ is the diagonal in Fig. 2.3.

Examples

Note: In the examples we use $A = 15 \times 10^6$, a value suitable for the average design.

- Choose a core for a ferrite transformer with the following parameters:
input voltage, RMS value: $V_{in} = 100$ V
input current, RMS value: $I_{in} = 5$ A
output voltage, RMS value: $V_{out} = 500$ V
RMS secondary current: $I_{out} = 1$ A
Using the equation (2.1) we have $\sum_{all\ windings} V_{rms} I_{rms} = 1000$,
 $a_{ch} = \left(\frac{1000}{15 \times 10^6} \right) = 0.0405$ m. We choose EE42/21/15 ferrite core with largest dimension $a_{ch,data} = 0.042$ m. This core can handle total volt-amps equal to $A a_{ch}^\gamma = 15 \times 10^6 \times 0.042^3 = 1111$ VA
- A ferrite ring core T87/54/14 with $a_{ch,data} = 0.087$ m can handle total volt-amps equal to $A a_{ch}^\gamma = 15 \times 10^6 \times 0.087^3 = 9877$ VA
If the core is used as a transformer with equal primary and secondary volt-amps, the primary volt-amps are 4938.5 VA.
- A ferrite pot core P30/19 with $a_{ch,data} = 0.030$ m can handle total volt-amps equal to $A a_{ch}^\gamma = 15 \times 10^6 \times 0.03^3 = 405$ VA.

Step 2) Calculate the Heat Dissipation Capability P_h

In this step, a rough estimation of the heat dissipation capability of the chosen core is made. The rule of thumb used is

The heat dissipation capability of a component can be approximated as the product of the two largest dimensions of that component in [m] and a constant 2500 W/m.

The total heat capability P_h is then

$$P_h = k_A a b \quad (2.2)$$

where

k_A is a coefficient, a typical value is 2500 W/m²

a and b are the two largest dimensions of the component in [m]

The expression in Equation (2.2) is not precise, but it gives a rough estimation of the allowed heat dissipation and it can be used in the fast design

approach. We do not use the full surface of the component as that requires a lot of detailed calculations, which are not so relevant. A much more precise approach is given in [Chapter 7 Thermal Considerations](#).

REMARK

For 50-Hz iron transformers, Equation (2.2) with $k_A = 2500 \text{ W/m}^2$ is a good approximation up to 40°C ambient temperature and 115°C hot spot temperature. For ferrite transformers, the dissipation is often quite well distributed between ferrite and copper, so that a temperature rise of 50°C can be allowed for $k_A = 2500 \text{ W/m}^2$.

Examples

1. For an EE42/15 ferrite core transformer, where both major dimensions are 0.042 m, the allowed dissipation is $P_h = 2500 \times 0.042 \times 0.042 = 4.41 \text{ W}$.
2. For a P30/19 ferrite core transformer the two largest dimensions are both 0.030 m and the result is $P_h = 2500 \times 0.03 \times 0.03 = 2.25 \text{ W}$.
3. For a single phase transformer, scrapless EI type laminated iron of 0.12 m, the two major dimensions 0.12 m and 0.10 m, the allowed total losses are $P_h = 2500 \times 0.12 \times 0.1 = 30 \text{ W}$.

Step 3) Copper Loss/Core Loss Ratio

We use the simplified assumption that the maximum efficiency, which means minimum losses at a given input or output power, is close to the point where the copper losses P_{cu} equal the core losses P_{fe} . This assumption allows us to find both copper and core losses:

$$P_h = P_{h,cu} + P_{h,fe} \tag{2.3}$$

$$P_{h,cu} = P_{h,fe} = \frac{P_h}{2} \tag{2.4}$$

where

P_h are total allowed losses found by Equation (2.2) (the dissipation capability of the component)

$P_{h,cu}$ are the allowed copper losses

$P_{h,fe}$ are the allowed core losses

The simple assumption presented by Equation (2.4) is true when

- the magnetic material is not saturated and the core losses are proportional to the square of the induction (as a first approximation)
- eddy current losses are low

Detailed study of the optimal copper loss/core loss ratio is presented in [Chapter 10](#).

Step 4) Calculate the Specific Core Losses $P_{fe,sp}$

By the next two steps, 4) and 5), we find the peak induction corresponding to the specific core losses in the core. The specific core losses $P_{fe,sp}$ can be calculated as follows:

- For iron-based cores, the specific losses are given per a unit weight:

$$P_{fe,sp,w} = \frac{P_{fe}}{V_c s_m k_{ff}} \tag{2.5}$$

where

V_c is the volume of the chosen core

s_m is the specific mass of the material

k_{ff} is the filling factor of the chosen core (typically 0.95 for classic magnet iron)

- For ferrites the filling factor k_{ff} is 1. The specific losses are given per volume:

$$P_{fe,sp,v} = \frac{P_{fe}}{V_c} \tag{2.6}$$

where

V_c is the volume of the chosen core

Step 5) Find the Peak Induction $B_{p,g}$ from Graphical Data

In data sheets of iron and ferrite cores, graphical dependencies of the specific losses are usually shown versus peak induction with frequency as a parameter. From those graphs, for a given frequency one can find the peak induction $B_{p,g}$ corresponding to the specific losses $P_{fe,sp}$ under sinusoidal excitation. Multiplying this induction by 2 gives us the allowed peak-to-peak induction. For more details concerning core losses, please refer to [Chapter 3](#). For symmetrical waveforms we can write

$$B_{pp} = 2 B_{p,g} \tag{2.7}$$

where

B_{pp} is peak-to-peak induction

It is important to check whether the graphs give typical or maximum losses, as material characteristics may vary depending on samples. We observed that data of material grades can change throughout years.

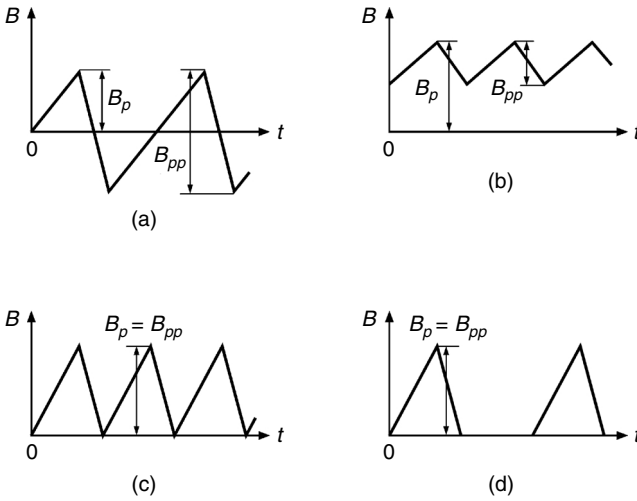


FIGURE 2.4

Typical wave forms and corresponding peak induction B_p .

a) $k_w = 0.5$; b) $k_w > 1$; c) $k_w = 1$; d) $k_w = 1$.

Step 6) Check if the Peak Induction B_p is Higher Than the Saturation Value B_{sat}

Symmetrical Waveforms

In *symmetrical waveforms*, see Fig. 2.4,a ($k_w = 1/2$, $k_w = B_p/B_{pp}$), the peak induction B_p is half of the peak-to-peak induction B_{pp} . Thus, we have $B_p = B_{p,g}$ ($B_{p,g}$ is found in the step 5), and for the check we can use $B_{p,g}$. We compare $B_{p,g}$ with the saturation level B_{sat} for the corresponding material:

$$B_{p,g} \leq B_{sat} \quad (2.8)$$

Most ferrites intended for energy conversion saturate at about 0.35 T (at 100°C). For laminated iron cores the saturation level is typically 1.5–1.7 T. The new soft magnetic materials, such as nanocrystalline iron, saturate at about 1.2 to 1.5 T. However, attention should be paid since the finished nanocrystalline core filling factor k_{ff} is about $k_{ff} = 0.5$, which results in a two times higher induction in the material than in the cross-sectional area of the core. For more detailed information, refer to [Chapter 3](#).

Asymmetrical Waveforms

In the case of *asymmetrical waveforms* (with DC flux, or even harmonics), the actual waveform has to be considered to find the peak induction B_p . Then we have

$$B_p = k_w B_{pp} = 2k_w B_{p,g} \quad (2.9)$$

where

the coefficient k_w depends on the specific wave forms of the application

Figure 2.4 shows some typical forms and corresponding peak induction B_p . The value of B_p has to be compared to the saturation level value B_{sat} :

$$B_p \leq B_{sat} \quad (2.10)$$

If the peak induction is higher than the saturation induction, then we have a saturation limited design case and the design continues with the corresponding procedure, described in the next section.

Step 7) Calculate the Winding Turns N_1

Let us consider an arbitrary voltage waveform $v(t)$ across a winding, as illustrated in Fig. 2.5. The integral of the voltage $v(t)$ during its positive half period, which is the area S shown in Fig. 2.5, is equal to the peak-to-peak flux linkage Ψ_{pp} :

$$\int_{t_1}^{t_2} v(t) dt = \Psi_{pp}, \quad \Psi_{pp} = N \Phi_{pp} \quad (2.11)$$

where

Ψ_{pp} is the peak-to-peak magnetic flux linkage, [Wb]

N is the number of turns

Φ_{pp} is the peak-to-peak magnetic flux

The peak-to-peak physical magnetic flux Φ_{pp} is equal to the product of the peak-to-peak induction B_{pp} and the effective cross sectional area A_e of the core:

$$\Phi_{pp} = A_e B_{pp} \quad (2.12)$$

Substituting Equation (2.12) into Equation (2.11), and because B_{pp} is two times $B_{p,g}$ ($B_{pp} = 2B_{p,g}$) for symmetrical cases, the primary turns number N_1 is presented as:

$$N_1 = \frac{\Psi_{pp}}{\Phi_{pp}} = \frac{\Psi_{pp}}{A_e B_{pp}} = \frac{\Psi_{pp}}{2 A_e B_{p,g}} \quad (2.13)$$

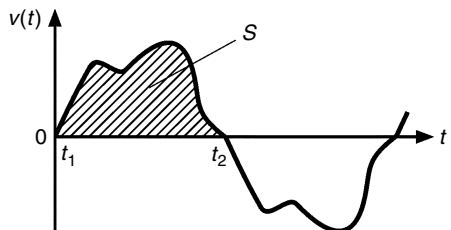


FIGURE 2.5
Arbitrary voltage waveform $v(t)$ across a winding.

Equation (2.13) is applicable for both primary and secondary winding turns. Depending on where the peak-to-peak flux linkage Ψ_{pp} is calculated, the result will be the respective number of turns.

Under sinusoidal excitation, Equation (2.13) is modified to:

$$N_1 = \frac{V_1 \sqrt{2}}{2\pi f A_e B_{p,g}} = \frac{V_1}{4.44 f A_e B_{p,g}} \quad (2.14)$$

where

V_1 is the RMS value of the voltage across the primary winding

f is the excitation frequency

A_e is the effective cross sectional area of the core

The number of the turns of the other windings is calculated according the desired voltages as

$$N_i = N_1 \frac{V_i}{V_1} \quad (2.15)$$

where

N_i are the number of turns of the i th winding

V_i is the RMS value of the voltage across the i th winding

Step 8) Distribute Allowed Total Copper Losses $P_{h,cu}$ Among the Windings

To distribute the allowed total copper losses $P_{h,cu}$ among the windings (primary and secondary windings, or more than one secondary winding) we introduce a coefficient α_i , which is equal to the relative part of the losses P_{cu} attributed to the i th winding:

$$\alpha_i = \frac{N_i I_{rms,i}}{\sum_{i=1}^n N_i I_{rms,i}} \quad (2.16)$$

$$P_{h,cu,i} = \alpha_i P_{h,cu} \quad (2.17)$$

where

$I_{rms,i}$ is the RMS current of the i th winding

$P_{h,cu,i}$ are the allowed losses of the i th winding

$P_{h,cu}$ are the allowed total losses, found by the equation (2.4)

Step 9) Determine Wire Diameter d_i

Knowing the allowed copper losses $P_{h,cu,i}$ distributed over every winding $P_{h,cu,i} = \alpha_i P_{h,cu}$, we determine a wire diameter d_i . We neglect the eddy currents

losses $P_{cu,eddy}$ and considering only the ohmic losses $P_{cu,ohm,i}$ in the wires, we assume $P_{h,cu,i} = P_{cu,ohm,i}$:

$$P_{h,cu,i} = P_{cu,ohm,i} = R_{0,i} I_{rms,i}^2 = \rho_c \frac{l_{T_i} N_i}{\pi d_i^2 / 4} I_{rms,i}^2 \quad (2.18)$$

$$d_i \geq \frac{2}{\sqrt{\pi}} I_{rms,i} \sqrt{\frac{\rho_c l_{T_i} N_i}{P_{cu,i}}} \quad (2.19)$$

where

$R_{0,i}$ is the DC resistance of the i th winding

$I_{rms,i}$ is the RMS current of the i th winding

ρ_c is the electrical resistivity of the wire (resistivity of copper)

l_{T_i} is the mean-length-per-turn of the i th winding

The available copper wire diameters are given in Appendix C at the end of the book. In practice, we select a *practical wire diameter* $d_{p,i}$ which is higher than the calculated by the Equation (2.19) value d_i and $d_{p,i}$ is the next available wire diameter. Since $d_{p,i} > d_i$, there are reduced ohmic losses, allowing some eddy current losses without exceeding the total allowed copper losses.

REMARKS

1. In transformer designs, when less than one full layer width is obtained, a good practice is to enlarge the diameter in order to achieve a full layer width (as far as allowed by the primary-secondary creepage insulation distance).
2. In some designs paralleling wires or using a Litz wire is necessary. In those cases the equation $d_{p,i}^2 p_i > d_i^2$ is to be used, where p_i is the number of the wires in parallel or the strands in a Litz wire.
3. In the realization of designs with parallel wires it is important to guarantee an equal current sharing as well as an arrangement providing the same flux linkage for every wire.

Step 10) Calculate the Actual Copper Losses P_{cu}

1) Ohmic Copper Losses

The actual ohmic losses $P_{cu,ohm}$ for all windings are inversely proportional to the square of the diameter of the wires and can be found by the expression:

$$P_{cu,ohm} = \sum_{i=1}^{all\ windings} R_{0,i} I_{rms,i}^2 = \sum_{i=1}^{all\ windings} \rho_c l_{T_i} N_i \left(\frac{4}{\pi d_{p,i}^2 p_i} \right) I_{rms,i}^2 \quad (2.20)$$

where

$I_{rms,i}$ is the RMS current of the i th winding

N_i is number of turns of the i th winding

p_i is the number of wires in parallel (or the number of strands in a litz wire)
 $\rho_c = 23 \times 10^{-9} \Omega\text{m}$ at 100°C ; $\rho_c = 17.24 \times 10^{-9} \Omega\text{m}$ at 25°C

Note that in case of Litz wire, the value l_{Ti} (mean-length-per-turn) is increased by about 5%.

For simplicity of notation, from now on, we drop the index i for the i th winding.

II) Low-Frequency Transverse Field Eddy Current Losses

The major part of the eddy current losses in a low frequency (LF) approximation for round wires can be explained by the presence of a uniform magnetic field component, which acts like an induction heating to the wire.

REMARKS

1. Note that we talk about a low frequency approximation of eddy currents, and that it does not mean that the eddy losses are low!
2. Low frequency (LF) approximation is applicable when the eddy currents induced in the winding do not considerably change the applied field inside the conductor.
3. In practice, the LF approximation is valid up to $d \leq 1.6 \delta$, (d is the wire diameter and δ is the penetration depth). For δ , see Equation (2.30).

To express the eddy current losses we use the following equation:

$$P_{cu,eddy}(t) = \frac{\pi l_w d_p^4}{64 \rho_c} \left(\frac{dB}{dt} \right)^2 \quad (2.21)$$

where

d_p is the practical diameter of the copper wire of the i th winding

B is the induction, assumed perpendicular to the considered wire

l_w is the conductor length of the i th winding ($l_w = N p l_{Ti}$)

Equation (2.21) is quite general and applicable for the cases with more complicated field distribution and also for non-sinusoidal waveforms [1,2,3]. The LF approximation and Equation (2.21) can also be used if the field is calculated by finite differences or finite element methods (FEM).

Figure 2.6 shows details of windings in a winding area, defining the parameters m , n , t_w , b , and h . Note that the parameter w is given in the data sheets as the minimum winding width (MWW) of a coil former.

Figure 2.7 shows common transformer and inductor shapes and the discussed dimensions. The number of layers m , the number of conductors in a layer n , and the field symmetry factor K are illustrated in Fig. 2.7.

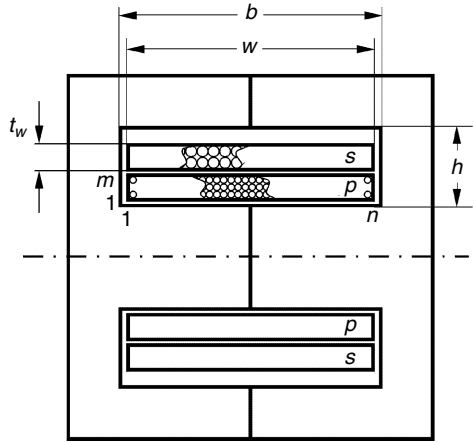


FIGURE 2.6

Details of a winding area, defining the winding area height h , the winding area width b , the winding thickness t_w and the minimum winding width w (MWW), (p -primary winding, s -secondary winding).

Definitions of the Values m_E , n_E , η , and λ

The parameter m_E is defined as an equivalent number of layers. The parameter n_E is defined as an equivalent number of turns in a layer.

- For p parallel wires a number of wires are present in the same layer, which will become an equivalent number of wires in a layer.

$$n_E = np, \quad m_E = m \tag{2.22}$$

- For the Litz wire one cannot count exactly the number of individual wires in a layer. We distribute the equivalent turns in both directions and then we have

$$n_E = n\sqrt{p}, \quad m_E = m\sqrt{p} \tag{2.23}$$

where

p is the number of paralleled strands

- The copper fill factor in the direction of the layer η can be defined as

$$\eta = \frac{d}{w} n_E \tag{2.24}$$

where

d is the wire diameter

w is the winding width (see Fig.2.6)

- The copper fill factor in the direction perpendicular to the layer λ can be defined as

$$\lambda = \frac{d}{h} m_E \tag{2.25}$$

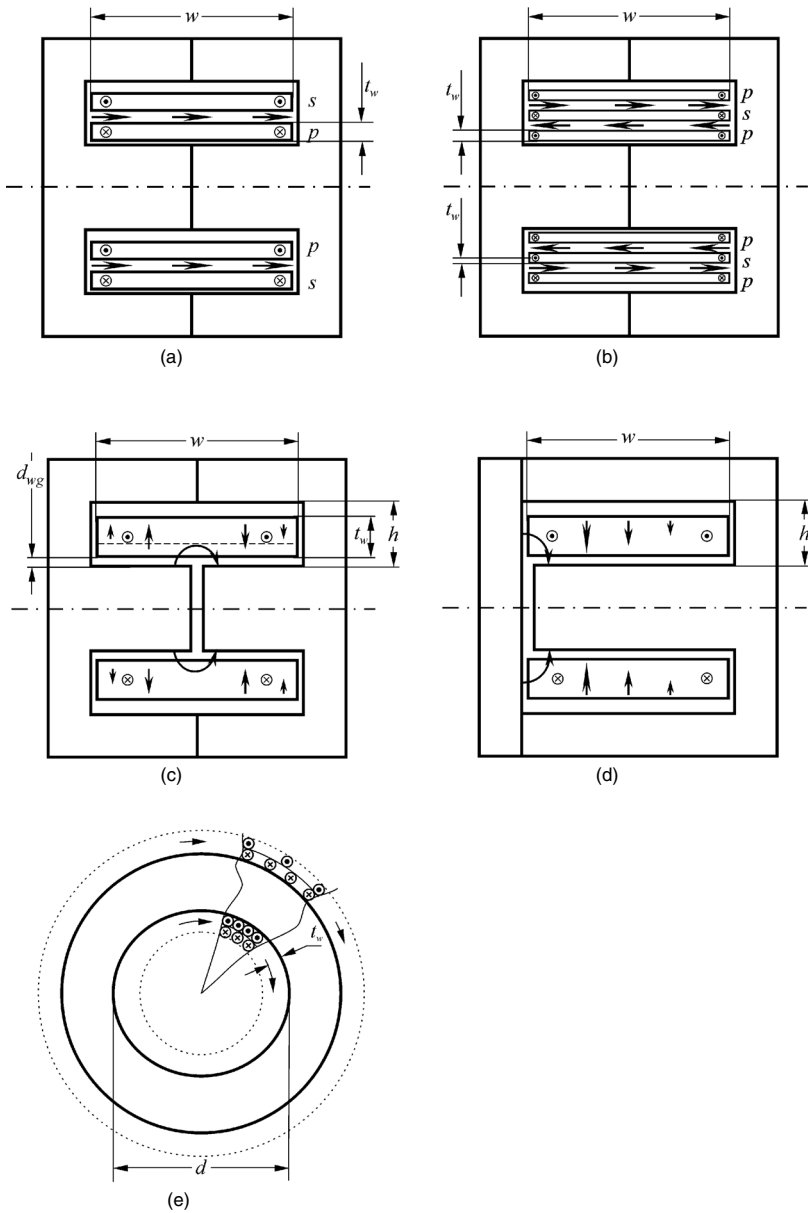


FIGURE 2.7

The usual transformers and inductor shapes and the discussed dimensions and field directions.

a) Normal transformer (reference case), $K = 1$ for both windings.

b) Secondary winding in an interleaved transformer (the secondary winding is sandwiched), $K = 2$ for secondary winding.

c) Center gapped inductor, $K = 2$.

d) EI core inductor, $K = 1$.

e) Ring core transformer or inductor, $K = 1$.

where

h is the window height (see Fig. 2.6)

We can also write for a transformer with one concentric primary and one secondary winding:

$$m_E n_E = N p \quad (2.26)$$

For interleaved windings in transformers (and no parallel wires) $m_E = m/K$, where K is the field symmetry factor, see Fig. 2.7. This presentation is necessary for half layers.

Usually, the field over the winding cross section area increases almost linearly from zero to its maximum value, so if we express the total losses by $(B_{\max})^2$, the result is to be divided by a factor of 3, see Appendix A. However, as not all field patterns behave like this, we add a factor k_F , and the result for eddy current losses becomes

$$P_{cu,eddy} = \frac{\pi l_w d_p^4 \omega^2 B_{\max}^2 k_F}{64 \rho_c 3} \quad (2.27)$$

where

$$B_{\max} \approx N \left(\frac{I_{ac} \mu_0}{w} \right)$$

Substitution of the expression of B_{\max} into the equation (2.27) yields

$$P_{cu,eddy} = \frac{l_w \frac{\pi d_p^4}{4} N^2 \left(\frac{2\pi f_{ap} I_{ac} \mu_0}{w} \right)^2 k_F}{48 \rho_c} \quad (2.28)$$

where

$k_F = 1$ for transformers

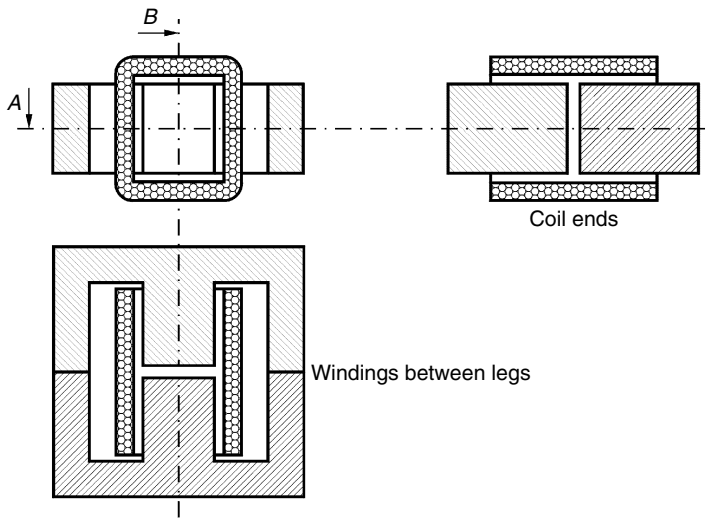
$k_F = 1$ also for inductors if the air gap is at a large distance from the layer compared to the layer width.

REMARK

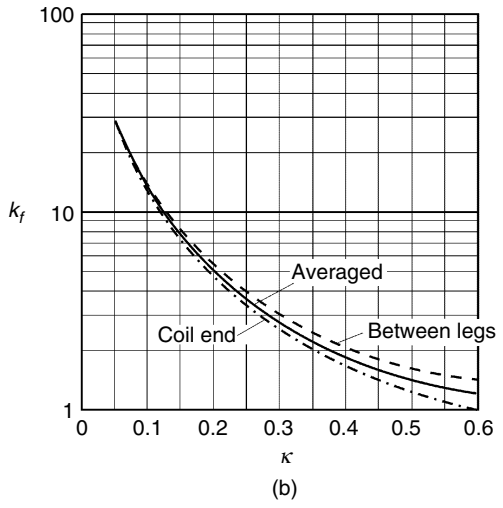
When the losses are quadratic with frequency, as it is in low frequency approximation, using $(di/dt)_{rms}$ instead of ωI is possible, thus avoiding the summing over the harmonic components. Then the apparent frequency necessary for Equation (2.28) is $f_{ap} = \frac{(di/dt)_{rms}}{2\pi I_{rms}}$.

Note that the eddy current losses are basically proportional to the third power of the number of turns for a given core, as the transverse field (the field perpendicular to the wire axis) is proportional to the number of turns N , and that the wire length is also proportional to N .

We denote k_F as *field factor*. For transformers, such as in Fig. 2.7,a) and b), the value of the field factor is $k_F \approx 1$. The factor k_F for inductors (e.g., EE and ETD cores) is highly dependent on the distance of the winding to the air gap, such as illustrated in Fig. 2.8. The corresponding high eddy current



(a)



(b)

FIGURE 2.8

2-D field factor k_f as a function of κ . Solid curve—typical average values of k_f ; Dashed curve—Field factor k_f for wires between legs, e.g., EE core, see Fig. 2.8, a; the eddy current losses are maximal; Dash-dotted curve—Field factor k_f for wires of coil ends, e.g., without legs, see Fig. 2.8, a; the eddy current losses are minimal.

losses are located close to the air gap and can cause local overheating. Thus, a thin layer coil close to the air gap has an especially high field factor k_F . The factor k_F is reduced for filled coils as the average distance to the air gap is increased.

REMARKS CONCERNING FIG. 2.8

1. The two extreme cases are shown:
 - Dashed curve—Field factor k_F for wires between legs (plane field pattern), e.g., EE core, see Fig. 2.8,b). The eddy current losses are maximal in this case.
 - Dash-dotted curve—Field factor k_F for wires of coil ends (axis-symmetrical field pattern), e.g., without legs, see Fig. 2.8,b). The eddy current losses are minimal in this case.
2. In this Chapter we use the average typical values shown by the solid curve in Fig. 2.8.

The factor k_F is also somewhat decreased in the coil ends because of the 3-D effect, as the transverse fields in the coil ends are lower in comparison with the fields in the coil inside the core.

We define a dimensionless parameter κ (pronounced kappa), which reflects the relative distance between the winding and the air gap. The parameter can be expressed as

$$\kappa = \frac{d_{wg} + \frac{t_w}{3}}{w/K} \quad (2.29)$$

where

d_{wg} is the distance between the winding and the leg, see fig 2.7c

t_w is the thickness of the winding, see fig 2.7c

K is the field symmetry factor, see Fig. 2.7

The factor k_F is mainly dependent on κ and has a low dependence on t_w and w in the cases when κ is kept constant. The factor k_F is derived in details in Appendix 5.A.3.

Note that as far as Equation (2.28) is valid, the losses are proportional to the square of $\omega I_{ac,lv}$ so they are proportional to di/dt . This is an interesting feature, as it allows us to use directly the RMS value of di/dt in these cases instead of summing all individual harmonics. Often the RMS value of di/dt is easy to compute. In the case of an inductor, it is the RMS voltage value across the inductor divided by its inductance $V_{L,rms}/L$. In the case of transformers, it is proportional to the voltage across the leakage inductance.

In the case of p parallel wires or Litz wire with p strands, we have p times more wires, but the transverse field remains the same. It is assumed that all

currents in the parallel wires are equal. Thus, in this case we have the following result $P_{cu,eddy,litz}$ compared to the original Equation (2.27):

$$P_{cu,eddy,litz} = P_{cu,eddy,orig} p \left(\frac{d_{p,litz}}{d_{p,orig}} \right)^4 = \frac{P_{cu,eddy,orig}}{p} = \frac{l_w \pi \frac{d_p^4}{4} N^2}{p 48 \rho_c} \left(\frac{2 \pi f I_{ac} \mu_0}{w} \right)^2 k_F \quad (2.30)$$

The advantage is that the losses $P_{cu,eddy}$ are inversely proportional to p , as for the same total cross section the term d_p^4 is inversely proportional to p^2 and, thus, we have $P_{cu,eddy,litz} = \frac{P_{cu,eddy,orig}}{p}$.

In the case of Litz wire, one has to take in account an increased wire length of about 5%. The wire diameter of the Litz wire is small and local fields are negligible, so the low frequency transverse field approximation is usually valid.

III) Wide Frequency Eddy Current Losses

The presented method for calculating eddy current losses includes 2-D effects, which provides an increased accuracy compared to 1-D approaches (such as Dowell type). Starting from Equation (2.28), two improvements can be done:

- At high frequency, the eddy currents in the wires generate fields, which influence the fields in the conductor itself and in other conductors. This fact leads to a reduction coefficient F_T in the equation for $P_{cu,eddy}$, see Appendix 2A.2. The letter T comes from the term *transverse* field.
- At low frequency, one can consider the real eddy current losses, caused also by the local fields around the wire and not only by the transverse fields. This fact yields a specific term and a reduction coefficient F_A in the equation for $P_{cu,eddy}$, see Appendix 2A.2. The letter A comes from the term *around*.

To be able to analyze eddy current losses in a wide frequency range, we introduce the penetration (skin) depth δ , given as

$$\delta = \sqrt{\frac{2 \rho_{cu}}{\omega \mu}} \quad (2.31)$$

where

$\omega = 2\pi f$ is the frequency of the applied magnetic field

μ is the permeability of the material (for copper $\mu \equiv \mu_0$), μ_0 is the permeability of vacuum; $\mu_0 = 1.25664 \times 10^{-6}$

$2\rho_{cu}$ is the electrical resistivity of the conducting material (copper) we use
 $2\rho_{cu} = 23 \times 10^{-9} \Omega\text{m}$ at 100°C; $\rho_c = 17.3 \times 10^{-9} \Omega\text{m}$ at 25°C

The penetration depth δ of copper (Cu) conductors is plotted in Fig. 2.9 as a function of frequency f for temperatures 25°C and 100°C.

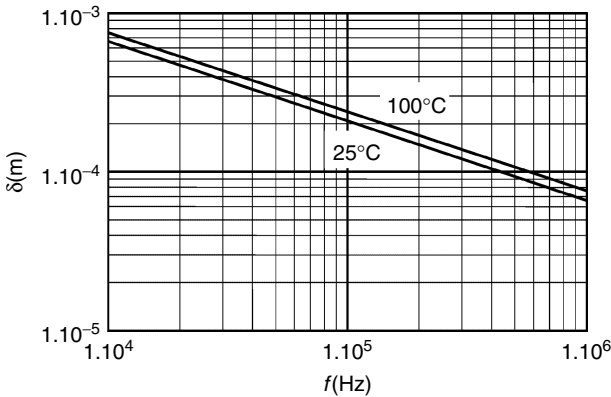


FIGURE 2.9 Penetration depth δ for copper wires as a function of frequency f , parameter temperature, $T = 25^\circ\text{C}$ and $T = 100^\circ\text{C}$.

Eddy Current Losses Factor k_c and the Wide Frequency Method

To extend the validity of Equation (2.27) for larger diameters and a wide frequency range, we derived the factor $k_c(m_E, \zeta, \eta, \lambda)$, which represents the ratio between the eddy current losses compared to the losses in the ohmic resistance of the winding of the magnetic component. The approach is called the **wide frequency method** for inductors and transformers, as it is applicable for all frequencies.

Using the previously introduced terms m_E , η , and λ , the eddy current losses are given by the following equation:

$$P_{eddy} = (R_0 I_{ac}^2) k_c(m_E, \zeta(f, d), \eta, \lambda) \quad (2.32)$$

where

the parameter ζ (the Greek letter zeta) represents the conductor diameter divided by the penetration depth

$$\zeta(f, d) = \frac{d}{\delta(f)} \quad (2.33)$$

In Equation (2.32) R_0 is the ohmic resistance of the winding,

$$R_0 = \rho_c l_T N \left(\frac{4}{\pi d_p^2 p} \right).$$

The details of the function $k_c(m_E, \zeta(f, d), \eta, \lambda)$ are given in Appendix 2A.2 and the full derivation is presented in Chapter 5. To allow an easy use of k_c , we provide here a few graphs.

REMARKS AND CONCLUSIONS CONCERNING EQUATION (2.32)

1. The results of the proposed equation are close to the known Quadrature-of-the-circle method of Dowell [4], but the proposed equation is more accurate in transformers (e.g., at low packing factors) and it can also handle inductor designs, where the Dowell method results in large errors.
2. For $\zeta < 1.6$, the low frequency approximation is valid and the losses increase proportionally to the frequency with an error below 10%.
3. In the transformer design, if $m_E > 2$ we can consider only the transverse field losses given by Equation (2.28).

Apparent Frequency Calculation

In Equation (2.32) the apparent frequency should be used.

1. In general, one has to sum the contribution of each current harmonic in order to calculate losses. In the presented method, for sinusoidal currents no corrections have to be made and the apparent frequency f_{ap} is the real one:

$$f_{ap} = f$$

2. For a symmetrical triangular current waveform, in the low frequency approximation we obtain the following apparent frequency f_{ap} :

$$f_{ap} = f \frac{2\sqrt{3}}{\pi} \approx 1.10f$$

3. At high frequency, the losses tend to increase with the root of frequency for a given current. In that case, the contribution of harmonics in the current is low and one can use the RMS value of the current instead of summing over all harmonics. For a symmetrical triangular current waveform this results in an apparent frequency f_{ap} :

$$f_{ap} \approx 1.025f$$

Reference Wire Diameter

The choice of 0.5 mm as a reference wire diameter is done in order to use a typical wire diameter for power electronics. The frequency, for which the penetration depth is equal to the reference diameter $d = \delta$, is 20 kHz. The limit of the low frequency (LF) approximation for the reference diameter $d = 0.5$ mm is 50 kHz, thus LF can be applied below 50 kHz for that wire diameter. These values are easy to remember. The diameters of wires in adjacent layers are taken equal and in a square fitting. This is the worst-case design, as a hexagonal fitting usually reduces the losses.

Equivalent Frequency Calculation

To use the provided graphs (Figs. 2.10–2.13) for any frequency, wire diameter, and conductor resistivity, the equivalent frequency of the considered case should be first found:

$$f_{eq} = f_{ap} \left(\frac{d_p}{0.5 \text{ mm}} \right)^2 \left(\frac{23 \times 10^{-9}}{\rho_c} \right) \quad (2.34)$$

where

- f_{ap} is the apparent frequency
- d_p is the practical wire diameter in [mm]
- ρ_c is the conductor resistivity in [Ωm]

If one is only interested in an order of magnitude of the eddy current losses, the waveform and resistivity change could be neglected, but the diameter effect has still to be taken into account by the following simplified expression:

$$f_{eq} \approx f \left(\frac{d_p}{0.5 \text{ mm}} \right)^2 \quad (2.35)$$

REMARK

Use Equation (2.35) only for fast design when reading from Fig. 2.10 to Fig. 2.13. The direct calculation of the coefficient k_c and the graphical method for obtaining it are explained in detail in the Appendix 2.A.2.

Transformer Cases and Examples

For the transformers the value of the coefficient k_c is

$$k_c \approx m_E^2 k_{ff} \quad (2.36)$$

where

the value of k_{ff} is found using Fig. 2.10 and Fig. 2.11. The number of parallel wires p reduces the DC resistance and thus increases k_c .

It is not recommended to use partially filled layers in transformer designs. If otherwise partially filled layers are used, the wires should be equally spread. The effect of the partially filled layers is reduced at high values of m_E .

The graphs shown in Fig. 2.10 and Fig. 2.11 concern a design example with a typical wire diameter of 0.5 mm and the normal frequency range for power electronics: 10 kHz to 10 MHz. For more than two layers ($m_E > 2$), the result is almost independent of the number of layers. The usual values of η in transformers are between 0.7 (typical for thin wires and Litz wire) and 0.9 (typical for $d > 0.5$ mm). For other values of η , a linear interpolation between

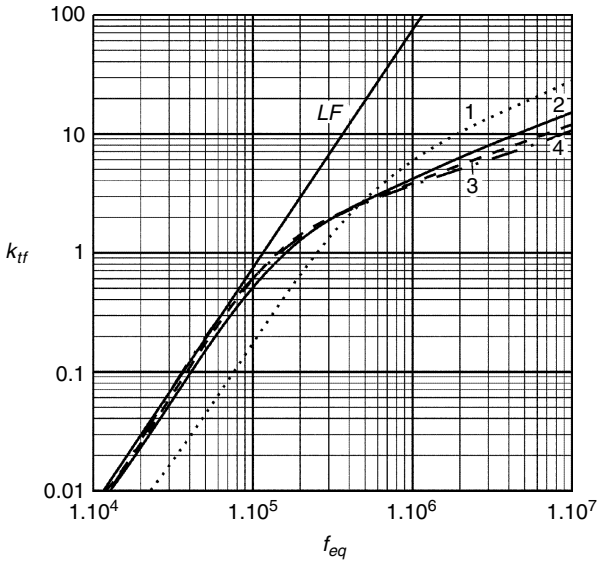


FIGURE 2.10

Transformer cases, typical transformer factor k_{Tf} for $d = 0.5$ mm, $\eta = 0.9$, $\rho = 23 \times 10^{-9}$ and $\lambda = 0.5$, 1) dotted line: half layer, $m_E = 0.5$; 2) solid line: single layer, $m_E = 1$; 3) dashed: two layers, $m_E = 2$; 4) dash-dot: three or more layers, $m_E > 2$. *LF* – low frequency approximation.

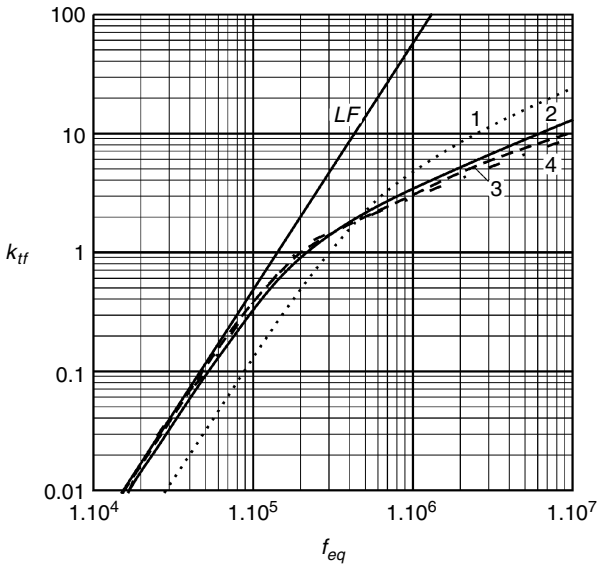


FIGURE 2.11

Transformer cases, typical transformer factor k_{Tf} for $d = 0.5$ mm, $\eta = 0.7$, $\rho = 23 \times 10^{-9}$ and $\lambda = 0.5$, 1) dotted line: half layer, $m_E = 0.5$; 2) solid line: single layer, $m_E = 1$; 3) dashed: two layers, $m_E = 2$; 4) dash-dot: three or more layers, $m_E > 2$. *LF* – low frequency approximation.

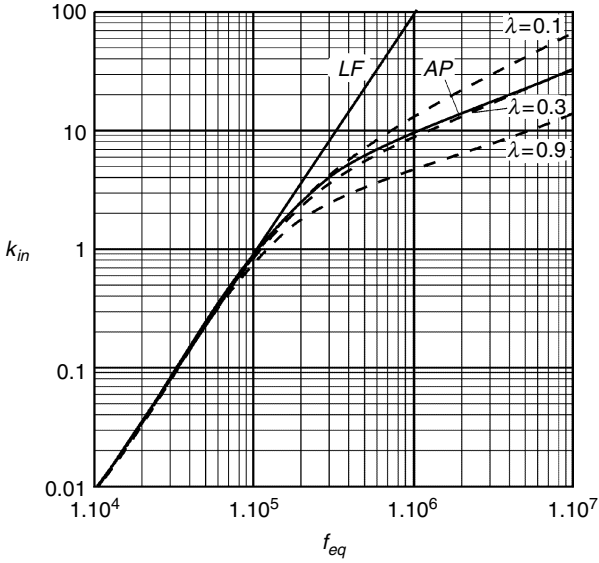


FIGURE 2.12

Inductor case, k_{in} as a function of f_{eq} for $\eta = 0.9$, $d = 0.5$ mm, $\rho = 23 \times 10^{-9}$, high m_E values, Straight full line *LF*: low frequency solution; Full curve *AP*: approximation of k_{in} used in Chapter 2; dashed curves: solutions given in the Chapter 5 for $\lambda = 0.1, 0.3, 0.9$.

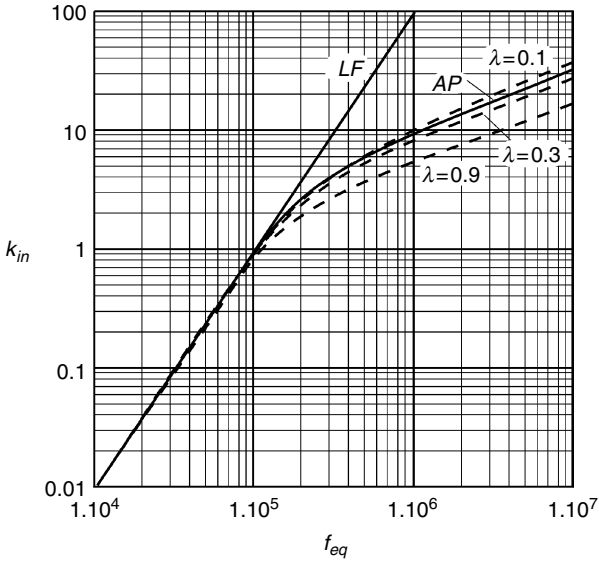


FIGURE 2.13

Inductor case, k_{in} as a function of f_{eq} for $\eta = 0.7$, $d = 0.5$ mm, $\rho = 23 \times 10^{-9}$, high m_E values, Straight full line *LF*: low frequency solution; Full curve *AP*: approximation of k_{in} used in Chapter 2; Dashed curves: solutions given in the Chapter 5 for $\lambda = 0.1, 0.3, 0.9$.

Fig. 2.10 and Fig. 2.11 can be done. The additional error due to that interpolation is below 2%.

A few **short examples** of transformer design show the use of the graphs in Fig. 2.10 and Fig. 2.11 or the corresponding equations in Appendix 2A.2.

- 1) *A single layer winding of a transformer uses a wire diameter of 0.9 mm and an outer diameter of 1 mm, the frequency is 30 kHz, the copper resistivity is $\rho = 23 \times 10^{-9} \Omega m$.*

We have $\eta = 0.9 \text{ mm}/1 \text{ mm} = 0.9$, so we use Fig. 2.10. We have to keep the same diameter/penetration depth ratio, i.e., to find the equivalent frequency $f_{eq} = 30 \text{ kHz} \times (0.9/0.5)^2 = 97.2 \text{ kHz}$.

For this frequency, we calculate k_c using the full equation of Appendix 2A.2. The result corresponds to $k_{jf} = 0.473$. Reading from Fig. 2.10 gives the same result. It is a single layer transformer, so $m_E = 1$ and we obtain $k_c = k_{jf} = 0.473$.

- 2) *The same wire diameters and resistivity, but a three-layer transformer winding, using a three times smaller winding width, the same turn number.*

We use the same values $\eta = 0.9$ and $f_{eq} = 97.2 \text{ kHz}$. It is a three-layer transformer, so $m_E = 3$. For three layers and more, we obtain $k_{jf} = 0.575$ (using Fig. 2.10. or the equation of the Appendix 2A.2) and we have $k_c = 3^2 k_{jf} = 5.17$. For comparison, using the full equation we obtain $k_c = 5.08$, which is close to that result.

- 3) *The same wire diameters and resistivity, but a half layer transformer design (the considered single layer secondary is sandwiched between two primaries).*

Using the same values $\eta = 0.9$ and $f_{eq} = 97.2 \text{ kHz}$, we calculate or read from Fig. 2.10 $k_{jf} = 0.166$. It is a half-layer transformer, so $m_E = 0.5$ and we have $k_c = 0.5^2 k_{jf} = 0.0415$. Using the full equation for k_c gives the same result. This value is much lower than cases 1) and 2). The reason is that in this design case the transverse field is zero and only local fields are present. In practical realizations, the half layer solutions do indeed perform well, but a noncareful winding (e.g., nonequal winding width of the layers) generates parasitic transverse fields that increase the losses considerably.

- 4) *A two-layer transformer winding of 0.5-mm diameter copper at 50 kHz and packing factor in the direction of the layer $\eta = 0.8$, copper resistivity $\rho_c = 23 \times 10^{-9} \Omega m$.*

We have the same diameter as the graphs, so the equivalent frequency is equal to the applied frequency. We obtain $k_{jf,0.9} = 0.170$ from Fig. 2.10 and $k_{jf,0.7} = 0.104$ from Fig. 2.11. To find $k_{jf,0.8}$ (for $\eta = 0.8$), we take the average of the two values $k_{jf,0.8} = \frac{0.104 + 0.170}{2} = 0.137$. Then we find $k_c = 2^2 k_{jf,0.8} = 0.549$. For comparison, using the full equation for k_c gives $k_c = 0.541$.

Inductor Cases and Examples

For the low frequency range, where the dependence of the losses on the frequency is quadratic, Equation (2.30) can be used. At higher frequency, the losses are lower than predicted by Equation (2.30). The field has parallel components to the layer as well as perpendicular components. In this chapter, a simplified expression is used for inductors, neglecting the field induced by the other conductors.

Thus, we define the following simplified eddy current loss factor k_c for inductors:

$$k_c = \left(\frac{p N d_p}{w} \right)^2 k_F k_{in}(f_{eq}) \quad (2.37)$$

where

k_F is the field factor, see Fig. 2.8

the coefficient k_{in} is found from Fig. 2.12 and Fig. 2.13

p is the number of wires in parallel (or the number of strands in a Litz wire).

The full equation presenting the eddy current loss factor k_c is given in the Appendix 2A.2.

REMARKS CONCERNING FIG. 2.12 AND FIG. 2.13

1. For the low frequency range ($f < 50$ kHz for $d = 0.5$ mm), where $d < 1.6\delta$, the parameters λ and η are not really important and the low frequency approximation is valid, see the straight line LF in Fig. 2.12 and Fig. 2.13.
2. In Fig. 2.12 and Fig. 2.13, we give the approximation of k_{in} for inductors (solid curve AP), which neglects the induced field of other wires and we use it in this chapter.
3. In Chapter 5 we directly calculate k_c in a more accurate way—the results are the dashed curves added to the graphs in Fig. 2.12 and Fig. 2.13.

We give a few short examples of inductor designs showing the use of the graphs in Fig. 2.12 and Fig. 2.13. In all examples the resistivity is $\rho = 23 \times 10^{-9} \Omega \cdot m$.

- 1) A single layer center gapped inductor with 40 turns has a winding width of 30 mm and $\eta = 0.9$. The wire diameter is $d = 0.8$ mm. The frequency is 25 kHz. The winding is wound directly on the coil former and the distance to the center leg is 1.5 mm.

The equivalent frequency for the given diameter is

$$f_{eq} = 25 \text{ kHz} \times (0.8/0.5)^2 = 64 \text{ kHz}.$$

The symmetry factor is $K = 2$ and the value of κ is $\kappa = \frac{1.5}{30/2} = 0.1$

For the found equivalent frequency $f_{eq} = 64$ kHz we calculate $k_{in} = 0.365$ by the full equations or read from the curve in Fig. 2.12. Using Fig. 2.8 or Equation (2.A.24) we find the field factor value $k_F = 12.5$. Then, we calculate

$$k_c = \left(\frac{pNd_p}{w} \right)^2 k_F k_{in} = \left(\frac{1 \times 40 \times 0.0008}{0.03} \right)^2 12.5 \times 0.365 = 5.19$$

2) *An inductor with the same wire diameter, frequency, turn number, core type, and η , but $\kappa \approx 0.3$*

This corresponds to a distance of 4.5 mm between the centerline of the winding and the center leg. Only k_F changes and its value is now $k_F = 2.77$, see Equation (2.A.24). We have

$$k_c = \left(\frac{pNd_p}{w} \right)^2 k_F k_{in} = \left(\frac{1 \times 40 \times 0.0008}{0.03} \right)^2 2.77 \times 0.3653 = 1.15$$

Although the wire length increases in this case compared to the previous one, and thus the DC resistance is also increased, a significantly lower AC loss is obtained. Moreover, the hot spot close to the air gap is avoided. However, even better k_c values can be obtained. A smaller diameter would result in smaller AC losses but paralleled wires or Litz wire can still give further improvements in both AC and DC resistance of the winding.

3) *A high-current DC inductor with a center gap is wound with $d = 2$ mm wire (2.22 outer diameter), and a high frequency component of 200 kHz is present. The number of turns is 24, 12 turns in each layer. The distance from the winding to the center leg is 1.5 mm, the winding thickness is 4.5 mm, the winding width is 30 mm, and the winding area height is 10 mm.*

The equivalent frequency for the given diameter is $f_{eq} = 200 \text{ kHz} \times (2/0.5)^2 = 3.2$ MHz.

In the case $K = 2$, the value of κ is

$$\kappa = \frac{t_{wg} + t_w/3}{w/2} = \frac{1.5 + 4.5/3}{30/2} = 0.2$$

Using Fig. 2.8 or Equation (2.A.24) we find $k_F = 5.19$. The value of η is $\eta = 0.8$. We interpolate between the two graphs in Fig. 2.12 and Fig. 2.13 or use the equation in the appendix to get k_{in} . We obtain $k_{in} = 17.48$. Then, we have

$$k_c = \left(\frac{pNd_p}{w} \right)^2 k_F k_{in} = \left(\frac{1 \times 24 \times 0.002}{0.03} \right)^2 5.19 \times 17.48 = 232$$

The value of k_c is very high and this type of inductor is definitely really not suitable to be used as an AC inductor! The example shows also that even for small high frequency components, the AC losses are much higher ($k_c = 232$) than the DC losses.

NOTE: We have $\lambda = 4.5/10 \approx 0.45$, this results in about 30% lower AC loss if the full equations of [Chapter 5](#) are used.

- 4) *The same design as 3), also 24 turns but 4 wires in parallel of 1 mm wire, the DC resistance is the same. The currents are equally divided among the 4 wires.*

The equivalent frequency for the given diameter $d = 0.5$ is $f_{eq} = 200 \text{ kHz}$ $f_{eq} = 200 \text{ kHz} \times (1/0.5)^2 = 800 \text{ kHz}$.

The values for η and k_F are the same as in 3): $\eta = 0.8$, $k_F = 5.19$. We read or calculate $k_{in} = 8.06$. Then, we find

$$k_c = \left(\frac{p N d_p}{w} \right)^2 k_F k_{in} = \left(\frac{4 \times 24 \times 0.001}{0.03} \right)^2 5.19 \times 8.06 = 428$$

The conclusion is that for this high frequency, the AC losses increase by taking more wires in parallel with the same total cross section: k_c is 428 in comparison with 232 in the previous case. *For really high frequency cases the eddy current losses tend to increase with the root of p .* This high frequency phenomenon is the inverse of what is experienced for the low frequency eddy current losses, where the losses decrease with p .

IV) Total Copper Losses

Now we calculate the sum P_{cu} of the obtained actual ohmic and eddy current losses for all windings:

$$P_{cu} = \sum_i P_{cu,i} = \sum_i \left(R_{0,i} \left(I_{dc,i}^2 + I_{ac,i}^2 + I_{ac,i}^2 k_{ci} \right) \right) \quad (2.39)$$

Step 11) Check if the Copper Losses P_{cu} are Lower Than the Allowed Copper Dissipation $P_{h,cu}$

We check if the total copper losses are lower than the thermally allowed copper dissipation:

$$P_{cu} \leq P_{h,cu} \quad (2.40)$$

If the total copper losses P_{cu} are lower than the allowed dissipation limit $P_{h,cu}$, then we continue with the step 13, otherwise we go to step 12.

Step 12) Is Improvement Possible?

The answer to this question is related to the type of technology one is willing to use. This means

- Which wire diameters are in stock or available?
- Is Litz wire allowed or not?
- Can one keep distance between the winding and the air gap?

The proposed design method normally guarantees a sufficiently low ohmic copper loss. If step 11 is not satisfied, it means that the eddy current losses are too high. So it is still worthwhile to investigate if one can reduce the total actual copper losses. In general, if $k_{eddy} < 0.5$, a small increase in diameter can be useful as the ohmic losses decrease and the eddy current losses may not increase too much. However, specific tricks to reduce the eddy current losses are possible. They are discussed in step 12a.

The choice of wire diameters and winding arrangements can be used to optimize the wire losses.

Step 12a) Optimize the Diameter and Winding Arrangement

I) Transformers

Possible improvements are

- If the design results in a single layer winding, the diameter of the wire can be increased in order to fill the layer completely, as far as it is tolerated by the creepage distance. This is a very efficient way to reduce the DC resistance. Thus, although k_{eddy} ($k_{eddy} = P_{cu,eddy}/P_{cu,ohm}$) may be high, the losses are reduced while increasing the diameter of the wire. If this trick is not sufficient, one can think of interleaving, where the secondary winding wound with thick wires (typically 2 times the penetration depth or more) is sandwiched by two primary windings of a lower diameter.
- If the design results in two or more layers, then it is useful to use p_i wires in parallel to reduce the eddy current losses. In this way, the diameter of the wires can be diminished with a factor $\sqrt{p_i}$ and thus eddy current losses reduced. Special care should be taken to make sure that the current in the wires is almost equal, which is usually obtained by symmetry. A special case of paralleling wires is Litz wire. In this case p_i becomes the number of strands. Some 5% increase of MLT has to be taken into account in the case of Litz wire and paralleling wires.

II) Inductors

Possible improvements are

- Using Litz wire or paralleled wires reduces the eddy current losses a lot in the usual cases.
- An important improvement can be reached while keeping some distance from the air gap. The graph of k_F (Fig. 2.8) gives an impression of this improvement.
- Designs with large ratio d_p/δ are possible if the AC current is much lower than the DC component.

In inductors with concentrated air gaps, the field close to the air gap is only slightly lower than the field in the air gap. Thus, the field close to the air gap can cause an induction heating of the windings by the transverse field at that place. Moreover, the field is usually not parallel to the layers, this means that the field has to tunnel between the wires. This fact increases in a significant way the losses in single layer designs. *So, using a single layer directly on the coil former, close to the air gap is the worst thing to do in inductor designs!*

Step 13) Check the Copper Filling Factor

We check if the core window area W_a is large enough to fit all the windings. We assume a copper filling factor $k_{cu} = 0.4$ for round conductors and $k_{cu} = 0.2$ for Litz wire and check the inequality:

$$\sum_{i=1}^n p_i N_i \frac{\pi d_{i,p}^2}{4} \leq k_{cu} W_a \quad (2.41)$$

If the window area is not large enough, we go to step 13a) and choose a larger core. For more detailed information concerning the copper filling factor, refer to [Chapter 4](#).

Step 13a) Choose a Larger Core

We choose a larger core in order to have a larger window area and higher dissipation possibility. Choosing a better material with lower losses or a higher saturation level may also be a sufficient step.

Step 14) Check if the Chosen Core Size in Step 1) is not Too High

To estimate if the chosen core size in step 1) is not too high, we use the inequalities

$$k_{eddy} = \frac{P_{cu,eddy}}{P_{cu,ohm}} = \frac{I_{ac}^2 k_c}{I_{dc}^2 + I_{ac}^2} \ll 0.5 \quad (2.42)$$

$$k_{cu} \ll 0.4 \quad (2.43)$$

and if both are true, then we go to step 14.a).

Step 14a) Choose a Smaller Core

We choose a smaller core size as the window area is hardly filled ($k_{cu} \ll 0.4$) and eddy currents losses are relatively low $k_{eddy} \ll 0.5$.

A low core size results in longer wires as we have to increase the turn number and, thus, higher wire diameters are to be chosen to keep the ohmic losses low. This results in higher eddy current losses. Therefore, we choose

a smaller core (step 14a), only if both the inequalities, Equations (2.42) and (2.43), are really met.

Step 15) Calculate the Total Air Gap Length Σl_g

Usually, inductors require an air gap to avoid saturation. An air gap is also required for transformers subjected to DC MMF (magneto-motive force).

When neglecting fringing field in a magnetic circuit with air gaps, the inductance L can be presented as

$$L = \frac{\mu_0 A_e N^2}{\sum l_g + l_e / \mu_c} \tag{2.44}$$

Then, for calculating small air gaps the following expression can be used:

$$\sum l_g = \frac{\mu_0 A_e N^2}{L} - \frac{l_e}{\mu_c} \tag{2.45}$$

where

Σl_g is the total length of the air gaps

μ_c is the permeability of the core material

μ_0 is the permeability of free space

A_e is the equivalent cross-sectional area of the magnetic circuit, see Appendix B

l_e is the equivalent magnetic path length in the core, see Appendix B

L is the wanted inductance

For large air gaps, the permeance of the other field paths (fringing paths) at the side of the air gap is to be considered. This permeance results in considerable deviations of Equation (2.45), which takes into account only the main magnetic path. In some cases, as the permeance of the fringing field paths is neglected, Equation (2.45) underestimates the necessary air gap length up to a factor of 2. Thus, practically, the total air gap length calculated by Equation (2.45) should be increased typically 1–2 times to obtain the necessary gap length $l_{g,actual}$:

$$\sum l_{g,actual} = (1-2) \sum l_g \tag{2.46}$$

Many parameters influence the necessary correction, but as a first approach, some rough approximation for a center gapped EE core or for an UA core can be made by using the experimental equation proposed by McLyman [5]:

$$L' = LF \tag{2.47}$$

$$F = 1 + \frac{l_g}{\sqrt{A_g}} \ln \left(\frac{2w_h}{l_g} \right) \tag{2.48}$$

where

- L is the inductance, found by Equation (2.44)
- L' is the inductance corrected for fringing flux
- F is the fringing factor
- l_g is the length of the air gap
- A_g is the cross-sectional area of the air gap
- w_h is the total width of the winding

REMARKS

1. It is not correct to compensate the fringing effect by decreasing the turn number. This results in a high induction value, the core might saturate, and the core losses will be higher;
2. If for obtaining the wanted inductance L , some of the already calculated parameters are to be changed (N , core size), then both core and copper losses have to be recalculated and compared with the allowed limits.

The real question is to find l_g when L is given, which corresponds to

$$\sum l_g = \frac{\mu_o A_c N^2}{L} F_{new} - \frac{l_c}{\mu_c} \quad (2.49)$$

Equation (2.49) results in solving a nonlinear equation, as F_{new} is also a function of l_g . However, a result very close to the final value is obtained by substituting the following value of F_{new} :

$$F_{new} = (F - 1)F + 1 \quad (2.50)$$

Parameter A_L

Often the manufacturers of ferrite cores consider the parameter A_L for center-leg gapped cores. The parameter A_L , corresponding to a defined gap length, is given in the data sheets. Then, the inductance value is presented as

$$L = A_L N^2 \quad (2.51)$$

where

- A_L is in fact the permeance of the magnetic circuit
- N is the turn number

Knowing the desired value of L , first we find A_L and then using the manufacture data, we obtain the corresponding gap length l_g :

$$A_L = \frac{L}{N^2} \Rightarrow l_g \quad (2.52)$$

REMARK

Such data are not always available, or in the first design a spacer gap is used (two air gaps in series in the flux path) so a more precise expression is necessary to find the wanted air gap length. Spacer gaps tend to give lower losses than center gaps, but they are not preferred as they generate a lot of leakage field outside the magnetic component, causing possible EMI problems.

2.1.2 Saturated Thermally Limited Design

In applications where the core losses are relatively low and the induction level is high, the design is thermally limited as well as saturation limited. Usually, these applications are low-frequency or pulse applications. Typical examples of such applications are AC filters, pulse transformers, and DC chokes.

We explain the steps of the saturated thermally limited design as they are given in the flowchart in [Fig. 2.2](#).

Step 1') Find the Peak-to-Peak Induction B_{pp}

To start the design, we find the peak-to-peak induction, as this value corresponds to the losses in the core. We need this value to evaluate the necessary core size.

To find the allowed B_{pp} , we first have to define the saturation induction B_{sat} . The practical use of a core is limited to an induction value, where the nonlinearity of the saturation does not deteriorate the waveforms too much. For transformers, this limit is the induction value for which the magnetizing current becomes excessive. For inductors, the limit corresponds to the point, where the differential inductance is significantly reduced, for example by a factor of 2. For ferrites for power conversion applications, the induction value of 0.35 T is a typical saturation value at a temperature of 100°C. Knowing B_{sat} we can find the allowed B_{pp} using the specific converter current and voltage waveforms.

Example

Let us consider a filter inductor in a step-down or step-up converter. If the DC component of the current of the inductor is $I_{L,DC}$ and the ripple peak current is $\Delta i_{L,peak}$, then the allowed B_{pp} is

$$B_{pp} = B_{sat} \frac{2 \Delta i_{L,peak}}{I_{L,DC} + \Delta i_{L,peak}} \quad (2.53)$$

Step 2') Choose a Core, Material, and Size

The next step of the design is to choose an appropriate core material and size. To choose the core size, we use again a simple scale law based on natural convection in air, which compares the total volt-amp rating of the component

to the product of a core characteristic size parameter a_{ch} , the operating frequency f , and the peak-to-peak induction B_{pp} :

$$S_{tot} = \sum_{all\ windings} V_{rms} I_{rms} = A_1 a_{ch}^\gamma f \frac{B_{pp}}{2} \Rightarrow a_{ch} = \left(\frac{S_{tot}}{A_1 f B_{pp}/2} \right)^{1/\gamma} \quad (2.54)$$

where

A_1 is a coefficient.

For ferrites, A_1 is in the range $A_1 = (5 - 15) \times 10^3$ when a_{ch} is in [m]; ($A_1 = (0.5 - 1.5) \times 10^{-3}$ when a_{ch} is in [cm])

a_{ch} is the largest dimension of the component, used as a scaling parameter

γ is an exponent, characterizing the material and shape of the core, $\gamma = 3.5$

f is the operating frequency in [Hz]

B_{pp} is the peak-to-peak induction in [T]

In Equation (2.54) we use the operating frequency f and the peak-to-peak induction B_{pp} as indications for the power handling ability of the component, and thus, the core size choice is more accurate in comparison with the non-saturated thermally limited design.

In Fig. 2.14 we show the possible ranges of the scaling parameter a_{ch} , upper value $a_{ch,u}$ ($A_1 = 5 \times 10^3$) and lower value $a_{ch,l}$ ($A_1 = 15 \times 10^3$), as a function of the total V-A rating S_{tot} of the component for two values of the peak-to-peak induction B_{pp} (0.7 T and 0.35 T).

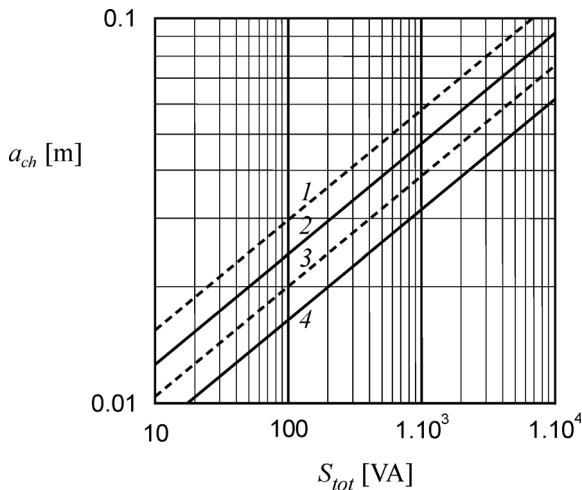


FIGURE 2.14

Core size estimation for a saturated, thermally limited ferrite core design at 25 kHz.

- 1: for $A_1 = 5 \times 10^3$ and $B_{pp} = 0.35$ T (single magnetization direction)
- 2: for $A_1 = 5 \times 10^3$ and $B_{pp} = 0.7$ T (double magnetization direction)
- 3: for $A_1 = 15 \times 10^3$ and $B_{pp} = 0.35$ T (single magnetization direction)
- 4: for $A_1 = 15 \times 10^3$ and $B_{pp} = 0.7$ T (double magnetization direction)

REMARKS

1. A not appropriate choice in step 2') will be noticed later in the next steps, which leads to a smaller or a larger core size.
2. The high values of A_1 are considered for better cooled applications. The low values of A_1 are typical for applications with a low filling factor k_{cu} (Litz wire, for instance) and a high DC component, where $B_{pp}/2 \ll B_p$;
3. Insulation requirements tend to decrease the coefficient A_1 .

Step 3') Find the Core Losses P_{fe} from Graphical Data

To find the core losses P_{fe} , we use the aforementioned graphic dependencies of the specific losses $P_{fe,sp}$ versus induction $B_{pp}/2$ with frequency f as a parameter. These graphs are usually provided by the core manufacturers. We find the specific losses $P_{fe,sp,w}$ from the graphs and then the core losses for iron-based cores are

$$P_{fe} = P_{fe,sp,w} V_c g k_{ff} \quad (2.55)$$

where

V_c is the core volume

g is the specific weight of the material, $g = 7800 \text{ kg/m}^3$

k_{ff} is the core filling factor

$P_{fe,sp,w}$ are the losses per unit weight

For ferrites it is common to specify the losses per unit volume:

$$P_{fe} = P_{fe,sp,v} V_c \quad (2.56)$$

where

$P_{fe,sp,v}$ are the losses per unit volume

Step 4') Find the Heat Dissipation Capability P_h of the Component

This step is similar to step 2 in the non-saturated thermally limited design. First, we calculate the component dissipation capability:

$$P_h = k_A a b \quad (2.57)$$

where

k_A is a coefficient, typical value 2500 W/m^2

a and b are the two largest dimensions of the component in [m]

The result of (2.57) is the allowed total losses in the case with ratio $P_{fe}/P_h = 0.5$, which corresponds to the non-saturated thermally limited design. However, the allowed dissipation is lower than the component dissipation capability

when the major part of the losses is concentrated in the windings. This is the case in the saturated thermally limited designs.

Step 5') Check the Ratio P_{fe}/P_h

We check if the core losses P_{fe} , found in step 3), are below half of the found component dissipation capability P_h :

$$P_{fe} < 0.5 P_h \tag{2.58}$$

and if it is so, we continue the design as a saturated thermally limited case.

If P_{fe} is not below $1/2$ of P_h , we consider the case as a non-saturated thermally limited design and start with step 1) of that design procedure.

Step 6') Estimate the Allowed Copper Dissipation Capability

Using the already found core losses P_{fe} from Equation (2.55) and component dissipation capability P_h from Equation (2.57), in this step we find the allowed copper losses $P_{h,cu}$ in the considered saturated limited case. Assuming the component allowed dissipation of $2/3$ of P_h , from Equation (2.57), for the case with zero core losses, we can depict the allowed copper dissipation $P_{h,cu}$ compared to the total dissipation capability P_h , as a linear function of the ratio P_{fe}/P_h , see Fig. 2.15. That function can be also expressed as

$$P_{h,cu} = \frac{2}{3} P_h - \frac{1}{3} P_{fe} \tag{2.59}$$

Now we find the allowed copper losses $P_{h,cu}$ graphically using Fig. 2.15 or analytically by Equation (2.59).

The next steps of the design are aimed at finding the number of turns, the wire diameter, and the copper losses. Thus, we go to step 7) of the non-saturated thermally limited design (see the flowchart shown in Fig. 2.2).

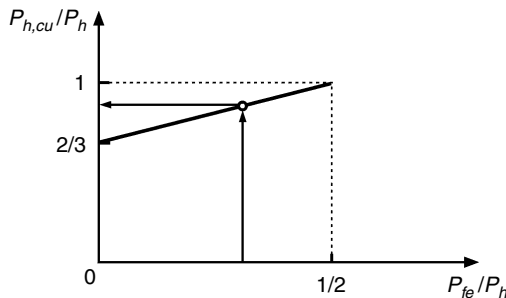


FIGURE 2.15

Dependence of the allowed copper loss/dissipation capability (the ratio $P_{h,cu}/P_h$) on the ratio P_{fe}/P_h .

2.1.3 Signal Quality Limited Design

Taking into account the specifics of the signal quality limited cases, they can be considered as non-saturated thermally limited cases or saturated thermally limited cases. The design temperature is typically close to ambient temperature if ferrites are used. This fact may lead to a different choice of ferrite grades according to the specific constraints.

Here we give some recommendations:

- *Current transformers:* There is limitation on the magnetizing current that can influence the current transfer ratio. This fact determines the size of the core. The number of turns is not a degree of freedom in these designs.
- *Accurate inductors:* The non-linearity has to be kept within some limits in such designs. After calculating the maximum induction, the case can be considered as a saturated thermally limited design.
- *Loss limited designs* in order to achieve high efficiency. These cases correspond to non-saturated thermally limited designs. Low loss at a low temperature ferrite grades have to be considered.

2.2 Examples

Two fully calculated examples are given here. Although it is still possible to calculate them with a pocket calculator and graphs, the most accurate way is to include the algorithm in a computer program. We use MathCAD, but Maple, Matlab, C, Pascal, and Basic types and spreadsheet programs can also be used.

2.2.1 Non-Saturated Thermally Limited Design Example

2.2.1.1 Design Steps

As an example of the non-saturated thermally limited design procedure, let us consider a transformer for a full bridge converter (Figs. 2.16 and 2.17). The converter is only used to do a voltage level conversion and a galvanic separation, not voltage control. In the converter, the series resonant capacitor is added to resonate with the leakage inductance of the transformer. This allows us to approximate the current by a sine wave.

The corresponding (ideal case) converter specifications are as follows:

Input DC voltage: $V_{in,DC} = 400 \text{ V}$

Output DC current: $I_{o,DC} = 3.6 \frac{2\sqrt{2}}{\pi} = 3.24 \text{ A}$

Output voltage: $V_o = 100 \text{ V}$

Operating temperature: $T = 100^\circ\text{C}$

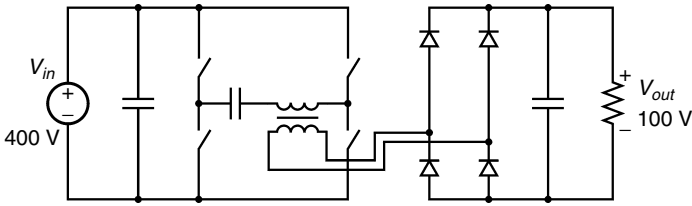


FIGURE 2.16
Full bridge DC/DC converter.

The transformer specifications are:

Operating frequency: $f_{op} = 100 \text{ kHz}$

Square wave primary voltage: $V_1 = 400 \text{ V}$

Square secondary voltage: $V_2 = 100 \text{ V}$

Output AC current: $I_2 = 3.6 \text{ A}$

Input AC current: $I_1 = 0.9 \text{ A}$

In a practical design, the resonance frequency is set somewhat higher than the switching frequency in order to obtain zero voltage switch behavior, and thus, the converter specifications are close to 300 W transferred power.

The design is likely to be a non-saturated thermally limited case as it is a high frequency application and there is no DC current in the transformer.

1) Using Equation (2.1) we find the total VA rating:

$$\sum_{\text{all windings}} V_{rms} I_{rms} = 400 \times 0.9 + 100 \times 3.6 = 720 \text{ VA}$$

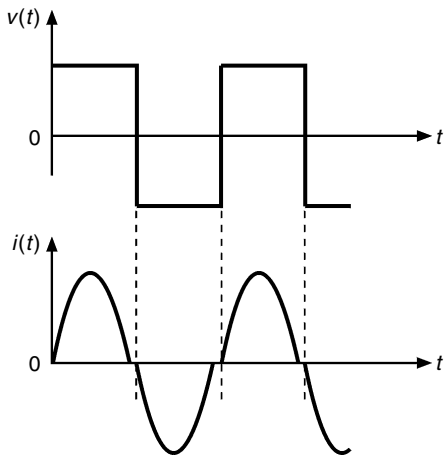


FIGURE 2.17
Voltage and current of the secondary winding of the full bridge converter.

and for $A = 15 \times 10^6$ the scale parameter a_{ch} is

$$a_{ch} = \sqrt[3]{720/15 \times 10^6} = 0.0364 \text{ m} = 36.4 \text{ mm}$$

An ETD34 core seems to be too small, so we choose a core shape ETD39, material grade 3F3 [6] with the largest dimension $a = b = 0.039 \text{ m}$. The core parameters (see the Appendix B at the end of the book) are

$$V_c = 11.5 \times 10^{-6} \text{ m}^3, A_e = 125 \times 10^{-6} \text{ m}^2, W_a = 174 \times 10^{-6} \text{ m}^2, \\ MLT = l_T = 69 \times 10^{-3} \text{ m}, MWW = 25.7 \text{ mm}$$

2) Using Equation (2.2) gives the total allowed dissipation:

$$P_h = 2500 \times 0.039^2 = 3.8 \text{ W}$$

3) The allowed copper and core losses are

$$P_{h,cu} = P_{h,fe} = P_h / 2 = 1.9 \text{ W}$$

4) The specific core losses are found by Equation (2.6):

$$P_{fe,sp,v} = \frac{1.9}{11.5 \times 10^{-6}} = 165 \text{ kW/m}^3$$

5) Find the peak induction of the data sheets for the ferrite core material 3F3, see Fig.2.18, using the obtained value $P_{fe,sp,v} = 165 \text{ kW/m}^3$.

We use the following two points:

- at 100°C, 100 kHz, and 0.1 T the core losses are 75 W/m³
- at 100°C, 100 kHz, and 0.2 T the core losses are 450 W/m³

The graph in Fig. 2.18 represents the Steinmetz equation $P_{sp,v} = k_{fe} f^\alpha B^\beta$, where

k_{fe} is the core loss coefficient

α is the frequency exponent

B is the peak-to-peak value of the induction AC waveform

f is the frequency

So, we can do a logarithmic interpolation to find the core loss exponent β in the Steinmetz equation, and then using that value of β we can calculate the wanted peak induction.

First, using the data of the two points, we can write

$$\beta = \log(450/75)/\log(0.2/0.1) = 2.58$$

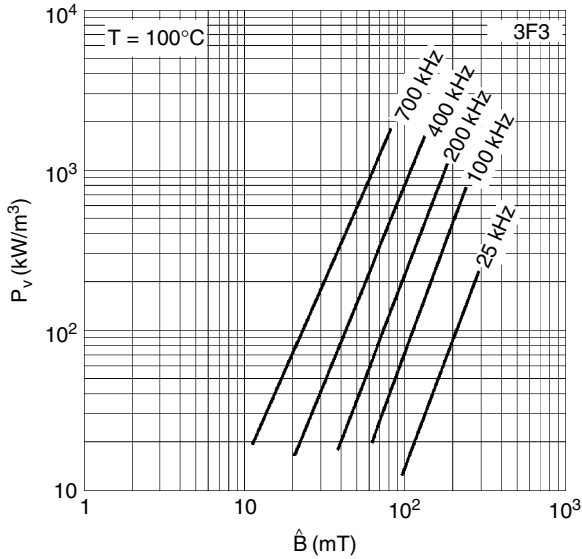


FIGURE 2.18

Specific core losses for the ferrite core material 3F3 as a function of peak-to-peak value of the induction B , frequency f is the parameter, $T = 100^\circ\text{C}$.

Second, using the found value for β , the peak induction level for

$$P_{fe,sp,v} = 165 \text{ kW/m}^3 \text{ is found:}$$

$$B_{p,g} = 0.1 \times (165/75)^{1/2.68} = 0.136 \text{ T}$$

6) The peak induction is lower than the saturation value $B_{sat} = 350 \text{ mT}$:

$$B_{p,g} < B_{sat}$$

7) To find the number of turns we need the peak-to-peak flux linkage Ψ_{pp} :

$$\Psi_{pp} = LI_{pp} = V_{in} \frac{T}{2} = 400 \frac{1}{2 \times 10^5} = 200 \mu\text{V} \cdot \text{s}$$

Using Equation (2.13) we calculate N_1 and N_2 :

$$N_1 = \frac{0.002}{2 \times (125 \times 10^{-6}) \times 0.136} = 58.8$$

$$N_2 = 58.8 \times \frac{100}{400} = 14.7$$

We choose $N_1 = 60$, $N_2 = 15$.

- 8) The V–A ratings of the primary and secondary windings are almost equal, so

$$P_{cu,1} = P_{cu,2} = 1.9/2 = 0.95 \text{ W}$$

- 9) Determine the wire diameters.

Using Equation (2.18) we find

$$d_1 \geq \frac{2}{\sqrt{\pi}} \times 0.9 \times \sqrt{\frac{(23 \times 10^{-9}) \times (69 \times 10^{-3}) \times 60}{0.95}} = 0.321 \text{ mm}$$

$$d_2 \geq \frac{2}{\sqrt{\pi}} \times 3.6 \times \sqrt{\frac{(23 \times 10^{-9}) \times (69 \times 10^{-3}) \times 15}{0.95}} = 0.643 \text{ mm}$$

For the primary winding we choose a wire diameter $d_1 = 0.335 \text{ mm}$. This diameter fits in a single layer design. The skin depth for 100 kHz is $\delta_{100\text{kHz}} = 0.241 \text{ mm}$, so the secondary winding copper losses for $d_2 = 0.65 \text{ mm}$ will be seriously increased by eddy current losses in that winding. In single layer transformers, we can increase the diameter to reduce losses instead of putting wires parallel. For the secondary winding we choose a diameter of 1.25 mm; this results in about the same winding width as the primary and we again have a single layer design. The chosen diameters are in accordance with DIN 46 435 and IEC 182-1, see Appendix C. The diameters are chosen in a way to fill one layer, as partial layers would result in losses, which are not described in this chapter.

- 10) Actual copper losses.

First we find the ohmic resistances of the two windings:

$$R_{dc,1} = (23 \times 10^{-9}) \frac{(69 \times 10^{-3}) \times 60}{\frac{\pi \times 0.000355^2}{4}} = 0.962 \ \Omega$$

$$R_{dc,2} = (23 \times 10^{-9}) \frac{(69 \times 10^{-3}) \times 15}{\frac{\pi \times 0.00125^2}{4}} = 0.0194 \ \Omega$$

We calculate the packing factor η using the external diameter of the wires (maximum overall diameter, Grade 2) and the diameter of the copper cross section (nominal diameter, see Appendix C).

$$\eta_1 = 0.355/0.411 = 0.864$$

$$\eta_2 = 1.25/1.349 = 0.927$$

Beware, this approach is allowed for transformers, not for inductors.

A check of the winding width using $w = dN$ gives:

$$d_{1,out} = 0.411 \text{ mm}, \quad w_1 = 0.411 \times 60 = 24.66 \text{ mm}$$

$$d_{2,out} = 1.349 \text{ mm}, \quad w_2 = 1.349 \times 15 = 20.2 \text{ mm}$$

The winding width is about 24.66 mm for primary, 20.2 mm for the secondary, and the minimum winding width (MWW) is 25.7 mm.

For an accurate design one can use the wide frequency equation, giving k_c directly, see the Appendix to that Chapter. The approach is fast when the equation is already programmed. Using Equation (A.2.11) the results are

- for the primary winding: $k_{c,1} = 0.1357$
- for the secondary winding: $k_{c,2} = 3.223$

Then for the copper losses we have

$$P_{c,1} = (1 + k_{c,1})R_1 \times (0.9)^2 = 0.885 \text{ W}$$

$$P_{c,2} = (1 + k_{c,2})R_2 \times (3.6)^2 = 1.062 \text{ W}$$

We can also use the graphical method. First, using Fig. 2.10 and Fig. 2.11 we find the values of $k_{f,1}$ and $k_{f,2}$. For both windings $p = 1$ and $m_E = 1$, so we have $k_c = k_{f,1}$.

- To find the primary winding value $k_{f,1}$, we first calculate the equivalent frequency:

$$f_{eq,1} = 100 \text{ kHz} \left(\frac{0.355}{0.5} \right)^2 = 50.4 \text{ kHz}$$

Then we find $k_{f,0.9} = 0.15$ from Fig. 2.10 for $\eta = 0.9$ and $k_{f,0.9} = 0.9$ from Fig. 2.11 for $\eta = 0.7$. The actual value of η for the primary is $\eta_1 = 0.864$. Using the found two values and interpolating for $\eta_1 = 0.864$, we obtain $k_{c,1} \approx 0.137$. For comparison, the result from the full equation of Appendix 2.A.2 is $k_{c,1} \approx 0.136$.

- For the secondary winding we calculate the equivalent frequency:

$$f_{eq,2} = 100 \text{ kHz} \left(\frac{1.25}{0.5} \right)^2 = 625 \text{ kHz}$$

Then we read $k_{f,2} = 3.18$ from Fig. 2.10 for $\eta = 0.9$. The actual value $\eta_2 = 0.923$ is very close to $\eta = 0.9$. The full equation of Appendix 2.A.2 gives $k_{c,2} \approx 3.22$.

Conclusions:

1. The graphs (Figures 2.10–2.13) can also be used to give a first approximation, neglecting small differences in η and in resistivity, thus allowing a fast check.

2. It is clear that the full equation results in more accuracy than the approximate graphical method.

11) Compare the total copper losses and the allowed copper losses:

$$P_{cu} = P_{c,1} + P_{c,2} = 1.95 \text{ W}$$

Although this power is higher than 1.9 W, it is very close to the limit of 1.9 W.

We know that the real mean length of turns l_T is considerably lower than the data of the manufacturer because a fully wound coil-former is considered to define this data value. Thus, the actual copper losses are lower and the found difference could be neglected. We checked the actual losses by the results of the experiment and by a more accurate value of l_T .

12) Is improvement possible?

The total copper losses are lower than the allowed copper losses, thus we do not look for an improvement at this step.

13) We calculate the resulting copper filling factor:

$$k_{cu} = \left(\sum_{i=1}^{\text{all windings}} N_i \frac{\pi d_{i,p}^2}{4} \right) / W_a = 0.14$$

We see that the filling factor is much lower than 0.4. However, if we want to use a smaller core size, it would be at a more expensive manufacturing cost.

The actual winding width of both windings is smaller than the available MWW = 25.7 mm, so there is still room for a limited creepage distance. If the creepage distance is not needed, lower losses can be obtained by spacing the conductors or using a somewhat larger wire diameter.

14) Check if the chosen core in step 1) is not too high.

In this case $k_{eddy} = k_c$ because there is no DC current component, so we have

$$k_{eddy,1} = k_{c,1} = 0.136 < 1$$

$$k_{eddy,2} = k_{c,2} = 3.223 > 1$$

The eddy current factor of the secondary is much bigger than 1, which is allowed in single layer designs as it avoids using a number of parallel wires or Litz wire.

The copper filling factor is low:

$$k_{cu} = 0.14$$

As a conclusion, improvements are possible but at the expense of a more complicated design.

2.2.1.2 Improvements of the Design

The following improvements of the design are feasible:

1. A possibility is to sandwich (interleave) the secondary between two primaries in parallel.

In this way, a half-layer winding is obtained for the secondary and only half of the MMF [A turn] is present in each primary. This results in a reduction close to a factor of 2 in the primary winding losses and somewhat more than a factor of 2 in the secondary winding losses. We obtain

$$1 + k_{c,2} \text{ (single layer case)} = 4.20 \text{ compared to} \\ 1 + k_{c,2} \text{ (half layer case)} = 1.95$$

Thus, the total copper losses are reduced by about a factor of 2. Or, while keeping the same total copper loss, the current (and the total power rating) can be increased by a factor of 1.4.

2. Improvements using Litz wire.

Let us consider a not interleaved design with 30 strands of 0.1 mm Litz wire. The equivalent number of layers for the primary winding for Litz wire is:

$$m_{E1} = \frac{pdN}{w\eta} = \frac{30 \times 0.0001 \times 60}{0.025 \times 0.7} = 10.28$$

We consider $\eta = 0.7$.

The eddy current factor is $k_{c,1} = 0.078$. The DC resistance is 0.424Ω , where 5% increase in the wire length is taken into account. The total primary copper losses are then 0.451 W.

The secondary winding contains 15 turns and every wire consists of 120 strands of 0.1 mm. Thus, we obtain

$$m_{E2} = \frac{pdN}{w\eta} = \frac{120 \times 0.0001 \times 15}{0.025 \times 0.7} = 10.28$$

We have the same copper losses as in the primary winding. Thus, the total copper loss in the Litz wire is 0.902 W. This value is much lower than the losses of the full wire design. The lower losses allow increasing the current (and power) by a factor of 1.5, compared to the original design.

3. Interleaved Litz wire designs or more strands in the Litz wire can still reduce losses. However, the use of Litz wire has other troubles of heat transfer, insulation, and soldering.

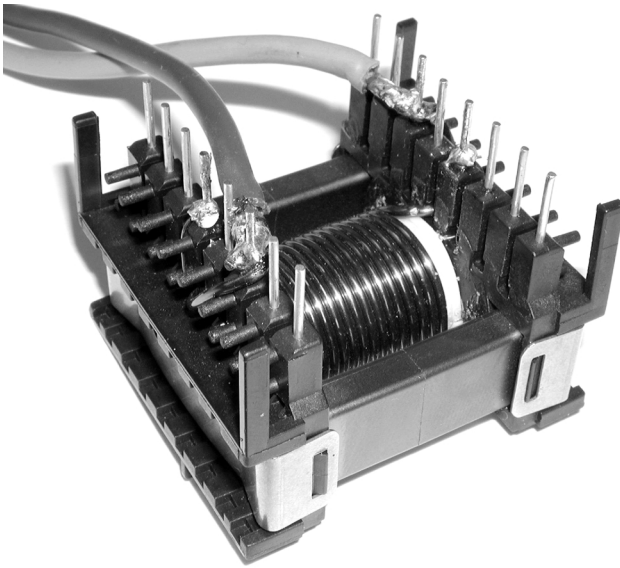


FIGURE 2.19
Photograph of the experimental transformer.

REMARKS CONCERNING LITZ WIRE DESIGNS

The window is more filled in the design with Litz wire. Also the leakage inductance in the Litz wire design is much higher than in the sandwich case, for a comparable rating. The increased leakage inductance may be an advantage or has to be avoided, depending on the design strategy of the converter.

2.2.1.3 Measuring and Validation of the Design

We made a transformer with the obtained specifications: core ETD39, material grade 3F3, primary winding turn number $N_1 = 60$, and secondary $N_2 = 15$ (Fig. 2.19). The primary winding was insulated from the secondary winding by two turns of 0.1 mm polyester insulation sheet.

We performed a no-load and a short circuit test on the built transformer. For more information concerning no-load and short circuit tests, refer to [Chapter 11, Measurements](#).

- Short circuit test

By this test we obtain the copper losses. The test was realized at a temperature of 100°C. The measurement was done at the primary side and the secondary was short-circuited, using a straight wire of the same type as the secondary winding. The results of the test are shown in [Table 2.1](#).

TABLE 2.1

Results of the Short Circuit Test on the Calculated and Built transformer

f , [kHz]	I , [A]	P_{cur} [W]
100	0.90	1.59

We see that the measured losses are lower than the calculated. The main reason is that in the fast method we use the data of the manufacturer for the mean turn length. If we introduce the real turn length, based on measurements of the winding diameters, we obtain the following mean length per turn values for the primary l_{T1} and for the secondary l_{T2} :

$$l_{T1} = (15.2 + 0.411)\pi = 50.0 \text{ mm}$$

$$l_{T2} = (20.2 - 1.349)\pi = 59.2 \text{ mm}$$

Here we use the measured outer diameter of the primary winding, which is 15.2 mm, and the measured outer diameter of the secondary winding of 20.2 mm. The wire diameters are

$$d_1 = 0.411 \text{ mm} \quad \text{and} \quad d_2 = 1.349 \text{ mm}$$

If we use the obtained values in the design, we get the following results:

$$R_{1dc} = 0.684 \quad R_{2dc} = 0.0166$$

$$P_{cu1} = 0.629 \quad P_{cu2} = 0.907$$

$$P_{cu} = 1.536 \text{ W}$$

The found value for the copper losses 1.536 W is very close to the measured value of 1.59 W. The remaining difference can be attributed to mechanical tolerances and the typical accuracy of about 3% of the proposed wide frequency method. For comparison, the measured values of the DC resistances at 100°C are $R_{1dcm} = 0.729$, $R_{2dcm} = 0.0159$. For the primary winding, the measured DC resistance is higher than the calculated one, which also reflects in the results for the losses.

The conclusion of the short circuit test is that the calculations and the measurements give almost the same results.

- No-load test

By this test we obtain the core losses. The test was realized also at temperature of 100°C, at square wave voltage 100 V. The voltage was applied at the secondary winding and the primary winding was open. The results for the core losses are shown in [Table 2.2](#). The measured value of 1.328 W for the core losses is lower than expected one because of three reasons:

TABLE 2.2

Results of No-Load Test on the Calculated and Built Transformer

f , [kHz]	U , [V]	P_{fe} , [W]
100	100.4	1.328

1. The practical number of turns is higher than the theoretic one $N_1 = 58.8$, thus the actual induction B is lower and the ratio reflecting on the core losses is:

$$ratio = \left(\frac{58.8}{60}\right)^\beta = \left(\frac{58.8}{60}\right)^{2.58} = 0.949$$

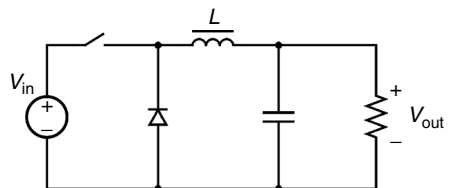
That is, the actual core losses are decreased with factor of 0.949.

2. There is tolerance between the manufacture data and the actual cores data. There is also some safety margin between typical and maximal values. Care should be taken if those safety margins are set to zero.
3. A 50% duty ratio square wave voltage generates 10–15% lower losses than a sine wave voltage for the same peak-to-peak induction. This fact is shown in [Chapter 3](#), Magnetic materials. Thus, we overestimate the core losses, while using the data for sine waves in the case, where we have square wave.

The conclusion of the no-load test is that the calculations do give a right order of magnitude but that measurements show lower core losses, allowing the core to be operated at somewhat higher ambient temperature or slightly higher currents, or allowing some tolerances on the manufacture data.

2.2.2 Saturated Thermal Limited Design Example

The second example is an inductor for a buck (step-down) converter. A buck converter is shown in Fig. 2.20 and the inductor current and voltage are given in Fig. 2.21.

**FIGURE 2.20**

A buck (step-down) DC/DC converter.

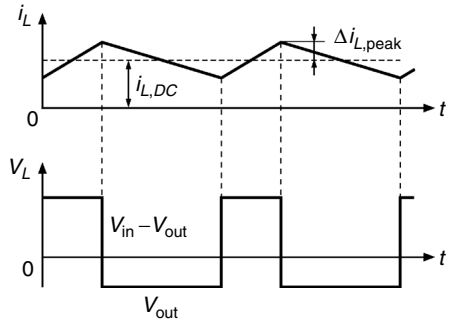


FIGURE 2.21
Voltage and current across the inductor in a step-down converter.

The purpose of the inductor is to reduce the current ripple to the load. This purpose defines a desired value of the inductance L . Usually, an air gap is used in order to prevent saturation of the core by the peak inductor current $i_{L,peak} = I_{L,DC} + \Delta i_{L,peak}$. The design results usually in a saturated thermal limited design. The core losses are smaller than the copper losses.

First, we calculate the parameters of the inductor used in the buck DC/DC converter (Fig. 2.20). The maximum power output is 450 W. However, a duty ratio of 50% results in the largest current ripple for the given frequency, so it can be considered as a worst-case design. We need a desired induction value and the RMS values of the voltage and current of the inductor. The specifications of the converter are

- Input voltage: $V_{in} = 210 \text{ V}$
- Output voltage: $V_{out} = 105 \text{ V}$
- Operating frequency: $f_{op} = 70 \text{ kHz}$
- Output current: $I_{out} = 3 \text{ A, DC}$
- Peak-peak inductor ripple current $I_{Lpp} = 2 \text{ A}$

The duty ratio of the transistor control D is:

$$D = \frac{V_{out}}{V_{in}} \Rightarrow D = \frac{105}{210} = 0.5$$

The inductor DC current component is

$$I_{L,DC} = I_{out} = 3 \text{ A}$$

The peak magnitude of the ripple in the inductor current $\Delta i_{L,peak}$ is

$$2 \Delta i_{L,peak} = \frac{V_L \Delta t}{L}$$

so, we can find the desired inductance value:

$$L = \frac{(V_{in} - V_{out})DT_{op}}{2\Delta i_{L,peak}}, \Rightarrow L = \frac{(150 - 75)(0.5)(20 \times 10^{-6})}{2 \times 1} \Rightarrow L = 375 \mu\text{H}$$

The AC RMS value of the inductor current is

$$I_{L,AC,rms} = \sqrt{(\Delta i_{L,peak})^2/3} = 0.577 \text{ A}$$

The RMS value of the inductor current is

$$I_{L,rms} = \sqrt{I_{L,DC}^2 + (\Delta i_{L,peak})^2/3} = 3.1225 \text{ A}$$

The RMS value of the inductor voltage is

$$\begin{aligned} V_{L,rms} &= \sqrt{D(V_{in} - V_{out})^2 + (1-D)V_{out}^2} \\ &= \sqrt{0.5(210 - 105)^2 + (1 - 0.5)105^2} = 105 \text{ V} \end{aligned}$$

All the input parameters of the inductor under design are

Wanted inductance value: $L = 375 \mu\text{H}$

AC RMS inductor current: $I_{L,AC,rms} = 0.577 \text{ A}$

Total RMS inductor current: $I_{L,rms} = 3.1225 \text{ A}$

RMS inductor voltage: $V_{L,rms} = 105 \text{ V}$

Operating frequency: $f_{op} = 70 \text{ kHz}$

Operating temperature: $T = 100^\circ\text{C}$

2.2.2.1 Design Procedure

Now we follow the design steps.

1') We find B_{pp} by

$$B_{pp} = B_{sat} \frac{2\Delta i_{L,peak}}{I_{L,DC} + \Delta i_{L,peak}} = 0.35 \frac{2 \times 1}{3 + 1} = 0.175 \text{ T}$$

2') We find the size parameter a_{ch} :

$$a_{ch} = \left(\frac{\sum_{\text{all windings}} V_{rms} I_{rms}}{A_1 f B_{pp}/2} \right)^{1/3.5} = \left(\frac{105 \times 3.1225}{(1 \times 10^4) (70 \times 10^3) \times 0.175/2} \right)^{1/3.5} = 0.03118 \text{ m}$$

Here we use $A_1 = 1 \times 10^4$. We choose a core shape ETD 34, material grade 3F3 [6] with the largest dimension $a = b = 0.034$ m. The core parameters are

$$V_c = 7.64 \times 10^{-6} \text{ m}^3, \quad A_m = 91.6 \times 10^{-6} \text{ m}^2,$$

$$W_a = 123 \times 10^{-6} \text{ m}^2, \quad MLT = 0.06 \text{ m}, \quad MWW = 0.021 \text{ m}.$$

3') We find the specific core losses $P_{fe,sp,v} = 33 \times 10^3$ from graphs for $f = 70$ kHz and $B_{p,g} = B_{pp}/2 = 0.175/2 = 0.0875$ T.

$$\text{Then } P_{fe} = P_{fe,sp,v} V_c = (33 \times 10^3) (7.64 \times 10^{-6}) = 0.25 \text{ W}$$

4') Find the total heat capability of the component:

$$P_h = 2500 ab = 2.94 \text{ W}$$

5') Check the ratio P_{fe}/P_h :

$$P_{fe} = 0.25 \text{ W} \ll P_h/2$$

The design is clearly a saturation thermal limited case.

6') Estimate the allowed copper losses using Equation (2.59):

$$P_{h,cu} = \frac{2}{3} P_h - \frac{1}{3} P_{fe} = \frac{2}{3} \times 2.94 - \frac{1}{3} \times 0.25 = 1.84 \text{ W}$$

7) Calculate the number of turns.

The number of turns is found by Equation (2.13), using

$$\Psi_{pp} = \frac{(V_{in} - V_{out})D}{f} = 750 \times 10^{-6} \text{ V} \cdot \text{s}$$

$$N = \frac{\Psi_{pp}}{A_m B_{pp}} = \frac{750 \times 10^{-6}}{(91.6 \times 10^{-6}) 0.175} = 46.8$$

We choose $N = 47$.

8) Distribute the copper losses.

In an inductor there is only one winding.

9) Determine a wire diameter:

$$d \geq \frac{2}{\sqrt{\pi}} I_{rms} \sqrt{\frac{\rho_c l_T N}{P_{cu}}}$$

$$d \geq \frac{2}{\sqrt{\pi}} \times 4.163 \times \sqrt{\frac{(23 \times 10^{-9}) \times (60 \times 10^{-3}) \times 47}{1.84}} = 0.661 \text{ mm}$$

The next available wire diameter in the table in Appendix C is 0.71 mm, the outer diameter is 0.789 mm. We try the design the 0.71 mm wire, directly wound on the coil former.

10) Calculate the actual ohmic and eddy current losses

In principle, we could sum over all individual current harmonics to find accurate eddy current losses. In this design we avoid that complication. We calculate the apparent frequency, which generates the same $(di/dt)_{rms}$ as in a sine wave:

$$f_{ap} = \frac{V_{L,rms}}{L I_{rms} 2\pi} = 77.2 \text{ kHz}$$

We start calculating k_c using the graphs.

$$\eta^2 m_E^2 = \left(\frac{p N p}{w} \right)^2 = \left(\frac{0.00071 \times 47 \times 1}{0.02123} \right)^2 = 2.47$$

The equivalent frequency is

$$f_{eq} = f_{ap} \left(\frac{d}{0.0005} \right)^2 = 155.6 \text{ kHz}$$

The distance from center leg to outer leg is 7.7 mm (measured on the core). The diameter of the coil former is 13.4 mm. The diameter of the center leg is 10.7 mm. The number of layers is almost 2 (we spread the wires of the second layer). With this information we can calculate κ .

$$\kappa = \frac{13.3/2 - 10.7/2 + \frac{0.789 \times 2}{3}}{21.2/2} = 0.17$$

We first consider the 2-D solution. The corresponding k_F is 6.31 found from the graph in Fig. 2.8. We read k_{in} from the graph (Fig. 2.12, $\eta = 0.9$) for the found equivalent frequency $f_{eq} = 155.6$ kHz. The value of λ is found as $\lambda = \frac{d^2 N p}{w h \eta} = 0.1737$. We find $k_{in} = 1.76$. Then we obtain the eddy current loss factor

$$k_c = \left(\frac{p N p}{w} \right)^2 K_F k_{in} = 2.47 \times 6.31 \times 1.76 = 27.4$$

Equation Approach

The packing factor η for the chosen 0.71 mm wire (in the layer direction for inductors) is $\eta = 0.71/0.789 = 0.899$, which is close to 0.9. Using the full equation of Chapter 2, the found value of k_c is 27.4.

We calculate the DC resistance:

$$R = \frac{0.06 \times 47 \times 23 \times 10^{-9}}{\frac{\pi 0.71^2}{4}} = 0.164 \Omega$$

Then the copper losses are

$$P_{cu} = R(3^2 + (1 + k_c)0.577^2) = 3.14 \text{ W}$$

- 11) Check if the copper losses are lower than the allowed copper dissipation: $3.14 \text{ W} > 1.88 \text{ W}$

The resulting copper losses are too high and they are concentrated close to the air gap, which could create a hot spot at the middle of the coil. Using a smaller diameter wire generates too much ohmic loss; a design with a larger wire diameter results in even worse eddy current losses.

- 12) Is improvement possible?

1. A solution is to keep some distance between the winding and the air gap, e.g., to increase κ . If the winding is wound on a 19.6-mm diameter coil former with the same wire diameter, then $\kappa = 0.468$. Thus, we have the field factor $k_F = 1.48$ and the copper losses are 1.85 W.
2. Another way to improve the design is to use an appropriate *Litz wire*, so that the losses are sufficiently low. For example, a design with Litz wire of 60 strands of 0.1 mm diameter, $\kappa = 0.21$, $k_F = 4.72$, and $k_c = 0.666$ results in 1.39 W total copper losses.

- 13) We calculate the resulting filling factor.

The winding area is 123 mm² and the filling factor is about 0.1 for the full wire design and 0.12 for Litz wire design.

- 14) Check if the core size is not too high.

A design with a smaller core (ETD29) can be possible but only using Litz wire.

- 15) Calculate the air gap length.

To find the length of the air gap, we use the McLyman equation, and the obtained result is: $l_g = 0.639 \text{ mm}$, without correction for fringing field. The first

calculated value of the fringing factor is $F = 1.28$. The final air gap is found using the iteration approach. We obtain $F_{new} = 1.357$, which is close to the above value. It is clear that the correction for fringing field was necessary. The final air gap is $l_g = 0.867$ mm.

In practice, the air gap is sometimes adjusted until the inductance of $375 \mu\text{H}$ is reached.

REMARK

The accuracy of the previous calculations is limited because of the limited accuracy of the mechanical dimensions (wire diameter, mean length per turn, core dimensions) and the ratio f_{ap}/f .

2.2.2.2 *Measurements and Validation of the Eddy Current Losses*

The main concern in the design is the eddy current loss. So, in the tests a higher AC current is applied, $I_{L,AC,rms} = 1$ A, to improve the measurement accuracy.

Three inductors are built and measured:

- Inductor 1: with 0.69 mm wire, wound directly on the coil former, so the winding is with 13.3 mm diameter, [Fig. 2.22,a](#).
- Inductor 2: with 0.71 mm wire, wound in a winding with diameter 19.6 mm, [Fig. 2.22,b](#).
- Inductor 3: using Litz wire of 60 strands of 0.1 mm wire diameter, wound directly on the coil former, [Fig. 2.22,c](#).

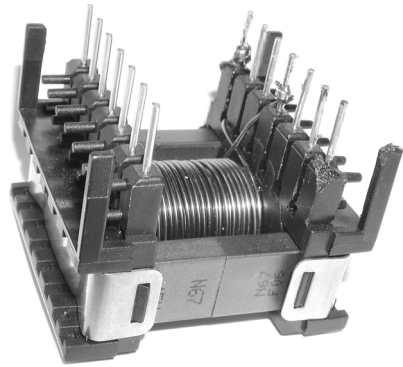
Adapted Calculations

We measured all the dimensions: the copper wire diameter (by measuring the DC resistance), the outer and inner diameters of the winding, the width of the winding, and the turn length. Then we used the obtained values to recalculate the losses. In [Table 2.3](#) we give the winding dimensions and the values of κ and k_f for the three measured designs.

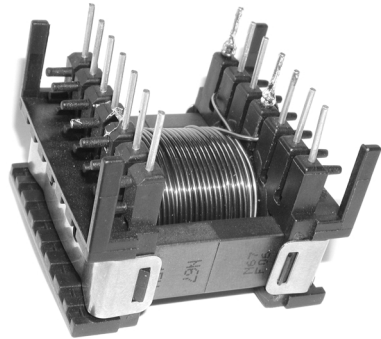
Oscilloscope Measurements

We use the oscilloscope method, see [Chapter 11 Measurements](#), for more details.

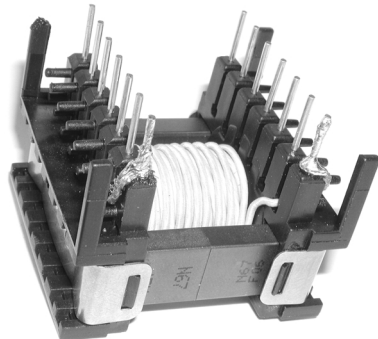
- *Core loss measurements.* The ferrite losses are low and a separate test is done to evaluate them. The magnetic path is closed (no air gap) and only an AC current component is applied generating the same flux as in the case with an air gap. Thus, the measured losses are the core losses (the copper losses are neglected as in a no-load test).



(a)



(b)



(c)

FIGURE 2.22

The three built and measured inductors, the core is ETD34, turn number $N = 47$:

- a) wire diameter $d = 0.69$ mm, the winding wound directly on the coil former;
- b) wire diameter $d = 0.71$ mm, the winding wound in a distance from the coil former;
- c) Litz wire, 60 strands of 0.1 mm wire diameter, the winding wound directly on the coil former.

- *Copper loss measurement.* We apply a 70-kHz, 50% duty ratio square wave in order to obtain 1A RMS value (3.46 A peak-to-peak).

The obtained results are shown in [Table 2.4](#) and compared with the calculated results using the equations in Chapter 2 and the equations in [Chapter 5](#), which are more accurate.

TABLE 2.3

The Winding Dimensions, the Values of κ and k_F for the Three Measured Inductors

Design case	Wire diameter, mm	Winding diameter, mm		κ	k_F
		outer	inner		
Inductor 1	0.69	13.3	16.3	0.165	6.57
Inductor 2	0.71	19.6	22.7	0.468	1.48
Inductor 3	60×0.1	13.3	18.7	0.21	4.72

TABLE 2.4

The Calculated and Measured AC Losses of the Three Experimental Inductors, the Core Losses are $P_{fe} = 0.75 W$ for all the Cases

Design case	Calculation, Ch2	Calculation, Ch5	AC copper losses
			by scope measurements
Inductor 1	3.03	2.99	2.65
Inductor 2	1.24	1.17	1.13
Inductor 3	0.196	0.196	0.27

REMARK

The typical error of the oscilloscope measurements, described in [Chapter 11](#), is about 0.15 W at the applied test frequency of 70 kHz. This explains the difference in the calculations and measurements.

2.3 Conclusions

We know that the design of magnetic components for power electronics comprises many steps and skills, but eddy currents usually determine the conductor choice in today's transformers and inductors. Simple rules, such as increasing the diameter of the wires to reduce copper losses, are not valid any more. Without a clear approach, the design of a magnetic component including eddy currents could be a labyrinth, which may result in tedious trial and error. This chapter guides the designer throughout the designs of inductors and transformers including eddy currents. Using graphs one can get a fast design, even with a simple calculator. More accurate solutions can be obtained using the full equations for k_c directly. This approach can be implemented by calculation programs (e.g., MathCAD).

The accuracy of the presented approach for calculating eddy current losses is already sufficient in many cases, although we propose a method using a limited amount of mathematical tools. We do not apply numerical methods directly; we use them in the derivation and validation of the proposed equations.

The given loss calculation method is based on 2-D analytical expressions and improved by finite element calculations. This approach results in good accuracy as well in both low and high copper filling factors and in low and high frequency. The method is an improvement of existing methods such as Dowell type [4], which are not applicable at low copper filling factors, very high frequency, and not in inductor designs!

In practice, the final accuracy in loss calculations is more limited by the mechanical tolerances of ferrite cores and windings than by the equations themselves.

Many effects are reflected in the proposed design approach. The following basic conclusions are derived:

- A design where saturation limit is reached is different from the cases where there are only thermal limits.
- A high total number of turns N reduces the core losses, but it increases the eddy current losses by about N^3 , as both the transverse field and the wire length are increased. This effect often appears in designs where the winding area is not filled.
- At low frequency approximation designs ($d < 1.6\delta$) the losses increase with the 4th power of the diameter of the wires, and they are quadratically dependent on frequency.
- A good approach to reduce the transformer losses is to use interleaved (sandwiched) windings. In such a design the MMF is reduced for the same length of the field line for the outside windings, and the field line length is increased for the inside winding.
- In high frequency transformers, single layer winding designs do perform better than more layer designs at high frequency. Thus, if the number of turns and the wire size allow it, the single layer design should be preferable. Increasing the wire diameter in a single layer transformer reduces the losses, even if the diameter is large compared to the penetration depth. But this last fact is not true for more layer windings.
- In gapped inductors, with high frequency currents, winding close to the air gap should be avoided, unless Litz wire is used. The combination of Litz wire and some distance to the air gap further improves the design. Increasing the wire diameters results in higher eddy current losses in almost all practical cases of inductor designs.

Appendix 2.A.1 Core Size Scale Law for Ferrites in Non-Saturated Thermal Limited Design

The core dissipation capability $P_{h,fe}$ based on natural convection in air is proportional to the square of the scaling parameter a_{ch} :

$$P_{h,fe} \sim a_{ch}^2 \quad (2.A.1)$$

The core losses P_{fe} are proportional to the induction in power β and to the volume of the core:

$$P_{fe} \sim B^\beta a_{ch}^3 \quad (2.A.2)$$

Equalizing $P_{h,fe} = P_{fe}$, we obtain

$$B \sim a_{ch}^{-1/\beta} \quad (2.A.3)$$

Equalizing the copper dissipation capability $P_{h,cu}$ and copper losses P_{cu}

$$P_{h,cu} \sim a_{ch}^2 \quad (2.A.4)$$

$$P_{cu} \sim J^2 a_{ch}^3, \quad (2.A.5)$$

we obtain the following expression for current density J :

$$J \sim a_{ch}^{-1/2} \quad (2.A.6)$$

The RMS value of the MMF is

$$MMF \sim a_{ch}^2 J \sim a_{ch}^{1.5} \quad (2.A.7)$$

Using the obtained dependence (2.A.7), we get the volt-amps rating of the component:

$$\sum_{all\ windings} V_{rms} I_{rms} \sim \Phi \times MMF \sim A(a_{ch}^2 B)a_{ch}^{1.5} = A a_{ch}^{3.5} a_{ch}^{-1/\beta} = A a_{ch}^{3.5-1/\beta} = A a_{ch}^\gamma \quad (2.A.8)$$

where

Φ is the RMS value of the magnetic flux in the core, $\Phi \sim a_{ch}^2 B$

From the equation (2.A.8) it follows that

$$\gamma = 3.5 - 1/\beta \quad (2.A.9)$$

Using Equation (2.A.9) for $\beta=2$, we obtain $\gamma=3$. In more accurate models the dissipation is less proportional to the surface (for instance $P_{h,fe} \sim a_{ch}^{1.8}$ and $P_{h,cu} \sim a_{ch}^{1.8}$), but also, β is usually higher than 2 for ferrites, usually $\beta=2.4-3$. Even then, for a case with $\beta=3$ and thermal dissipation $P_h \sim a_{ch}^{1.8}$, we again obtain $\gamma=3$.

Appendix 2.A.2 Eddy Current Losses for Wide Frequency

2.A.2.1 Approximation of k_c

The eddy current loss factor k_c is defined as

$$k_c(m_E, \zeta(f), \eta, \lambda, k_F) = \frac{P_{eddy}}{R_0 I_{ac}^2} \quad (2.A.10)$$

In [Chapter 5 Eddy Currents](#), a function presenting k_c is derived, which gives eddy current losses in round wires. It combines

- The analytical low frequency solutions
- The analytical solution for a round, current carrying free wire
- The analytical solution for a round conductor in a transverse field
- The high filling high frequency rule
- More than 100 well-chosen finite element computations to tune the remaining parameters, matching better than 10%, typically 3%; the computations are based on infinite layers with square fitting

The function of k_c takes into account the major part of all 2-D effects and it is applicable for all values of η and λ and for all frequencies from very low to very high.

2.A.2.2 Transformers

2.A.2.2.1 Direct Calculations

For transformers, the function is expressed as

$$k_c = \frac{1}{16} \zeta^4 \left[\eta^2 \left(\frac{m_E^2 - \frac{1}{4}}{3} \right) \frac{\pi^2}{4} k_F E_T + \frac{1}{48} F_A \right] \quad (2.A.11)$$

where the quantities m_E , η , and λ are already defined in [Chapter 2](#)

A value of $\lambda = 0.5$ can be chosen for Equation (2.A.11). For lower values, the result is almost identical. For λ tending to 1, the eddy current factor k_c is slightly higher, but this increase is mainly due to the tuning with finite element models based on square fitting.

The parameters and functions in Equation (2.A.11) are described as follows:

- The coefficient k_F , named as field factor, is derived in [Chapter 5](#). For transformers it is close to 1 (for $\eta > \lambda$, which is usually the case in transformers).

- The parameter ζ is the ratio between diameter and penetration depth, and it is used in defining the functions F_T and F_A :

$$\zeta = \frac{d}{\delta(f)} = \frac{d}{\sqrt{\frac{2\rho}{\omega\mu_0}}} = \frac{d}{\sqrt{2\pi f\mu_0}} \quad (2.A.12)$$

- The function F_T is given as

$$F_T(\zeta, \eta, \lambda) = \frac{1}{\sqrt{1 + \frac{G_T(\zeta)}{1024} \left(1 + \frac{\pi^2}{12} F_i \chi^2 - \left(1 - \frac{\eta^2}{12} \right) (\lambda^{10} + \eta^{10}) \chi^{10} \right)^4}} \quad (2.A.13)$$

where

$$F_i(\eta, \lambda) = \eta^2 \quad \text{for } \eta > \lambda$$

This relation is usual with transformers.

- The function F_i represents the dipole effect of the induced eddy currents. This effect has the tendency to reduce the losses at high frequency and high filling in the direction of the layer.
- The function $\chi(\zeta)$ used in Equation (2.A.13) represents the influence of the penetration depth on the dipole effect and it is defined as

$$\chi(f) = \frac{1}{1 + \frac{1.4}{\zeta(f)}} \quad (2.A.14)$$

- The function F_A is expressed as

$$F_A(\zeta, \eta, \lambda) = \frac{1}{\sqrt{\left((1 + 1.3537\eta^4) \right)^2 + \frac{G_A(\zeta)}{36864} \left(1 - \frac{\pi}{12} (\eta^{2.5} + 0.3\lambda^{10}) \right)^4}} \quad (2.A.15)$$

- The quantities G_T and G_A are given as

$$G_T(\zeta) = \zeta^6 + 2.7\zeta^5 - 1.3\zeta^4 - 17\zeta^3 + 85\zeta^2 + 43\zeta \quad (2.A.16)$$

$$G_A(\zeta) = \zeta^6 + 6.1\zeta^5 + 32\zeta^4 + 13\zeta^3 + 90\zeta^2 + 110\zeta \quad (2.A.17)$$

The function F_T and the quantity G_T are introduced to realize a 1% approximation of the exact analytical solution of the losses in a transverse field (the approximation avoids the use of Bessel functions and it is more flexible).

The functions F_A and the quantity G_A are introduced to realize a 0.4% approximation of the exact analytical solution of the losses of a free current carrying conductor.

Note that

- ζ is proportional to the root of the frequency, the consequence is that k_c is proportional to the square of the frequency at low frequency and to the root of the frequency at high frequency
- For transformers with concentric windings, k_F is close to 1, even when the coil ends (3-D effect) are considered

Although the equations are not very simple, they do not use complicated functions. They are very fast by their analytical nature.

2.A.2.2.2 Graphical Transformer Method

The presented direct calculation is more accurate than the graphical method. However, for simple calculations some details can be neglected and a function k_{tr} is derived to allow a graphical representation:

$$k_{tr}(m_E, \zeta(f, d), \eta, \lambda) = \frac{k_c}{m_E^2} \quad (2.A.18)$$

To display this function, a reference diameter (0.5 mm) and a reference resistivity ($23 \times 10^{-9} \Omega\text{m}$) are chosen. The diameter is quite typical in power electronics, whereas 1mm wires are already large. The resistivity corresponds to copper at 100°C, which is a normal temperature in power electronics designs. Other diameters and resistivities can be chosen by calculating an equivalent frequency, based on the fact that the result is identical for a given ζ . Curves are given for $m_E = 0.5, 1, 2,$ and 10 , see [Fig. 2.10](#) and [Fig. 2.11](#). For $m_E > 2$, the curves are almost identical. Using these graphs we obtain k_{tr} and then, substituting it into Equation (2.A.18) we find k_c .

2.A.2.3 Inductors

2.A.2.3.1 Direct Calculations

In inductors, due to the presence of air gaps, the transverse field is usually much higher than in transformers for similar windings. Also, half-layer solutions are not realistic in inductors. This means that the local fields can be neglected, which simplifies the expression of k_c to

$$k_c = \frac{1}{3.16} \zeta^4 \left(m_E^2 \eta^2 \frac{\pi^2}{4} k_F F_T \right) \quad (2.A.19)$$

More accurate presentation is given in [Chapter 5](#).

For inductors, the field factor k_F is highly dependent on the distance between the windings and the air gap. The dependence is shown graphically in [Fig. 2.8](#) and it is also derived in [Chapter 5](#).

The full field problem in inductors is quite involved as the leakage field has main components in the layer direction as well as in the direction perpendicular to it. If the field components are parallel to the layers, the field is reduced (screening effect). If the fields are perpendicular to the layer, the losses are increased (tunneling effect).

A further simplification is not to take these effects in account and to take the solution of eddy current losses of a free wire in a transverse field, without considering the field induced by the eddy currents of other wires. This simplifies the expression of F_T to F_{Tb} .

$$F_{Tb}(\zeta) = \frac{1}{\sqrt{1 + \frac{G_T(\zeta)}{1024}}} \quad (2.A.20)$$

where

F_{Tb} is the simplified presentation of F_T for a single wire

REMARK

For inductors a simplified presentation of G_T is possible instead of Equation (2.A.16). It is given as

$$G_T(\zeta) = (\zeta + 0.37)^6 \quad (2.A.21)$$

Note that with those simplifications, the solution is not dependent on η and λ anymore.

2.A.2.3.2 Graphical Inductor Method

For simple calculations some details can be neglected and a function k_{in} is created to allow a graphical representation:

$$k_{in}(m_E, \zeta(f, d)) = \frac{k_c}{\eta^2 m_E^2 k_F} \quad (2.A.22)$$

With the simplifications

$$k_{in} \approx \frac{1}{16} \frac{\pi^2}{4} F_{Ts}(\zeta) \quad (2.A.23)$$

To display this function, a reference diameter of 0.5 mm and a reference resistivity ($23 \times 10^{-9} \Omega\text{m}$) are chosen.

The factor k_F , is mainly dependent on the distance to the air gap, winding width, and thickness of the winding. For a given distance to the air gap, a 2-D modeling with yoke and side legs (close to the pot cores) results in some

overestimation of the k_F value. The lowest value of k_F corresponds to coil ends, where neither yoke nor side legs are present. In practical cores (EE, ETD cores), a situation in between the two extreme cases is observed, so we advise taking the average value.

We define a parameter κ , which is relevant to the factor k_F :

$$\kappa = \frac{d_{wg} + t_w / 3}{w/K} \tag{2.A.23}$$

The function k_F can be approximated as

$$k_F(\kappa) = \frac{3.44(0.505 - \kappa)^2 + 0.688}{\kappa} \tag{2.A.24}$$

Using the graphs, we obtain k_{in} and k_F and then, substituting them into Equation (2.A.22), we find the wanted value of k_c .

Appendix 2.A.3 Mathcad Example Files

Here we present a MathCAD example file, which calculates eddy current losses in a transformer and an inductor windings, see Fig. 2.A.1. The two windings are identical with the same number of turns and wire diameter 0.5 mm. The windings are wound on the same core and subjected to the same currents and frequency.

The MathCAD example file for calculating eddy current losses in a transformer is shown in Fig. 2.A.2. Figure 2.A.3 shows the MathCAD example file for calculating eddy current losses in an inductor.

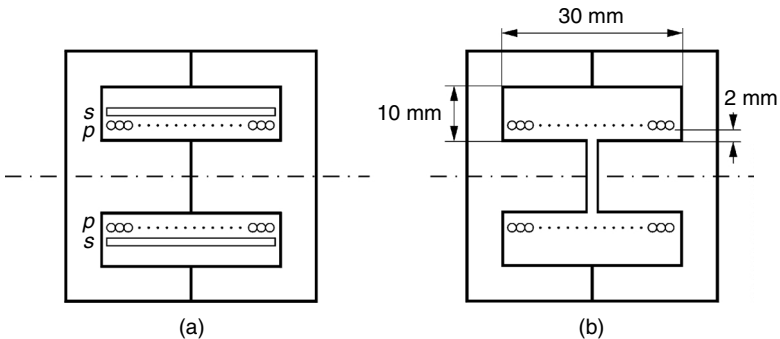


FIGURE 2.A.1

The transformer a) and inductor b) constructions used in the MathCAD example files.

**Calculating the losses of a similar winding in a similar transformer and inductor core,
one layer coil of 0.5 mm wire, 54 turns**

1. Transformer, only one winding is considered

Results on right side:

$$d := 0.0005 \quad \rho := 23 \cdot 10^{-9} \quad f := 100000 \quad \text{lac} := 1 \quad \mu_0 := 4 \cdot \pi \cdot 10^{-7} \quad h := 0.01$$

$$m := 1 \quad p := 1 \quad N := 54 \quad w := 0.03$$

$$f_{ap} := \frac{2 \cdot \sqrt{3}}{\pi} \cdot f \quad K := 1 \quad KF := 1 \quad mE := m \quad nE := \frac{N \cdot p}{mE}$$

$$\eta := \frac{d \cdot nE}{w} \quad \lambda := \frac{d \cdot mE}{h}$$

$$\lambda = 0.05 \quad nE = 54$$

$$\eta = 0.9$$

$$lw := 1 \quad \delta(f) := \sqrt{\frac{2 \cdot \rho}{2 \cdot \pi \cdot f \cdot \mu_0}} \quad \zeta(f, d) := \frac{d}{\delta(f)} \quad \chi(f, d) := \frac{1}{1 + \frac{1.5}{\zeta(f, d)}}$$

$$\delta(f) = 2.4137 \times 10^{-4}$$

$$R0 := \frac{\rho \cdot lw}{\left(\frac{d^2 \cdot \pi}{4}\right)}$$

$$R0 = 0.1171$$

$$f_{ap} = 1.1027 \times 10^5$$

The value of λ is not really important if $\lambda < \eta$

$$GT(f, d) := \zeta(f, d)^6 + 2.7 \cdot \zeta(f, d)^5 - 1.3 \cdot \zeta(f, d)^4 - 17 \cdot \zeta(f, d)^3 + 85 \cdot \zeta(f, d)^2 - 43 \cdot \zeta(f, d)$$

$$GT(f, d) = 282.6246$$

$$GA(f, d) := \zeta(f, d)^6 + 6.1 \cdot \zeta(f, d)^5 + 32 \cdot \zeta(f, d)^4 + 13 \cdot \zeta(f, d)^3 + 90 \cdot \zeta(f, d)^2 + 110 \cdot \zeta(f, d)$$

$$GA(f, d) = 1.6306 \times 10^3$$

$$Fi(\eta, \lambda) := \eta^2 \quad \eta \text{ must be higher than } \lambda$$

$$Fi(\eta, \lambda) = 0.81$$

$$FA(f, d, \eta, \lambda) := \frac{1}{\sqrt{\left(1 + 1.3537\eta^4\right)^{-2} + \frac{GA(f, d)}{36864} \cdot \left[1 - \frac{\pi}{12} \cdot \left(\eta^{2.5} + \lambda^{10} \cdot 0.3\right)\right]^4}}$$

$$FA(f, d, \eta, \lambda) = 1.8303$$

$$FT(f, d, \eta, \lambda) := \frac{1}{\sqrt{\left[1 + \frac{GT(f, d)}{1024} \cdot \left[1 + \frac{\pi^2}{12} \cdot Fi(\eta, \lambda) \cdot \chi(f, d)^2 - \left(1 - \frac{\pi^2}{12}\right) \cdot \left(\lambda^{10} + \eta^{10}\right) \cdot \chi(f, d)^{10}\right]\right]^4}}$$

$$FT(f, d, \eta, \lambda) = 0.7859$$

Eddy current loss factor kc

$$kctr(mE, f, d, \eta, \lambda, KF) := \frac{1}{16} \cdot \zeta(f, d)^4 \cdot 1 \cdot \left[\frac{mE^2 - \frac{1}{4}}{3} \right] \cdot \frac{\pi^2}{4} \cdot FT(f, d, \eta, \lambda) \cdot KF + \frac{1}{48} \cdot FA(f, d, \eta, \lambda)$$

Total copper losses per a meter wire length in a winding

$$kctr(mE, f, d, \eta, \lambda, 1) = 0.4958$$

$$P_{cubr} := (1 + kctr(mE, f, d, \eta, \lambda, 1)) \cdot R0 \cdot \text{lac}^2$$

$$P_{cubr} = 0.1752$$

FIGURE 2.A.2

MathCAD example file for calculating eddy current losses in a transformer.

2. Center leg gapped inductor, one layer winding

Results on right side:

$d := 0.0005$ $\rho := 23 \cdot 10^{-9}$ $f := 100000$ $l_{ac} := 1$ $\mu_0 := 4 \cdot \pi \cdot 10^{-7}$ $h := 0.01$

$w := 0.03$ $N := 54$ $p := 1$ $K := 2$ $mE := 1$

$nE := \frac{N \cdot p}{mE}$ $f_{ap} := \frac{2 \cdot \sqrt{3}}{\pi} \cdot f$ $\lambda = 0.05$ $\eta := \frac{d \cdot nE}{w}$ $\lambda = 0.05$ $\eta = 0.9$
 $nE = 54$

$l_w := 1$ $\delta(f) := \sqrt{\frac{2 \cdot \rho}{2 \cdot \pi \cdot f \cdot \mu_0}}$ $\zeta(f, d) := \frac{d}{\delta(f)}$ $\chi(f, d) := \frac{1}{1 + \frac{1.5}{\zeta(f, d)}}$ $\delta(f) = 2.4137 \times 10^{-4}$

$R_0 := \frac{\rho \cdot l_w}{\left(\frac{d^2 \cdot \pi}{4}\right)}$ $R_0 = 0.1171$

$K := 2$ (center gapped core)

$GI(f, d) := \zeta(f, d)^6 + 2.7 \cdot \zeta(f, d)^5 - 1.3 \cdot \zeta(f, d)^4 - 17 \cdot \zeta(f, d)^3 + 85 \cdot \zeta(f, d)^2 - 43 \cdot \zeta(f, d)$ $GI(f, d) = 282.6246$

$FTb(f, d, \eta, \lambda) := \frac{1}{\sqrt{1 + \frac{GI(f, d)}{1024}}}$ $\kappa := \frac{0.002 + \frac{0.0006}{3}}{\frac{w}{K}}$ $\kappa = 0.1467$

$KF := \frac{3.5 \cdot (0.5 - \kappa)^2 + 0.69}{\kappa}$ $KF = 7.6838$

$k_{cin}(N, f, d, \eta, \lambda, KF) := \frac{1}{16 \cdot 3} \cdot \zeta(f, d)^4 \cdot \left(\frac{p \cdot N \cdot d}{w}\right)^2 \cdot \frac{\pi^2}{4} \cdot FTb(f, d, \eta, \lambda) \cdot KF$ $k_{cin}(N, f, d, \eta, \lambda, KF) = 5.2153$

$P_{cuin} := (1 + k_{cin}(N, f, d, \eta, \lambda, KF)) \cdot R_0 \cdot l_{ac}^2$ $P_{cuin} = 0.728$

Note1: Inductor winding loss compared to transformer winding loss : $\frac{P_{cuin}}{P_{ctr}} = 4.1552$

Note2: Inductor winding eddy current loss factor k_c compared to transformer eddy current loss factor k_c : $\frac{k_{cin}(N, f, d, \eta, \lambda, KF)}{k_{ctr}(mE, f, d, \eta, \lambda, 1)} = 10.5193$

FIGURE 2.A.3
 MathCAD example file for calculating eddy current losses in an inductor.

References

- [1] Snelling, E.C., *Soft Ferrites, Properties and Applications*, 2nd ed., Butterworths, London, 1988.
- [2] Sullivan C.R., Computationally efficient winding loss calculation with multiple windings, arbitrary waveforms, and two-dimensional or three-dimensional field geometry, *IEEE Transactions on Power Electronics*, vol. 16, No. 4, January 2001, pp. 142–150.
- [3] Erickson, R.W., and Maksimovic D., *Fundamentals of Power Electronics*, 2nd ed., KAP, Norwell, MA, 2001.
- [4] Dowell P.L., Effects of eddy currents in transformer windings, *Proc. Inst. Elect. Eng.*, vol. 113, No. 8, August 1966, pp.1387–1394.
- [5] McLyman, Col. Wm. *Transformer and Inductor Design Handbook*, Marcel Dekker, New York, 1988.
- [6] www.ferroxcube.com

3

Soft Magnetic Materials

In this chapter we present different magnetic materials used in power electronics. The manufacturing process, magnetic properties, and specific applications are discussed. The losses in the magnetic materials are considered in detail since they are very important for selection of the right material type and size in the design of high efficiency magnetic components.

Iron-based soft magnetic materials, such as laminated cores, powdered iron, and carbonyl iron cores are considered together with amorphous and nanocrystalline materials. Amorphous and nanocrystalline materials combine a high peak induction and low high frequency losses.

Ferrites are still a common choice in power electronics, as they have low losses in a wide frequency range (up to 3 MHz for power ferrites) because of their high specific resistivity (usually 1 Ωm and higher).

In this chapter the peak values of the induction are used in the discussions. The permeabilities are all relative except for the values of μ and μ_0 .

3.1 Magnetic Core Materials

The history of magnetism begins centuries before Christ with the discovery of the magnetic properties of a natural mineral called magnetite (Fe_3O_4). In 1600 William Gilbert published the first scientific study on magnetism: *Die Magnete*. The new science of electromagnetism was founded by the later contributions by Oersted, Faraday, Maxwell, and Hertz.

The development of soft magnetic materials for industrial purposes started with laminated iron and continues with powdered and carbonyl iron, ferrites, amorphous materials, and the newest nanocrystalline materials. The historical development of the soft magnetic materials is shown in [Fig. 3.1](#).

In power electronics there are two basic classes of materials used for magnetic cores for transformers and inductors:

- The first class of materials are alloys of iron and they contain some amounts of other elements, such as silicon (Si), nickel (Ni), chrome (Cr),



FIGURE 3.1
The history of soft magnetic materials.

and cobalt (Co). These materials are referred to as *ferromagnetic* materials. The values of the saturation induction begin at 1.4 T, and for some of the materials the values are near 1.9 T. The electrical resistivity of these alloys is only slightly higher than good conductors, such as copper or aluminum.

- The second class of magnetic materials are ferrites (*ferrimagnetic*). Ferrites are ceramic materials, basically soft magnetic oxide mixtures of iron and other magnetic elements, such as manganese (Mn), zinc (Zn), nickel, and cobalt. They are characterized by a high resistivity. The order of magnitude of the resistivity is at least 10^6 higher than the first class.

Depending on the applications, the desirable properties of the magnetic materials are different. In most soft magnetic material applications high permeability and saturation induction and low coercivity and power loss are preferable. Mechanical properties of the materials are also important. Usually it is not possible to have all the desirable properties in a single material, so for a given application the choice of the material is usually a compromise.

3.1.1 Iron-Based Soft Magnetic Materials

In this section we discuss the first class of materials often referred to as ferromagnetic materials.

3.1.1.1 Laminated Cores

The magnetic cores that use magnetic materials with high electrical conductivity are made from stacks of many thin laminations, electrically insulated from each other by a thin insulating coating. Laminations are used to reduce the eddy currents in AC applications and in DC applications with superimposed AC components. In pure DC applications, the core can be laminated to reduce the manufacturing cost. For laminated cores, a core stacking factor is defined as the ratio of the cross-sectional area of the soft magnetic material to the cross-sectional area of the core (typical values are 0.9 to 0.95).

Iron-Silicon Alloys

The main purpose of adding silicon to iron is to reduce the conductivity of iron and in that way to reduce the eddy-current loss in the alloy. The second beneficial effect of alloying iron with silicon is reducing magnetostriction and, thus, reducing the acoustic noise caused by cyclic stresses resulting from magnetostriction strains in AC applications.

The disadvantages of alloying silicon with iron are

- decreasing the saturation induction
- high silicon content results in a very brittle core
- reducing the life time of the punched material

The normal high silicon content is about 3%; above this content the mechanical processing is more complex. The practical useful limit of silicon content is about 6.5%. This content combines low losses with a low magnetostriction.

Grain-Oriented Silicon Steel

In the laminated cores, the magnetic flux passes in the direction along the laminations and it is beneficial to provide the highest permeability along this direction (in the plane of the laminations) and to decrease the permeability in the direction perpendicular to lamination plane. Grain-oriented silicon steel is mainly used for transformer and inductor cores. In general, iron cores are called isotropic when the same magnetic properties are observed in the rolling direction and in the direction perpendicular to it. Grain-oriented steel is anisotropic with high permeability and low loss in the rolling direction.

Over the last years the reduction of the core loss of grain-oriented silicon steel has been achieved mainly by the improvement of crystalline orientation, the development of thinner-gauge materials, and the development of magnetic domain refining techniques. According to [1], the extremely low core loss of 0.35–0.65 W/kg at 1.7 T and 50 Hz is obtained for 3.5% silicon grain-oriented steel of 0.15 mm thickness.

Iron-Nickel Alloys

There are three groups of nickel-iron alloys used for magnetic cores [2]. The first alloy contains 80% nickel (Permalloy, Mumetal) and exhibits the highest permeability. The alloy consisting of 50% nickel (Isoperm) has the highest saturation induction, near 1.6 T. The electrical resistivity of the alloy consisting of 36% nickel (Invar) is the highest and is about 0.7–0.8 $\mu\Omega\text{m}$.

The applications of iron-nickel alloys are in the transformers and inductor cores at audio frequencies. Some of the high permeability alloys (Mumetal) with relative permeability up to 300,000 are used for magnetic screening.

Iron-Aluminum and Iron-Cobalt Alloys

Other iron alloys are iron-aluminum and iron-cobalt alloys. The alloy $\text{Fe}_{65}\text{Co}_{35}$ exhibits the highest saturation induction of about 2.45 T and it is used in electromagnet pole tips.

Manufacturers of special grades of magnetic strip alloys are Magnetics [3], Vacuumschmelze [4],[5], NKK, and TDK.

3.1.1.2 Powdered Iron and Carbonyl Iron Cores

Powdered Iron

Iron powder is obtained directly from iron with low carbon content. The iron powder is resin bonded, which also limits the temperature. Powdered iron cores consist of small iron particles electrically isolated from each other. The size of the particles (less than a skin depth in their largest dimension even at moderate frequency) results in a quite high resistivity of the material and, thus, it leads to low eddy currents. In general, there are two kinds of eddy currents in powdered iron cores:

- eddy currents limited in the volume of the particles (micro currents);
- eddy currents in the bulk material (macro currents).

The powdered iron has a high saturation induction in the range 1–1.3 T. The usual initial permeability is in the range 1–200 [6].

Typical applications of powdered iron are DC filter inductors, where a high induction and a low permeability are possible and some damping (loss) is tolerated.

Manufacturers of iron powder cores are Magnetics [3] and Micrometals [7].

Carbonyl Iron

Carbonyl iron cores are obtained by heating carbonyl iron $\text{Fe}(\text{CO})_5$. The carbon monoxide splits off and the material has a microspherical, onionlike structure. The obtained material still has 0.8% carbon. This carbon has an adverse effect on hysteresis losses. To obtain low carbon contents, a further reduction of the carbon is performed afterward. The material has a relatively low permeability, which is in the range 1–50. Specific advantages of the carbonyl iron are its almost constant permeability versus magnetic field and frequency and its temperature stability ($-55^\circ + 150^\circ\text{C}$). The quality factor Q ($Q = j\omega L/R$) is very high even for frequencies above 100 MHz. The saturation induction is high (above 1.9 T). The losses per volume are higher than the ferrite's losses at the same induction level. The double logarithmic core loss graphics available in data sheets are straight lines. The following fit equation is often used to present the graphic data:

$$P_{\text{loss}} = k_{fe} f^\alpha B^\beta \quad (3.1)$$

where

P_{loss} the average power loss per unit volume

B is the peak induction

f is the frequency of the sinusoidal excitation

In equation (3.1) typical values for carbonyl iron are $k_{fe} = 0.3\text{--}0.7$, $\alpha = 1.15$, $\beta = 2.1\text{--}2.2$ this corresponds to a loss of 1000–3000 kW/m³ at 0.1 T, 100 kHz.

In comparison, good ferrites have 50–100 kW/m³ at 0.1 T, 100 kHz. At several MHz, and higher induction, the difference is less.

The carbonyl iron shows low hysteresis losses up to very high frequencies (10 MHz) and can be used in high frequency applications. Main applications are in EMI/RFI devices and in high linearity RF current sensing.

Typical shapes for powdered iron and carbonyl are ring cores and pot cores.

The advantage of powdered iron and carbonyl iron soft magnetic materials is that they can be easily processed (drilling, sawing, grinding) without the need of special tools. The tolerance of the dimensions of the powdered iron and carbonyl iron cores is lower in comparison with ferrites.

3.1.1.3 Amorphous Alloys

Amorphous soft magnetic materials are alloys of iron and other magnetic or transition metals such as cobalt, nickel, boron, silicon, niobium, and manganese. The alloys are known mainly by the following trade names: VITROVAC® [4], METGLAS® [8].

Production Process and Microstructure Characteristics

Amorphous alloys exhibit special chemical, mechanical, and magnetic properties due to their amorphous structure. Atoms in the amorphous structure are in complete disorder and no crystalline order exists in the structure. This type of structure is typical for liquids, molten metals, or glass. Amorphous metals are therefore called metallic glasses. The alloys are produced as thin ribbons directly from a melt. The hot molten metal with a temperature of around 1300°C is compressed on a cooling roller that rotates at high speed (100 km/h) (Fig. 3.2). When the liquid metal is rapidly quenched, the amorphous structure freezes up to a certain extent. In the manufacturing process the high cooling speed of about 10⁶ K/s prevents the formation of crystals and the amorphous structure is kept for a wide temperature range.

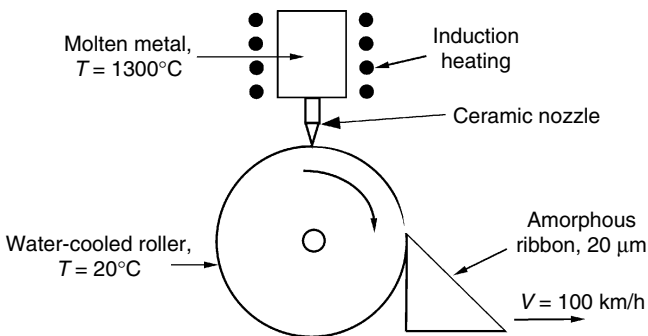


FIGURE 3.2

Rapid quenching technology for producing amorphous thin ribbon—the first step for obtaining nanocrystalline thin ribbon structure.

Magnetic Properties

Amorphous materials exhibit linear hysteresis loops with low coercivity and a saturation induction of 0.7–1.8 T [7]. The values of the saturation induction are almost completely retained at high frequency. The initial permeability of the material (up to 150,000 for some alloys) as well the remanence induction ratio B_r/B_s are adjustable in a wide range by field annealing. By annealing the amorphous ribbon with high frequency, high values of the DC permeability are obtained, such as a DC permeability up to 800,000 for the iron-nickel based alloy 2826MB METGLAS® [7]. Although the permeability reduces at high frequency, a relative permeability of about 1000 is still attained even at 1 MHz. The low permeability alloys have a wider frequency range and some of them are applicable above 1 MHz. The amorphous materials have relatively low losses with small temperature dependence or even a negative temperature coefficient.

The Curie temperature (the temperature at which the material loses its magnetic properties) of the amorphous materials is in the range of 350–450°C.

Applications

The small thickness of about 10–50 μm combined with the relatively high resistivity of 1.2–2.0 $\mu\Omega\text{m}$ (for comparison, the resistivity of pure iron is about 0.08 $\mu\Omega\text{m}$) makes the material suitable for high frequency applications. For high frequency applications, iron-based cores, such as MicroLite® and Powerlite® (based on Metglas materials), and cobalt-based cores, such as VITRO-VAC® and MagnaPerm® are used. The MicroLite® toroidal cores are available with distributed gap, which results in a distinct RFI advantage compared to conventional air gapped cores. Other high-frequency applications of amorphous metal cores are for common-mode RFI suppression chokes; flyback and push-pull transformers, active power factor correction common mode chokes, saturable reactors, and uninterruptible power supply inductors; high power outdoor industrial ballasts; and welding power supplies.

Low frequency applications of amorphous iron-based cores are in utility and industrial energy-efficient transformers as they have lower losses than the best grain-oriented steel grades (about 0.25 W/kg at 1.4 T, for amorphous materials). The amorphous cores permit very low no-load losses in transformers. The efficiency of amorphous iron-based dry-type transformers is as high as 99.5% [10]. The high permeability makes them a preferred material for current sensors in leakage current detectors.

Shapes

Amorphous alloys are mainly available in toroidal cores. Usually the cores are supplied epoxy coated and suitable for direct winding. Air-gapped and U-shape cores are also available [7]. U-shaped cores are also referred to as C-cores or cut cores, when they are made from a bobbin. For power electronics, the external dimensions today are from a few mm up to 130 mm for outer diameters and between 8 mm and 35 mm for the core height. The core

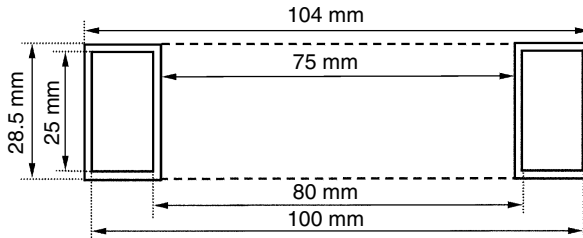


FIGURE 3.3
Core dimensions of core type 100-W342, alloy VITROPERM 500 F.

stacking factor, defining the ratio between the effective cross-sectional area A_e and the physical cross-sectional core area A_c (without coating) $k_{sf} = A_e/A_c$ is around 0.8. The finished core sizes and the finished core cross sectional area A_f define the total core filling factor $k_{ff} = A_e/A_f$ which is in the range 0.44–0.60.

In fact, the total core filling factor is equal to the product of the core stacking factor and the core packaging factor (coating).

Example

Fig. 3.3 shows the cross-sectional view of a tape wound amorphous core [4]. The effective iron cross-sectional area given in the manufacturer data sheets is $A_e = 190 \text{ mm}^2$. The core stacking factor k_{sf} is

$$k_{sf} = A_e/A_c = 190/(25 \times 10) = 0.76 \quad (3.2)$$

where

A_e is the effective cross-sectional area of the soft magnetic material

A_c is the physical cross-sectional area of the magnetic core

The total core filling factor k_{ff} is then

$$k_{ff} = A_e/A_f = 190/(28.5 \times 14.5) = 0.46 \quad (3.3)$$

where

A_f is the finished core cross-sectional area (in this case, after coating of the core)

The effective filling factor is much lower than for coated ferrite ring cores. As the density of metallic cores is high (about 7500 kg/m^3) and the density of ferrites is about 4800 kg/m^3 , the resulting average density of a wound core becomes similar to the average density of ferrite cores.

3.1.1.4 Nanocrystalline Magnetic Materials

In the last decade much work has been done with the aim of introducing new soft magnetic materials, called nanocrystalline materials, which enjoy more and more acceptance in modern power electronics. The first

nanocrystalline material was invented in 1988 by Yoshizawa et al. from Hitachi Metals Laboratory [11]. The alloy composition originally proposed is $\text{Fe}_{73.5}\text{Cu}_1\text{Nb}_3\text{Si}_{13.5}\text{B}_9$.

The advantages of iron-based nanocrystalline materials lie in the high values of the saturation induction, the reduction of volume of the magnetic components, the low heat dissipation, and the stable operation up to 120°C.

The first commercial names of nanocrystalline materials are known as VITROVAC® and VITROPERM® from VAC [4] and FINEMET® from Hitachi Metals [9].

Production Process and Microstructure Characteristics

The material is a two-phase structure consisting of an ultra fine grain phase of FeSi embedded in an amorphous minority phase. During the production process, a continuous, originally amorphous ribbon of only 20–25 micrometers in thickness is produced. The nanocrystalline structure is obtained by a specific annealing procedure usually under the presence of a transversal and/or longitudinal magnetic field. The thermal treatment affects the magnetic properties as a consequence of the structural changes produced within the amorphous state. During the thermal treatment at temperatures about 500° to 600°C, the initially achieved amorphous structure forms ultrafine crystals with a typical size of only 7–20 nm and therefore the material is called nanocrystalline. The soft magnetic properties of the nanocrystalline material combine the high saturation induction of conventional silicon steel and low high-frequency losses of ferrites.

The material itself is brittle and additional mechanical protection is necessary, provided by suitable epoxy coating or by plastic core boxes. There are several nano-ribbon trade names: VITROPERM® with nominal composition $\text{Fe}_{73.5}\text{Cu}_1\text{Nb}_3\text{Si}_{15.5}\text{B}_7$ [4,12,13], FINEMET® with nominal composition $\text{Fe}_{73.5}\text{Cu}_1\text{Nb}_3\text{Si}_{13.5}\text{B}_9$ [14], NANOPERM® consisting of Fe-M-B (M = Zr, Nb at 5–7%, and B of 2–6%) [15, 16]. The major manufactures of nano-ribbons are in Germany and in Japan.

Magnetic Properties

Nanocrystalline soft magnetic materials exhibit a linear hysteresis loop with coercivities smaller than 2 A/m and a saturation induction of 1.2–1.5 T [15]. The initial permeability of the material is adjustable in the range of 15,000 to 150,000. The remanent induction ratio B_r/B_s is also controllable depending on the specific needs of the different applications. By magnetic field annealing with transverse (perpendicular to the circumferential direction of a core) and longitudinal (parallel to the circumferential direction of a core) fields, almost rectangular and flat loops can be obtained.

The properties of nanocrystalline materials and their possible features are summarized in Fig. 3.4.

The material reveals a relatively high electrical resistivity of about 1.2 $\mu\Omega\text{cm}$. Combined with a ribbon thickness of 15–25 μm , this results in a proper frequency dependence of the permeability and low eddy current losses. The permittivity of the material is low due to its metallic conductivity. The low

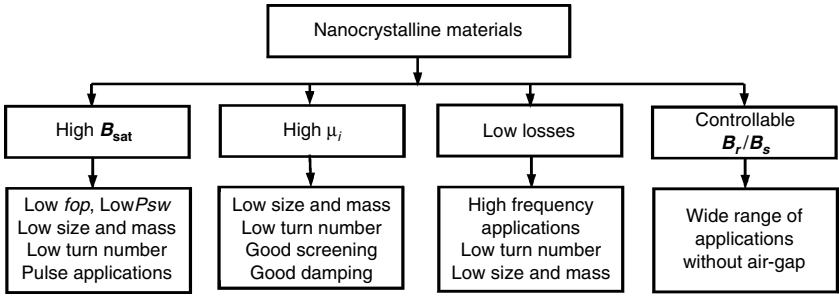


FIGURE 3.4
Properties of nanocrystalline materials and their possible feature.

core losses and the static hysteresis properties yield a favorable dynamic behavior of the nanocrystalline materials up to 150 kHz and more.

Figure 3.5 shows a graph of the losses as a function of the induction for two frequencies. It is remarkable that for the nanocrystalline materials the losses are almost purely quadratic with the induction.

Temperature Behavior

The dependence of the initial permeability μ_i of the nanocrystalline soft magnetic materials on the temperature is almost linear and the difference in the temperature range, -40°C to 120°C , is about 6% [13]. For comparison, the same curves of ferrites and permaloys show a high level temperature dependence, which has to be additionally considered during the component

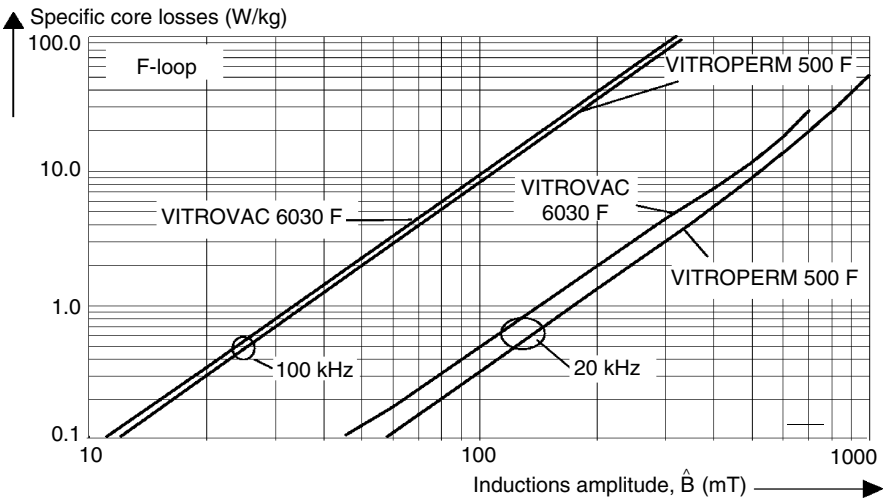


FIGURE 3.5
Specific core losses of nanocrystalline material VITROPERM and amorphous material VITROVAC, ribbon thickness 20 μm , with permission of Vacuumschmelze, GMBH.

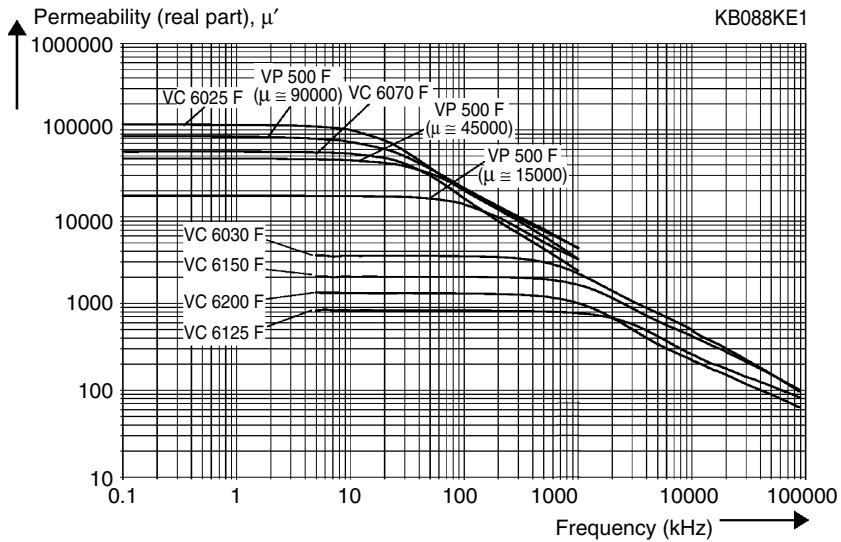


FIGURE 3.6 Permeability of nanocrystalline material VITROPERM, ribbon thickness 20 μm , with permission of Vacuumschmelze, GMBH.

design. The Curie temperature of the material is about 600°C and additionally contributes to its temperature stability. Figure 3.6 shows the permeability as a function of the frequency for some nanocrystalline materials.

Shapes

The material itself is brittle and additional mechanical protection is necessary, provided by suitable epoxy coating or by plastic core boxes. Nanocrystalline cores are made in similar shapes as amorphous materials: toroidal cores, air-gapped, and U-shape cores. The core stacking factor k_{sf} is typically about 0.8 and the total core filling factor k_{ff} is in the range 0.45–0.55.

Applications

There is no doubt that the nanocrystalline soft magnetic materials are a good choice for magnetic component design in electronics and power electronics when their price is competitive.

1. Power electronics

The applications of nanocrystalline materials with the most added value are these with high peak induction and EMC applications, where a high permeability in a wide range is useful. The nanocrystalline materials can combine a high permeability in the 100 kHz range together with the 10 MHz range, which is difficult to obtain with ferrites.

Typical applications of the nanocrystalline soft magnetic materials are (Fig. 3.7)

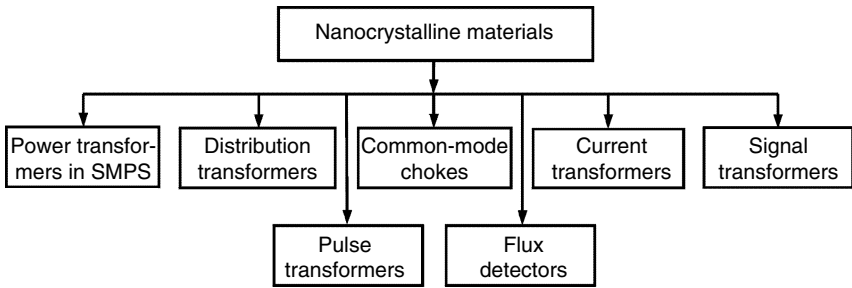


FIGURE 3.7
Applications of nanocrystalline materials.

- power transformers in SMPS (switched mode power supplies)
- distribution transformers
- common-mode chokes
- high precision current transformers
- signal transformers

In comparison with amorphous alloys, nanocrystalline alloys are a better choice for power transformers and common mode chokes because of the higher saturation induction and the lower cost [17]. The high saturation induction allows a lower operating frequency f_{op} and thus low switching losses P_{sw} . Nanocrystalline cores reveal good high frequency damping properties because of their low losses, high saturation induction, and high initial permeability.

2. Pulse transformers in ISDN.

Pulse transformers are used in integrated service digital network (ISDN) terminal equipment. The role of the pulse transformers is to isolate electrically the network circuit from the terminal equipment. The high saturation induction B_{sat} and the high initial permeability μ_i of the nanocrystalline soft magnetic materials allow miniaturization of the transformers. As a result, the mass-size parameters of the nanocrystalline core pulse transformers are much better in comparison with traditional MnZn ferrites transformers.

3. Flux gate magnetic detectors.

The magnetic properties of the nanocrystalline materials allow manufacturing flux gate magnetic detectors with high output voltage, high precision, and low size.

3.1.2 Ferrites

Currently ferrites are still the soft magnetic materials most widely used in power electronics.

The most important characteristic of ferrites, as compared to other magnetic materials, is the high volume resistivity of the material. In high frequency applications eddy current losses are usually dominant and increase approximately with the square of the frequency. These losses are inversely proportional to the resistivity. Therefore the high resistivity of the ferrites is the factor most contributing to their wide application in high frequency magnetic components.

Production Process and Microstructure Characteristics

Ferrites are dark gray or black ceramic materials. They are chemically inert, brittle, very hard, and difficult to process, except with water-cooled diamond tools. The general chemical formula is MeFe_2O_3 , where Me represents one or more divalent transition metals, such as manganese, zinc, nickel, cobalt, or magnesium. The most common combinations are manganese and zinc (MnZn) or nickel and zinc (NiZn). MnZn ferrites are characterized by a high permeability and high saturation induction levels and they are applicable up to a few MHz. NiZn ferrites are, in general, used in higher frequency ranges (above 1 MHz) and are suitable for low induction levels.

The raw materials used to produce ferrite cores are oxides or carbonates of the constituent metals. The base materials are weighed into the correct proportions and mixed to obtain a uniform distribution of all the components. The pre-fire (calcine) of the mixed oxides forms the ferrite at about 1000°C. The pre-sintered material is then milled to a specific particle size. A small amount of organic binder is added. Most ferrites are formed by pressing and as a result, so called green cores are obtained. Further in the process, the green cores are sintered at a temperature between 1150°C and 1300°C. After sintering, the ferrite core has the required magnetic properties. The finishing operations in the manufacturing process are burnishing, grinding, providing air-gap, annealing, and coating, depending on the specific form and application. The dimensions of the cores are typically within 2% of nominal due to 10–20% shrinkage.

Magnetic Properties

The relations between B [T] and H [A/m] (magnetization curves) are material properties. Although they have a physical origin, the properties are influenced by the manufacturing process. So, for practical applications, the dependency of B - H loops on frequency and temperature are measured on samples. For such characteristics one can refer to data from manufacturers [18–22].

The magnetic properties of the ferrites are isotropic. By various pressing, injection molding, and/or grinding techniques, a wide range of different shapes can be formed.

The saturation induction of the ferrites is in the range 0.25–0.45 T for the different material grades. The initial permeability is in the range 1000–15,000 and there are new materials reported with values above 20,000 [23]. Generally, the permeability of ferrites increases with the frequency to a maximum value at the Curie temperature and then drops sharply. Because of the isolation between the crystals in the structure, the bulk resistivity of ferrites is high: 0.1–10 Ωm for MnZn ferrites and 10^4 – 10^6 Ωm for NiZn ferrites. The

resistivity depends strongly on the temperature and the measuring frequency. The resistivity increases with increasing temperature. At high frequencies the crystal boundaries are short-circuited by the capacitances and the resistivity decreases.

Low Induction Level (Signal Level) Parameters

Specific parameters used in ferrite data books are the loss factor ($\tan \delta/\mu_i$), the hysteresis material constant η_B [1/T], and the inductance factor A_L [nH]. In material grade specifications, the loss factor ($\tan \delta/\mu_i$) includes residual and eddy current losses but not hysteresis losses. The hysteresis losses are described by the hysteresis loss factor ($\tan \delta_h/\mu_e$), which can be calculated using

$$\frac{\Delta \tan \delta_h}{\mu_e} = \eta_B \Delta \hat{B} \tag{3.4}$$

where

- \hat{B} is peak induction
- μ_e is effective permeability

REMARK

Cores with larger air gaps have a lower μ_e and lower $\tan \delta_h$.

For induction values above 10 mT the hysteresis losses become predominant. Their part in the total losses can be found by means of two measurements, usually at 1.5 mT and 3 mT induction levels. Then the hysteresis material constant η_B is found from

$$\eta_B = \frac{\Delta \tan \delta}{\mu_e \Delta B}, \quad \eta_B = \frac{(\tan \delta)_{3\text{mT}} - (\tan \delta)_{1.5\text{mT}}}{\mu_e (3\text{ mT} - 1.5\text{ mT})} \tag{3.5}$$

See also [Chapter 1](#), section 1.2.4.

High Induction Level (Power Level) Parameters

For high induction, the losses in the ferrites are based on experimental data and can be modeled depending on temperature, induction, and frequency. The general form of the loss per unit volume, termed the specific loss $P_{sp,v}$, is

$$P_{sp,v} = k_{fe} f^\alpha B^\beta \tag{3.6}$$

where

- k_{fe} is core loss coefficient, $k_{fe} = F(f, B, T)$
- α is frequency exponent
- β is core loss exponent
- B is the peak-to-peak value of the induction AC waveform
- f is the frequency

The constants k_{fe} , α , and β depend on material grade, induction, and temperature. For a constant value of k_{fe} the double logarithmic core loss graphics are straight lines. At high induction levels the losses are almost proportional

to B^3 . Equation (3.6) is often used as an interpolation equation for graphical data. The losses are given for peak induction with sinusoidal voltage. For other waveforms, the peak-to-peak induction divided by two is used. For square wave voltages, this approach results in typical errors of 10 to 15%. However, usually the accuracy of loss models is also limited due to the spreading on the material grade characteristics.

Since the frequency exponent α is strongly dependent on the frequency, the core loss coefficient k_{fe} in Equation (3.6) differs enormously for the high frequency range.

Ferrites also show a temperature dependence of their permeability, which can change up to 1.5 times between signal levels (few mT) and intermediate induction levels, such as 0.1–0.2 Tesla.

More precise results concerning temperature dependence can be obtained by the following expression:

$$P_{sp,v} = k_{fe} f^\alpha B^\beta (c_1 T^2 - c_2 T + c_3) \quad (3.7)$$

where

T is the core temperature in °C

c_1, c_2, c_3 are specific coefficients [24]

The values of the coefficients $c_1, c_2,$ and c_3 are much different for the different material grades and are usually not available in the data sheets. It is important to look carefully at the data of the temperature characteristics of different ferrite grades, as the losses can easily increase by a factor of 2 if a grade with an incorrect temperature is chosen. In a lot of designs, ferrite grades with a minimum loss at about 100°C are used, as this is often a worst-case temperature of the ferrite in the design.

Shapes

There are a number of different shapes for ferrites. In Appendix B at the end of the book the most frequently used shapes are given with the corresponding data.

TABLE 3.1

Magnetic and Operating Properties of Some Iron-Based Soft Magnetic Materials in Use in Electronics

Material	FeSi, laminated	NiFe, nickel steel, laminated		Powdered iron	Carbonyl iron	
Contents	3–6% Si	Permaloy 80% Ni	Isoperm 50% Ni	Invar 30–40% Ni	95% Fe bulk	92.5% Fe bulk
Permeability, μ_t	1000–10000	10000	3000	2000	1–500	1–50
B_{peak} , T	1.9	1	1.6	0.6	1–1.3	1.6–1.9
ρ , $\mu\Omega\text{m}$	0.4–0.7	0.15	0.35	0.75		>10 ⁶
P_{loss} , W/kg	0.3–3 at	24 at	22 at	21 at		60 at
Curie temp. T_c , °C	1.5 T/50 Hz 720	0.2 T/5 kHz 500	0.2 T/5 kHz 500	0.2 T/5 kHz 500	700	0.02 T/1 MHz 750

TABLE 3.2

Magnetic and Operating Properties of Ferrites, Amorphous, and Nanocrystalline Soft Magnetic Materials

Material	Ferrites	Amorphous s.m.m.		Nanocrystalline s.m.m.
Contents	MnZn, NiZn bulk	73.5% Fe, ribbon thickness 5–25 μm	70–73% Co, ribbon thickness 25 μm	73.5–90% Fe, ribbon thickness 20 μm
Permeability, μ_i	100–20000	10000–150000	10000–150000	15000–20000
B_{peak} , T	0.3–0.45	0.7–1.8	0.5–0.8	1.2–1.5
ρ , $\mu\Omega\text{m}$	10^2 – 10^4 MnZn 10^7 – 10^9 NiZn	1.2–2	1.4–1.6	0.4–1.2
P_{loss} , W/kg	12 at 0.2 T/20 kHz 60 mW/cm ³	18 at 0.2 T/ 20 kHz	7–18 at 0.2 T/ 20 kHz	5 at 0.2 T/20 kHz
Curie temp. T_c , °C	125–450	350–450	400	600

3.2 Comparison and Applications of the Core Materials in Power Electronics

The magnetic and operating properties of the soft magnetic materials discussed here are summarized in Table 3.1 and Table 3.2. The comparison and the applications of some soft magnetic materials in power electronics are shown in Fig. 3.8.

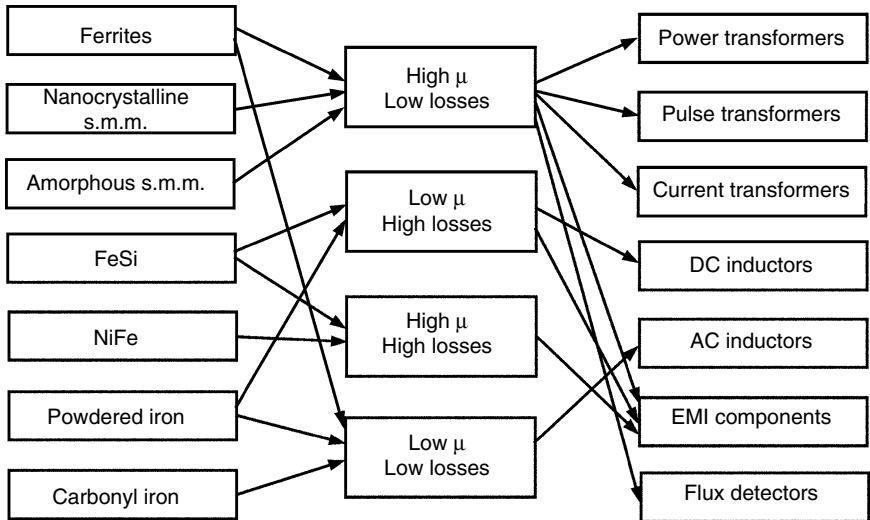


FIGURE 3.8 Applications of various soft magnetic materials.

3.3 Losses in Soft Magnetic Materials

In this section, a more general approach for modeling losses in soft magnetic materials is given.

According to classical loss separation, the total loss is decomposed into a sum of hysteresis, eddy current, and residual loss components. This decomposition permits loss mechanisms to be treated separately, as if they were independent of each other.

3.3.1 Simplified Approach for Laminated Steel Cores

In simplified models, the core losses are traditionally separated into hysteresis losses and eddy current (Foucault) losses. This should be considered as curve fitting in losses, proportional to frequency and losses and proportional to the square of the frequency at constant induction B . For a first approximation, they are also quadratic with the induction. For steel, these losses are usually specified at 50 Hz and 1.5 T peak value of the induction B :

$$P_v = (B_p/1.5)^2 \left(P_{vh} \frac{f}{50} + P_{vf} \left(\frac{f}{50} \right)^2 \right) \quad (3.8)$$

The losses at 50 Hz are the sum of hysteresis losses P_{vh} and eddy current (Foucault) losses P_{vf} . The coefficients P_{vh} and P_{vf} in Equation (3.8) should be considered as curve fitting constants in 50 Hz. In high quality grades P_{vh} is dominant

The losses are at least 0.5 W/kg at 1.5 T for grain-oriented steel of 0.3 mm and up to 20 W/kg for non-silicon soft iron of 0.65 mm. For high-frequency applications, ultra thin silicon steel has been used down to 50 μm (~2 mills = 0.002 in) thickness.

When the excitation frequency rises, a reduced penetration depth is observed. The frequency at which the penetration depth δ equals half the sheet thickness is called the cut-off frequency f_{co} :

$$\delta = \sqrt{\frac{2}{2\pi f \mu \sigma}}, \quad \delta = d/2 \Rightarrow f_{co} = \frac{4\rho}{\pi \mu d^2} \quad (3.9)$$

where

d is the thickness of the iron sheet

For commonly used sheets intended for 50-or 60-Hz applications, the cut-off frequency f_{co} is close to 400 Hz.

3.3.2 Hysteresis Losses

Hysteresis in the B - H characteristics of the magnetic materials is the central feature among their properties. The size of the B - H loop depends on the

range of the applied H field. The *hysteresis loss* P_H corresponds to the dissipation in the DC measurements, i.e., it is equal to the work done on the magnetic material by the applied field. The area inside the B - H loop is the actual energy loss for a cycle of the applied H field. The higher values of B , respectively H , result in the larger enclosed area of the B - H loop. When an alternating H field is applied, the loss per unit time is the energy enclosed by the loop multiplied by the exciting frequency. The hysteresis loss is approximately proportional to frequency:

$$P_H = f \oint B \, dH \quad (3.10)$$

$$P_H = k_h f B^\beta \quad (3.11)$$

where

k_h is the hysteresis loss coefficient

β is the core loss exponent: for a very small induction amplitude (e.g., 1 mT), $\beta = 2$; for larger amplitudes, $\beta = 1.5$ – 2 for iron and $\beta = 2$ – 3 for ferrites

The area of the hysteresis loop increases with the frequency. This means that the relation P_H/f increases with frequency at constant B level.

The reduction of the hysteresis loss can be realized by reducing the hindrances to domain wall movement [25]. There is some compromise as in thin sheets the hysteresis losses increase while the thickness decreases.

Further description of the physical mechanisms that cause hysteresis and lead to hysteresis loss is beyond the scope of this book. Detailed characterization of magnetic hysteresis and mathematical presentation of the phenomenon are presented by Bertotti in [25].

3.3.3 Eddy-Current Losses

All magnetic materials have some electrical conductivity, and the conductivity of iron-based magnetic materials is relatively high. As a result, the flux within the core induces an internal voltage $d\Psi/dt$ that drives circulating currents around the paths, as shown in Fig. 3.9.

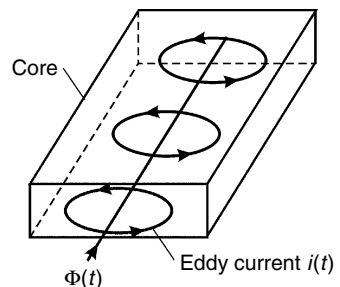


FIGURE 3.9
Eddy currents in a magnetic core.

These currents are termed *eddy currents* and corresponding effects are termed *eddy current effects*. If a field is suddenly applied, the eddy currents flow in directions such that the magnetic field generated by them is opposite to the applied (primary) field. As illustrated in Fig. 3.9 this field is generated in the opposite direction and superimposes with the applied field and thus, the resulting magnetic field in the core decreases exponentially inside the core. The resulting shielding effect increases with the rate of change of the applied magnetic field. The characteristic penetration depth is called *skin depth*. The value of the skin depth is given by

$$\delta = \sqrt{\frac{2}{\omega \mu \sigma}} = \sqrt{\frac{2\rho}{\omega \mu}} \quad (3.12)$$

where

$\omega = 2\pi f$, f is the frequency of the applied magnetic field

μ is the permeability of the magnetic material

σ is the electrical conductivity of the magnetic material

The skin effect is important for defining the geometry of the cross-sectional area of the core. If the cross-sectional dimensions of the core are large compared to the skin depth expressed by the equation (3.12), then the applied magnetic field is carried mainly by the surface area and the inner part of the core carries very little of the flux. As a result, the AC reluctance of the core for that frequency is increased and the main role of the core, to provide low reluctance path for the applied field, is significantly deteriorated. At 50 Hz, for iron, the skin depth is in the order of 1 mm.

The eddy currents with density J cause *eddy current losses* per volume $J^2\rho$, where ρ is the specific resistance of the core material. For a given thickness and material, the eddy current losses P_{ec} depend on the amplitude induction B_{\max} , on the frequency f , and on the internal resistivity ρ of the core material. As the eddy current losses per volume are proportional to the square of the induced voltage, the eddy current losses are proportional to $(fB_{\max})^2$. According to Snelling [26], eddy current losses can be expressed as

$$P_{ec} = k_e \frac{f^2 B_{\max}^2}{\rho} \quad (3.13)$$

where

k_e is a dimensionless eddy currents loss coefficient

B_{\max} is the amplitude induction of the applied field

ρ is the internal resistivity of the core

Equation (3.13) is only an approximation of the actual eddy current losses, as the impedance of some magnetic materials is not pure resistive and thus it depends on frequency. In most of the magnetic materials, the core permeance magnitude decreases with increasing frequency f . This implies that beyond some frequency, the eddy current loss dependence on frequency is higher than f^2 at constant induction level.

The microstructure and the construction of the magnetic cores in power electronics are considered in order to reduce the eddy current effects. To increase the resistivity of most magnetic steel a percentage of Si is added to the iron. Ferrites are appropriate core materials for high frequency applications because of their high resistivity, so that laminating ferrite cores is not required.

3.3.3.1 Eddy Current Losses in Laminated Cores

Iron-based magnetic materials have a low resistivity of about 0.4–0.8 $\mu\Omega\text{m}$. A way to decrease the density of eddy currents is by using cores made from stacks of many thin laminations. The laminations carry little flux and have short paths and, thus, a low induced voltage $V \sim d\Psi/dt$ is generated, resulting in lower specific eddy current losses. The same effect of reducing eddy current effects is obtained in amorphous and nanocrystalline magnetic cores by winding up a thin (10–100 μm) ribbon. This specific structure makes amorphous and nanocrystalline magnetic materials suitable for high frequency applications in spite of their still relatively low resistivity (1.2–2 $\mu\Omega\text{m}$).

The solutions and presentation of eddy current losses in sheets can be found in literature for two different approaches:

1. Low frequency approximation, where the average field inside the magnetic conductor is only slightly different from the applied field. This is already a good approximation when the thickness d of the magnetic sheet is smaller than the skin depth δ ;
2. Arbitrary frequency, a short discussion of which is given here, and the basics are given in the appendix of this Chapter.

Low Frequency Approximation of Eddy Current Losses in Laminated Cores

In the low frequency approximation, according to Bertoti [25] and the appendix to this chapter, the specific eddy current losses $P_{ec,\sin}$ in laminated cores under **sinusoidal** induction $B(t) = B_{\max} \sin(2\pi ft)$ are

$$P_{ec,\sin} = \frac{\pi^2}{6} V_c \sigma d_t^2 f^2 B_{\max}^2 \quad (3.14)$$

where

$P_{ec,\sin}$ are the eddy current losses per unit volume

V_c is the core volume

d_t is the thickness of the lamination

In a more general case, where the induction B changes with a constant rate in each half period $dB/dt = \pm 4f B_{\max}$ (i.e., under **triangular** induction waveform), the specific eddy current losses are

$$P_{ec,\text{tri}} = \frac{4}{3} V_{fe} \sigma d_t^2 f^2 B_{\max}^2 \quad (3.15)$$

according to [25] and the appendix to this chapter.

The ratio $P_{ec,\text{tri}}/P_{ec,\sin}$ is $8/\pi^2$, e.g., $P_{ec,\text{tri}}/P_{ec,\sin} = 0.811$.

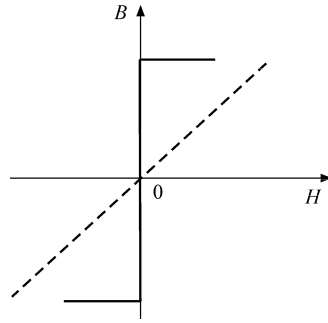


FIGURE 3.10
Linear and step like magnetization law.

3.3.3.2 Eddy Current Losses in Laminated Cores at Arbitrary Frequencies

The expression for eddy current losses for an arbitrary frequency and a linear magnetization law is given by Bertotti [25] as

$$\frac{P_{ec}}{f} = \frac{\pi}{2} V_c \frac{g B_{\max}^2}{\mu} \frac{\sinh g - \sin g}{\cosh g - \cos g} \quad (3.16)$$

where

$$g = \sqrt{\pi \sigma \mu d^2 f} \text{ is a dimensionless parameter}$$

This is a special case of the wide frequency model, where only the eddy current losses are considered and where the change in permeability or reactive power and hysteresis losses are not taken into account.

In the case $g \ll 1$ (i.e., low frequency case) Equation (3.16) results in Equation (3.14).

When the magnetization law is a steplike function, see Fig. 3.10, the case is close to a real heavy saturation mode. According to [25], in the case of sinusoidal induction the eddy current losses are

$$P_{ec, \text{step}} = \frac{\pi^2}{4} V_{fe} \sigma d^2 f^2 B_{\max}^2 \quad (3.17)$$

The comparison of this result with Equation (3.14) gives

$$P_{ec, \text{step}} = \frac{3}{2} P_{ec, \text{sin}} \quad (3.18)$$

From Equation (3.18) it is clear that in the case of heavy saturation the eddy current losses are proportional to $(f B_{\max})^2$, such as in the low frequency approximation case but increased by a factor 3/2

3.3.4 Anomalous (Residual, Excess) Losses

Under AC measurement conditions there are extra losses that do not match Equation (3.14). These losses can be expressed by a third term, anomalous losses, in the total loss presentation:

$$P = P_H + P_{ec} + P_a \quad (3.19)$$

According to the different magnetic materials, the third term in the decomposition of the losses in Equation (3.19) is attributed to different mechanisms in the magnetization process.

In magnetic steels and other iron-based materials these losses are called *excess losses* and are attributed to the consequence of the existence of magnetic domains. The excess losses are caused by the induced eddy currents in the vicinity of active domain walls in motion under the influence of the applied external field. According to [25] the excess losses P_e can be presented as

$$P_e \sim C (f B_{\max})^{3/2} \quad (3.20)$$

where

C is a parameter depending on a given material and the geometry of the magnetic core

For ferrites, the third category in the loss separation is termed *residual losses*. The residual losses P_r are associated with magnetic relaxation and (spin and dimensional) resonances in the ferrite. The relative importance of the residual losses to the total losses is strongly dependent on the frequency. At MHz frequencies, the residual losses dominate the ferrite dissipation. Decreasing the residual losses is persuaded by using fine-grained ferrites.

The loss separation is important in the description of the losses because each of the contributing terms exhibits a different, distinctive power law dependence on the frequency f and on the amplitude induction B_{\max} .

3.4 Ferrite Core Losses with Non-Sinusoidal Voltage Waveforms

In usual data ferrite core losses are given under sinusoidal excitation, however in power electronic converters the non-sinusoidal voltage waveforms, such as square voltage waveforms, are much more common. Therefore, we discuss ferrite core losses with non-sinusoidal voltage waveforms

The macroscopic mechanisms responsible for the losses in magnetic cores are discussed in the classical books [2,25,27] and also are summarized and updated in [28]. A practical approach for computing high-frequency ferrite core losses for arbitrary voltage waveforms is presented in [29,30]. The articles [31,32] present a technique to predict more accurately the magnetic core losses for pulsed operation.

Practical disadvantages of most of the proposed methods are the required additional measurements for a given material and the parameter calculations. The most popular equation for ferrite losses is known as the Steinmetz equation [33]:

$$P_{\text{loss}} = k f^\alpha \hat{B}^\beta \quad (3.21)$$

where

\hat{B} is the peak induction

P_{loss} is the average power loss per unit volume

f is the frequency of the sinusoidal excitation

For commonly used power ferrites, $\alpha = 1.2\text{--}2$ and $\beta = 2.3\text{--}3$. For square waves of 50% duty ratio Equation (3.21) shows a decreased accuracy but still remains a good approximation. But with a duty ratio D of 5% (or 95%), our calorimetric experiments showed more than doubled losses compared to sine waves and the prediction of Equation (3.21). Thus, it is obvious that in such cases Equation (3.21) cannot be used.

3.4.1 Identification of the Steinmetz Equation

In ferrite materials, there is some dependence of the batch and also manufacturer data change in time for the same grade. To avoid this problem, we measure the samples.

Real materials do not always fit perfectly to the Steinmetz equation. In practice, this means that α (and β) are frequency dependent. Usually they increase with frequency. The consequence is that k also changes.

To define a working (investigation) area, the reference frequency of 100 kHz is defined with a reference power and induction of 0.1 T, for which we can write

$$P = k_{\text{ref}} B^\beta f^\alpha = P_{\text{ref}} \left(\frac{B}{B_{\text{ref}}} \right)^\beta \left(\frac{f}{f_{\text{ref}}} \right)^\alpha \quad (3.22)$$

The coefficient β is fitted at the reference frequency (100 kHz), for the reference induction (0.1 T), and for other levels (0.05 and 0.15 T). The coefficient α is determined using the losses at the reference induction at a higher frequency of 250 kHz as is lies between the second and third harmonic.

Here we give the values α and β for two ferrite grades: 3F3 and N67, obtained after measuring the corresponding cores. The found value of β at 100°C is higher than the value at 25°C. The value of α is higher at 100 kHz than at 25 kHz. The values are shown in [Table 3.3](#).

The parameters α and β are close to the actual manufacture data sheets.

3.4.2 Natural Steinmetz Extension for Ferrite Core Losses with Non-Sinusoidal Voltage Waveforms

In a quasi-static approach, no power loss is generated during moments where B is constant. The losses can be represented as a surface in the B/H loop.

TABLE 3.3

Measured Material Constants at the Reference Point

Material Grade	k_{ref}	α	β	Operational conditions
3F3	0.0482	1.842	3.06	100°C, 100 kHz
N67	0.1127	1.76	2.94	100°C, 100 kHz
3F3	17.26	1.31	2.9	100°C, 25 kHz

A natural way to include the frequency dependence is to include a dependence of losses on dB/dt . We propose the following loss model called the Natural Steinmetz Extension:

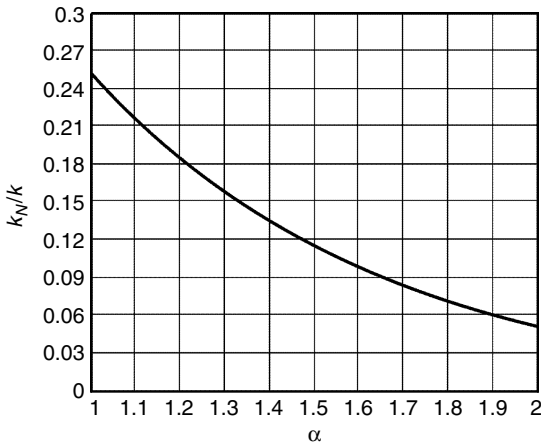
$$P_{NSE} = \left(\frac{\Delta B}{2}\right)^{\beta-\alpha} \frac{k_N}{T} \int_0^T \left|\frac{dB}{dt}\right|^\alpha dt \quad (3.23)$$

where the coefficients α and β are defined using the approach given in the previous subsection.

Equation (3.23) is consistent with the Steinmetz equation, Equation (3.21), for sine waves, if k_N is defined as

$$k_N = \frac{k}{(2\pi)^{\alpha-1} \int_0^{2\pi} |\cos \theta|^\alpha d\theta} \quad (3.24)$$

The ratio k_N/k is shown in Fig. 3.11 as a function of α , for α in the range of 1–2.

**FIGURE 3.11**The ratio k_N/k as a function of α .

We call the model given by Equations (3.23) and (3.24) a natural extension of the Steinmetz equation (NSE).

For a square wave voltage with duty ratio D , Equation (3.23) can be simplified to

$$P_{\text{NSE}} = k_N (2f)^\alpha \hat{B}^\beta (D^{1-\alpha} + (1-D)^{1-\alpha}) \quad (3.25)$$

where

f is the operating frequency

\hat{B} is the peak induction

D is the duty ratio of the square wave voltage

NOTE: The second and third harmonics are dominant at moderate values of duty ratio D . For extreme values of D (95%), a higher value of α gives better matching to the actual losses.

The modified Steinmetz equation (MSE) presented in [34,35] and later in [36] is also a good prediction of losses with non-sinusoidal waveforms. The losses in the MSE are given as

$$P_{\text{MSE}} = k f_{\text{eq}}^\alpha \hat{B}^\beta f \quad (3.26)$$

where

f_{eq} is an equivalent frequency

f is the operating frequency

α and β are the exponents, derived under sine excitation

The equivalent frequency in the MSE, Equation (3.26), is defined as

$$f_{\text{eq}} = \frac{2}{\left(2\pi \frac{B_{\text{pp}}}{2}\right)^2} \int_0^T \left(\frac{dB}{dt}\right)^2 dt \quad (3.27)$$

where

B_{pp} is peak-to-peak induction value

$T = 1/f$ is the period of the operating frequency

The specific loss predictions (P_V losses per unit volume) calculated by NSE, Equation (3.25), are shown in Fig. 3.12, Fig. 3.13, and Fig. 3.14 for the ferrite grades 3F3 and N67 at 100 kHz and 25 KHz, 0.1 T. The same graphs show the experimental measurements for square voltage waveforms with $D = 50\%$ – 95% . The computed results of the MSE, Equation (3.26), and the classical Steinmetz Equation (3.21) with corresponding α and β for sine wave are also shown in the same graphs. The experiments were made with an ETD 44 core, 3F3 material grade and an EE42 core, N67 material grade. For more details about the measuring set up, refer to Chapter 11 and to [37,38].

The given comparisons show that the matching for NSE is within 5% for duty ratio D up to 90%. The small difference for $D = 95\%$ can be explained

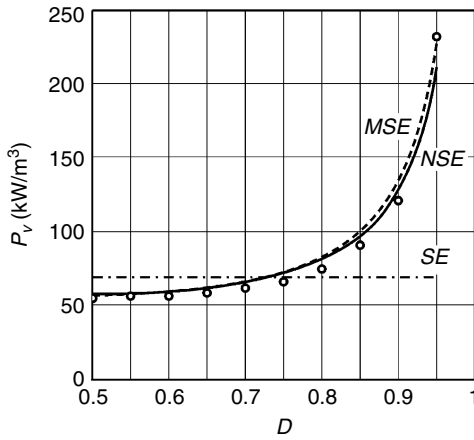


FIGURE 3.12

Specific ferrite core losses with square voltage waveforms for ferrite grade 3F3 at 100 kHz, 100°C, 0.1 T as a function of the duty ratio D : the experiments are the circles; the natural Steinmetz extension is the solid curve (NSE) for $\alpha = 1.842$; $\beta = 3.06$; the modified Steinmetz equation [34] is the dashed curve (MSE); classical Steinmetz Equation (3.21) is the dash-dot curve (SE).

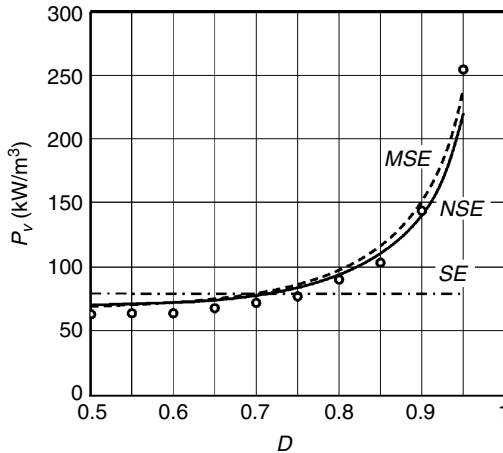


FIGURE 3.13

Specific ferrite core losses with square voltage waveforms for ferrite grade N67 at 100 kHz, 100°C, 0.1 T as a function of the duty ratio D : the experiments are the circles; the Natural Steinmetz Extension is the solid curve (NSE) for $\alpha = 1.76$; $\beta = 2.94$; the modified Steinmetz equation [34] is the dashed curve (MSE); classical Steinmetz Equation (3.21) is the dash-dot curve (SE).

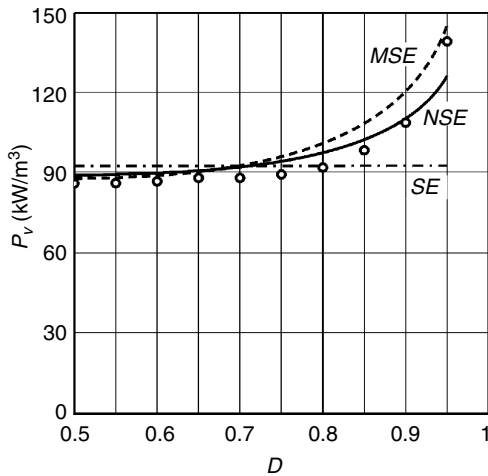


FIGURE 3.14

Specific ferrite core losses with square voltage waveforms for ferrite grade 3F3 at 25 kHz, 100°C, 0.2 T as a function of the duty ratio D : the experiments are the circles; the natural Steinmetz extension is the solid curve (NSE) for $\alpha = 1.31$; $\beta = 2.9$; the modified Steinmetz equation [34] is the dashed curve (MSE); classical Steinmetz Equation (3.21) is the dash-dot curve (SE).

by the high frequency content at that point and the fact that material characteristics show a higher α at higher frequencies.

Note that NSE and MSE show the same numerical results for $\alpha = 1$ (pure hysteresis losses) and for $\alpha = 2$ (pure Foucault losses).

REMARK

DC magnetization increases the losses for the same B_{pp} induction value. However, it is not usual in practice to have large B_{pp} and large DC components combined.

3.5 Wide Frequency Model of Magnetic Sheets Including Hysteresis Effects

In the classical loss separation theory, the permeability and the losses are described in a separate way. There is however a relation between the frequency characteristic of the active and reactive power and between the angle and frequency characteristic of the permeability. Impedance functions have no poles or zeros in the right half plane and are minimum phase. The complex permeability associated with hysteresis losses has a nearly constant angle,

whereas its magnitude decreases with increasing frequency. A one-dimensional approach is known using complex tanh functions [39].

We use the theory of impedances and the theory of one-dimensional homogeneous transmission lines to find a general function in which energy losses (hysteresis and eddy currents) and reactive power are combined and used to derive complex analytical functions describing the losses.

In this section, we are limited to the linear case. The theory is derived using complex analytical functions as they give much shorter expressions and are still easy to handle in today's mathematical software. More mathematical details are presented in Appendix D at the end of the book.

3.5.1 Constant Loss Angle Impedance

First, we consider a constant loss angle impedance function for the description of the hysteresis losses. The hysteresis effect can be characterized by a constant loss angle δ_h of the complex impedance of the material over a wide frequency range. The mathematical function with constant loss angle, which satisfies the requirements of impedance functions, is

$$z_h(s) = s \mu_h(s) = \mu_{hr} s^{1-2\delta_h/\pi} \quad (3.28)$$

where

- δ_h is the loss angle (in radians)
- s is the Laplace operator ($s = j\omega$)
- μ_{hr} is the hysteresis reference permeability

The hysteresis reference permeability μ_{hr} is a real constant and is fitted such that Equation (3.28) matches the data at a reference frequency, e.g., 100 kHz. For $\delta_h = 0$, the material is loss-less and has a constant permeability.

For a low loss angle, the amplitude of the permeance is almost independent of the frequency and the losses are almost proportional with the frequency.

High loss angles (combined with a high permeance) are present in some amorphous alloys, grain-oriented FeSi steels, and Ni-Fe alloys. In these cases an important frequency dependence of the permeability is also observed. By the frequency dependence, the major part of the anomaly losses are explained as well. Equation (3.28) tends to give an infinite permeance at zero frequency. This corresponds to a flux without current, known as a remanent flux. However, as it is a singularity point of the function, it should not be used to describe the behavior at DC inductance.

If the considered core has some parasitic air gap, a loss-less parallel permeability μ_g can be paralleled in the full model. This additional permeability does not affect the losses.

The nonhomogenous materials can also behave like a series connection of different reluctances, which results in paralleling permeabilities with a different loss angle.

3.5.2 Transmission Line Approach with Constant Loss Angle Material

The transmission line theory gives us an equation, which takes into account the one-dimensional approach of magnetic material, where the flux penetrates from the outer sides.

Using the one-dimensional transmission line theory, the following equation for a loss-less μ_c complex permeability μ_c can be derived:

$$z_c(s) = s\mu_c(s) = \frac{2}{d} \sqrt{\frac{s\mu}{\sigma}} \tanh\left(\sqrt{s\mu\sigma} \frac{d}{2}\right) \quad (3.29)$$

where

- σ is the electrical conductivity
- d is the lamination thickness

Similar expressions are used in [39], [40], and [41]. At high frequencies, the permeance reduces with the root of the frequency, and the angle tends to $\pi/4$.

Equation (3.28) is an intrinsic material characteristic and can be included in the transmission line model of Equation (3.29). This results in complex permeability μ_c :

$$z_c(s) = s\mu_c(s) = \frac{2}{d} \sqrt{\frac{\mu_{hr} s^{1-2\delta_h/\pi}}{\sigma}} \tanh\left(\sqrt{\sigma \mu_{hr} s^{1-2\delta_h/\pi}} \frac{d}{2}\right) \quad (3.30)$$

This function combines low and high frequency properties and is still consistent with the theory of passive impedances. One can see that the permeance goes to infinity when the frequency goes to zero. Some high permeance materials exhibit such behavior while the permeance is still increasing below 50 Hz.

NOTES:

- The angle of the resulting permeability is δ_h at low frequency and tends to $45^\circ + \delta_h/2$ at very high frequency.
- For iron based materials, a typical loss angle close to $\delta_h = \pi/6$ is observed.
- For amorphous and nanocrystalline materials, a loss angle close to $\delta_h = 50^\circ$ is typical.
- For $\delta_h = 45^\circ$, the losses at low frequency increase with the frequency to the power 1.5, which would be equivalent to the previously cited anomalous losses.

3.5.3 Wide Frequency Complex Permeability Function

At very low frequency, materials can exhibit some permeability limitation. This limitation can be loss-less if it is a parasitic air gap. We call this limitation the parallel permeability μ_g . One could intuitively consider this as taking

into account the parasitic air gap in a perfect core. This parallel permeability is defined by the reference permeability μ_{gr} and loss angle δ_g :

$$z_g(s) = s\mu_g(s) = \mu_{gr} s^{1-2\delta_g/\pi} \quad (3.31)$$

If it is a part of the material characteristics, μ_g usually represents losses. Note that for $\delta_g = 0$, the permeability μ_g is real and constant. With δ_g on the order of 1%, this behavior corresponds to amorphous and nanocrystalline materials.

The wide frequency complex permeability μ_w is thus given as follows:

$$\mu_w(s) = \frac{1}{\frac{1}{\mu_c(s)} + \frac{1}{\mu_g(s)}} \quad (3.32)$$

The model does have the following features:

- It explains both low and high frequency behavior, loss angle, and amplitude of the permeability in one expression.
- It gives an answer how it is possible to have loss angles that exceed $\pi/4$ (45°) in the high-frequency range, which is observed in most of materials.
- It includes effects, which are known as excess losses.
- It has only four parameters (for a given resistivity and thickness): μ_{hr} , δ_{hr} , μ_{gr} , and δ_g .

The model has its limitations:

- It is based on linear theory, thus it is valid at a given induction level and when the induction does not change much over the thickness.
- The resistivity of the material can change depending on the depth in the sheet.
- Even under sinusoidal flux excitation, harmonics are introduced. Those harmonics caused by the non-linearity of the magnetic material are not modeled.

3.5.4 Real, Reactive, and Apparent Power

The wide frequency model gives useful information, including the reactive power and the wide frequency behavior of the material.

The knowledge of the permeability allows calculating the complex power per unit volume $S_v(j\omega)$ under sinusoidal flux [m³]:

$$S_v(j\omega) = H H^* j\omega \mu_w(j\omega) = \frac{B}{\mu_w(j\omega)} \frac{B^*}{\mu_w^*(j\omega)} j\omega \mu_w(j\omega) = \left(\frac{1}{\sqrt{2}} \hat{B} \right)^2 \frac{j\omega}{\mu_w^*(j\omega)} \quad (3.33)$$

where

\hat{B} is the peak induction

H_{rms} is the effective value of the magnetic field

Using Equation (3.33), we can calculate the apparent power of the fundamental component $|S(j\omega)|$, the power loss $\text{Re}(S(j\omega))$ at sinusoidal flux excitation, and the reactive power $-\text{Im}(S(j\omega))$ of the fundamental component.

3.5.5 Dependence on Saturation Level

As far as the permeability variation due to the change in induction is negligible, the derived equations are applicable for a wide frequency range. With increasing frequency however, the induction level at the side edge of the sheet becomes significantly higher than the average induction in the sheet. The ratio between the average induction B , compared to the induction on the side edges, is denoted as $K_w(s)$. We have to compare the wide frequency permeability with the permeability when the thickness would be zero. Thus, for $K_w(s)$ we obtain

$$K_w(s) = \frac{\tanh\left(\sqrt{\sigma \mu_{hr}} s^{1-2\delta_h/\pi} \frac{d}{2}\right)}{\sqrt{\sigma \mu_{hr}} s^{1-2\delta_h/\pi} \frac{d}{2}} \quad (3.34)$$

The coefficient $K_w(s)$ is an indication of the ratio between the outer sides induction level and the average induction level in the cross section of the magnetic core.

For the frequency range, where $K_w(s)$ is close to unity, the linear model can be used.

But, for example, for an average induction level of 1 T and a $K_w(s) = 0.3$, it is clear that a serious local saturation will occur close to the surface of the sheet.

3.5.6 Wide Frequency Model Curves of Typical Materials

Three examples of wide frequency model curves are computed using a MathCAD program. The material parameters used in the wide frequency model for the description of the soft magnetic materials are given in [Table 3.4](#).

3.5.6.1 Silicon Steel

Silicon Steel of 0.35 mm Thickness

Example 1 considers 3% silicon steel of 0.35 mm thickness. The effect of a parallel permeability μ_g is ignored (set to infinite). When the thickness and the resistivity are given, only two parameters are left: the hysteresis loss angle δ_h and the hysteresis reference permeability μ_{hr} . Two values of the

TABLE 3.4

Material Parameters in the Wide Frequency Model for the Description of Soft Magnetic Materials

Quantity	Example 1	Example 2	Example 3
	3% Si steel, 0.35 mm	3% Si steel, 0.1 mm	Nanocrystalline, Vitroperm 500 F
d [mm]	0.35	0.1	0.021
ρ [Ωm]	0.5×10^{-6}	0.5×10^{-6}	1.15×10^{-6}
density [kg/m^3]	7500	7500	7300
δ_h [$^\circ$]	30	30	50
μ_{ir}	2×10^4 and 10^5	2×10^4 and 10^5	250×10^6
δ_g [$^\circ$]	0	0	0.025
μ_g	infinite	infinite	18000
$ \mu_r $ at 50 Hz (calculated)	2907 and 13810	2939 and 14640	—
$ \mu_r $ at 10 kHz (calculated)	—	—	15000

hysteresis reference permeability were chosen: 20,000 and 100,000. These two values have been chosen to illustrate the influence of the permeability. The computed curves for different functions are shown in [Fig. 3.15](#).

Silicon Steel of 0.1 mm Thickness

Example 2 resembles the *Example 1* except for the thickness, here the thickness is 0.1 mm. The improvement in losses and permeability is clear for high frequencies, see the computed curves, [Fig. 3.16](#). Note that a factor 2 reduction in thickness has the same effect as a factor 4 increase in specific resistivity.

3.5.6.2 Nanocrystalline Material

Example 3 shows the curves for the nanocrystalline material Vitroperm 500 F. The computed curves, [Fig. 3.17](#), can be compared with the manufacture data given in [Fig. 3.5](#) and [Fig. 3.6](#). As the material is quite linear, the predicted values can be quite close to the measured quantities. The values of μ_g have been adjusted in order to obtain a permeability of 15,000 at 10 kHz. When comparing the graphs, note that the scale of the losses in *Example 3* is shifted by a factor 10 to lower losses compared to *Examples 1* and *2*, describing silicon steel sheets.

Amorphous and nanocrystalline materials are thin ribbons (about 20 μm), so the argument of the value of \tanh is low and equal to its argument up to 100 kHz, thus the penetration depth is high compared to the thickness. This effect is reflected in the parameter K_w . As the core filling factor for thin ribbons is lower than for ferrites, the induction level of 0.5 T could be compared with ferrite data in the range of 0.3–0.35 T for the same outer dimensions of a core.

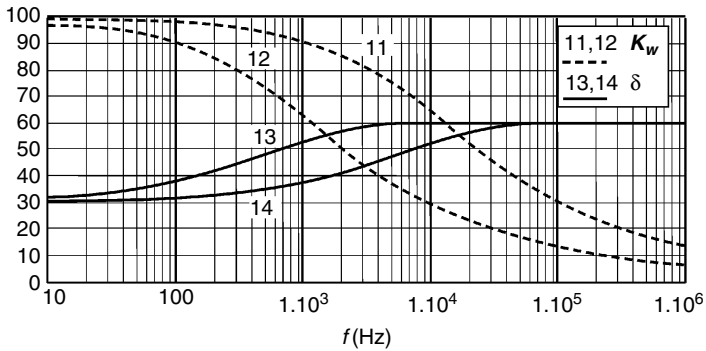
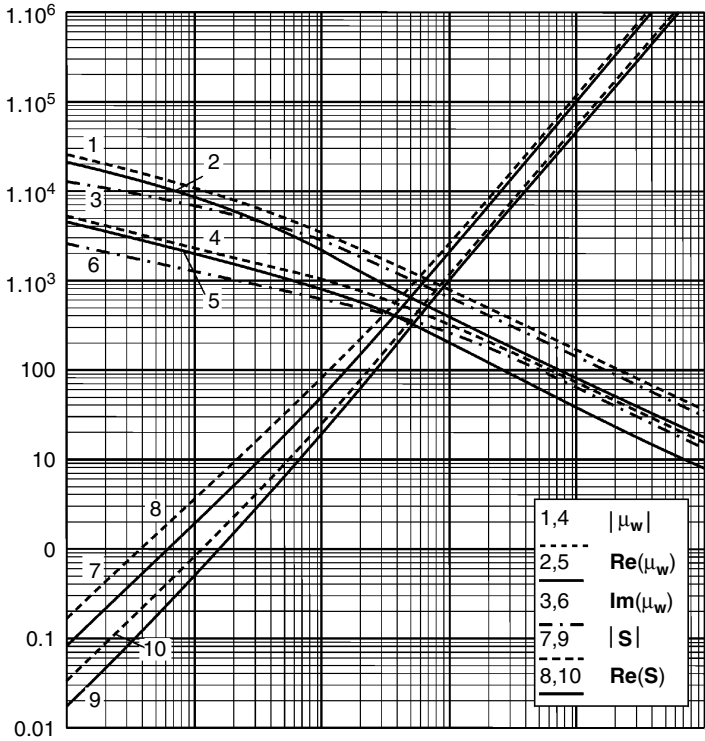


FIGURE 3.15

Computed curves of the wide frequency model for magnetic sheets, 0.35 mm 3% Si steel, Example 1.

Curves 1, 2, 3, 9, 10, 12, and 13 correspond to a material with $\mu_{hr} = 10^5$; curves 4, 5, 6, 8, 9, 11, and 14 correspond to a material with $\mu_{hr} = 2 \times 10^4$.

1,4: magnitude of the permeability: $|\mu_w|$

2,5: real part of the permeability: $\text{Re}(\mu_w)$

3,6: imaginary part of the permeability: $-\text{Im}(\mu_w)$

7,10: power loss at 0.5 T: $\text{Re}(S(j\omega))$

8,9: apparent power at 0.5 T: $|S(j\omega)|$

11,12: ratio average/peak induction: K_w

13,14: loss angle δ : $\arg(\mu_w)$

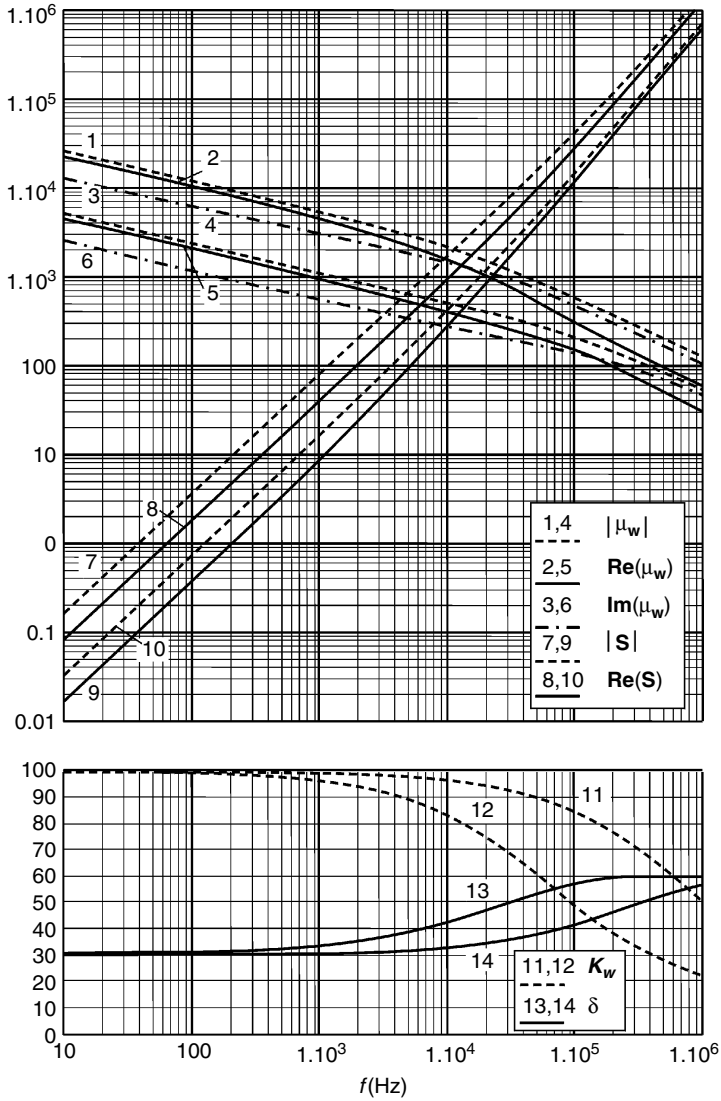


FIGURE 3.16

Computed curves of the wide frequency model for magnetic sheets, 0.1 mm 3% Si steel, Example 2. Curves 1, 2, 3, 9, 10, 12, and 13 correspond to a material with $\mu_{hr} = 2 \times 10^4$. Curves 4, 5, 6, 8, 9, 11, and 14 correspond to a material with $\mu_{hr} = 2 \times 10^4$.

- 1,4: magnitude of the permeability: $|\mu_w|$
- 2,5: real part of the permeability: $\text{Re}(\mu_w)$
- 3,6: imaginary part of the permeability: $-\text{Im}(\mu_w)$
- 7,10: power loss at 0.5 T: $\text{Re}(S(j_w))$
- 8,9: apparent power at 0.5 T: $|S(j_w)|$
- 11,12: ratio average/peak induction: K_w
- 13,14: loss angle δ : $\arg(\mu_w)$

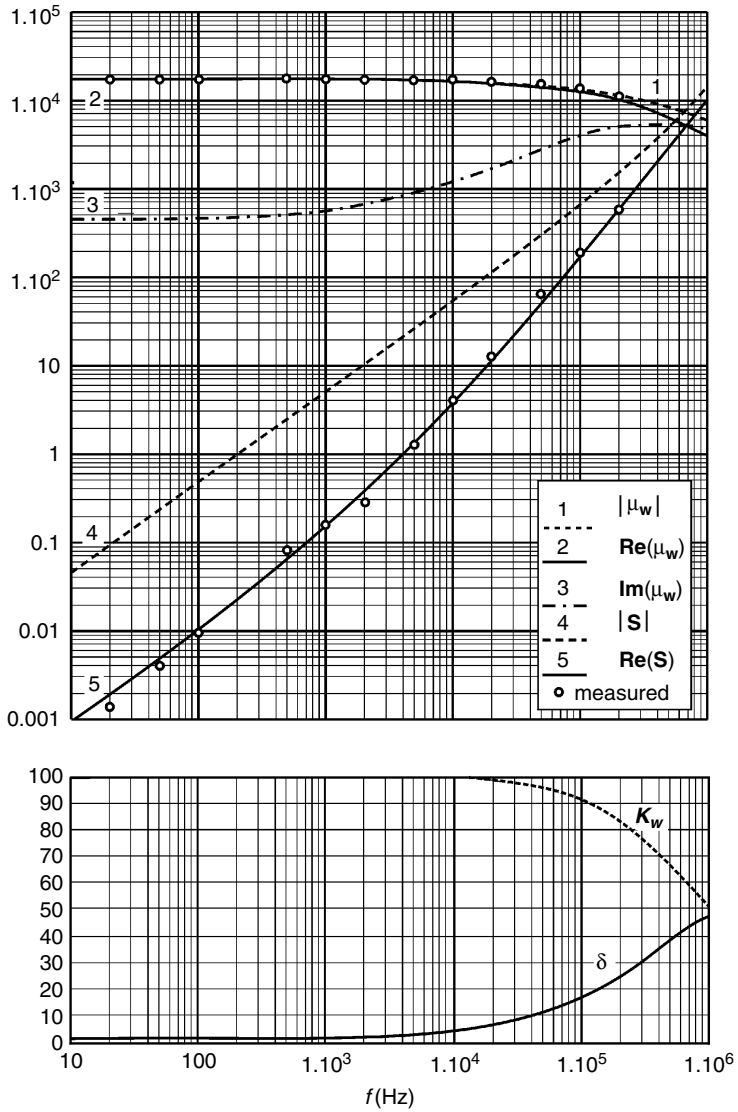


FIGURE 3.17

Computed curves of the wide frequency model for on nanocrystalline Vitroperm500F, Example 3.

- 1: magnitude of the permeability: $|\mu_w|$
- 2: real part of the permeability: $\text{Re}(\mu_w)$
- 3: imaginary part of the permeability: $-\text{Im}(\mu_w)$
- 4: power loss at 0.5 T: $\text{Re}(S(j_\omega))$
- 5: apparent power at 0.5 T: $|S(j_\omega)|$
- K_w : average/peak induction ratio
- δ : loss angle, $\arg(\mu_w)$

3.5.6.3 Wide Frequency Model for Ferrites

Similar models are possible for ferrite materials. If no capacitive (the high permittivity of ferrites) and resonance effects are modeled, the models are good up to a few MHz only. The properties of ferrites have been well documented in data sheets during the past decades.

The conductivity of ferrites is low, so in general there is no need to laminate ferrites (ferrimagnetic), such as ferromagnetic sheets. At very high frequency however there can be some benefit of laminating ferrites. Also, ferrites with a thickness of more than 20 mm begin to have cooling problems.

Appendix 3.A Power and Impedance of Magnetic Sheets

In principle, the main derivations for power as a function of the field H , for general conductors, given later in Appendix 5.1, are also valid for magnetic sheets. One difference is that magnetic sheets are bad electrical conductors as their penetration depth is low because of the high relative permeability. The fact that the magnetic sheets sometimes carry current is usually not intentional but a result of a bad construction. The term *applied current* corresponds in fact to an outside current, which generates an average magnetic field, see Fig. 3A.1. Another difference is that magnetic materials are usually described by the magnetic induction B and the permeability μ .

NOTE: Here we use RMS values for H and B variables.

Figure 3A.1 shows a magnetic sheet in an average H -field. The average value of H_{top} and H_{bot} , see Fig. 3A.1, is denoted by H_{av} : $H_{av} = (H_{top} + H_{bot})/2$. For the apparent power $S(s)$, according to Equations (5A.20) and (5.A25) in Appendix 5.1 we can write

$$\begin{aligned} S(s) &= 2bl_c Z_0(s) |H_{av}|^2 \tanh\left(\gamma(s) \frac{d}{2}\right) \\ &= 4R_0 b^2 \frac{1+j}{\delta(\omega)} \frac{b}{2} \tanh\left(\frac{1+j}{\delta(\omega)} \frac{d}{2}\right) |H_{av}|^2 \end{aligned} \quad (3A.1)$$

where

d is the thickness of the sheet

b is the width of the sheet

$Z_0(s)$ is the characteristic impedance of the material, $Z_0(s) = \left(\frac{s\mu}{\sigma}\right)^{1/2}$

σ is the specific conductivity of the material

R_0 is the resistance of the material

$\gamma(s)$ is a propagation function, $\gamma(s) = (s\mu\sigma)^{1/2} = (1+j)/\delta(\omega)$

$\delta(\omega)$ is the penetration depth, $\delta(\omega) = \sqrt{2/\omega\mu\sigma}$

$s = j\omega$

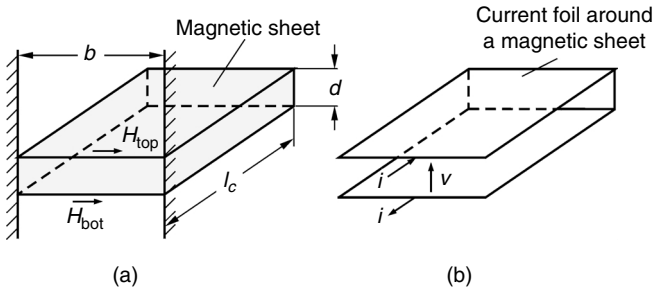


FIGURE 3A.1

A magnetic sheet in an average H -field (a) caused by a fictitious current foil around the sheet (b).

The induced voltage V around the sheet is the apparent power divided by $MMF. = H_{av}^* b$,

$$V = \frac{S(s)}{H_{av}^* b} = 2l_c H_{av} Z_0(s) \left(\tanh\left(\gamma(s) \frac{d}{2}\right) \right) \quad (3A.2)$$

where

l_c is the length of the sheet, see Fig. 3A.1

H_{av}^* is the complex conjugate of H_{av} .

The integral of the voltage is the flux Φ :

$$\Phi = 2l_c H_{av} \frac{Z_0(s)}{s} \tanh\left(\gamma(s) \frac{d}{2}\right) \quad (3A.3)$$

The averaged induction B_{av} is then

$$B_{av} = \frac{\Phi}{A_{sh}} = \frac{\Phi}{l_c d} = 2 \frac{H_{av}}{d} \frac{Z_0(s)}{s} \tanh\left(\gamma(s) \frac{d}{2}\right) \quad (3A.4)$$

where

$A_{sh} = l_c d$ is the cross sectional area of the sheet

The corresponding average complex permeability μ_c is

$$\mu_c = \frac{B_{av}}{H_{av}} = 2 \frac{Z_0(s)}{ds} \tanh\left(\gamma(s) \frac{d}{2}\right) \quad (3A.5)$$

Using the penetration depth $\delta(\omega)$, we can write

$$\mu_c = \mu(1-j) \frac{\delta(\omega)}{d} \tanh\left(\frac{1+j}{2} \frac{d}{\delta(\omega)}\right) \quad (3A.6)$$

Note that μ is an intrinsic material constant and that μ_c is a property of a magnetic sheet. A negative imaginary part of μ_c corresponds with positive power losses.

One can also express the apparent power as a function of B_{av} :

$$S(j\omega) = V_c j\omega \frac{1}{\mu} |B_{av}|^2 \frac{1+j}{2} \frac{d}{\delta(\omega)} \coth\left(\frac{1+j}{2} \frac{d}{\delta(\omega)}\right) \quad (3A.7)$$

where

V_c is the volume of the magnetic material

Also the impedance $Z(s)$ of a magnetic sheet can be calculated using Equation (3A.1). Note that this impedance is not obtained by feeding a current into the sheet, but with a current i , which generates an average magnetic field, $H_{av} = i/b$, and observing the voltage of top and bottom close to the sheet, see Fig. 3A.1. The impedance of a magnetic sheet $Z(s)$ is then

$$Z(s) = 2 \frac{l_c}{b} Z_0(s) \tanh\left(\gamma(s) \frac{d}{2}\right) \quad (3A.8)$$

$$Z(j\omega) = \frac{l_c d}{b} j\omega\mu(1-j) \frac{\delta(\omega)}{d} \tanh\left(\frac{1+j}{2} \frac{d}{\delta(\omega)}\right) \quad (3A.9)$$

With the Taylor expansion given in Appendix 5.1, we can look at the first two terms of this impedance:

$$Z(j\omega) = \frac{l_c}{db} \left(j\omega\mu d^2 + \frac{1}{12} \omega^2 \mu^2 \sigma d^4 \right) \quad (3A.10)$$

NOTE: The impedance value, given by Equation (3A.10) is for one sheet and one turn.

This can be used for frequencies, where the thickness $d = 1.5\delta$. The second term in the Taylor expansion corresponds to the eddy current losses. The first term represents the low frequency approximation of the reactive part of the impedance.

Note that the space between sheets is normally composed by air and also gives a contribution to the reactive power:

$$S_{air}(s) = s\mu b l_c |H_{air}|^2 \Delta y \quad (3A.11)$$

For a number of sheets, with an applied EMF, the losses are

$$S(j\omega) = P(j\omega) - jQ(j\omega) = \frac{V^2}{Z(j\omega)} = V^2 Y(j\omega) \quad (3A.12)$$

where

$Y(j\omega) = 1/Z(j\omega)$ is the admittance of one sheet and one turn, which can be presented as

$$Y(j\omega) = \frac{1}{j\omega L_m} + \frac{1}{R_m} \quad (3A.13)$$

For the loss calculation one is used to formulate it by the peak value of the induction \hat{B} and with a magnetizing inductance L_m in parallel to the core loss resistance. The reason is that the magnetizing reactance becomes highly nonlinear close to saturation and that the core loss resistance shows much less dependence on saturation. This corresponds to a parallel representation (admittance) of the transmission line:

$$Y(j\omega) = \frac{1}{R_m} - \frac{j}{\omega L_m} = \frac{1}{Z(j\omega)} \\ = \frac{b}{l_c d} \frac{1}{j\omega\mu} \frac{1+j}{2} \frac{d}{\delta(\omega)} \coth\left(\frac{1+j}{2} \frac{d}{\delta(\omega)}\right) \quad (3A.14)$$

For high frequencies, the function \coth will tend to 1 and the behavior of $Y(j\omega)$ is quite clear.

For low frequencies, we can make a Taylor series as a function of a relative frequency ω_r .

$$Y(j\omega) = \frac{b}{l_c d} \frac{1}{\mu} \frac{1}{\omega_a} \left[\frac{1}{j\omega_r} + \frac{1}{6} - \frac{j\omega_r}{180} - \frac{\omega_r^2}{3780} + \frac{j\omega_r^3}{75600} + \frac{\omega_r^4}{1496880} \right] \quad (3A.15)$$

where

$$\omega_a \text{ is the absolute frequency, for which the penetration depth } \delta \text{ equals the} \\ \text{thickness of the sheet } \delta = d, \omega_a = \frac{2}{\sigma\mu d^2} \\ \omega_r \text{ is the relative frequency } \omega_r = \frac{\omega}{\omega_a}; \text{ for } \omega_r = 1, \delta = d, \omega_r = \frac{\omega\sigma\mu d^2}{2}$$

The first two terms in Equation (3A.15) are the low frequency magnetizing inductance L_m and the parallel resistance, by which the low frequency eddy current losses can be modeled. For the magnetizing inductance L_{m1} , using the first term of Equation (3A.15) and multiplying with N_1^2 and N_f , we can write

$$L_{m1} = \frac{l_c d \mu N_f N_1^2}{b} \quad (3A.16)$$

where

$$N_1 \text{ is the primary number of turns} \\ N_f \text{ is the number of sheets}$$

The second term from Equation (3A.15) gives for R_{m1}

$$R_{m1} = \frac{12 l_c N_f N_1^2}{db\sigma} \quad (3A.17)$$

The results from Equations (3A.16) and (3A.17) correspond with the usual models [25] of eddy current losses.

The power loss in the sheet is then

$$P(\omega) = \frac{V_{m1}^2}{R_{m1}} = \frac{db \sigma V_{m1}^2}{12 l_c N_f N_1^2} = \frac{d^2 b \sigma V_{m1}^2}{12 A_c N_1^2} \quad (3A.18)$$

where

$A_c = N_f A_{sh} = N_f l_c d$ is the effective cross sectional area of the core

This result can also be obtained if one states that the eddy currents do not influence the induction inside the sheet at the low frequency approach, which is defined by $d \leq 1.5\delta$. In that case, the current density is zero in the middle and increases in a linear way to the sides of the sheets.

Note that in this approximation, the losses are quadratic with the RMS voltage at the magnetizing reactance.

For sinusoidal waveforms, the losses can be presented as a function of the peak induction \hat{B} . First, we express \hat{B}

$$\hat{B} = \frac{\sqrt{2} V_{m1}}{\omega N_1 S_{fe}} = \frac{\sqrt{2} V_{m1}}{2 \pi f N_1 S_{fe}} \quad (3A.19)$$

Then we can write

$$P_{\sin} = \frac{\pi^2 d^2 f^2 V_c \hat{B}^2}{6\rho} \quad (3A.20)$$

For a square wave emf, the induction is triangular and the peak value \hat{B} is

$$\hat{B} = \frac{V_{m1}}{N_1 A_c} \frac{1}{4f} \quad (3A.21)$$

This equation leads to the following result for the losses P_{tri} in that case

$$P_{tri} = \frac{4 d^2 f^2 V_c \hat{B}^2}{3\rho} \quad (3A.22)$$

Equations (3A.20) and (3A.22) are known in literature [25].

References

- [1] Kubota, T., Fujikura, M., and Ushigami, Y., Recent progress and future trend on grain-oriented silicon steel, *Journal of Magnetism and Magnetic Materials*, vol. 215–216, 2000, pp. 69–73.
- [2] Jiles, D., *Introduction to Magnetism and Magnetic Materials*, Chapman & Hall, London, UK, 1991.
- [3] www.mag-inc.com/
- [4] Cores and Components Databook 2000, Vacuumschmelze GmbH & Co. KG.

- [5] www.vacuumschmelze.com
- [6] www.icm1.com
- [7] www.micrometals.com
- [8] www.metglas.com
- [9] www.hitachi.com/
- [10] Hasegawa, R., Present status of amorphous soft magnetic alloys, *Journal of Magnetism and Magnetic Materials*, vol. 215–216, 2000, pp. 240–245.
- [11] Yoshizawa, Y., Oguma, S., and Yamauchi, K., New Fe-based soft magnetic alloys composed of ultrafine grain structure, *Journal of Applied Physics*, vol. 64, 1988, pp. 6044–6046.
- [12] Ferch, M., Soft magnetic materials in todays power electronic designs, *PCIM*, 6/2000, pp. 64–70.
- [13] Petzold, J., and Klinger, R., Nanocrystalline materials in common-mode chokes, *PCIM*, 7/2000, pp. 50–51.
- [14] Yoshizawa, Y., Oguma, S., Hiraki, A., and Yamauchi, K., Development of soft magnetic materials “FINEMET” composed of ultrafine grain structure, *Hitachi Metals Technical Review*, vol. 5, 1989, pp. 13–20.
- [15] Makino, A., Hatanai, T., Naitoh, Y., and Bitoh, T., Applications of nanocrystalline soft magnetic material Fe-M-B (M = Zr, Nb) alloys NANOPERM, *IEEE Transactions on Magnetics*, vol. 33, No. 5, Sept. 1997, pp. 3793–3798.
- [16] Mazaleyrat, F., and Varga, L., Ferromagnetic nanocomposites, *Journal of Magnetism and Magnetic Materials*, vol. 215–216, 2000, pp. 253–259.
- [17] Herzer, G., Nanocrystalline soft magnetic materials, *Journal of Magnetism and Magnetic Materials*, vol. 112, 1992, pp. 258–262.
- [18] www.epcos.com
- [19] www.ferroxcube.com
- [20] www.tokin.com
- [21] www.ferrite.de
- [22] www.fair-rite.com
- [23] Lucke, R., Advances in the development and production of highest permeability ferrite aterials, *Journal de physique*, IV, 1998, Pr2.437–440.
- [24] Mulder, S.A., Fit Formulae for power loss in ferrites and their use in transformer design, *PCIM’93, Proceedings of the 29th Power Conversion Conference*, 22–24 June 1993, Nurnberg, Germany, pp. 345–359.
- [25] Bertotti, G., *Hysteresis in Magnetism*, Academic Press, San Diego, CA, 1998.
- [26] Snelling, E.C., *Soft Ferrites, Properties and Applications*, 2nd ed., Butterworths, London, 1988.
- [27] Boll, R., Soft magnetic materials, in *The Vacuumschmelze Handbook*, Heyden & Son Ltd., London, 1979, pp. 13–108.
- [28] Goodenough, J.B., Summary of losses in magnetic materials, *IEEE Transactions on Magnetics*, vol. 38, No. 5, Sept. 2002, pp. 3398–3408.
- [29] Roshen, W., Ferrite core loss for power magnetic component design, *IEEE Transactions on Magnetics*, vol. 27, No. 6, Nov. 1991, pp. 4407–4415.
- [30] Devin, D., Sorting out losses in high frequency magnetic design, *Power Electronic Technology*, vol. 28, No. 5, May 2002, pp. 55–60.
- [31] Jamerson, C., Core loss calculations, *Power Electronic Technology*, Vol. 28, No. 2, Feb. 2002, pp. 14–24.
- [32] Severns, R., Additional losses in high frequency magnetics due to non ideal field distributions, *APEC’92, 7th Annual IEEE Appl. Power Electronics Conf.*, 1992, pp. 333–338.

- [33] Steinmetz, C.P., On the law of hysteresis, *AIEE Transactions*, vol. 9, pp. 3–64, 1982, Reprinted under title A Steinmetz contribution to the ac power revolution, in *Proceedings of IEEE*, vol. 72, No. 2, 1984, pp.196–221.
- [34] Brockmeyer, A., Dimensionierungswerkzeug für magnetische Bauelementein Stromrichteranwendungen, Ph.D. thesis, Aachen, University of Technology, Germany, 1997.
- [35] Brockmeyer, A., Albah, M., and Durbaum, T., Remagnetization losses of ferrites materials used in power electronic applications, PCIM'96, Nurnberg, Germany, 21–23 May, 1996, pp. 387–394.
- [36] Li, J., Abdallah, T., and Sullivan, C., Improved calculation of core loss with nonsinusoidal waveforms, IEEE, IAS 36th Annual Meeting, Chicago, September 30–October 4, 2001, pp. 2203–2210.
- [37] Van den Bossche, A., Valchev, V., and Georgiev, G., *Measurement and Loss Model of Ferrites with Non-sinusoidal Waveforms*, Proceedings of PESC-04, Aachen, Germany, June 20–25, cd-rom.
- [38] Van den Bossche, A., Valchev, V., and Georgiev, G., *Ferrite Losses with Square Wave Voltage Waveforms*, Proceedings of OPTIM-04, Brasov, Romania, May 20–22, cd-rom.
- [39] Lebourgeois, R., Bérenguer, S., Ramiarinjaona, C., and Waeckerlé, T., Analysis of the initial complex permeability versus frequency of soft nanocrystalline ribbons and derived composites, *Journal of Magnetism and Magnetic Materials*, vol. 254–255, January 1, 2003, pp. 191–194.
- [40] Bozorth, R.M., *Ferromagnetism*, New York, Van Nostrand, Princeton, 1951, p. 443.
- [41] Lammeraner, J., and Stafl, M., *Eddy Currents*, Iliffe Books, London, 1966.

4

Coil Winding and Electrical Insulation

A beginning designer of magnetic components has to face a few questions concerning the windings of the components: how much copper can be wound on a given core, how many turns for one layer are available, and what kind of insulation should be used in the design. Some experience and the trial-and-error approach can improve the result. In this chapter a more systematic view about coil winding aspects is given to facilitate the design.

The filling factor, the hexagonal and orthogonal wire fitting, the possible number of layers, and the wire length are considered.

We discuss the spread standards concerning wires, as well as the thermal requirements and standards of magnetic modules. In the United States the AWG (American Wire Gauge) is spread. The standard widely used in Europe is EN 60317 (old IEC 317).

In this chapter we assume that the winding axis is horizontal so that we can view cross sections and see the layers horizontally. Basically the approach is given for concentric layers. The application to coils with different sections is similar. Regardless, it makes sense to make a drawing of the cross section to know how the wires are arranged.

Coil winding is closely related to electrical insulation. Therefore, special attention is given to breakdown in air and solid materials.

Here we do not discuss ring cores, but many presented items are similar and applicable to them, when referring to the inside area of the core. Ring cores are usually wound by hand or by specialized equipment.

4.1 Filling Factor

The total copper cross-sectional area equal to the product of the number of turns N and the wire cross section A_{cu} (in some data it is denoted as A_w) is always less than the window area of the core W_a . The ratio of the total copper cross-sectional area and the core window area is called the copper filling factor:

$$k_{cu} = \frac{NA_{cu}}{W_a} \quad (4.1)$$

The copper filling factor k_{cu} is usually considered for each winding. Indeed, primary and secondary windings can be of very different natures. They can have a different diameter, and windings in round, Litz, and foil windings are possible.

The copper filling factor depends on the following aspects:

- The type of coil former used
- The insulation thickness of the used wire compared to the wire diameter
- Whether round or rectangular coil formers are used
- The creepage distance and insulation sheets between layers
- The accuracy of the winding equipment

In general, a net total copper section of 30% to 80% can be obtained for a given available core winding area W_a , e.g., $k_{cu} = 0.3\text{--}0.8$. For round conductors the copper filling factor is in the range $k_{cu} = 0.5\text{--}0.7$. Practical values for Litz wire are $k_{cu} = 0.3\text{--}0.4$. Usually, the high voltage magnetic components have a low filling factor in comparison with low voltage applications.

The best method of compact winding is to use a coil former with ripples on the bottom. In this way one avoids wire crossings. The ripples absorb the wire thickness tolerances. When the coil former is designed with the nominal diameter, the right result can be obtained only if the final delivery of the wire is like this design. So, for a good design one should take the maximum diameter into account. Another way to increase the filling factor is to use baking wire. In this way a self-supporting coil can be manufactured without a coil former.

Here, a perfect winding arrangement is assumed so that no chaotic winding is possible, e.g., where one wire can block the place of a whole layer. In circular (round) coil formers, a good winding arrangement is quite easily obtained. In rectangular coil formers, some manufacturers use ribbons in the bottom of the coil former to obtain a better arrangement. To obtain a good winding, it is also imperative that intermediate connections are made in the coil ends and not in the winding area of the coil. Note that obtaining a good winding with thin wires is difficult.

In a lot of designs for power electronics, the winding area W_a is not completely filled. Generally it is a good practice to perform a compact winding. It reduces the length for one turn, but it also reduces air between layers, which is an advantage for obtaining a good heat transfer. However, at high frequency ($d \gg \delta$) low eddy current losses may be obtained when the wires are spaced perpendicular to the field direction. Also it is not always possible to fill layers with the given number of turns. Sometimes it is better to adapt the wire thickness to still obtain full layers. An important advantage of winding a full layer is the fact that all wires are well fixed. Wires can move when the winding is injected with thermoplastic materials.

In this section we discuss the different arrangements of the wires and the influence of those arrangements on the copper filling factor.

REMARK

Here we will use the terms k_{sq} and k_{hx} for the filling factor to denote the ratio between the total copper cross-sectional area and the available winding area (no insulation between layers is considered). This available winding area is less than the core window area W_a . The difference is the sum of the areas of the coil former, the necessary creepage distance, and other spaces.

4.1.1 Round Wires

In the arrangement of the round wires there are basically two different kinds of fittings: square and hexagonal.

4.1.1.1 Square Fitting

Ideal Case

In this case the wires fit in a square grid as shown in Fig. 4.1.a. The theoretical filling factor for square fitting k_{sq} is

$$k_{sq} = \frac{\pi}{4} \left(\frac{d_{cu}}{d_o} \right)^2 = 0.7854 \left(\frac{d_{cu}}{d_o} \right)^2 = \frac{\pi}{4} \eta \lambda \tag{4.2}$$

where

- d_o is the outer diameter of the enameled copper wire;
- d_{cu} is the effective diameter of the copper wire;
- η is the horizontal packing factor;
- λ is the vertical packing factor.

In the ideal case, when the insulation thickness is zero and $d_{cu} = d_o$, the filling factor for square fitting reaches its maximum value: $k_{sq} = \frac{\pi}{4} = 0.7854$.

The horizontal packing factor is

$$\eta = \frac{d_{cu}}{d_o} \tag{4.3a}$$

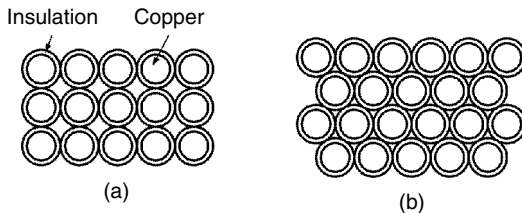


FIGURE 4.1 Different fitting of wires in the coil-former: (a) square fitting (b) hexagonal fitting.

The vertical packing factor in that case is the same as the horizontal one:

$$\lambda = \frac{d_{cu}}{d_o} \quad (4.3b)$$

Layer Approach

To find the number of wires in one layer we use the following expression:

$$n_h = \text{ent} \left(\frac{w \eta}{d_o} \right) \quad (4.4)$$

where

w is the available width of the coil-former, in data sheets it is also known as *MWW*

η is the horizontal spacing filling factor, $\eta = 0.8-1$, typically 0.9;

ent is the function giving the greatest integer less than the value in the brackets

The number of layers is

$$n_v = \text{ent} \left(\frac{h \lambda - n_i d_s}{d_o} \right) \quad (4.5)$$

where

h is the available height for the considered winding in the coil former;

λ is the vertical spacing filling factor and it is close to 1 if there is no insulating sheet between the layers;

d_s is the thickness of the insulating sheet;

n_i is the number of insulating sheets.

The total maximum number of turns N is

$$N = n_h n_v \quad (4.6)$$

where

n_h and n_v are, respectively, the number of wires in one layer and the number of the layers.

4.1.1.2 Hexagonal Fitting

Ideal Case

We can use partly the same approach as in the previous section. The theoretical filling factor for hexagonal fitting k_{hx} is

$$k_{hx} = \frac{\pi}{2\sqrt{3}} \left(\frac{d_{cu}}{d_o} \right)^2 = 0.9069 \left(\frac{d_{cu}}{d_o} \right)^2 = \frac{\pi}{4} \eta \lambda \quad (4.7)$$

In the ideal case when $d_{cu} = d_o$, the filling factor for hexagonal fitting reaches its maximum value: $k_{hx} = \frac{\pi}{2\sqrt{3}} = 0.9069$.

The maximal horizontal packing factor is

$$\eta = \frac{d_{cu}}{d_o} \quad (4.8)$$

The maximal vertical packing factor is

$$\lambda = \frac{2}{\sqrt{3}} \frac{d_{cu}}{d_o} = 1.155 \frac{d_{cu}}{d_o} \quad (4.9)$$

The value of the vertical packing factor given by Equation (4.8) can be higher than one. This represents the fact that more layers could be possible than the available total winding height divided by the outer wire diameter.

Layer Approach

The number of wires in the horizontal direction (in one layer) is given again as

$$n_h = \text{ent} \left(\frac{w\eta}{d_o} \right) \quad (4.10)$$

Taking into account that the first and the last half layers are still square fitting, the number of layers is

$$n_v = \text{ent} \left(\left(\frac{h}{d_o} - 1 \right) \frac{2}{\sqrt{3}} \right) + 1 \quad (4.11)$$

The total possible number of turns N is

$$N = n_h n_v \quad (4.12)$$

where

n_h and n_v are, respectively, the number of wires in one layer and the number of the layers

In hexagonal fitting no insulating sheets are assumed between layers, as normally the fitting is not improved compared to square if such insulation is used. With rectangular coil formers, often some air is present in the middle of a plane section, which reduces the vertical spacing filling factor λ . This is particularly true for thick wires.

4.1.1.3 Practical Case

Concerning the number of the layers n_v , in practice a winding arrangement between hexagonal and square is usually obtained. A winding arrangement close to the hexagonal can be achieved mainly in the case of a circular coil former.

In the case of a rectangular coil former, and when winding different layers from left to right and backwards, the wires of the second and higher layers have to jump two times a turn, generating a square fitting on that place. Generally the jump occurs in a long section, which is usually the winding section. Statistically, the cross section consists of a mix of about 50% hexagonal and 50% square fitting. Using the Equations (4.5) and (4.10) and assuming no insulation between layers, the number of layers for this case is

$$n_v = \text{ent} \left(\frac{h}{d_o} \left(\frac{1}{\sqrt{3}} + \frac{1}{2} \right) \right) + 1 = \text{ent} \left(\frac{h}{d_o} 1.0774 \right) + 1 \quad (4.13)$$

REMARKS ABOUT w AND h

1. There can be a large difference between the allowed winding width w and the width of the core window. So the maximum value of w is a characteristic parameter of the coil former but not of the core itself.
2. The allowed value of w can be limited by the need of creepage distances for galvanic insulation.
3. The height h is the value for one winding, not for the whole transformer. The sum of the different layers must not exceed the available total height, because some air distance has to be provided for the insulation to the core.
4. Windings of a thick wire cannot follow the bottom of a square coil former, usually some air remains between the coil former and the first layer.

The filling factor for square and hexagonal fitting of a coil is given in [Fig. 4.2](#) as a function of wire diameter. The graph is obtained using the data from Appendix C of the book (Grade 1 is used as insulation standard). However, the result given in [Fig. 4.2](#) has to be lowered by a stacking factor of 5% to 10% because of two factors:

- a wire in a winding takes more space than its nominal diameter;
- the tolerances in the wire diameter decrease the filling factor.

Therefore, the values given in [Fig. 4.2](#) can be used as a first approximation.

4.1.2 Foil Windings

Foil winding is often preferred when the necessary effective copper cross section is high. The foil windings have very low eddy current losses for fields

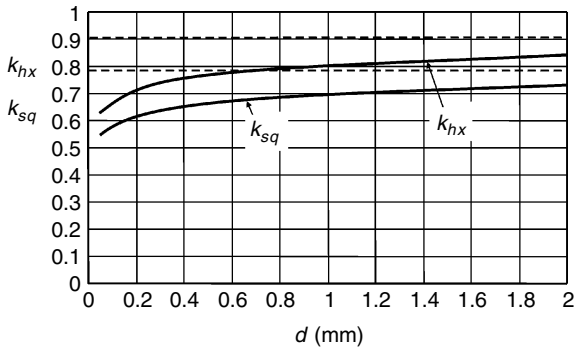


FIGURE 4.2

Filling factor for square and hexagonal fitting as a function of wire diameter; dashed lines present the ideal case without insulation, Grade 1 is used as insulation standard, see Appendix C.

parallel to the foil. Care should be taken for end (edge) effects and fringing field of air gaps, for more details refer to [Chapter 8](#).

The foil can be insulated by insulation sheets or by varnish. The vertical filling factor, dependent on the insulation thickness, is

$$k_v = \frac{t_{cu}}{t_{cu} + d_{ins}} \quad (4.14)$$

where

t_{cu} is the thickness of the copper of the foil

d_{ins} is the thickness of the foil insulation

As long as the thickness of the foil insulation is much lower than the copper foil, high filling factors can be obtained. The usual insulation thickness for thin copper foils is a multiple of $50 \mu\text{m}$ (Europe) or 2 mils ($= 50.8 \mu\text{m}$). Aluminum foils can also be used; however, care should be taken to ensure good electrical contacts. This can be made by pressure or by a nickel surface.

The major problem in manufacturing foil windings is the labor-intensive handling of the place where the foil is connected to the contacts of the coil former. Also foils can be enameled as wires, but it is again a manufacturing problem for the contacts.

4.1.3 Wires with Rectangular Cross Section

Wires with rectangular cross section are used for high currents. They are preferred in large 50-Hz transformers. The rectangular cross section wires are easier to handle than the square cross section wires. The filling factors of the rectangular cross section wires can be very high, especially if the changes from one layer to another are done in the coil ends. The rectangular

cross section wires have enamel insulation or combined glass-fiber epoxy insulation.

4.1.4 Litz Wires

Litz wires are used in order to reduce the eddy currents at high frequencies. A Litz wire contains from 4, 7, and so on to several hundreds of strands, which are insulated from each other. The strands are assembled in groups of strands. Every group is insulated a second time as a whole by a woven texture or a foil. For typical numbers and diameters, see Appendix C3 at the end of the book.

The advantages of the Litz wires are lower high-frequency losses and easier bending compared to the full wires. One of the disadvantages is a low filling factor, as the strands in the wires are small and the insulation takes more space. Another disadvantage is the low thermal conductivity of Litz wire wound winding.

The insulating material of the Litz wires can usually be removed by a high soldering temperature. Indeed, it is not practical to remove the insulation of each strand. But this manipulation can reduce the available insulation class for the Litz wires. However, in practical cases often the coil former is the limiting factor with respect to the insulation temperature requirements.

4.2 Wire Length

The wire length considered in this section is derived for a round wire wound component. For foil wound and rectangular cross section conductors the results are nearly the same.

4.2.1 Circular Coil Formers

The wire length l_w , summed over the number of layers n_v , is

$$l_w = \sum_{i=1}^{n_v} 2\pi r_i n_{h,i} \quad (4.15)$$

where

r_i is the radius of the i th layer

$n_{h,i}$ is the turn number of the i th layer

For an equal number of wires per layer we can write

$$l_w = 2\pi n_h n_v \sum_{i=1}^{n_v} r_i = 2\pi N r_{i,av} = \pi N (r_{\min} + r_{\max}) = N l_{av} \quad (4.16)$$

where

N is the number of the turns

l_{avr} is the mean length per turn (MLT) also l_T is used before

$r_{min} + r_{max} = d_{avr}$ is the average diameter of the winding

According to Equation (4.16), the mean length per turn (MLT) l_{avr} based on the average diameter d_{avr} determines the total length of the wire. Manufacturers often give the average turn length for a full coil former (MLT), see Appendix A at the end of the book. The given MLT value is usually the worst-case value.

If in a winding the last layer contains a lower number of wires than the other full layers, then the total length is somewhat lower.

4.2.2 Rectangular Coil Formers

The wire length of one turn can be approximated by four lines and four quarters of a circle.

Then, the total wire length l_w is determined by the mean length per turn (MLT) l_{avr} :

$$l_w = \pi N (h_{min} + h_{max}) + 2N (a + b) = N (\pi (h_{min} + h_{max}) + 2 (a + b)) = N l_{avr} \quad (4.17)$$

where

a and b are the sides of the coil former

h_{min} and h_{max} are the minimum and maximum available height above the coil former, see Fig. 4.3

If one uses h values based on practical filling factors, normally the length will be somewhat overestimated, as the fitting on the corners is usually hexagonal.

The angles of a rectangular coil former should be rounded. The radius should not be smaller than the radius of the wire; however, the minimum

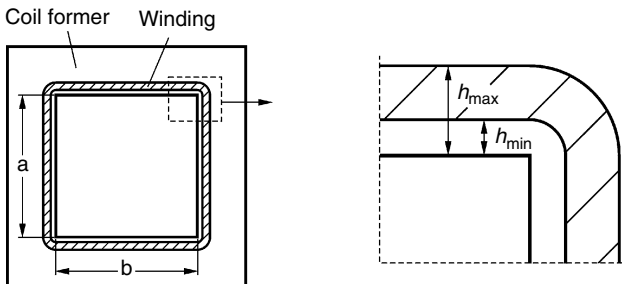


FIGURE 4.3
Determining the total wire length in rectangular coil formers.

radius should be 0.2 mm at least. When winding on a rectangular coil former, one should be aware of the fact that the wires make contact mainly at the four angles, which reduces the filling factor and increases the thermal resistance to the core.

4.3 Physical Aspects of Breakdown

Here we present fundamentals concerning physical aspects of breakdown.

4.3.1 Breakdown Voltage in Air

The breakdown voltage of air for a homogeneous field for a distance d_s is given by [1]:

$$V_s = 2441 \times 10^3 \times \rho d_s + 66.1 \times 10^3 \sqrt{\rho d_s} \quad (4.18)$$

where

V_s is the voltage in [V]

ρ is the relative density of air referenced to 101.3 kPa and 20°C, for water contents of 11 g per m³

d_s is the distance [m]

The relative density of air ρ can be presented by the following expression:

$$\rho = \frac{p}{101.3} \frac{293}{T + 273} \quad (4.19)$$

where

p is the pressure [kPa]

T is the air temperature [°C]

The breakdown voltage of air for homogeneous fields at 20°C, 101.3 kPa, versus the product of density ρ and distance d_s is shown in Fig. 4.4.

Let us consider the dielectric strength.

DEFINITION

The dielectric strength of an insulating material is the maximum value of the electrical field that can be applied without irreversible phenomena, such as a breakdown, in which the voltage can not be applied again. It is the ratio between the breakdown voltage and the distance: V_s/d_s [V/mm].

One can notice that the dielectric strength of air, which is the first derivat of the graph in Fig. 4.4, increases with decreasing distance.

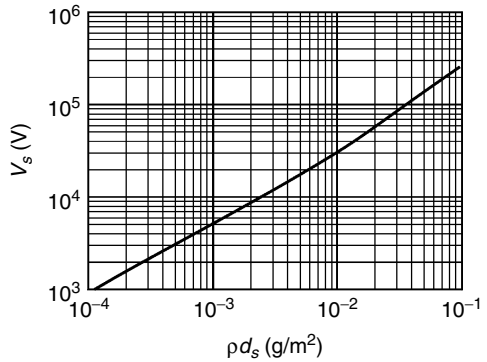


FIGURE 4.4
Breakdown voltage in a homogeneous field in air, 20°C, 101.3 kPa.

REMARKS

1. Equation (4.18) is valid within the range of $10^{-4} \text{ m} < \rho d_s < 0.15 \text{ m}$, for DC or AC voltages with frequency below 1000 Hz.
2. For nonhomogenous fields, the breakdown voltage is much lower, typically a factor 0.1 to 0.3 of the breakdown voltage in the homogeneous field case described by Equation (4.18).

Example

A typical problem is corona discharge in the parasitic air spaces. This can occur between layers of a transformer, inside capacitors, or in other conductor arrangements. To illustrate this we consider the following example.

Two flat conductors are separated by an insulating foil of 0.3 mm and a variable air distance d , see Fig. 4.5. The insulating foil has a breakdown voltage of 15 kV and a relative permittivity $\epsilon_{r,f} = 3$. The field is assumed to be homogenous and the air density is normal. What is the worst case air distance and the worst case peak voltage at which discharge in air occurs?

ANSWER

The breakdown voltage in the air is given by Equation (4.18). The voltage drop in the foil V_f is

$$V_f = V_s \frac{d_f}{d_s} \frac{1}{\epsilon_{r,f}} \tag{4.20}$$

Then, using Equations (4.18) and (4.20), the total voltage V_{tot} is expressed as

$$V_{tot} = V_s + V_f = V_s + V_s \frac{d_f}{d_s} \frac{1}{\epsilon_{r,f}} = \left(2441 \times 10^3 \times \rho d_s + 66.1 \times 10^3 \sqrt{\rho d_s} \right) \left(1 + \frac{d_f}{d_s} \frac{1}{\epsilon_{r,f}} \right) \tag{4.21}$$

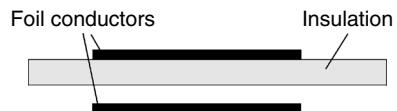


FIGURE 4.5
Flat conductors separated by an insulating sheet and air.

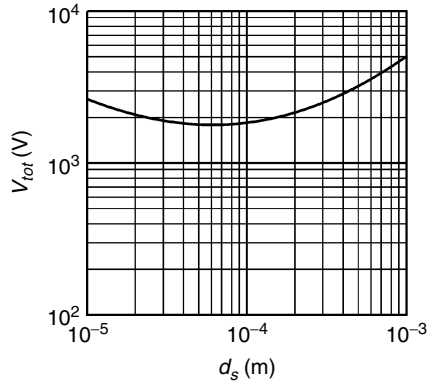


FIGURE 4.6
Total peak breakdown voltage of the example as a function of the distance d_s .

The total breakdown voltage V_{tot} as a function of the distance d_s is shown in Fig. 4.6.

From Fig. 4.6 we find that the worst case distance is about 60 μm , and the worst case total voltage is 1.75 kV peak. At that point, the voltage across the air is only 690 V peak and the E-field in the insulation is 3.55 kV/mm, which is about nine times lower than the breakdown E-field of the foil. The conclusion of the example is that corona discharges can occur much earlier than the breakdown of an insulating foil, even for a homogenous field.

4.3.2 Breakdown Voltage in Solid Insulation Material

Volume Breakdown

The best insulation materials can withstand optimal conditions from a hundred kV/mm up to one MV/mm. Practical materials reach a few tens of kV/mm. Under severe circumstances, such as water trees, at about 1 kV/mm the insulation aging process occurs. Therefore, the maximal theoretically achievable dielectric strength has only small practical importance.

A practical expression for the breakdown voltage in solid materials has been proposed in [2]:

$$V_d = V_r \left(\frac{d}{d_r} \right)^\alpha \quad (4.22)$$

where

V_d is the breakdown voltage [V]

V_r is the reference voltage [V]

d is the thickness of the sample [m]

d_r is reference thickness [m]

α is an exponent, $\alpha = 0.5$ according to [2]

For $\alpha = 0.5$ Equation (4.22) is known as the Tauscher equation [2]. In the same reference the equation is validated on materials such as glass fiber filled polyester, polyamide film (thickness: 0.1–2 mm). According to Equation (4.22),

the dielectric strength is not a constant but decreases when the thickness increases. This seems to be the main reason for high dielectric strength values of foils compared to potting insulators made with similar materials. In fact, they are tested in different thickness and the thickness for foil is lower.

Example

A foil of $d_r = 50 \mu\text{m}$ thickness has a breakdown voltage of 10 kV. What is the breakdown voltage of a $d = 200 \mu\text{m}$ foil made of the same material?

ANSWER

We use Equation (4.22) for $\alpha = 0.5$:

$$V_{d,200} = V_{r,50} \left(\frac{d}{d_r} \right)^\alpha = 10000 \left(\frac{200}{50} \right)^{0.5} = 10000 \times 2 = 20 \text{ kV} \quad (4.23)$$

The expected breakdown voltage is found to be 20 kV and not 40 kV as one would expect if the dielectric strength was constant.

REMARK

In practical cases one has also to consider possible mechanical damage, aging, environment pollution, and so on. To obtain a valuable breakdown property at high thickness, often materials with a high degree of purity are used at high thicknesses or a several layer design is utilized.

For most materials, the dielectric strength is reduced by a factor of 2 in their temperature operating range. The temperature aging can also cause breakdown in a material.

In practice, often a breakdown occurs at quite low values of the electric field. The cause is often mechanical stresses or a defect at the actual border of the insulating material. Typical factors for decreasing the dielectric strength are

- gas enclosures
- conductors with a small radius (point effect)
- foreign particles (metal particles, salt pellets, residue of the polymerization process)
- partial discharges at the surface
- electrical tree or water trees

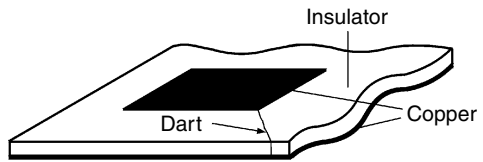
Surface Breakdown Along Solid Insulating Materials

The surface of an insulator usually has a lower dielectric strength compared to the volume itself. Often, the dielectric strength along the surface is lower even than the strength in air. In practical cases one should also take into account external pollution, which additionally decreases the breakdown voltage values. Insulators for all climates are also tested with salt smog.

In quite favorable circumstances, for instance inside instruments and equipment, the breakdown voltage value of 2–3 mm/kV is necessary.

FIGURE 4.7

A dart in the case of asymmetrical conductors insulated with a thin insulator, e.g., the two sides of a PC board.



A very specific case happens with a thin insulator (plate or foil) with asymmetric conductors on both sides, see Fig. 4.7. If the shorter conductor is charged quickly, a dart type discharge occurs at the edge of the conductor (usually at the corner). This dart gives a new field concentration, which continues the process. The dart can propagate over a long distance because a part of the insulation foil is charged like a capacitor. For example, with a 30-kV, 50 Hz supply, a flashover distance of about 20 cm can be reached over a foil of 0.2 mm, and the foil itself remains intact. The effect is also known to occur at the end of a slot in electrical machines. For medium voltage machines, sometimes an intermediate semi-conductive zone is used to smooth the field.

4.3.3 Corona Discharge

In a capacitor with a dielectric sheet and some air distance, the electrical field in the air is ϵ_r times higher than in the dielectric. As the dielectric strength of air is much lower than the strength of the usual dielectrics, it is clear that a first discharge occurs in the air. This happens only once in DC but happens two times during a period in AC. The discharge produces ozone and nitrogen oxides, which attack the insulation material, and a slow degradation process occurs. The effect is known as corona discharge.

Typical places for such phenomena are non-impregnated or partially impregnated wire wound components. The peak-to-peak voltage across two adjacent wires is important. Usually the risk becomes real for voltages of 500 V peak-to-peak between wires.

Partial discharge measurement set-up can be used to evaluate the corona risk.

4.4 Insulation Requirements and Standards

As the physical phenomenon are difficult to be estimated clearly, some safety factor must be included in order to meet the insulation requirements.

4.4.1 Basic, Supplementary, and Reinforced Insulation

Basic standards, such as IEC65 [3], are drawn up especially for insulating materials. A typical standard, which also contains requirements for magnetic components, is the standard for safety of information technology equipment IEC950 [4].

In these standards the following different terms are defined for the kind of insulation: operational (Op) insulation, basic (B) insulation, supplementary (S) insulation, double (D) insulation, and reinforced (R) insulation. In the standard IEC 950 the following definitions are given:

- Op: necessary for proper functional operation
- B: to avoid electrocution
- S: to avoid electrocution when the basic insulation fails
- D: Double insulation equal to: $B + S$
- R: Single insulating system, which properties are equivalent to double insulation

Three different pollution degrees of the environment are specified:

1. environment without dust and humidity
2. common environment, applicable for the most of the equipment
3. environment containing dust or dry dust, which becomes conducting at expected condensation

4.4.2 Standard Insulation Distances

Here we consider the standard insulation distances clearance and creepage distance. The distance through insulation is considered in subsection 4.3.2 and the electric tests are discussed in subsection 4.4.3.

4.4.2.1 Clearance

Clearance is defined as the shortest distance between two conductors, or between a conductive part and the bounding surface of the equipment, measured through air. *Bounding surface* is the outer surface of the electrical enclosure, considered as though metal foil were pressed into contact with accessible surface of insulation material.

Clearance is shorter than the creepage distance, defined later, because air is a better insulator than the surface of the insulator itself. A quite elaborate description of clearance is given in IEC950 [4]. In [Table 4.1](#) we tabulate only a selection of the available data. The insulating distance depends on the mains voltage, on the insulated working voltage, and on the pollution degree.

According to the definition in [4], the *working voltage* is the highest voltage to which the insulation under consideration is, or can be, subjected when the equipment is operating at its *rated* voltage under conditions of normal use. The working voltage in magnetic components is the highest voltage between primary circuits and secondary circuits, between primary circuits and the body of the equipment, and between secondary circuits and the body of the equipment.

In [Table 4.1](#) a few typical cases are given; the distances are in mm, pollution degree 2.

TABLE 4.1

Minimum Clearances for Different Voltages and Insulation Types [4]

Maximum insulated secondary side working voltage [V]		Clearance [mm]					
		Primary voltage between 150 and 300 V RMS (Transient 2500 V)			Primary voltage between 300 and 600 V RMS (Transient 4000 V)		
		Pollution degree 1, 2			Pollution degree 1, 2, 3		
V_{peak}	V_{RMS}	Op	B/S	R	Op	B/S	R
71	50	1.0	2.0	4.0	2.0	3.2	6.4
210	150	1.4	2.0	4.0	2.0	3.2	6.4
420	300	1.7	2.0	4.0	2.5	3.2	6.4
840	600	3.0	3.2	6.4	3.0	3.2	6.4
1400	1000	4.2	4.2	6.4	4.2	4.2	6.4

In some circumstances smaller distances can be tolerated than those tabulated in Table 4.1. Note that pollution degree 3 requires higher insulation distances than the given in Table 4.1. Also, the presence of additional peak voltages from a power electronic converter increases the required distance.

4.4.2.2 Creepage Distance

Creepage distance is the shortest distance between two conductors, or between a conductive part and the bounding surface of the equipment, measured along the surface of the insulation.

In a pure environment (pollution degree 1) the creepage distance can be equal to the clearance distance (generally true for mica, quartz, ceramics). But the required distance may increase a lot for pollution degree 2 or 3.

A number of distances are listed in Table 4.2 for pollution degree 3 and a material susceptible to creepage paths. The creepage paths are tracks where flashover is possible.

Concerning electronic printed circuit boards (PCB) with additional coating, the creepage distance is shorter than the values tabulated in Table 4.2. The PCBs are tested on dielectric strength.

TABLE 4.2

Creepage Distance, Operational, Basic and supplementary Insulation, Pollution Degree 2 and 3, for the material groups IIIa and IIIb [4]

Working voltage* [V]	Creepage distance to the secondary side [mm] PD = 2	Creepage distance to the secondary side [mm] PD = 3
200 to 250	2.5	4.0
250 to 300	3.2	5.0
300 to 400	4	6.3
400 to 600	6.3	10
600 to 1000	10	16

*This is the highest voltage between points, DC or AC RMS value.

4.4.3 Electric Strength Tests

Considerable progress has been made in the development of tests to evaluate insulating materials. Here we give the required voltages for electric strength tests. All voltages mentioned section are RMS values. If the electric strength test is performed with DC voltage, then the tested voltage should be $V_{DC,Test} = \sqrt{2} V_{rms}$. The test voltage is applied progressively during the test. The RMS values of test voltage depending on the working voltage (RMS values) are tabulated in Table 4.3.

For working voltages higher than those tabulated in Table 4.3, one can directly refer to the corresponding standard. During the test no flashover is tolerated (corona is permitted).

If the equipment contains radio interference filters, then it is tested in DC voltage. For practical reasons (portable testers, cost), mostly DC tests are used.

For the operation insulation itself (Op), these tests can be omitted as long as the requirements for clearances and creepage distances are fulfilled.

TABLE 4.3

RMS Values of Test Voltages Depending on the RMS Values of the Working Voltage V_w

	Test voltage, RMS values [V]		
	$V_w = 0$ to 130 V	$V_w = 131$ to 250 V	$V_w = 251$ to 1000 V
Insulation Type: Op	1000	1500	$\cong 114.5 \cdot U^{0.4638}$
Insulation Type: B/S	1000	1500	$\cong 114.5 \cdot U^{0.4638}$
Insulation Type: R	2000	3000	3000

4.4.4 Leakage Currents

Usually, magnetic components have very low leakage currents, typically below 1 μ A in DC or currents corresponding with 0.1 to 10 nF in AC. Due to the presence of high frequencies in power electronics, even a parasitic capacitance of a few nF can result in currents of a few mA. The leakage current is often increased by discharge resistors, voltage surge arrestors, and parallel capacitors.

The total leakage current of information technology equipment in normal operation is limited as follows:

- normal equipment: <0.25 mA
- hand held equipment: <0.75 mA
- movable equipment: 3.5 mA
- stationary, pluggable equipment: 3.5 mA
- stationary equipment, with a special warning label for leakage current: 5% of input current

In industrial equipment higher leakage currents are usually tolerated than those stated previously.

However, one should be aware of

- the EMC regulations and requirements
- the need to reduce the earth currents a sufficient level below the trip level of leakage current protection devices

4.5 Thermal Requirements and Standards

There are a few classes of insulation with respect to the thermal requirements:

- Class A: The maximum temperature in the component is not allowed to exceed 100°C. A high diversity of materials can be used, where each material is of class A.
- Classes E, B, F, H: The materials have to fulfil stringent rules and need a special certification.

REMARK

If one uses self-adhesive systems, one should be aware of the possible electrolytic corrosion action of the adhesive. With thin enamel layers on copper, the adhesive can corrode the copper. The standards that address these issues are VDE 0203 and DIN53489 [5].

4.5.1 Thermal Evaluation of Insulation Materials and Systems

The IEC 216 standard is a guideline for the determination of thermal endurance properties. The maximum operating temperatures of some installation materials are tabulated in Table 4.4 at 25°C ambient temperature. There is a difference between the general standard IEC 85 [6] and the standard for equipment IEC 950 [4].

TABLE 4.4

Maximum Operating Temperatures of Some Insulation Materials at 25°C Ambient Temperature

Installation materials	Maximum allowed temperature [°C]
Rubber, PVC (cord, normal type)	75°C
Rubber	60°C
PE, PVC	70°C
XLPE	90°C
Paper-lead	80°C
Butyl rubber	85°C

Thermal Evaluation of Insulation Systems

The description of an insulating material as being of a particular thermal class does not mean that each material used in a system (or a device) has the same thermal capability. Problems of incompatibility between materials may decrease the appropriate temperature limit of the system below that of the individual materials. On the other hand, in an isolating system the thermal performance of the insulating materials could be increased by the protective character of the other materials used in that system.

Very few test procedures for thermal evaluation are standardized. The IEC 505, IEC 610, and IEC 791 [7] can help as a guideline for the determination of thermal endurance properties.

Responsibility for Selection and Assignment

The manufacturer has the responsibility for the selection of appropriate insulation materials of a component. Only sufficient experience or adequate acceptable tests provide bases for assigning rational temperature limits for the insulation.

4.5.2 Requirements and Standards for Inductive (Magnetic) Modules

We must differentiate between the thermal classification of an inductive module and the terminal classification of the wire of the inductive module. The reason is that the endurance of the insulation of inductive modules is affected by many factors such as temperature, electrical and mechanical stresses, vibration, deleterious atmospheres and chemicals, moisture, dirt, and radiation. This means that an inductive module could have a lower thermal class than the wires used in it. The thermal class of the inductive modules is specified according to the IEC 85 standard [6]. The thermal class of the wires is specified according to the IEC 317 [7] standard.

Certain basic thermal classes are recognized and widely spread throughout the industrial world. These thermal classes are tabulated in Table 4.5.

TABLE 4.5
Thermal Classes for Inductive Modules

Thermal class	Maximum allowed temperature [°C]
Y	90
A	105
E	120
B	130
F	155
H	180
200	200
220	220
250	250

REMARKS

- Temperatures over 250°C should increase by 25°C intervals and corresponding classes should be consistent with that requirement.
- The old class C, used in the past for all temperatures above 180°C, is replaced by the above mentioned thermal classes.
- The tabulated temperatures are the actual temperatures of the insulation and not the temperature rises.
- When a thermal class describes an inductive module, it represents the maximum temperature that is allowed under rated nominal load. The insulation used in the device is subjected to the same standard maximum temperature. Thus, it should have thermal capability at least equal to the temperature associated with the thermal class of the device.

4.5.3 Standards for Wires

The copper diameter d_{cu} of enameled copper wire is standardized. In the U.S. the AWG (American Wire Gauge) [8] is frequently used, please refer to section C2 of Appendix C at the end of the book. The standard widely used in Europe is EN 60317 [7] (old IEC 317), refer to section C1 of Appendix C. The basic description is EN60317-0. There is also a special standard depending on the enamel type, e.g., EN60317-20. In Europe, the E10 mechanical series are used, refer to section C1 of Appendix C. Depending on the required insulation level, a varnish layer is needed, which increases the outer diameter d_o .

The IEC 317 standard specifies also the thermal class of magnet wires. In the standard IEC 317-0 a lot of general requirements for magnet wires are specified, such as bending properties, etc. The major given specifications are bare material diameter, enamel thickness, resistance per meter, and high voltage characteristics. We give some explanations concerning those specifications.

Bare Material Diameter

Not all possible diameters can be ordered. The IEC 317 standard specifies two series of diameters: the R20 and the R40 series. The R20 series are the preferred diameters. The R40 series can be ordered but are the exceptions. However, most of the suppliers of magnet wires have both the R20 and R40 series in their standard program.

NOTE: At additional cost the suppliers can deliver wires with improved (reduced) tolerances on resistance and wire diameter. The actual production techniques are more refined now than they were 10 years ago.

Enamel Thickness

The IEC standard specifies 3 grades concerning the enamel thickness: Grade 1, Grade 2, and Grade 3. For most applications only Grade 1 and Grade 2 are

used. A high grade number means better high voltage characteristics. For example, a wire with a diameter of 0.25 tested at room temperature according to IEC 851 is guaranteed up to 2100 V at Grade 1, up to 3900 V at Grade 2, and up to 5500 V at Grade 3.

Resistance Per Meter

Depending on the wire size, different equations are used to determine the minimum and maximum values of the resistance per meter. However, the nominal value is always calculated with a specific resistance of $\rho_c = 17.24 \times 10^{-9} \Omega\text{m}$ at 25°C.

Thermal Classes of Magnet Wires

The index of the IEC standard describes the enamel type and accordingly the temperature index. The temperature index means that the wire can be used during that specific temperature for at least 20,000 hours.

The most common enamel types are discussed in the following standards:

1. IEC 317–20: This standard describes polyurethane enamel insulation, class 155.
2. IEC 317–51: This standard describes modified polyurethane enamel insulation class, 180.
3. IEC 317–13: This standard describes enamel insulation made of polyester with a polyamide overcoat, class 200.
4. IEC 317–26: This standard describes polyamide enamel insulation, class 200. Although only standardized up to 200°C, all the suppliers guarantee 220°C during 20,000 hours for this enamel wire type.

NOTE: With increasing thermal properties also the chemical resistance is increasing.

In Table 4.6 we give an overview of the maximum operating temperature of a copper wire in normal operating. The temperature is registered by

TABLE 4.6

Thermal Classes for Copper Wires Depending on Thermal Properties of the Insulation

Class	Maximum temperature According IEC 85	Maximum temperature* Resistance method	Maximum temperature** Thermocouple method
A	+105°C	+100°C	+90°C
E	+120°C	+115°C	+105°C
B	+130°C	+120°C	+110°C
F	+155°C	+140°C	+130°C
H	+180°C	+165°C	+155°C

* Resistance method, thermocouple for motors, according IEC 950.

** Thermocouple method for transformers, according IEC 950.

resistance measurement in 25°C ambient temperature. The tolerated temperature by thermocouple measurement is 10°C *lower* in transformers but *equal* to the resistance measurement method for electrical motors. The maximum allowed temperature rise is the temperature value of [Table 4.6](#) after subtracting an ambient temperature of 25°C.

4.6 Magnetic Component Manufacturing Sheet

Often, wrong series or prototypes are made due to a too limited communication between the designer and the manufacturer. The origin of these errors is the common practice to specify only the number of turns and the wire diameter for small 50 or 60 Hz transformers. But this information is not sufficient for power electronics magnetic components!

Here we consider some important items to be included in magnetic component design information.

Coupling

Often errors are made in the coupling between windings. The coupling is defined when the starting pin and the stop pins are specified, assuming that the same winding direction is maintained.

Air Gaps

Usually, first breadboard designs are made with a spacer, as it is not easy to cut ferrites at that level. However, the series manufacturing is normally done with a center gap. Therefore, it is not sufficient to specify just the total gap length. Unpunctuality in these specifications generates inductance errors, close to a factor of 2, refer to [Chapter 8](#) for more details. In fact, the designer wants to realize a given permeance (A_L) value by creating an air gap. At low air gaps, the permeance measurement is more accurate than the measurement of the air gap, so it is advisable to specify the A_L value or to measure the final component.

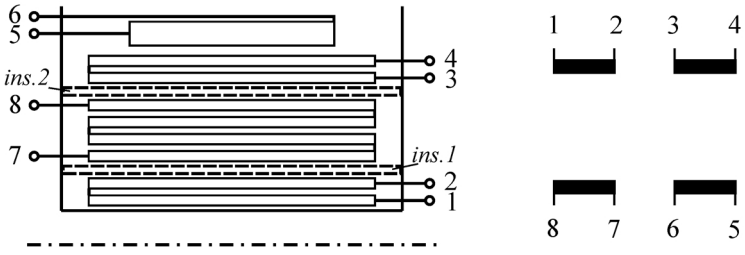
Impregnating

Another important fact is impregnating a magnetic component. The performance of a transformer is not the same if it is impregnated. Impregnation increases the lifetime of the insulation but also the parasitic capacitance, which may not be suitable. The most used materials for impregnation are polyester, or epoxy resins. Recently, silicones are also used for impregnation. The advantage of the latter materials is the flexibility and the high maximal operating temperature. The disadvantage is the price and the lower resistance to chemicals.

Magnetic component manufacturing sheet

Company:
Reference:
Date (dd/mm/yy): /.../.../.../
Person:

Core type:	E20/10/6
Coil former	8 pins, hor.
Core material	3F3....
Centre gap, [mm]	0.1 mm *
Spacer, [mm]: *
A_L value, [nH]: *
*only one position filled in	



a) Cross section view of the coil b) Pin configuration, seen from former with windings and insulation bottom

Magnetic Component Manufacturing Table:

Winding number	Start Pin	End Pin	Number of turns	Wire diameter* thickness [mm]	Insulation type	Remarks
1	1	2	50	0.15	Grade 2	Secondary winding
Insulation 1			2	0.1	Class B	sheet
2	7	8	100	0.15	Grade 2	Primary winding
Insulation 2			2	0.1	Class B	sheet
3	3	4	50	0.15	Grade 2	Secondary winding 2
4	5	6	6	0.35	Grade 2	Sense winding

*This is the diameter of the bare copper

Impregnation: yes/no type:

Remarks: white dot at a pin 1

FIGURE 4.8
Magnetic component manufacturing sheet.

Partially Filled Layer

A layer that is partially filled can be realized in different ways. Thus, the different realizations have impact on the total performance of the component. The designer should use some of the following relevant aspects to specify the right manufacturing:

- winding on one side of the coil, which is the easiest way of winding
- spread along the winding width, thus low leakage inductance with other layers
- avoiding to wind in the middle, thus decreasing eddy current losses in the presence of an air gap

Manufacturing sheet

Here we give an example of a magnetic component-manufacturing sheet. It contains the aforementioned aspects, such as coupling, air gaps wire diameters insulation type and thickness, core material and coil former type see [Fig. 4.8](#).

References

- [1] Segur, P., *Techniques de l'ingénieur*, Gaz Isolants, Paris, France, D 2531-10, 6, 1990.
- [2] Salmon, E.R., Dielectric strength of an insulation material—Is it a constant? *IEEE Electrical Insulation Magazine*, Vol. 5, No. 1, Jan/Feb 1989.
- [3] IEC General, Metrology and measurement. Physical phenomena, Other standards related to electricity and magnetism, Catalogue of IEC publications 1997, International Electrotechnical Commission, 17.220.99, Bureau Central de la CEI, Geneva, Switzerland, 1991.
- [4] IEC 950, Safety of information technology equipment, including electrical business equipment, 2nd ed., Bureau Central de la CEI, Geneva, Switzerland, 1991.
- [5] DIN, Deutsches Institut für Normung, Berlin, Germany, www.vde-verlag.de
- [6] IEC 85, Thermal evaluation and classification of electrical insulation, Bureau Central de la CEI, Geneva, Switzerland, 1991.
- [7] International Electrotechnical Commission, Switzerland, www.iec.ch
- [8] American National Standards Institute, Washington, DC, www.ansi.org

5

Eddy Currents in Conductors

5.1 Introduction

Eddy current effects in conductors were recognized at an early time. At the end of the nineteenth century, it was known that a conductor of a (telegraphic) coaxial cable has an increased AC resistance for higher frequencies and that the inductance reduces with frequency [1]. The method that was applied used mathematical series and the derivative of the current. This approach is different from the methods we use now, but the result was correct.

Eddy currents have long been recognized in electrical machines as well. For example, the starting torque in squirrel cage induction motors is improved by a rotor resistance increase and inductance decrease caused by the eddy currents. In large machines and transformers, eddy currents have a big impact on the process of manufacturing coils because of efforts to avoid them, for example, paralleling wires and R obel bars.

Although some physical properties were known before, the real breakthrough of ferrites came after 1945 in the Netherlands [2]. Using ferrites, the magnetic components could be made much smaller since the main flux path was not going through the conductors and, thus, most of the eddy currents could be avoided. In classical electronics, more attention was given to the total core losses and the Q-factor than to a detailed analysis of eddy current losses [3].

Current Power Electronics Needs

Because of improvements in semiconductors and soft switching topologies, much higher switching frequencies are now possible, compared to 20 years ago. As a result, most of the actual designs of magnetic components in power electronics are highly influenced by eddy currents.

Skin Effect

At high frequencies, the major part of the current flows in a thin outer layer (skin) of the conductor, so the phenomenon is called *skin-effect*.

Proximity Effect

The effect by a transverse field is called *proximity effect*. The eddy current losses in wires close to each other are much larger than in a free wire or the central wire in a coaxial arrangement. A similar increase in losses appears when magnetic materials are close to conductors. The major part of losses in wires can be explained by the presence of a transverse field. This allows simplified approximations such as in [Chapter 2](#).

Air Gap Effects

The most intense losses appear when the flux is concentrated by a magnetic circuit with an air gap and some conductors are close to that air gap. This is often the case with gapped inductors and transformers. If one does not pay special attention to this phenomenon, it often results in a local melting of the coil former.

Eddy Current Losses in Conductors

In general, other field patterns are also possible and we can talk about eddy currents or about *eddy current losses*. A way to reduce the eddy currents is using Litz wire. The word *Litz* is derived from the German word *Litzendraht* and refers to wire consisting of a number of separately insulated strands twisted or bunched together such that each strand tends to take all possible positions in the cross section of the entire conductor; it is also called *bunched wires*.

The presence of eddy currents is a linear effect. Voltage and current remain proportional and active and reactive power losses are quadratic with currents or fields. The complex impedance functions related to eddy currents are linear and passive. Thus, they contain neither poles nor zeroes in the right half plane. The mathematical functions associated with them are analytical (minimum phase impedance function). This means that Bode laws are applicable and that real and imaginary parts are related to each other. For example, neglecting capacitive effects, if the resistance increases with frequency, then the inductance must decrease with frequency.

Only a few exact analytical explicit solutions of eddy currents are known and we give some of the most useful ones. Although they are not always that simple, they are worthwhile and give automatically analytical functions (both real and imaginary part of the impedance) when the complex formulation is used. Using modern mathematical programs (MathCAD, Maple, Matlab, Mathematica) makes the implementation of the approach easier.

Many approximations are possible, such as low frequency approximation, high frequency approximation, Quadrature of the circle method of Dowell [4], splitting in orthogonal components. The finite element methods and finite difference methods can also be seen as approximations, as they discretize the space and solve an idealized local field problem. We observe a good interaction between finite element and classical methods. The knowledge

of the classical theory can reduce the amount of cases for simulation for one side and the finite elements methods can solve geometries and problems not solvable by analytical solutions for the other side.

We propose a *wide frequency approximation*, which starts from analytical solutions of special cases and is finetuned by finite elements. The focus is on the losses (the real part of the power). The imaginary part, corresponding to the inductance, is easier to measure so that modeling is less important.

Practical experiments are often difficult; if the design is well done, the eddy current losses are only a fraction of the total losses and they have to be separated from the losses of magnetic materials and the temperature dependence of copper and core losses. With the right approximations, very fast and quite accurate calculations can be done. This allows using such an approach in an optimizing design, where many cases can be calculated in a short time.

Mathematical derivations are given in the Appendix at the end of this chapter.

5.2 Basic Approximations

In order to avoid extensive mathematical computation and to improve the intuitive understanding, some approximations of the effects are shown.

An important quantity in eddy currents theory is the penetration depth δ given as

$$\delta = \sqrt{\frac{2\rho_c}{\mu\omega}} \quad (5.1)$$

where

$\omega = 2\pi f$ is the frequency of the applied magnetic field

μ is the permeability of the material (for copper $\mu \cong \mu_0$)

ρ_c is the electrical resistivity of the conducting material (copper) we use

$\rho_c = 23 \times 10^{-9} \Omega\text{m}$ at 100°C ; $\rho_c = 17.24 \times 10^{-9} \Omega\text{m}$ at 25°C

The ratio between a characteristic dimension of the conductor (the diameter for round wires) and the penetration depth for the corresponding frequency is a parameter for estimation if low or high frequency approximations can be done. In Fig. 5.1 the penetration depth is shown as a function of frequency.

5.2.1 Low Frequency Approximation

In this type of approximation, the field of the induced eddy currents is neglected. Thus, the basic field is assumed to penetrate completely through the conductors. This simplifies the mathematical solution, as the induced

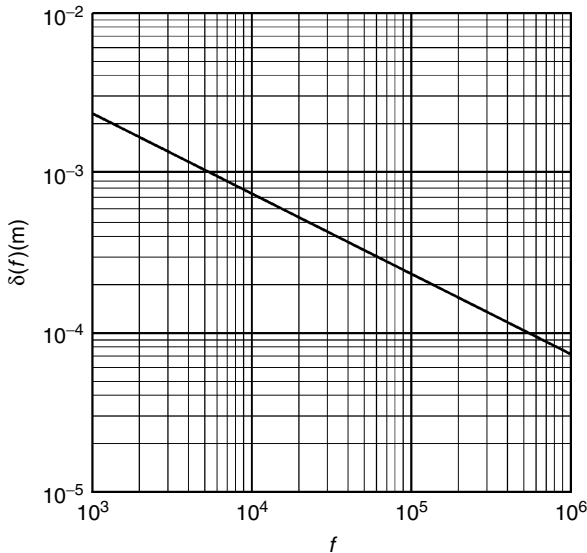


FIGURE 5.1

Penetration depth δ as a function of frequency for copper conductors, $\rho_c = 20 \times 10^{-9} \Omega\text{m}$, $T \approx 66^\circ\text{C}$.

current can be computed with the aid of the DC field pattern. If an analytical exact solution for all frequencies exists, the low frequency approximation will give the first term in the Taylor expansion (series). In power electronic components, a large part of the impedance is not influenced by eddy currents, so that most of the time, the change in inductance can be neglected. The low frequency approximations are usually applicable (lower than 5% on the resistance increase) if the largest dimension of the conductor is lower than 1.6 times the penetration depth. If a low frequency approximation is allowed, the losses can be represented by a parallel resistor to the considered type of inductance. This approach simplifies greatly the circuit modeling.

It should be emphasized that the statement "The low frequency eddy current approximation is allowed" does not mean at all that the eddy current losses are low!

5.2.2 High Frequency Approximation

If an AC H-field is applied parallel to the surface of a plane conductor, this field will be attenuated along the depth in the conductor. If the thickness of the conductor is much larger than the penetration depth δ , the **losses** in the conductor can be associated with an equivalent thin layer with thickness δ , which has a fictitious homogenous current not affected by eddy currents. The equivalent inductance would be explained by an equivalent fictitious increase of the area of the air by $\delta/2$. *Note the difference: for resistive part δ is used and for the inductive part, $\delta/2$!*

For an infinite frequency, no field is penetrating into the conductor. This can be simulated by taking permeability equal to zero inside the conductor or stating that the field must be parallel to the surface (Dirichlet boundary condition in numerical problems).

5.2.3 Superposition of Losses

The superposition of fields can be done in eddy current problems, as the phenomenon is linear. However, in general, for the calculation of the losses, the superposition of losses from different field types is not allowed. Nevertheless, simply adding losses of different field types is an interesting feature.

Let us consider the following calculation of an average power over a conductor cross section:

$$P = \frac{l_c}{T} \int_{t,ref}^{t,ref+T} \int_{conductorsection} \rho (J_a(x, y, t) + J_b(x, y, t))^2 dx dy dt \quad (5.2)$$

$$P = \frac{l_c}{T} \int_{t,ref}^{t,ref+T} \int_{conductorsection} \rho [J_a(x, y, t)^2 + J_b(x, y, t)^2 + 2J_a(x, y, t)J_b(x, y, t)] dx dy dt \quad (5.3)$$

where

$J_a(x, y, t)$ is the current density generated by a field $H_a(x, y, t)$
 $J_b(x, y, t)$ is the current density generated by a field $H_b(x, y, t)$

To add the losses without taking into account mixed products, it is sufficient that the following integral vanishes:

$$\int_{time} \int_{conductorsection} J_a(x, y, t) J_b(x, y, t) dx dy dt = 0 \quad (5.4)$$

The usual reasons and conditions that make the superposition of losses allowed are as follows:

- The wire and the field problem have a symmetry axis; one current density is even (or constant) and the other current density is odd across that symmetry axis.
- Two different frequencies are applied.
- The current densities of the same frequency have 90° phase difference. This can be the case with a magnetizing field and a leakage

field in a transformer if the transformer has a low leakage inductance and the load is resistive.

- In general, when the functions of the current densities in space are orthogonal.

If the superposition of losses is applied where it is not allowed, the losses can range from zero up to two times the expected ones.

5.2.4 Wide Frequency Approximation

If a low frequency solution and a high frequency solution exist, the transition between low and high frequency is usually smooth and even if no exact solution exists, still some approximations can be used. A way to finetune the approximations is to use finite element solutions or known analytical cases.

5.3 Losses in Rectangular Conductors

Here only some major highlights are shown; the mathematical derivation and more details can be found in Appendix 5.A.1 at the end of this chapter.

5.3.1 Exact Solution For a Current Carrying Rectangular Conductor in a Transverse Field

The conductor is placed between two walls of magnetic material with infinite permeability (Fig. 5.2,a). All field lines are perpendicular to the walls, which allows a one-dimensional solution. The case is also equivalent to a field pattern, where several conductors are present between walls of a magnetic material with infinite permeability (Fig. 5.2,b) or a large (infinite) number of conductors are placed in a layer (Fig. 5.2,c).

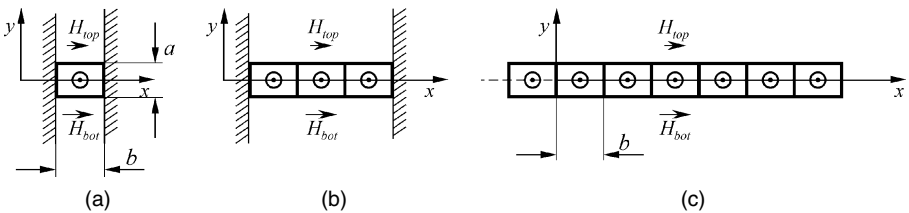


FIGURE 5.2

Rectangular conductor subjected to a horizontal field, in parallel to the layer: a) Single conductor; b) Several conductors; c) Many conductors.

Note that we do not look at the field outside the conductors. This means that the fictitious current return path can be thought of just as a thin layer above and below the conductor. The choice of the place of the return path does only influence the inductive part in the one-dimensional approach.

We consider the complex apparent power given as

$$S = P - jQ = VI^* \quad (5.5)$$

where

P is the real power

Q is the reactive power

I^* is the complex conjugate of the current

As found in Appendix 5.A.1, the losses of a rectangular conductor are

$$S(s) = 2bl_c Z_0(s) \left(\left| \frac{H_{top} - H_{bot}}{2} \right|^2 \coth\left(\gamma(s) \frac{a}{2}\right) + \left| \frac{H_{top} + H_{bot}}{2} \right|^2 \tanh\left(\gamma(s) \frac{a}{2}\right) \right) \quad (5.6)$$

where

l_c is the length of the conductor

a is the thickness of the conductor, see Fig. 5.2

b is the width of the conductor, see Fig. 5.2

$\sigma = 1/\rho$ is the specific conductivity of the conductor

ρ is the specific resistivity of the conductor (for copper:

$$\rho = 17.3 \times 10^{-9} (1 + 0.0039(T - 25))$$

T is the temperature in °C

$$s = j\omega = j 2\pi f$$

H_{top} is the H -value at the top of the conductor in the x -direction

H_{bot} is the H -value at the bottom of the conductor in the x -direction

The following quantities, impedance, propagation function, and penetration depth, are defined as

$$Z_0(s) = \left(\frac{s\mu}{\sigma} \right)^{1/2} = \sqrt{j} \sqrt{\frac{\omega\mu}{\sigma}} = \frac{1+j}{\sqrt{2}} \sqrt{\frac{\omega\mu}{\sigma}} = \frac{1+j}{\sigma\delta(\omega)} = \frac{1-j}{2} j\omega\mu\delta(\omega) \quad (5.7)$$

$$\gamma(s) = (s\mu\sigma)^{1/2} = \frac{1+j}{\sqrt{2}} \sqrt{\omega\mu\sigma} = \frac{1+j}{\delta(\omega)} \quad (5.8)$$

$$\delta(\omega) = \sqrt{\frac{2}{\omega\mu\sigma}} = \sqrt{\frac{2\rho}{\omega\mu}} \quad (5.9)$$

The aforementioned type of formulation, Equation (5.6), is interesting by its symmetry. The formulation is quite general as not only current in the conductor but also other applied fields are allowed. In the appendix, more

details and other formulations are given. We can rewrite Equation (5.6) using the current I in the conductor and the average transverse field H_{av} :

$$S(s) = 2bl_w Z_0(s) \left(\left(\frac{|I|}{2b} \right)^2 \coth \left(\gamma(s) \frac{a}{2} \right) + |H_{av}|^2 \tanh \left(\gamma(s) \frac{a}{2} \right) \right) \quad (5.10)$$

$$H_{av} = \frac{H_{top} + H_{bot}}{2}, \quad H_{top} - H_{bot} = I/b \quad (5.11)$$

The advantage of the previous formulation is that no phase relationship between the average transverse field and the current must be known (no time orthogonality required), as Equation (5.10) and Equation (5.6) use orthogonal functions in space.

The contribution of the air between the conductors to the apparent power is given as

$$S_{air} = s\mu_0 bl_c |H|^2 \Delta y \quad (5.12)$$

For m superimposed layers carrying the same current, $H = 0$ below the lowest one, the impedance can be calculated compared to the DC resistance:

$$Z = R_0 \frac{1+j}{2} \frac{a}{\delta(\omega)} \left(\coth \left(\frac{1+j}{2} \frac{a}{\delta(\omega)} \right) + \left(\frac{4m^2 - 1}{3} \right) \tanh \left(\frac{1+j}{2} \frac{a}{\delta(\omega)} \right) \right) + \frac{j\omega\mu l_c}{b} \sum_n a_{m,air} m^2 \quad (5.13)$$

The equation is also valid for $m = 0.5$. This is the case where the magnetic field is zero in the middle of the each conductor of the layer. The case is referred to as a *half layer*.

The last term at the right side of Equation (5.13) (the sum) gives the contribution of the field between the conductors.

5.3.2 Low Frequency Approximation

5.3.2.1 Current Carrying Conductor Without Transverse Field

For a low frequency approximation, the exact solution can be written using Taylor expansion. The even terms with respect to the frequency ω contribute to the resistance. The first term is the DC resistance; the third term gives the low frequency eddy current part. The first and third terms are

$$R(\omega) = \frac{l_c}{ab\sigma} \left(1 + \frac{a^4 \omega^2 \mu^2 \sigma^2}{720} \right), \quad R_{DC} = R_0 = \frac{l_c}{ab\sigma} \quad (5.14)$$

The odd terms with respect to ω present the inductance. Here we give only the first term:

$$L = \frac{1}{12} \frac{\mu l_w a}{b} \quad (5.15)$$

The second term in Equation (5.14) is quadratic with the frequency, so this type of loss is quadratic with the derivative of the current. These results can also be obtained assuming that

- the field fully penetrates the conductor and generates an e.m.f.
- the average current density generated by eddy currents is always zero; if it is not so, the constraint of the applied current is not maintained

Using Appendix 5.A.1, more terms in the expansion can be calculated. However, the exact equation is easier to apply than adding a number of terms. Compared to the exact solution, Equations (5.14) and (5.15) give a higher inductance and higher resistance for increasing frequencies.

5.3.2.2 Conductor Without Current in a Transverse Field

The losses $P_{tr,jf}$ in a rectangular conductor without current with fields in the x and y directions is given by

$$P_{tr,jf} = \frac{l_c}{12} \mu^2 \omega^2 \sigma \left(a^3 b |H_{av,x}|^2 + a b^3 |H_{av,y}|^2 \right) \quad (5.16)$$

where

$P_{tr,jf}$ are the losses using the low frequency approximation

$H_{av,x}$ is the average transverse field in x direction

$H_{av,y}$ is the average transverse field in y direction

No DC loss is present in this case. In the low frequency approximation for m superimposed layers, the power loss expressed by the DC resistance is

$$R = R_0 \left(1 + \frac{a^4 \omega^2 \mu^2 \sigma^2}{720} + \frac{a^4 \omega^2 \mu^2 \sigma^2}{48} \frac{4m^2 - 1}{3} \right) \quad (5.17)$$

The LF inductance for m superimposed layers is

$$L = \frac{\mu l_c a}{3b} m^2 + \sum_m \frac{\mu l_c a_{m,air}}{b} m^2 \quad (5.18)$$

The first term in Equation (5.18) originates in the energy of the average static field in the conductor. The second term in Equation (5.18) is the contribution of the inductance of the air between the conductors.

5.3.3 High Frequency Approximation

5.3.3.1 Ideal Case

The eddy currents generate a field that tends to neutralize the field inside the conductor. The losses are equivalent to the conduction process in a thin layer of the conductor on both sides of the conductor, as the problem is symmetrical. Using Equation (5.13), the impedance of a conductor without transverse field is presented:

$$Z(j\omega) = \frac{R_0 a}{2\delta(\omega)}(1+j) \quad (5.19)$$

where

R_0 is the DC resistance of the series connection of the conductors

This result corresponds to a conducting layer with thickness δ on the top and bottom of the conductor. The imaginary part (reactance) equals the resistive part and both increase with the root of the frequency.

Using Equation (5.13), the HF approximation of the resulting impedance for m superimposed layers is

$$Z(j\omega) = \frac{R_0 a}{\delta(\omega)}(1+j) \left(\frac{2m^2+1}{3} \right) \quad (5.20)$$

This result can also be obtained using the equivalent currents in the thickness of the penetration depth shown in Fig. 5.3.

We can denote by F the sum of the squares of the current ratio of the upper and lower surface current compared to the conductor current: $F = (I_{bot}^2 + I_{top}^2)/I^2$. Table 5.1 presents the increase in eddy current losses due to the high frequency effects.

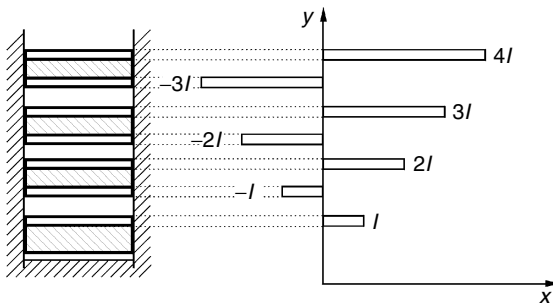


FIGURE 5.3

High frequency approximation of series connected wires in a slot with current I . The currents shown flow in an equivalent penetration depth.

TABLE 5.1

The Increase in Eddy Current Losses Due to the High Frequency Effects

Conductor number m :	1	2	3	4	5
$F = (I_{\text{bot}}^2 + I_{\text{top}}^2)/I^2$	1	1 + 4	4 + 9	9 + 16	16 + 25
ΣF^2	1	6	19	44	85
$m(2m^2 + 1)/3$	1	6	19	44	85

REMARK

The DC resistance is increased by a factor of m while using m layers.

5.3.4 Spaced Conductors

5.3.4.1 Classical Approach

The approximation is derived under the condition that b' is still small compared to a and to the penetration depth δ , so that the H -field is still almost horizontal.

Conductors do need insulation, which corresponds to a minimum distance between the conductors. For conductors spaced with air or insulation, the classical approach is to enlarge the conductor in the x -direction to fill the air and to adapt the conductivity to get the same DC resistance. In this way the penetration depth and other quantities depending on the conductivity are changed. The following terms are used, see Fig. 5.4:

- a is the thickness of the conductor
- b is the width of the conductor
- b' is the slot width or distance between center lines of the conductor
- b/b' is the (horizontal) filling factor

The penetration depth is then defined as

$$\delta'(\omega) = \sqrt{\frac{2\rho b'}{\omega\mu b}} \tag{5.21}$$

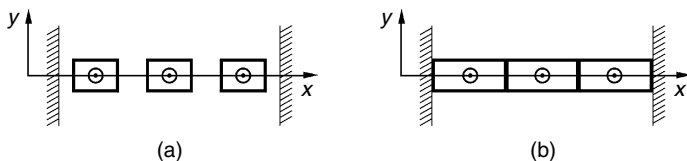


FIGURE 5.4

Spaced conductors. a) Symmetrical arrangement of conductors; b) enlarging the conductors in the x -direction.

The adapted characteristic impedance and the propagation function can be written as

$$Z'_0(s) = \left(\frac{s\mu}{\sigma'} \right)^{1/2} = \sqrt{j} \sqrt{\frac{\omega\mu}{\sigma}} \sqrt{\frac{b}{b'}} = \frac{1+j}{\sqrt{2}} \sqrt{\frac{\omega\mu}{\sigma}} \sqrt{\frac{b}{b'}} \quad (5.22)$$

$$\gamma'(s) = (s\mu\sigma')^{1/2} = \frac{1+j}{\sqrt{2}} \sqrt{\frac{\omega\mu\sigma b}{b'}} = \frac{1+j}{\delta'(\omega)} \quad (5.23)$$

At decreasing b/b' and increasing frequency the conditions are not satisfied, but for $a = b$ and $b/b' > 0.5$ the approximation is still feasible. Equations (5.21), (5.22), and (5.23) can be substituted in the exact solutions presented by Equations (5.6), (5.10), and (5.13). By this substitution, the exact equations become only wide frequency approximations. The exact problem with several conductors is a two-dimensional problem and it is not easily solved analytically.

This type of method was first applied in slots of electrical machines, where rectangular conductors are placed vertically in a slot, as they are easily inserted in this way. The horizontal dimension is smaller than the penetration depth, and the distance between the conductors is low. Under these conditions, the approach is a good approximation.

5.3.4.2 Low Filling Factor and High Frequency

The previous conditions are not always present in practical arrangements.

At low filling factors, which are close to a standalone conductor, vertical fields are also present and Equation (5.10) does not contain all losses, thus underestimating the total losses. In Equations (5.22) and (5.23), if b/b' is sufficiently low, the losses tend to zero, which does not correspond to the reality of standalone conductors.

This conclusion shows that the classical approach leads to erroneous results at low filling factors, as it neglects the vertical field components. The best approach is to use finite element methods to solve problems with rectangular conductors at low filling factors. If by some means, the top, bottom, and side H -fields can be estimated, Equation (5.6) can be extended and quite good approximations can be obtained.

5.4 Quadrature of the Circle Method for Round Conductors

We called the next method the *Quadrature of the circle* after a historical mathematical problem that couldn't be solved: to construct a square with the same surface as a circle by means of a ruler and a pair of compasses. Since we have a solution for rectangular conductors, if we can convert a circle to a square, we could use the already derived method to approximate the eddy current losses. This method is often referred to as the *Dowell method*.

The way of presenting here is slightly different from the *classical Dowell*, as we prefer using orthogonal functions, since the superposition of losses can easily be applied. An improvement of that method is possible by using other functions. We call it *improved quadrature of the circle method (IQOC)*.

5.4.1 Equivalent Rectangle Principle

Following the principle of equivalent rectangles, the original round conductor is approximated by a square with the same surface, Fig. 5.5 η is the horizontal filling factor, $\eta = \frac{d}{b'}$. This assumption allows maintaining the same DC losses while using the same resistivity. To obtain the equivalent square, we use

$$a = b = \sqrt{\pi r^2} = \sqrt{\frac{\pi d^2}{4}} = \frac{\sqrt{\pi}}{2} d \quad (5.24)$$

The square can be enlarged to a rectangle, which fits the available area, Fig. 5.5, such as in the rectangular conductors with space to the core material (the slot).

5.4.2 Adapted Equations

The equations for the impedance of m superposed conductors can be reformulated. We introduce directly the (copper) diameter of the wire d . For the contribution of air between the layers, the distance between the conductors has to be increased with the difference of a and d .

The conductor impedance Z_{cond} can be presented as

$$Z_{cond} = R_0 \frac{1+j}{2} \frac{\sqrt{\pi}}{\delta'(\omega)} d \left(\coth \left(\frac{1+j}{2} \frac{\sqrt{\pi}}{\delta'(\omega)} d \right) + \left(\frac{4m^2 - 1}{3} \right) \tanh \left(\frac{1+j}{2} \frac{\sqrt{\pi}}{\delta'(\omega)} d \right) \right) \quad (5.25)$$

DC resistance and local field loss \uparrow transverse field loss \uparrow

The adapted penetration depth is

$$\delta'(\omega) = \sqrt{\frac{2\rho}{\omega\mu} \frac{b'}{d} \frac{2}{\sqrt{\pi}}} \quad (5.26)$$

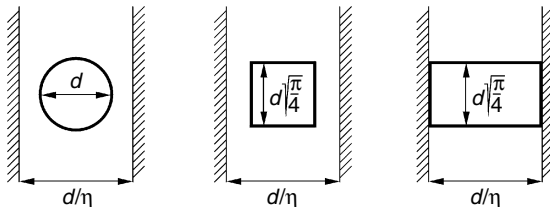


FIGURE 5.5
A circle, the equivalent square, and the equivalent rectangle.

The air impedance Z_{air} is given as

$$Z_{air} = \frac{\omega \mu l_c}{b} \sum_m \left(a_{m,air} + d \frac{\sqrt{\pi}}{2} \left(1 - \frac{\sqrt{\pi}}{2} \right) \right) m^2 \quad (5.27)$$

Then, we have

$$Z = Z_{cond} + Z_{air} \quad (5.28)$$

Those equations can be reformulated using the original penetration depth again and showing the dependency on $\eta = d/b'$ in a separate function. This simplifies the equation as the real penetration depth is used and not something dependent on both frequency and η .

$$g_D(\eta) = \left(\frac{\pi}{4} \right)^{3/4} \eta^{1/2} \quad (5.29)$$

$$Z_D(f, \eta) = R_0 \frac{1+j}{2} \frac{g_D(\eta)d}{\delta(f)} \left[\coth \left(\frac{1+j}{2} \frac{g_D(\eta)d}{\delta(f)} \right) + \left(\frac{4M^2 - 1}{3} \right) \tanh \left(\frac{1+j}{2} \frac{g_D(\eta)d}{\delta(f)} \right) \right] \quad (5.30)$$

5.4.3 Low Frequency Approximation

For low frequency approximation, using the equations of Appendix 5.A.1, the resistive part $R_{ac,lf}$ of the impedance of m superposed round conductors is presented as

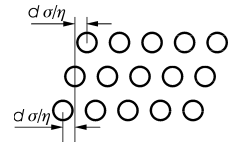
$$\frac{R_{ac,lf}}{R_0} = 1 + \frac{1}{180} \left(\frac{\omega \mu \sigma}{2} \right)^2 \frac{\left(\frac{\pi d^2}{4} \right)^3}{b'^2} + \left(\frac{4m^2 - 1}{3} \right) \frac{1}{12} \left(\frac{\omega \mu \sigma}{2} \right)^2 \frac{\left(\frac{\pi d^2}{4} \right)^3}{b'^2} \quad (5.31)$$

The transverse field part, the third term in Equation (5.31), can also be calculated directly in a homogenous field, as in low frequency, the eddy currents do not influence the transverse field.

REMARKS CONCERNING EQUATION (5.31)

- It can be shown that Equation (5.31) overestimates the low frequency losses of a pure transverse field by a factor $\pi/3$ in that case.
- For the local field losses (the second term) the deviations are larger than $\pi/3$. Equation (5.31) indicates that those losses tend to zero for large b' values, which is not true for local eddy current losses, as a free wire also has losses.

FIGURE 5.6
 Conductor arrangement for several layers,
 variable shift of wires of different layers.



For low frequency approximation, we derive accurate 2-D solutions (see next sections). This permits us to verify the accuracy of Equations (5.25), (5.30), and (5.31) for low frequency. We checked a transformer design with primary and secondary windings with opposite currents and the same wire diameter. The (vertical) distance between the layers equals the horizontal distance, and it is given as the copper diameter d divided by η (Fig. 5.5). The wires in Fig. 5.6 are shifted to make an average between the different arrangements (square and hexagonal fitting). Analyzing square fitting only, results in much more loss at lower filling factors. However, this worst case is not realistic, as actual coils are not wound in square fittings. To compare different arrangements, we use a three-field method that has a high accuracy for low frequency problems. This method is discussed later in the chapter.

Accuracy of Dowell Method

From the comparison in Fig. 5.7 one can see that the Dowell method seriously underestimates the losses at low filling factors (low values of η). At low filling factors the approximation is better for a higher number of layers m .

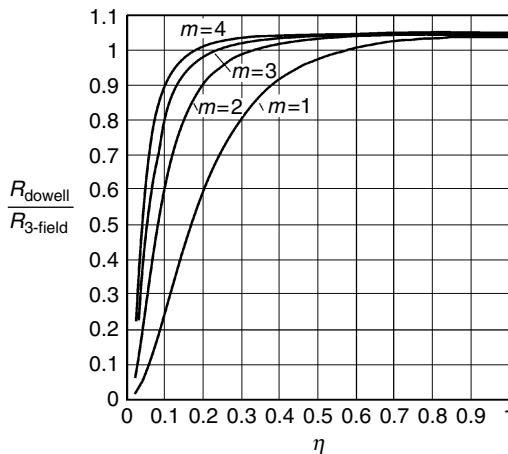


FIGURE 5.7
 Dowell method low frequency conductor resistance increase divided by the resistance found by the low frequency three field method, see section 5.7.2 (the method is accurate for low frequency cases), m is the layer number. The conductors are shifted.

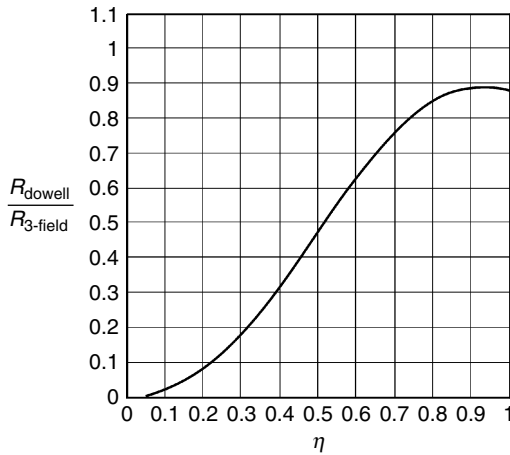


FIGURE 5.8

Dowell method low frequency conductor resistance increase divided by the resistance found by the low frequency three field method for a half layer ($m = 0.5$).

The reason is that the approximation of the local field in the Dowell presentation, Equation (5.30), is not accurate enough. The quite good matching of the single layer at high filling factor is because of the combination of overestimating the transverse field and underestimating the local field.

The lack of accuracy of the local field estimation is more noticeable if a half layer is considered: the losses of a primary layer that is sandwiched by two secondary layers. In this case $m = 0.5$. One can see that for this case, the third term in Equation (5.30) is zero.

If we compare this solution again with the accurate three-field method, we have the result shown in Fig. 5.8.

From Fig. 5.8 we see that *in the Dowell method, the low frequency local field loss is underestimated for all filling factors for half layers*. The reason is that only fields parallel to the layers are considered in the Dowell method, and that at low filling factors the losses do not tend to zero.

When the conductors are not shifted, which means a square fitting, there is a maximum of 2.5% loss increase for a half layer and less than one percent in one and more layers.

5.4.4 Improved Quadrature of the Circle Method

Knowing what is wrong in the Dowell method described in the previous section, we can try to correct the inaccuracies. Thus, we present an Improved Quadrature of the circle method (IQOC). The method avoids the disadvantages of the classical Dowell method.

We define two g -functions, a local one g_A (A refers to around) and a transverse field one g_T (T comes from transverse). The functions are formulated as follows:

$$g_T(\eta) = \frac{\sqrt{\pi\sqrt{3}}}{2\sqrt{2}} \sqrt{\eta} \quad (5.32)$$

$$g_A(\eta) = \left(\frac{15}{64} (1 + \eta^4 1.3537) \right)^{1/4} \quad (5.33)$$

We can put both functions in Equation (5.30) to get an improved quadrature of the circle approximation of the impedance:

$$Z_{iqoc}(f, \eta) = R_0 \frac{1+j}{2\delta(f)} \left[g_A(\eta) d \coth\left(\frac{1+j}{2} \frac{g_A(\eta)d}{\delta(f)} \right) + \left(\frac{4M^2 - 1}{3} \right) g_T(\eta) d \tanh\left(\frac{1+j}{2} \frac{g_T(\eta)d}{\delta(f)} \right) \right] \quad (5.34)$$

NOTES:

- The g_T function is adapted to remove the typical $\pi/3$ error of the Dowell approach for a transverse field.
- The g_A function fits the low frequency approximation for a free wire for η tending to zero. It has been tuned to fit the half layer case. It is significantly different from the original Dowell presentation.

Figure 5.9 shows the plot of the g -function of the Dowell method and the g -functions of the introduced IQOC method.

When using the IQOC method *with variable shifted wires*, the matching with the low frequency three field method becomes very good. The deviation is lower than 0.1% for the whole range of filling factors and layers! We must admit that finding those functions was a combination of luck and some knowledge.

If the conductors are not average shifted, the eddy current losses of one or more layers may increase up to 1% for a square fitting ($\chi = 0$) and decrease up to 1% for $\chi = 0.5$.

Figure 5.10 shows the ratio between the IQOC method results for eddy current losses compared to the three field method results.

For a half layer the differences become +2.5% for $\sigma = 0$ and -2.5% for $\sigma = 0.5$ on eddy current losses.

NOTE: Keeping more distance between the layers than between wires decreases the eddy current losses very little in low frequency.

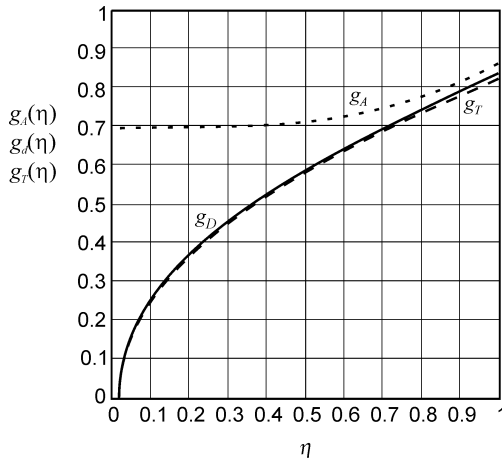


FIGURE 5.9
Plot of the g -function of the Dowell method and of the introduced IQOC method.

The following remarks should be considered with respect to accuracy of the presented IQOC method:

- In this approach, end effects are neglected (we assume an infinite permeability on left and right side)
- The distance between the layers (their center lines) equals the distance between the center of the wires in the layer; those distances are changed equally in the investigation
- No partially filled layers are present

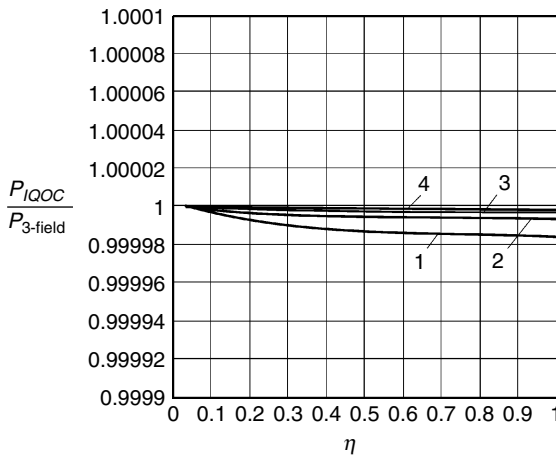


FIGURE 5.10
The ratio between the IQOC method results for eddy current losses compared to the three field method results. Curves from bottom to top: 1, 2, 3, and 4 layers.

- The high frequency accuracy is not improved by the IQOC method
- It is still a 2-D solution, some curvature and differences at the coil ends remain
- The method is difficult to use in inductor design in the presence of air gaps as the transverse field is mainly not parallel to the layers

5.4.5 Discussion of Quadrature of the Circle Methods

Conclusions for Classical Dowell Method

The Dowell method contains several types of approximations:

- Transition from round to square conductors (this is not the major cause of error) creates up to about 10% deviation of the eddy current loss
- Transition from square to rectangle shapes that causes additional error
- The method solves accurately designs, where there is no distance between the winding and the magnetic material at the sides
- There are possible vertical components of fields, especially in inductors with air gap, that are not considered
- Neglecting vertical components in the local fields
- The effects connected with extending the solution from 2-D to 3-D are neglected

However, the Dowell method fails for inductors with concentrated air gaps, as the transverse field is mainly influenced by effects of the air-gap. The method also has a poor accuracy for low filling factors and for half layer designs.

Other attempts have been made to improve the Dowell methods, including end effects [5]. However, the method [5] is based on multivariable regression and many data, and it is not easy to implement. Usually, most of the proposed methods are suitable mainly for eddy currents caused by transformer-like fields without air gaps.

The Dowell method has been used for a long time by many designing engineers. In fact, at usual filling factors, the approximation is accurate enough for practical designs. The reasons for this are the following:

- This is a wide frequency approximation, giving a resistive and inductive part of the impedance.
- At high filling factors and low frequency range, no underestimation is observed, except for half layers.
- Due to tolerances in diameter, the exact position of wires and the temperature, and 3-D effects, it was difficult to find those differences by measurements.

However, the method fails for inductors with concentrated air gaps, as the transverse field is mainly influenced by effects of the air-gap.

Conclusions for IQOC Method

The IQOC method avoids some of the drawbacks of the classical Dowell method at low frequency. This is because of the following:

- The 2-D local fields are well modeled, so that the typical large error at half layers is avoided.
- The typical $\pi/3$ error due to the transition from round to square shapes is also avoided.

The improved quadrature of the circle method has *additional merits*:

- It does not underestimate the losses at low filling factors.
- The half layer is better modeled than in the classical Dowell method.

As both methods are somewhat limited in accuracy, one can think of adapting the equations. However, our opinion is that one can obtain a much better global accuracy starting from the known 2-D analytical solutions. Such solutions are developed in the next sections of this chapter. The proposed method is long, but it also supports inductors with air gaps. The method is used in [Chapter 2](#).

5.5 Losses of a Current Carrying Round Conductor in 2-D Approach

In this section, we consider a conductor having neither another conductor close to it nor magnetic material. In this way, there is no average transverse field across the wire.

5.5.1 Exact Solution

The problem of a current carrying cylinder was described in [6].

We first define a parameter ξ (the Greek letter xi), which can also be related to the penetration depth δ

$$\xi = \sqrt{\frac{\mu\omega}{\rho}} r_o = \frac{\sqrt{2}}{\delta} r_o \quad (5.35)$$

where

r_o is the conductor radius

The solution for the impedance of the current carrying round conductor is

$$R(\omega) + j\omega L(\omega) = \bar{Z}(\omega) = \frac{\rho l_c}{2\pi r_o^2} j^{\frac{3}{2}} \xi \frac{J_0\left(j^{\frac{3}{2}} \xi\right)}{J_1\left(j^{\frac{3}{2}} \xi\right)} \quad (5.36)$$

Or also

$$\bar{Z}(\omega) = \frac{\rho z}{2\pi r_o^2} j^{\frac{3}{2}} \xi \frac{\text{ber}_0(\xi) + j \text{bei}_0(\xi)}{\text{ber}_1(\xi) + j \text{bei}_1(\xi)} \quad (5.37)$$

where

J_0, J_1 is a Bessel function of order zero and order 1, complex argument
 $\text{ber}_0, \text{bei}_0$ are the real and imaginary part of the Bessel-function, of order 0
 in the Kelvin form

$\text{ber}_1, \text{bei}_1$ are the real and imaginary part of the Bessel-Kelvin, of order 1 in
 the Kelvin form

$j = \sqrt{-1}$ is the complex number

μ is absolute permeability

l_c is the length of the considered conductor

For the graph, Fig. 5.11, we use the relative impedance $Z_r(\omega)$:

$$Z_r(\omega) = \frac{Z(\omega)}{R_0} \quad (5.38)$$

where

R_0 is the DC resistance

Note that the graph can be used for any other diameters as well; for a wire with diameter $d = \alpha \times 0.5$ mm, the applied frequency must be multiplied with α^2 to obtain the equivalent frequency $f_{eq} = f \alpha^2$ to be used to read the relative impedance $Z_r(\omega)$ on the graph in the Fig. 5.11. Note that for $f_{eq} = 20$ kHz and the considered case, the penetration depth equals the conductor diameter.

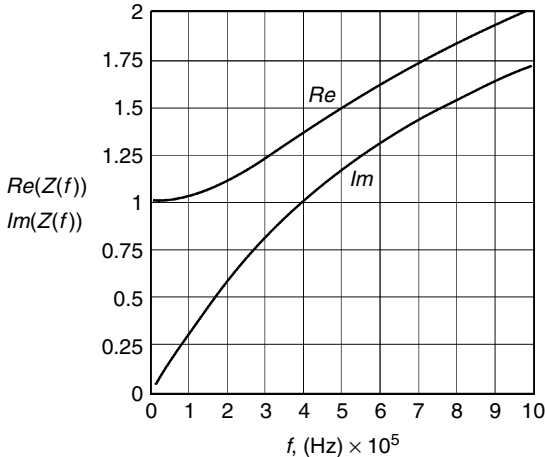


FIGURE 5.11

Real and imaginary part of the impedance of a 0.5-mm diameter free wire as a function of the frequency [Hz], $\rho = 20 \times 10^{-9}$.

5.5.2 Low and High Frequency Approximation

In the Taylor expansion, the first term after the constant term is quadratic with frequency. So, in the equation of the resistance R_l in *low frequency approximation*, there is a 4th power dependence on the penetration depth:

$$R_l(\omega) = R_o \left[1 + \frac{1}{48} \left(\frac{r_o}{\delta} \right)^4 \right] = R_o \left[1 + \frac{1}{192} (\omega \mu \sigma r_o^2)^2 \right] \quad (5.39)$$

Fig. 5.12 shows the area A for the calculation of the *high frequency approximation* of the resistive part. For high frequency approximation, one can use the skin depth principle, see Fig. 5.12, so the active area is

$$A = \pi(r_o)^2 - \pi(r_o - \delta)^2 = \pi(d - \delta)\delta \quad (5.40)$$

Then, the resistive part for the high frequency R_h is

$$R_h = \omega L_l = \frac{l_w \rho}{\pi(d - \delta)\delta} \quad (5.41)$$

It is clear that the approximation makes no sense if $\delta > 0.5 d$.

The field inside a conductor with a homogenous current density is linear increasing with the radius. The low frequency reactance of the internal field is known to be

$$X_l = \omega L_l = \frac{\omega l_c x}{8 \pi} \quad (5.42)$$

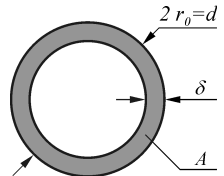
For high frequency, the reactance is

$$X_h = \omega L_h = \frac{l_c \mu_0 \delta / 2}{\pi d} \quad (5.43)$$

Note, that the penetration depth for the inductance should be considered as $\delta/2$. This fact is verified in Fig. 5.13, which shows the low frequency approximation, the high frequency approximation, and the exact solution.

FIGURE 5.12

The equivalent active area A used for the resistive part of the impedance in the high frequency approximation.



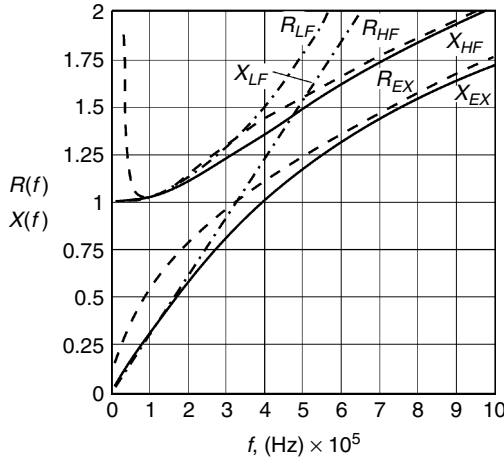


FIGURE 5.13

Comparison of the exact solution and low and high frequency approximations for the real and imaginary part of the impedance of a 0.5-mm diameter free wire as a function of the frequency. The wire length is 9.81 m and the total DC wire resistance is 1 Ω .

Exact solution: full line, EX.

Low frequency approximation: dash-dot line, LF.

High frequency: dash line, HF.

5.5.3 Wide Frequency Approximation

Not everyone likes to work with Bessel type functions. Therefore, here we present another approximation solution. We concentrate on the resistive part of the power. The advantage is that the new expression can help the intuition of the engineer. The resistive part is given as

$$R_{wf} = R_0 \left[1 + \frac{1}{48} \left(\frac{\zeta}{2} \right)^4 \frac{1}{\sqrt{1 + \frac{G_A(\zeta)}{36864}}} \right] \quad (5.44)$$

where

$$\zeta = \frac{d}{\delta(f)} = \frac{d}{\sqrt{\frac{2\rho}{\omega\mu_0}}} = \frac{d}{\sqrt{\frac{2\rho}{2\pi f\mu_0}}} \quad (5.45)$$

ζ is the diameter/penetration depth ratio and the polynomial function G_A is given as

$$G_A(\zeta) = \zeta^6 + 6.1\zeta^5 + 32\zeta^4 + 13\zeta^3 + 90\zeta^2 + 110\zeta \quad (5.46)$$

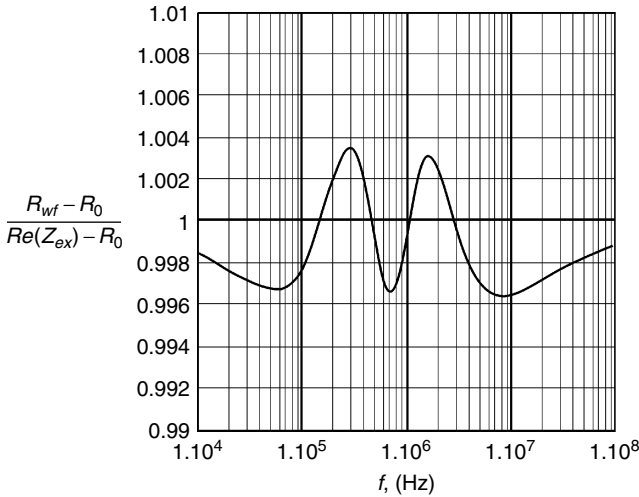


FIGURE 5.14

Deviation of the resistive part of the wide frequency approximation from Equation (5.44) compared to the exact Equations (5.36) and (5.37) for a current carrying free wire. Diameter $d = 0.5$ mm, $\rho = 20 \times 10^{-9}$ Ω m.

The coefficient in polynomial function G_A is tuned to give a 0.4% accuracy in the wide frequency approximation. The numbers 48 and 36864 are not tuning constants but result from exact analytical limits to low and high frequency.

Figure 5.14 shows the deviation of the resistive part of the wide frequency approximation from Equation (5.44) compared to the exact Equations (5.36) and (5.37) with Bessel functions.

5.6 Losses of a Round Conductor in a Uniform Transverse AC Field

This type of field is usually the main cause of eddy current losses in round conductors. As this field generates an odd current density across the conductor, the losses can be superposed on losses with an even current density, resulting from the field from the current through the conductor itself. The intensity of the transverse field can be changed by eddy currents in other conductors or by the presence of magnetic materials.

5.6.1 Exact Solution

If we consider an applied field in the x -direction, the induced current density will be an odd function of y -direction. Thus, it is orthogonal to the field

caused by the current flowing through the conductor, which generates an even current density function.

Expressing the active and reactive power of a conductor in a transverse field is not an easy mathematical problem. It needs more than five pages with Bessel equations and a Lommel integral [6]. Anyhow, the solutions are known and can be applied now. We limit ourselves to the case where the permeance of the conductor is equal to the permeance of free air (nonmagnetic conductors). We give the mathematical solution and compare it with low and high frequency approximations.

The power loss is expressed as

$$P(\xi) = 2\sqrt{2} \pi \rho H^2 \xi \frac{\text{ber}_1(\xi)(\text{bei}_2(\xi) - \text{ber}_2(\xi)) - \text{bei}_1(\xi)(\text{ber}_2(\xi) + \text{bei}_2(\xi))}{\text{ber}_0(\xi)^2 + \text{bei}_0(\xi)^2} \quad (5.47)$$

H is the undisturbed (for away) magnetic field

An auxiliary function F is introduced in order to present the reactive power. This function is given as

$$F(\xi) = \text{ber}_1(\xi)(\text{ber}_2(\xi) + \text{bei}_2(\xi)) + \text{bei}_1(\xi)(\text{bei}_2(\xi) - \text{ber}_2(\xi)) \quad (5.48)$$

Then, the reactive power is

$$Q(\xi) = \omega \mu_0 \pi \frac{d^2}{4} H^2 \frac{\frac{2\sqrt{2}}{\xi} F(\xi) + \frac{4}{\xi^2} \text{ber}_1(\xi)^2 + \text{bei}_1(\xi)^2}{\text{ber}_0(\xi)^2 + \text{bei}_0(\xi)^2} \quad (5.49)$$

The active and reactive powers of a conductor in a transverse field are shown in Fig. 5.15 as functions of the frequency.

The choice of a field of 1000 A/m is not arbitrary. It could be generated at half the conductor height by a current of 1 A in a slot width of 0.5 mm. Adding both types of losses (the transverse field and own field) is not a final solution as the proximity of other wires or magnetic material still affects the losses in the considered wire.

5.6.2 Low Frequency Approximation

In contradiction to the involved exact solution, the low frequency approximation can be quite easily calculated and presented analytically.

At low frequency, the power losses can be approximated by

$$P_{LF}(f) = \frac{l_c \pi (\omega \mu_0 H)^2 d^4}{64 \rho} \quad (5.50)$$

where

l_c is the conductor length

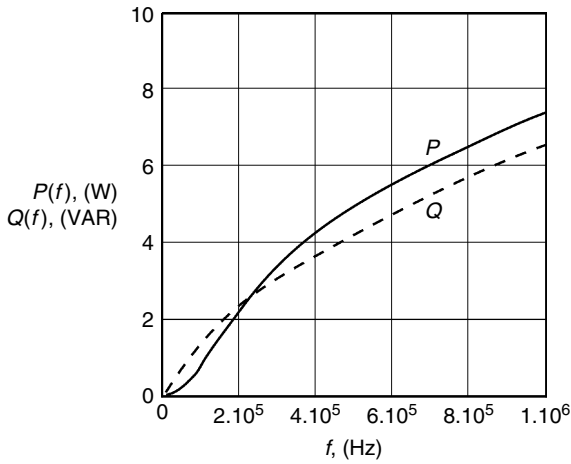


FIGURE 5.15

Active power in [W] and reactive power in [VAR] of a wire $d = 0.5$ mm, in a uniform transverse field of 1000 A/m, as a function of the applied frequency. The length is 9.81 m, the DC wire resistance is 1 Ω .

In this equation, H is an RMS value. One can see that the losses are in fact proportional to the RMS value of the derivative of the H -field.

At low frequency, the eddy currents do not change considerably the field inside the conductor. The energy inside the conductor is the energy of the field, multiplied by the pulsation frequency ω . This factor can also be recognized in Equation (5.44). Out of this observation, the reactive power can be computed at low frequency:

$$Q_{LF}(f) = l_c \omega \mu_0 \frac{\pi d^4}{4} H^2 \quad (5.51)$$

One can see that Equation (5.50) corresponds to the first part of Equation (5.16).

5.6.3 High Frequency Approximation

For the high frequency approximation, it can be demonstrated that the surface current is distributed in a sinusoidal way along the circumference of the conductor. The maximum surface current density is two times the undisturbed field. Using the penetration depth, the power loss at the high frequency approximation can be computed:

$$P_{HF}(f) = \frac{2\pi l_c H^2 \rho (d - \delta(f))}{\delta(f)} \quad (5.52)$$

Figure 5.16 shows the matching of low and high frequency loss approximation together with the exact solution. Note that, if the correction of the penetration depth on the diameter is not done, the matching is not so good.

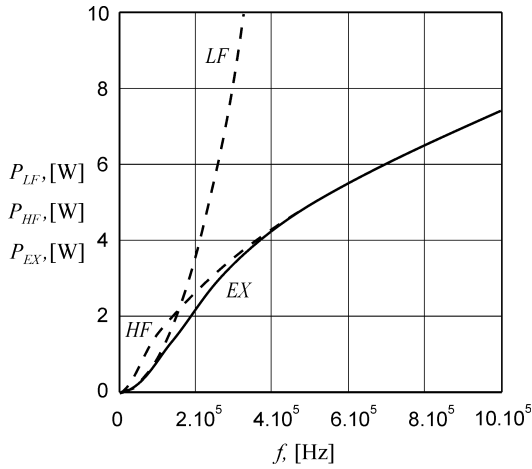


FIGURE 5.16

High and low frequency approximation and the exact solution of losses for a wire $d = 0.5$ mm in a field of 1000 A/m. The wire length is 9.81 m, the DC wire resistance is 1 Ω .

HF: high frequency approximation.

LF: low frequency approximation.

EX: exact solution.

5.6.4 Wide Frequency Approximation

Here we present wide frequency approximation. We use the function

$$G_T(\zeta) = \zeta^6 + 2.7\zeta^5 - 1.3\zeta^4 - 17\zeta^3 + 85\zeta^2 - 43\zeta \quad (5.53)$$

Then, we obtain

$$\frac{R_{wf}}{R_0} = \frac{l_c \pi^2 \frac{d^2}{4} \zeta^4 \left(\frac{B}{\mu_0} \right)^2}{16 \left[1 + \frac{G_T(\zeta)}{1024} \right]^{1/2}} \quad (5.54)$$

where

R_0 is the DC resistance

R_{wf} is the obtained resistance using the presented wide frequency approximation

Equation (5.54) is quite similar to Equation (5.44) for the skin effect. It satisfies the low and high frequency limit for the exact solution of a conductor in a transverse field. The factors 16 and 1024 are not tuning constants but a consequence of the exact low and high frequency limits. The coefficients in G_T are adapted to the exact solution match to an error on eddy current loss, less than 1%, see Fig. 5.17.

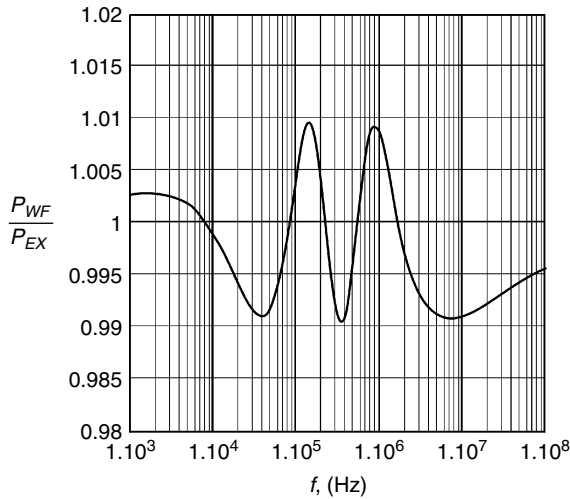


FIGURE 5.17

Deviation of the wide frequency approximation of the losses of a free round conductor in a uniform transverse field. Comparison to the exact solution. Diameter $d = 0.5$ mm, $\rho = 20 \times 10^{-9}$ Ωm .

5.6.5 Discussion

The conductor losses in a transverse field are exactly known and presented analytically for a free conductor if the applied uniform transverse field can be calculated.

Besides the transverse field losses and the skin-effect losses, other components are present when conductors are close to each other or close to a magnetic material. In order to consider those effects, in the next sections we propose analytical methods valid in low frequency approximation. The methods are tuned in intermediate and high frequency by finite element calculations.

5.7 Low Frequency 2-D Approximation Method for Round Conductors

5.7.1 Direct Integration Method for Round Wires

The method is discussed in detail in Appendix 5.A.2. This method is an exact solution

- at low frequency approximation, where the eddy currents practically do not influence the field inside the conductor
- when the conductors do have a circular cross section
- when the problem can be converted to a 2-D plane problem, where no magnetic materials are present

The last requirement can be obtained in rectangular winding areas by mirroring.

We consider m layers with N_m conductors in a layer. To have the possibility to investigate a number of winding constructions, we use the winding arrangement and specifications shown in Fig. 5.18. We use complex numbers to identify the center of the conductors. This method is used because the formulation of the Biot-Savart law gets particularly simple. The first conductor in each layer has the (complex) coordinate $q_m = q_{mx} + j q_{my}$.

The field induced by the other conductors in a considered point from a conductor n in layer m , with coordinates $z = x + jy$, is

$$H_{ext} = \frac{-j i}{2 \pi (z - (q_m + n s_m))^*} \quad (5.55)$$

$$\Phi_{ext}(z) = \frac{\mu_0 i_m}{2 \pi} \sum_{m=1}^M \sum_{n=1}^{N_m} \varepsilon(m - m_c, n - n_c) \ln \left(\frac{(z - (q_m + n s_m))^*}{(q_m + n_c s_{mc} - (q_m + n s_m))^*} \right) \quad (5.56)$$

where

$\varepsilon(m - m_c, n - n_c) = 0$ for ($m = m_c$ AND $n = n_c$)

$\varepsilon(m - m_c, n - n_c) = 1$ for all other cases

n is the number of the conductor, which field is considered

m is the layer of the conductor, which field is considered

n_c is the number of the conductor in which we calculate the flux

m_c is the layer of the considered conductor

M is the total number of layers

N_m is the total number of conductors in the m -th layer

* is used for a complex conjugate value

The contribution of the flux of the considered conductor itself is

$$\Phi_{int}(z) = \frac{\mu_0 i_1}{4 \pi} \left(\frac{|z - (z_{mc} + n_c s_{mc})|^2}{r_{mc}^2} \right) \quad (5.57)$$

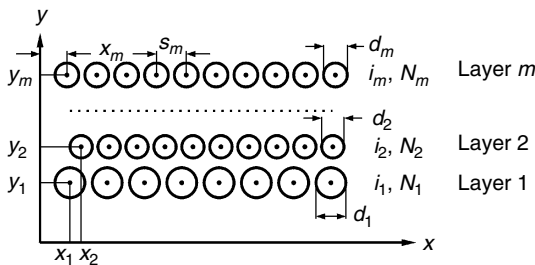


FIGURE 5.18

An arbitrary winding arrangement.

Then the total flux in a considered point is

$$\Phi_{\Sigma}(x, y) = \Phi_{ext}(x, y) + \Phi_{int}(x, y) \quad (5.58)$$

The average flux is an integrating constant and has to be removed, as it leads to the eddy current component, which would generate a nonzero total current contribution:

$$\Phi_{av}(x, y) = \frac{1}{\pi r_1^2} \int_{-r_1}^{r_1} \int_{-\sqrt{r_1^2 - y^2}}^{\sqrt{r_1^2 - y^2}} \Phi_{\Sigma}(z - (z_{mc} + n_c s_{mc})) dx dy \quad (5.59)$$

Then we consider the following flux

$$\Phi(x, y) = \Phi_{\Sigma}(x, y) - \Phi_{av}(x, y) \quad (5.60)$$

The eddy current losses are obtained using the induced *EMF* and the resistivity

$$P_{eddy} = \frac{(2\pi f)^2}{\rho} \int_{-r_1}^{r_1} \int_{-\sqrt{r_1^2 - y^2}}^{\sqrt{r_1^2 - y^2}} (\Phi(z - (z_{mc} + n_c s_{mc})))^2 dx dy \quad (5.61)$$

This power is the low frequency eddy current loss in the considered conductor. *The method is very accurate, as only one numerical surface integral is needed.* However, the solution is not very fast due to this numerical integral and since the flux can be generated by many conductors.

No special approximations (except low frequency eddy current) are done, so this type of solution can be used to check other solutions!

5.7.2 Three-Field Approximation

The external fields change smoothly inside the conductor. This allows approximating the direct integral method with simplified functions.

A rough simplification is to consider only a homogenous transverse field calculated at the center of the conductor with Equation (5.56). This can be called a zero order approximation. The losses associated with the transverse field are

$$P_{eddy,tr} = \frac{\pi r_m^4 (2\pi f)^2 \mu_0^2 (|H_{tr}|)^2}{4\rho} \quad (5.62)$$

A better approach is obtained using also the first derivative. Together with the homogenous transverse field, there are three types of fields, which can be shown to be orthogonal, see Fig. 5.19. We consider the first derivative of the field at the center of a conductor. The field is generated from the external conductors. We take the derivative of Equation (5.55) to z and we have

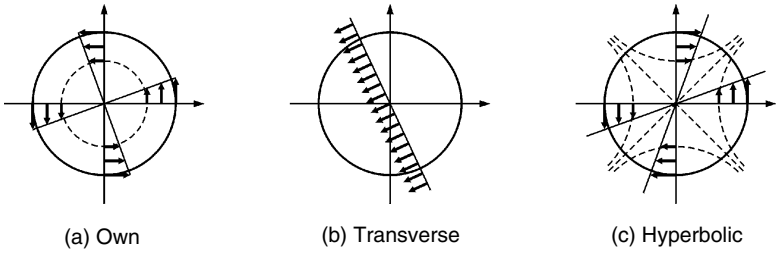


FIGURE 5.19
The three orthogonal fields, comprised in the proposed three-field approximation.

$$H'_{hy,m} = \frac{dH_{hy,m}}{d(z)} \tag{5.63}$$

$$H'_{hy,m} = \frac{i_m}{2\pi} \sum_{m=1}^M \sum_{n=1}^{N_m} \varepsilon(m - m_c, n - n_c) \frac{1}{((z_{mc} + n_c s_{mc}) - (z_m + n s_m))^2} \tag{5.64}$$

The obtained type of field is called hyperbolic (H_{hy}), as the field lines follow hyperbolas, see Fig. 5.20. The losses associated with the hyperbolic field are

$$P_{eddy,hy} = \frac{\pi r_m^6 (2\pi f)^2 \mu_0^2 |H'_{hy}|^2}{24 \rho_m} \tag{5.65}$$

The field caused by the current contributes also to the first derivative in the center of the conductor. However, it has a singularity point in the middle, so we calculate its contribution in a separate way. Then, the losses associated with the one field are

$$P_{eddy,own} = \frac{\pi r_m^2 (2\pi f)^2 \mu_0^2 (i_m/2\pi)^2}{24 \rho_m} \frac{1}{2} \tag{5.66}$$

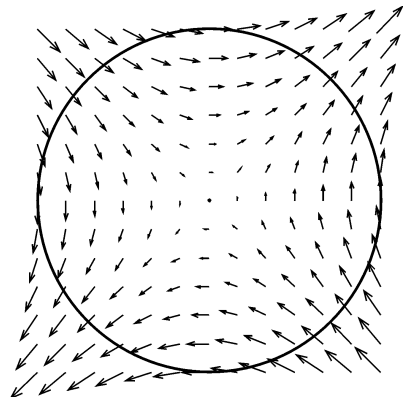


FIGURE 5.20
The field lines of the hyperbolic field.

Now we can write the total power losses for one conductor:

$$P_{eddy,\Sigma} = P_{eddy,tr} + P_{eddy,own} + P_{eddy,hy} \quad (5.67)$$

The three-field method has the advantage of being very fast, as neither numerical integrals nor functions have to be computed. Besides that, computing the magnitudes can be avoided, as the square contains no functions, for example

$$|H_{tr}|^2 = \text{Re}(H_{tr})^2 + \text{Im}(H_{tr})^2 \quad (5.68)$$

The method has an error, which is usually below 0.1% compared to the integral method for normal field problems. In Appendix 5.A.2, the validation of the method is discussed. The accuracy is somewhat limited by the presence of higher mode fields, which do not contribute to a derivative in the center of the conductor.

5.7.3 Solution in a Magnetic Window Using Mirroring

In the previous section, the solutions were derived ignoring magnetic materials. Often this result is still quite good for eddy currents caused by leakage fields in transformers. When conductors are surrounded by material with infinite permeability, we know that the H -field is perpendicular to the walls. This property can be used to remove the walls from the magnetic problem. A wall at the bottom, corresponding to $y = 0$ can be removed by injecting the same currents at positions mirrored to $y = 0$. In this way, the fields will be perpendicular to the x -axis and the same field problem is obtained inside the window. A new wall is created at $y = -yw$, w is the window width. A mirroring can be done across the y -axis so that the wall at $y = 0$ is removed, and a new wall is created at $x = -xw$. One can continue mirroring like this, pushing the walls always farther away. However, after the first two times mirroring, the problem becomes symmetrical, in such way that mirroring becomes equal to shifting by $2yw$ in the y direction or $2xw$ in the x -direction. This is easier to implement in programs. [Figure 5.21](#) illustrates the described mirroring approach.

Normally, a lot of mirroring would be needed before reaching 0.1% accuracy in all cases. After the mirroring at the x -axis and y -axis, the H -field is perpendicular to the x - and y -axis by symmetry, and $H = 0$ at the origin.

The additional mirroring is needed to fulfill the perpendicularity of H at $x = xw$ and $y = yw$. A way to check this feature is to look at the corners $(xw, 0)$, $(0, yw)$, and (xw, yw) . Far away mirrors do generate smooth functions, which tend to make $H = 0$ at the corners. This effect can be simulated by creating a smooth compensating function that has that effect. In this way, less time-consuming mirrors are needed. By the special choice of the function it cancels the field at the four corners of the window and other symmetrical points $(0, 0)$, $(\pm xw, 0)$, $(0, \pm yw)$, and $(\pm xw, \pm yw)$.

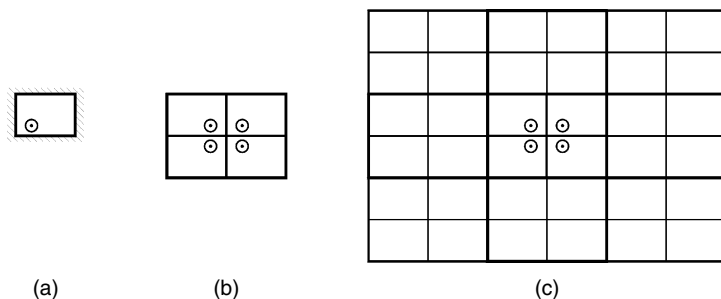


FIGURE 5.21
Mirroring a window with magnetic walls.

For inductors with an air gap, a counter *MMF* is placed at the air gap. In that case, it is considered as a first layer.

The analysis is not intended for problems where the total *MMF* is non-zero. This is the case when studying eddy currents of magnetizing currents in transformers without air gap. This problem is not compatible with an infinite permeability.

5.7.4 Suppression of the First Infinite Sum

When mirroring in two directions, two sums are cascaded. This fact reduces the speed of the calculation. To remove the first sum the following equation can be used:

$$\frac{\pi}{\tan\left(z \frac{\pi}{a}\right)} = \sum_{n=-\infty}^{+\infty} \frac{1}{z + an} \quad (5.69)$$

The equation is applicable for the transverse field, for $z \neq 0$. The transverse field of other conductors, for $z = 0$, is zero, so it does not have to be calculated.

For the hyperbolic field, for $z \neq 0$, we can use this series:

$$\frac{\pi}{\sin\left(z \frac{\pi}{a}\right)} = \sum_{n=-\infty}^{+\infty} \frac{1}{(z + an)^2} \quad (5.70)$$

For $z = 0$, in the middle of a conductor, there is a contribution of the same layer that has to be calculated by a mathematical limit:

$$\frac{\pi^2}{3} = \sum_{n=-\infty, \neq 0}^{+\infty} \frac{1}{(an)^2} \quad (5.71)$$

A lot of calculation time can be saved using these methods. This is the case for the graphs, which are generated to compare with the quadrature of the circle method. For example, a graph with 100 points (changing filling factor), 50 shifts in relative position of wires, and 10 infinite layers, can be generated in about one second using MathCAD 11 and a Pentium 4, 2 GHz PC.

A consequence of the aforementioned sums is that the main effect of induced fields is caused by the layer in the direction of the field. In the presence of different layers, when the relative position of the wires is shifted (so it means no pure square or hexagonal wire fitting), the average effect of the losses due to the distance between layers is very small in the low frequency case.

5.8 Wide Frequency Method for Calculating Eddy Current Losses in Windings

5.8.1 High Frequency Effect of Other Wires, Using Dipoles

At high frequency, the field induced by the *eddy currents* of other wires is not negligible. At very high frequency ($\delta \ll d$), the eddy currents will even cancel any field inside a conductor. We consider a transverse field applied to a single, infinite layer of conductors. For simplicity, we consider the field in the x -direction and a conductor with complex coordinates $z = 0$. Here, not all intermediate steps are mentioned in order to shorten the explanation. For a standalone wire, a sinusoidal surface current density cancels the field inside the wire. The maximum value of that current density $\sigma(\theta)$ is twice the inverse of the applied field:

$$\sigma(\theta) = \sigma_{\max} \sin(\theta) = 2 H_{\text{ext}} \sin(\theta) \quad (5.72)$$

where

θ is the angle with x -axis

H_{ext} is the applied field

The induced field of the n^{th} conductor generates a field outside the wire. This field is identical to the field of a dipole, see Fig. 5.22:

$$H_{\text{exti}} = \frac{-r_o^2 \frac{\sigma_{\max}}{2}}{((z - ns)^*)^2} \quad (5.73)$$

where

s is the distance between the center lines of the conductors, the step

the term $-r_o^2 \frac{\sigma_{\max}}{2}$ is the dipole moment of the current

n is the number of the conductors in the layer

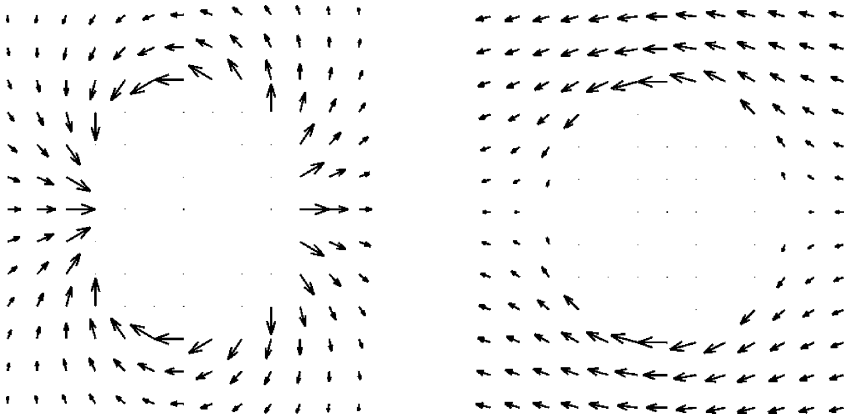


FIGURE 5.22

A vector plot of the dipole field shown in a), and the dipole field with an applied homogenous field in the $-x$ direction, shown in b); scale $\frac{1}{2}$ for the arrows in b).

The field H_{exti} attenuates or increases the field applied to other wires. Thus, we start from an unknown sinusoidal surface current, which is the same in each conductor.

One can demonstrate that the field generated by the other wires H_m , in the middle of a considered wire, is

$$H_m = -r_o^2 \frac{\sigma_{\max}}{2} \frac{\pi^2}{12} \left(\frac{d}{s}\right)^2 \quad (5.74)$$

Here the effect of other than homogenous transverse fields is neglected. The sum of the induced fields, H_i , of an infinite row of conductors on the x -axis, including the field inside the conductor, is

$$H_i = \left(\frac{\pi^2}{12} \left(\frac{d}{s}\right)^2 + 1 \right) \left(-r_o^2 \frac{\sigma_{\max}}{2} \right) \quad (5.75)$$

In Equation (5.75) we recognize a factor that increases the field compared to a single wire for a given σ_{\max} . This results in the fact that a lower current density is sufficient to cancel the fields inside the wire compared to a single wire case. The attenuation factor for a transverse field in the x -direction AF_x is

$$AF_x = \left(\frac{\pi^2}{12} \left(\frac{d}{s}\right)^2 + 1 \right) \quad (5.76)$$

We have the corresponding effect on losses $F_{T,hf,x}$ for a transverse field in the x -direction:

$$F_{T,hf,x} = \left(1 + \frac{\pi^2}{12} \left(\frac{d}{s} \right)^2 \right)^{-2} \quad (5.77)$$

where

$F_{T,hf,x}$ is the high frequency coefficient

The field parallel to a layer seems in this way to be *screened* by the current distributions of the wires in that layer. It can be noted that the dipoles induce an almost negligible field outside the conductor area ($y > d/2$ and $y < -d/2$). This fact is especially true if one takes the average over the shift positions of different conductors. This type of effect is typical with transformers. As the thickness of a layer is usually much lower than the winding width, the effect is dominant.

Concerning the field perpendicular to a layer, in the y -direction, a similar solution is possible, but the current is increased compared to the single wire problem. The resulting effect on losses $F_{T,hf,y}$ in this case is

$$F_{T,hf,y} = \left(1 - \frac{\pi^2}{12} \left(\frac{d}{s} \right)^2 \right)^{-2} \quad (5.78)$$

In this case, the field between the wires is increased. The flux has to *tunnel* between the wires, causing an increased H -field and more losses. This effect is present in center-gapped inductors. In a major part of the winding, the field is rather perpendicular to the layers.

It is convenient to consider a filling factor in the direction of the layer, denoted as η , and a filling factor perpendicular to the layer named λ . Now we want again to give definitions of the coefficients η and λ :

$$\eta = d/s_x, \quad \lambda = d/s_y \quad (5.79)$$

Both coefficients are illustrated in [Fig. 5.23](#).

The previous presentation of the filling factors can be used to solve single layer cases. We define the function F_i as

$$F_i = \eta^2 \quad \text{for } \lambda = 0 \quad (5.80)$$

$$F_i = -\lambda^2 \quad \text{for } \eta = 0 \quad (5.81)$$

Then we can rewrite the resulting effect on losses $F_{T,hf,y}$ as

$$F_{T,hf,y} = \left(1 - \frac{\pi^2}{12} F_i(\eta, \lambda) \right)^{-2} \quad (5.82)$$

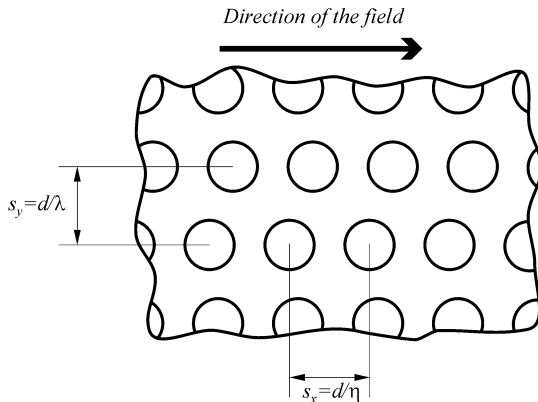


FIGURE 5.23

Definition of the filling factors η and λ of conductors in a winding area. The ratio $\eta = d/s_x$ is in the horizontal direction, and the ratio $\lambda = d/s_y$ is in the vertical direction in the illustrated field case.

These extreme cases set the limits for F_i : $-1 < F_i < 1$.

The general analytical case, where η and λ are both non-zero is not simple to analyze analytically. These cases and the frequency dependence at intermediate frequencies are more easily obtained by tuning with finite elements. The condition $\delta \ll d$ is usually not fulfilled in power electronics so that the actual frequencies are often in the region between low and high frequency approximation.

5.8.2 Wide Frequency Method, Tuning with Finite Element Solutions

Although the pure analytical solutions help to find the nature of the functions, they usually do not give practical solutions for general 2-D (and 3-D) problems. However, analytical approximations can still be made when tuning with finite elements is provided. The used method is current driven, this means that we consider that the currents (or *MMF*) are given, although voltages and inductance may be frequency dependent. This allows starting from low frequency and obtaining a good approximation at high frequency.

5.8.2.1 A Wire in a Transverse Field

In this case, an average *H*-field is applied, and the situation corresponds with a wire in an infinite layer with layers above and below it. The considered layer itself does not carry current. According to the way of implementing, the case corresponds to a square fitting of wires, which has the tendency to overestimate losses.

Figure 5.24 shows finite element modeling of a wire in a transverse field, $d = 0.5$ mm.

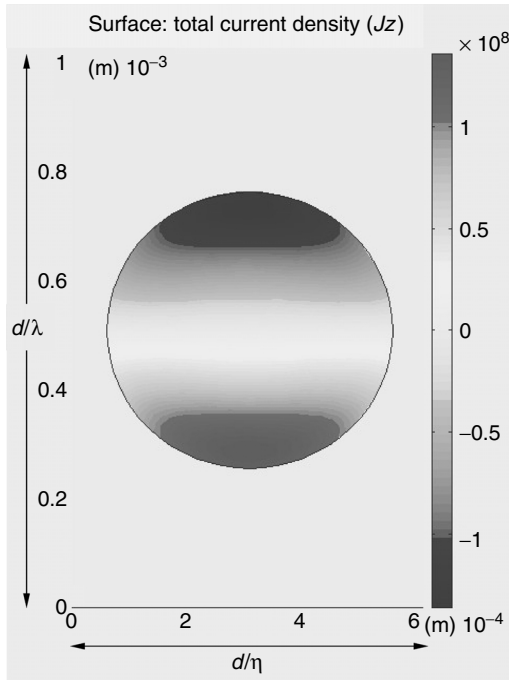


FIGURE 5.24

Finite element modeling of a wire in a transverse field, $d = 0.5$ mm; $\lambda = 0.5$; $\eta = 0.8$.

A function F_T (T for transverse fields) is found as the ratio between the wide frequency approximation and the low frequency approximation. Then the losses of a single wire in a transverse field P_{tr} are given as

$$P_{tr} = \frac{l_c \rho}{16} (\zeta)^4 \pi F_T(\zeta, \eta, \lambda) (\mu_0 H_{rms})^2 \quad (5.83)$$

Note that $F_T \cong 1$ at low frequency cases. We propose the following presentation of F_T :

$$F_T = \frac{1}{\sqrt{1 + \frac{G_T(\zeta)}{1024} \left(1 + \frac{\pi^2}{12} F_i(\lambda, \eta) \chi(\zeta)^2 - \left(1 - \frac{\pi^2}{12} \right) (\lambda^{10} + \eta^{10}) \chi(\zeta)^{10} \right)^4}} \quad (5.84)$$

where F_i is the effect of induced field by dipoles compared to the direction of the layers.

The function F_T has only three parameters: ζ , η , and λ . The relative diameter compared to the penetration depth is

$$\zeta(f) = \frac{d}{\delta(f)} \quad (5.85)$$

The function χ (pronounced *chi*) takes the frequency dependence of the dipole effect in account and is defined as

$$\chi(\zeta) = \frac{1}{1 + 1.5\zeta(f)} \quad (5.86)$$

The function F_i can be approximated as

$$F_i(\eta, \lambda) = \eta^2 \quad \text{for } \eta > \lambda \quad (5.87)$$

$$F_i(\eta, \lambda) = -\lambda^2 + 2\eta\lambda \quad \text{for } \eta \leq \lambda \quad (5.88)$$

The following situations are relevant:

- For $\eta \gg \lambda$, the case corresponds to the screening effect case, which is typical for transformers
- For $\eta \ll \lambda$, the case corresponds to the tunneling effect case, which is present in gapped inductors
- Special cases: $F_i = 1$ for $\eta = 1$; $F_i = -1$ for $\lambda = 1$ and $\eta = 0$
- The function F_i and its derivatives are continuous for $\eta = \lambda$
- The factor $2\eta\lambda$ is a result of the finite element tuning

FEM Tuning Conditions

We performed FEM tuning of the function in equation (5.84), (using MATLAB and also checked with GETDP) of the proposed analytical method. The following conditions and ranges are considered:

- The ratio λ/η was set in the range 0.1, 0.5, 1, 2, 10.
- The maximum values of η and λ were set to 0.2, 0.5, 0.7, 0.8, 0.9, and 0.999.
- The tested frequencies were 20 kHz, 50 kHz, 100 kHz, 200 kHz, 500 kHz, 1000 kHz, and 10 MHz.
- The wire diameter was $d = 0.5$ mm.

The resulting set of problems simulated corresponds to 210 cases, in the described wide range of parameters.

Accuracy of the Simulations

Up to 1 MHz (for that frequency the diameter is lower than seven times the penetration depth), the typical error is about 3%, maximum 10%. At higher frequencies, the deviation is somewhat larger. In those cases the finite elements solutions show larger losses, mainly because the finite element simulations

were done for a square fitting, whereas the analytical solutions take an averaged variable shift into account.

Conclusions

- The low frequency and high frequency cases at low filling factors fit easily, as they are close to known analytical solutions.
- Some additional terms were added to take the losses of the local fields in account at high frequency.

5.8.2.2 A Wire in a Half Layer

In this case, no average transverse field is considered across the conductor. The conductor carries current I . The conductors above and below the considered conductor carry half of the current in the reverse direction. This situation is often referred to as a *half layer*. The case includes not only the losses of a current carrying free wire but also losses due to the local field of the conductors around it, although no average field is present.

The half layer situation is orthogonal with the losses of a transverse field (even and odd current distributions), which permits adding those losses. Figure 5.25 shows finite element modeling of a current carrying conductor with current I and two return conductors each carrying current $-I/2$.

The function F_A is also presented as the ratio between the wide frequency approximation and the low frequency approximation of a free wire problem. The index A comes from fields close *around* the conductor. Using the function F_A , the losses of a free wire in a half layer are given as

$$P_A = \frac{l_w \rho}{16 \times 12} (\zeta)^4 F_A(\zeta, \eta, \lambda) I_{rms}^2 \quad (5.89)$$

where

l_w is the wire length

The function F_A is defined as

$$F_A = \frac{1}{\sqrt{\left(1 + 1.3537 \eta^4\right)^{-2} + \frac{G_A(\zeta)}{36864} \left(1 - \frac{\pi}{12} (\eta^{2.5} + 0.3 \lambda^{10})\right)^4}} \quad (5.90)$$

Conclusions of the Comparisons

- At low frequency, the term $(1 + 1.3537 \eta^4)^{-2}$ allows very good matching (better than 0.1%) with the three-field method calculations of a continuous (average shifted) layer. At low frequency (and $\eta = 1$), the losses are about two times higher than the case of the free wire only.

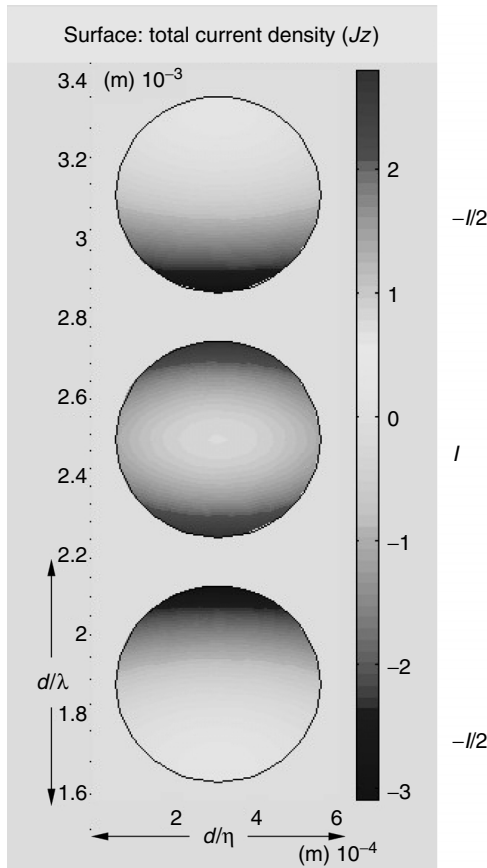


FIGURE 5.25

Finite element modeling of a current carrying conductor with current I and two return conductors each carrying current $-I/2$.

- At high frequency, high filling factors $\lambda = 1$ and $\eta = 1$, the losses seem to be about 2–3 times higher than the case of the free wire only. This increase is similar to the low frequency case.

In the case of a half layer, no transverse field is present. The losses of a free wire do not accurately predict the losses at normal filling factors.

5.8.2.3 Losses in the General Case of a Transformer Winding

In a transformer, the transverse field is caused by the other layers and by half of the field increase across the considered layer. This allows compiling an equation that predicts the losses taking into account the above facts. We did solve similar problems for rectangular cross sections. Not all details in the calculation are given here; for more details see the Appendix 5A.

For transformers, the ratio of the eddy current losses compared to the AC losses in the DC resistance is denoted as **eddy current factor** $k_{c,tr}$:

$$k_{c,tr} = \frac{P_{eddy}}{R_0 I_{ac}^2} \quad (5.91)$$

and we have the following presentation for $k_{c,tr}$

$$k_{c,tr}(m, \zeta, \eta, \lambda) = \frac{1}{16} (\zeta)^4 \left(\eta^2 \frac{m^2 - \frac{1}{4}}{3} \frac{\pi^2}{4} F_T(\zeta, \eta, \lambda) + \frac{F_A(\zeta, \eta, \lambda)}{48} \right) \quad (5.92)$$

where m is the number of layers, perpendicular to the field direction

Taking into account the typical length of field lines, η and λ can be approximated by

$$\eta = \frac{nd}{w} \quad (5.93)$$

where

w is the winding width

n is the number of conductors in a layer

$$\lambda = \frac{md}{h} \quad (5.94)$$

where

h is the winding height

m is the number of layers

Note that η and λ , m , n , d , w , and h are **not independent**. The parameters are linked by the equations (5.93) and (5.94).

The eddy current losses are then given as

$$P_{eddy} = (R_0 I_{ac}^2) k_{c,tr}(m_E, \zeta(f, d), \eta, \lambda) \quad (5.95)$$

Accuracy Limitation

The winding width w is chosen as the flux returns even if the winding area width is larger, so the winding area width is less relevant than the winding width. The winding height h is used as in the y -direction the field lines go from the center leg to the outer leg. The definition of λ is not important for transformers as it is mainly relevant when $\lambda > \eta$, which is usually not the case in transformers. In the coil ends, h is virtually higher, which results in even lower λ . In practice, the accuracy is often 10% or better and is even more limited by the knowledge of the exact mechanical

parameters (such as exact wire diameter and winding width, temperature) than the error of the approximation method.

5.8.2.4 Losses in an Inductor Winding

In usual transformers, the transverse field is mainly parallel to the layer. This is a reasonable assumption for transformers. However, for inductors this is usually not the case. The fields perpendicular to layers do induce more losses as they tunnel between the wires. The transverse field is mainly caused by the presence of an air gap.

In a large part of the inductor winding, the field is even rather perpendicular to the layers.

To present the inductor winding losses, we define a correction **field factor** k_F with contributions in the x -direction (parallel to the layer) and y -direction (perpendicular to the layer) as follows

$$k_{Fx} = \frac{\int_{winding} H_x^2}{\frac{1}{3} \left(\frac{NI}{wK} \right)^2} \quad (5.96)$$

$$k_{Fy} = \frac{\int_{winding} H_y^2}{\frac{1}{3} \left(\frac{NI}{wK} \right)^2} \quad (5.97)$$

where

k_{Fx} and k_{Fy} are x and y components of the coefficient k_F

H_x is the transverse field in the layer direction

H_y is the transverse field in the direction perpendicular to the layer

K is the symmetry factor (= 2 for EE, = 1 for EI cores)

N is the turn number

If the influence of the direction can be neglected, a global value k_F can also be defined:

$$k_F = \frac{\int_{winding} H_{tr}^2}{\frac{1}{3} \left(\frac{NI}{wK} \right)^2} \quad (5.98)$$

$$k_F = k_{Fx} + k_{Fy} \quad (5.99)$$

where

H_{tr} is the transverse field value

REMARKS

1. The factor k_F for transformers and multiple layer windings, where the transverse field linearly increases across the winding, is $k_F \cong 1$.
2. For usual concentric wound transformers the factor $k_{Fx} \cong 1$ and $k_{Fy} \cong 0$. This is also true for multiple layer windings, where the field is parallel to the layers and linearly increasing across the winding.
3. For inductors the values k_{Fx} and k_{Fy} are of the same order of magnitude.

Full Equation for Inductors

Using the introduced coefficients, the eddy current loss factor $k_{c,in}$ for inductors can be presented as

$$\begin{aligned}
 k_{c,in}(m, \zeta, \eta, \lambda) = & \frac{1}{16} (\zeta)^4 \left(\eta^2 \frac{m^2 - \frac{1}{4} \pi^2}{3} k_{Fx} F_T(\zeta, \eta, \lambda) \right) \\
 & + \frac{1}{16} (\zeta)^4 \left(\lambda^2 \frac{n^2 - \frac{1}{4} \pi^2}{3} k_{Fy} F_T(\zeta, \lambda, \eta) \right) \\
 & + \frac{1}{16} (\zeta)^4 \left(\frac{F_A(\zeta, \lambda, \eta)}{48} \right)
 \end{aligned}
 \tag{5.100}$$

Equation (5.100) is called *the full equation for inductors*. The factors k_{Fx} and k_{Fy} can be determined analytically in some special cases or derived using finite elements. The factors take the H-field in account at low frequency. Together with the filling factors η and λ , a good estimate of the high frequency losses is obtained. The details are given in the appendix. Here we give the following approximation presentations of the factors k_{Fx} and k_{Fy} :

$$k_{Fx}(\kappa) = \frac{1.55(0.38 - \kappa)^2 + 0.517}{\kappa}
 \tag{5.101}$$

$$k_{Fy}(\kappa) = \frac{1.88(0.609 - \kappa)^2 + 0.126}{\kappa}
 \tag{5.102}$$

The parameter κ is the characteristic distance ratio, defined as

$$\kappa = \frac{d_{wl} + t_w/3}{w/K} \quad (5.103)$$

where

d_{wl} is the distance between the winding and the core leg

t_w is the winding thickness

h is the height of the window

w is the width of the window

K is symmetry factor (equals 2 for EE, 1 for EI cores)

The parameter κ is defined in such way that the field factor is quite insensitive (<10%) for changes in t_w and h for constant κ .

Simplified Equation for Inductors

Simplifications of Equation (5.100) are possible. Usually the local field losses F_A are negligible as the transverse field losses are usually much more. For intermediate frequencies, and for large values of m and n , Equation (5.100) can be approximated by

$$k_{c,in}(m, \zeta, \eta, \lambda) = \frac{1}{16} (\zeta)^4 \left(\frac{N^2 d^2}{3w^2} \frac{\pi^2}{4} k_F F_{Tb}(f, d) \right) \quad (5.104)$$

with the simplified function F_{Tb} corresponding to the free wire losses:

$$F_{Tb}(f, d) = \frac{1}{\sqrt{1 + \frac{G_T(f, d)}{1024}}} \quad (5.105)$$

and the following approximation of k_F

$$k_F(\kappa) = \frac{3.5(0.5 - \kappa)^2 + 0.69}{\kappa} \quad (5.106)$$

Equation (5.104) is called *the simplified equation for inductors*. This simplification was used in [Chapter 2](#) for inductors. The advantage is its simplicity and the fact that η and λ do not have to be evaluated. The simplification can be allowed, as the fields of an inductor are a mix between parallel and perpendicular fields. This type of simplification is not allowed in transformers, as it would result in a systematic overestimation of losses as it neglects the screening effect.

Accuracy

The typical accuracy on the eddy current losses calculation is about 10% for low frequency cases and about 20% at high frequency. However, in practice, the main cause of error is the accuracy of the mechanical dimensions, as for instance k_{Fx} and k_{Fy} are very sensitive to the distance to the center leg. The eddy current loss is only a part of the total loss, so that good global designs can still be made.

The method has decreased accuracy for inductors with a low number of turns (e.g., lower than 5). The reason is that the derivation of k_{Fx} and k_{Fy} uses a homogenous current distribution, which is a bad approximation at a low number of turns. Regardless, such cases are easy to analyze using finite elements.

5.8.3 High Frequency, High Filling Factor Relations

For $\eta = 1$ and for a frequency tending to infinite, the field at the horizontal wire diameter tends to zero. This effect results in a defined ratio (not the value itself) of losses between the layers, as it is solved in section 5.3.4 of this chapter. The found relationship is valid also for round wires, although the losses are not the same in the case of round wires compared to rectangular conductors. Thus, we can present the additional loss factor in k_c for m layers compared to the value of k_c for one layer.

For $\eta = 1$, independent of λ , and a frequency tending to infinite (e.g., for a penetration depth lower than 1% of the diameter) the following relation should be met:

$$\lim_{f \rightarrow \infty} \left(\frac{k_c(m, f)}{k_c(1, f)} \right) = \left(\frac{2m^2 + 1}{3} \right), \quad \text{for } 0 < \lambda < 1, \text{ each value of } m \quad (5.107)$$

where

$k_c(1, f)$ is the eddy currents factor for one layer

When the approximation is derived, this property was taken in account, although the frequency, where it appears, is often beyond the actual applications of power electronics. Figure 5.26 shows the dependence of the ratio $k_c(m, f)/k_c(1, f)$ on λ for high frequency.

Using Equations (5.84) and (5.90), the following relation between the tuning coefficients can be derived:

$$\lim_{f \rightarrow \infty} \left(\frac{F_A(f)}{F_T(f)} \right) = 3\pi^2, \quad \text{for } 0 < \lambda < 1 \quad (5.108)$$

Note that the 1-D approximation and both quadrature of the circle methods (Dowell and IQOC) also satisfy the high frequency, high filling factor relations stated in that section.

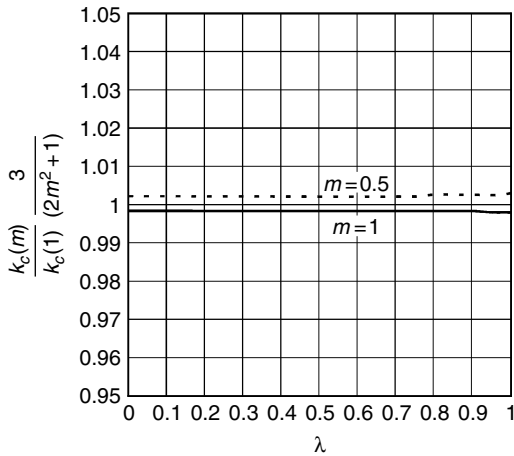


FIGURE 5.26
The dependence of the ratio $k_c(m, f)/k_c(1, f)$ on λ for high frequency.

5.8.4 Summary of the Wide Frequency Method

Assembling the elements of previous sections, we can summarize the wide frequency method. To extend the validity of Equation (2.27) for larger diameters, and a wide frequency range, the factor $k_c(m_E, \zeta, \eta, \lambda)$ is derived, which represents the ratio between the eddy current losses compared to the losses in the ohmic resistance of the winding of a magnetic component. The factor k_c is expressed with full and simplified equations for inductors.

We get a reduction of the parameters by using the relative diameter ζ . The effect of induced currents (the dipole effect) is frequency dependent. We take such an effect into account by an empirical (tuned by finite element simulation) factor χ . The effect of induced field by dipoles compared to the direction of the layers is reflected by the function F_i . The adaptation factor for transverse field losses is denoted as F_T and the adaptation factor for field around (local field) losses is F_A .

The field factor k_F reflects the type of the field problem. This field factor is close to 1 for transformers. The factor k_F is highly dependent on an equivalent relative distance to the center leg, thus for inductors typical values of k_F are in the range 0.6–15.

5.8.5 Comparison of Analytically Based Methods

5.8.5.1 Low Frequency Methods

Low frequency methods can use different approaches of field calculation but take only the static field solution in account. They are easy to apply, as they need less parameters and less computing time in finite elements. An additional

advantage is that the losses are proportional to the square of the derivative of the current, which simplifies the modeling to a parallel loss resistor. Therefore, it is still worthwhile to look in which conditions low frequency methods are applicable. The solution is compared to the wide frequency method (WFM).

Method Considering Only the Transverse Field

When the diameter is lower than 1.6 times the penetration depth, the transverse field losses can be well described using the low frequency approximation for transverse field, with an accuracy even better than 10%. The deviation is the defined function F_T . The largest deviation occurs at a high filling factor in the direction of the field. This is the case in a single layer, well filled transformer. The lowest deviation occurs when the filling factor in the direction of the field is low and it is high in the direction perpendicular to the field.

Both extreme cases are shown in Fig. 5.27 compared to a single wire low frequency solution. For the example of 0.5-mm wire, extreme case of $\eta = 1, \lambda = 0$ (transformer case) at 50 kHz, a 10% deviation is observed. At this frequency the ratio diameter/penetration depth is 1.57, but the ratio is usually above 1.6 for realistic fillings.

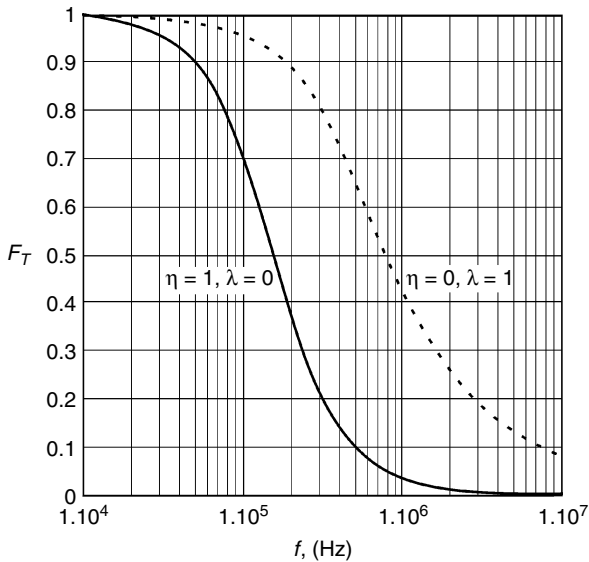


FIGURE 5.27

The coefficient F_T as a function of the frequency, the solution for a single wire $d = 0.5$ mm, $\rho = 20 \times 10^{-9} \Omega\text{m}$.

Full line: $\eta = 1, \lambda = 0$ (field parallel to a single layer);

Dashed line: $\eta = 0, \lambda = 1$ (field perpendicular to a single layer).

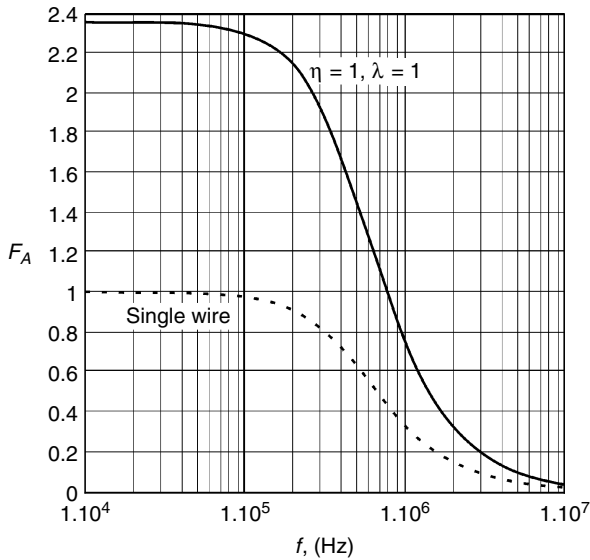


FIGURE 5.28

The coefficient F_A as a function of the frequency, the solution of a single wire $d = 0.5$ mm, $\rho = 20 \times 10^{-9} \Omega\text{m}$.

Full line: highly filled window ($\eta = \lambda = 1$);

Dashed line: a single wire solution.

Three Field Method

Methods considering only transverse fields are always approximation methods. Those methods result in significant errors for a half layer, a single layer, and for low filling factor problems. A way to improve the accuracy is to consider also the space derivative of the field in the center of a conductor. This approach leads to field separation of three types of field.

Figure 5.28 shows the correction factor of the losses of a half layer winding compared to a single wire low frequency solution. The deviation is the defined function F_A . We see that the solution of a single wire is only right at very low filling and is increased by a factor of 2.35 for low frequency at a full filling (and up to 1.9 at $\eta = 0.9$). The ratio remains about the same at high frequency. This is an argument to cancel the myth that the total losses can be found by adding the transverse field losses to the solution of a free wire only.

For single layer and more layers, the transverse field losses dominate and the relative effect of local field losses is small when the filling factor is not too low.

5.8.5.2 Wide Frequency Method and Quadrature of Circle Methods

The wide frequency method also takes 2-D high frequency effects into account, whereas the quadrature of the circle methods are based on 1-D

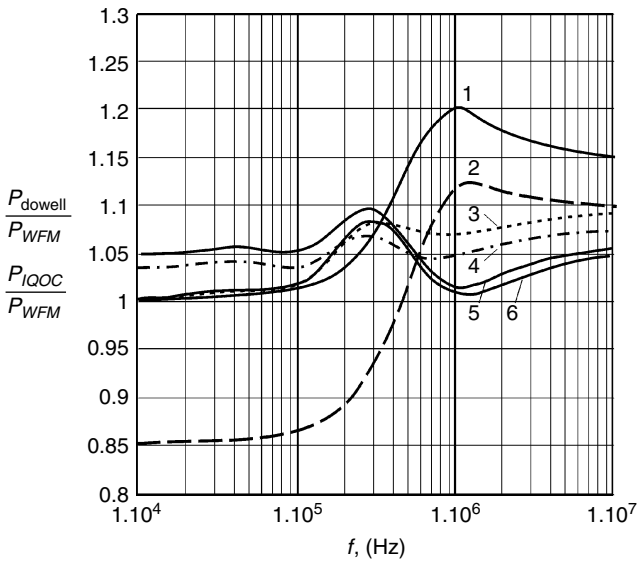


FIGURE 5.29

Losses given by the Dowell approximation and by the IQOC method compared to the WFM, $\eta = 0.8$, ($0 < \lambda < 0.8$), typical for transformers, $d = 0.5$ mm:

- 1: P_{IQOC}/P_{WFM} , $m = 0.5$; 2: P_{dowell}/P_{WFM} , $m = 0.5$;
 3: P_{IQOC}/P_{WFM} , $m = 1$; 4: P_{dowell}/P_{WFM} , $m = 1$;
 5: P_{IQOC}/P_{WFM} , $m = 3$; 6: P_{dowell}/P_{WFM} , $m = 3$.

methods. The IQOC method is corrected for low frequency and local fields. A few examples give an impression of the deviation of the eddy current losses obtained by the Dowell method, IQOC method, and the WFM.

Comparison for the Cases with Transformer Type of Field

In Fig. 5.29 we show the comparison of the eddy current losses of Dowell approximation and IQOC method compared to the wide frequency method. The comparison is made for $\eta = 0.8$, ($0 < \lambda < 0.8$), which filling factors are typical for transformers. The wire diameter is 0.5 mm.

Figure 5.30 shows Dowell approximation and IQOC method compared to the WFM for $\eta = 0.4$, ($0 < \lambda < 0.4$), $d = 0.5$ mm. The cases are typical for transformers at very low filling factors. The comparisons illustrated in Fig. 5.29 and Fig. 5.30 show the following conclusions for transformers:

- The quadrature of the circle methods perform reasonably well at high filling factors $\eta > 0.7$ and above (the errors are lower than 25%).
- The Dowell method significantly underestimates the half layer eddy current losses, but those losses are low compared to single layer losses.

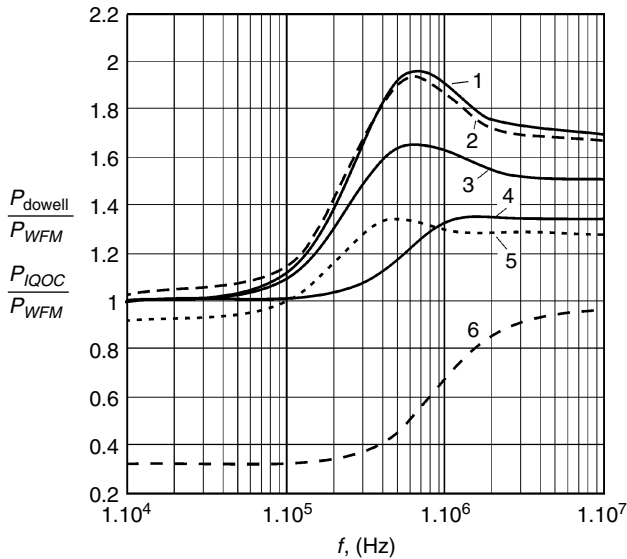


FIGURE 5.30

Losses given by the Dowell approximation and by the IQOC method compared to the WFM, $\eta = 0.4$, ($0 < \lambda < 0.4$). The cases are typical for transformers at very low filling factors, $d = 0.5$ mm.

- 1: P_{IQOC}/P_{WFM} , $m = 3$; 2: P_{dowell}/P_{WFM} , $m = 3$;
- 3: P_{IQOC}/P_{WFM} , $m = 1$; 4: P_{IQOC}/P_{WFM} , $m = 0.5$;
- 5: P_{dowell}/P_{WFM} , $m = 1$; 6: P_{dowell}/P_{WFM} , $m = 0.5$.

- The IQOC method performs well in low frequency and has the tendency to overestimate at high frequency.

The major conclusion is that one should avoid using the quadrature of circle methods at low filling factor, as the deviations get significant.

Comparison for the Cases with Inductor Type of Field

- One should **not apply** quadrature of circle type of methods to inductors!
- The factor k_F is neglected in the classical way of describing quadrature of circle methods, which results in severe underestimations (e.g., factor of 10) when winding close to the air gap.
- The number of layers is usually low; it is very normal to have $\lambda = 0.1-0.3$ and $\eta = 0.9$.
- For a large frequency range, one better uses the wide frequency method of 5.8. or finite element solutions including skin-effect. For low frequency, one can use the three-field method based on Biot Savart law like in appendix 5.A.2.4 or combine the three-field method and a static finite element solution.

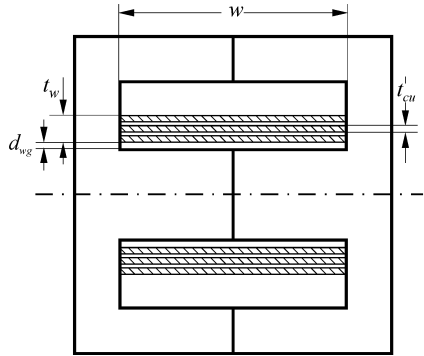


FIGURE 5.31
An ideal foil wound winding.

5.9 Losses in Foil Windings

5.9.1 Homogenous Field Parallel to the Foil

The ideal case supposes that the field lines are parallel to the foil surface. An ideal foil wound winding is shown in Fig. 5.31. This can be obtained if the tip of the foil almost touches the magnetic material (e.g., using enameled copper foil in a pot core or open box), so that the field lines are parallel to the foil surface. In transformers with a turns ratio equal to 1, the same effect can be reached by alternating a primary and a secondary foil, in this case the field lines are also parallel to the foil and very low eddy current losses can be obtained.

The equations in section 5.3 for rectangular conductors can be used and the impedance of the winding can be calculated, as the number of layers equals the number of turns here:

$$R_h + jX_h = R_0 \frac{1+j}{2} \frac{t_{cu}}{\delta(\omega)} \left(\coth \left(\frac{1+j}{2} \frac{t_{cu}}{\delta(\omega)} \right) + \left(\frac{4N^2 - 1}{3} \right) \tanh \left(\frac{1+j}{2} \frac{t_{cu}}{\delta(\omega)} \right) \right) + \frac{j\omega\mu_0 l_T}{w} \sum_m a_{m,air} m^2 \quad (5.109)$$

where

R_0 is the DC resistance of the foil conductor

N is the turn number, equal to the number of layers in the case

t_{cu} is the thickness foils, a is used for conductors

l_T is the length of a turn

w is the foil width

δ is the penetration depth

m is the m^{th} conductor, start counting from no field (outer side)

$a_{m,air}$ space distance below the m^{th} conductor (side towards increasing field)

The real part of the equation shows the resistive part of the impedance. Note that this resistive part also contains the DC resistance. The imaginary part shows the leakage reactance coupled with the winding:

$$X_{\sigma} = \omega L_{\sigma} \quad (5.110)$$

NOTE: The leakage inductance will not be considered in the next sections.

A way to approximate the ideal conditions for inductors is to use foil windings without a coil former in pot cores, or to cover the outside coil ends with ferrite plates. A special construction is the box type, where the mid-leg is removed, e.g., a planar core with removed mid-leg.

A way to approximate the ideal conditions for transformers is to use interleaved windings, so that the field lines have a very short return path outside the foil.

Care should be taken for incoming and outgoing connecting strips or wires because if not carefully designed, they may have a considerable part in the total losses.

5.9.2 Induced Losses by Air Gaps

5.9.2.1 Analytical Modeling

We consider the following simplified ideal 1-D case:

- The tip of the foil winding is very close to the magnetic material
- The air gap is in the center leg
- The air gap length is small compared to the distance from the center leg to the foil
- The penetration depth is low compared to the total copper thickness t_w of the winding
- If the winding comprises more than one turn, both the thickness of the foil and the insulation distance of the winding should be considerably lower than the penetration depth

With these conditions, a simplified modeling is possible.

NOTE: When the total copper thickness is higher than the penetration depth, the foil screens the field perpendicular to it. This case can be modeled as a material with a zero permeability perpendicular to the foil.

The average current density corresponds to a homogenous field, and it is discussed in section 5.9.1 of this chapter. For the remaining part of the current density, the currents are not generating voltage at the end of the winding. The circulating currents are short-circuited internally. For these type of currents, the winding can be replaced by a homogenous short-circuited turn with a copper thickness equal to t_{cu} , winding thickness t_w , see Fig. 5.32, and an adapted resistivity ρ' :

$$\rho' = \rho \frac{N t_{cu}}{t_w} \quad (5.111)$$

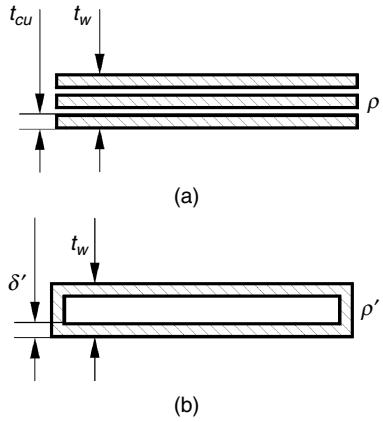


FIGURE 5.32 Replacing the foil winding shown in a), by an equivalent short circuited winding shown in b), for nonhomogenous current densities, where the average density is absent.

where

t_{cu} is the foil thickness

t_w is the foil winding thickness

This adapted resistivity corresponds to an adapted penetration depth:

$$\delta'(f) = \delta(f) \sqrt{\frac{t_w}{N t_{cu}}} \quad (5.112)$$

Figure 5.32 shows the discussed transformation.

As by the defined conditions the thickness of winding is much larger than the penetration depth, and the penetration depth is small compared to the foil thickness, one can solve the field problem using the 2-D Biot-Savart solution and mirroring. Here we omit the details of the derivation.

The surface current density $\sigma(x)$ [A/m] equals the H -field parallel to the layer [A/m], as the perpendicular field is almost zero at a deepness of a few penetration depths. The surface current density, for an infinite foil (N turns of a current I), due to a single air gap is given as

$$\sigma(x) = \frac{NI}{2d_{wg}} \frac{1}{\cosh\left(\frac{x\pi}{2d_{wg}}\right)} \quad (5.113)$$

where s is the distance from the center leg to the foil, see Fig.5.31

The loss corresponding to the current density of a concentrated air gap for a foil of width w in a window with the same width w is

$$P_g(d_{wg}) = \frac{\rho' l_T (NI_{ac})^2}{\delta'} \left\{ \int_{-p/2}^{+p/2} \left[\sum_{k=-\infty}^{+\infty} \frac{1}{2d_{wg} \cosh\left(\frac{(x+kp)\pi}{2d_{wg}}\right)} \right]^2 dx - \frac{1}{p} \right\} \quad (5.114)$$

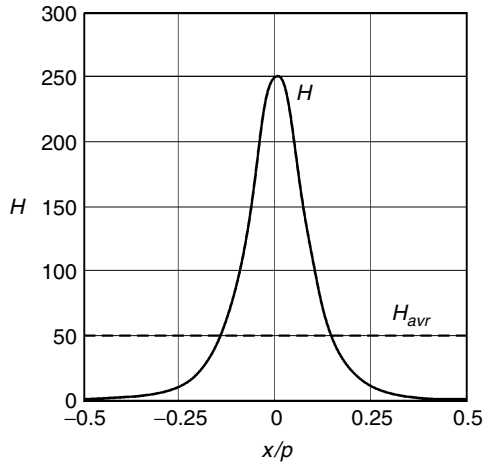


FIGURE 5.33

The field H_g due to the concentrated air gap as a function of the distance x/p in the x -direction.

Full line is the H_g -field; dotted line is the average H_g -field, both in [A/m]; for $NI = 1$, $d_{wg} = 2$ mm, $p = 20$ mm.

where p is the periodicity in the field pattern. It equals the winding area width w in the case of a single air gap: $p = w$.

The loss corresponding to the average current is removed, as it is orthogonal and it corresponds to a homogenous field parallel to the layer (this issue is discussed in the section 5.9.1 of this Chapter). For an easier calculation, an additional coefficient K_g is defined and then we can rewrite Equation (5.114):

$$P_g(d_{wg}) = \frac{\rho' l_T (NI_{ac})^2}{\delta' \pi d_{wg}} K_g \left(\frac{d_{wg}}{p} \right) \quad (5.115)$$

The coefficient K_g tends to 1 for low values of d_{wg} . Hence, for low d_{wg} , the considered losses are almost inversely proportional to d_{wg} . Figure 5.34 shows K_g as a function of the ratio d_{wg}/p .

In Fig. 5.33 we show the field H_g due to the concentrated air gap as a function of the distance in the x -direction.

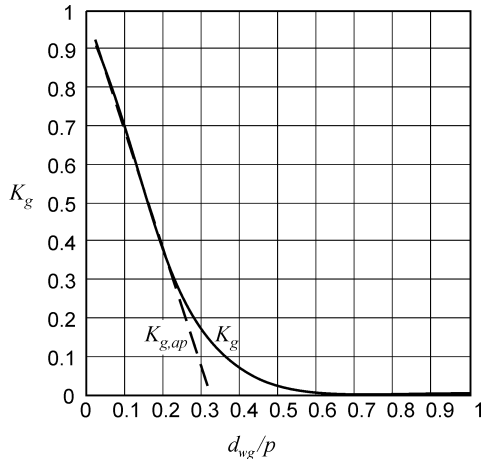


FIGURE 5.34

The coefficient K_g (full line) and an approximation of $K_{g,ap}$ (dashed line) for low values of d_{wg} as a function of the ratio d_{wg}/p , $K_{g,ap} = 1 - \pi d_{wg}/p$.

Means to reduce the effect of the air gap field are

- Keep some distance between the winding and the mid-leg. However, this approach increases the DC resistance of the foil.
- Use several smaller air-gaps, e.g., multiple air gaps, thus p is reduced by the symmetry.
- Use a mid-leg with low permeability, e.g., equally distributed air gap.
- Put the air gap in the outer legs. However, this results in higher far-away fields, which could generate EMI (Electro Magnetic Interference) problems.

REMARKS

- Other effects that can be handled in a similar way: one single primary turn in round wire, with a secondary in foil winding.
- When the radius of the foil is much larger than the radius of the center leg, an overestimation of the losses will occur as the field is reduced by the larger surface for the leakage flux (3-D-effect).

5.9.3 Tip Currents in Foil Conductors

We neglect the effects of the air gap in this section. In general, the approximation of spaced conductors given in Chapter 5 is not applicable in a normal way as the width of the foil is much longer than the penetration depth.

If the foil tips are at some distance from the magnetic material, a field component H_{tip} is present perpendicular to the foil, see Fig. 5.35. This field component is neutralized at some distance from the top by a tip current in

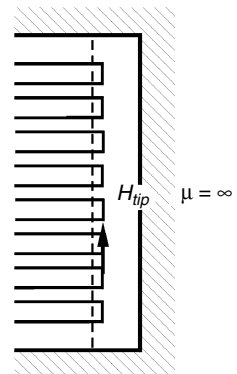


FIGURE 5.35
Field H_{tip} at the tips of foil conductors.

a penetration depth. The corresponding losses for one side of foil winding $P_{tip,1}$ for small distances to the core are given as

$$P_{tip,1} = \rho' l_T H_{tip,a}^2 \frac{t_w}{\delta'(f)} \quad (5.116)$$

where

- l_T is the mean length of turn
- t_w is the thickness of the foil winding
- $\delta'(f)$ is the adapted penetration depth

Foil Inductors

For inductors with small distances from the foil to the core, $H_{tip,a}$ can be estimated as

$$H_{tip,a} = \frac{N I_{ac} e_a}{(w + e_a + e_b) t_w} \quad (5.117)$$

where

- I_{ac} is the total AC current in the foil
- $H_{tip,a}$ is the field in the 'a' tip of the foil
- e_a and e_b are the distances from the foil tips to the core, see Fig. 5.36
- w is the width of the copper foil
- t_w is the thickness of the foil winding

Substituting Equation (5.117) in Equation (5.116), we obtain the tip losses

$$P_{tip} = \frac{\rho' l_T}{\delta' t_w} \frac{N^2 I_{ac}^2 (e_a^2 + e_b^2)}{(w + e_a + e_b)^2} \quad (5.118)$$

At larger distances to the core-foil tip, the tip losses can be very high. Anyhow, there is a maximum of those losses when almost all the current is concentrated in the tip. This maximum can be approximated as

$$P_{tip,max} \approx \frac{\rho' l_T}{\delta'(f) t_w} \frac{N^2 I_{ac}^2}{2} \quad (5.119)$$

As the losses are large in this case, this type of construction should only be used when the AC component in the current is small compared to the DC component.

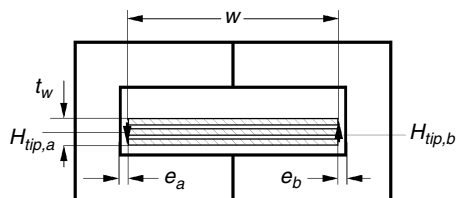


FIGURE 5.36
Foil winding arrangement and dimensions.

Foil Transformers

For transformers, it is difficult to realize a small distance between the foil tips and the core. The reason is that the transformer windings need more connections. Fortunately, the length of the field lines at the top is limited as this field is a leakage field.

For transformers, a practical order of magnitude can be set:

$$e_a = e_b = K_t t_w \quad (5.120)$$

where

$K_t = 0.5-1$ and the lowest K_t values correspond to interleaved windings
 t_w is the thickness of the foil winding

Conclusions Concerning Tip Currents

1. The tip losses in foil windings can be significantly reduced while interleaving primary and secondary, as in this way the thickness of the winding is reduced.
2. The current flowing in the tips reduces the average current in the foil.

5.9.4 Conclusions for Foil Windings

The tip currents tend to reduce the homogenous field, which should be taken into account. Using the previous sections of this chapter, for the transformer winding number 1 we can present the eddy current losses as

$$P_1 = I_{ac}^2 \left(\frac{w}{w + 2K_t t_{w1}} \right)^2 R_h + \frac{I_{ac}^2 N^2 \rho' l_T}{\delta'(f) t_w} \frac{2(K_t t_{w1})^2}{(w + 2K_t t_{w1})^2} \quad (5.121)$$

Using sections 5.9.1 and 5.9.3, we can write for an inductor winding with a center leg gap

$$P = I_{ac}^2 \left(\frac{w}{w + e_a + e_b} \right)^2 R_h + \frac{I_{ac}^2 \rho' l_f N}{\delta' \pi s} K_s \left(\frac{s}{p} \right) + \frac{I_{ac}^2 \rho' l_f}{\delta' t_w} \frac{(e_a^2 + e_b^2)}{(w + e_a + e_b)^2} \quad (5.122)$$

REMARK

For simplicity, we neglected the combination of the effects of air gaps and tip currents.

Although very low eddy current losses are possible in a proper design, it is not always easy to realize transformers and inductors having low parasitic effects such as low tip currents and low effects of nonhomogenous current distributions.

The best use of foil windings can be obtained in the following conditions:

- The foil tips close to the core
- The foil winding placed far away from air gaps
- For transformers, interleaving primary and secondary windings
- For transformers with mixed foil and wire windings: avoid winding close to the tips

5.10 Losses in Planar Windings

Planar windings are usually obtained by etching (multilayer) printed circuit boards (PCB). The windings are perpendicular to the magnetic legs, see Fig. 5.37. In an experimental set-up one can also bend copper foils under 45° .

Advantages of the Planar Cores

- The planar cores can be incorporated in the PCB design and, thus, no winding action is needed anymore. In addition, the parasitic capacitance and leakage inductance are well defined, as the relative position of the wires is accurate.
- For transformers, low losses and low leakage inductance can be obtained by interleaving primary and secondary windings (multi-layer PCB).

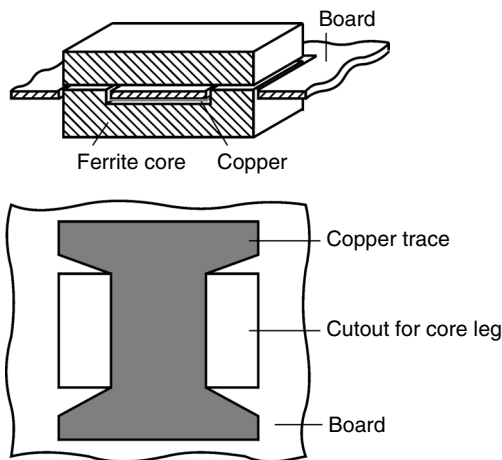


FIGURE 5.37
A planar core and a winding.

- The planar cores (and the windings) could be cooled by a heat sink.
- Planar cores have a low thickness, so the heat transfer is better.

Losses in Planar Magnetic Components

In general, similar types of losses occur as in foil windings. However, the planar windings are often less close to the ideal cases, so that the use of numerical (3-D finite element) models is interesting. The designs are particularly suited for high frequency applications and for applications with a low number of turns.

Specifics

For transformers, usually a crepage distance and thickness trough insulation are required. These distances are easily obtained if the primary is in one layer of the PCB and the secondary is in another layer. If several layers or interleaved windings are used, metallizations through holes are necessary. In this case, the design includes crepage distances and distance trough insulation and it gets more involved.

For inductors, care should be taken to avoid the proximity of the air gap. The air gap can cause currents induced by fringing fields.

Planar designs are often made with planar cores. When using PCB, usually a very low copper filling factor is obtained. Therefore, it is possible that other types of windings (such as Litz wire) could have lower copper losses in the same core. However, in that case one loses the ability of easy manufacturing.

Appendix 5.A.1 Eddy Current 1-D Model for Rectangular Conductors

A one-dimensional (1-D) approach can help to find solutions for eddy currents in conductors and magnetic materials. The basic mathematics are close to RL transmission lines and one-dimensional dynamic heat problems. Care has been taken to obtain orthogonal functions, so that losses can be added. This appendix builds up the theory using Maxwell and Poynting laws. Thus, the conditions under which the methods are derived become clear.

Both conductors and magnetic sheets can be subjected to an average magnetic field and both have losses due to eddy currents. The theory unifies the eddy currents in current carrying conductors and in magnetic

field conducting sheets and cores. The equations are similar, the main differences are

- the magnetic sheets have a higher permeability and they normally do not carry current.
- the behavior of conductors is much more linear than the behavior of magnetic materials.

Inside magnetic materials and in conductors, capacitive effects can usually be neglected. In this section, the hysteresis and the excess losses in magnetic materials are also not considered.

Complex *RMS* values for *E* and *H* are used (when they are not explicit time dependent).

Some properties of mathematical functions used are given in Appendix D at the end of the book.

5.A.1.1 Basic Derivations

Figure 5.A.1 shows a conductor with infinite permeability material on its left and right side. A reference plane at $y = 0$ is placed in the middle of the conductor. From the laws of Maxwell in differential form [7], in 2-D, we can derive the following equations:

$$\frac{\partial E(y, t)}{\partial y} = -\mu \frac{\partial H(y, t)}{\partial t} \tag{5A.1}$$

$$\frac{\partial H(y, t)}{\partial y} = -\sigma E(y, t) \tag{5A.2}$$

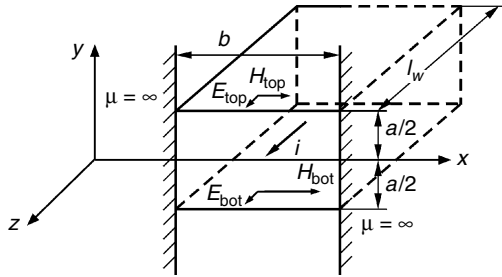


FIGURE 5A.1

A conductor with infinite permeability material on the left and right side. *H* field in the *x*-direction, *E* field in the *z*-direction.

where

$E(y, t)$ is the electric field in the time domain, [V/m]

$H(y, t)$ is the magnetic field in the time domain, [A/m]

σ is the specific conductivity, $\sigma = 1/\rho$, [Ω m]

μ is the permeability, $\mu = \mu_r \mu_0$, for copper and aluminium $\mu_r = 1$, [s Ω m]

We consider the Laplace transformation in the time domain:

$$E(y, s) = \int_0^{\infty} E(y, t) e^{-st} dt \quad (5A.3)$$

$$H(y, s) = \int_0^{\infty} H(y, t) e^{-st} dt \quad (5A.4)$$

where

$E(y, s)$ is the electric field in the Laplace domain, [Vrms/m]

$H(y, s)$ is the magnetic field in the Laplace domain, [Arms/m]

s is the Laplace operator ($s = j\omega$ for sinusoidal signals) [1/s]

Transforming Equations (5A.1) and (5A.2), we obtain:

$$\frac{dE(y, s)}{dy} = -\mu s H(y, s) \quad (5A.5)$$

$$\frac{dH(y, s)}{dy} = -\sigma E(y, s) \quad (5A.6)$$

Differentiating (5A.6) and substituting in (5A.5) and vice versa give

$$\frac{d^2 E(y, s)}{dy^2} = \gamma(s)^2 E(y, s) \quad (5A.7)$$

$$\frac{d^2 H(y, s)}{dy^2} = \gamma(s)^2 H(y, s) \quad (5A.8)$$

where

$$\gamma(s) = (s \mu \sigma)^{1/2} \quad (5A.9)$$

The function $\gamma(s)$ is called *the propagation function* and it has the dimension [m^{-1}]. The general solution for the differential equations is in the form

$$E(y, s) = A(s) e^{-\gamma(s)y} + B(s) e^{+\gamma(s)y} \quad (5A.10)$$

$$H(y, s) = \frac{A(s)}{Z_0(s)} e^{-\gamma(s)y} - \frac{B(s)}{Z_0(s)} e^{+\gamma(s)y} \quad (5A.11)$$

Here $A(s)$ and $B(s)$ are coefficients, independent of y . The function $Z_0(s)$ is called *characteristic impedance* of the conductor material and is expressed as

$$Z_0(s) = \left(\frac{s\mu}{\sigma} \right)^{1/2} \quad (5A.12)$$

This impedance is complex here as the medium is not loss-less. For $y = 0$, the reference plane, we consider the following reference values for E and H :

$$E_{ref}(s) = A(s) + B(s) \quad (5A.13)$$

$$H_{ref}(s) = \frac{A(s) - B(s)}{Z_0(s)} \quad (5A.14)$$

Solving with respect to $A(s)$ and $B(s)$ results in

$$A(s) = \frac{E_{ref}(s) + Z_0(s) H_{ref}(s)}{2} \quad (5A.15)$$

$$B(s) = \frac{E_{ref}(s) - Z_0(s) H_{ref}(s)}{2} \quad (5A.16)$$

Using Equation (5A.10), the E and H fields can be expressed by E_{ref} and H_{ref} .

$$E(y, s) = E_{ref}(s) \cosh(\gamma(s)y) - Z_0(s) H_{ref}(s) \sinh(\gamma(s)y) \quad (5A.17)$$

$$H(y, s) = H_{ref}(s) \cosh(\gamma(s)y) - \frac{E_{ref}(s)}{Z_0(s)} \sinh(\gamma(s)y) \quad (5A.18)$$

We can derive an equation for the top fields. We assume fields E_{top} and H_{top} at the top of the conductor for $y = a/2$, see Fig. 5A.1. Then, we can write

$$E_{top} = E_{ref}(s) \cosh\left(\gamma(s)\frac{a}{2}\right) - Z_0(s) H_{ref}(s) \sinh\left(\gamma(s)\frac{a}{2}\right) \quad (5A.19)$$

$$H_{top} = H_{ref}(s) \cosh\left(\gamma(s)\frac{a}{2}\right) - \frac{E_{ref}(s)}{Z_0(s)} \sinh\left(\gamma(s)\frac{a}{2}\right) \quad (5A.20)$$

The same equations are valid for the bottom of the conductor $y = -a/2$. The local power flow through a surface can be calculated using the Pointing vector, showing the direction and the magnitude of the instantaneous power:

$$dP(y, t) = (\mathbf{E}(y, t) \times \mathbf{H}(y, t)) \cdot d\mathbf{S} \quad (5A.21)$$

Using this equation, we can calculate the complex apparent power flowing through a conductor:

$$S = P - jQ = VI^* = \int_O (\mathbf{E}(y,s) \times \mathbf{H}^*(y,s)) \cdot d\mathbf{S} \quad (5A.22)$$

where

- P is the active (real) power
- Q is the reactive power
- O is the side surface of the conductor
- $*$ denotes the complex conjugate value

At the sides of the conductor, the H -field is perpendicular to the surface and it does give **no contribution to the power**. The magnetic field is non-zero only at the top and the bottom and it contributes to the complex power S of the conductor:

$$S = (E_{bot} H_{bot}^* - E_{top} H_{top}^*) b l_c \quad (5A.23)$$

where

- b is the width of the conductor/sheet
- l_w is the length of the conductor/sheet

We can also look at the power through the reference plane ($y = 0$). Interesting cases are situations where the power at the reference plane is zero. It is sufficient that the fields E or H are zero at the reference plane. We calculate the **power coming from the top** in both cases:

- $H_{ref} = 0$. This case happens when $H_{top} + H_{bot} = 0$. Using Equations (5A.19) and (5A.20), we obtain

$$\frac{S}{b l_c} = E_{ref}^* \cosh\left(\gamma(s) \frac{a}{2}\right) H_{top} = Z_0(s) |H_{top}|^2 \coth\left(\gamma(s) \frac{a}{2}\right) \quad (5A.24)$$

The practical case corresponding to this case is a current carrying conductor without average magnetic field. The E -field is an odd function of the distance to the reference plane.

- $E_{ref} = 0$. This case happens if $H_{top} = H_{bot}$. Using Equations (5A.19) and (5A.20), we can write

$$\frac{S}{b l_c} = E_{ref}^* \sinh\left(\gamma(s) \frac{a}{2}\right) H_{top} = Z_0(s) |H_{top}|^2 \tanh\left(\gamma(s) \frac{a}{2}\right) \quad (5A.25)$$

The practical case corresponding to that case is a transverse field without current in the conductor or sheet. The E -field is an even function of the distance to the reference plane. The cases, when E or H are zero at the

reference plane, give orthogonal current distributions as they are even and odd functions of y . Hence, we can calculate the total losses as a superposition of both cases, for both top and bottom power:

$$S(s) = 2bl_w Z_0(s) \left(\left| \frac{H_{top} - H_{bot}}{2} \right|^2 \coth\left(\gamma(s) \frac{a}{2}\right) + \left| \frac{H_{top} + H_{bot}}{2} \right|^2 \tanh\left(\gamma(s) \frac{a}{2}\right) \right) \quad (5A.26)$$

This equation is quite important as it solves the losses in the 1-D model for a given field at the top and bottom. The imaginary part describes the negative reactive power. This is the reactive power in the conductor. The complex power above or below the conductor in a homogenous field H for a vertical section Δy can be expressed as

$$S_{air} = s\mu_0 bl_c |H|^2 \Delta y \quad (5A.27)$$

In practice, we know that the difference between the top and bottom field comes from the current in the rectangular conductor itself. So, we can use this fact

$$I = \oint_{\text{around a conductor}} H dl = H_{top} b - H_{bot} b = (H_{top} - H_{bot}) b \quad (5A.28)$$

$$S(s) = 2bl_c Z_0(s) \left(\left(\frac{|I|}{2b} \right)^2 \coth\left(\gamma(s) \frac{a}{2}\right) + |H_{av}|^2 \tanh\left(\gamma(s) \frac{a}{2}\right) \right) \quad (5A.29)$$

We give the coefficients with a number of variants in how they can be written

$$H_{av} = \frac{H_{top} + H_{bot}}{2} \quad (5A.30)$$

$$Z_0(s) = \left(\frac{s\mu}{\sigma} \right)^{1/2} = \sqrt{j} \sqrt{\frac{\omega\mu}{\sigma}} = \frac{1+j}{\sqrt{2}} \sqrt{\frac{\omega\mu}{\sigma}} = \frac{1+j}{\sigma\delta(\omega)} = \frac{1-j}{2} j\omega\mu\delta(\omega) \quad (5A.31)$$

$$\gamma(s) = (s\mu\sigma)^{1/2} = \frac{1+j}{\sqrt{2}} \sqrt{\omega\mu\sigma} = \frac{1+j}{\delta(\omega)} \quad (5A.32)$$

Here the penetration depth $\delta(\omega)$ is defined as

$$\delta(\omega) = \sqrt{\frac{2}{\omega\mu\sigma}} = \sqrt{\frac{2\rho}{\omega\mu}} \quad (5A.33)$$

Within the limits (rectangular conductor, without air, one-dimensional), the preceding equations can be used in all kinds of 1-D cases. The H -field (in the x -direction) can be generated by other conductors, which might carry currents with another phase angle, or by an air gap. Note that for $s = 0$, the

power reflects the power losses of the DC resistance. Thus, using the DC resistance yields

$$S(s) = R_0 \frac{1+j}{\delta(\omega)} \frac{a}{2} \left(|I|^2 \coth\left(\frac{1+j}{\delta(\omega)} \frac{a}{2}\right) + 4b^2 |H_{av}|^2 \tanh\left(\frac{1+j}{\delta(\omega)} \frac{a}{2}\right) \right) \quad (5A.34)$$

Then, the impedance of the conductor can be computed using that power. This presentation makes sense if the average field H_{av} can be expressed as a function of the current in the conductor.

The impedance is

$$Z = R_s + j\omega L_s \quad (5A.35)$$

where

Z is the impedance of the conductor

R_s, L_s are the equivalent series resistance and inductance

Then we can write

$$Z = 2bl_c Z_0(s) \left(\left(\frac{1}{2b}\right)^2 \coth\left(\gamma(s) \frac{a}{2}\right) + \left(\frac{|H_{av}(I)|}{|I|}\right)^2 \tanh\left(\gamma(s) \frac{a}{2}\right) \right) \quad (5A.36)$$

Presented by the DC resistance and penetration depth, the impedance is

$$Z = R_0 \frac{1+j}{\delta(\omega)} \frac{a}{2} \left(\coth\left(\frac{1+j}{\delta(\omega)} \frac{a}{2}\right) + \left(\frac{2b|H_{av}(I)|}{|I|}\right)^2 \tanh\left(\frac{1+j}{\delta(\omega)} \frac{a}{2}\right) \right) \quad (5A.37)$$

The last two equations are important for the cases where the relationship between the transverse field and the current is known. The case is usual for inductors. But also in transformers in no-load tests or a short circuit test, only one current is present. In the next two sections, we have examples where the average field and the current are related.

5.A.1.2 Single Conductor in a Slot

Figure 5A.2 shows an arrangement for a conductor in a slot or winding area with a high permeability material on three sides. For a single conductor in a slot the field at the bottom is zero, $H_{bot} = 0$. The average field is $H_{av} = I/(2b)$. Using the function properties at the end of this appendix, the corresponding impedance is

$$Z = \frac{l_c}{b} Z_0(s) (\coth(\gamma(s)a)) \quad (5A.38)$$

or

$$Z = \frac{l_c}{b} \sqrt{\frac{s\mu}{\sigma}} \left(\coth(\sqrt{s\mu\sigma} a) \right) = \frac{l_c}{b\sigma} \frac{(1+j)}{\delta(\omega)} \coth\left(a \frac{(1+j)}{\delta(\omega)}\right) \quad (5A.39)$$

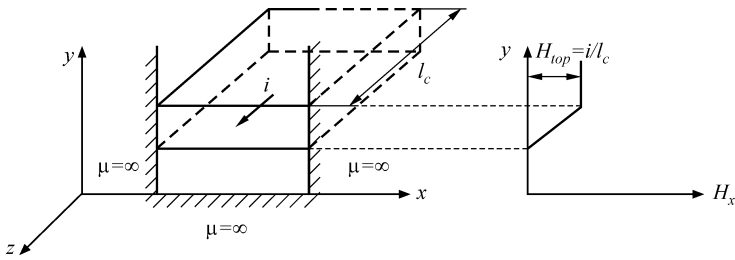


FIGURE 5A.2

A single conductor in a slot and the static field H_x in the x -direction.

For ω tending to zero, the value of Z tends to the DC resistance ($\coth(z) \rightarrow 1/z$), then we have

$$R_0 = \frac{l_c}{ab\sigma} \quad (5A.40)$$

For high values of ω , we have $\coth(z) \rightarrow 1$, and then using Equation (5A.31) we obtain

$$Z(j\omega) = \frac{l_c(1+j)}{b\sigma\delta(\omega)} = \frac{j\omega l_c(1-j)\delta(\omega)}{2a} \quad (5A.41)$$

Conclusions from Equation (5A.41) are

- The equivalent resistance is the resistance of a thin layer with thickness δ and width b on the top of the conductor.
- The real and the imaginary parts are equal and the phase angle equals 45° .
- The equivalent inductance is the inductance of a thin layer of air with thickness $\delta/2$ on top of the conductor. The equivalent length for the inductance is b ; the equivalent area is $A_m = l_w \delta/2$. Attention should be paid to the fact that *the equivalent air thickness to far the inductance is only $\delta/2$!*

We can rewrite Equation (5A.34) in a real and an imaginary part, which means a series equivalent circuit:

$$R_s = \frac{R_0 a}{\delta(\omega)} \frac{\sinh(2a/\delta(\omega)) + \sin(2a/\delta(\omega))}{\cosh(2a/\delta(\omega)) - \cos(2a/\delta(\omega))} \quad (5A.42)$$

$$L_s = \frac{R_0 a}{\omega\delta(\omega)} \frac{\sinh(2a/\delta(\omega)) - \sin(2a/\delta(\omega))}{\cosh(2a/\delta(\omega)) - \cos(2a/\delta(\omega))} \quad (5A.43)$$

Equations (5A.38), (5A.42), and (5A.43) are compatible with [6] and [8] for single conductors and several publications afterwards. Although Equations

(5A.42) and (5A.43) are real functions, they are not so easy to handle. As an example try to compute the value or the derivative for ω tending to 0!

Another problem with the equations of a single conductor in a slot is that the field problem is not split in orthogonal functions. Thus, care should be taken when these functions are used in various situations. Although the solution for a single wire is quite simple, it gets more complicated when other conductors are present, as the decomposition is not orthogonal and mixed products are present.

5.A.1.3 Superimposed Rectangular Conductors in a Slot

We consider the case of several superposed conductors carrying the same current, Fig. 5A.3.

Each conductor is subjected to its own field and to the field of the conductors below it. For the m th conductor the average field is

$$H_{av} = \left(m - \frac{1}{2}\right) \frac{I}{b} = F \frac{I}{2b} \quad (5A.44)$$

where

$$F = 2m - 1$$

The losses are dependent on H_{av}^2 . To obtain the total losses we sum over all the conductors. Thus, we need the sum of F^2 . Table 5A.1 shows the sum ΣF^2 .

We use Equation (5A.29), where we substitute the average field from Equation (5A.44). The total conductor length is ml_c . The total impedance for the series connection of the conductors is then

$$Z = \frac{1}{2b} l_c Z_0(s) m \left(\coth\left(\gamma(s) \frac{a}{2}\right) + \left(\frac{4m^2 - 1}{3}\right) \tanh\left(\gamma(s) \frac{a}{2}\right) \right) \quad (5A.45)$$

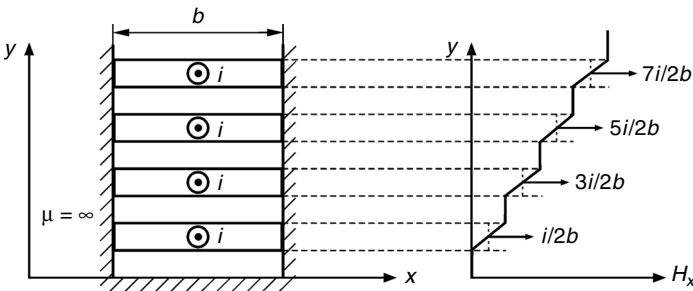


FIGURE 5A.3

Several conductors in a slot and the static field H_x in the x -direction.

TABLE 5A.1

The Sums ΣF^2

Conductor number	1	2	3	4	5
F	1	3	5	7	9
F^2	1	9	25	49	81
ΣF^2	1	10	35	84	165
$m(4m^2 - 1)/3$	1	10	35	84	165

We can introduce the DC resistance of the total wire and the penetration depth, then we obtain

$$Z = R_0 \frac{1+j}{\delta(\omega)} \frac{a}{2} \left(\coth\left(\frac{1+j}{\delta(\omega)} \frac{a}{2}\right) + \left(\frac{2b|H_{av}(I)|}{|I|}\right)^2 \tanh\left(\frac{1+j}{\delta(\omega)} \frac{a}{2}\right) \right) \quad (5A.46)$$

It can be verified that the case without average field corresponds to $m = 1/2$. This case occurs when the conductor is mirrored at the bottom of the slot, with no H -field in the middle of the conductor. This is often referred to as a half layer. It corresponds to minimal losses for a given current.

It is clear that the losses due to the transverse field increase a lot with increasing the number of layers m . Figure 5A.4 shows the result of Equation (5A.46) and various numbers of layers, for $R_0 = 1$. Fig. 5A.4 shows resistive and reactive

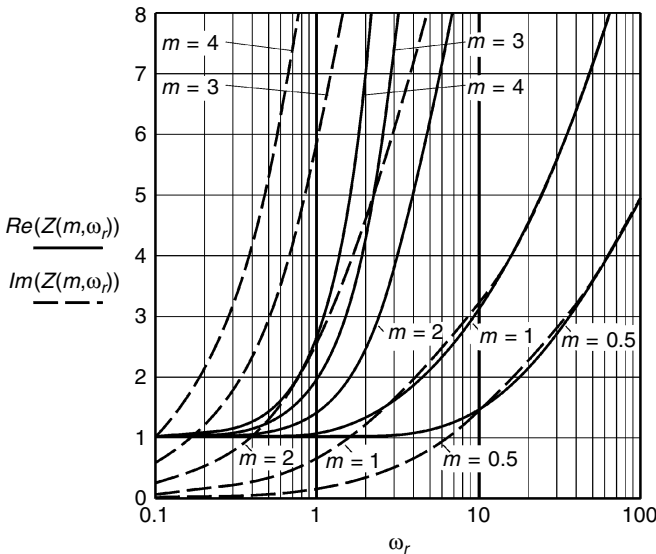


FIGURE 5A.4

Resistive and reactive impedance of m rectangular conductors in a slot, compared to the DC resistance, as a function of a relative frequency ω_r , $\omega_r = 1$ corresponds to $a = \delta$. The case $m = 0.5$ is without transverse field.

impedance of m rectangular conductors in a slot, compared to the DC resistance, as a function of a relative frequency ω_r . We use the relative frequency $\omega_r = \frac{\omega}{\omega_a}$ for $\omega_r = 1$, $\delta = a$, and $\omega_r = \frac{\omega \sigma \mu a^2}{2}$. The absolute frequency ω , is defined as the frequency for which the penetration depth δ equals the thickness of the conductor $\delta = a$, $\omega_a = \frac{2}{\sigma \mu a^2}$.

For $m = 0.5$, the impedance is identical to the case $m = 1$ if one chooses the frequency four times higher. Note that the resistive part increases almost in a quadratic way with m . The resistive part of the impedance depends on ω^2 for low frequency and increases with the root of the frequency $\sqrt{\omega}$ at high frequencies.

The conclusion is that for a given winding area when the field is in one direction, the losses are mainly dependent on the number of turns. There is a slight advantage to using a single layer in low frequency cases.

5.A.1.4 Taylor Expansion and Low Frequency Approximation for Superimposed Rectangular Conductors in a Slot

The complex functions can be expanded (for instance using MathCAD) in Taylor series as a function of the frequency ω . This can be done in a symbolic way. For that purpose, we use again the relative frequency; for $\omega_r = 1$ the penetration depth δ just equals the thickness a of the conductor:

$$\delta(\omega_a) = a \quad \omega_a = \frac{2}{\mu \sigma a^2} \quad \omega_r = \frac{\omega}{\omega_a} = \frac{\omega \mu \sigma a^2}{2} \quad (5A.47)$$

where ω_a is the absolute frequency, defined as the frequency, for which the penetration depth δ equals the thickness of the conductor $\delta = a$.

For a *current without field* we can write

$$Z = R_0 \sqrt{\frac{j\omega_r}{2}} \coth\left(\sqrt{\frac{j\omega_r}{2}}\right) = R_0 \frac{(1+j)}{2} \sqrt{\omega_r} \coth\left(\frac{(1+j)}{2} \sqrt{\omega_r}\right) \quad (5A.48)$$

$$\begin{aligned} \frac{Z}{R_0} = & 1 + \frac{j}{6} \omega_r + \frac{1}{180} \omega_r^2 - \frac{j}{3780} \omega_r^3 - \frac{1}{75600} \omega_r^4 \\ & + \frac{j}{1496880} \omega_r^5 + \frac{691}{20432412000} \omega_r^6 + \dots \end{aligned} \quad (5A.49)$$

The first term of the expansion from Equation (5A.40) is simply the resistance of the conductor. The second term is the low frequency inductance:

$$L = \frac{l_c}{12} \frac{\mu a}{b} \quad (5A.50)$$

The third term is the low frequency resistance increase compared to the DC resistance. The first and third term together yield

$$R(\omega) = \frac{l_c}{ab\sigma} \left(1 + \frac{a^4 \omega^2 \sigma^2 \mu^2}{720} \right) \quad (5A.51)$$

The impedance for the *transverse field* is

$$Z = \left(\frac{2H_{av}b}{I} \right)^2 R_0 \sqrt{\frac{j\omega}{2}} \tanh\left(\sqrt{\frac{j\omega}{2}}\right) \quad (5A.52)$$

$$\begin{aligned} \sqrt{\frac{j\omega_r}{2}} \tanh\left(\sqrt{\frac{j\omega_r}{2}}\right) &= 0 + \frac{j}{2}\omega_r + \frac{1}{12}\omega_r^2 - \frac{j}{60}\omega_r^3 - \frac{17}{5040}\omega_r^4 \\ &+ \frac{j31}{45360}\omega_r^5 + \frac{691}{4989600}\omega_r^6 + \dots \end{aligned} \quad (5A.53)$$

For a *single conductor* in a slot the impedance is

$$Z = R_0 \sqrt{\frac{j\omega_r}{2}} \left(\coth\left(\sqrt{\frac{j\omega_r}{2}}\right) + \tanh\left(\sqrt{\frac{j\omega_r}{2}}\right) \right) = R_0 \sqrt{j\omega_r} \coth\left(\sqrt{j\omega_r}\right) \quad (5A.54)$$

$$\begin{aligned} \frac{Z}{R_0} &= 1 + \frac{j2}{3}\omega_r + \frac{4}{45}\omega_r^2 - \frac{j16}{945}\omega_r^3 - \frac{16}{4725}\omega_r^4 \\ &+ \frac{j64}{93555}\omega_r^5 + \frac{88448}{638512875}\omega_r^6 + \dots \end{aligned} \quad (5A.55)$$

Conclusions concerning Equations (5A.52) and (5A.54) are

- The first three terms are representative for the low frequency approximation.
- The presence of the fourth term already reduces the inductance with the frequency and does not fit in the low frequency model any more. For comparison, this deviation appears earlier in the transverse field case.
- Up to a thickness a of about 1.6δ , the first three terms are sufficient for 10% accuracy on the eddy current losses.
- The losses in the low frequency model are quadratic with the frequency and with voltage, so they can be modeled as a resistor in parallel to the considered inductance. This fact allows an easy circuit modeling.

At low frequency, the transverse field solution is quite independent of the amount of air around the conductor, as far as there is a means to find an average field value between the upper and lower side. This means also that a low frequency approximation can also be used for fields being in a different direction compared to the x -axis. The transverse field is split in two components, one in the x -direction and one in the y -direction. The generated current distributions are odd in the x -direction (for H_x) and even in the y -direction (for H_y), which tends to give orthogonal functions, so that losses can be superposed.

The power losses $P_{tr,lf}$ at low frequency in the transverse field cases are

$$P_{tr,lf} = \frac{l_c}{12} \mu^2 \omega^2 \sigma \left(a^3 b |H_{av,x}|^2 + a b^3 |H_{av,y}|^2 \right) \quad (5A.56)$$

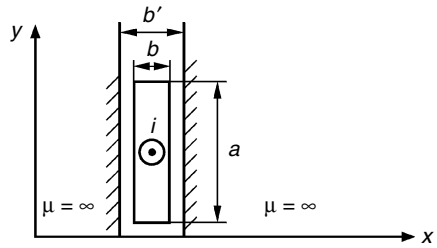


FIGURE 5A.5
A rectangular conductor with air.

Often one likes to see the power losses presented by the DC resistance

$$P_{tr,lf} = \frac{R_0}{12} \omega^2 \mu^2 \sigma^2 a^2 b^2 \left(a^2 |H_{av,x}|^2 + b^2 |H_{av,y}|^2 \right) \quad (5A.57)$$

5.A.1.5 Approximation for Rectangular Conductors with Air

In real cases, conductors do have insulation or space in between and they are spaced to the magnetic materials. In these cases exact analytical solutions are not obvious.

5.A.1.5.1 Classical Approach

The classical approach starts the derivation considering a narrow space and a narrow conductor. If the space and the conductor width are small compared to the penetration depth, the H -field is still in the x -direction. Figure 5A.5 shows an example.

The type of approximation possible assumes that the magnetic field is in the x -direction. The problem can be translated in the problem of a single conductor with conductivity for horizontal fields reduced with the amount of air. This adapted conductivity is then given as

$$\sigma' = \frac{b}{b'} \sigma \quad (5A.58)$$

The adapted conductivity results also in an adapted penetration depth $\delta'(\omega)$, characteristic impedance $Z'_0(s)$, and propagation function $\gamma'(s)$, expressed as

$$\delta'(\omega) = \sqrt{\frac{2\rho b'}{\omega\mu b}} \quad (5A.59)$$

$$Z'_0(s) = \left(\frac{s\mu}{\sigma'} \right)^{1/2} = \sqrt{j} \sqrt{\frac{\omega\mu b}{\sigma b'}} = \frac{1+j}{\sqrt{2}} \sqrt{\frac{\omega\mu}{\sigma}} \sqrt{\frac{b}{b'}} \quad (5A.60)$$

$$\gamma'(s) = (s\mu\sigma')^{1/2} = \frac{1+j}{\sqrt{2}} \sqrt{\frac{\omega\mu\sigma b}{b'}} = \frac{1+j}{\delta'(\omega)} \quad (5A.61)$$

The following remarks should be considered:

- The predicted losses are not accurate for low ratio b/b' . For a free conductor, the predicted losses are zero, which does not correspond to the reality.
- There is no physical meaning of the adapted penetration depth. At very high frequency, the physical penetration depth inside the conductor will still be the original one.

Although the method is not really applicable for low values of the ratio b/b' , still some reasonable accuracy is obtained in normal cases. For one layer, reference [9] compares the approximation with finite elements solutions. The simplified conclusions are

- For $b/b' > 0.8$, the losses are overestimated up to about 2.5%.
- For $b/b' = 0.5$, the losses are underestimated about 1% for low frequency; and overestimated up to 10% at intermediate frequencies.

In fact, we would not recommend using the method for values of b/b' lower than 0.5 values as both large underestimations and overestimations can occur. This constraint is usually not limiting for conductors in a layer. But, in practice, this means that the approximation is not good for fields in the y -direction of the winding area, where it is likely to have more air than conductors. Such fields are usual in inductors with concentrated air gap.

Appendix 5.A.2 Low Frequency 2-D Models for Eddy Current Losses in Round Wires

5.A.2.1 Low Frequency Approach

For a low frequency (LF) approach, the eddy currents induced in the winding do not considerably change the applied field in the winding. This field penetrates in the conductor and the losses in round wires are quadratic with frequency. The low frequency approach results in about 10% error on eddy current losses when $d \leq 1.6\delta$, d is the wire diameter and δ is the penetration depth for the applied frequency [10]. In that LF range, the proposed exact analytical solution has more realistic field patterns compared to the classical Dowell method [6] and is more accurate for low frequencies, as the method is derived directly for round wires. The main problem of the classical 1-D methods [3] is that the fields are only homogeneous in a layer in ideal cases. In the scientific literature 2-D analytical approximations are mainly focused on uniform transverse fields (proximity losses) and also on the own field of a wire (skin-effect losses) [11–14].

Methods of extending the design to nonsinusoidal waveforms for transformer and inductor design are given in [15–17].

Here we present an approximation method for calculating eddy current losses in round wires using a 2-D low frequency approach.

- First, we derived an exact solution containing the sums of the contributions of fluxes induced by the individual wires. The losses in a wire can be found using one single surface integral. However, that integral slows the calculation down.
- To speed up the calculation, we developed an approximation method using three fields: a uniform transverse, a rotational, and a hyperbolic field. These fields are easy to compute and the calculation is very fast, as neither integral nor functions have to be computed.

Within its limitations, the accuracy of the approximation in normal winding configurations is usually better than 0.1%. Features of the proposed three-field approximation method are the low computational time and the possibility to investigate and optimize the following design aspects: the difference in losses, dependent on the distance between layers; hexagonal or square fitting of the wires; the influence of the fields of air gaps; and the influence of the distance to the magnetic materials.

5.A.2.2 Defining a 2-D Winding Arrangement

We use complex numbers to represent the place of conductors and distance vectors. To have the possibility of testing easily a number of winding arrangements (Fig. 5A.6), we define for the m th layer:

- The center of the first conductor of the m th layer has a complex coordinate $z_{m,1} = x_m + jy_m$.
- The distance between the centers of the conductors is s_m .
- The current in the conductors is i_m .

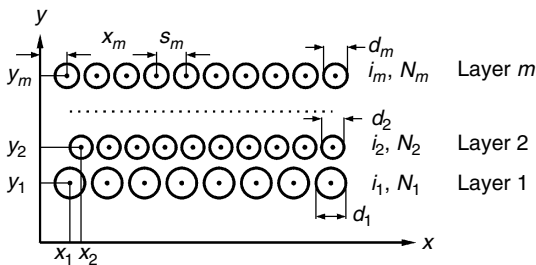


FIGURE 5A.6

An arbitrary winding arrangement.

- The number of conductors of the layer m is N_m .
- m is the considered layer.
- There are M layers in total.

The presence of an air gap can be reasonably modeled as a fictitious conductor without eddy currents with a current equal to the m.m.f. (magneto-motive force) across the air gap.

5.A.2.3 Eddy Current Losses by The Direct Integration Method

The field generated by a current i in a single conductor in the LF case, inside the conductor is

$$H_{in} = \frac{a}{r} \frac{i j}{2 \pi r} \quad (5A.62)$$

where

i is the current in the conductor

r is the radius of the conductor

a is the distance vector from the considered point to the center of the conductor ($|a| < r$)

j is the imaginary unit (= positive y -axis, rotates the vector, $+90^\circ$)

The field generated by a current i in a single conductor outside the conductor ($a > r$) in the LF case is

$$H_{ext} = \frac{i j}{2 \pi a^*} \quad (5A.63)$$

where

a^* is the complex conjugate of a , $a^* = x - jy$, ($|a^*| = |a| > r$)

The resulting field of a number of conductors in a considered conductor (cc) is the sum of the inside field of the considered conductor (own field) and the outside fields of all the other conductors in the winding. The considered conductor is in the layer m_c and has the number n_c .

The flux Φ at a point in the space at a distance a_2 from a current carrying conductor is

$$\Phi = \mu \int \frac{H}{j} dl = \mu \operatorname{Re} \left\{ \int_{a_1}^{a_2} \frac{i}{2 \pi a^*} da \right\} = \frac{\mu i}{2 \pi} \left(\ln(|a_2|) - \ln(|a_1|) \right) = \frac{\mu i}{2 \pi} \ln \left(\left| \frac{a_2}{a_1} \right| \right) \quad (5A.64)$$

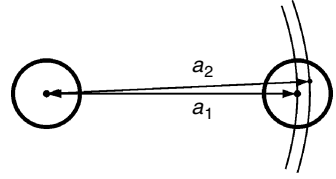
where

a_1 is the distance vector between the centers of the two conductors, see [Fig.5 A.7](#)

a_2 is the distance vector between the point (z) and the center of the n^{th} conductor

FIGURE 5A.7

The distance vector a_1 between the centres of the two conductors and the distance vector a_2 between the center of the n th conductor and the point (x, y) .



Note that the result does not change if a complex conjugate is used.

The flux $\Phi(z)$ of the n th conductor of the m th layer ($z_{m,n}$), generated in a point (z) of the considered conductor ($z_{mc,nc}$ -layer m_c , number n_c):

$$\Phi_{m,n}(z) = \frac{\mu i_m}{2\pi} \ln \left(\frac{z - z_{m,n}}{z_{mc,nc} - z_{m,n}} \right) \quad (5A.65)$$

where

n is the number of the conductor, which field is considered

m is the layer of the conductor, which field is considered

n_c is the number of the conductor in which we calculate the flux

m_c is the layer of the considered conductor

In a point (z) the sum of the external fluxes $\Phi_{m,n}(z)$ of all the conductors is

$$\Phi_{ext}(z) = \frac{\mu}{2\pi} \sum_{m=1}^M i_m \sum_{n=1}^{N_m} \varepsilon(m - m_c, n - n_c) \ln \left(\frac{z - z_{m,n}}{z_{mc,nc} - z_{m,n}} \right) \quad (5A.66)$$

where

$\varepsilon(m - m_c, n - n_c) = 0$ for $(m = m_c \text{ AND } n = n_c)$ and $\varepsilon(m - m_c, n - n_c) = 1$ for all other cases

The contribution of the flux of the considered conductor itself is

$$\Phi_{int}(z) = \frac{\mu i_{mc}}{4\pi} \left(\frac{|z - z_{mc,nc}|^2}{r_{mc}^2} \right) \quad (5A.67)$$

Then we obtain the total flux from internal and external currents:

$$\Phi_{\Sigma}(z) = \Phi_{ext}(z) + \Phi_{int}(z) \quad (5A.68)$$

Eddy currents in wires flow in the axial direction of the wire. The magnitude of the current density is the derivative of the flux to the time divided by the specific resistivity ρ . The integrating constant in the flux must be chosen in a way that the induced eddy current over the wire section is zero.

To remove the integrating constant we subtract the average value of the flux Φ_{av} over the cross section surface $S = \pi r^2$ of the wire. The average value of the flux for the considered conductor is

$$\Phi_{av} = \frac{1}{\pi r_{mc}^2} \int_{-r_1}^{r_1} \int_{-\sqrt{r_1^2 - y^2}}^{\sqrt{r_1^2 - y^2}} \Phi_{\Sigma}(z_{mc,nc} - (x + jy)) dx dy \quad (5A.69)$$

Note that for circular conductors, this contribution comes from the field from the internal current.

Now we can express the resulting flux $\Phi(z)$, which generates eddy currents:

$$\Phi(z) = \Phi_{\Sigma}(z) - \Phi_{av} \quad (5A.70)$$

The local eddy current loss/volume is integrated over the conductor surface to give the power loss for a considered conductor per unit length:

$$P_{eddy} = \frac{(2\pi f)^2}{\rho_m} \int_{-r_1}^{r_1} \int_{-\sqrt{r_1^2 - y^2}}^{\sqrt{r_1^2 - y^2}} (\Phi(z_{mc,nc} - (x + jy)))^2 dx dy \quad (5A.71)$$

where

f is the excitation frequency

ρ_m is the resistivity of the conductor

The proposed method allows using the most practical arrangements even in cases that are not possible to analyze with methods that suppose that the field direction is parallel to the layers, such as Dowell's method.

The calculation speed of the method is feasible (a few minutes for 50 wires, using MathCAD) as only one surface integral has to be computed numerically. Regardless, the method is fast enough to be used as a way to check more approximate methods.

5.A.2.4 The Proposed Three Orthogonal Fields Method

A way to fasten the integral is to approximate it with a first order approximation. In general, however, the first derivatives to x and y are not orthogonal, so the losses cannot be added. Therefore we propose to use the following set of three fields, see Fig. 5A.8:

- the one field of a single current carrying conductor, which contains the first derivatives in a single rotation direction
- the uniform transverse field
- the hyperbolic field, which contains the first derivatives in an opposite rotation direction

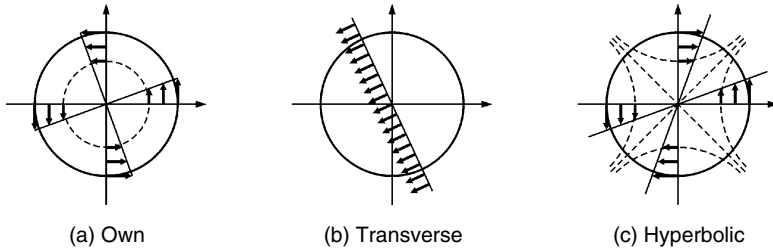


FIGURE 5A.8
The three orthogonal fields, comprised in the proposed three-field approximation.

It can be shown that these fields correspond to the following resulting current distributions:

- a current density independent of the orientation θ , mode 0
- a current density changing with $\sin(\theta - \varphi_1)$, mode 1
- a current density changing with $\sin(2\theta - \varphi_2)$, mode 2

Those three components are orthogonal, as their mixed products vanish when integrated over the conductor.

The field H generated by the other conductors of all layers can be approximated by its value at the center of the conductor H_0 and its derivatives of H in space (Taylor expansion):

$$H = H_0 + \frac{dH}{dz} a + \frac{d^2H}{d^2z} a^2 + \dots \quad \text{and also} \quad H = H_0 + \frac{dH}{dz^*} a^* + \dots \quad (5A.72)$$

5.A.2.4.1 The Field of the Conductor

The field at a point inside the considered conductor imposed by the current in the same conductor is

$$H_{in} = \frac{a}{r_m^2} \frac{i_{mc} j}{2\pi} \quad (5A.73)$$

5.A.2.4.2 The Transverse Field

If the field H_0 is applied to the whole conductor section we call it a transverse field H_{tr} . The total transverse field resulting from all the conductors in the center of the considered conductor is

$$H_{tr} = \frac{j}{2\pi} \sum_{m=1}^M i_m \sum_{n=1}^{N_m} \varepsilon(m - m_c, n - n_c) \frac{1}{z_{mc,nc}^* - z_{m,n}^*} \quad (5A.74)$$

This field is applied over the conductor area (Fig. 5A.8,b).

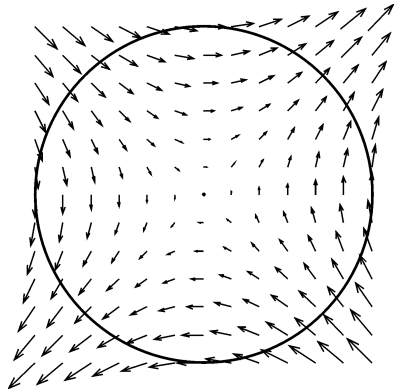


FIGURE 5A.9
Hyperbolic field distribution in a round conductor for $\left| \frac{dH}{dz^*} \right| = 1$.

5.A.2.4.3 The Hyperbolic Field

The derivative to the distance of the field generated by the other conductors of all layers in the center of the considered conductor is

$$\frac{dH}{dz^*} = \frac{-j}{2\pi} \sum_{m=1}^M i_m \sum_{n=1}^{N_m} \varepsilon(m - m_c, n - n_c) \frac{1}{(z_{mc,nc}^* - z_{m,n}^*)^2} \quad (5A.75)$$

This presentation corresponds to the following field contribution according to Equation (5A.72).

$$H_1 = \frac{dH}{dz^*} a^* \quad (5A.76)$$

Therefore we denote the deviation caused by the derivate of the field by other conductors as a hyperbolic field, given as

$$H_{hy} = \frac{dH}{dz^*} a^* = H'_{hy} a^* \quad (5A.77)$$

Equation (5A.77) results in a field pattern where the field lines follow hyperbolas (Fig. 5A.9). Note that, as the field does not contain the field of the current, the rotational field of this component is zero. So, the hyperbolic field component does not contribute to the average value of the MMF.

5.A.2.4.4 Residual Field

The difference between the actual fields, as used in the integral method and the sum of the three fields is called residual field (2nd and higher order in Taylor expansion). This field is usually low. It is zero in the middle of the conductor, and also its first derivatives are zero. In the validation we can look at the relevance of this residual field for the accuracy of the method.

5.A.2.4.5 Eddy Current Losses by the Three Orthogonal Fields

Considering the fields (H_{in}, H_{tr}, H_{hy}) , we can find the eddy current losses due to each of the three components as we did for the direct integral method before—calculate the flux Φ , subtract the average value of the flux Φ_{av} , and integrate the eddy current loss over the conductor surface to obtain the power loss per unit length for the considered conductor.

- For the field of a single current carrying conductor (the own field), the eddy current losses are

$$P_{eddy,own} = \frac{\pi r_m^2 (2\pi f)^2 \mu_0^2 (i_m / 2\pi)^2}{24 \rho_m} \quad (5A.78)$$

This is the first term of the Taylor series of the exact wide frequency *skin effect loss* of a free wire [11,18].

- For the transverse field losses we obtain the losses for unity length, which corresponds to [13]:

$$P_{eddy,tr} = \frac{\pi r_m^4 (2\pi f)^2 \mu_0^2 |H_{tr}'|^2}{4 \rho_m} \quad (5A.79)$$

This is the first term of the Taylor series of the exact wide frequency solution of the *proximity losses* of a free wire in a uniform transverse field [11,18].

- The hyperbolic field losses are

$$P_{eddy,hy} = \frac{\pi r_m^6 (2\pi f)^2 \mu_0^2 |H_{hy}'|^2}{24 \rho_m} \quad (5A.80)$$

The solution is found by calculating the flux of the hyperbolic field and the corresponding eddy current losses. The hyperbolic field is usually not considered in analytical solutions in literature, which means that these solutions do not attain a first order approximation accuracy of the field.

- The total losses are then

$$P_{eddy,\Sigma} = P_{eddy,own} + P_{eddy,tr} + P_{eddy,hy} \quad (5A.81)$$

Note that this result does only use sums, multiplications, and divisions; no functions have to be computed. For example, the operation of the square of a modulus, used in Equation (5A.79) can be written as

$$|H_{tr}'|^2 = \text{Re}(H_{tr}')^2 + \text{Im}(H_{tr}')^2 \quad (5A.82)$$

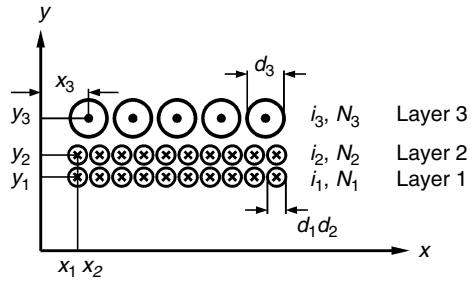


FIGURE 5A.10
Two-winding transformer arrangement for the calculated example.

5.A.2.5 Validation of the Proposed 3-Field Approximation

To validate the proposed approximation method, eddy current calculation, we take an example with the following parameters, see Fig. 5A.10:

- the first layer (primary winding) $N_1 = 10$, $i_1 = 1A$, $d_1 = 0.25$ mm, $s_1 = 0.30$ mm, $x_1 = 0.15$ mm, $y_1 = 0$
- the second layer (primary winding) $N_2 = 10$, $i_2 = 1A$, $d_2 = 0.25$ mm, $s_2 = 0.30$ mm, $x_2 = 0.15$ mm, $y_2 = 0.30$ mm;
- the third layer (secondary winding) $N_3 = 5$, $i_3 = -4A$, $d_3 = 0.5$ mm, $s_3 = 0.60$ mm, $x_3 = 0.30$ mm, $y_3 = 0.80$ mm .
- $\rho_m = 20 \times 10^{-9} \Omega\text{m}$

The frequency is $f = 50$ kHz, so we have a LF case, as the penetration depth for 50 kHz is $\delta_{50 \text{ kHz}} = 0.338$ mm and for $d_3 = 0.5$ mm the limit $d \leq 1.6\delta$ is met.

In Table 5A.2 we give the found values of the eddy current losses in each conductor of the third layer by the proposed approximation approach $P_{eddy,ap}$ and the direct integration method $P_{eddy,in}$ and the deviation between two values. The found deviation is due to the residual field but remains below 0.1%. This accuracy is quite satisfactory, taking into account the very low computation time of the proposed method. In examples with more layers, the accuracy improves, as the main losses are due to transverse fields.

TABLE 5A.2

Eddy Current Losses in Each Conductor of the Third Layer of the Example (See Fig. 5A.10), Given by the Proposed 3-Field Method $P_{eddy,ap}$ and Direct Integration Method $P_{eddy,in}$ and the Deviation Between Them

Losses/m [W]	1-st conductor	2-nd conductor	3-rd conductor	4-th conductor	5-th conductor
$P_{eddy,ap}$	0.116425372	0.15459682	0.167083425	0.15459682	0.116425372
$P_{eddy,in}$	0.116522823	0.15461503	0.167100871	0.15461503	0.116522823
$P_{eddy,ap} - P_{eddy,in}$	-0.00083632	-0.00011775	-0.00010440	-0.00011776	-0.00083632
$\frac{P_{eddy,ap} - P_{eddy,in}}{P_{eddy,in}}$					

The time for calculating the losses in all conductors for this arrangement of 25 conductors with the integral method is 1 min and 15 sec. With the proposed three-field method we can calculate a problem with 10^3 conductors for the same calculating time. We observed that this time is proportional with the square of the total number of the conductors.

5.A.2.6 Extension of the Obtained Solution

Note that the examples are derived without the presence of magnetic material. One can take into account mirroring techniques or use the finite elements method to calculate the transverse field contribution, but this is beyond the scope of this appendix.

If different conductors carry different currents with harmonics, each current can be written in a Fourier sine and cosine expansion. The contributions of all the sine components for each frequency are orthogonal in time with the cosine contributions. By this property all power loss contributions can be added.

This means that problems of transformer windings with phase-shifted currents can be solved. Remember that we consider frequencies where $d \leq 1.6\delta$. The approach overestimates losses if higher frequencies are present.

Appendix 5.A.3 Field Factor For Inductors

A field factor k_F is used to take transverse field losses into account in non-homogenous fields due to air gaps, such as in inductors. The factor k_F has been chosen in the way that it is close to 1 for transformers and also for inductors if the winding is far away from the air gap.

5.A.3.1 2-D Analytical Approximation of the Field Factor k_F

If the layer is wound using the full winding width of the winding area, the field of the winding can be presented as a superposition of linear increasing field by the winding and a field caused by the air gap, mirrored at the walls of the core.

The gap is modeled with a concentrated *MMF* at the center of the gap:

$$H(z) = \frac{j}{2\pi} \frac{NI}{z^*} \quad (5A.83)$$

where

$z = x + jy$ is the complex coordinate of a point

Mirroring at $y = 0$ doubles the current. Mirroring in the x direction is periodic with a (the window width) and mirroring in y direction is with a period of $2h$ (the window height, see [Fig. A5.11](#)).

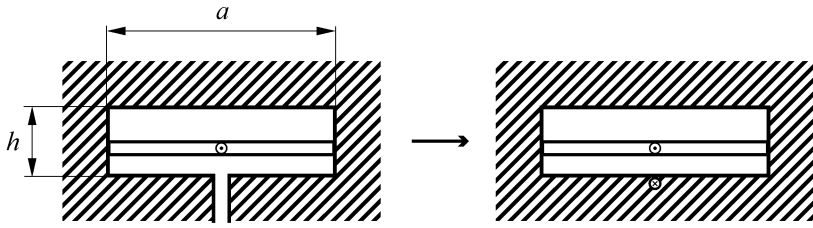


FIGURE 5A.11
Inductor core window and dimensions.

The field of the gap is given as:

$$H_g(z) = \frac{2jNI}{2\pi} \sum_{k=-\infty}^{\infty} \sum_{m=-\infty}^{\infty} \frac{1}{z^* + 2jk h + a m} \quad (5A.84)$$

One of the infinite sums in Equation (5A.84) can be changed into a function, which improves the accuracy and speed:

$$H_g(z) = \frac{2jNI}{2\pi} \sum_{k=-\infty}^{\infty} \frac{\pi}{a} \cot \frac{(z^* + 2jk h)\pi}{a} \quad (5A.85)$$

The winding is modeled by a current density. When it is mirrored in the x direction, it becomes independent of x . We have the field of the window H_w

$$\begin{aligned} H_w(z) &= 0 \quad \text{for } \text{Im}(z) < d_{wg} \\ H_w(z) &= NI \quad \text{for } \text{Im}(z) > d_{wg} + t_w \\ H_w(z) &= NI \frac{\text{Im}(z) - d_{wg}}{t_w} \quad \text{for } d_{wg} + t_w > \text{Im}(z) > d_{wg} \end{aligned} \quad (5A.86)$$

The sum of H_g and H_w (the field of the winding) is the resulting field H in the window area:

$$H(z) = H_g(z) + H_w(z) \quad (5A.87)$$

It can be verified that H has no tangential component at the walls. The vector of the field H is shown in Fig. 5A.12, the amplitude is limited to 50 A/m.

The square of the field in the x -direction, averaged over the cross section is

$$\langle H_x^2 \rangle_{av} = \frac{1}{t_w a/2} \int_{d_{wg}}^{d_{wg}+t_w} \int_a^{a/2} (\text{Re}(H(z, d_{wg}, t_w)))^2 dx dy \quad (5A.88)$$

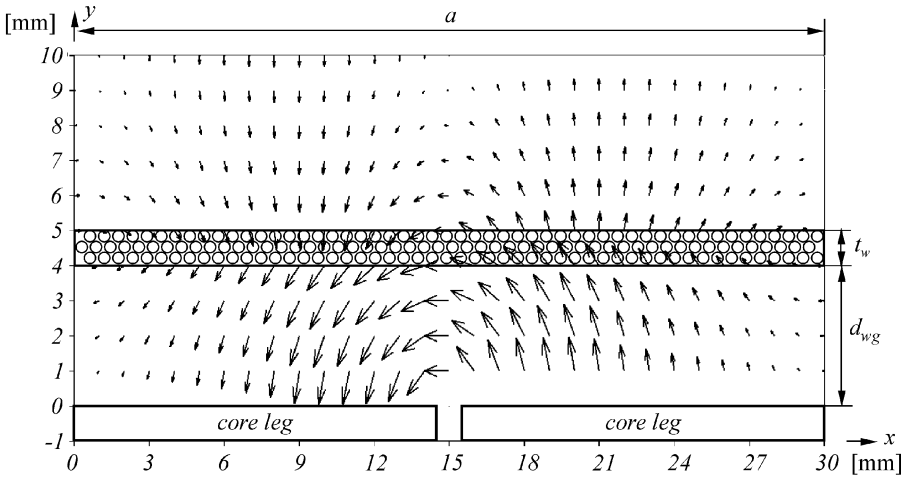


FIGURE 5A.12

Field vector in x -axis and y -axis, the winding is between 4 and 5 mm. The winding area is 30 mm wide and 10 mm high. The m.m.f. is set to 1 A turn.

The square of the field in the y -direction, averaged over the cross section is

$$\langle H_y^2 \rangle_{av} = \frac{1}{t_w a/2} \int_{d_{wg}}^{d_{wg}+t_w} \int_a^{a/2} (\text{Im}(H(z, d_{wg}, t_w)))^2 dx dy \quad (5A.89)$$

If the winding is far away from the air gap, the field across the winding increases linearly and the averaged square of the field then is

$$\langle H^2 \rangle_{av} = \frac{1}{3} \left(\frac{NI}{a} \right)^2 \quad (5A.90)$$

This equivalent field is used as a reference solution. Two contributions of the field factor k_F are defined as

$$k_{Fx} = \frac{\langle H_x^2 \rangle_{av}}{\frac{1}{3} \left(\frac{NI}{w} \right)^2} \quad (5A.91)$$

$$k_{Fy} = \frac{\langle H_y^2 \rangle_{av}}{\frac{1}{3} \left(\frac{NI}{w} \right)^2} \quad (5A.92)$$

For the field in the x direction the filling factor η is relevant. The filling factor λ is relevant for the field in the y direction.

5.A.3.2 Simplified Approach

When both field directions parallel and perpendicular to the layer generate about the same losses, a simple presentation of k_F can be used:

$$k_F = k_{Fx} + k_{Fy} \quad (5A.93)$$

REMARKS

- This simplification is allowed at low frequency.
- In high frequency simplified approach, we consider if the field is parallel or perpendicular to the layer and not to the higher order local fields when the filling is high. This approach is allowed as k_{Fx} and k_{Fy} are usually of the same magnitude in inductors, whereas k_{Fx} dominates in transformers.
- In the simplified approach for inductors one can use the losses of a single wire in a transverse field. This approach is used in [Chapter 2](#).
- The approach gives sufficient accuracy for most of the cases.

5.A.3.3 Parallel and Perpendicular Components of k_F

In this approach we separate the field component in a component parallel and a component perpendicular to the layer.

The analytical approximations of k_F , k_{Fx} and k_{Fy} are

$$k_F(\kappa) = \frac{3.44(0.505 - \kappa)^2 + 0.688}{\kappa} \quad (5A.94)$$

$$k_{Fx}(\kappa) = \frac{1.55(0.38 - \kappa)^2 + 0.517}{\kappa} \quad (5A.95)$$

$$k_{Fy}(\kappa) = \frac{1.88(0.609 - \kappa)^2 + 0.126}{\kappa} \quad (5A.96)$$

In [Fig. 5A.13](#), [Fig. 5A.14](#), and [Fig. 5A.15](#) we show factors k_F , k_{Fx} , and k_{Fy} as a function of the factor κ for different cores (rectangular and round legs) and for different locations of the windings: between legs and coil ends.

In [Table 5A.3](#) we show the values of k_F , in [Table 5A.4](#) the values of k_{Fx} and in [Table 5A.5](#) the values of k_{Fy} for the different cores and cases.

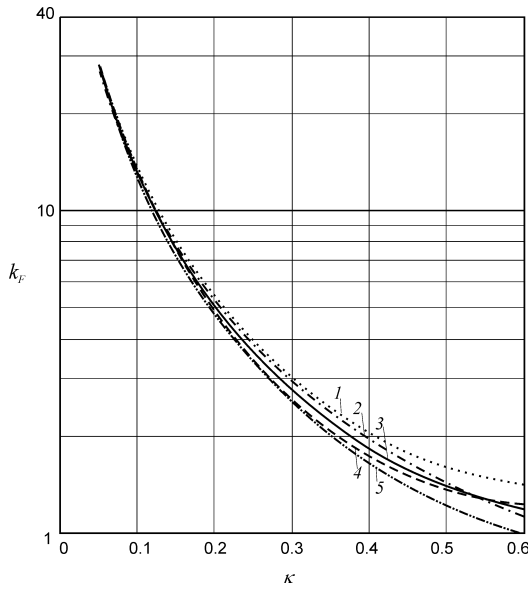


FIGURE 5A.13

The field factor k_F as a function of κ .

- 1: 2-D plane solution for windings between legs, for example: in EE core designs, Figure 2.8, cut A.
- 2: 2-D plane solution for coil ends, example: in EE core designs, Figure 2.8, cut B.
- 3: average curve, given by the analytical approximation.
- 4: axis-symmetrical solution for windings between legs, for example: Pot core designs, ETD core designs, cut A.
- 5: axis-symmetrical solution for coil ends, example: ETD core designs, cut B.

TABLE 5A.3

The Values of the Coefficient k_F for Different Values of κ

κ	k_{F_r} 2-D plane Between legs	k_{F_r} 2-D plane Coil ends	$k_{F, average}$	k_{F_r} Axis- symmetrical Between legs	k_{F_r} Axis- symmetrical Coil ends
0.05	28.3315	27.7809	28.2293	28.7165	28.0884
0.1	13.0077	12.5958	12.671	12.75	12.3303
0.15	7.8694	7.5813	7.4945	7.3945	7.1328
0.2	5.3515	5.159	5.0058	4.8343	4.6785
0.25	3.9065	3.7782	3.607	3.419	3.3243
0.3	3.0061	2.9127	2.75	2.5748	2.5066
0.35	2.4183	2.3348	2.1956	2.0482	1.9813
0.4	2.0245	1.9306	1.8236	1.7108	1.6283
0.45	1.7585	1.6382	1.5678	1.4918	1.3826
0.5	1.5809	1.421	1.3897	1.3497	1.2071
0.55	1.4681	1.2565	1.2658	1.2595	1.0791
0.6	1.4062	1.1303	1.184	1.2149	0.9845

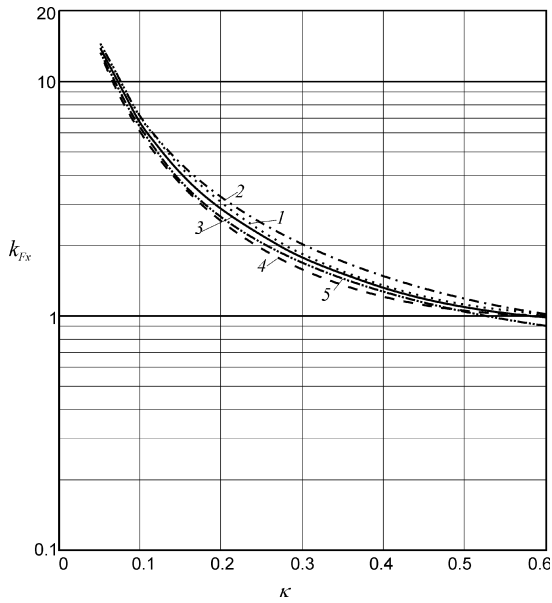


FIGURE 5A.14

The field factor k_{Fx} as a function of κ .

- 1: 2-D plane solution for windings between legs, for example: in EE core designs, Figure 2.8, cut A.
- 2: 2-D plane solution for coil ends, example: in EE core designs, Figure 2.8, cut B.
- 3: average curve, given by the analytical approximation.
- 4: axis-symmetrical solution for windings between legs, for example: Pot core designs, ETD core designs, cut A.
- 5: axis-symmetrical solution for coil ends, example: ETD core designs, cut B.

TABLE 5A.4

The Values of the Coefficient k_{Fx} for Different Values of κ

κ	k_{Fx} 2-D plane Between legs	k_{Fx} 2-D plane Coil ends	$k_{Fx, average}$	k_{Fx} Axis- symmetrical Between legs	k_{Fx} Axis- symmetrical Coil ends
0.05	14.4764	14.4715	13.8627	13.2515	13.2515
0.1	6.8142	6.8737	6.4151	5.9558	6.0167
0.15	4.2453	4.3592	3.9767	3.5987	3.7036
0.2	2.9864	3.1384	2.8111	2.4956	2.6238
0.25	2.2639	2.4363	2.1551	1.8940	2.0263
0.3	1.8137	1.9902	1.7507	1.5388	1.6599
0.35	1.5198	1.6866	1.4859	1.3196	1.4177
0.4	1.3229	1.4689	1.3053	1.1810	1.2483
0.45	1.1899	1.3065	1.1784	1.0929	1.1241
0.5	1.1011	1.1814	1.0875	1.0376	1.0298
0.55	1.0447	1.0827	1.022	1.0046	0.9561
0.6	1.0138	1.0034	0.9772	0.9944	0.8973

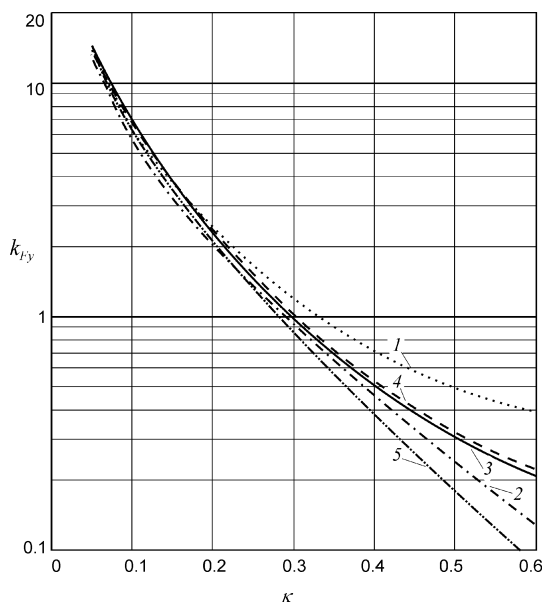


FIGURE 5A.15

The field factor k_{Fy} as a function of κ .

- 1: 2-D plane solution for windings between legs, for example: in EE core designs, Figure 2.8, cut A.
- 2: 2-D plane solution for coil ends, example: in EE core designs, Figure 2.8, cut B.
- 3: average curve, given by the analytical approximation.
- 4: axis-symmetrical solution for windings between legs, for example: Pot core designs, ETD core designs, cut A.
- 5: axis-symmetrical solution for coil ends, example: ETD core designs, cut B.

TABLE 5A.5

The Values of the Coefficient k_{Fy} for Different Values of κ

κ	k_{Fy} 2-D plane Between legs	k_{Fy} 2-D plane Coil ends	$k_{Fy, average}$	k_{Fy} Axis- symmetrical Between legs	k_{Fy} Axis- symmetrical Coil ends
0.05	13.8551	13.3094	14.3666	15.4650	14.8369
0.1	6.1935	5.7221	6.2559	6.7942	6.3136
0.15	3.6241	3.2221	3.5178	3.7958	3.4292
0.2	2.3651	2.0206	2.1948	2.3387	2.0547
0.25	1.6426	1.3419	1.4519	1.5250	1.2980
0.3	1.1924	0.9225	0.9994	1.0360	0.8467
0.35	0.8985	0.6482	0.7097	0.7286	0.5636
0.4	0.7016	0.4617	0.5183	0.5298	0.3800
0.45	0.5686	0.3317	0.3894	0.3989	0.2585
0.5	0.4798	0.2396	0.3022	0.3121	0.1773
0.55	0.4234	0.1738	0.2438	0.2549	0.1230
0.6	0.3924	0.1269	0.2068	0.2205	0.0872

References

- [1] Vashy, A., *Traité d'Électricité et de Magnétisme*, Tome premier Paris, Librairie polytechnique, Baudry et Cie, 15, rue de saints pères, 15, 1890, Chapitre III, §174 Cas d'un câble à conducteurs concentriques and § État variable du courant dans un circuit.
- [2] Snoek, J.L., *New Developments in Ferromagnetic Materials*, Elsevier Publishing Company, Inc., New York and Amsterdam, 1947.
- [3] Snelling, E.C., *Soft Ferrites: Properties and Applications*, 2nd ed., Butterworth, London, 1988.
- [4] Dowell, P.L., Effects of eddy currents in transformer windings, *IEE Proceedings*, vol. 113, No. 8, August, 1966, pp. 1387–1394.
- [5] Frederic, R., Modelisation et simulation de transformateurs pour alimentations a decoupage, PhD thesis, Universite Libre de Bruxelles, 2000, vol. 1 and vol. 2.
- [6] Lammeraner, J., and Stafl, M., *Eddy Currents*, Iliffe Books, London, 1966.
- [7] Foglier, 1996, *The Handbook of Electrical Engineering*, REA Staff of Research and Education Association, Piscataway, NJ, ISBN 0-87891-981-3.
- [8] Lebourgeois, R., Bérenguer, S., Ramiarinjaona, C., and Waeckerlé T., Analysis of the initial complex permeability versus frequency of soft nanocrystalline ribbons and derived composites, *Journal of Magnetism and Magnetic Materials*, vol. 254–255, January 1, 2003, pp. 191–194.
- [9] Frederic, R., A closed-form formula for 2-D ohmic losses calculation in SMPS transformers, *IEEE Transactions on Power Electronics*, vol. 16, No. 3, May 2001, pp. 437–444.
- [10] Valchev, V., and Van den Bossche, A., Design method for power electronic magnetic components including eddy current losses, 1st International Congress, MEET-MARIND, Varna, Bulgaria, 7–11 October, 2002, pp. 311–321.
- [11] Wallmeier, P., Frohlike, N., and Grotstollen, H., Improved analytical modelling of conductive losses in gapped high-frequency inductors, *IEEE-IAS Annual Meeting*, 1998, pp. 913–920.
- [12] Severns, R., Additional losses in high frequency magnetics due to non ideal field distributions, *APEC'92, 7th Annual IEEE Applications Power Electronics Conference*, 1992, pp. 333–338.
- [13] Sullivan, C.R., Winding loss calculation with multiple windings, arbitrary waveforms and 2-D field geometry, *IEEE IAS Annual Meeting*, 1999, pp. 2093–2099.
- [14] Carsten, B., Designing filter inductors for simultaneous minimization of dc and high frequency ac conductor losses, *PCIM'94, Dallas, TX*, 17–22 Sept. 1994, pp. 19–37.
- [15] Hurley, W.G., Gath, E., and Breslin, J.G., Optimised transformer design: inclusive of high-frequency effects, *IEEE Transactions on Power Electronics*, vol. 13, No. 4, July 1998, pp. 651–658.
- [16] Hurley, W.G., Gath, E., and Breslin, J.G. Optimising the ac resistance of multi-layer transformer windings with arbitrary current waveforms, *IEEE Transactions on Power Electronics*, vol. 15, No. 2, March 2000, pp. 369–376.
- [17] Petkov, R., Optimum design of a high-power, high-frequency transformer, *IEEE Transactions on Power Electronics*, vol. 11, No. 1, January 1996, pp. 33–42.
- [18] Ferreira, J., Analytical computation of AC resistance of round and rectangular litz wire windings, *IEEE Proceedings—B*, vol. 139, No. 1, 1992, pp. 21–25.

6

Thermal Aspects

In this chapter we discuss the heat transfer aspects that determine the magnetic component operating temperature. The component operating temperature is the sum of the ambient temperature and the component temperature rise.

In power electronics not all designs require the maximum accuracy, and often only an order of magnitude is necessary with respect to thermal dimensioning. Therefore, we present three different levels of approaches for thermal design. Level 0 and level 1 approaches don't need special knowledge in heat transfer. These approaches are simple, but they are not to be dismissed. Because of the uncertainties in the convection coefficient, sometimes it makes no sense to use a more elaborate approach. We start the chapter with level 0 and level 1 designs, so those readers who desire a fast approach to thermal design will find the necessary sections immediately after this introduction.

The three mechanisms of heat transfer, conduction, convection, and radiation, are presented together with the basic heat transfer laws. Equivalent electrical circuits giving the analogy between the heat flow process in magnetic components and the corresponding electrical quantities are considered and explained in details. The level 2 design, including a thermal resistance network presentation of a magnetic component, is discussed based on the already introduced fundamentals. This thermal resistance network can be completed with thermal inertia of the different parts of the component. The complete model allows the analysis of different operating modes:

- Steady-state conditions, long-term operation under full continuous load
- Transient thermal behavior, short-term operation under a heavy load
- Adiabatic loading conditions, where a very high load is applied for a very short time interval, and, thus, no real heat transfer occurs except a rise in component temperature.

The characteristic features of the heat transfer in magnetic components are given special treatment in this chapter. An improved thermal modeling of

convection and radiation heat transfer for magnetic components for power electronics is also presented.

6.1 Fast Thermal Design Approach (Level 0 Thermal Design)

In some cases it is quite time consuming to calculate all the surfaces and the necessary parameters for an accurate heat transfer estimation. One can simply observe how much power could be dissipated for a given core size (i.e., what is the dependence of the allowed dissipated power on the dimensions of the core). We denote this approach as 'level 0' design. Experimental data concerning data for 50 Hz transformers indicates that allowed dissipation can be approximated by the following empirical equation:

$$P_{loss} = p \times a \times h, \quad [W] \quad (6.1)$$

where

p is a coefficient for 'specific dissipation' and falls within the range of 1500–2500 [W/m²];

a is the largest horizontal dimension of the core, [m];

h is the height of the core, [m].

REMARKS

1. In Equation (6.1) the core sizes a and h are in [m], and the obtained result for the allowed dissipation P is in [W].
2. The other (smaller) horizontal dimension of the core is not considered, as the horizontal surfaces are always less efficient than the vertical surfaces are for heat transfer.
3. If the copper winding dimensions are higher than the core dimensions, then the copper dimensions are used in Equation (6.1). This is the case for ring and core (shell) type transformers and inductors.
4. The magnetic component is assumed to be in vertical position, and the axis of the coil former is vertical. This is usually the best position for heat transfer.

Equation (6.1) is derived after considering the allowed power dissipation for scrap metal iron-type transformers at 40°C ambient temperature and 115°C hot spot temperature in the copper, using manufacturer data [1]. The derived dependence of the coefficient p (an average value for different stack width and core grade) on the characteristic dimension of the core a ($a = h$ for the cores in the data considered) is shown in Fig. 6.1. The influence of the width of the stack (the third dimension of the core) on the value of p is only a few percent. For small 50 Hz transformers almost all losses are in the copper, and, thus,

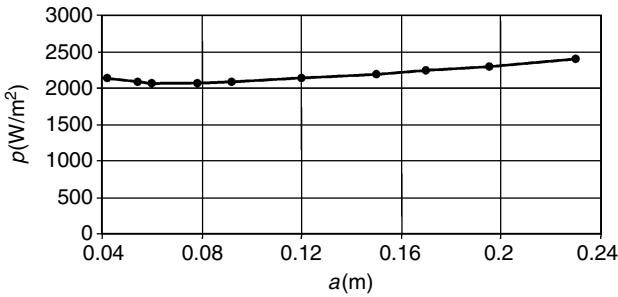


FIGURE 6.1

Values of specific dissipation p [W/m^2], equation (6.1), versus the largest horizontal dimension a [m], for 50 Hz scrapples transformers at 40°C ambient temperature and 115°C hot spot temperature in the copper, by data used from [1].

the core open surface, which is usually even higher than the copper open surface, is not used effectively for dissipation. This results in low values for p .

6.1.1 Specific Dissipation p for Ferrites

A higher value of p can be tolerated for ferrites because the total losses are more equally distributed between the copper and core, even for small sizes; thus, a better dissipation is realized. From one side, the ambient temperature of ferrites is often higher than that of 50 Hz iron transformers because the ferrite core components are usually used in closed-box equipment. Therefore, the ambient temperature of 60°C is more realistic for ferrites, which results in a low allowed temperature rise of about 50°C for copper. But from the other side, the typical ferrite cores have characteristic dimension values below 60 mm, which facilitate the heat transfer.

Keeping in mind all mentioned considerations about ferrite dissipation specifics, a value of p in the range of $p = 2000\text{--}2500$ can be used in most of the designs with ferrite cores. For safety, in the applications with an ambient temperature higher than 60°C we suggest a value in the range of $p = 1500\text{--}2000$.

Examples

- For an ETD39 ferrite core with both major dimensions equal to 0.039 m, the allowed dissipation is

$$P_{\text{loss}} = 2500 \times 0.039 \times 0.039 = 3.8 \text{ W} \quad \text{for } p = 2500.$$

- For an EE65 ferrite core with both major dimensions equal to 0.065 m, the obtained result is

$$P_{\text{loss}} = 2500 \times 0.065 \times 0.065 = 10.56 \text{ W} \quad \text{for } p = 2500.$$

- For a ring core (toroid) T102/65/25 mounted vertically with $a = h = 0.102 + 0.004 = 0.106$ m (0.004 m copper winding thickness), the obtained result is $P_{loss} = 2500 \times 0.106 \times 0.106 = 28$ W for $p = 2500$. In this case, from one side the open surface is not $A = ah$, but from the other side the actual open surface is higher than $A = \pi a^2/4$ because of the inner surface of the component, so the approximation used is still accurate enough.

6.1.2 Conclusion About Level 0 Thermal Design

The level 0 design approach allows a rapid check of the allowable dissipation of a magnetic component. The advantage is that the calculation is simple and can even be done in one's head. However, wherever more accuracy is needed one should not stick to this level, but use the more elaborate level 1 or level 2 designs.

6.2 Single Thermal Resistance Design Approach (Level 1 Thermal Design)

For a better understanding of heat transfer process in magnetic components, we can associate the thermal quantities and equations to an electrical analogy presented in Table 6.1. Using that analogy, we can present a heat transfer system by an electrical analog circuit. In this circuit the heat transfer rate is represented by current, the temperature difference is represented by voltage, and the thermal resistances are represented by electrical resistances.

The level 1 approach represents a magnetic component by a single thermal resistance that is temperature dependent (see Fig. 6.2). The heat transfer rate q is equal to the total power losses in the component P_{loss} . The temperature rise ΔT is the difference between the temperature of the component hot spot T_{hs} and the ambient temperature T_a .

Using Fig. 6.2 and the analogy with electrical quantities we can write

$$P_{loss} = \frac{\Delta T}{R_\theta} \tag{6.2}$$

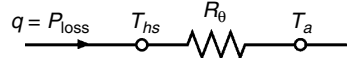
TABLE 6.1

Analogy Between Thermal and Electrical Quantities

Thermal quantities and laws	Electric quantities and laws
Heat transfer rate, q (or P_{loss}), [W]	Current, I , [A]
Temperature difference ΔT , [°C]	Potential difference, Voltage, V , [V]
Thermal resistance, R_θ , [°C/W]	Resistance, R , [Ω]
$q = \Delta T/R_\theta$, [W]	$I = V/R$

FIGURE 6.2

Electrical analog circuit of heat transfer in a magnetic component, using only one thermal resistance.



where

P_{loss} is the total power loss, equal to the sum of the core and copper losses

ΔT is the temperature rise, $\Delta T = T_{hs} - T_a$

R_θ is the total thermal resistance of the component

The thermal resistance paths for convection and radiation are in parallel for a magnetic component, so the value R_θ is

$$\frac{1}{R_\theta} = \frac{1}{R_{\theta,conv}} + \frac{1}{R_{\theta,rad}} = h_c A + h_R A = A(h_c + h_R) \quad (6.3)$$

where

A is the total open area of the magnetic component, [m²]

h_c is the convection heat transfer coefficient of the component

h_R is the radiation heat transfer coefficient of the component

The temperature rise ΔT is then

$$\Delta T = T_{hs} - T_a = P_{loss} R_\theta = \frac{P_{loss}}{A(h_c + h_R)} \quad (6.4)$$

where

T_{hs} is the component hot spot temperature

T_a is the ambient temperature

NOTE: The convection and radiation heat transfer coefficients are not constants; rather, they are temperature dependent. Some manufacturers give thermal resistances for cores, but care should be taken if no temperature difference is provided since the thermal resistances depend on the temperature difference ΔT .

To find the allowed dissipation P_{loss} when the surface of the component A and the temperature rise ΔT are known the following empirical equation can be used:

$$P_{loss} = (\Delta T)^{1.1} A \quad (6.5)$$

where A is in [cm²] and P_{loss} is in [mW].

The purpose of Equation (6.5) is to directly present the influence of the temperature difference and the area on the dissipation capability. A dependence similar to that of Equation (6.5) is proposed in [1].

Example

Let us consider a magnetic component with an EE42 core set. The total open surface of the component is: $A = 2 \times 42^2 + 4 \times 42 \times 15 + 8 \times 29 \times 8 = 7904 \text{ mm}^2 =$

79.04 cm². If we take $\Delta T = 50^\circ\text{C}$, then we obtain: $P_{\text{loss}} = (50)^{1.1} \times 79.04 = 5844 \text{ mW} = 5.844 \text{ W}$. By comparison, the accurate approach given later in section 5 of this chapter, and applied for the same construction and conditions, results in $P_{\text{loss}} = 5.35 \text{ W}$ [2].

6.3 Classic Heat Transfer Mechanisms

There are three heat transfer mechanisms: conduction, convection and radiation. In this section we will define these mechanisms and present the primary physical laws that govern their behavior.

6.3.1 Conduction Heat Transfer

Conduction heat transfer is the energy transfer from a high temperature region to a low temperature region of a body along a temperature gradient. The *heat transfer rate* q is proportional to the cross-sectional area A through which heat is being conducted and to the temperature gradient $\frac{\partial T}{\partial x}$ in the direction of the heat flow (normal to A):

$$q \sim A \frac{\partial T}{\partial x} \quad (6.6)$$

A positive constant k , called *thermal conductivity*, is introduced and then

$$q = -k A \frac{\partial T}{\partial x} \quad (6.7)$$

where

q is the heat transfer rate, [W]

k is the conductivity of the material, [W/m·°C]

A is the cross-sectional area through which heat is being conducted, [m²]

Equation (6.7) is known as Fourier's law. The negative sign indicates that the heat flows downhill on the temperature slope. The key parameter in Equation (6.7) is the thermal conductivity.

Using the energy balance of a unit volume, the general three-dimensional heat equation is

$$\frac{\partial^2 T}{\partial x^2} + \frac{\partial^2 T}{\partial y^2} + \frac{\partial^2 T}{\partial z^2} + \frac{E}{k} = \frac{1}{\alpha} \frac{\partial T}{\partial t} \quad (6.8)$$

where

E is the generated energy per unit volume, [W/m³]

$\alpha = \frac{k}{\rho c_p}$ is the thermal diffusivity of the material, [m²/s]

TABLE 6.2Thermal Conductivity of Some Materials at $T = 100^\circ\text{C}$, [3] and [4]

Material	Conductivity k , [W/m · °C]
Aluminum, Al	206
Ferrites (MnZn, NiZn)	3.8
Iron (pure), Fe	67
Carbon steel, C \approx 0.5%	52
Carbon steel, C \approx 1.5%	36
Invar, Ni = 36%	10.7
Nickel steel, Ni \approx 80%	35
Nickel (pure), Ni	83
Copper (pure), Cu	379
Tin	59
Lead, Pb	33
Silver	440
Zinc (pure), Zn	109
Magnesium (pure)	168
Glass	0.78
Epoxy resin (unfilled)	0.25
Epoxy resin (filled)	1.1
Polyethylene	0.33
Polyvinylchloride	0.09
Polypropylene	0.16
Polyimide film	0.40
Transformer oil	0.12
Cardboard	0.04
Kraft paper	0.11
Fiber, insulating board	0.05
Asbestos	0.07–0.17
Wood	0.11–0.15
Water, H ₂ O, at $T = 20^\circ\text{C}$	0.60
Air, at $T = 30^\circ\text{C}$	0.026
Air, at $T = 70^\circ\text{C}$	0.030
Carbon dioxide, CO ₂	0.022
Oxygen, O ₂	0.033
Hydrogen, H ₂	0.21

Selection out of tables of Holman J.P. *Heat transfer*, 8th ed. McGraw-Hill New York, 1997 [3] and Flanagan, W.M. *Handbook of transformer design and applications*, 2nd ed. McGraw-Hill New York, 1992 [4] (with permission of McGraw-Hill).

ρ is the material density, [kg/m³]

c_p is the material specific heat, [J/kg · °C]

The quantity α characterizes the *diffusivity* of the heat through the material. A high α means a high thermal conductivity k or a low thermal capacity ρc_p and α leads to faster heat diffusion through the material.

The values of k given in data sheets and used in practice are usually obtained by experiments because the analytical approach does not yield accurate results. The thermal conductivity of some materials are given in Table 6.2 at $T = 100^\circ\text{C}$.

6.3.2 Convection Heat Transfer

Convection heat transfer is a complex process involving conduction to the boundary level of the convecting fluid. The physical mechanism of convection is related to heat conduction through a thin boundary layer of fluid adjacent to the heated body surface. The heat transfer rate is determined by the velocity of the fluid blowing the heated surface and the type of fluid (air, water, oil). The convection process also includes the changes in the fluid density with the temperature, the viscosity, and the motion of the fluid.

Newton's law of cooling gives a simple expression for the overall process of convection heat transfer:

$$q = h_c A(T_w - T_a) \quad (6.9)$$

where

q is the heat transfer rate by convection, [W]

h_c is the convection heat transfer coefficient of the material, [W/m²·°C]

A is the surface of the heated body, [m²]

T_w is the temperature of the surface (the wall)

T_a is the ambient temperature

The convection heat transfer coefficient is sometimes denoted as thin film conductance because of the heat conduction process between the heated body and the thin boundary film of fluid.

6.3.2.1 Natural and Forced Convection

If the heated body is exposed to the ambient room air without any external source of movement, then the movement of the air is caused only by the density gradients near the body surface. This type of convection is called *natural*, or *free*, *convection*. If there is a fan blowing air over the heated body, then the process is called *forced convection*.

6.3.2.2 Convection Heat Transfer Coefficient h_c

In Equation (6.9) the key parameter is the convection heat transfer coefficient h_c . For vertical plates h_c is usually given as a function of the height H of the plate and is expressed as

$$h_c = 1.42 \left(\frac{\Delta T}{H} \right)^{1/4} \quad (6.10)$$

where

ΔT is the temperature rise $T_w - T_a$, [°C]

H is the height of the component, [m]

The classical book of Holman [3] gives detailed information for calculating h_c for various surfaces in both laminar and turbulent flow cases, which can

be used for a more precise estimation of the convection heat transfer coefficient. However, most of the approaches in [3] are difficult to apply in the design of magnetic components.

To clarify the uncertainties about the convection heat transfer coefficient h_c , we carried out experimental investigations, and the results are given in section 5 of this chapter.

6.3.3 Radiation Heat Transfer

The physical mechanism of radiation heat transfer is different from the mechanism of conduction and convection heat transfer, where the heat is transferred through a material medium (fluid). The mechanism of radiation heat transfer is electromagnetic radiation, and heat can be transferred even through a vacuum area. The heat transfer by radiation is described by the Stefan-Boltzmann law of thermal radiation:

$$q = \varepsilon \sigma A T^4 \quad (6.11)$$

where

q is the heat transfer rate by radiation, [W]

ε is the emissivity of the radiating surface

σ is the Stefan-Boltzmann constant, $\sigma = 5.67 \times 10^{-8} \text{ W/m}^2 \cdot \text{K}^4$

T is the absolute temperature, [K]

A is the radiating area (for magnetic components this is the component open surface), [m^2].

The factor ε (emissivity) represents the ratio between the heat transfer rate q for a given surface and a black surface for which $\varepsilon = 1$. Painted surfaces of almost all colors have the emissivity of about 0.9. The emissivity of a bright, metal surface is much lower, at about 0.05–0.1.

The radiant energy exchange between a hot body with absolute temperature T_1 and an enclosing body with absolute temperature T_2 is proportional to the difference in the absolute temperatures to the fourth power:

$$q = \varepsilon \sigma A (T_1^4 - T_2^4) \quad (6.12)$$

where

T_1 is the absolute temperature of the hot body

T_2 is the absolute temperature of the enclosing body

The wavelength of the temperature radiation for the surface temperature of magnetic components is in the infrared range.

Table 6.3 lists emissivity values of various surfaces for temperatures near the operating temperatures of magnetic components (around 100°C).

To unify the equations for the heat transfer rate q of the three heat transfer mechanisms, given by Equations (6.7), (6.9), and (6.12), Equation (6.12) can be simplified to

$$q = h_R A (T_1 - T_2) \quad (6.13)$$

TABLE 6.3

Total Emissivity of Some Surfaces Near 100°C, [3] and [4]

Material	Emissivity ϵ
Aluminum, polished	0.04
Aluminum, oxidized	0.25
Brass (CuZn), polished	0.03
Not brilliant brass	0.2
Ferrites	0.95
Copper, polished	0.052
Copper, not brilliant	0.40
Copper, covered with oxide layer	0.78
Cast iron	0.7
Steel, polished	0.066
Steel, with oxide layer	0.80
Sheet steel	0.55
Tinned sheet steel	0.04–0.06
Nickel, polished	0.072
Paint, all colours	0.90–0.94
Rubber	0.94
Porcelain	0.92
Enamel	0.9
Enameled copper	0.8
Isolation paper	0.9

Selection with permission out of tables of Holman J.P. *Heat transfer*, 8th ed. McGraw-Hill New York, 1997 [3] and Flanagan, W.M. *Handbook of transformer design and applications*, 2nd ed. McGraw-Hill New York, 1992 [4] (with permission of McGraw-Hill).

where

h_R is the radiation heat transfer coefficient:

$$h_R = \frac{\epsilon \sigma (T_1^4 - T_2^4)}{T_1 - T_2} = \frac{\epsilon 5.67 \times 10^{-8} (T_1^4 - T_2^4)}{T_1 - T_2} \quad (6.14)$$

6.4 Thermal Design Utilizing a Resistance Network

Level 2 Thermal Design

A more detailed presentation of the heat transfer in magnetic components requires a network consisting of several thermal resistances. Using the analogy of the electrical circuits and quantities, we can present a heat transfer system by a detailed equivalent circuit. This kind of circuit is useful for a better representation of the heat transfer process and for calculation of the

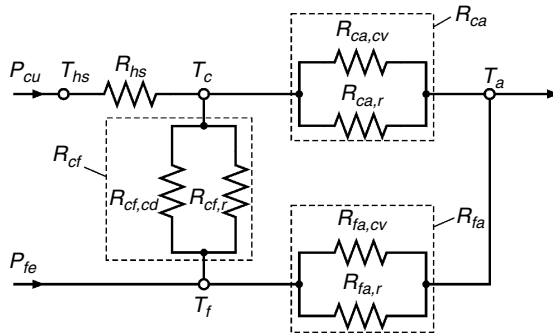


FIGURE 6.3

Electrical analog circuit of heat transfer in a magnetic component, using a resistance network (level 2).

temperature rise in magnetic components. The key parameters are the thermal coefficients k , h_c and h_r , which depend on the temperature and the geometry of the magnetic component.

Assumption: All copper surfaces have the same temperature, and all core surfaces also have the same temperature.

6.4.1 Thermal Resistances

Here we present a resistance network (see Fig. 6.3) that includes the following thermal resistances:

- $R_{\theta,hs}$ which represents the conduction heat transfer between the hot spot, is assumed to be in the copper windings and the copper coil surface. For simplicity, the surface temperature of the copper is considered to be uniform. This resistance is determined mainly by the parasitic air gaps in the coil. $R_{\theta,hs}$ is expressed as

$$R_{\theta,hs} = \frac{l_{cw}}{k(A_{cf} + A_{ca})} \quad (6.15)$$

where

l_{cw} is the equivalent air gap representing the air in windings and parasitic air gap between the windings and the coil-former; l_{cw} depends on the wire type, the insulation, and the temperature profile inside the coil
 A_{cf} is area of the copper coil surface in the slot (the surface realizing the conduction between the coil and the core), or the copper-to-ferrite area
 A_{ca} is the area of the copper coil open surface (the open surface that transfers heat directly to the ambient air), or the copper-to-ambient area
 k is the air thermal conductivity; $k = 0.031 \text{ W/m} \cdot \text{C}^\circ$ at 100°C , and $k = 0.026 \text{ W/m} \cdot \text{C}^\circ$ at 30°C [3]

TABLE 6.4

Values of the Emissivity of the Investigated Surfaces

	Aluminium surfaces, ϵ_{al}	Unpolished copper, ϵ_{cu}	Enameled copper, ϵ_{en}	Black painted surfaces, ϵ_{bp}
Emissivity	0.07	0.14	0.81	0.925

- $R_{\theta,cf}$ This thermal resistance is the inverse of the sum of the inverses of the conduction and radiation thermal resistances between the copper-coil surface in the slot and the core (copper-to-ferrite thermal resistance), $R_{\theta,cf,cd}$ and $R_{\theta,cf,r}$, respectively:

$$\frac{1}{R_{\theta,cf}} = \frac{1}{R_{\theta,cf,cd}} + \frac{1}{R_{\theta,cf,r}} \quad (6.16)$$

The value of $R_{\theta,cf,cd}$ is:

$$R_{\theta,cf,cd} = \frac{l_{cf}}{k A_{cf}} \quad (6.17)$$

where

l_{cf} is the equivalent air gap corresponding to the air space between the coil and the core

The value of $R_{\theta,cf,r}$ is

$$R_{\theta,cf,r} = \frac{1}{h_{R,cf} A_{cf}} = \frac{T_c - T_f}{\epsilon \sigma (T_c^4 - T_f^4) A_{cf}} \quad (6.18)$$

where

$h_{R,cf}$ is radiation heat transfer coefficient of the coil

T_c is the absolute temperature of the coil, [K]

T_f is the absolute temperature of core, [K]

ϵ is the emissivity of the coil surface; $\epsilon = 0.8$ (see Table 6.4)

σ is the Stefan-Boltzmann constant; $\sigma = 5.67 \times 10^{-8} \text{ W/m}^2 \cdot \text{K}^4$

REMARK

Let us consider $R_{\theta,cf,r}$ together with $R_{\theta,cf,cd}$. These resistances are in parallel. A simple example with $l_{cf} = 3 \text{ mm}$, $T_c = 374 \text{ K}$ and $T_f = 373 \text{ K}$ (one degree difference between coil and core temperatures) results in almost the same thermal resistances:

$$R_{\theta,cf,cd} / A_{cf} = \frac{l_{cf}}{k} = \frac{0.003}{0.031} = 0.097$$

$$R_{\theta,cf,r} / A_{cf} = \frac{1}{0.9 \times 5.67 \times 10^{-8} (374^4 - 373^4)} = 0.094.$$

- $R_{\theta,ca}$ This thermal resistance is a combination of the convection and radiation thermal resistances between the coil open surface and the ambient air (*copper-to-ambient* thermal resistance), $R_{\theta,ca,cv}$ and $R_{\theta,ca,r}$ respectively. These resistances are in parallel so:

$$\frac{1}{R_{\theta,ca}} = \frac{1}{R_{\theta,ca,cv}} + \frac{1}{R_{\theta,ca,r}} \quad (6.19)$$

The values of $R_{\theta,ca,cv}$ and $R_{\theta,ca,r}$ are as follows:

$$R_{\theta,ca,cv} = \frac{1}{h_c A_{ca}} \quad (6.20)$$

$$R_{\theta,ca,r} = \frac{1}{h_{R,ca} A_{ca}} = \frac{T_c - T_a}{\varepsilon \sigma (T_c^4 - T_a^4) A_{ca}} \quad (6.21)$$

where

- $h_{R,ca}$ is the radiation heat transfer coefficient of the open coil area
- T_c is the absolute temperature of the open coil area, [K]
- T_a is the absolute temperature of ambient air, [K]
- ε is the emissivity of the open coil surface; $\varepsilon = 0.8$ (see [Table 6.4](#)).

- $R_{\theta,fa}$ This thermal resistance is a combination of the convection and radiation thermal resistances between the core open surface and the ambient air (*ferrite-to-ambient* thermal resistance), $R_{\theta,fa,cv}$ and $R_{\theta,fa,r}$ respectively. These resistances are also in parallel so:

$$\frac{1}{R_{\theta,fa}} = \frac{1}{R_{\theta,fa,cv}} + \frac{1}{R_{\theta,fa,r}} \quad (6.22)$$

The value of $R_{\theta,fa,c}$ is

$$R_{\theta,fa,c} = \frac{1}{h_c A_{fa}} \quad (6.23)$$

where

- A_{fa} is the core end surface (the core open surface transferring heat to the ambient air), or ferrite-to-ambient area

The value of $R_{\theta,fa,r}$ is

$$R_{\theta,fa,r} = \frac{1}{h_{R,fa} A_{fa}} = \frac{T_f - T_a}{\varepsilon \sigma (T_f^4 - T_a^4) A_{fa}} \quad (6.24)$$

where

- $h_{R,fa}$ is radiation heat transfer coefficient of the core end
- T_f is the absolute temperature of the core end, [K]
- ε is the emissivity of the core surface; $\varepsilon = 0.9-0.95$ (see [Table 6.2](#))

The equivalent circuit comprising the above-mentioned thermal resistances is presented in Fig. 6.3.

NOTE: For components with forced convection or cooled by heat sinks, an additional thermal resistance should be included between the hot spot point in the core and the core surface.

6.4.2 Finding Temperature Rise

There are two sources of heat in a magnetic component: the copper losses P_{cu} and the core losses P_{fe} (see Fig. 6.3). To find the temperature rise ΔT in the magnetic component we use the *superposition principle*.

First, we find the temperature rise $\Delta T_{c,f}$ in the coil caused by the core losses P_{fe} . The losses are assumed to be a current source in the equivalent circuit of that process (Fig. 6.3). We have to find the ‘potential difference’ $\Delta T_{c,f} = T_c - T_a$ caused by the losses P_{fe} . Using the known electrical laws and Fig. 6.4, we find $P_{fe,c}$

$$P_{fe,c} = \frac{P_{fe} R_{fa}}{R_{ca} + R_{cf} + R_{fa}} \quad (6.25)$$

$$\Delta T_{c,f} = P_{fe,c} R_{ca} = P_{fe} \frac{R_{fa} R_{ca}}{R_{ca} + R_{cf} + R_{fa}} \quad (6.26)$$

Second, we find the temperature rise $\Delta T_{c,c}$ in the copper caused by the copper losses P_{cu} . The heat transfer process is represented by the equivalent circuit shown in Fig. 6.5. Using Fig. 6.5, we find:

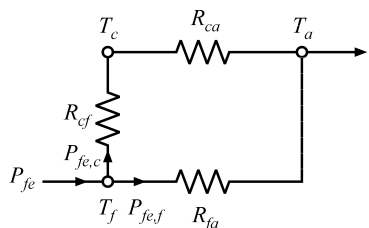
$$\Delta T_{c,c} = P_{cu} R_{eqv} = P_{cu} \left(R_{hs} + \frac{R_{ca}(R_{cf} + R_{fa})}{R_{ca} + R_{cf} + R_{fa}} \right) \quad (6.27)$$

Now, knowing the temperature rises caused by copper and core losses, we can find the total temperature rise ΔT as a sum of these values:

$$\Delta T = \Delta T_{c,c} + \Delta T_{c,f} = P_{cu} \left(R_{hs} + \frac{R_{ca}(R_{cf} + R_{fa})}{R_{ca} + R_{cf} + R_{fa}} \right) + P_{fe} \frac{R_{fa} R_{ca}}{R_{ca} + R_{cf} + R_{fa}} \quad (6.28)$$

FIGURE 6.4

Electrical analog circuit for finding the temperature rise $\Delta T_{c,f}$ in coil caused by the core losses P_{fe} .



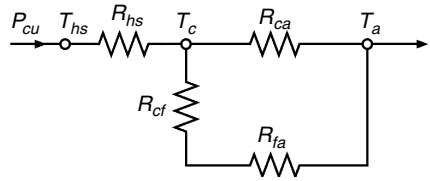


FIGURE 6.5
Electrical analog circuit for finding the temperature rise $\Delta T_{c,c}$ in the coil caused by the copper losses P_{cu} .

Equation (6.28) allows us to find the temperature rise in a magnetic component for given values of the copper and core losses. Sometimes a few iterations are necessary in practice to find the exact temperature rise, as the thermal resistances used in Equation (6.28) and the core and copper losses are temperature dependent.

6.5 Contribution to Heat Transfer Theory of Magnetic Components

The thermal design of magnetic components is usually somewhat neglected, as it is often not clear exactly which theory and coefficients should be used. Also, the experiments are time-consuming and not easy. In a real design many construction details that complicate the modeling are present. This is true for classical approaches as well as for numerical methods. Here we want to present some reference expressions and conclusions to be used for fine-tuning classical and other methods.

Both the classical approaches [4,5,6] and the new thermal models [7,8] have their advantages and applications. In the *isotherm surface model* (all open surfaces of the component have the same temperature) the total heat transfer rate q , which shows the heat dissipating capability of a component, can be presented as follows:

$$q = q_a + q_r + q_c \quad (6.29)$$

where

q_d, q_r, q_c are the already discussed conduction, radiation and convection transfer rates

Substituting, we obtain

$$q = k A_k \frac{T_w - T_a}{l_k} + \varepsilon \sigma A_r (T_w^4 - T_a^4) + h_c A_c (T_w - T_a) \quad (6.30)$$

where

k is the *conductivity* of the material, [W/m²K]

A_k is the cross-sectional area through which heat is being conducted, [m²]

l_k is the equivalent length of the conduction heat transfer path

ε is the *emissivity* of the radiating surface

σ is the Stefan-Boltzmann constant, $\sigma = 5.67 \times 10^{-8} \text{ W/m}^2 \cdot \text{K}^4$
 A_r is the radiating area; i.e., the component open surface, $[\text{m}^2]$
 h_c is the *convection heat transfer coefficient* of the material, $[\text{W/m}^2 \cdot \text{°C}]$
 A_c is the open surface of component, $[\text{m}^2]$; $A_c = A_r$
 $T_w - T_a = \Delta T$ is the temperature rise; T_w is the surface temperature of the component, and T_a is the ambient temperature.

The conduction heat transfer can usually be neglected in the heat transfer from a magnetic component to the ambient air, so we will focus only on the radiation and convection heat transfers.

The uncertainties in the coefficients k , ε , and h_c result in an insufficient accuracy of Equation (6.30) applied to magnetic components. In particular, the coefficients h_c and ε are quite critical. The well-known expression of the coefficient h_c is

$$h_c = 1.42 \left(\frac{\Delta T}{L} \right)^{0.25} \quad (6.31)$$

where

ΔT is the temperature rise $T_w - T_a$, $[\text{°C}]$

L is the height of the component, $[\text{m}]$

This equation is valid only under specific conditions, and some factors limit its validity for magnetic component design:

- The convection heat transfer is a quite complex process, and Equation (6.31), which was derived for infinite surfaces, is not completely applicable for magnetic components.
- The conductivity, viscosity, and density of air are assumed to be constant in the temperature range for which the expression is used, but this assumption is only an approximation.
- Equation (6.31) is not valid for natural convection in an enclosed space or in close proximity of other heated surfaces. Usually the *ambient temperature* is adapted to some average temperature inside the enclosure.

Example

For an EE42 core with $L = 0.042 \text{ m}$, and for a temperature rise of $\Delta T = 50\text{°C}$ the value of the convection heat transfer coefficient, according to Equation (6.31), is $h_c = 8.34 \text{ [W/m}^2 \cdot \text{°C]}$. According to the references [9,10], the typical values of h_c are spread in the range of 6–10 $[\text{W/m}^2 \cdot \text{°C}]$ for cores used in power electronics!

The above-mentioned limitations of Equation (6.31) and the uncertainties in the values of ε and h_c result in an inaccuracy of about 20–30% in the estimation of convection and about 15% in the estimation of the total heat transfer! This inaccuracy can really influence some designs.

6.5.1 Practical Experience

We carried out some experiments to investigate the values of emissivity ε for some surfaces typical to power electronics components (see the appendix to this chapter). The main results are summarized in [Table 6.4](#).

Our conclusions from the experiments and the results concerning the position and location of the magnetic components are:

- The location of a magnetic component directly on the PCB (printed circuits board) improves the heat transfer, and the temperature rise is 6–8% lower by comparison to the case when the component does not touch the PCB.
- The dissipating ability hardly depends on the position (vertical or horizontal) of a magnetic component.
- In high ambient temperatures the allowed temperature rise ΔT for the same dissipated power P_{diss} is slightly lower because of the increased radiation heat transfer.

For more details see the appendix to this chapter.

6.5.2 Precise Expression of the Natural Convection Coefficient h_c

Magnetic components are never *infinite* or *thin* plates like the shapes in the classical heat transfer. So, the heat transfer coefficient h_c could be well-defined but still different from the classical thermal approach for horizontal and vertical plates. Here we present improved thermal modeling of convection heat transfer for magnetic components for power electronics.

6.5.2.1 Derivation of Convection Coefficient h_c

The convection process is a quite complex phenomenon. Properties of air, such as heat conductivity k , kinematic viscosity ν and specific weight (density) ρ , that influence the convection process change a lot in the considered temperature range of 250–400 K. Thus, the heat transfer parameters, Nusselt number Nu , Grashof number Gr , Prandtl number Pr and Rayleigh number Ra , which are used in classical convection heat transfer theory, are quite affected by the temperature, and, as a result, the simplified proportionality $h_c \sim (\Delta T/L)^{0.25}$ is not observed in the real experiment.

The accurate dependence of h_c on ΔT is different than the one given in the simplified relation of Equation (6.31). To obtain a good matching between the classical expressions and Equation (6.31) the exponents in it should be precisely adapted. We consider the following approximation:

$$h_c = C \frac{(\Delta T)^{\alpha_T}}{L^{\alpha_L}} \quad (6.32)$$

where the exponents α_T and α_L will not be 0.25 as they are in Equation (6.31). To complete the expression of Equation (6.32) and to derive the dependence of h_c on the pressure p , the ambient temperature T_a , and the position (horizontal or vertical) of the component, we propose the following expression:

$$h_c = C \left(\frac{p}{p_{ref}} \right)^{\alpha_p} \left(\frac{T_a}{T_{a,ref}} \right)^{\alpha_{Ta}} \frac{(\Delta T)^{\alpha_T}}{L^{\alpha_L}} \quad (6.33)$$

where the exponents α_p and α_{Ta} and the coefficient C , which depends on the position, are to be found.

The precise values of the exponents α_T , α_L , α_p and α_{Ta} and the coefficient C were found using table data and analytical matching (see the appendix to this chapter). Each exponent was found individually by comparing the results obtained by a classical complete presentation of h_c and the results of an expression consisting of an adaptation coefficient and the corresponding quantities of ΔT , T_a , L , p .

Using the found values of α_T , α_L , α_p , α_{Ta} and C we give the following complete expression for the convection coefficient h_c :

$$h_c = C \left(\frac{p}{p_{ref}} \right)^{0.477} \left(\frac{T_a}{T_{a,ref}} \right)^{-0.218} \frac{(\Delta T)^{0.225}}{L^{0.285}} \quad (6.34)$$

where

C is $C_h = 1.53$ for horizontal position and $C_v = 1.58$ for vertical position of the component in an open enclosure ; $C_e = 1.35$ in a closed enclosure (closed box)

L is the total distance passed by the air cooling the component (see Fig. 6.6)

ΔT is the temperature rise, $\Delta T = T_w - T_{a,r}$ [K]

p_{ref} is the reference pressure at sea level, $p_{ref} = 101.32 \text{ kPa}$

$T_{a,ref}$ is the reference ambient absolute temperature, $T_{a,ref} = (273.15 + 25) \text{ K}$

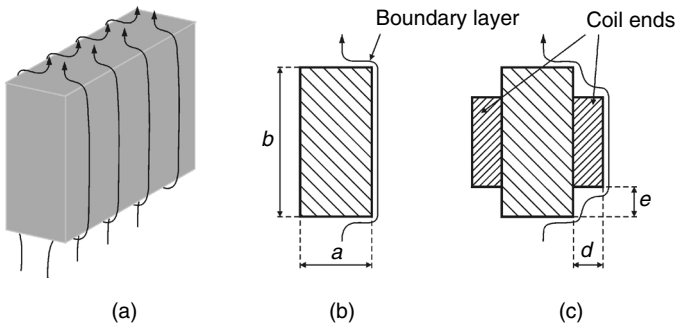


FIGURE 6.6

Parameter L as the total distance of the boundary layer: b) $L = a + b$; c) $L \cong a + b - 2e + 2\sqrt{d^2 + e^2}$.

The found exponent $\alpha_T = 0.225$ matches well the results for convection of vertical and horizontal plates in the considered temperature range of 250–400 K obtained by software included in [3]. Note that convection decreases for the same temperature rise ΔT when the ambient temperature T_a increases. However, that dependence is quite small in comparison with the dependence of radiation on T_a .

The value $\alpha_p = 0.5$ can also be used in Equation (6.34), as it gives only a very small difference in comparison with $\alpha_p = 0.477$. A similar dependence of $h_c \sim \sqrt{p}$ can also be found in [3].

The derived expression of Equation (6.34) can also be used in more complex thermal models including inner thermal resistances and different copper and iron temperatures, representing the complexity in the construction details of the component.

More details of the presented approach can be found in [2,11,12].

6.5.2.2 Dependencies of h_c on the Parameter L and on the Position and Shape

Here we give the details of the proposed dependencies of h_c on the parameter L and on the position and shape of a component, included in Equation (6.34).

Dependence of h_c on Parameter L

The dependence for combined vertical and horizontal surfaces, which is the case of magnetic components, includes three new aspects:

1. A more precise exponent for L in the considered range of $L = 10$ – 400 mm is $\alpha_L = 0.285$ with 4% deviations with respect to the experimental results. The deviations are at the end of the range. By comparison, the exponent $\alpha_L = 0.25$ results in deviations above 22% in the considered range.
2. The parameter L is the total distance passed by the air cooling the component (e.g., the length of the boundary flow layer of the component (see Fig. 6.6)). In general L could be described as “half of the length of the shortest path around a vertical midsection of the object.” Notice that L is not the height of the component. For example, in the box-shaped model with EE42 dimensions the parameter L is $L = a + b = 57$ mm (see Fig. 6.6b). For the EE core transformer shape, as one general parameter for the whole surface we propose $L \cong a + b - 2e + 2\sqrt{d^2 + e^2}$ (see Fig. 6.6c). For an EE42 transformer we obtain $L \cong a + b - 2e + 2\sqrt{d^2 + e^2} = 64$ mm.
3. Magnetic components are often mounted above a PC board. For simplicity, we keep the same L and surface in Equations (6.34) and (6.30) for magnetic components mounted directly on a PC board. Our investigations show that when the component is mounted on

a PC board the total thermal heat transfer of the component is improved by about 6–8% in comparison with the case when the component is above the PC board. On one hand, the contribution of the bottom surface toward the total heat transfer is low and mainly determined by the air conductivity. On the other hand, the conduction heat transfer to the PC board seems to be relevant, certainly if some copper traces are present. However, the detailed investigation of this case is beyond the scope of this book.

Dependence of h_c on the Position of Component and on Enclosure

The difference in convection for horizontal and vertical position of a component is proved to be low by the experiments. This difference can be presented by different values of the coefficient C for both positions. The experimentally obtained values are $C_h = 1.53$, $C_v = 1.58$, respectively, for the horizontal and vertical positions of the model in an open enclosure. The obtained value for a closed enclosure (closed box with dimensions of 0.5 m \times 0.3 m and a height equal to 0.3 m), when the convection is lower than in an open box, is $C_e = 1.35$.

Dependence of h_c on the Shape of the Component, the ‘Envelope Surface’

For the magnetic component shapes we propose specific equivalent surfaces to be used to present more accurately the convection and radiation heat transfer instead of the full open surface of the component. For radiation, this surface S_{rad} is close to the component *envelope* surface. The surface between the corners is reduced because in those regions the surfaces radiate to each other and the actual radiating surface is lower than the total surface (see Fig. 6.7a). For convection, the equivalent surface S_{con} includes completely the vertical parts of the component because all of the vertical surfaces act effectively in the convection process (see Fig. 6.7b).

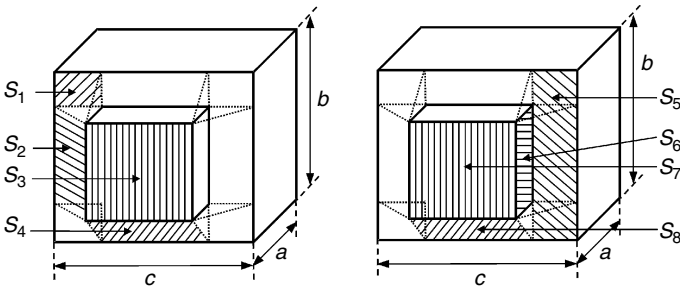


FIGURE 6.7
 The equivalent surfaces of an EE core transformer:
 a) the ‘envelope’ surface for radiation, $S_{env} = S_{rad} = 2ab + 2ac + 2(4S_1 + 2S_2 + S_3 + 2S_4)$.
 b) the equivalent surface for convection, $S_{con} = 2ab + 2ac + 2(2S_5 + 2S_6 + S_7 + 2S_8)$.

TABLE 6.5

The Surfaces and the Parameter L for an EE42 Core Transformer

EE42	Box	Transformer	Difference transformer/box
Total surface, [$10^{-6} \cdot \text{m}^2$]	6048	7904	30%
$S_{env} = S_{rad}$, [$10^{-6} \cdot \text{m}^2$]	6048	6895	14%
S_{con} , [$10^{-6} \cdot \text{m}^2$]	6048	7324	21%
Parameter L , [$10^{-3} \cdot \text{m}$]	57	64.26	12.7%

The *envelope* surface $S_{env} = S_{rad}$ and the equivalent surface for convection S_{con} of an EE core transformer, in accordance with Fig. 6.7, are

$$S_{env} = S_{rad} = 2ab + 2ac + 2(4S_1 + 2S_2 + S_3 + 2S_4) \tag{6.35}$$

$$S_{con} = 2ab + 2ac + 2(2S_5 + 2S_6 + S_7 + 2S_8) \tag{6.36}$$

The box surface S_{box} is $S_{box} = 2ab + 2ac + 2bc$. The values of those three surfaces and the parameter L for an EE core transformer are tabulated in Table 6.5.

The measured difference in dissipation between a transformer and a corresponding black-painted box is only about 10.5%. This difference is well-explained by the proposed equivalent surfaces for the heat transfer of a transformer, the difference in the characteristic parameter L , and the difference in the global emissivity for both cases.

6.5.3 Forced Convection

6.5.3.1 Classical Approach

Because of the complicated nature of the flow-separation processes it is not possible to analytically calculate the average heat transfer coefficients in forced convection heat transfer. However, some experimental data, [3,13], indicate that the average heat transfer coefficients for flow across cylinders can be calculated with the following expression:

$$\frac{h_c d}{k_f} = C \left(\frac{u_\infty d}{\nu_f} \right)^n Pr_f^{1/3} \tag{6.37}$$

where

h_c is the mean convection heat transfer coefficient

d is the height of the magnetic component

C and n are constants

u_∞ is the velocity of the approaching flow

ν_f is the cinematic viscosity evaluated at the film temperature

Pr_f is the Prandtl number evaluated at the film temperature

k_f is the air thermal conductivity evaluated at the film temperature

TABLE 6.6

Properties of Air at Atmospheric Pressure

T , [K]	$\nu \cdot 10^6$, [m ² /s]	k , [W/m · °C]	Pr
300	15.69	0.02624	0.708
350	20.76	0.03003	0.697
400	25.90	0.03365	0.689

Part of a table with permission of: Holman J.P. *Heat transfer*, 8th ed. McGraw-Hill New York, 1997 [3] (with permission of McGraw-Hill).

The cinematic viscosity is defined as

$$\nu_f = \frac{\mu_f}{\rho_f} \quad (6.38)$$

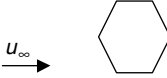
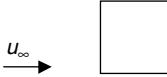
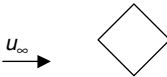
where μ_f is the dynamic viscosity and ρ_f is the density, both properties evaluated at the film temperature.

To facilitate the use of Equation (6.37) we tabulate the values of cinematic viscosity ν , thermal conductivity k , and the Prandtl number of air at atmospheric pressure (see Table 6.6).

The coefficients C and n are tabulated in Table 6.7, depending on the geometry of the object. Here the object is considered to be infinite in one of its dimensions, and its cross-section is considered in Table 6.7. The values given in the Table 6.7 are found using the Reynolds number Re_f evaluated at the film temperature T_f :

$$Re_f = \frac{\rho_f u_\infty d}{\mu_f} \quad (6.39)$$

TABLE 6.7Copnstants C and n Used for Forced Convection Presentation Given by Equation (6.37)

Geometry	Cases	C	n
	Case 1	0.246	0.588
	Case 2	0.102	0.675
	Case 3	0.153	0.638

Part of a table of: Holman J.P. *Heat transfer*, 8th ed. McGraw-Hill New York, 1997 (with permission of McGraw-Hill) [3].

The film temperature T_f is defined as

$$T_f = \left(\frac{T_w + T_\infty}{2} \right) \quad (6.40)$$

where

T_w is the surface temperature of the component

T_∞ is the temperature of the approaching flow

Now, having found h_c , we can present the convection heat transfer q as

$$q = h_c A (T_w - T_\infty) \quad (6.41)$$

where A is the approached-by-the-flow area of the magnetic component; $A = dl$, where l is the horizontal length of the component.

The first advantage of Equation (6.37) is that it allows investigation of the influences of the parameters, such as air pressure and the kind of the fluid, on the value of the convection coefficient. The second advantage is that the coefficients C and n give the dependence on how the flow approaches the surface; for instance, the diagonal flow of case 1 in Table 6.7 provides much better cooling in comparison with the side flow of case 2.

6.5.3.2 Adapted Approach

To simplify the calculations of Equation (6.37) we propose the following expression for forced convection in air at atmospheric pressure:

$$h_c = (3.33 + 4.8 u_\infty^{0.8}) L^{-0.288} \quad (6.42)$$

where L is the total distance of the boundary layer of the component (see Fig. 6.6).

Equation (6.42) is consistent with the classical reference [10] up to $u_\infty = 12$ m/s, as well as with Equation (6.37), case 2 [3]. The advantage of Equation (6.42) is that it combines both natural and forced convection processes. The offsets of the corresponding curves, when the velocity of the approaching flow u_∞ is zero, correspond to the values of the natural convection coefficient h_c given by Equation (6.34) of the previous section. Fig. 6.8 presents the convection coefficient h_c for different values of the parameter L for a temperature difference of 30°C, in accordance with Equation (6.42). Fig. 6.8 gives a fast result for the forced convection coefficient h_c , including the scale effect of the component size.

In forced cooling there are a lot of details to be considered to find the accurate heat transfer, such as the position and orientation of the component relative to the nearby components. Thus, the accuracy of Equation (6.42), which is about 10–15%, is quite acceptable for most designs in power electronics.

Concerning forced convection, some warnings should be given:

- The forced convection reduces the surface-to-ambient thermal resistance, but does not change the internal hot spot-to-ambient thermal resistance.

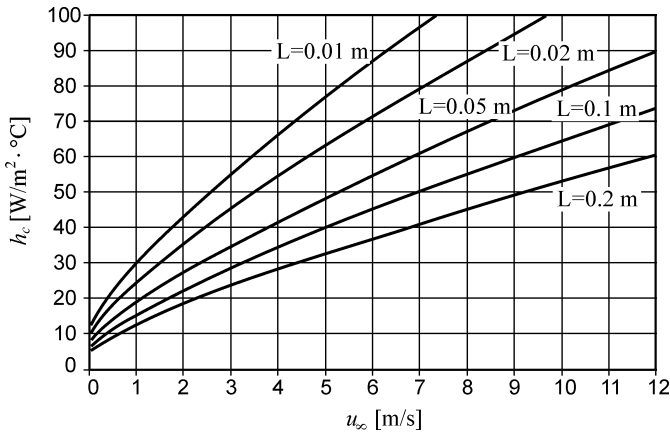


FIGURE 6.8 Convection coefficient h versus the flow velocity u_∞ , for different values of the parameter L , the temperature difference of 30°C , in accordance with equation 6.42.

- An intensive forced cooling results in a high temperature gradient within the component. In extreme cases the thermal stresses caused by such a cooling can break the ferrites or reduce the lifetime of the insulation.

6.5.4 Relationship with Thermal Resistance Networks

The accurate expressions for convection and radiation heat transfer for magnetic components given in the previous sections can be used in the resistance network shown in Fig. 6.3. To separate the copper-to-ambient and core-to-ambient resistances, one has to separate the surfaces corresponding to copper and to the core. A pragmatic solution is to attribute resistances proportionally to the respective core and copper surfaces. The other resistances in the resistance network are the same as they are defined in Section 6.4.1 of this chapter.

6.6 Transient Heat Transfer

In this section we consider the basic aspects of transient heat transfer and their applications in magnetic components design.

6.6.1 Thermal Capacitances in Magnetic Components

The thermal resistance network can be completed by thermal capacitances of the magnetic component parts. The thermal capacitance is analogous to the electrical capacitance in a circuit that is equivalent to the thermal transfer.

To find thermal capacitance C_θ of a component part we need the value of specific heat c and the mass m of that part:

$$C_\theta = c \rho V = c m \quad (6.43)$$

where

ρ is the material density, [kg/m³]

V is the volume of the element, [m³]

m is the mass of the element, [kg]

The thermal capacitance of the component C_θ is the sum of the thermal capacitances of all of the parts of the component:

$$C_\theta = C_{\theta, cu} + C_{\theta, fe} + C_{\theta, co} + C_{\theta, i} = c_{cu} m_{cu} + c_{fe} m_{fe} + c_{co} m_{co} + c_i m_i \quad (6.44)$$

where

$c_{cu}, c_{fe}, c_{co}, c_i$ are the specific heat values for the copper, the core, the coil-former, and the insulation, [kJ/kg · °C];

$m_{cu}, m_{fe}, m_{co}, m_i$ are the values of the mass of the copper, the core, the coil-former, and the insulation, [kg].

REMARKS

1. For short time processes the thermal resistances can be neglected, and the model of the component comprises only its thermal capacitances.
2. The thermal capacitances are mainly determined by the weight of the magnetic component elements, as all values of their specific heat capacitances (ρc) are close to each other.
3. The values of the thermal capacitances are usually more accurate than the values of the thermal resistances.

Values for the specific heat c and the density ρ (at 20°C) of some common materials are given in [Table 6.8](#) [3].

6.6.2 Transient Heating

After starting the heat generating process (the operating process) in the magnetic component some time must elapse before the equilibrium temperature is to be reached. The temperature rise ΔT of the magnetic component increases from the start of the magnetic component operation, following an exponential law defined by the thermal time constant τ_θ of the component. The same time constant defines the cooling process of the component.

The transient dependence of the temperature rise of a magnetic component on time $\Delta T(t)$ can be expressed as

$$\Delta T(t) = \Delta T(1 - e^{-t/\tau_\theta}) \quad (6.45)$$

TABLE 6.8Specific Heat c and Density ρ of Some Common Materials at 20°C, [3]

Material	Specific heat c_p , [kJ/kg · °C]	Density ρ , [kg/m ³]
Aluminum, Al	0.896	2707
Ferrites (MnZn, NiZn)	1.07	4800
Iron (pure), Fe	0.452	7897
Carbon steel, C ≈ 0.5%	0.465	7833
Carbon steel, C ≈ 1.5%	0.486	7753
Invar, Ni ≈ 40%	0.46	8137
Nickel steel, Ni ≈ 80%	0.46	8618
Nickel (pure), Ni	0.45	8906
Copper (pure), Cu	0.383	8954
Tin	0.226	7304
Lead, Pb	0.13	1137
Silver	0.234	1052
Zinc (pure), Zn	0.384	7144
Glass fiber	0.84	32
Polyethylene	2.1	930
Polyvinylchloride	1.1	1700
Polypropylene	1.9	1150
Polyimide film	—	1420
Asbestos	0.816	500
Water, H ₂ O, at $T = 30^\circ\text{C}$	4.296	918
Air, at $T = 30^\circ\text{C}$	1.0056	1.177
Carbon dioxide, CO ₂	0.871	1.80
Oxygen, O ₂	0.92	1.3
Hydrogen, H ₂	14.43	0.082

Selection out of tables of Holman J.P. *Heat transfer*, 8th ed. McGraw-Hill New York, 1997 (with permission of McGraw-Hill) [3].

where

τ_θ is the thermal time constant of the magnetic component

ΔT is the steady-state temperature rise over the ambient temperature

It should be noted that the temperature rise values in Equation (6.45) are the average values across the component.

The thermal time constant τ_θ of a magnetic component is

$$\tau_\theta = R_\theta C_\theta \quad (6.46)$$

where

R_θ is the average thermal resistance of the component [°C/W]

C_θ is the average thermal capacitance of the component [kJ/°C].

Knowing the value of τ_θ is useful in the case of short-term overloading of the magnetic component. If we know the rated (nominal) values of the temperature rise ΔT_N and losses $P_{loss,N}$, we can find the thermal resistance:

$$R_\theta = \frac{\Delta T_N}{P_{loss,N}} \quad (6.47)$$

And then, for a given value of the overloading losses $P_{loss,ov}$, we can find the corresponding steady-state temperature rise ΔT_{ov} :

$$\Delta T_{ov} = R_{\theta} P_{loss,ov} = \frac{P_{loss,ov}}{P_{loss,N}} \Delta T_N \quad (6.48)$$

Now we can find the dependence of the temperature rise on time in the overloading conditions:

$$\Delta T(t) = \Delta T_{ov} (1 - e^{-t/\tau_{\theta}}) = \frac{P_{loss,ov}}{P_{loss,N}} \Delta T_N (1 - e^{-t/R_{\theta}C_{\theta}}) \quad (6.49)$$

Using Equation (6.48) and substituting $\Delta T(t) = \Delta T_N$, we can also find the time interval Δt , after which the temperature rise under overloading conditions will reach the allowed (nominal) temperature rise:

$$\Delta t = R_{\theta} C_{\theta} \ln \frac{P_{loss,ov}}{P_{loss,ov} - P_{loss,N}} \quad (6.50)$$

6.6.3 Adiabatic Loading Conditions

If a winding is subjected to a large current for a short time interval and no heat transfer occurs in a magnetic component, we call these conditions and that process *adiabatic loading*. The critical parameter under such conditions is the highest allowed temperature of the wire insulation or the allowed temperature of the coil-former. Assuming that there is no heat transfer in the magnetic component, the thermal process can be represented by charging a capacitor equal to the thermal capacity of the windings by a current source. The current source in this case are the copper losses (see Fig. 6.9).

Considering Fig. 6.9, we can write

$$\int_0^t (i(t))^2 R dt = \Delta T_{cu} C_{cu} \quad (6.51)$$

$$I^2 R \Delta t = \Delta T_{cu} C_{cu} \quad (6.52)$$

$$\Delta T_{cu} = \frac{I^2 R \Delta t}{C_{cu}} \quad (6.53)$$

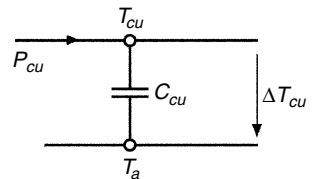


FIGURE 6.9
Equivalent circuit for adiabatic loading.

TABLE 6.9

Allowed Highest Operating Temperatures of Some Isolation Types and Coil Former Materials

Materials	Highest operating temperature, [°C]
Polybutileneterephthalate (PBT)	155
Thermoplastic polyester	150
Polyamide (PA)	85–130
Liquid crystal polymer (LCP)	155
Phenolformaldehyde (PF)	150–180

Selection out of a table of Holman J.P. *Heat transfer*, 8th ed. McGraw-Hill New York, 1997. (with permission of McGraw-Hill) [3].

where

I is the RMS value of the winding current during the time interval Δt , [°C]

R is the (AC) resistance of the wire, [Ω]

ΔT_{cu} is the temperature rise, $\Delta T_{cu} = T_{cu} - T_a$; T_{cu} is the copper temperature, [°C]

C_{cu} is the thermal capacity of the windings, $C_{cu} = c_{cu} m_{cu}$; for pure copper the specific heat is $c_{cu} = 0.383$ at 20°C.

The highest allowed temperatures of some insulation types and coil-formers given in Table 6.9 are in the range 85–180°C.

6.7 Summary

Three different levels for thermal design are presented. The level 0 and level 1 thermal designs do not need special knowledge in heat transfer. These approaches are relatively simple. Because of the uncertainties in the convection coefficient, sometimes it makes no sense to use a more elaborate approach. The level 2 design, including a thermal resistance network presentation of a magnetic component, is based on the already introduced fundamentals.

An improved thermal modeling for convection and radiation heat transfer is proposed. The model includes a precise dependence of the convection coefficient h_c on the temperature rise ΔT , on the ambient temperature T_a , on the pressure, on the dimensions and position of the magnetic component, and on the type of enclosure. The model uses an extended representation of h_c , but with more precise values of the exponents of the parameters ΔT and characteristic dimension L . Use of the definition of the characteristic parameter L and reduced surfaces, instead of the totally open surface of a transformer, contributes to the accurate modeling of the convection and radiation heat transfer. The proposed isotherm surface model can also be used as an element in more complex, multiple thermal resistance models of magnetic components.

A level 3 approach includes a finite element presentation of radiation and convection on all surfaces, and conduction in all the component parts. The design requires knowledge of FEM (Finite Element Methods). Presenting this type of design is not within the scope of this book.

Appendix 6.A Accurate Natural Convection Modeling for Magnetic Components

Most of the authors [3,14] give the following simplified expression for h_c :

$$h_c = C \left(\frac{\Delta T}{L} \right)^{1/4} \quad (6A.1)$$

where

C is in the range of 1.32–1.42 for vertical surfaces and $C = 0.59$ for horizontal surfaces

ΔT is the temperature rise, $\Delta T = T_s - T_{ar}$, [K]

L is the height of the component, [m]; in classical theory L is a characteristic dimension equal to the height of an infinite vertical surface

For magnetic components the values of h_c are given in a wide range of 6–10 [W/m²·°C] for a temperature rise of $\Delta T = 50$ [K] [8,9,10]

We present a study, and its results, of the natural convection process and the convection heat transfer coefficient h_c . The results are relevant to the design of magnetic components for power electronics and other equipment.

6.A.1 Experimental Set Up

The two experimental shapes used are:

- A box- (parallelepiped-) type shape with dimensions 42/42/15 mm, which are the outer dimensions of an EE42 core set
- A transformer-like shape, the dimensions of which are exactly the dimensions of an EE42 core transformer with a fully wound coil-former

The experimental models were made from copper of 1 mm thickness. The temperature was measured by NTC thermistors. Two heating resistors inside the model were used to heat the model, see Fig. 6A.1. The model is close to an isothermal surface model because the thermal conductivity of copper is quite high.

NOTE: The detailed set up, experimental results, and analytical presentations are given in [2].

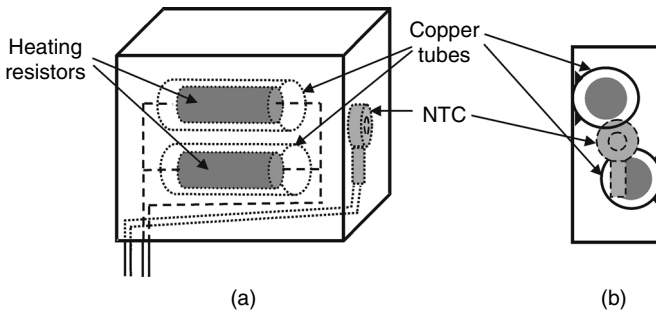


FIGURE 6A.1

A sketch of the experimental box model, a) transparent view; b) side cross section.

6.A.2 Thermal Measurements with the Box-Type Model

The objective of the experiments carried out with the box-type model was to collect enough data to derive a more precise expression for h_c . The experiment was conducted with four different surfaces of the model: new, but unpolished copper; enameled copper, which is the real open surface of windings; a black-painted surface, which has an emissivity close to the emissivity of transformer iron and ferrites; and a bright, aluminium-covered model.

To find the influence of the horizontal and vertical surface areas on the coefficient h_c , the measurements were taken for both the horizontal and vertical orientation of the model. The values of emissivity coefficients were found to be the following: black painted surface: $\epsilon_{en} = 0.925$; enameled copper: $\epsilon_{en} = 0.81$; unpolished copper: $\epsilon_{cu} = 0.14$; and bright aluminium: $\epsilon_{al} = 0.07$.

6.A.3 Thermal Measurements with the EE Transformer Type Model

6.A.3.1 Thermal Measurements at an Ambient Temperature of 25°C

A set of measurements was taken for a model that completely resembles a real transformer with respect to its surfaces. The surfaces of the model corresponding to the ferrite surfaces were black painted, and the surfaces corresponding to the coil-ends were enameled copper. Fig. 6A.2 shows the experimental results obtained for the vertical and horizontal positions of the model, and for the case when the model is on a PCB.

6.A.3.2 Thermal Measurements at an Ambient Temperature of 60°C

The final set of thermal measurements was taken at an ambient temperature of 60°C in a closed enclosure. The model was put in a black-painted, closed box with a constant temperature inside.

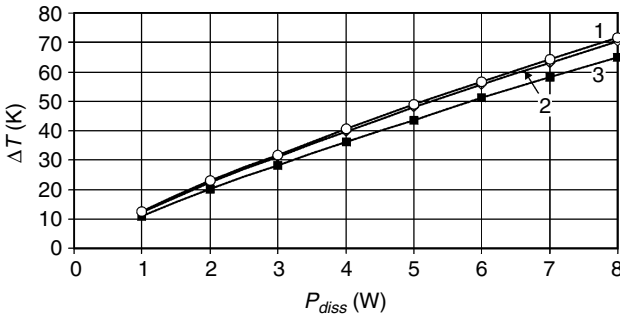


FIGURE 6A.2

Measured temperature rise ΔT as a function of the dissipated power P_{diss} transformer model, EE core 42/42/15 mm, the results are normalized to 25°C ambient temperature.

- 1: black painted and enameled model, horizontal position;
- 2: black painted and enameled model, vertical position;
- 3: black painted and enameled model on PCB.

The results and conclusions of the experiments conducted are mentioned above in Section 6.5 of this chapter.

6.A.4 Derivation of an Accurate Presentation of the Convection Coefficient h_c

A plot of the experimental results is a poor match to a curve-fitting plot based on the widely used Equation (6.10). The reason is that the convection process is a quite complex phenomenon. Properties of air, such as heat conductivity k , kinematical viscosity ν , and specific weight (density) ρ , that influence the convection process vary a lot in the considered temperature range of 250–400 K (see Table 6A.1, [3]). Thus, the heat transfer parameters, Nusselt number Nu , Grashof number Gr , Prandtl number Pr and Rayleigh number Ra , which are used in classical convection heat transfer theory, are quite influenced by the temperature, and, as a result, the simplified proportionality

TABLE 6A.1

Properties of Air: Heat Conductivity k , Viscosity ν and Density ρ in the Temperature Range 250–400 K [3]

Temperature, [K]	250	300	350	400
Conductivity k , [W/m · K]	0.02227	0.02624	0.03003	0.03365
Kinematic viscosity ν , [10^{-6} m ² /s]	11.31	15.69	20.76	25.29
Density ρ , [kg/m ³]	1.4128	1.1774	1.0091	0.8826
Prandtl number Pr , [.]	0.722	0.708	0.697	0.689

of $h_c \times (\Delta T/L)^{0.25}$ is not observed in the real experiment. The definitions for Prandtl number Pr , Grashof number Gr and Rayleigh number Ra are

$$Pr = \frac{\nu}{\alpha} \quad (6A.2)$$

$$Gr = \frac{g \left(\frac{2}{T_s + T_a} \right) (T_s - T_a) L^3}{\nu^2} \quad (6A.3)$$

$$Ra = Gr Pr \quad (6A.4)$$

where

ν is kinematic viscosity, [m²/s]

α is an accommodation coefficient, [s/m²]

g is gravity, $g = 9.81$ [m/s²]

The convection coefficient h_c is defined by the Nusselt number Nu as follows:

$$h_c = Nu \frac{k}{L} \quad (6A.5)$$

where

k is the thermal conductivity

One precise presentation of the Nusselt number, applicable over a wide range of the Rayleigh number, has been provided by Churchill and Chu [15]:

$$Nu = 0.68 + \frac{0.670 Ra^{1/4}}{(1 + (0.492/Pr)^{9/16})^{4/9}} \quad \text{for } Ra < 10^9 \quad (6A.6)$$

Substituting Equations (6A.2), (6A.3), and (6A.4) into Equation (6A.6) and then substituting the obtained relation for the Nusselt number in Equation (6A.5) results in the following expression for h_c :

$$h_c = \left[0.68 + \frac{0.670 \left\{ g \left(\frac{2}{T_s + T_a} \right) (T_s - T_a) L^3 Pr / \nu^2 \right\}^{1/4}}{\{1 + (0.492/Pr)^{9/16}\}^{4/9}} \right] \frac{k}{L} \quad (6A.7)$$

REMARK

For the temperature dependency of ν and α , the average value of these quantities for ambient and surface temperature is used.

From Equation (6A.7) it is clear that:

- the exponent, giving the final dependence of h_c on temperature rise, is lower than 0.25, as T_s , ν , Pr , and k are quite temperature dependent
- the exponent giving the dependence of h_c on the height L is higher than 0.25 because of the additional term 0.68 in Equations (6A.6) and (6A.7)

The above conclusions imply the need for more precise values of these exponents. Considering these facts, *our investigation aims are the following:*

1. To obtain more precise values for the exponents in a simplified expression of h_c :

$$h_c = C \frac{(\Delta T)^{\alpha_T}}{L^{\alpha_L}} \quad (6A.8)$$

where the exponents α_T , α_L and the coefficient C are to be found (note that α_T and α_L are not equal like in Equation (6A.1))

2. To extend Equation (6A.8) and to derive the dependence of h_c on the pressure p , on the ambient temperature T_a , and on the orientation (horizontal or vertical) of the component; i.e., to define a complete presentation of h_c in the following way:

$$h_c = C \left(\frac{p}{p_{ref}} \right)^{\alpha_p} \left(\frac{T_a}{T_{a,ref}} \right)^{\alpha_{T_a}} \frac{(\Delta T)^{\alpha_T}}{L^{\alpha_L}} \quad (6A.9)$$

where the exponents α_p and α_{T_a} and the coefficient C (depending on the orientation) are to be found.

First, using MathCAD and table data [3], we derive the following analytical expressions: $k = f_1(T)$, $\mu = f_2(T)$, $\rho = f_3(T)$, $Pr = f_4(T)$, which match the corresponding table data very well, and the difference is smaller than 0.1% (μ is dynamic viscosity, $\nu = \mu/\rho$). Second, those expressions are substituted in Equation (6A.9), and we obtain the complete classical expression for h_c :

$$h_c = F(\Delta T, T_a, L, p) \quad (6A.10)$$

In eq. (6A.9), the values of the exponents α_T , α_L , α_p and α_{T_a} , are matched to fit (6A.7) which results in the final equation (6A.11):

$$h_c = C \left(\frac{p}{p_{ref}} \right)^{0.477} \left(\frac{T_a}{T_{a,ref}} \right)^{-0.218} \frac{(\Delta T)^{0.225}}{L^{0.285}} \quad (6A.11)$$

where

C is $C_h = 1.53$ for horizontal orientation and $C_v = 1.58$ for vertical orientation of the component

L is the total distance passed by the air cooling the component (see Fig. 6.6)

ΔT is the temperature rise, $\Delta T = T_s - T_a$, [K]

p_{ref} is the reference pressure at sea level

$T_{a,ref}$ is the reference ambient temperature, $T_{a,ref} = 25 + 273$ °C

REMARK

The value $\alpha_p = 0.5$ can also be used in Equation (6A.11), as it gives only a very small difference in comparison with $\alpha_p = 0.477$.

6.A.5 Comparison of the Experimental Results and Proposed Thermal Modeling

The experimental results were compared with the analytical curves obtained by the final fit formulae (Equation (6A.11)) and by using the proposed *envelope* surface for both convection and radiation for the transformer-shaped model. The experimental and theoretical curves for the unpolished and black-painted, enameled transformer models in an open and closed enclosure are shown in Fig. 6A.3 for an ambient temperature of $T_a = 25^\circ\text{C}$. The results for an ambient temperature of $T_a = 60^\circ\text{C}$, closed enclosure, for the black-painted, enameled transformer model are shown in Fig. 6A.4. In all

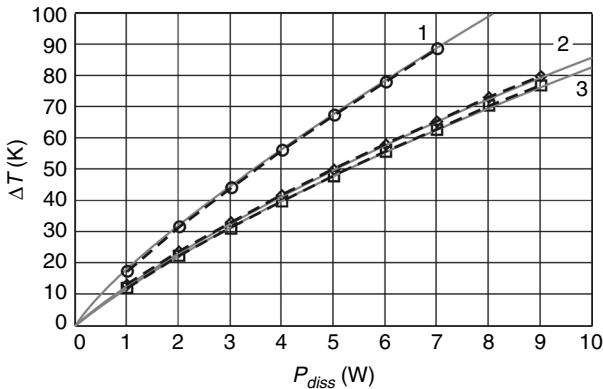


FIGURE 6A.3

Temperature rise ΔT as a function of the dissipated power P_{diss} for a transformer, EE core 42/42/15 mm, $T_a = 25^\circ\text{C}$,

1: unpolished surface in an open enclosure;

2: enameled-black painted surface in a closed enclosure (a closed box);

3: enameled-black painted surface in an open enclosure.

Solid (gray) curves are the model results; dash curves are experimental results.

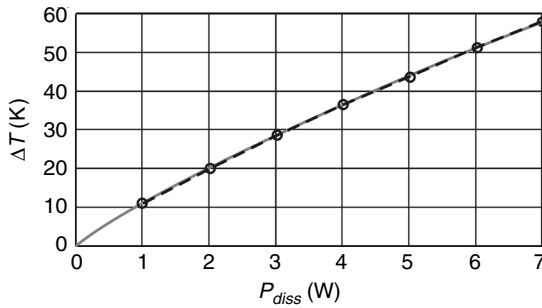


FIGURE 6A.4

Temperature rise ΔT as a function of the dissipated power P_{diss} for a transformer, EE core 42/42/15 mm, $T_a = 60^\circ\text{C}$, enameled-black painted surface in a closed enclosure (closed box). Solid (gray) curves are model results; dash curves are the experimental results.

cases the matching between the experimental results and the model results is very good. The closeness of the match proves the validity of the proposed expression for h_c , the found values of the emissivity of enameled and unpolished copper and black-painted surface, as well as the proposed approach for using the *envelope* surface for real magnetic components.

References

- [1] Waasner, *Trafo-Steckerkerne Trafo-Kernbleche Zubehor*, Katalog T 15/1-87, Berlin, 1987, pp. 35–105.
- [2] Van den Bossche, A., Valchev, V., and Melkebeek, J., Improved thermal modeling of magnetic components for power electronics, *European Power Electron. J.-EPE*, 12:2, 7–11, 2002.
- [3] Holman, J.P., *Heat Transfer*, 8th ed., McGraw-Hill, New York, 1997.
- [4] Flanagan, W.M., *Handbook of Transformer Design and Applications*, 2nd ed., McGraw-Hill, New York, 1992.
- [5] McLyman, W.T., *Transformer and Inductor Design Handbook*, 2nd ed., Marcel Dekker, New York, 1988.
- [6] Snelling, E.C., *Soft Ferrites and Applications*, 2nd ed., Butterworths, London, 1988, pp. 22–64, 176, 191, 202.
- [7] Odendaal, W.G. and Ferreira, J.A., A thermal model for high-frequency magnetic components, *IEEE Transactions on Industry Applications*, vol. 35. No. 4, July/August 1999, pp. 924–930.
- [8] Petkov, R., Optimum design of a high power, high frequency transformer, *IEEE Transactions on Power Electronics*, vol. 11. No. 1, January 1996, pp. 33–42.
- [9] Mulder, A.S., Fit formulae for power loss in ferrites and their use in transformer design, in proceedings of *Power Conversion*, Nurnberg, June, 1993, pp. 345–359.
- [10] Richter, R., *Elektrische Maschinen, Allgemeine Berechnungselemente, Die Gleichstrommaschinen*, Springer, Berlin, 1924, pp. 318–321.

- [11] Valchev, V. and Van den Bossche, A., Accurate natural convection model for magnetic components, *Microelectronics Reliability*, vol. 43, No. 5, May 2003, pp. 795–802.
- [12] Van den Bossche, A., Valchev, V., and Melkebeek, J., Thermal modelling of E-type magnetic components, *IECON'2*, Sevilla, Spain, November 5–8, 2002, pp. 1312–1317.
- [13] Hilperr, R., Wärmeabgabe von geheizten Drahten und Röhren, *Forschung Geb. Ingenieurwes.*, Berlin, vol. 4, 1933, p. 220.
- [14] Hurley, W. G., Wolfe W. H., and Breselin J.G., Optimized transformer design: Inclusive of high-frequency effects, *IEEE Transactions on Power Electronics*, vol. 13, No. 4, July 1998, pp. 651–659.
- [15] Churchill S. and Chu, H.H., Correlating equations for laminar and turbulent free convection from a vertical plate, *International Journal of Heat and Mass Transfer*, vol. 18, 1975, pp. 1323–1330.

7

Parasitic Capacitances in Magnetic Components

This chapter presents the parasitic capacitances in the magnetic components, their measurements and some approaches to decrease the values of these usually undesired capacitances. At very high frequency even parasitic capacitances are not sufficient to describe the complete behavior of the magnetic component, as propagation or transmission-line effects become important. Such effects are also encountered in wide band current probes [1],[2]. Thus, at very high frequency, it is advisable to use special measurement techniques such as an impedance analyzer, (discussed in [Chapter 11](#), Measurements). A specific view on EMC filter components is presented in [3] and [4].

At high frequencies or high voltages the parasitic capacitances cannot be neglected and should be taken into account in the magnetic components design and applications. We will discuss, consecutively, the typical capacitances influencing the design:

- Capacitances between the windings (inter capacitance);
- Own capacitance of the windings (intra capacitance);
- Capacitance between the windings and the magnetic material (the core).

REMARK

In this chapter we consider mainly the low frequency effects of the parasitic capacitances.

7.1 Capacitance Between Windings: Inter Capacitance

The capacitances between the windings are also denoted as **inter capacitances** of the windings in a magnetic component.

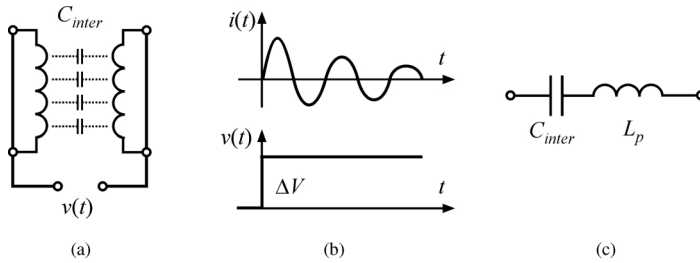


FIGURE 7.1

The effect of the inter capacitances C_{inter} in an isolating transformer. (a) the isolating transformer; (b) the common mode current $i(t)$ at step voltage $v(t)$; (c) the equivalent circuit for common mode current.

7.1.1 Effects of the Inter Capacitance

The capacitance between windings often generates common mode currents in galvanic insulated converters. This is a typical case of EMI (Electro Magnetic Interference) generation. Often it is even a matter of safety to obtain low common mode currents, especially in medical equipment. Another typical example of the requirement of low capacitance transformers is the supply of the high side drivers in bridge converters.

Here we will explain the mechanism of the inter capacitance influence. Let us consider the transformer shown in Fig. 7.1. When we apply a step in the common mode voltage between the primary and secondary windings (see Fig. 7.1a) we have the common mode current shown in Fig. 7.1b. By the step voltage ΔV , an average charge $Q = \Delta V C_{inter}$ is injected. The RMS value of the corresponding current is usually quite high $I_{rms} \gg f \Delta V C_{inter}$, as ringing occurs, causing the charge to oscillate forward and backward. The parasitic capacitance C_{inter} resonates with a parasitic leakage inductance L_p , see the equivalent series scheme in Fig. 7.1,c. To decrease the RMS common mode current, a damping common mode choke can be added to the circuit.

7.1.2 Calculating Inter Capacitances and the Equivalent Voltage

The inter capacitance can be expressed as

$$C_{inter} = \epsilon_o \epsilon_r \frac{S}{d} \quad (7.1)$$

where

S is the area between the windings

d is the distance between the wires of the adjacent layers

ϵ_o is the permittivity of the air

ϵ_r is the relative permittivity

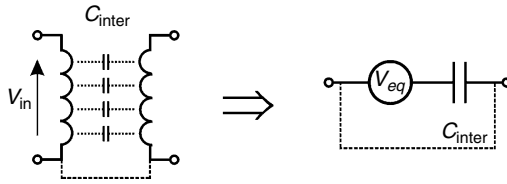


FIGURE 7.2
Equivalent circuit of a transformer with respect to common mode voltages.

Note that d is not constant, and that ϵ_r also depends on the enamel, insulating sheets, impregnating varnish, and air, so, in fact, a quite complex field problem is present.

We will start with estimating the transmitted charge. If a winding is excited with an AC voltage, then a total charge is present, depending on the voltages V' and V'' between the adjacent surfaces. The total charge Q is

$$Q = \int (V' - V'') \epsilon_o \epsilon_r \frac{dS}{d} \tag{7.2}$$

where

- $V' - V''$ is the voltage between adjacent wires of different layers
- d is the distance between the wires of the adjacent layers
- dS is an elementary surface

To present a transformer with respect to common mode voltages and currents, we can use the equivalent circuit shown in Fig. 7.2. Using Equations (7.1) and (7.2), the equivalent voltage V_{eq} from Fig. 7.2 can be calculated as

$$V_{eq} = \frac{Q}{C_{inter}} \tag{7.3}$$

However, the inter capacitance is easily measured using a low frequency test. In practice, the test is much easier to be carried out than the calculating the value.

7.1.3 Measuring Inter Capacitances

Usually, the measurements can easily be done with a capacitance meter, or an RLC tester at low frequency (1 kHz or lower), where the voltages induced in the windings by the capacitive currents are negligible. Care should be taken with the internal capacitance influence of the measurement device.

Measurements of very low capacitances (10pF and lower) require special measurement techniques such as the methods described in [Chapter 11](#).

7.2 Self-Capacitance of a Winding: Intra Capacitance

The capacitances of the windings are also denoted as **intra capacitances**. First, we will show the negative effects of these capacitances on the performance of a circuit in which the magnetic component is included.

7.2.1 Effects of Intra Capacitance

This capacitance is usually not desired and one tries to keep it low. The intra capacitance of a magnetic component results often in parallel resonances with magnetizing or leakage inductances of the component.

Let us consider the boost (step up) converter illustrated in Fig. 7.3a. The inductor voltage and current are shown in Fig. 7.3b for discontinuous mode. The ripples in these voltage and current waveforms are due to the resonance between the intra capacitance of the winding C_{intra} and the inductance L of the inductor. Here we should also take into account the outer body capacitance of the semiconductor device, which is, in fact, in parallel with C_{intra} for the AC component. These ripples are narrow band disturbances, which are harmful with respect to the EMC (Electro-Magnetic Compatibility) of the converter. In some cases, the ripples can even cause instability in the feedback

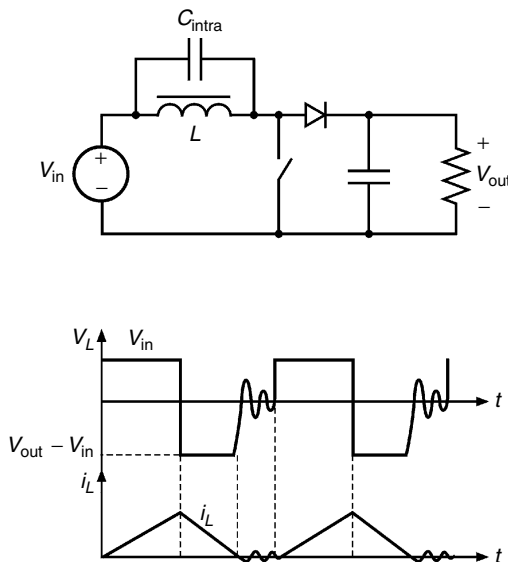


FIGURE 7.3

The effect of the intra capacitance C_{intra} : (a) boost converter; (b) inductor voltage V_L and current i_L wave forms, discontinuous mode.

control of the converter while the open loop gain can have a locally inverted gain [5]! The problem is really relevant when the resonant frequency of the circuit consisting of C_{intra} and L is not very high in comparison to the switching frequency. To decrease the amplitude of the ripples a damping should be realized by additional components.

In some designs the switching frequency can be close to the resonant frequency of the converter. This is typically true for converters from low to high voltage. Such converters are often designed to operate near the resonant frequency of the high voltage winding; thus, fewer primary switch currents are necessary in the primary side to operate the converter.

7.2.2 Calculating Intra Capacitances of a Winding

At low frequency, the capacitance between layers can be converted to an equivalent capacitance between the terminals. To calculate the capacitance, the method using the energy of a capacitor is often preferable because it seems to be the easiest one. Assume a sinusoidal voltage applied to the terminals of a winding. Using the voltage distribution between turns of the different layers, the elementary energy can be estimated and integrated to obtain the total energy W of the equivalent capacitor C_{intra} , representing the intra capacitance of the winding:

$$W = \frac{C_{intra} v^2}{2} \quad (7.4)$$

$$W = \int \frac{(v' - v'')^2 \epsilon_o \epsilon_r}{2d} dS \quad (7.5)$$

where

W is the total energy accumulated in the equivalent capacitor C_{intra}

$v' - v''$ is the voltage between adjacent wires of different layers

d is the distance between the wires of the adjacent layers

The elementary energy is integrated over the surface between the different layers. Then, using Equations (7.4) and (7.5), the equivalent capacitance C_{intra} , converted to the primary winding, is

$$C_{intra} = \frac{2W}{v^2} \quad (7.6)$$

where

v is the voltage across the considered winding

The practical problem is that the distance between two adjacent layers is not constant (d is not constant in Equation 7.5), and, also, there is usually some air between the windings. The solution is to do a practical test to

measure the capacitance between layers. This can be done by cutting the link between the layers and then measuring the capacitance between the layers such as an inter capacitance.

Usually, the voltage between the conductors of the layers increases linearly. In this case, the intra capacitance between two layers can be approximated based on Equations (7.2), (7.5), and (7.6):

$$C_{intra} = \frac{1}{3} \sum C_{intra,i} \quad (7.7)$$

where $C_{intra,i}$ is the capacitance between every two adjacent layers of the considered winding.

REMARK

In the ferrite core components, the capacitance of the wires is not the only factor that contributes to the equivalent intra capacitance. The resonant properties of the ferrite material itself can also increase the apparent equivalent intra capacitance.

7.2.3 Measuring Intra Capacitances of Windings

Measurement of the intra capacitance of a winding is usually realized by measuring a resonant frequency. In this case, the capacitance of the measuring device should also be taken in account. A sine wave generator can be used, along with a series resistor. Depending on the considered equivalent scheme, different tests can be used.

7.2.3.1 Single Parasitic Capacitance Model

This model is mainly applicable to inductors, as they have only two terminals. In transformers with a low and a high voltage winding, the major effect is in the high voltage winding. To reduce the influence of the capacitance of the probe on the results, it is advisable to measure the resonant frequency f_r using the low voltage winding of the transformer with open high voltage winding, as it is shown in Fig. 7.4. Thus, the parasitic capacitance can be modeled as a single capacitor in that high voltage winding (see Fig. 7.4).

For an inductor it is sometimes easy to add one turn to the core. The measurement is possible on this single turn in the same way, since it is used as a low voltage winding fed by a sine generator. The device being tested is fed with a sine wave generator with a resistor, which is much higher than the resonant impedance (typically $> 10 \text{ k}\Omega$). Then:

$$C_{intra} = \frac{1}{L_1 (2\pi f_r)^2} - \left(\frac{N_2}{N_1} \right)^2 C_{probe} \quad (7.8)$$

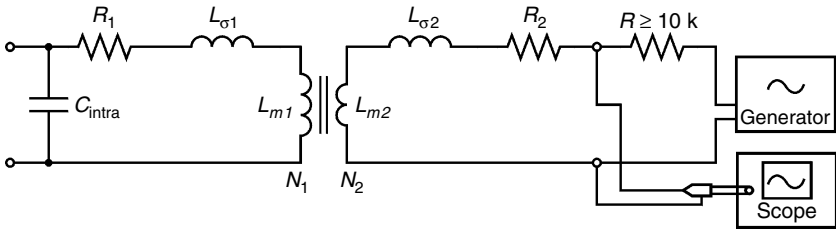


FIGURE 7.4

Measurement using a single parasitic capacitance equivalent circuit, the transformer is fed at the low voltage winding.

where

$L_1 = L_{m1} + L_{\sigma1}$ is the inductance of the high voltage winding, measured at low frequency (see Fig. 7.4)

f_r is the measured resonant frequency

$N_1 \gg N_2$; N_1, N_2 are the turn numbers of the primary and secondary windings, respectively

C_{probe} is the capacitance of the probe.

Note that we don't include $L_{\sigma2}$ in Equation (7.8) because the current of the secondary winding, where the generator is placed, is very small in comparison with the current in the resonant circuit consisting of L_1 and C_{intra} .

7.2.3.2 Model with a Parasitic Capacitance for Each Winding

This is a typical scheme for transformers with a turn ratio close to 1 and a few windings. All the windings are short-circuited except the measured winding. In Fig. 7.5 this is the primary winding, and the measured capacitance in the case is $C_{intra,1}$. The capacitance can be estimated in a similar way as described in Section 7.2.3.1. For each measurement, the generator is connected to the respective windings. The inductance to be considered for the calculation is the equivalent series leakage inductance $L_{\sigma,e}$ seen from that winding. This

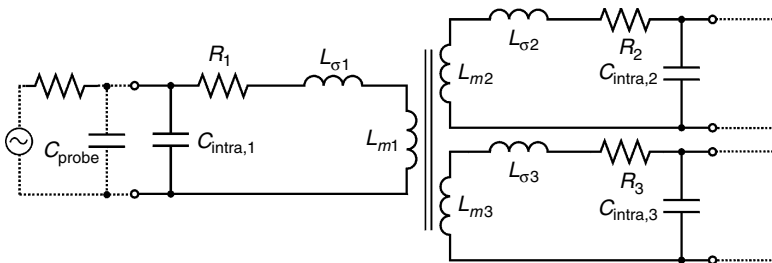


FIGURE 7.5

Equivalent circuit with a capacitance at each winding, measurement circuit in dots.

inductance should be measured at a sufficiently high frequency to avoid errors due to series resistance of the winding, as the magnetizing inductance L_m is not always high compared to resistances (see Chapter 11). Then the parasitic capacitance C_{intra} of the measured winding is

$$C_{intra} = \frac{1}{L_{\sigma,e} (2\pi f_r)^2} - C_{probe} \quad (7.9)$$

where $L_{\sigma,e}$ is equivalent series leakage inductance measured at the excited (measured) winding.

The measurements as described in Section 7.2.3.2 are not easy. To improve the accuracy in this case one can also use impedance analyzer.

7.3 Capacitance Between the Windings and the Magnetic Material

Up to now we neglected the capacitances between the windings and the magnetic material in the calculations. Sometimes the core is ground to reduce the capacitive transfer between the windings. Grounding or not grounding of the core influences both inter and intra capacitances, and thus, it influences the resonant frequency of the magnetic component. When the core (the magnetic material) is ground, the capacitances increase and vice versa.

The capacitance between the windings and the magnetic material is discussed also in [3].

7.4 Practical Approaches for Decreasing the Effects of Parasitic Capacitances

7.4.1 Low Intra-Capacitance Windings

Obtaining a low intra capacitance of a winding is realized by a higher distance between layers, a low number of turns per layer, and a low value of ϵ_r . Impregnating or immersion in oil of the winding increases this capacitance considerably because of increasing ϵ_r .

Here we give a construction approach to decrease the intra capacitance using a special way of winding (see Fig. 7.6). In this case the voltage between the adjacent turns is always $v'' - v' = v/2$, where v is the total voltage across the layers. Then the total intra capacitance of the winding is found as

$$C_{intra} = \frac{1}{4} \sum C_{intra,i} \quad (7.10)$$

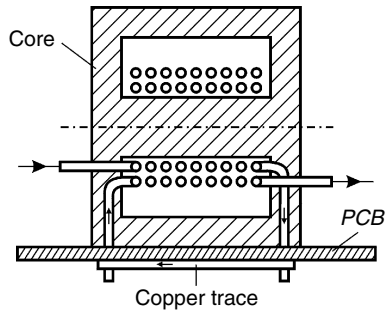


FIGURE 7.6

A coil former construction to decrease intra capacitance of a winding.

where $C_{intra,i}$ is the capacitance between every two adjacent layers of the considered winding. This value is somewhat decreased in comparison to the value $C_{intra} = \frac{1}{3} \sum C_{intra,i}$ in the common way of winding.

Other advantages of such a design are:

- The maximum voltage between the adjacent turns is always equal to $\frac{1}{2}$ of the total voltage, applied over the winding;
- The winding pitch has the same direction; thus, obtaining hexagonal fitting is easy, which contributes to a better heat transfer in the winding;
- This arrangement is better with respect to corona effect. Also, the arrangement reduces the partial discharges, which are harmful for the lifetime of the component.

7.4.2 Decreasing the Effects of the Inter Capacitance

A good design idea is to decrease the inter capacitance itself. One way is to provide more distance between primary and secondary windings. This can be realized by putting more insulating material between primary and secondary windings in concentric windings. One can also wind in separate rooms. However, good solutions for capacitance reduction often result in increasing a lot both leakage inductance and eddy current losses of the magnetic component.

A method to decrease the effect (capacitive current) of the inter capacitance of a transformer is to wind the windings symmetrically in a way that the adjacent layers of the primary and secondary winding contain the same number of turns (see Fig. 7.7).

To find the effect of the inter capacitance, we consider only the two adjacent layers at the border between primary and secondary because these layers act as a screen for the other layers. In the construction shown in Fig. 7.7, the voltage between the adjacent turns of the two boundary layers of the primary and secondary windings and the reference point is the same. Thus, there is

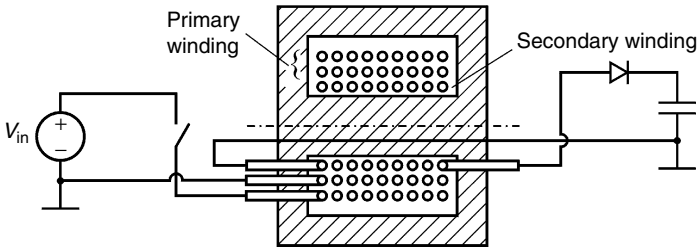


FIGURE 7.7

Symmetrical adjacent layers of the primary and secondary windings in order to decrease the common mode currents.

no voltage between the adjacent turns of the primary and the secondary windings. So, if we use the equivalent scheme illustrated in Fig. 7.2, the equivalent voltage V_{eq} in it is zero, which means that there is (almost) no common mode current in that case.

In some cases it is difficult to reduce the effect of the parasitic inter capacitance only by the design of the magnetic component. Another solution is to add an additional external capacitance as it is shown in Fig. 7.8. In this case a 'capacitive voltage divider' is obtained, and the equivalent common mode current is much lower. The typical value of the additional external capacitor is 2.2nF (at 2 kV or more). If the common mode choke has an inductance of 1mH, then a resonant frequency below 150kHz is obtained. Together with some damping (low $\tan\delta$) of the common mode choke, the EMC requirements can be satisfied.

The proposed method for decreasing the parasitic inter capacitance by adding an external capacitor is not advisable for supplies for high side drivers in bridge converters, or other applications where a high dv/dt is applied between both sides of the galvanic separation.

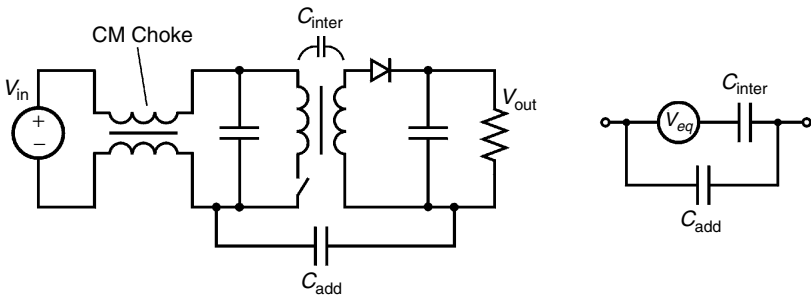


FIGURE 7.8

A method to suppress the effects of inter capacitance by adding an external capacitance.

7.4.3 Screening

Screens are sometimes used to decrease the capacitive currents. This effect is obtained by lowering the equivalent voltage V_{eq} , in spite of the usually higher values of the parasitic capacitances. Screens can be considered as single turn windings. In screens, eddy currents can also be induced. All this implies that making high quality magnetic components is still an art.

References

- [1] Van den Bossche, A. and Ghijselen, J., EMC combined di/dt current probe, *IEEE International Symposium On Electromagnetic Compatibility*, August 21–25, 2000, Washington, D.C., CD-ROM.
- [2] Sergeant, P. and Van den Bossche, A., High sensitivity 50 Hz-1 MHz probe for B and dB/dt, *IEEE International Symposium on Electromagnetic Compatibility*, Vol. 1, Minneapolis, August 19–23, 2002, pp. 55–60.
- [3] Goedbloed, J.J., *Electromagnetische Compatibiliteit*, 3rd ed., Kluwer Technische Boeken, Antwerpen, 1993, pp. 86–92.
- [4] Tihanyi, L., *Electromagnetic Compatibility in Power Electronics*, Butterworth-Heinemann, Oxford, 1995, pp. 275–309.
- [5] De Gussemé, K., Van de Sype, D.M., Van den Bossche, A.P., and Melkebeek, J.A., in *Proceedings of the 34th Annual IEEE Power Electronics Specialists Conference (PESC03)*, Acapulco, 2003, pp.1685–1690.

8

Inductor Design

This chapter treats the specific aspects related to inductors, in general, and the design of special inductors.

The inductance of air coils and toroidal cores is presented at the beginning. Air coils were historically important and are still used if accurate values are needed, as they are not influenced by the characteristic of magnetic materials. Compared to air coils, much higher energy and apparent power densities are obtained using coils with cores of magnetic materials. With high permeability materials, air gaps are necessary to improve the energy storage. Usual shapes for laminated iron are given in this chapter. For inductors with air gaps, methods to estimate the additional permeance due to fringing fluxes are also presented.

In the second part of the chapter we discuss the design details for different kinds of inductors. We present the differences in design of DC inductors, HF (high frequency) inductors, and combined DC-HF inductors. A few examples are given:

- the requirements of an inductor in a buck converter
- a coupled common mode inductor
- a flyback transformer

At the end of the chapter we include appendices, concerning fringing coefficients for gapped wire wound inductors and details in the design of the mixed DC-HF inductors.

8.1 Air Coils and Related Shapes

8.1.1 Air Coils

Air coils have several applications, such as:

- inductors with high peak currents and low duty ratio
- accurate coils, as there is no influence of the magnetic material characteristics, such as a low initial permeability and saturation

- inductors with very large dimensions employed in distribution grids
- commutating inductors (in thyristor and resonant commutation circuits)

The typical shapes of air coils are:

- solenoids
- toroidal air coils
- air coils with rectangular winding cross section

In designs with small dimensions care should be taken, as the air coils usually have more DC resistance and more eddy current losses than designs with magnetic materials.

8.1.2 Solenoids

For long solenoids, where the length is much larger than the diameter (see Fig. 8.1), as a first approximation, the reluctance of the flux return path (flux path outside the coil) can be neglected as the return path reluctance is typically 5 to 20 times less than the internal reluctance of the central part. The central path for the flux is indeed much narrower than the external return path. Thus, the inductance of a solenoid, neglecting the reluctance of the outside flux path, is:

$$L = \mu_0 N^2 \frac{A}{l} \quad (8.1)$$

where

$\mu_0 = 4\pi 10^{-7}$ [H/m] is the permeability of free space

N is number of turns

A is the cross sectional area of the coil [m²], $A = \pi d^2$

l is the length of the coil [m]

The accuracy of Equation (8.1) is not high, except if the return path is closed with high permeability magnetic material.

If the internal volume of the coil is filled with a high permeability material then only the return path is considered. In this case the inductance of the coil is typically increased 5 to 10 times. This type of construction combines a low DC resistance and a high power/weight ratio. However, the stray

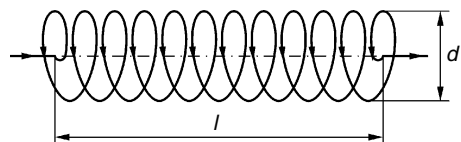


FIGURE 8.1

A solenoid air coil, l is the length, d is the diameter of the coil.

fields are really high so that this type of construction is not compatible with EMC requirements.

8.1.3 Toroidal Coils

When a solenoid is 'bent' to a toroidal shape (see Fig. 8.2a) and the ends are joined together, the coil is called a 'toroid'. The inductance of a toroidal air coil can be calculated by Equation (8.2). In that case it is permissible to neglect the return path. If the internal volume is filled with a magnetic material with relative permeability μ_r , the inductance is increased by a factor μ_r and it becomes:

$$L = \mu_0 \mu_r N^2 \frac{A}{l_c} \tag{8.2}$$

where

- l_c is the average length of the magnetic part
- N is the number of turns
- μ_r is the relative permeability inside the toroid
- μ_0 is the relative permeability inside the toroid

If a toroidal shape is filled with *high-permeability material*, it is called a toroidal core or a ring core. It is easily saturated as the magnetic circuit is closed. When using *low-permeability materials*, the energy storage is good. However, it is not easy to find low-permeability materials that combine low

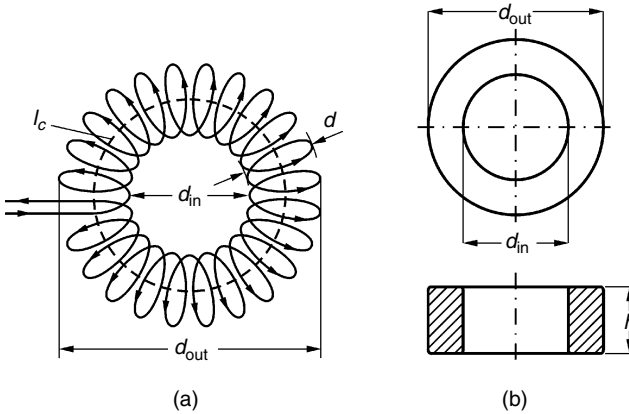


FIGURE 8.2

Toroid coils.

(a) a toroidal air coil: l_c is the length, d is the diameter of the winding, d_{in} , d_{out} are inner and outer diameters of the coil;

(b) a toroidal core with rectangular cross section of the winding.

loss at high induction, so materials must be carefully chosen. The use of an air gap allows for the use of high-permeability materials in combination with good energy storage, but the advantage of low stray fields is lost.

For toroidal cores with rectangular cross section (see Fig. 8.2b), one can easily correct for the curvature. To find the inductance first we will find the flux linkage $\Psi = \Phi N$. The total MMF of the coil is $MMF = Ni$. The physical flux is:

$$\Phi = \mu_0 \mu_r b \int_{d/2}^{D/2} \frac{Ni}{2\pi r} dr = \frac{\mu_0 \mu_r h N i \ln(d_{out}/d_{in})}{2\pi} \quad (8.3)$$

The inductance in that case is:

$$L = \frac{\Psi}{i} = \frac{\Phi N}{i} = \mu_0 \mu_r N^2 \frac{h \ln(d_{out}/d_{in})}{2\pi} \quad (8.4)$$

where

d_{in} , d_{out} are inner and outer diameters of the coil (see Fig. 8.2b)

h is the height of the coil

The advantage of toroidal coils is that their outside field is virtually zero. Also, the voltage at the terminals is not influenced by external fields. A special exception is the case of a wire through the coil aperture. In an open circuit, the output voltage of the inductor will be proportional to the derivative of the current. If no magnetic material is present, the toroid can be seen as a closed Rogowski coil.

The typical disadvantage of toroidal *air* cores is that the energy density is also very low compared to other air coils, such as air coils with rectangular cross sections.

8.1.4 Coils with Rectangular Cross Sections

8.1.4.1 General Case

An air coil with a rectangular cross section is shown in Fig. 8.3. The experimental formula of Welsby proposed in [1] gives a quite accurate result for

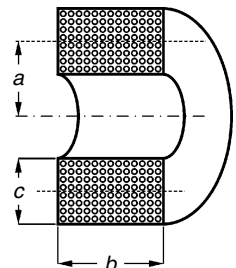


FIGURE 8.3
Cylindrical air coil with rectangular winding cross section.

the inductance value:

$$L = \frac{\mu_0 N^2 \pi a^2}{b} \frac{1}{1 + 0.9(a/b) + 0.32(c/a) + 0.84(c/b)} \quad (8.5)$$

where

- a is the distance between the axis of the winding area and the axis of the coil (for a, b and c see Fig. 8.3)
- b is the width of the winding cross section
- c is the height of the winding cross section

The accuracy of Equation (8.5) is usually better than 2%. The expression also gives good results for solenoids (small c) and disc coils (small b). For small values of c , Equation (8.5) is similar to the approximation for the solenoid, but a distance of $0.9a$ has been added to b to compensate for the reluctance of the return path. However, Equation (8.5) is not accurate in the cases where both parameters c and b are small compared to a .

Cylindrical coils generate high stray fields. In practice, this means that some conductive shielding around the circuit should be provided. This reduces the inductance and increases the losses. In the presence of iron enclosures acoustic noise can also occur.

8.1.4.2 ‘Four Square’ Cylindrical Air Coil

Brooks proposes an air inductor with a ‘four square’ cross section shown in Fig. 8.4 [1]. The proposed that the coil construction obtains maximal induction L for a given wire length l_w . The optimal shape is close to the coil with a ‘four square’ cross section and the inductance is:

$$L = 2.029 \mu_0 c N^2 \quad (8.6)$$

The ‘four square’ shape is close to the minimum wire length for a given DC resistance and inductance at ambient temperature, but it is not optimal with regard to thermal aspects and eddy current losses, where solenoid type (long) coils exhibit better performance.

Other cross-sectional areas such as hexagonal winding cross section or a circular winding cross section give almost no improvements; hardly a 1% increase in the inductance value can be obtained for the same wire length.

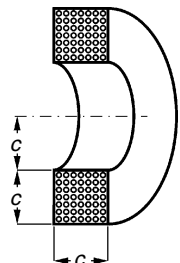


FIGURE 8.4
“Four square” cylindrical air coil.

8.2 Inductor Shapes

For frequencies below 1 kHz laminated iron inductors are still considered in power electronics. Typical applications are smoothing inductors at the DC or AC side of grid-connected rectifiers (intended to reduce harmonics), energy storage in DC link converters, and low-frequency lamp ballasts. The advantages are the low cost, the high saturation induction, and the availability in large sizes. Inductors with laminated iron sheets are somewhat different in construction and assemblage compared to iron sheet transformers. In most types they need more mechanical construction elements than transformers. In general, care should also be taken to avoid short circuit paths for circulating currents into construction parts, which would heat up the mechanical construction element such as bolts. A normal design peak induction of laminated iron is 1.5 T.

Here we present usual inductor shapes used for laminated iron cores.

- EI (Fig. 8.5)

The EI shape is called scrapless if the lamination dimensions of the E- and I-part fit to each other. In that case the laminations are made by punching without loss of material. All dimensions are multiples of a characteristic dimension (thickness of the I-part). The center leg cross-sectional area is equal to the sum of the outer legs. For non scrapless E-I types, the height of the winding area is larger than the thickness of the I-part. The air gap can be obtained with a distance between E- and I-parts. This distance is realized by a so-called “spacer.” If only the center leg is shortened, the gap is then referred to as a “center-leg gap.” In the commercial products, normally a center-leg gap is utilized because of both the reduced leakage field and the acoustical noise. To obtain the same inductance, the center-leg gap length has to be more than twice the spacer thickness due to “fringing” field effects (to be discussed in greater detail later in the chapter).

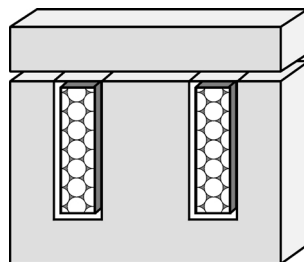


FIGURE 8.5
An EI laminated iron inductor.

- UU shape (Fig. 8.6)

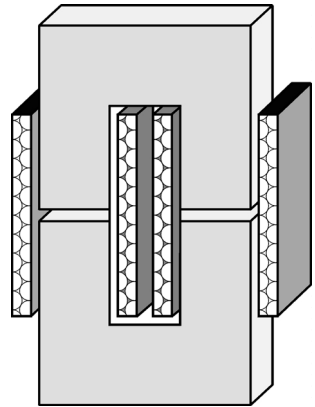


FIGURE 8.6
A UU laminated iron inductor.

In the UU shapes, normally both legs are wound with equal coils. The advantage of a UU shape is having air gaps close to the point where the MMF is produced. This equalizes the induction along the iron path, thus avoiding bottlenecks.

- 4I shape (Fig. 8.7)

The 4I construction has four air gaps. The windings are located on both side legs. The iron is easy to cut without special tooling. It is typically used for large cores.

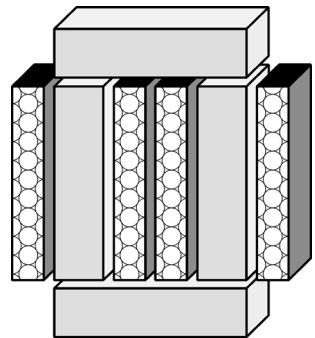


FIGURE 8.7
A 4I laminated iron inductor.

- M-shape (Fig. 8.8)

M-shapes can be manufactured with (inductor) or without (transformer) air gaps. The advantage of this type is that it has almost no stray field. Also, no special mechanical pieces are needed to hold the parts together. The acoustical noise is limited as the mechanical construction is stiff.

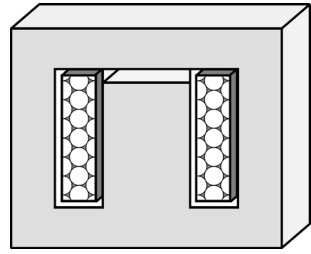


FIGURE 8.8
A M-type laminated iron inductor.

8.3 Typical Ferrite Inductor Shapes

A special appendix at the end of the book is dedicated to this subject. This is Appendix B and it gives geometrical data of a selection of commonly used ferrite core shapes. In the tables we present the data concerning the following parameters:

- l_e – effective magnetic path
- A_e – effective magnetic area
- A_{min} – minimum magnetic area
- W_a – minimum winding area
- MLT – mean length per turn
- MWW – minimum winding width (also denoted in the book as w)

8.4 Fringing in Wire-Wound Inductors with Magnetic Cores

Basically ferrite types of inductors are considered here, as they are the most usual ones in power electronics.

8.4.1 Center Gapped, Spacer and Side Gapped Inductors

Figure 8.9 shows different arrangements of gapped inductors.

The *center gap* inductors (Fig. 8.9a) are common in industrial designs, as they generate less EMI than inductors with gaps in the side legs. However making center gaps needs special diamond tools with water-cooling. Also, the center leg is not easy to adapt.

In practice, the first laboratory prototypes are often made using *spacers*, Fig. 8.9b. The advantage is that one can easily change the air gap throughout the design of the circuit. These inductors induce lower eddy current losses

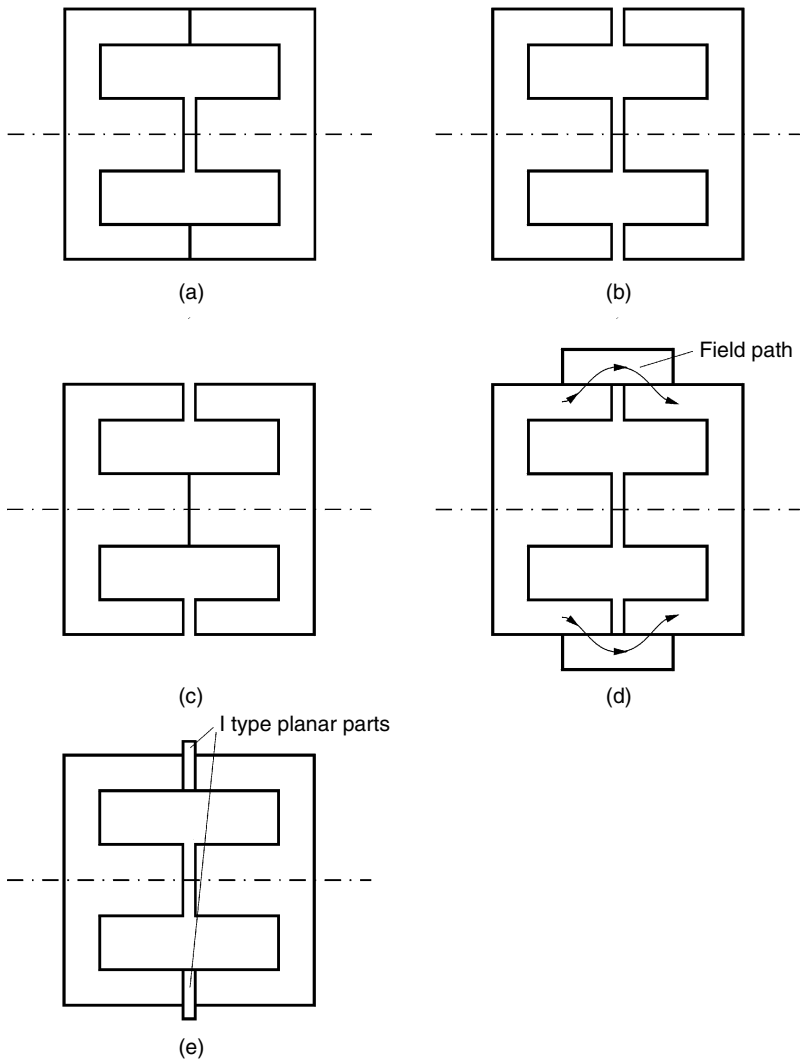


FIGURE 8.9

Different ways to realize air gaps in EE cores.

- (a) A center gapped inductor;
- (b) A spacer gapped inductor;
- (c) A side gapped inductor;
- (d) An inductor with side shunts;
- (e) An inductor with planar I type core parts in the side legs.

than center gap inductors do. The disadvantage is that they produce more stray field at some distance from the core.

Some problems can arise when the production goes from prototype with spacers to series production using a center gap. The first problem is that the required center gap length is more than twice the spacer thickness. The

second problem is that the eddy current losses in the conductors increase. It may be a good idea to take the losses of a center gap into account even when designing a prototype with a spacer, thereby avoiding troubles afterwards.

Cores with *only side gaps* (Fig. 8.9c) usually induce still lower eddy current losses than cores with spacers. A problem with cores having only side gaps is that the center leg carries the biggest flux (losses) and it is easily saturated (also due to the higher temperature inside the magnetic component).

A practical way to *simulate a center gap* for experiments is to use shunted outer legs (see Fig. 8.9d) or by using parts of planar cores in the side legs (see Fig. 8.9e). While using spacers or shunted outer legs, the inductance can easily be adapted by trial and error. Often, the inductance will be higher than expected due to fringing fields. If the number of turns is well designed, one should not reduce the number of turns, but increase the air gap. The reason is that the difference in the inductance value is due to the permeance of the air gap. Reducing the number of turns at high fringing fields would cause an early saturation of the core.

8.4.2 Simplified Approach to the Center Gapped Inductors

Inductors with full wire or Litz wire windings are the most common constructions. For the calculation of the inductance in a simplified approach for small air gaps, if only the main flux path is considered, and one can use a simple expression for the inductance of a coil. This yields the following equation:

$$L = \mu_0 N^2 \frac{A_g}{\sum l_g + l_{fe}/\mu_r} \quad (8.7)$$

where

$\sum l_g$ is the sum of the air gap lengths in the flux path

A_g is the cross section of the air gap, equal to core cross section

l_{fe} is the equivalent length of the flux path in core material

μ_r is the relative permeability of the core material

N is the number of turns

In Equation (8.7) μ_r depends on the type of magnetic material, the induction saturation level, and the type of applied voltage and current waveforms. For more details concerning μ_r , see [Chapter 3](#).

However, for normal air gaps, the permeance of other field paths (fringing paths) out of the air gap is not negligible. It results in much larger values for L than predicted by Equation (8.7). In almost all designs of gapped inductors for power electronics the fringing field should be considered, and, thus, the expression (8.7) gives a poor approximation in most practical cases.

A better approximation for gapped UU and gapped EE cores (the gap is in the excited leg or legs) is McLyman's equation [2]:

$$L' = L \cdot X_f, \quad X_f = 1 + \frac{l_g}{\sqrt{A_g}} \ln\left(\frac{2w}{l_g}\right) \quad (8.8)$$

where

L' is the inductance value corrected for fringing

X_f is fringing factor

w is the total width of the winding (layer width)

l_g is the air gap length

The accuracy of Equation (8.8) can be increased using a tuning coefficient q for round and rectangular cross-sections:

$$L'_q = L X'_f, \quad X'_f = 1 + \frac{q l_g}{\sqrt{A_g}} \ln\left(\frac{2w}{l_g}\right) \quad (8.9)$$

where

$q = 0.85-0.95$ for round cores (for example ETD-core)

$q = 1-1.1$ for rectangular cores (for example EE-core)

The values of q are fine-tuned using manufacturer data and compared with the results of Finite Elements Method (FEM) [3] solutions. The results of Equations (8.7), (8.8), and (8.9) and the manufacturer data for an EE42/21/15 core (12/15 mm center leg) are shown in Fig. 8.10. The value of the coefficient q is 1.05. The same comparison between the results of Equations (8.7), (8.8),

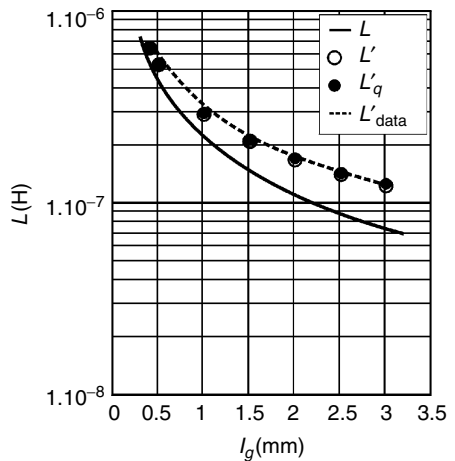


FIGURE 8.10

Comparison of the inductance value L obtained by Equations (8.7), (8.8), and (8.9) and the manufacturer data for EE42/21/15 core, $q = 1.05$.

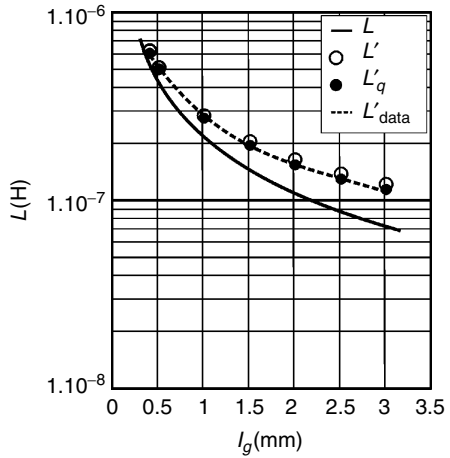


FIGURE 8.11
 Comparison of the inductance value L obtained by Equations (8.7), (8.8), and (8.9) and the manufacturer data for ETD44 core, $q=0.85$.

and (8.9) and the manufacturer data for an ETD44 core (15 mm center leg) are shown in Fig. 8.11 ($q = 0.85$).

The advantage of the above approach is that it is quite easy and that it gives a rapid idea of the effect of fringing when using a center gap. The drawback is that it is only applicable for center-gapped inductors, whereas the extension to inductors having air gaps in the side legs is not easy.

Detailed general methods for calculating gapped inductors are presented in [4,5,6,7].

8.4.3 Improved Approximation for Fringing Permeances of Gapped Inductors

Here we discuss analytical approximations for fringing flux calculations around the air gaps of inductor cores.

8.4.3.1 Fringing Coefficients

It is clear that in a 2-D problem, the fringing permeance is proportional to the third dimension (the permeance Λ is $\Lambda = 1/\mathfrak{R}$, where \mathfrak{R} is the reluctance of a magnetic path). The fringing permeance leads mainly to a correction on the permeance of the air gap and it is of a small consequence to the remaining core permeance. The permeance of an air gap is:

$$\Lambda_g = \mu_0 \frac{A_g}{l_g} + \mu_0 \sum_{all\ sides} C_g F \tag{8.10}$$

where

- Λ_g is the permeance of the air gap
- S_g is the surface of the air gap
- C_g is a part of the total core circumference

l_g is the total length of air gap

F is the fringing coefficient corresponding to the given part of C_g (see the Appendix 8.A.1).

We provide analytical expressions for the fringing coefficient F for several basic cases of air gap designs and the proposed coefficients can be used to calculate most usual symmetrical and asymmetrical cases of gapped inductors. The values of the fringing coefficient F for the basic cases and for the symmetrical and asymmetrical cases are given in the Appendix 8.A.1 at the end of this Chapter. The appendix presents the derivation of the expressions and comparison with finite element calculations.

8.4.3.2 Equivalent Surface

A graphical interpretation can be used to incorporate the effect of fringing. The corner effects are not considered. The fringing coefficient F multiplied by l_g can be seen as a border to enlarge the original cross section with an area to obtain the real permeance:

$$\frac{1}{\mathfrak{R}_g} = \Lambda_g = \mu_o \frac{A'_g}{l_g} \quad (8.11)$$

where

A'_g is the enlarged air gap area corresponding to the fringing field

For a single air gap the total permeance of the magnetic circuit is:

$$\Lambda_g = \frac{1}{\frac{l_g}{\mu_o A'_g} + \frac{l_c}{\mu_r A_m}} \quad (8.12)$$

where A_m is the effective cross-sectional area of magnetic circuit.

In the presented solution, we only include the 2-D effects. In 3-D presentation we also have a contribution of corner permeances, which results in an increase of permeance. However, in 3-D presentation the field lines return closer to the gapped leg, resulting in only a small increase by corner contributions.

NOTE: Increasing the mathematical accuracy of the expressions has its limits, as the tolerances of the mechanical dimensions often influence the result significantly.

8.4.3.3 Single and Multiple Air Gap Cases

If more than one air gap is present, a reluctance network can be used to describe the permeance of the full magnetic circuit (or the reluctance $\mathfrak{R}_g = 1/\Lambda_g$).

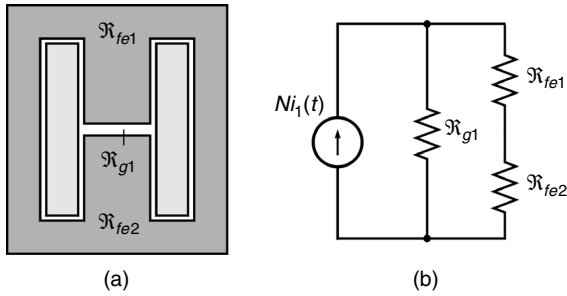


FIGURE 8.12

An EE-core set with a centre leg air gap, Example 1, N -turn number; i -current.

- (a) Flux path definition;
- (b) The reluctance network.

Example 1

The case with a center gap, where the yoke to yoke reluctances vanish, is shown in Fig. 8.12.

Example 2

For a multiple air gap in the center leg the magnetic circuit is represented by the reluctance network shown in Fig. 8.13.

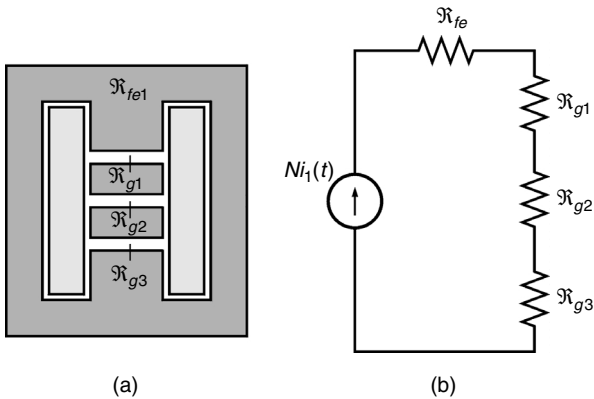


FIGURE 8.13

An EE-core set with a multiple air gap at the centre leg, Example 2.

- (a) Flux path definition;
- (b) The reluctance network.

Example 3

This example addresses the use of a spacer to increase the air gap. In that way air gaps are created in all legs (see Fig. 8.14).

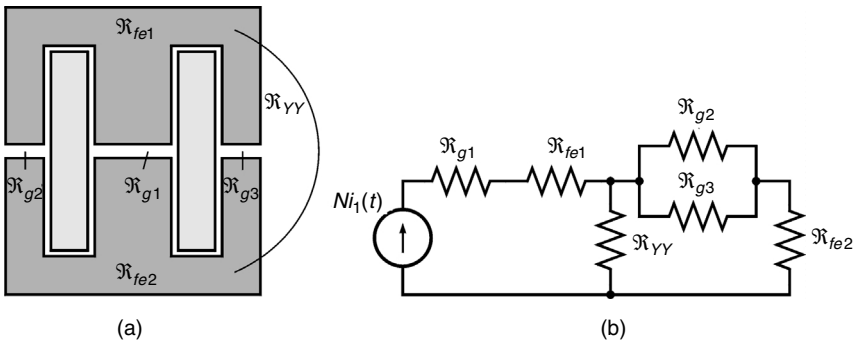


FIGURE 8.14
 A spacer gaped EE-core set, Example 3.
 (a) Flux path definition;
 (b) The reluctance network.

Example 4

A UU-core set. The MMF of both legs can be equal or different (even zero). It is clear that in the symmetrical case the top to bottom permeance does not influence the result (see Fig. 8.15).

REMARK

While using multiple air gaps, care should be taken with the heat transfer of the magnetic core pieces in the center leg. The air gap should be filled by preference with thermally conductive, but electrically isolating materials.

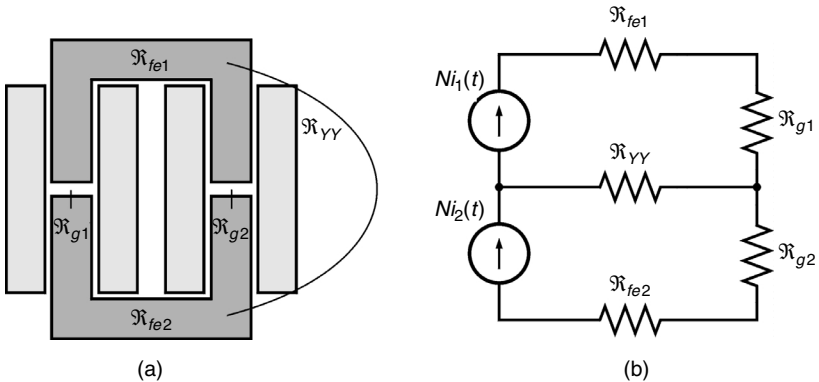


FIGURE 8.15
 A gapped UU-core set, Example 4.
 (a) Flux path definition;
 (b) The reluctance network.

8.5 Eddy Currents in Inductor Windings

8.5.1 Referring to Described Methods

The major part of the eddy current losses in inductors is caused by transverse field. For the center-gapped EI and EE inductors some methods are already given in the book.

In [Chapter 2](#) an approximated method is presented, which introduces a factor k_F to take into account the increased losses due to the air gap. In [Chapter 5](#) the method is refined as the losses caused by an H -field in the direction of the layer or perpendicular to it are sensitive to the field factors in the direction of the layers and perpendicular to it. The method includes the field factors k_{Fx} and k_{Fy} .

Inductors with spacers could have about two times less eddy current losses by fringing compared to center gapped ones. Indeed, the m.m.f. of the air gap is divided in two air gaps, each inducing two times less field, so resulting in two contributions of about one quarter. However, the field problem is a full 3-D one.

8.5.2 Multiple Air Gap Inductors

Up to now, while calculating k_F , the symmetry factor K value was equal to 1 for EI-cores, and 2 for EE-cores. But if N_g multiple air gaps are used, the field pattern can have symmetry with $K = 2N_g$ sections with the same field type. For such cases approximately the same type of calculation for k_F can be adopted using the new K value. The effect is that for the same distance to the center leg, the parameter κ increases a lot if K increases, thus the resulting eddy current losses are comparable to a transformer case winding with $k_F \approx 1$.

NOTE: Often three air gaps are used (cutting each leg one time with a diamond band saw) and this approach reduces the losses already a lot.

One possible problem while using multiple air gaps is that the ferrite pieces are not well cooled and can create a hot spot. In a ferrite core, too-high temperatures result in lower saturation levels and higher specific losses, which could lead to a thermal run-away. A good practice is to fill the 'air gaps' with thermally conductive insulating materials.

8.5.3 Avoiding Winding Close to the Air Gap

Different arrangements of windings in the window area of an inductor are shown in [Fig. 8.16](#)

- a fully filled winding area, case A
- a partly filled winding area, case B
- a partly filled winding area, sufficient distance to the air gap, case C

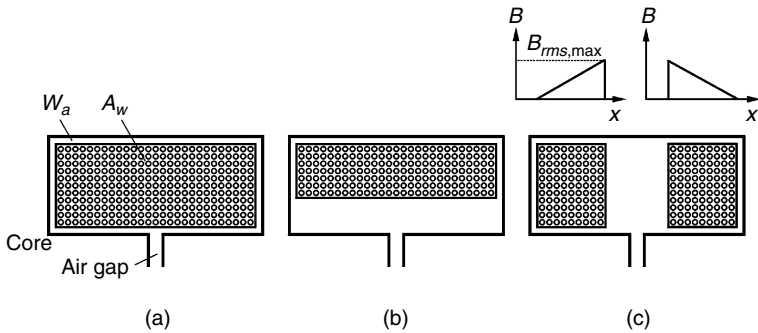


FIGURE 8.16

Different arrangements of windings in the window area of an inductor:

- (a) A fully filled winding area, case A;
- (b) A partly filled winding area, case B;
- (c) A partly filled winding area, sufficient distance to the air gap, case C.

The arrangements shown in Fig. 8.16b and Fig. 8.16c are intended to reduce the eddy current losses in the windings.

Figure 8.16b shows a solution, where some distance between the winding and the center leg is kept. This is described in [Chapter 2](#) and is reflected in the calculations through the use of a global field factor coefficient k_F . More details are given in [Chapter 5](#) regarding the use of the field factor coefficients k_{Fx} and k_{Fy} depending on the horizontal and the vertical direction. The eddy current losses are substantially reduced by this approach. The disadvantage is that the mean length of turn and the DC resistance are increased.

Figure 8.16c shows another solution to keep distance from the air gap. The advantage of this type is that the mean length of turn is equal to the value for a fully filled area. It also avoids a hot spot in the middle of the winding area.

8.6 Foil Wound Inductors

A high-frequency foil inductor with substantial AC current requires careful design to avoid high AC conduction losses. In the ideal case, when the field is parallel to the foil, a low level of high-frequency eddy current loss can be obtained.

In the general case, there are three different types of winding loss effects (mechanisms) that can be distinguished in gapped inductors with foil windings (see also [Chapter 5](#)):

1. Losses due to the homogeneous field parallel to the foil
2. Losses due to a non-homogeneous field parallel to the foil; this field usually has its origin in the fringing field at the air gap
3. Losses due to the field at the tips (edges) of the foil

The *low value* of the first type of losseffect is the attractive feature of foil windings. However, the second and the third effects are of real importance, and they can cause the main part of the winding losses at high frequencies.

8.6.1 Foil Inductor—Ideal Case

Figure 8.17 shows a foil inductor with a pot core. To be classified as an ideal case, the width of the foil must be equal to the width of the winding area. The tips of the foil touch the high permeability material over the whole circumference. The center leg is made from a low permeability material (or air), thus acting as a distributed air gap. This is the best solution for the air gap fringing problems. In this case the field lines are parallel to the conductors. The resultant AC resistance in the uniformly distributed gap design is low.

In the discussed ideal case, the theory of a rectangular conductor is perfectly applicable, as all fields are parallel to the foil surface. Shapes like EE and ETD can nearly meet the ideal case conditions when no coil-former is used (a negligible distance to the top and bottom of the magnetic core can be obtained), and the conductor edges are covered with ferrite plates. The low-permeability center leg can be simulated by using multiple air gaps.

NOTES:

1. If the center leg of planar cores is removed a kind of hollow box is obtained, where foil windings can be inserted while the conductor edges are covered with ferrite.
2. In general, to reduce the thickness of the insulation one can use enameled copper foil.

For the ideal case of Fig. 8.17 an analytical solution exists to determine the inductance of the inductor. For simplicity, a homogenous current density in the winding cross-sectional area and a constant thickness are assumed. In this case an exact analytical result can be obtained using symbolic integration of the integral of the stored energy divided by $\frac{1}{2}i^2$ the inductance is:

$$L = \mu_0 \frac{N^2}{w} \left(\mu_r A_1 + A_2 + \frac{1}{3} t_w \left(l_{\min} + \frac{l_{\max} - l_{\min}}{4} \right) \right) \quad (8.13)$$

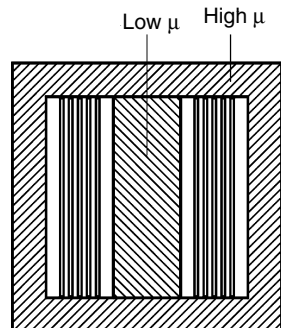


FIGURE 8.17

A foil inductor—ideal case.

where

L is the total inductance of the coil

μ_r is the relative permeability of the center leg

A_1 is the cross-sectional area of the center leg

A_2 is the area of the surface between the first winding and the center leg

l_{\min} is the perimeter length inside the first turn (the closest turn to the center leg)

l_{\max} is the perimeter length outside the last turn

The field problem of this particular shape is a unique one. The form of (8.13) was the simplest form we could obtain. It corresponds to an equivalent length of turn measured at $1/4^{\text{th}}$ of the thickness of the winding. Although the equation was derived for axis-symmetrical problems, it remains true for a variable curvature case (but also with constant current density and keeping t_w constant). The winding can be also a combination of straight and axis-symmetrical parts, such as for a rectangular mid-leg.

NOTE:

- The above-defined equivalent length is also applicable for eddy current type of losses.
- The equivalent length is different from the length we would have if we calculate the DC resistance, as then we have to consider the length at $1/2^{\text{th}}$ of the thickness.

8.6.2 Single and Multiple Air Gap Design in Foil Inductors

Materials with low permeability have some disadvantages, as they often have a lower saturation induction level or higher specific losses than high permeability materials (for example ferrites). Therefore, the use of a distributed air gap is often a good compromise. Discretely distributed air gap design is a solution to decrease the perpendicular field component near the foil edges. A single air gap inductor is shown in Fig. 8.18.

(NOTE: We don't consider the edge (tip) losses here, and, therefore, we take the ideal case when the foil winding touches top and bottom of the core.)

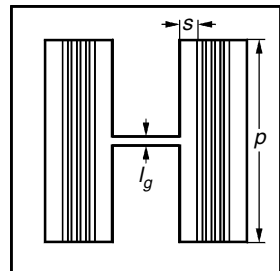


FIGURE 8.18

Single air gap in a foil wound inductor.

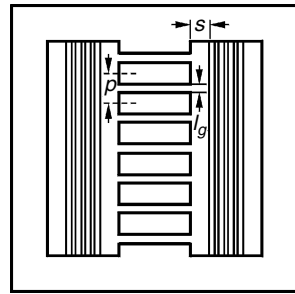


FIGURE 8.19
Discretely distributed air gap in a foil wound inductor.

Figure 8.19 shows a discretely distributed air gap inductor, where the air gap is in the center leg. The air gaps are placed near the foil, but the length of the air gaps is very small compared to the lumped air gap design. The investigations presented in [8] show that AC resistance of the layers that are near the air gaps is still quite high compared to that of the other layers. This is a result of the eddy currents induced by the fringing field of the air gaps. When the distance between the foil and the air gaps (denoted by s in Fig. 8.18) is decreased and the foil is subjected to the fringing field, the AC losses are increased significantly. The influence of the distance s and the other geometric parameters l_g and p on the eddy current losses of the foil are discussed in Chapter 5.

8.6.3 Eddy Current Losses in Foil Windings of Gapped Inductors

A more detailed view of the different air gap designs and the losses at high-frequency foil inductors are presented in Chapter 5 and in [8,9,10,11].

8.6.4 Planar Inductors

Planar configurations are often applicable for inductors because of packing constraints, thermal considerations, and improved production technology. Often the planar constructions use printed circuit board windings. Figure 8.20 shows an example of a planar inductor with an air gap. In some cases the design parameters are achievable without air gaps (or distributed gaps). Depending on the inductance value, low-permeability materials may be necessary.

A planar inductor configuration is likely to be subjected to high eddy current losses in windings. Gaps in the magnetic path tend to introduce a perpendicular field. To obtain acceptable eddy current losses, the conductors should be placed a sufficient distance from the air gaps. The best solution for the planar inductors is to use a *low-permeability material* to realize a distributed gap [12,13]. Such a construction is shown in Fig. 8.21. Another solution is to use *discretely distributed air gaps* as shown in Fig. 8.22. In that kind of construction the design and loss are similar to that of the foil inductors with discretely distributed air gaps presented in the previous section.

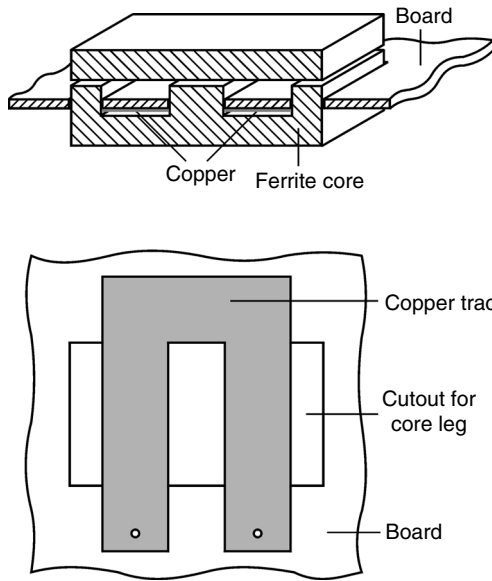


FIGURE 8.20
A planar inductor with an air gap.

One difference is the loss at the coil ends. The current density at the coil ends close to the center leg is higher than the outer edges; therefore, higher eddy current losses are expected (but the perpendicular field can be low, as the inner side is close to the high μ material, ferrite). The outer edges are also subjected to the same kind of losses, but the current density is lower because of the smaller radius. Accurate loss estimation in planar inductors requires 3-D FEM calculations.

In cases where printed circuit board windings are used, a higher number of turns can be obtained by several layers or more turns in one layer. An advanced design can even use different thicknesses for the different layers, in which the thicker layers are away from the air gap in order to reduce the eddy current losses.

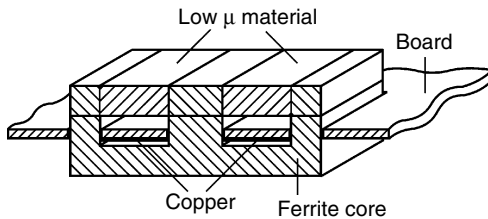


FIGURE 8.21
A planar inductor with a low permeability distributed gap.

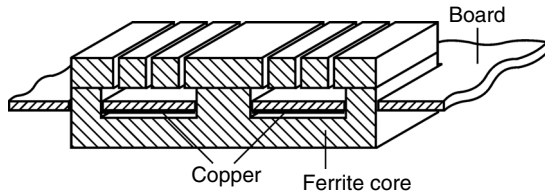


FIGURE 8.22
A planar inductor with discretely distributed air gaps.

Making windings parallel in planar inductors is not easy. It is worthwhile to mention that for inductor design, planar cores can be used in combination with round wires, Litz wires, or foil conductors. In many practical cases the final result is better when using these kinds of windings instead of using printed circuit board windings only.

8.7 Inductor Types Depending on Application

8.7.1 DC Inductors

True DC inductors do not exist. If one uses an inductor, there is always some AC component of the current, which requires higher AC impedance. Applications where the AC current components are small are typically EMI filters and continuous conduction mode inductors with low peak-to-peak AC currents.

Example

In an inductor the peak-to-peak AC current ripples are about 10% of the DC current value. For a triangular current waveform, we obtain a resulting RMS current value of about 3% of the DC current. And, if the eddy current factor is $k_c = 100$ (thick wires, several layers such as in short example of [chapter 2](#)) some additional copper losses of 10% can still occur in the component. In some cases the k_c value can even be several hundred. Thus, one should not be quick to say that an inductor is a true DC inductor.

Low frequencies such as 50, 60, 100, and 120 Hz can often be considered as almost DC for eddy currents and for ferrite materials. These frequencies are typical for low-frequency components in grid-connected applications.

DC inductors are usually wound using full wires and are nearly filled. The approach has the advantage of obtaining a high filling factor and, thus, low losses due to the DC resistance.

For cores in DC inductors, it is beneficial to use materials with a high saturation induction, such as low-frequency ferrite grades or iron powder. The advantage of iron-powder materials is that they combine a low permeability

(distributed air gap) and a high saturation. The iron-powder cores are proposed in several types:

- Soft-iron type, saturation up to 1.4 T.
- Iron with Silicon alloy (Sendust, Kool-mu), saturation of about 1.1 T.
- Fe-Ni types (Permalloy), saturation of about 0.8 T.
- Nanocrystalline powder iron (expensive).

The soft-iron type has the advantage of high saturation. However, care should be taken if a large low-frequency component is also present, such as inverter output filters at low frequency losses. At 60 Hz AC, 1 T, the losses may be 40–100 mW/cm³, depending on the material grade. This is about 5 to 13 W/kg, which is much higher than the losses of good transformer iron. The reason is that hysteresis losses increase when the size of the domain walls decreases. The other powder grades have reduced losses, but also have reduced saturation induction. Powder materials are preferable in the MHz areas, as they have smooth characteristics and do not exhibit capacitive resonant frequencies that reduce the permeability.

At intermediate frequencies it may be useful to have iron losses in EMC filter inductors so that the amplitude of parasitic resonances can be reduced. With intermediate frequencies, we mean frequencies lower than the switching frequencies but higher than the DC or low frequency component. Those resonances increase the EMI spectrum, but they are also a risk for instabilities in the control of converters.

8.7.2 HF Inductors

An HF (high-frequency) inductor is a typical component in resonance converters. We also denote AC inductors as high frequency inductors, where the eddy current losses in the wires are not negligible. This is usually the case in the frequencies actually used in power electronics.

REMARKS CONCERNING HF INDUCTORS

- The full-wire design is usually not the preferred choice for HF inductors.
- At least some distance to the air gap should be taken.
- The preferred design is parallel wires (but avoiding circulating currents) or Litz wire.
- Usually the winding area is not filled completely, as it would generate too much eddy current loss.

As a number of turns per layer is used, one has to choose a small wire diameter to reduce the eddy current losses, which automatically results in a design where the low-frequency approximation is valid. The latter can

simplify the design because simplified equations can be used. Also, the modeling is easier since the eddy current losses can be modeled as a resistor in parallel with the inductor.

The drawbacks of *Litz wire designs* are the low filling factor and poor thermal conductivity due to the presence of more insulation material. Also, the Litz wire is more fragile in the winding process and harder to solder. At a high current and for a limited number of turns one can also consider using *foil windings*, taking care of tip and fringing losses.

The current and voltage of the HF inductors are both alternating, and there is no DC component of the current. The main difference between the HF inductors and the filter inductors is that the loop $B(t) = F(H(t))$ of the HF inductors is high, i.e., under large excitation, but the of the DC (filter) inductors is a so-called minor loop. The core losses in HF inductors are large and should be considered for the total component dissipation. The copper losses are also high due to the high AC resistance in that kind of inductors. The design of an HF inductor is a typical, non-saturated, thermally limited design (see [Chapter 2](#)).

8.7.3 Combined DC-HF Inductor

In the combined DC-HF inductors the losses of the HF component are usually not negligible compared to the DC or LF losses. This type of inductor is very normal in power factor controllers, buck and boost converters. It concerns continuous-mode operation with high ripples, border-mode, or discontinuous operation.

8.7.3.1 Classical Solutions

The DC or low-frequency component in the current would benefit from full wires, but then the eddy current losses are the bottleneck of the design. Using Litz wire is possible, but it results in a larger DC resistance due to the lower filling factor. One can also use one winding close to the air gap to “screen” the frequency magnetic field, where the remaining winding area is used to put a parallel winding, which carries almost only DC current. In [14], arrangements are proposed where a foil winding or a single layer round wire winding is used as an “HF screen” with multiple or distributed air gap.

8.7.3.2 Special, Combined Design: Litz Wire–Full Wire Inductor Winding

Here we propose a Litz wire winding to screen the HF magnetic field, while using a single air gap design. The special, combined design: Litz wire–full wire solution is proposed in details in the appendix 8.A.2 of this chapter. We screen the HF m.m.f of the air gap using Litz wire; the remaining part of the winding area is filled with full wire. This type of solution combines the benefits of Litz wire and full wire. Moreover, if a special arrangement can be achieved, only the HF losses in the Litz wire have to be calculated. The special arrangement is given in [Fig. 8.23](#); it was first proposed in [15].

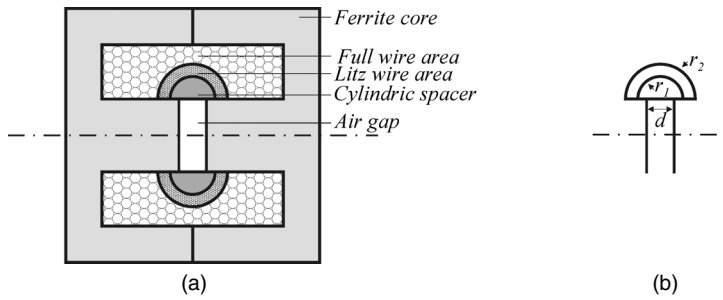


FIGURE 8.23
 Cross section of the combined Litz wire-Full wire inductor.
 (a) full cross section;
 (b) details of the air gap.

The design asks that almost all the HF m.m.f. would be cancelled by the Litz winding. Thus, almost all of the HF current would flow in the Litz wire. The average flux per turn in the Litz winding is somewhat lower than in the full wire. This leads to a number of turns in the Litz wire that is slightly higher than in the full wire. In practice, there is always some local leakage flux that also causes some voltage drop, so the number of turns of the Litz wire can be almost equal to the number of turns in the full wire.

A practical solution is to do a test while feeding the Litz wire with an HF voltage and measure the difference in voltage between the windings. This voltage should be low; if not, one can adapt one turn.

8.7.3.3 Analytical Modeling of the Combined Full-Wire-Litz-Wire Inductor

In the appendix 8.A.2 an analytical model is proposed. It permits one to predict the losses and the required number of turns of both the Litz wire and the full wire winding.

$$P_{cu,eddy,Litz}(t) = \frac{\pi l_w d_s^4 p}{64 \rho_c} \left(\frac{\mu_0 \varepsilon f N_L I}{2\pi r_1} \right)^2 \frac{1}{3} k_L \left(\frac{r_2}{r_1} \right) \quad (8.14)$$

where

- p is the number of strands
- d_s is the diameter of the strands

The experiments show that, although the DC resistance of the Litz wire winding is much higher than the DC resistance of the full wire, much lower losses are obtained by the combination of both types of wires.

Figure 8.24 shows the coil former before and after winding with Litz wire.

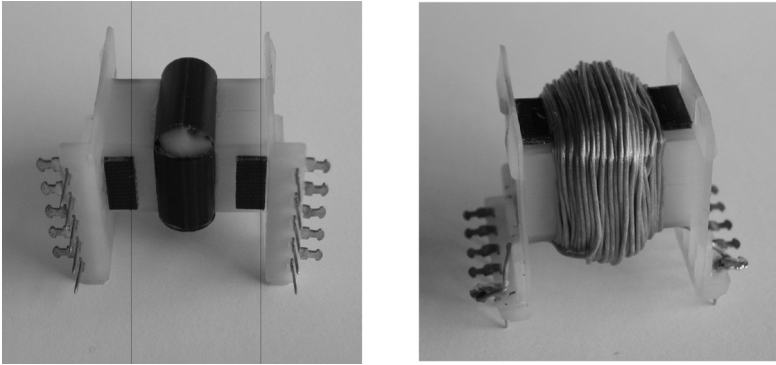


FIGURE 8.24

Coil former of the combined inductor before and after winding with Litz wire.

8.8 Design Examples of Different Types of Inductors

8.8.1 Boost Converter Inductor Design

An inductor (a DC choke) is usually employed in DC/DC converters. Such a boost converter is shown in Fig. 8.25, and the inductor current and voltage are shown in Fig. 8.26. The purpose of the inductor in this topology is to reduce the current ripple and to realize the voltage increase from its input value to the required output value. This purpose defines a desired value of the inductance L . An air gap is used in order to prevent saturation of the core by the peak inductor current $I_{L,peak} = I_{L,DC} + \Delta I_{peak}$. The core losses are smaller than the copper losses. Therefore, such a design can be defined as a *Saturated, Thermally Limited Design* according to the classification given in Chapter 2, Fig. 2.1.

The basic constraints of the design are:

- to obtain a given inductance value L
- to keep the induction peak value B_p below the saturation value B_{sat}
- to keep the temperature limited

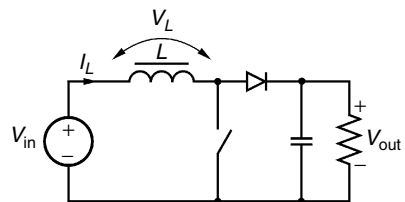


FIGURE 8.25

A boost DC/DC converter.

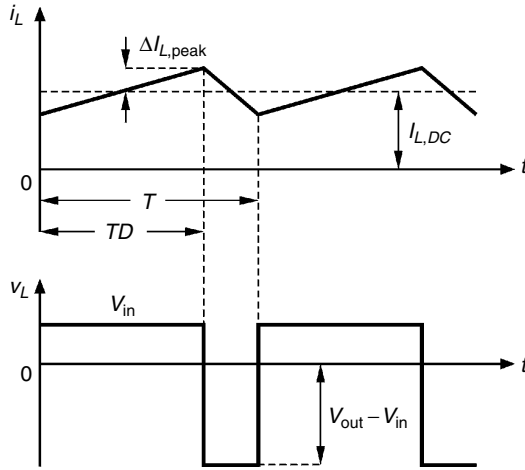


FIGURE 8.26
Inductor current and voltage waveforms.

Here we calculate the design parameters of an inductor. We need a desired induction value and the RMS values of the voltage and current of the inductor. The specifications of the example converter are

- Input voltage: $V_{in} = 100 \text{ V}$
 Output voltage: $V_{out} = 400 \text{ V}$
 Operating frequency: $f_{op} = 20 \text{ kHz}$
 Output power: $P_{out} = 1 \text{ kW}$

The peak magnitude of the ripple in the inductor current is envisaged to be equal to 20% of the inductor DC component.

The duty ratio D of the switch control is:

$$\frac{V_{out}}{V_{in}} = \frac{1}{1-D} \Rightarrow D = \frac{V_{out} - V_{in}}{V_{out}} = 0.75 \quad (8.15)$$

The inductor DC current component is:

$$I_{L,DC} = \frac{I_{out}}{1-D} = \frac{P_{out}/U_{out}}{1-D} = 10 \text{ A} \quad (8.16)$$

The peak magnitude of the ripples in the inductor current $\Delta I_{L,peak}$ is:

$$\Delta I_{L,peak} = \frac{V_{in} D T_{op}}{2L} \quad (8.17)$$

where T_{op} is the operating period, $T_{op} = 1/f_{op}$.

Since we want $\Delta I_{L,peak}$ to be equal to 20% of $I_{L,DC}$, we can find the desired inductance value:

$$L = \frac{V_{in} DT_{op}}{2 \Delta I_{L,peak}}, \quad \Delta I_{L,peak} = 0.2 I_{L,DC} \Rightarrow L = \frac{V_{in} DT_{op}}{0.4 I_{L,DC}} \Rightarrow L = 937 \mu H \quad (8.18)$$

The RMS value of the inductor current is:

$$I_{L,rms} = \sqrt{I_{L,DC}^2 + (\Delta I_{L,peak})^2 / 3} = 10.07 A \quad (8.19)$$

The RMS value of the inductor voltage is:

$$V_{L,rms} = \sqrt{D V_{in}^2 + (1-D)(V_{out} - V_{in})^2} = 173.2 V \quad (8.29)$$

Now we have all the input parameters of the inductor under design:

Wanted inductance value: $L = 937.5 \mu H$
 RMS inductor current: $I_{L,rms} = 10.07 A$
 RMS inductor voltage: $V_{L,rms} = 173.2 V$
 Operating frequency: $f_{op} = 20 \text{ kHz}$

To continue the design, one can follow the design procedure presented in [Chapter 2](#).

If the case is a low-frequency design ($d < 1.6\delta$), the eddy current losses in the winding can be calculated using the apparent frequency:

$$f_{ap} = \frac{V_{L,rms}}{2 \pi L} = \frac{173.2}{2 \pi \times 937.5 \times 10^{-6}} = 29.4 \text{ kHz} \quad (8.21)$$

If the low frequency condition ($d < 1.6\delta$) is not fulfilled, the calculated apparent frequency is a worst-case frequency value.

8.8.2 Coupled Inductor Design

A coupled inductor is a filter inductor having multiple windings. The inductor is designed to have a high inductance for common mode currents and a negligible inductance for differential currents. Possible applications are a coupled inductor in a two-output forward converter, or common mode chokes. Figure 8.27 gives an example of a common mode choke, which is,

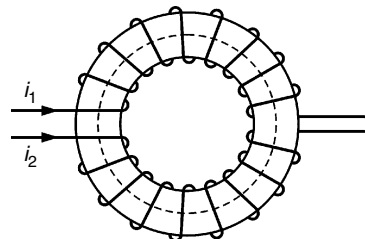


FIGURE 8.27

A common mode choke as a coupled inductor example.

in fact, a coupled inductor. The inductors are wound on the same core. There is a significant DC-current (or low-frequency) component in both windings. The size of the B - H loop is small, as the inductor current ripples are small compared to the DC-current component.

We split the field patterns into two types:

- Magnetizing field induced by the sum of the currents in both windings $i_1 + i_2$
- Leakage field induced by the difference between the currents in both windings $i_1 - i_2$

The magnetizing field flows along a high-permeance path (using the core). The leakage field encounters a low-permeance path (through air). It is useful to split the currents in two components:

- a common mode component, i_{com}
- a differential mode component, i_{dif}

The two current components are:

$$i_{com} = \frac{i_1 + i_2}{2} \quad \text{and} \quad i_{dif} = \frac{i_1 - i_2}{2} \quad (8.22)$$

$$L_{com} = N_1^2 \Lambda_m = N_2^2 \Lambda_m \quad (8.23)$$

$$L_{dif} = N_1^2 \Lambda_\sigma = N_2^2 \Lambda_\sigma \quad (8.24)$$

Here the magnetizing permeance Λ_m is a value given by the manufacturer (A_L value).

In respect to I_{com} , the magnetic device behaves as an inductor with two parallel windings. We follow the loss calculation given in [Chapter 2](#). The winding width w is equal to the inner circumference of the core. The saturation value for I_{com} is very low, as a suitable flux path is provided.

In respect to I_{dif} , the magnetic device behaves as a transformer. The primary and the secondary windings are far from each other. The design of the transformer part is not easy, as the field pattern is a real 3-D type. The saturation value for I_{dif} is not very high, as the leakage permeance is not very low. Thus, it is advisable to check this value. The practical leakage permeance for ring cores is almost proportional to the inner diameter d_{int} . The proportionality factor A is almost independent from the material and somewhat dependent on how the core is actually wound. The leakage permeance is approximated as

$$\Lambda_\sigma = A d_{int} \text{ } [\mu\text{H}] \quad (8.25)$$

where

A is typically $2.3 \mu\text{H/m}$;
the inner diameter d_{int} is in [m].

The eddy current losses of the two components (the common-mode component i_{com} , and the differential-mode component i_{diff}) can be added. The summation of losses is usually allowed, as the common-mode and differential-mode currents contain different frequencies. Without splitting into common mode and differential mode, the design would be difficult.

Example

A ferrite ring core has the following dimensions (coating included):

1. Internal diameter: 18.4 mm
2. External diameter: 32.7 mm
3. Height: 13.3 mm

Both windings have 20 turns. The common mode or magnetizing permeance Λ_m is found as $2.0 \mu\text{H}/\text{turn}^2$. The differential mode permeance is about $2.3 \mu\text{H} \times 0.019 \text{ m} = 44 \text{ nH}/\text{turn}^2$. The common-mode inductance is calculated as:

$$L_{com} = 20^2 \cdot 2.0 \mu\text{H} = 800 \mu\text{H}$$

The differential-mode inductance is found:

$$L_{diff} = 20^2 \cdot 44 \text{ nH} = 17.6 \mu\text{H}$$

By comparison, the measured values on the built inductor are: $L_{com} = 874 \mu\text{H}$ and $L_{diff} = 17.4 \mu\text{H}$. The measurements are made by putting the windings in series and anti-series and dividing the result by four.

8.8.3 Flyback Transformer Design

A flyback transformer operates as an inductor with two windings; therefore, we discuss it in this chapter. It could also be denoted as a coupled inductor in which the current waveforms are well known. The first winding carries current while the switch S conducts, and the second winding carries current while the diode D conducts (see Fig. 8.28: A flyback converter). Although the device has two interacting windings and is depicted by the same symbol as a transformer, a more descriptive name of that magnetic component is a *two-winding inductor*. The major difference between a transformer and a flyback transformer is that the currents in a flyback transformer do not flow simultaneously in both windings as in a usual transformer. The purpose of the flyback transformer is to store energy during the conduction interval of the switch and to inject it to the output during the conduction interval of the diode.

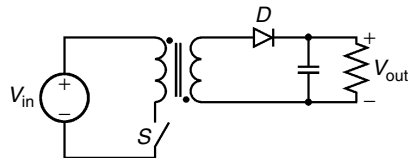


FIGURE 8.28
A flyback converter.

The B - H loop depends on the current mode of the converter. In DCM (Discontinuous Current Mode) the loop is larger than in CCM (Continuous Current Mode) and the core losses are higher. In a flyback transformer two types of fields are present simultaneously:

- The magnetizing field with energy storage action such as in an inductor
- The leakage field that performs a transformer action

However, it is not obvious that the losses could be separated in magnetizing and leakage type. Let us assume that the total field across the winding is a sum of the magnetizing field $B_m(t)$ and the leakage field $B_l(t)$:

$$B(t) = B_m(t) + B_l(t) \quad (8.26)$$

The eddy current losses are mainly determined by the square of the transverse field $B(t)$. Then, we can write:

$$P_{eddy} \sim B_m^2(t) + B_l^2(t) + B_m(t)B_l(t) \quad (8.27)$$

To be able to separate losses, the mixed product (the third term in Equation (8.27)) should be zero in average. A way to obtain this is to distribute the magnetizing m.m.f. between primary and secondary windings in such a way that the mixed product vanishes when averaged over time. Figure 8.29 shows a decomposition of the fields of the primary and secondary windings, which allows considering both types of fields in the device, the inductor and the transformer types. This approach allows presenting the eddy current losses more clearly and precisely.

The following relations are considered for Fig. 8.29:

$$\begin{aligned} F_1 &= N_1 i_1 \\ F_2 &= N_2 i_2 \\ F_1 &= F_{m1} + F_{l1} \\ F_2 &= F_{m2} + F_{l2} \\ F_m &= N_1 i_1 + N_2 i_2 \\ F_{l1} &= -F_{l2} \\ F_{m1} &= F_{m2} = \frac{F_m}{2} \end{aligned} \quad (8.28)$$

where

F_1, F_2 are the m.m.f. of the primary and secondary windings, respectively
 F_{m1}, F_{m2} are the magnetizing field components of the primary and secondary windings

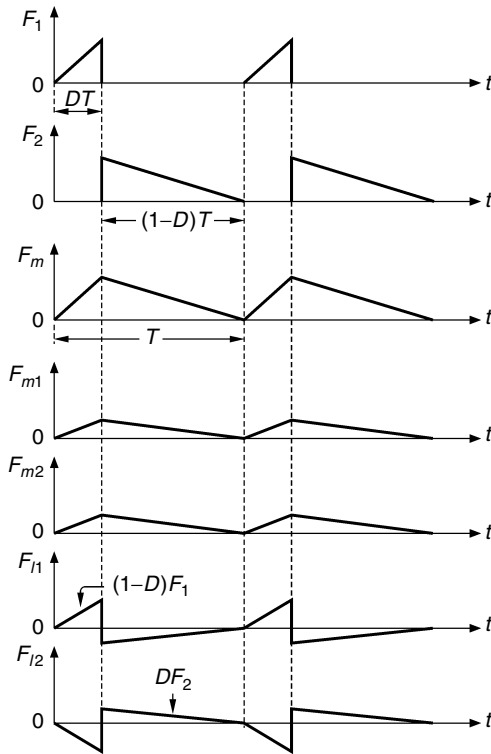


FIGURE 8.29

Decomposition of the currents of the primary and secondary windings in a flyback transformer.

F_{11}, F_{12} are the leakage field components of the primary and secondary windings

F_m is the total magnetizing field in the component

The choice of $F_{m1}, F_{m2}, F_{11}, F_{12}$ is made in such way that the mixed product of F_{m1} and F_{11} does vanish when averaged over one period and also for F_{m2} and F_{12} . This allows the superposition of the magnetizing type current losses and the leakage type current losses without considering the mixed products.

Considering the magnetizing fields F_{m1} and F_{m2} , we analyze the inductor type of field in the device. This allows presenting and calculating the eddy current losses associated with fringing fields near the air gap for each of the windings. While considering the leakage fields F_{11} and F_{12} , the transformer type of field is analyzed, and we obtain the corresponding losses.

REMARK

- In a single-center-gap design, it is better to put the thinnest winding (or Litz wire) close to the air gap and the thickest winding (or foil

conductor winding) at a sufficient distance from the air gap. By this arrangement, the eddy current losses due to the fringing field are reduced.

Now we can calculate the losses separately for the magnetizing field and leakage field and sum them. For the magnetizing field, the calculation can be done by the solutions given for an inductor. For the leakage field, the field pattern is the same as in a transformer.

There are two reasons why flyback converters are not preferred for high power applications:

- The leakage inductance between primary and secondary windings causes switching-off losses in the transistor. It is difficult to reduce this leakage inductance, as an insulation voltage is often required between primary and secondary, and, also, a low capacitance between primary and secondary is preferred. These constraints increase the distance between the primary and secondary windings and thus increases the leakage inductance.
- The magnetic design of the component leads to a compromise, as both field patterns are present in a single component, and, thus, they make the design more difficult.

8.A.1 Fringing Coefficients For Gapped-Wire-Wound Inductors

Here we propose calculations of fringing coefficients along the sides of an air gap. The accuracy of the mathematical approximations of the inductance, obtained using the proposed equations, is usually better than 3% for a wide variety of parameters. The approximations are derived with a fully filled window. The real accuracy using practical windings is slightly lower, as the winding area is not fully filled but sufficient for the usual designs. Windings at some distance to the air gap show higher fringing; windings at a shorter distance to the air gap show a lower fringing. We compare the solutions with experiments and an overall good matching is obtained. Influences are parasitic air gaps when the gap is set to zero, mechanical tolerances, and differences between data of different manufacturers for the same air gaps.

8.A.1.1 Basic Cases

8.A.1.1.1 Basic Case 1

In the basic case 1 the conductors are surrounded by magnetic material except at the air gap (see [Fig. 8A.1](#)). The current density in the conductor

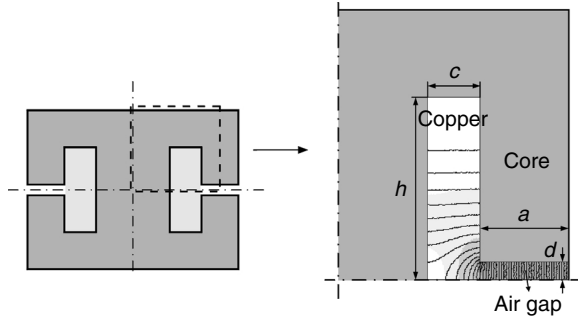


FIGURE 8A.1
Magnetic field in the basic case 1 (conductors surrounded by a core).

area (copper) is assumed to be homogenous. The permeability of magnetic material is assumed to be infinite. Then, the coefficient F_1 is given by the following approximation:

$$F_1(d, c, h) = \frac{2}{\pi} \ln \left(\left(\frac{1}{c} \right) + \left(\frac{1}{d} \right) \right) + \frac{(h-d)^2(h-0.26d-0.5c)}{3ch^2} + \frac{c}{3h} \quad (8A.1)$$

where

F_1 [] is the fringing coefficient for the basic case 1

d [m] is the air gap distance to the reference plane

c [m] is the thickness of winding

h [m] is the width of the winding, see Fig. 8A.1

NOTE: The appendix is derived on an independent basis, the definitions of the dimensions (c , h , d) are different with respect to the definitions used in the other chapters.

Equation (8A.1) corresponds to analytical solutions when c is small or when $d = h$, and also for a small d . The tuning constants (0.26 and 0.5) are fitted using the software *Finite Element Method Magnetics (FEMM3.1)* [3]. For small d , Equation (8A.1) is symmetrical with respect to c and h .

The fringing coefficient F_1 is shown in Fig. 8A.2 as a function of the ratio d/h , and c is a parameter ($c/h = 0.5, 1, 2$).

8.A.1.1.2 Basic Case 2

In the basic case 2 the winding touches the core, but all other sides of the winding are surrounded by air (see Fig. 8A.3). In this case the fringing field

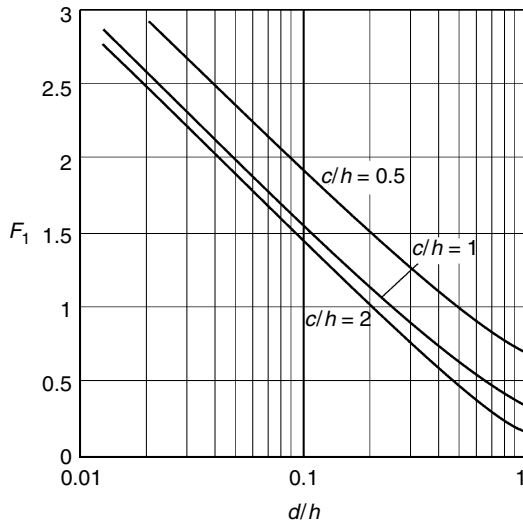


FIGURE 8A.2
Fringing coefficient F_1 as a function of the ratio d/h , c is a parameter ($c/h = 0.5, 1, 2$).

is also mainly concentrated near the air gap. The fringing coefficient F_2 is approximated as:

$$F_2(d, c, h) = \frac{2}{\pi} \ln \left(\sqrt{\frac{0.44(h^2 + c^2) - 0.218dh + 0.67cd + 0.33hc + 0.7825d^2}{d^2}} \right) \quad (8A.2)$$

For a small d , Equation (8A.2) is symmetrical with respect to c and h .

Note that cases 1 and 2 are similar when c is equal to h . This is normal since in case 2 almost no field lines are present outside the conductor area when $c = h$, so the presence of ferrite walls does not influence the result too

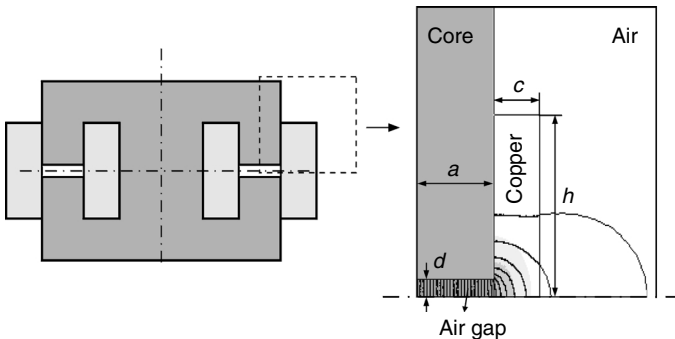


FIGURE 8A.3
Magnetic field in the basic case 2 (conductors in open area).

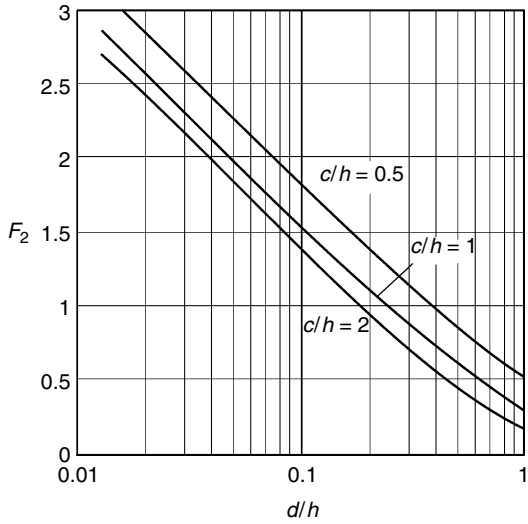


FIGURE 8A.4
Fringing coefficient F_2 as a function of the ratio d/h , c is a parameter ($c/h = 0.5, 1, 2$).

much. The correspondence between the analytical approximations and the finite elements solutions is within 2% for both cases.

The fringing coefficient F_2 is shown in Fig. 8A.4 as a function of the ratio d/h , and c is a parameter ($c/h = 0.5, 1, 2$).

8.A.1.1.3 Basic Case 3

The basic case 3 represents a new problem as no conductors are present (see Fig. 8A.5), and the m.m.f. (magnetomotive force) can be put in the air gap. This is the case of the outside legs without windings (for instance cores EE, ETD, ER cores). The total height is now larger than the winding height so

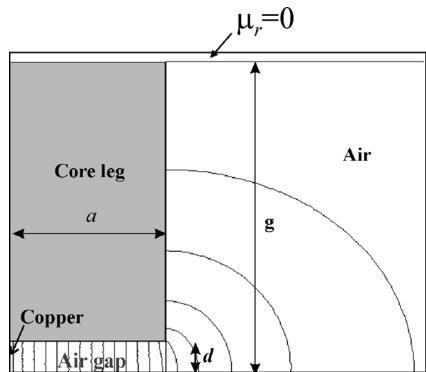


FIGURE 8A.5
Magnetic field in the basic case 3, typically outer legs.

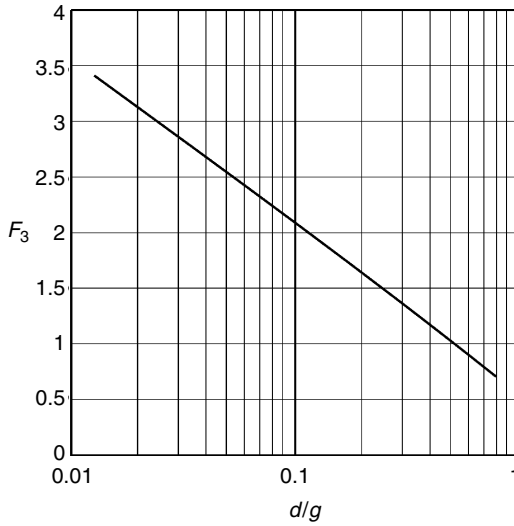


FIGURE 8A.6
Fringing coefficient F_3 as a function of the ratio d/g .

we use g , instead of h . The fringing coefficient is approximated as:

$$F_3(d, g) = \frac{1}{\pi} a \cosh \left[3.4 \left(\frac{g}{d} \right)^2 + 1.3 \right] \quad (8A.3)$$

The fringing coefficient F_3 is shown in Fig. 8A.6 as a function of the ratio d/g .

8.A.1.1.4 Basic Case 4

The basic case 4 represents a top to bottom problem, where there are no conductors (see Fig. 8A.7). This field pattern occurs when the m.m.f of yoke-yoke is not zero. It cannot be separated from the case 3. Case 3 and case 4, together, present the full problem. Although it is theoretically not obvious, in practice the field problems of case 3 and case 4 are de-coupled for normal values of d ($d < 0.8 g$). The fringing coefficient F_4 is given as:

$$F_4(a, g) = \frac{1}{\pi} a \cosh \left[1.4 \left(\frac{a}{g} \right)^{0.38} + 1 \right] \quad (8A.4)$$

From Equation (8A.4) it is seen that, when a is small, the value of F_4 decreases and almost vanishes.

The contribution of F_4 to the total permeance is usually low, except for cases such as planar EE or EI ferrites with a spacer.

For real cases (3-D), a good choice for a is a half of the core thickness. Together with the circumference, this will somewhat over-estimate the top

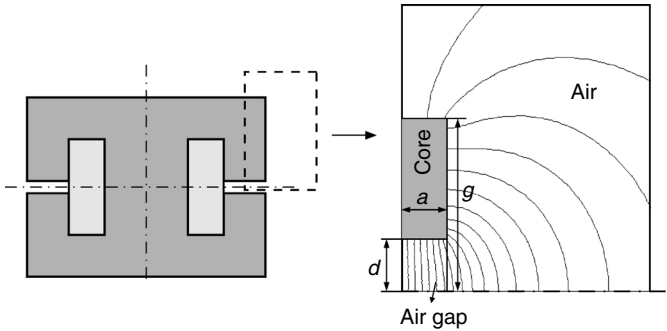


FIGURE 8A.7
Magnetic field in the combination of basic case 3 and case 4.

or bottom surface, thus compensating for the lack of corner contributions. Note that the exact value of a does not have a high influence on the result.

The basic case 4 can also be used in combination with the basic case 2 if the outer legs are wound and if the m.m.f between yokes is non-zero. This appears in the case of spacer-gapped UU cores if only one leg is wound.

The fringing coefficient F_4 is shown in Fig. 8A.8 as a function of the ratio a/g . The correspondence with finite elements is within 4%.

8.A.1.2 Symmetrical Cases

In general, all symmetrical cases can be split into two asymmetrical cases where the line of symmetry is replaced by $\mu = \infty$.

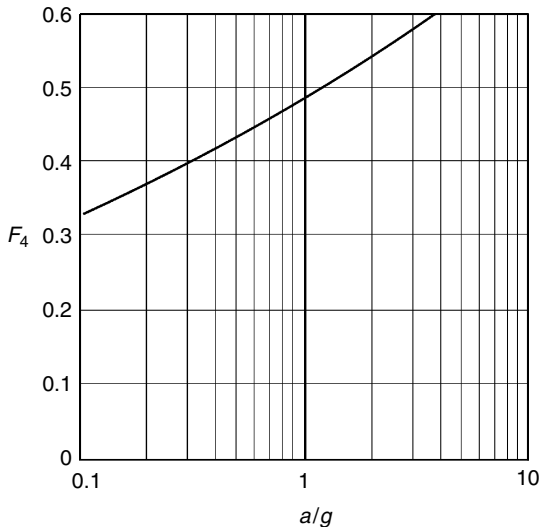


FIGURE 8A.8
Fringing coefficient F_4 as a function of the ratio a/g .

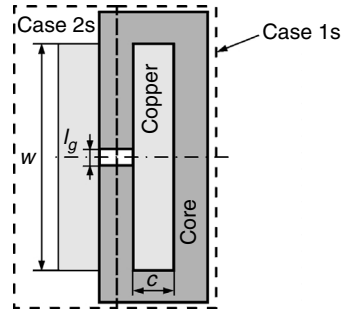


FIGURE 8A.9
 Cross section of the core presenting case 1s
 and case 2s.

8.A.1.2.1 Case 1s

In the symmetrical case 1 of a wound center leg with an air gap in the middle, each side has a field pattern identical to basic case 1. In this case $d = l_g/2$. Thus, the permeance of the air gap should be divided by two, and the corresponding fringing coefficient F_{1s} is:

$$F_{1s}(l_g, c, w) = \frac{F_1(l_g/2, c, w/2)}{2} \quad (8A.5)$$

(See Fig. 8A.9 for the definitions of c and w .)

8.A.1.2.2 Case 2s

The symmetrical case 2 represents two times the basic case 2. The corresponding fringing coefficient F_{2s} is:

$$F_{2s}(l_g, c, w) = \frac{F_2(l_g/2, c, w/2)}{2} \quad (8A.6)$$

Fig. 8A.9 shows a cross section of the core for case 1s and case 2s. For simulation we use axial symmetry with respect to the center of the core.

8.A.1.2.3 Case 3s

In this case the height of the magnetic part is g . This external height g is somewhat higher than the internal height h (or the winding width w). The case is close to the basic case 3. The fringing coefficient F_{3s} is:

$$F_{3s}(l_g, g) = \frac{F_3(l_g/2, g/2)}{2} \quad (8A.7)$$

8.A.1.2.4 Case 4s

This is the case where a top-to-bottom magnetic field part is present. Figure 8A.10 shows a cross section of the core for the symmetrical case 3s and case 4s:

$$F_{4s}(a_t, g) = \frac{F_4(a_t/2, g)}{2} \quad (8A.8)$$

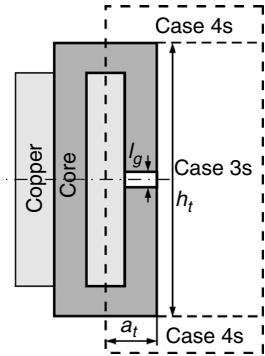


FIGURE 8A.10
 Cross section of the core presenting case 3s and case 4s.

8.A.1.3 Application to Gapped Rectangular Cores

The basic and symmetrical cases can be combined in all design constructions to obtain the inductance (center-gapped cores, spacer-gapped cores, UU cores and so on).

We give an example for a center gapped EE-core. In the window itself, usually case 1 type of field is observed. At the coil ends, perpendicular to the plane, case 2 type is present, see Fig. 8A.11. The permeance contribution in corner volumes still has to be added; however, it is small. Taking in account the above-stated remarks, the total permeance for a rectangular-gapped center-leg case is:

$$\Lambda_{\text{centre}} = \frac{1}{2} \mu_0 [2F_1 q + 2p_c F_2 + A_c] \quad (8A.9)$$

A_c : center leg cross section

8.A.1.4 Application to Center Gapped Rectangular Cores

In Fig. 8A.12 we show the fringing coefficients F_1 , F_2 and F_3 for a spacer gapped rectangular core.

The series connection of the permeances by the spacers can also be calculated:

$$A_{\text{spacer}} = \frac{1}{2} \mu_0 \left(\frac{1}{\frac{1}{2F_1 q + 2p_c F_2 + A_c} + \frac{1}{2F_1 q + 2F_3 q + 4F_3 p_s + 2A_s}} \right)$$

A_s : side leg cross section

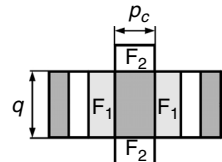


FIGURE 8A.11
 The fringing coefficients F_1 and F_2 at the cross section of a gapped rectangular centre leg.

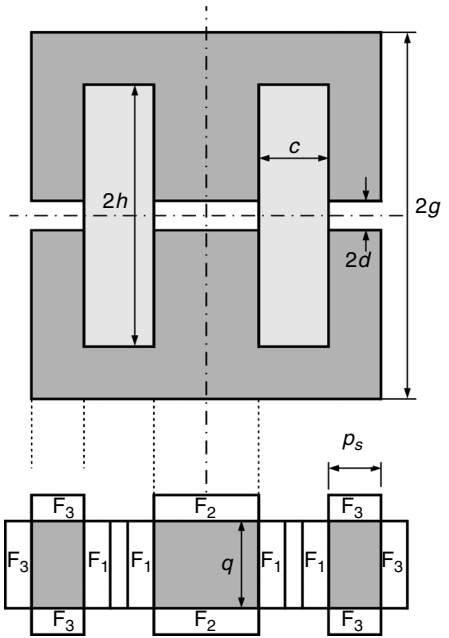


FIGURE 8A.12

The fringing coefficients F_1 , F_2 and F_3 at a spacer gapped rectangular legs inductor.

8.A.1.5 Application to Center Gapped Round Cores

In center gapped round leg cores (ETD, PM, RM) a mix of case 1 and case 2 are present; however, it is not evident where each field type stops. Close to the air gap, the field of case 1 and case 2 are not different. The main difference is present when the ratio h/c is small. A good choice is to determine an angle at an equivalent radius of $c/4$, see Fig. 8A.13. Thus, we take a contribution of case 1 or case 2 proportionally to the arc covered by the ferrite at the radius $r = r_1 + c/4$:

$$\alpha_1 = a \sin\left(\frac{q/2}{r_1 + c/4}\right) \quad (8A.10)$$

$$\alpha_2 = \frac{\pi}{2} - \alpha_1 \quad (8A.11)$$

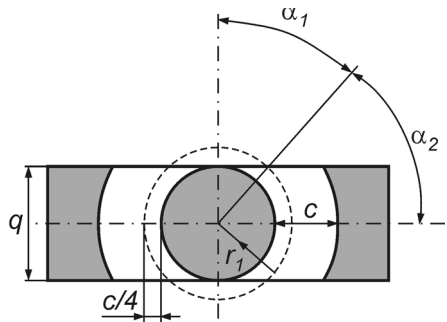


FIGURE 8A.13

Geometry of a center gapped round leg.

where

q is the thickness of the core.

For a symmetrical case, the total permeance of the center leg is given as:

$$\Lambda_{\text{round},s} = \mu_0 \left[\left(\frac{\alpha_1 F_{1s} + \alpha_2 F_{2s}}{\pi/2} \right) 2\pi r_1 \right] \quad (8A.12)$$

In principle, the method slightly underestimates the fringing, as there is more return surface available in the fringing flux path in 3-D as compared to a 2-D case.

8.A.2 Analytical Modeling of Combined Litz-Wire–Full-Wire Inductors

Here we discuss mainly the eddy current losses in the Litz-wire winding in the proposed combined Litz-wire–full-wire inductors. The solution is based on 2-D simulations, combined with the correct mean length of turn. The Litz-wire area is limited by distances to the air gap; i.e., the inner and outer radii. For high frequency, we assume that only the Litz wire carries current, so almost no field is present for a radius greater than the outer radius of the Litz-wire winding. By these assumptions, the field lines through the Litz-wire area are also almost circles.

The H-field depends on the enclosed m.m.f., and it is inversely proportional to the distance to the air gap:

$$H = \frac{N_L i}{2\pi r} \frac{r_2^2 - r^2}{r_2^2 - r_1^2} \quad (8A.13)$$

where

N_L is the number of Litz-wire turns

r_1 is the inner radius of the Litz-wire area

r_2 is the outer radius of the Litz-wire area

We denote the field at the radius r_1 by H_1 , and it is given as

$$H_1 = \frac{N_L i}{2\pi r_1} \quad (8A.14)$$

Inside the area of the Litz wire the H field is:

$$H = H_1 \frac{r_1}{r} \frac{r_2^2 - r^2}{r_2^2 - r_1^2} \quad (8A.15)$$

The square of the field integrated over the surface of the Litz area is (obtained with the help of by symbolic integration):

$$\int_{S_{\text{litz}}} H^2 dV = \pi \frac{H_1^2 r_1^2}{4(q^2 - 1)} \left[1 - 3q^2 + \frac{4q^2 \ln(q)}{(q^2 - 1)} \right] \quad (8A.16)$$

where

$$q = \frac{r_2}{r_1}$$

S_{litz} is the surface of the Litz area

We divide the result of Equation (8A.16) by the Litz-wire area to get an average square of the field:

$$\langle H^2 \rangle_{S_{\text{litz}}} = \pi \frac{H_1^2}{2(q^2 - 1)^2} \left[1 - 3q^2 + \frac{4q^2 \ln(q)}{(q^2 - 1)} \right] \quad (8A.17)$$

We define a factor k_L , which is only dependent on q :

$$k_L(q) = 3 \frac{\langle H^2 \rangle_{S_{\text{litz}}}}{H_1^2} \quad (8A.18)$$

Note that the factor k_L approaches 1 for thin Litz-wire areas. The factor k_L is shown in Fig. 8A.14 as a function of the ratio $q = r_2/r_1$. Since the purpose is to reduce eddy current losses, it is normal to have Litz-wire strand diameters $d \ll 1.6\delta$. Thus, the following expression, based on the low-frequency

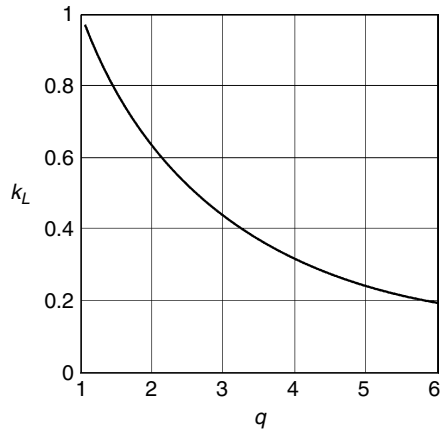


FIGURE 8A.14

Factor k_L as a function of $q = r_2/r_1$.

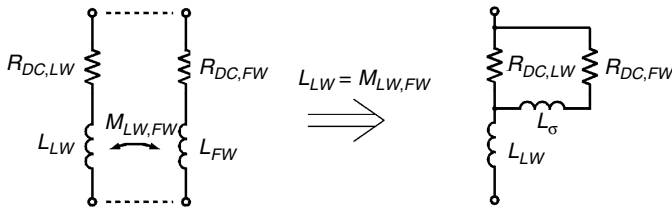


FIGURE 8A.15

Simplified equivalent scheme of the combined Litz-wire full wire inductor.

$R_{DC,LW}$ – the DC resistance of the Litz wire;

$R_{DC,FW}$ – the DC resistance of the full wire;

L_{LW} and L_{FW} the self inductances of the Litz wire and the full wire respectively;

$M_{LW,FW}$ the mutual inductance Litz wire – full wire.

eddy current loss approximation of Chapter 5 and [16,17], can be used for p strands:

$$P_{LF}(f) = \frac{l_c \pi (\omega \mu_0 H)^2 d^4}{64 \rho} p \quad (8A.19)$$

$$P_{cu,eddy,Litz} = \frac{\pi l_w d_s^4 p}{64 \rho_c} \left(\frac{\mu_0 N_L \omega I}{2 \pi r_1} \right)^2 \frac{1}{3} k_L \left(\frac{r_2}{r_1} \right) \quad (8A.20)$$

where

p is the number of strands

d_s is the diameter of the strand

l_w is the length of the Litz wire

REMARK

The simplified equivalent scheme of the combined Litz-wire–full-wire inductor is shown in Fig. 8A.15. It is valid when the number of turns is chosen to obtain an induced voltage in the full wire which is almost equal to the Litz wire voltage ($L_{LW} = M_{LW,FW}$).

The length of the Litz wire l_w should be multiplied by a factor of about 1.05 since the Litz-wire strand is internally longer than the outside length of the wire.

8.A.2.1 Example of a Combined Litz-Wire–Full-Wire Inductor

An inductor is built for an application with DC RMS current $I_{LF} = 5$ A, and a high-frequency component $I_{HF} = 1$ A RMS, at 100 kHz and a 50% duty ratio. The current waveform is triangular, and the peak-to-peak current is $I_{pp} = 3.46$ A. This waveform corresponds to $(di/dt)_{rms} = 0.693$ A/ μ s. The core is EE42/15-type, ferrite material N67, and the available winding area is 7.5×16.3 mm.

The inductor design corresponds to a step-up chopper operation of 100 kHz, 210 V DC, 5 A DC in, and 420 V DC out. A quite high air gap of 5 mm is

chosen in order to permit a high allowable peak current. The saturation current is about 10 A. By its specifications, the inductor could also be used in a continuous-mode, single-phase, power-factor-correction circuit of about 1050 W, at an input voltage of 210 V_{rms}. The number of turns of the Litz winding is 60 and each Litz wire contains 30 strands of 0.1 mm diameter each. The distance from the Litz winding to the ferrite is about 1.5 mm (which is not modeled). The full-wire winding contains two windings of 59 turns of 0.8 mm wire in parallel, one at the left side and one at the right side of the coil former. To test if the correct turns ratio of full wire to Litz wire is realized, a voltage can be applied on the Litz wire, observing the open-circuit voltage at the full wire.

An equivalent scheme of the inductor is shown in Fig. 8A.15. By the special choice of the turns ratio, the equivalent scheme can be reduced to an L-scheme. This scheme well describes the behavior up to high frequencies. The eddy current losses could be described with a parallel resistor to the inductors L_L and L_σ .

8.A.2.2 Experimental Results

A coil corresponding to the example was built. A cylindrical spacer was used before winding the Litz wire in order to keep distance to the air gap. The Litz wire was impregnated with epoxy before winding the full wire. The low-frequency inductance is measured as:

$$L_L = 300 \mu H, \quad L_\sigma = 300 \mu H$$

To have sufficient accuracy on AC losses, we apply only the AC voltage (in this case, a square wave voltage with a full bridge converter).

For comparison and in proof of the design advantages, a second coil former is made without Litz wire, with two times 60 turns of 0.8 mm wire in parallel. The same ferrite core with a 5 mm air gap is used in the measurements. The ferrite losses are 0.9 W, measured when the air gap is filled with a piece of ferrite and using a coil former with a normal winding of 60 turns of the same Litz wire. The losses are measured with a flow calorimeter [18] to an accuracy of 5%. The copper losses of the combined inductor are:

$$P_{cu,com} = 1.61 - 0.9 = 0.71 \text{ W}$$

and this value is about five times lower compared to the copper losses of the full-wire-only inductor:

$$P_{cu} = 4.3 - 0.9 = 3.2 \text{ W.}$$

The results of the measurements on the combined inductor and on the inductor without Litz wire are summarized in Table 8A.1.

The DC current of 5 A adds about 2.42 W to the copper losses, but the calculations and the experiments show that the total losses of the combined

TABLE 8A.1

Measurements on the Combined Inductor and on the Inductor Without Litz wire, Ferrite Losses are 0.9 W

Applied DC Voltage	Measurements on the combined inductor, total losses			Measurements on an inductor without Litz wire			Calculated losses in the Litz wire	
	peak current [A]	rms current [A]	Power loss [W]	Peak current [A]	rms current [A]	Power loss [W]	P_{eddy} in the Litz wire, [W]	P_{cu} (total) in the Litz wire, [W]
210 V	1.75	1.01	1.61	1.5	0.80	4.3	0.114	0.634

inductor can be dissipated without forced cooling. The experiments show that a comparable coil without Litz wire, but still taking 6.5 mm distance from the air gap, with an applied voltage of 210 V generates a 4.3 W copper loss, which is already too much for the copper loss, so no DC current can be added!

REMARKS

- We do not compare the inductor to an inductor without distance to the air gap. This would result in excessive losses and melt the coil former close to the gap.
- Inductors using only Litz wire are also possible, but less are performing than the combined Litz-wire–full-wire inductors. One reason is that the DC resistance increases a lot. Another reason is that a wire with a high number of strands has to be used.
- It is true that the proposed shape is harder to manufacture, but this is often the price to pay for a combination of high power density and low losses.

8.A.2.3 Conclusion

The design of a single-air-gap, combined Litz-wire–full-wire inductor is described. It is designed for mixed HF/DC current. The realization of a special shape results in a significant reduction in the copper losses.

References

- [1] Murgatroyd, P.N., The Brooks inductor: A study of optimal solenoid cross sections, *IEE Proceedings*, vol. 133, pt. B, no. 5, September 1986.
- [2] McLyman, Col. Wm., *Transformer and Inductor Design Handbook*, Marcel Dekker, New York, 1988.

- [3] Meeker, D., Finite Element Method Magnetics (FEMM), <http://femm.berlios.de/>
- [4] Evans, P.D. and Saied, B.M., Calculation of effective inductance of gapped core assemblies, *IEE Proceedings*, vol. 133, no. 1, 1986, pp. 41–45.
- [5] Chandler, P.L, Yan, X., and Paterson, D.J., Novel high-power ferrite inductor design with improved design accuracy and overall performance, IEE 32nd Annual PESC, vol. 4, pp. 2090–2094, 2001.
- [6] Rahmi-Kain, A., Keyhani, A., and Powell, J., Minimum loss design of 100 kHz inductor with Litz wire, IAS Conference Proceedings, New Orleans, 1997, CD-ROM.
- [7] Van den Bossche, A., Valchev, V., and Filchev, T., Improved approximation for permeances of gapped inductors, IEE-IAS 37th Annual Meeting, Pittsburgh, October 13–18, 2002, CD-ROM.
- [8] Kutkut, N.H. and Divan, D.M., Optimal air-gap design in high-frequency foil windings, *IEE Transactions on Power Electronics*, vol. 13, No. 5, September 1998, pp. 942–949.
- [9] Kutkut, N.H., A simple technique to evaluate winding losses including two-dimensional edge effects, *IEE Transactions on Power Electronics*, vol. 13, No. 5, September 1998, pp. 950–957.
- [10] Nysveen, A. and Hernes, M., Minimum loss design of a 100 kHz inductor with foil windings, EPE Conference Proceedings, 1993, pp 106–111.
- [11] Valchev, V. and Van den Bossche, A., Eddy current losses and inductance of gapped foil inductors, IECON'02, Sevilla, Spain, November 5–8, 2002, pp. 1190–1195.
- [12] Daniel, L. and Sullivan, C.R., Design of microfabricated inductors, *IEE Transactions on Power Electronics*, vol. 14, no. 4, July 1999, pp. 709–716.
- [13] Hu, J. and Sullivan, C.R., AC resistance of planar power inductors and the quasidistributed gap technique, *IEE Transactions on Power Electronics*, vol. 16, no. 4, July 2001, pp. 558–567.
- [14] Carsten, B., Designing filter inductors for simultaneous minimization of DC and high frequency AC conductor losses, PCIM'94, Dallas, TX, September 17–22, 1994, pp. 19–37.
- [15] Van den Bossche, A., Design of inductors with both DC and HF components, IEE Benelux meeting, Eindhoven, The Netherlands, October 1, 2003, CD-ROM.
- [16] Sullivan, C.R., Computationally efficient winding loss calculation with multiple windings, arbitrary waveforms, and two-dimensional or three-dimensional field geometry, *IEE Transactions on Power Electronics*, vol. 16, no. 4, January 2001, pp. 142–150.
- [17] Pollock, J.D., Abdallah, T., and Sullivan, C.R., Easy-to use CAD tools for Litz-wire winding optimisation, APEC, February 9–13, 2003, CD-ROM.
- [18] Van den Bossche, A., Flow calorimeter for power electronic converters, EPE Conference, Graz, August 27–29, 2001, CD-ROM.

9

Transformer Design

9.1 Transformer Design in Power Electronics

The design of a transformer in power electronics has many aspects, most of which are discussed in different chapters of the book.

In this chapter, we discuss mainly specific issues concerning transformer design. Many properties of the transformer influence the design of the power electronic converter, such as magnetizing inductance, leakage inductance, voltage, current, frequency, power loss, insulation voltage, parasitic capacitance, and so on. Parasitic properties often play an important role in the function of the transformer in power electronic converters.

9.2 Magnetizing Inductance

Usually the magnetizing flux determines the no-load current of the transformer. In general, the magnetic material is non-linear. For simplicity, we do not consider hysteresis losses in the magnetic material here.

The presence of an air gap is a property of inductors, and it is not discussed here.

9.2.1 Basics

We use the flux linkage presented as:

$$\Psi(i(t)) = \int (v(t) - Ri(t))dt, [\text{Vs}] \quad (9.1)$$

The amplitude-magnetizing inductance L_a can be represented by the peak current I_p :

$$L_a(I_p) = \frac{\Psi_p}{I_p}, [\text{H}] \quad (9.2)$$

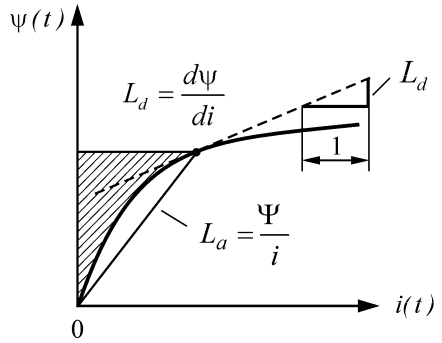


FIGURE 9.1
Peak flux linkage ψ_p as a function of the peak current I_p and definitions of L_a and L_d .

This representation is usually used to determine the peak magnetizing current, and it corresponds to the amplitude (chord) permeability of the material (see Fig. 9.1). The shaded area corresponds to the energy stored in the coil.

The differential magnetizing inductance L_d is defined as

$$L_d(i) = \frac{d\Psi}{di} = \frac{V}{\frac{di}{dt}}, \text{ [H]} \quad (9.3)$$

where

V and i are the coil voltage and current.

It corresponds to the incremental (differential, reversible) permeability of the material, and it is used to determine ripple currents superposed on a DC magnetizing current.

NOTE: At normal induction levels (0.1–0.2 T), the amplitude-magnetizing inductance L_a of ferrites is typically 1.5 times higher than it is at the low-induction amplitude of a few mT, which is a typical induction level of Henry meters.

The differential inductance can drop very fast once the core is close to saturation (0.35–0.4 T for power ferrites). The following relations should be considered:

- At low induction levels $L_a(I) < L_d(I)$
- At high induction levels $L_a(I) > L_d(I)$

REMARK

For linear materials $L_a(I) = L_d(I)$.

The *saturation point* is dependent on the criterion for saturation. If no special requirements are given, a practical criterion for power electronics is to use the point where the differential inductance is reduced by a factor of two, compared to its maximum value.

9.2.2 Design

The instantaneous flux linkage Ψ , divided by the number of turns results in an instantaneous average flux/turn Φ :

$$\Phi = \frac{\Psi_1}{N_1}, [\text{Wb}] \quad (9.4)$$

The peak flux is determined by (see also [figure 2.5](#) in [chapter 2](#)):

$$\Phi_p = \frac{\Psi_{p1}}{N_1} = B_p A_m, [\text{Wb}] \quad (9.5)$$

where

A_m is the minimum core cross-sectional area.

This equation usually determines the number of turns. In the saturation-limited designs $B_p = B_{sat}$. If the design is non-saturated, then B_p can be determined by the allowed core losses (see Chapter 2).

The flux Φ_p is also called *physical flux*. It is also the flux in the core if the leakage fluxes are neglected. Note that it is advisable to make a difference in units between the flux linkage [Vs] and the flux for one turn [Wb].

PERMEANCE

The ratio of the physical flux Φ_p and the peak m.m.f. F_p [A turn] is the permeance Λ . This permeance is also known as A_L value in the ferrite data:

$$\Lambda = A_L = \frac{\Phi_p}{F_p} = \frac{\Psi_{p1}}{N_1 I_{p1}} \quad (9.6)$$

The defined (non-linear) permeance gives the relationship between the peak flux linkage and the peak magnetizing current. This allows to determine the peak magnetizing current which is often a contribution in the turn-off current of transistors. The permeance Λ is defined as:

$$\Lambda = \mu_r \mu_0 \frac{A_e}{l_e} \quad (9.7)$$

where

A_e is the area of the equivalent magnetic cross section

l_e is the equivalent magnetic path length

μ_r is the relative permeability (the amplitude or differential value can be used depending on needs, see [Chapter 3](#)).

The equivalent magnetic cross section A_e and the equivalent magnetic path length l_e correspond to a fictitious ring core, which would have the same permeance and the same losses. This value is usually given by the manufacturer. The effective cross section is usually slightly higher than the section of the mid leg, which usually corresponds to the minimum cross section.

Now we can write a simplified equation for the magnetizing inductance of the primary winding:

$$L_{m1} = N_1^2 \mu_r \mu_0 \frac{A_e}{l_e} \quad (9.8)$$

9.3 Leakage Inductance

Leakage inductance can be very harmful in some designs, such as fly-back converters. In contrast, in some resonant converters it is used to improve the waveforms in the switching transistors, and should have a determined value.

9.3.1 Leakage Inductance of Concentric Windings

In this construction case, the field pattern is quite well-defined, and the leakage inductance can be accurately estimated.

The easiest way to determine the leakage inductance is by using the stored energy near the leakage field. To do this, we need an idealized short circuit test, where the sum of the ampere-turns in primary and secondary are zero. In this case, the energy in the magnetizing inductance is zero.

The H field between the two windings is:

$$H_a = N_1 \frac{I_1}{w} = N_2 \frac{I_2}{w} \quad (9.9)$$

where

w is the winding width (see Fig. 9.2)

H_a is the magnetic field between the windings

N_1, N_2 are the number of turns

NOTE: Here we neglect the reluctance of the flux return path, which is usually a good approximation.

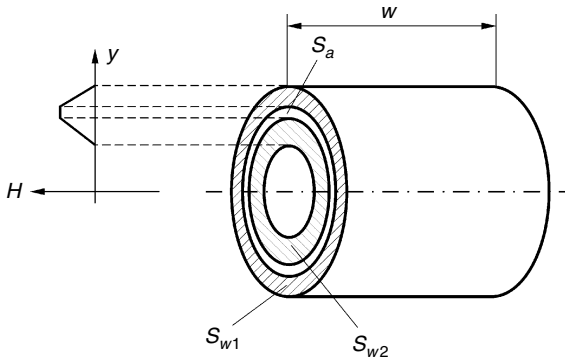


FIGURE 9.2

Concentric windings, dimensions and cross sections.

The corresponding energy is:

$$W_a = \frac{1}{2} \mu_0 \int_{\text{Volume}} H_a^2 dV \quad (9.10)$$

$$W_a = \frac{1}{2} \mu_0 H_a^2 V_a \quad (9.11)$$

where

V_a is the volume between the windings

In the windings themselves, the field is linearly increasing from the outside to the space between the windings. This part of the field gives a three times lower contribution in energy/volume.

$$W_a = \frac{1}{2} \frac{1}{3} \mu_0 H_a^2 V_w \quad (9.12)$$

where

V_w is the volume of the windings.

The total energy in the leakage field equals:

$$W_\sigma = \frac{1}{2} L_\sigma I^2 \quad (9.13)$$

Hence, using Equations (9.9) and (9.13) we obtain:

$$L_{\sigma 1} = \mu_0 \left(V_a + \frac{V_{w1} + V_{w2}}{3} \right) \left(\frac{N_1}{w} \right)^2 \quad (9.14)$$

where

V_{w1} is the volume of the primary winding

V_{w2} is the volume of the secondary winding

w is the winding width

If we represent the volumes by the cross-sectional surface of the cylinders S and their height w (see Fig. 9.2), then we can write:

$$L_{\sigma 1} = \mu_0 \left(S_a + \frac{S_{w1} + S_{w2}}{3} \right) \frac{N_1^2}{w} \quad (9.15)$$

Using the same approach, the leakage permeance can be defined as:

$$\Lambda_\sigma = \mu_0 \left(S_a + \frac{S_{w1} + S_{w2}}{3} \right) \frac{1}{w} \quad (9.16)$$

Equation (9.16) allows us to define an equivalent length l_{eq} and an equivalent cross section of the leakage path S_{eq} :

$$l_{eq} = w \quad (9.17)$$

$$S_{eq} = \left(S_a + \frac{S_{w1} + S_{w2}}{3} \right) \quad (9.18)$$

Although the method seems simple, the accuracy is often better than 10%. The practical problem, usually, is to get all mechanical dimensions right. Leakage inductances can be more easily measured than copper losses, so it is sometimes easier to measure the inductance than to get the exact dimensions of the magnetic component.

Note that the leakage inductance of concentric windings is hardly different, whether the core is present or not. The reason for this is that the area for the flux between the windings is small compared to the return path outside, even if there is no core. However, if the core is removed, there might be a measurement problem, as the resistance of the winding is not negligible compared to the magnetizing inductance (see [Chapter 11](#), Measurements).

9.3.2 Leakage Inductance of Windings in Separate Rooms

9.3.2.1 General Case

This type of winding is preferred if a high-insulation voltage is present or if a low-parasitic capacitance between windings is pursued. Figure 9.3 shows a transformer with windings in separate rooms. As the distance between primary and secondary is high, one can expect a high leakage permeance. An accurate estimation is not as easy as in the concentric-windings cases. Often a practical test is necessary to determine the permeance, or a 3-D finite-element computation could solve the problem.

The transverse field across the windings is quite high. So, high transverse-field eddy current losses can be expected. This type of winding should be used in combination with Litz wire.

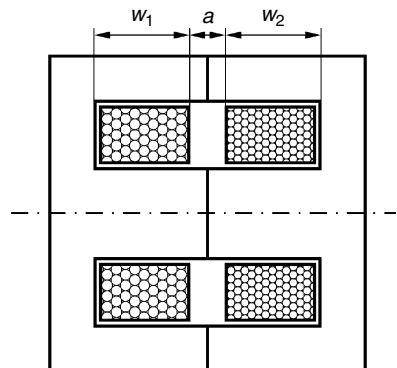


FIGURE 9.3
A transformer with windings in separate rooms.

9.3.2.2 Axis-Symmetrical Case

This is the case when the windings are in separate rooms, in a closed pot core (see [Fig. 9.4](#)). In this case the leakage field has an analytical solution. The same energy method can be used here as was used for concentric windings.

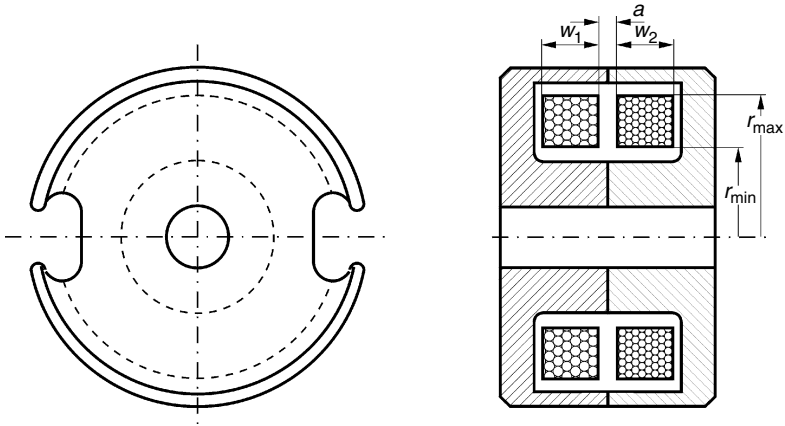


FIGURE 9.4

Transformer windings in separate rooms in an (almost) closed pot core, axis-symmetrical case.

Let us first calculate the maximum H -field close to the center leg. We consider the ideal case where the winding touches the legs (r_{min} is lower and r_{max} is higher than the values shown in Fig. 9.4). It can be demonstrated that the field in the air between the windings is:

$$H(r) = \frac{NI}{r \ln\left(\frac{r_{max}}{r_{min}}\right)} \quad (9.19)$$

where

r_{min} is the minimum radius of the winding area (see Fig. 9.4)

r_{max} is the maximum radius of the winding area

Using the energy method, the leakage inductance can be calculated as:

$$L_{\sigma 1} = 2 \pi \mu_0 N_1^2 \frac{a + \frac{w_1 + w_2}{3}}{\ln\left(\frac{r_{max}}{r_{min}}\right)} \quad (9.20)$$

where

a is the distance between the primary and secondary winding

w_1 is the width of the primary winding

w_2 is the width of the secondary winding.

Note that in cores with round center legs, but with outer legs that do not cover the winding completely (ETD, RM, PQ cores, EP cores), Equation (9.20) can also be used to obtain a maximum value of the leakage inductance.

9.3.3 Leakage Inductance in T, L and M Models of Transformers

The model of a transformer can be described using simple or more involved schemes.

9.3.3.1 T Transformer Model

If the transformer is symmetrical, the traditional model attributes a part of the leakage to the primary winding and the other part to the secondary winding.

In Fig. 9.5 we show an extended T model.

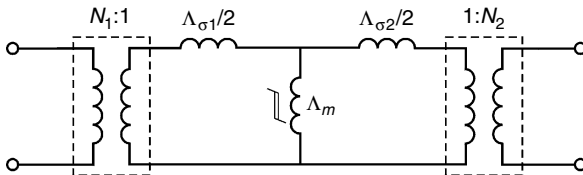


FIGURE 9.5
An extended T model of a transformer.

9.3.3.2 L Transformer Model

If the leakage inductance is small (maximum of a few percent) compared to the magnetizing reactance, then the scheme can be simplified to an L-scheme (see Fig. 9.6).

An L scheme can also be a more accurate model than a symmetrical T-scheme in some cases. One example is a ring core with a primary winding close to the core and a secondary winding above the primary. It is clear that in this case the primary winding is better coupled with the core than the secondary winding.

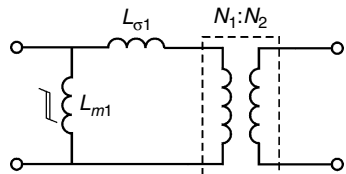


FIGURE 9.6
L model of a transformer.

9.3.3.3 M Transformer Model

Some designs have large leakage inductances. This is the case in some common-mode suppression inductors. In those cases, saturation can occur at either the primary or secondary side. This effect is easily represented by

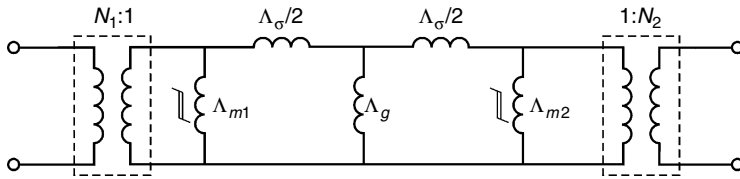


FIGURE 9.7
M model of a transformer.

the *M* transformer model (see Fig. 9.7). The saturable parts are well coupled with windings, whereas the air gap exhibits neither saturation nor core losses.

If the core contains an air gap, a small, central-magnetizing inductance can also be present. This is the case in non-contact, rotational axis, power transmission using two pot cores and an air gap.

9.4 Using Parallel Wires and Litz Wires

In power electronics large currents are often handled, and the eddy currents losses can dominate. A way to reduce eddy currents is to use more wires of smaller diameter in parallel.

In general, it is useful to use parallel wires or windings if they carry the same e.m.f. (electromotive force) or flux. If the e.m.f. is somewhat different and the leakage inductance between the paralleled windings (or wires) is small, then severe circulating currents can flow, which may be worse than the eddy current losses in the original design.

9.4.1 Parallel Wires

Just winding several (*p*) wires together is one possibility. Currents are shared if each wire has about the same distance to the other layer (or to an air gap). Practically, winding two wires in parallel is easy, but more than four wires is not advisable.

Here we discuss low-frequency and high-frequency cases separately.

9.4.1.1 Low Frequency Case: $d < 1.6 \delta$

The low frequency case is typical in designs with several layers. When using *p* parallel wires we can distinguish the following specific cases:

- A) Maintaining the same number of layers, increase the winding width with *p*.

In this case, the transverse field is reduced by a factor *p* but the amount of wires increases by a factor *p*. The result is that the eddy

current losses are reduced with a factor p . So, it is interesting to fill the layers.

B) Increase the number of layers with p .

The DC losses reduce almost with a factor p . However, in this case, the transverse field in the wires remains the same but the number of layer increases, and the eddy current losses will increase almost with a factor p . This is tolerated if the eddy current losses are low.

C) Keep the same total cross section of the conductor.

The field remains the same but the wire diameter reduces with a factor \sqrt{p} . This results in a reduction of transverse field losses r with a factor p^2 .

D) The general case.

We can use the equation of [Chapter 2](#) and [5](#), which give more nuance and more accurate results for a variable p , diameter, and number of layers.

9.4.1.2 High Frequency Case: $d > 2.7\delta$

This may be the case in single layer designs. The use of parallel wires with the same total cross section may even increase the eddy current losses. *In the case of a single layer transformer, it is usually not beneficial to use parallel wires.* A better approach is to use the highest diameter that fills the layer completely. The solution is to use the equations of the proposed wide-frequency method. In cases where windings carry both high-frequency and DC currents, it is useful to screen the HF field by a single layer and to have a second winding charring only DC. In this solution the influence of internal circulating currents is reduced.

9.4.2 Parallel Windings Using Symmetry in the Magnetic Path

A way to reduce eddy current losses is to reduce the conductor thickness. This approach will result in greater ohmic losses, so one will have to put wires in parallel to keep ohmic losses low. Normally, in designs that are subjected to eddy currents, there is an optimal wire thickness. In practice, this means that *the winding area is hardly filled if single wires are used.*

One can use the natural symmetry of shapes to wind different coils that will carry the same current. Without interleaving, a number of windings with the same number of turns can be put in parallel without circulating currents. Here we give the possible number of parallel windings for different cores:

- EE and EI types (see [Fig. 9.8a](#)): two parallel windings
- UU types (see [Fig. 9.8b](#)): four parallel windings;
- Multiple air gaps, if well arranged: two times more parallel windings than the number of gaps.
- Ring cores: in principle, an infinite number of paralleled windings.

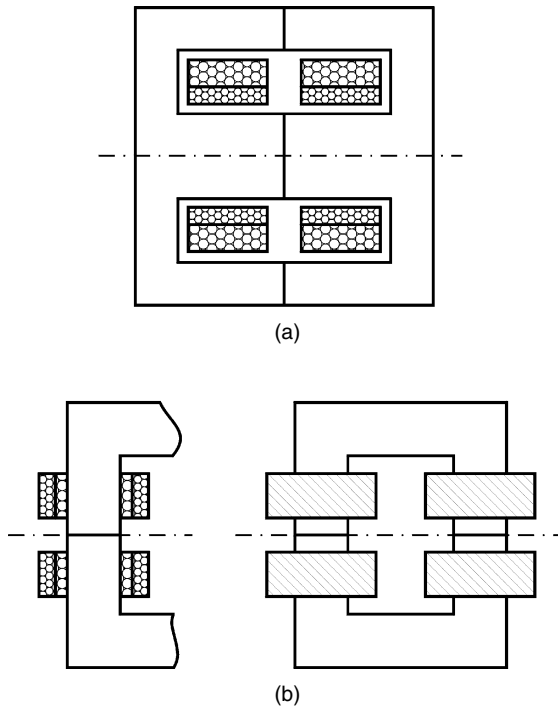


FIGURE 9.8

Possible number of paralleled windings for different cores, (a) EE core set: 2 windings, (b) UU core set: 4 windings.

9.4.3 Using Litz Wire

A way to parallel more wires is to use Litz wire, also called bunched conductors. Each Litz wire contains a number of strands that are individually insulated, and all the strands use their positions in the section equally. Therefore, in the typical transverse fields, each wire has the same flux. The advantage of Litz wire is that much lower eddy currents losses are usually generated, as the diameter of the individual strands is small. The disadvantages of Litz wire are a lower filling factor, a lower thermal conduction, and, usually, a lower temperature grade. The DC resistance increases by about 5% as the wire length increases.

We consider Litz wire containing p strands. In low-frequency approximation, for the same total wire cross section, Litz wire reduces the eddy current loss by a factor p . We can give a practical design aspect with an example:

9.4.3.1 Example in the Low-Frequency Approximation

We want to increase the current in an existing (poorly filled) transformer design by a factor of α , while trying to maintain the same ohmic and eddy current loss within the same core size.

To have the same ohmic losses we would have to increase the diameter by a factor of α . However, this would increase the eddy current loss by a factor of α^4 due to the diameter increase and, additionally, by a factor of α^2 due to the transverse field increase! Hence, to maintain the original eddy current loss, we would need a reduction factor of α^6 . The required Litz wire diameter is α^{-2} times the original wire. For example, if we want to double the current ($\alpha = 2$) and the required number of strands is 64, then the required Litz wire diameter should be four times smaller than the original diameter.

NOTE THAT:

- Large design improvements need many strands in the Litz wire.
- Litz wire can have a different temperature rating and a lower thermal conductance, so the design result may be slightly different than proposed.

9.4.4 Half Turns

Using half turns to equalize currents in different windings is a quite special technique.

Half windings are possible in EE cores, as they have two apertures for the windings. A winding of 3.5 turns has, for example, three turns in the left winding area and four turns in the right winding area. Usually, such half windings have to be avoided in designs. They tend to saturate the side legs as the m.m.f is not fully compensated by the secondary winding. However, when two such turns are put in parallel, an equal m.m.f. in both sides can be obtained again (e.g., having 3 + 4 turns on the left side and 4 + 3 on the right side). This winding is possible in vertically mounted coil formers. In that case, even when the winding is non-symmetric, the currents in the parallel windings are almost equal, as the leakage inductance between the windings is high since it contains one turn around each leg.

9.5 Interleaved Windings

This approach is only applicable to transformers, not to inductors.

If the design is changed from Primary/Secondary (P/S) to (P1, S1, S2, P2 or P1, S1, P2, S2) with the same type of wires, both the ohmic losses and the eddy current losses will be reduced by a factor of two. In practice, the thermal capability of the component is not improved significantly in the case of interleaving, so the current handling capability is increased by a factor of $\sqrt{2}$.

REMARKS

1. In the case of a center-gapped transformer, the inner primary winding will carry almost all of the magnetizing current.

2. The additional windings will have higher turn length.
3. The energy method can be used to compute the leakage inductance, and the leakage inductance usually decreases inversely proportionally to the number of interleavings in parallel.
4. The parasitic capacitance is almost proportional to the number of interleavings in parallel.

9.6 Superimposing Frequency Components

The actual voltage and current waveforms in power electronics are usually non-sinusoidal. When a phenomenon is linear, and not time-dependent, a complex waveform can be separated in Fourier components to analyze its behavior with a transfer function and to analyze losses.

This is the case with leakage inductance (mainly in air) and eddy currents in conductors. The individual Fourier components in frequency are orthogonal, and the losses caused by them can be superimposed. Also, sine and cosine Fourier components are orthogonal and can be analyzed separately (see orthogonality in [Chapter 5](#)).

Magnetized inductance and core losses are usually non-linear, and the orthogonality is not present.

9.6.1 Magnetic Materials

The peak-to-peak inductance and the frequency are the main parameters that determine the core losses (see [Chapters 2](#) and [3](#)). They are usually measured and shown in double-logarithmic graphs by the manufacturers. As long as the curves are close to straight lines, they can be modeled by the Steinmetz equation.

For ferrites, a dependence of the waveform, itself, for a given peak-to-peak inductance has also been observed (see [Chapter 3](#) and [[1](#)], [[2](#)], [[3](#)]). Methods of extending to non-sinusoidal waveforms for transformer and inductor design are given in [[4](#)], [[5](#)], [[6](#)]. High-frequency-loss analysis based on Preisach modelling is presented in [[7](#)].

9.6.2 Eddy Currents in Conductors

In the scientific literature, 2-D analytical approximations are mainly focussed on uniform transverse fields (proximity losses) and on the field of a wire (skin-effect losses) [[8](#)], [[9](#)], [[10](#)].

A current waveform can be separated into frequency components and cosine and sine components. The reference for the cosine and sine must be the same for all windings.

The individual losses of the Fourier components can be added without taking into account the interaction of mixed products, as superposition is allowed.

9.6.2.1 General Solution

The Fourier expansion of each component in a transformer current can be written as:

$$i(t) = I_0 + \sum_{n=1}^{\infty} (A_n \sqrt{2} \cos(\omega t) + B_n \sqrt{2} \sin(\omega t)) \quad (9.21)$$

The losses of each component presented by I_0, A_n, B_n can be calculated and summed, as the contributions are orthogonal. This way of proceeding is mathematically correct, but it takes time to be implemented.

In the *low-frequency approximation*, the terms can be calculated as described below. The eddy currents are proportional to the derivative of the current. This means that the losses can be modeled as a resistor parallel to the leakage inductance. One way to consider this fact is to define an apparent frequency f_{ap} that will result in the same losses as a sine wave at that apparent frequency with the same current RMS value.

As an example, we consider a triangular current waveform (see Fig. 9.9). The RMS value of this current is:

$$I_{rms} = \frac{I_{pp}}{2\sqrt{3}} \quad (9.22)$$

where

I_{pp} is the peak-to-peak value of the current.

The square RMS di/dt value is

$$\left(\frac{di}{dt}\right)_{rms}^2 = \frac{(I_{pp})^2}{T^2} \left(\frac{1}{D} + \frac{1}{1-D}\right) \quad (9.23)$$

$$\left(\frac{di}{dt}\right)_{rms}^2 = \frac{12 I^2}{T^2} \left(\frac{1}{D} + \frac{1}{1-D}\right) \quad (9.24)$$

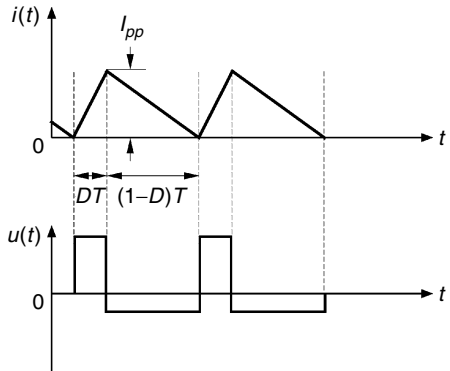


FIGURE 9.9

An asymmetric triangular current waveform of a coil and voltage across the coil.

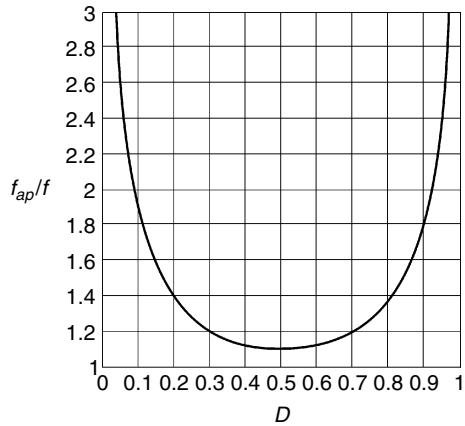


FIGURE 9.10

The ratio between the apparent frequency f_{ap} and the switching frequency f as a function of the duty cycle ratio D .

where

D is the duty ratio, which is equal to the ratio of the rising edge to the total period (see Fig. 9.9).

For a sine wave we have:

$$\left(\frac{di}{dt}\right)_{rms}^2 = \left(\frac{2\pi}{T}\right)^2 I_{rms}^2 \quad (9.25)$$

Then, combining Equations (9.24) and (9.25), we obtain the apparent frequency:

$$\frac{f_{ap}}{f} = \sqrt{\frac{12\left(\frac{1}{D} + \frac{1}{1-D}\right)}{(2\pi)^2}} = \frac{1}{\pi} \sqrt{\frac{3}{D(1-D)}} \quad (9.26)$$

This ratio between the apparent frequency and the switching frequency is shown in Fig. 9.10.

For $D = 0.5$, the ratio f_{ap}/f is 1.103, which is not so high of a value. At extreme values of D the difference is more significant, but in most converters the peak-to-peak current, or the RMS ripple current, reduces at extreme D ; thus, the resulting eddy current losses are often even lower than at $D = 0.5$.

9.7 Superimposing Modes

Transformers in power electronics may have more than two windings. We illustrate this fact by an example of a push-pull converter with two primary windings and one secondary winding (see Fig. 9.11).

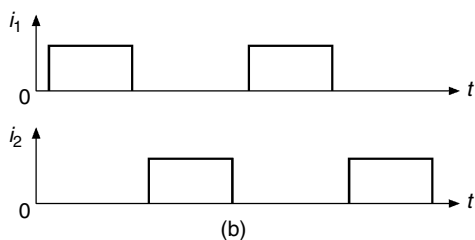
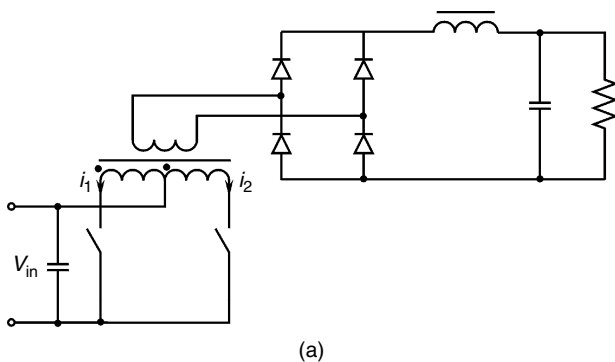


FIGURE 9.11 Push-pull converter and the corresponding current waveforms.

Both primary windings contain similar harmonics (see Fig. 9.12), and they cannot be considered separately for the loss calculation. The eddy current losses can be present in a winding, even if it does not carry current, as some transverse fields of other windings are present in that winding.

One solution is to expand the currents in Fourier components as mentioned above, but it takes a lot of implementation time and does not give much insight.

Another way is to divide the current into a common mode part and a differential mode part. Common mode i_{cm} and differential mode i_{dm} currents are expressed as

$$i_{cm} = \frac{i_1 + i_2}{2} \quad (9.27)$$

$$i_{dm} = \frac{i_1 - i_2}{2} \quad (9.28)$$

$$i_{dm} + i_{cm} = i_1 \quad (9.29)$$

$$i_{dm} - i_{cm} = i_2 \quad (9.30)$$

These currents are orthogonal, as they are even and odd functions in time.

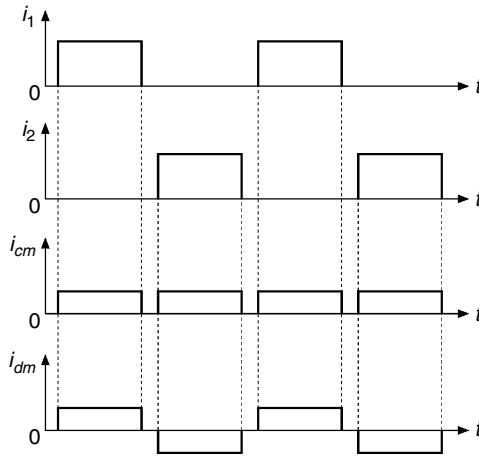


FIGURE 9.12

Common mode i_{cm} and differential mode current i_{dm} waveforms in the currents of a push-pull converter.

The common mode part contains a *DC* component and even harmonics of the switching frequency. The differential mode part contains only odd components of the switching frequency.

The field pattern in the case is quite different (see Fig. 9.13):

- The common mode current corresponds to the field of two single layers with opposite currents.
- The differential mode current corresponds to a two-layer primary winding containing only AC current, with a secondary winding carrying the opposite current.

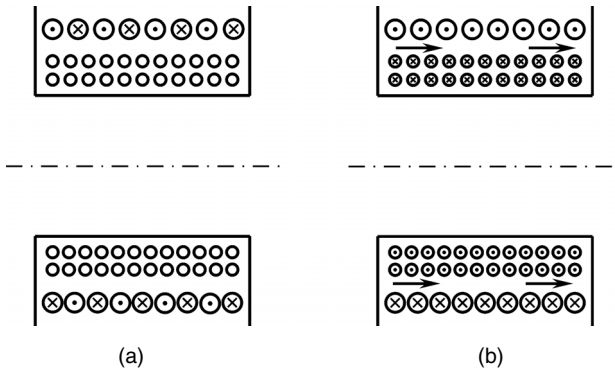


FIGURE 9.13

Common mode (a) and differential mode fields (b) in a transformer.

The advantage of splitting into modes is that the eddy current problem is divided into simpler problems.

References

- [1] Van den Bossche, A., Georgiev, G.B., and Valchev, V., Ferrite losses with square voltage waveforms, OPTIM'04, Brasov, Romania, May 20–23, 2004, CD-ROM.
- [2] Li, J., Abdallah, T., and Sullivan, C., Improved calculation of core loss with nonsinusoidal waveforms, IEEE, IAS 36th Annual Meeting, Chicago, September 30–October 4, 2001, pp. 2203–2210.
- [3] Van den Bossche, A., Valchev, V., and Georgiev, G.B., Measurement and loss model of ferrites with non-sinusoidal waveforms, PESC'04, Aachen, Germany, June 20–25, 2004, CD-ROM.
- [4] Hurley, W.G., Gath, E., and Breslin, J.G., Optimized transformer design: Inclusive of high-frequency effects, *IEEE Transactions on Power Electronics*, vol. 13, no. 4, July 1998, pp. 651–658.
- [5] Hurley, W.G., Gath, E., and Breslin, J.G., Optimising the AC resistance of multilayer transformer windings with arbitrary current waveforms, *IEEE Transactions on Power Electronics*, vol. 15, no. 2, March 2000, pp. 369–376.
- [6] Petkov, R., Optimum design of a high-power, high-frequency transformer, *IEEE Transactions on Power Electronics*, vol. 11, no. 1, January 1996, pp. 33–42.
- [7] Cheng, K.W.E., Lee, W.S., Tang, C.Y., and Chan, L.C., Dynamic modelling of magnetic materials for high frequency applications, *ELSEVIER Journal of Materials Technology*, vol. 139, 2003, pp. 578–584.
- [8] Wallmeier, P., Frohleke, N., and Grotstollen, H., Improved analytical modelling of conductive losses in gapped high-frequency inductors, IEEE-IAS Annual Meeting, 1998, pp. 913–920.
- [9] Severns, R., Additional losses in high frequency magnetics due to non ideal field distributions, APEC'92, 7th Annual IEEE Applied Power Electronics Conference, 1992, pp. 333–338.
- [10] Apeldoorn, O. and Kriegel, K., Optimal design of transformers for high power high frequency applications, EPE95, Sevilla, Spain, 1995, pp 1007–1014.

10

Optimal Copper/Core Loss Ratio in Magnetic Components

Most of magnetic component designs are a trade-off between induction level B and core losses on one hand, and copper, ohmic, and eddy current losses on the other hand [1,2,3]. This trade-off results in a point of maximum efficiency placed between 50 and 100% of the nominal load. Depending on the design philosophy (the starting point), different types of cost functions and constraints can be defined:

- Loss minimization at constant copper volume and core shape
- Loss minimization at constant copper wire cross section
- Capitalization of losses such as cumulative energy consumption; in this case partial load and no load are also important
- Worst case designs with maximum temperatures
- A part of optimization in a system, such as a power converter or an appliance

The purpose of this chapter is to discuss several most frequently appearing cases and to give results that can be used to check whether the design is close or far away from the optimal one with respect to loss minimization.

NOTE: It is assumed that, after an initial design, the main parameters of the magnetic component under development are already known. By using these found parameters, the core and copper losses can be found and included in an optimization process of adjusting the turn numbers and copper wire cross area. The practical optimization is often discrete; the choice of core shapes, number of turns and wire thickness is not continuous, but is limited to what the manufacturer offers.

Readers can look at the contents of the chapter to find their specific case.

10.1 Simplified Approach

In this section we give a simplified approach, corresponding to level 0 in the context of this book.

10.1.1 Transformer

For copper losses, the resistance can be calculated by the wire cross section. The resistance of (pulled) copper wire is

$$R = \rho l_w / A_{cu} \text{, } [\Omega] \quad (10.1)$$

where

$$\rho = 18(1 + 0.0374(T_c - 20))10^{-9} \Omega\text{m}$$

l_w is the wire length [m]

A_{cu} is the area of the wire cross section, [m²]

T_c is temperature, [°C]

$$\text{For } T = 20^\circ\text{C} \Rightarrow \rho = 18 \times 10^{-9} \Omega\text{m.}$$

$$\text{For } T = 100^\circ\text{C} \Rightarrow \rho = 23.4 \times 10^{-9} \Omega\text{m,}$$

which is 30% more than the value of ρ for 20°C.

The cost function to be considered is the total power losses. Assuming a level for core and copper losses, we derive the condition at which that level is the optimal one. The total power losses are given by the sum of core and copper losses, and the aim is to be minimal:

$$P_{tot} = P_{cu} + P_{fe} = \min \quad (10.2)$$

The constraint, or boundary condition, is that the output power P_{out} must be achieved. The copper volume V_{cu} is also assumed to remain constant, and then

$$P_{out} = V_{out} I_{out} = \text{constant} \quad (10.3)$$

$$V_{cu} = A_{cu} l_w = \text{constant} \quad (10.4)$$

where

A_{cu} is the total cross section, [m²]

l_w is the wire length [m]

V_{cu} is copper volume [m³]

Note that the constant copper volume constraint normally results in a constant length/turn ratio.

The core losses can be modeled in various ways. In the simplified approach we assume that the losses are quadratic, with an induction level B :

$$P_{fe} \sim B^2 \quad (10.5)$$

We neglect the magnetizing current, so the primary and secondary currents are proportional to each other. In practice this means a non-saturated transformer design without an air gap. Then increasing the wire length by ε (the relative number of turns, see Equation (10.7)) increases the copper losses also by ε . To keep the total copper volume constant, we also have

to reduce the copper cross-sectional area by ε , which results in increasing the total copper losses by ε^2 . The same increase in number of turns with a factor ε results in a peak induction decreased by a factor of ε . Then, if the core losses are assumed to decrease in a quadratic way with B , the same losses decrease by a factor of ε^2 . Finally, the dependence of the total power losses P_{tot} on ε is

$$P_{tot} = P_{cu} \varepsilon^2 + \frac{P_{fe}}{\varepsilon^2} = \min \quad (10.6)$$

where

ε is the relative number of turns:

$$\varepsilon = \frac{N + \Delta N}{N} = \frac{N_{new}}{N_{old}} \quad (10.7)$$

The derived dependence of Equation (10.6) is shown in Fig. 10.1.

Setting the derivative of P_{tot} to zero with respect to ε gives the condition that is used to adjust the design to the optimum:

$$P_{cu} = \frac{P_{fe}}{\varepsilon^4}, \quad \varepsilon = \sqrt[4]{P_{fe}/P_{cu}} \quad (10.8)$$

If, in a first attempt, the core losses and the copper losses are not equal, then Equation (10.8) gives the factor ε to use for changing the number of turns so as to obtain the optimal case.

If $P_{fe} = P_{cu}$ then $\varepsilon = 1$, which means that the number of turns is optimal and does not have to be changed.

In practice, if the design is not saturation limited, the condition of Equation (10.8) means that the minimum power losses, or optimal efficiency in the simplified case, are obtained when the copper losses are equal to the core losses:

$$P_{cu,opt} = P_{fe,opt} \quad (10.9)$$

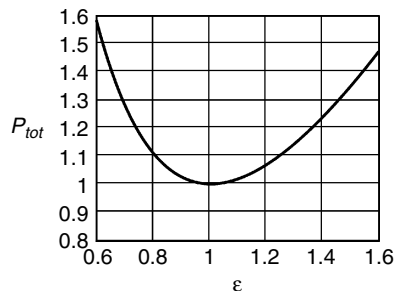


FIGURE 10.1

Total losses P_{tot} depending on the relative change of the number of turns ε .

10.1.2 Inductor

For inductors, an approach similar to that described in the previous section can be used. However, when the number of turns changes, the air gap should be adapted (the permeance of the magnetic path) in order to maintain the same inductance value and the same voltage and current at the inductor terminals. The change in magnetic path when changing the air gap length is neglected with respect to the core losses. Applying the above considerations yields minimum losses when:

$$P_{cu,opt} = P_{fe,opt} \quad (10.10)$$

10.2 Loss Minimization in the General Case

In the general case, the core losses mainly depend on the frequency and on the peak induction level:

$$P_{fe} = k f^\alpha \hat{B}^\beta \quad (10.11)$$

where

k is core loss coefficient, $k = F(f, B, T)$

T is the temperature

f is the frequency

α is frequency exponent

\hat{B} is the induction peak value of the AC waveform

β is core loss exponent

The ohmic copper losses are

$$P_{cu} = \sum_{\text{windings}} \rho_{cu} \frac{l_{cu}}{S_{cu}} I_{rms}^2 \quad (10.12)$$

Imagine an optimal magnetic-component design with core losses $P_{fe,opt}$ and copper losses $P_{cu,opt}$. Let us present the general core and copper losses by their optimal values. When increasing the number of turns by a factor of ε , the induction B in the core is decreased by a factor of ε because the flux linkage is kept constant; that is, the induction is proportional to ε^{-1} . Thus, considering Equation (10.11), the core losses are inversely proportional to ε^β :

$$P_{fe} = P_{fe,opt} \varepsilon^{-\beta} \quad (10.13)$$

The copper losses can be represented by their optimal value and ε as

$$P_{cu} = P_{cu,opt} \varepsilon^\gamma \quad (10.14)$$

where

γ is a coefficient, the value of which is in the range of 1–3.

The value of γ can vary depending on the constraint (e.g. constant copper volume, constant wire section, or as a result of eddy current calculation). Equation (10.14) means that a 1% increase in the number of turns results in a $\gamma\%$ increase in copper losses. For example, for $\gamma=2$, a 1% increase of number of turns results in a 2% increase in copper losses.

Combining Equations (10.13) and (10.14) we can write

$$P_{tot} = \frac{P_{fe}}{\epsilon^\beta} + P_{cu,opt} \epsilon^\gamma \quad (10.15)$$

For the optimal design the total losses P_{tot} should be minimal for $\epsilon = 1$. The minimum of P_{tot} is obtained by taking the derivative with respect to ϵ and setting it equal to zero:

$$\frac{d}{d\epsilon}(P_{fe} + P_{cu}) = 0 \quad (10.16)$$

Solving Equation (10.16) gives

$$\frac{P_{fe,opt}}{P_{cu,opt}} = \frac{\gamma}{\beta} \epsilon^{\gamma+\beta} \quad (10.17)$$

Substitution of $\epsilon = 1$ into Equation (10.17) results in

$$\frac{P_{fe,opt}}{P_{cu,opt}} = \frac{\gamma}{\beta} \quad (10.18)$$

Compared to the total losses, the optimal core and copper losses in the general case are:

$$P_{fe,opt} = \frac{\gamma}{\gamma + \beta} P_{tot} \quad (10.19)$$

$$P_{cu,opt} = \frac{\beta}{\gamma + \beta} P_{tot} \quad (10.20)$$

10.3 Loss Minimization Without Eddy Current Losses

In these cases we assume low eddy current losses and neglect them.

10.3.1 Constant Copper Volume

Here we consider loss minimization in a constant copper volume condition and neglect eddy current losses. For the constant copper volume design, the

coefficient γ is $\gamma = 2$ because the wire length increases almost proportionally with ε and the wire cross section decreases proportionally with ε , which means that the ohmic copper losses increase with ε^2 . Accepting this value, we neglect the eddy current losses and the fact that only discrete values for the wire cross-section are possible. Then

$$P_{cu,opt} = \frac{\beta}{2 + \beta} \quad (10.21)$$

$$P_{fe,opt} = \frac{2}{2 + \beta} \quad (10.22)$$

Assuming quadratic dependence of the core losses on the peak induction, the value of the core losses coefficient is $\beta = 2$, and we find the solution of 50% core and 50% copper from the simplified approach.

For laminated, non-saturated iron, β is usually in the range of 1.6–2, so iron losses can be somewhat higher than 50%.

For most ferrites $\beta = 2\text{--}3$ which results in core losses lower than 50%.

10.3.2 Constant Wire Cross Section

Here we consider loss minimization in the constant wire-cross-section condition. We can use almost the same approach as in the previous section. For most of high frequency transformers and inductors the winding area is not completely filled, and one can change the wire length (the number of turns) without changing the diameter of the wire. These conditions correspond to a coefficient value of $\gamma = 1$. The substitution of this value into Equations (10.19) and (10.20) gives the following results:

$$P_{fe,opt} = \frac{1}{1 + \beta} P_{tot} \quad (10.23)$$

$$P_{cu,opt} = \frac{\beta}{1 + \beta} P_{tot} \quad (10.24)$$

In fact, $\gamma > 1$ as the average turn length increases with the number of turns, which results in an increased core loss optimum and a correspondingly decreased copper loss optimum.

For $\beta = 2$ we find the following optimal ratios: $P_{fe,opt} = P_{tot}/3$ and $P_{cu,opt} = 2P_{tot}/3$.

10.3.3 Equal Core and Copper Surface Temperatures

The condition in this case is one with equal core and copper surface temperatures. In this case, the thermal heat transfer between the core and the copper can be neglected. This approach allows a different temperature inside the copper winding (hot spot) than at the surface. The losses will

be proportional to the thermal conductance between the core or copper and the ambient air. We can write

$$T_{fe} = T_{cu}, \quad T_{fe} = P_{fe} R_{\theta,fe}, \quad T_{cu} = P_{cu} R_{\theta,cu} \quad (10.25)$$

$$P_{fe,opt} R_{\theta,fe} = P_{cu,opt} R_{\theta,cu} \quad (10.26)$$

$$P_{fe,opt} = \frac{R_{\theta,cu}}{R_{\theta,cu} + R_{\theta,fe}} P_{tot} \quad (10.27)$$

$$P_{cu,opt} = \frac{R_{\theta,fe}}{R_{\theta,cu} + R_{\theta,fe}} P_{tot} \quad (10.28)$$

In Equations (10.25), (10.26), (10.27), and (10.28) $R_{\theta,fe}$ and $R_{\theta,cu}$ are the core-to-ambient and copper-to-ambient thermal resistances, respectively.

With shell-type transformers based on EE or EI shapes, the core surface area is usually about two times that of the outer copper coil. If the radiation heat transfer coefficient h_R and the convection heat transfer coefficient h_c are similar, then about two times more core losses than copper losses results:

$$P_{fe,opt} \approx \frac{2}{3} P_{tot}, \quad P_{cu,opt} \approx \frac{1}{3} P_{tot} \quad (10.29)$$

Note that this ratio usually results in a maximum power transfer and not a loss minimization.

10.4 Loss Minimization Including Low-Frequency Eddy Current Losses

Almost all actual designs in power electronic converters are subjected to eddy currents. This is particularly true with frequencies above 20 kHz and AC currents of several amps. This fact results in a compromise between eddy current losses, ohmic losses, and core losses.

10.4.1 Constant Copper Wire Cross Section

The total losses in a magnetic component can be presented as

$$P_{tot} = P_{fe} + P_{cu,ohm} + P_{cu,eddy} \quad (10.30)$$

where $P_{cu,ohm}$ are the copper losses, which would not be present if the copper losses were only caused by the DC resistance. At a constant diameter, $P_{cu,ohm} \sim \epsilon$, an increase in ϵ leads to an almost proportional increase in the wire length. Here we neglect the increase in the mean length of turn.

The low-frequency eddy current losses $P_{cu,eddy}$ are estimated to be proportional to the number of turns and proportional to the square of the total MMF, which is also proportional to the number of turns [4,5]. As a result, a cubic dependence of $P_{cu,eddy}$ on ε is assumed: $P_{cu,eddy} \sim \varepsilon^3$. This dependence is true in low-frequency approximation (LF) of eddy-current phenomenon. For a more detailed discussion of low-frequency approximation please refer to Chapter 5. The low-frequency model for eddy current losses that we use there satisfies the purpose of this chapter. The approximation is applicable if the general field has not changed significantly by increasing the number of turns (for example, the change from one to two layers leads to a significant change in the field). Using the above considerations and the core loss equation, we obtain the dependence of P_{tot} on ε

$$P_{tot} = \frac{P_{fe}}{\varepsilon^\beta} + P_{cu,ohm} \varepsilon + P_{cu,eddy} \varepsilon^3 \quad (10.31)$$

Taking the derivative of P_{tot} with respect to ε , setting it to zero, and substituting $\varepsilon = 1$, which corresponds to the minimum for $\varepsilon = 1$, yields the following expression:

$$P_{fe} = \frac{P_{cu,ohm} + 3P_{cu,eddy}}{\beta} \quad (10.32)$$

From Equation (10.32) it follows that a high eddy current loss tends to decrease the copper-to-core loss ratio.

REMARK

If the diameter is optimized (so not a constant copper cross section), the wire cross section is usually selected to perform the equation:

$$P_{cu,eddy} = \frac{P_{cu,ohm}}{2} \quad (10.33)$$

Combining Equations (10.31), (10.32), and (10.33) results in the following representation of the optimal losses as parts of the total loss:

$$P_{fe,opt} = \frac{5}{5+3\beta} P_{tot} \quad (10.34)$$

$$P_{eddy,opt} = \frac{\beta}{5+3\beta} P_{tot} \quad (10.35)$$

$$P_{ohm,opt} = \frac{2\beta}{5+3\beta} P_{tot} \quad (10.36)$$

Assuming $\beta = 2$, leads to the following optimal copper/core ratio in this case:

$$P_{fe,opt} = \frac{5}{11} P_{tot}, \quad P_{ohm,opt} = \frac{4}{11} P_{tot}, \quad P_{eddy,opt} = \frac{2}{11} P_{tot} \quad (10.37)$$

10.4.2 Constant Copper Wire Volume

The case is quite similar to the previously discussed case. As was mentioned above, the low frequency eddy current losses $P_{cu,eddy}$ are proportional to the third power of ε in the constant-wire-cross-section case. In the discussed case there is additional dependence. Increasing the number of turns leads to a decrease in the wire cross section and, correspondingly, to a decrease in $P_{cu,eddy}$ squared, because the low-frequency eddy current losses are proportional to the square of the wire cross-sectional area. Finally, the low-frequency eddy current losses $P_{cu,eddy}$ in this case are proportional to ε .

The ohmic losses $P_{cu,ohm}$ are proportional to the square of ε in this case because increasing the number of turns leads to an increase in the copper wire length and to a decrease in the copper wire cross-sectional area. Using the expression for the dependence of the core losses on ε , the total losses can be represented as

$$P_{tot} = \frac{P_{fe}}{\varepsilon\beta} + P_{cu,ohm} \varepsilon^2 + P_{cu,eddy} \varepsilon \quad (10.38)$$

Differentiation of P_{tot} with respect to ε and substitution of $\varepsilon = 1$ result in:

$$P_{fe} = \frac{2P_{cu,ohm} + P_{cu,eddy}}{\beta} P_{tot} \quad (10.39)$$

REMARK

Using Equation (10.39) and assuming that the diameter is optimized, e.g., $P_{cu,eddy} = P_{cu,ohm}/2$, the optimal losses are found as

$$P_{fe,opt} = \frac{5}{5+3\beta} P_{tot} \quad (10.40)$$

$$P_{eddy,opt} = \frac{\beta}{5+3\beta} P_{tot} \quad (10.41)$$

$$P_{ohm,opt} = \frac{2\beta}{5+3\beta} P_{tot} \quad (10.42)$$

Considering $\beta = 2$, the optimal copper-to-core ratio in this case can be represented as

$$P_{fe,opt} = \frac{5}{11} P_{tot}, \quad P_{ohm,opt} = \frac{4}{11} P_{tot}, \quad P_{eddy,opt} = \frac{2}{11} P_{tot} \quad (10.43)$$

10.4.3 Variable Wire Cross Section and Number of Turns

As the eddy current losses increase with the conductor cross section, an optimal section can be found that *does not fill the copper winding area*, so both the number of turns and the copper cross section can be chosen.

We introduce a relative section area $\zeta = S_{new}/S_{old}$, S is the wire cross-sectional area [m²]. As was mentioned above, the low-frequency eddy current losses $P_{cu,eddy}$ are proportional to the number of turns and proportional to the square of the total MMF. Hence, in this case $P_{cu,eddy}$ are proportional to the third power of ε . Using Equation (10.13) and the mentioned dependencies, the total losses can be represented as

$$P_{tot}(\varepsilon) = \frac{P_{fe}}{\varepsilon^\beta} + P_{cu,ohm} \frac{\varepsilon}{\zeta} + P_{cu,eddy} \varepsilon^3 \zeta^2 \quad (10.44)$$

Differentiation of P_{tot} with respect to ε and ζ gives

$$dP_{tot} = \frac{\partial P_{tot}}{\partial \varepsilon} d\varepsilon + \frac{\partial P_{tot}}{\partial \zeta} d\zeta \quad (10.45)$$

$$dP_{tot} = \left(-\beta \frac{P_{fe}}{\varepsilon^{\beta+1}} + \frac{P_{cu,ohm}}{\zeta} + 3\varepsilon^2 \frac{P_{cu,eddy}}{\zeta^2} \right) d\varepsilon + \left(-\frac{P_{cu,ohm}}{\zeta^2} + 2\varepsilon^3 \zeta P_{cu,eddy} \right) d\zeta \quad (10.46)$$

Substituting $\varepsilon = 1$, $\zeta = 1$ and setting $\frac{\partial P_{tot}}{\partial \varepsilon}$ to zero yields

$$P_{fe} = \frac{P_{cu,ohm} + 3P_{cu,eddy}}{\beta} \quad (10.47)$$

Substituting $\varepsilon = 1$ and $\zeta = 1$ and setting $\frac{\partial P_{tot}}{\partial \zeta}$ to zero gives

$$P_{cu,eddy} = \frac{P_{cu,ohm}}{2} \quad (10.48)$$

By using Equations (10.47) and (10.48), the optimal losses in this case are found as

$$P_{fe,opt} = \frac{5}{5+3\beta} P_{tot} \quad (10.49)$$

$$P_{eddy,opt} = \frac{\beta}{5+3\beta} P_{tot} \quad (10.50)$$

$$P_{ohm,opt} = \frac{2\beta}{5+3\beta} P_{tot} \quad (10.51)$$

In the typical case, when $\beta = 2$, the optimal losses are

$$P_{fe,opt} = \frac{5}{11} P_{tot}, \quad P_{ohm,opt} = \frac{4}{11} P_{tot}, \quad P_{eddy,opt} = \frac{2}{11} P_{tot} \quad (10.52)$$

Equation (10.52) gives the same results as the remarks in the two previous subsections give.

10.4.4 More General Problems with Eddy Currents

In the previous sections, a low-frequency approximation is used for the eddy current losses. The low-frequency approximation tends to over-estimate the losses at high frequency. If the dependency of copper losses on the diameter is known and can be approximated by equations in a way similar to Equations (10.13) and (10.14), then Equations (10.17) to (10.20) are still valid. This usually results in higher eddy current parts than in Equation (10.50), especially for round wires. For a high-frequency design with a limited penetration depth, a wire diameter increase is often beneficial. In the case of rectangular wire sections, lower optimal eddy current parts are observed [5].

10.5 Summary

This chapter presents a survey concerning the optimal copper-to-core loss ratio in magnetic components for power electronics. The proposed results provide a minimal loss design for the most frequently appearing cases. The optimization process includes adjusting the turn numbers and copper wire cross-sectional area. The obtained results concerning the optimal copper-to-core loss ratio are summarized in Tables 10.1 and 10.2.

TABLE 10.1

Optimal Core and Copper Losses for Different Cases, Constant Core Shape, Variable Number of Turns

	$P_{fe,opt}/P_{tot}$	$P_{cu\ ohm,opt}/P_{tot}$	$P_{cu\ eddy,opt}/P_{tot}$
General case	$\frac{\gamma}{\gamma + \beta}$		$\frac{\beta}{\gamma + \beta}$
Constant copper volume $\gamma = 2$	$\frac{2}{2 + \beta}$		$\frac{\beta}{2 + \beta}$
Constant wire cross area $\gamma = 1$	$\frac{1}{1 + \beta}$		$\frac{\beta}{(1 + \beta)}$
Equal core and copper temperature	$\frac{R_{\theta,cu}}{R_{\theta,cu} + R_{\theta,fe}}$		$\frac{R_{\theta,fe}}{R_{\theta,cu} + R_{\theta,fe}}$
Variable wire cross section, including low frequency eddy current approach	$\frac{5}{5 + 3\beta}$	$\frac{2\beta}{5 + 3\beta}$	$\frac{\beta}{5 + 3\beta}$

TABLE 10.2

Optimal Core and Copper Losses for Special Cases, $\beta = 2$, Constant Core Shape, Variable Number of Turns

	$P_{fe,opt}/P_{tot}$	$P_{cu\ ohm,opt}/P_{tot}$	$P_{cu\ eddy,opt}/P_{tot}$
Constant copper volume $\gamma = 2$	1/2	1/2	0
Constant wire cross area, $\gamma = 1$	1/3	2/3	0
Equal core and copper temperature, core surface equal to 2 times open coil surface	2/3		1/3
Variable wire cross area, including a low frequency eddy current approach	5/11	4/11	2/11

10.6 Examples

1. A 50 Hz single-phase transformer of 3 kW has 94 W core losses and 47 W copper losses at full load. Saturation is not taken into account. Assume the copper volume to be constant and the wire diameter to be variable. The core losses are assumed to be quadratic with the voltage per turn. How much should one decrease or increase the number of turns to obtain maximum efficiency at full load? What are the new losses?

SOLUTION

$\beta = 2$ and using Equation (10.8) we find $\varepsilon = \sqrt[4]{94/47} = 1.189$. The new number of turns $N_{new} = 1.19 N_{old}$. The new core losses and also the new copper losses are 66.5 W, and the total losses are 133 W, compared to the 141 W originally.

REMARK

One should verify whether the additional copper heat could be removed.

2. In the data sheets for ferrite cores, one can see that the losses (3F3 grade) increase with $B^{2.5}$. What is the optimal copper-to-core loss ratio for maximum efficiency if eddy current losses can be neglected and copper volume is constant?

SOLUTION

This is the case described in Section 10.3.1. Using Table 10.1, we find that the optimal copper-to-core loss ratio for maximum efficiency is $P_{cu\ ohm,opt}/P_{fe,opt} = \beta/2 = 1.25$.

3. The same question as in Example 2, but with constant copper diameter.

SOLUTION

This is the case described in Section 10.3.2. Using the [Table 10.1](#), we find that the optimal copper-to-core loss ratio for maximum efficiency in that case is $P_{cu, opt} / P_{fe, opt} = \beta = 2.5$.

4. An EE42 core has a copper surface-to-ambient thermal resistance of 50 K/W and a ferrite-to-ambient thermal resistance of 20 K/W. What are the maximum copper and core losses it can tolerate if the surface temperature of the copper and the core is kept at 100°C and the ambient temperature is 50°C?

SOLUTION

This is the case described in Section 10.3.3. The total allowed losses are

$$P_{fe} = \frac{T_{fe}}{R_{\theta, fe}} = \frac{100 - 50}{20} = 2.5 \text{ W}, \quad P_{cu} = \frac{T_{cu}}{R_{\theta, cu}} = \frac{100 - 50}{50} = 1 \text{ W},$$

$$P_{tot} = P_{fe} + P_{cu} = 3.5 \text{ W}.$$

By comparison, if we do not know the thermal resistances we use Equations (10.27) and (10.28), and we obtain: $P_{fe, opt} \cong \frac{2P_{tot}}{3} = 2.33 \text{ W}$ and $P_{cu, opt} \cong P_{tot}/3 = 2.33$, which is close to the found result.

References

- [1] Apeldoorn, O. and Kriegel, K., Optimal design of =tTransformers for high-power high-frequency applications, EPE 95, Sevilla, Spain, September 19–21, 1995.
- [2] Snelling, E. C., *Soft Ferrites, Properties and Applications*, 2nd ed., Illiffe Books, London, 1988.
- [3] McLyman, W.T., *Transformer and Inductor Design Handbook*, 2nd ed., Marcel Dekker, New York, 1988.
- [4] Dowell, P.L., Effects of eddy currents in transformer windings, IEE Proceedings B, 113:8, 1387–1394, 1966.
- [5] Lameraner, J. and Staffl, M., *Eddy Currents*, Illiffe Books, London, 1966, pp. 105–160.

11

Measurements

“Measurement is not only a technique but also an art”

Plato (428-347 B.C.) was already describing “the art of measurement” (From “Protagoras” [380 B.C.]):

“Now suppose happiness to consist in doing and choosing the greater, in not doing or in avoiding the less, what would be the saving principle of our life? Would it not be in *the art of measuring*; or the power of appearance? Is not the latter deceiving us, interpreting things in many ways, regretting our actions and choices relative to of things great and small? But *the art of measurement* would remove the effect of appearances, and, showing the truth, would procure rest to our soul based on truth and would thus save the happiness of our life. Would not mankind generally acknowledge that the art which accomplishes this result is *the art of measurement*?”

11.1 Introduction

This chapter treats the measurements on inductors and transformers. Measurements in high frequency are discussed, as they are the main item in magnetic components for power electronics.

Even if the design of a component is carried out carefully, measurements should be made to check it. Measurements can also be simply imposed by standards. One should be aware of the fact that measurements are always limited in accuracy and that the act of measuring does disturb the measured quantity. When magnetic components are measured in real converters, voltage slopes and high frequency fields can perturb the measurements.

We consider measurement of temperature, power loss, impedance, inductance, and parasitic capacitance.

11.2 Temperature Measurements

Temperature measurements can be made to check the design. The place of the expected hot spot temperature (the hottest point of the component) is also a point of discussion. In some converters limitations of the hot spot temperature results in a compromise with electrical insulation requirements. Indeed, increasing the electrical insulation leads to a worse thermal conduction.

Temperature Conversion Equations

The equation for conversion from Fahrenheit to Celsius is

$$^{\circ}\text{C} = (F - 32) \times 5/9 \quad (11.1)$$

where

$^{\circ}\text{C}$ is the temperature in Celsius degrees

F is the temperature in Fahrenheit degrees.

The Celsius–Kelvin (absolute temperature scale) conversion is

$$^{\circ}\text{C} = K - 273.15, \quad 273.15K = 0^{\circ}\text{C} \quad (11.2)$$

where

K is the temperature in Kelvin degrees.

The usual possibilities for temperature measurements in magnetic components are:

- Thermocouple measurement
- Thermistor measurements
- NTC thermistor measurement
- Glass fiber optic measurement
- Infrared surface temperature measurement
- Thermal paint and strips
- Winding resistance measurement.

11.2.1 Thermocouple Measurement

Seebeck discovered the principle that some voltage arises at the end of two wires when junctions of different materials are at different temperatures. This principle is used in thermocouples. Thermocouples are mechanically and thermally robust and are not subjected to self-heating. The temperature range of a thermocouple is more than large enough for most common applications: -200°C to $+1250^{\circ}\text{C}$. The thermocouples however, use a very low voltage and are subjected to disturbances of the power converter. Thus, the measured values are sometimes not valid during operation of the converter. The accuracy of the measurement can be reduced because the thermocouples could be heated up by eddy currents, and also because they can be cooled down by their own wires.

The most common thermocouple is the K-type: Nickel/Chromium (+) combined with Nickel/Aluminum (-), also known as chrome-constantan, or “yellow type.” According to the international code, the negative (nonmagnetic) wire has the yellow color, the positive (magnetic) wire is red, and the cover is brown. The voltage change is about 40 $\mu\text{V}/^\circ\text{C}$, so an amplifier is necessary. Using an appropriate amplifier avoids the need of a reference temperature.

Data for thermocouples are available in the standard EN60584-1 [1] (formerly IEC 584-1).

The initial accuracy of thermocouples is not high, about 2.5 $^\circ\text{C}$ for the K type, 0.5 $^\circ\text{C}$ for J type. However the inaccuracy is mainly a temperature offset, which can be taken into account. The advantage of thermocouples is the cheap basic material. However, the low voltage output limits their use for measurements in magnetic components.

11.2.2 PT100 Thermistor Temperature Measurement

Thermistors are devices widely applicable to measure temperature.

As an example, we consider frequently used Pt100 thermistors. For the temperature dependence of the resistance of industrial Pt100 thermistors, the following approximation can be made according to EN60751 (formerly IEC 751):

$$R_{pt} = 100 \times \left(1 + 3.90830 \times 10^{-3} \times T - 5.775 \times 10^{-7} \times T^2 \right) \quad (11.3)$$

where

R_{pt} is the resistance value in [Ω];

T is the temperature in [$^\circ\text{C}$].

Equation (11.3) shows about 0.39% resistance change for 1 $^\circ\text{C}$.

The Pt100 resistance thermometer is divided into two accuracy classes:

- Class A: $(0.15 + 0.002 |T|)$ $^\circ\text{C}$; the temperature T is in [$^\circ\text{C}$];
- Class B: $(0.30 + 0.005 |T|)$ $^\circ\text{C}$; the temperature T is in [$^\circ\text{C}$].

Often bridge configurations are used to convert the resistance to voltage. The resistance of the Pt100 thermistors is low and the relative voltage change is not high. Therefore the Pt100 thermistors are used in a four-wire measurement or in a three-wire system. The four-wire measurement has two current contacts and two voltage contacts. The three-wire measurement assumes the voltage drop in the two current wires to be equal.

In the range of 0–200 $^\circ\text{C}$, the reverse equation, which gives the temperature as a function of the resistance, is

$$T = 0.00109 \times (R - 100)^2 + 2.5543 \times (R - 100) \quad (11.4)$$

where

R is in [Ω] and T is in [$^\circ\text{C}$].

The reverse equation fits the original one, Equation (11.3), to better than 0.05°C in the range of $0\text{--}200^{\circ}\text{C}$.

The Pt100 thermistors are accurate devices, but they suffer the same drawback of all thermistors, that of using low voltages. Another drawback is the use of more than two wires. Self-heating, and cooling by its own wires, can also create inaccuracy. Therefore Pt100 thermistors are not very suitable for measuring in actual power devices and in magnetic components.

11.2.3 NTC Thermistor Temperature Measurement

The negative temperature coefficient resistors (NTC) consist of polycrystalline mixed oxide ceramic. The typical NTC resistance change is about -3.3 to -5.7% per 1 K, which gives a good sensitivity. Their usual range of use is -80°C to $+250^{\circ}\text{C}$, best between 0 and 105°C .

The resistance of an NTC can be approximated by the following equation:

$$R_T = R_{T_r} e^{B\left(\frac{1}{T} - \frac{1}{T_r}\right)} \quad (11.5)$$

where

T is the temperature in [K], ($0^{\circ}\text{C} = 273.15$ K)

T_r is the reference temperature in [K]

R_T is the resistance at the temperature T

R_{T_r} is the resistance at the temperature T_r

B is a constant dependent on form and material; B is in the range $2900\text{--}5000$ K.

Table 11.1 presents the ratio R/R_{25} given by manufacturer data and the same ratio obtained by Equation (11.5). From Table 11.1, it is seen that by using Equation (11.5) a quite feasible temperature accuracy is obtained in the whole considered range of -20°C to 105°C .

The accuracy of NTC thermistors is high, about $0.2\text{--}0.5^{\circ}\text{C}$. But care should be taken to use the correct data of the manufacturer, the parameter B and the reference temperature; and to use a notion of the self-heating (the order of magnitude is about 1 K/mW).

Note that PTC thermistors also exist, but they are mainly intended for protection, as their resistance changes more than 10 times in a few degrees at the 'switching' temperature, which is usually above 100°C .

PN-junctions could also be used for temperature measurement. This idea is not fantastic, due to the large EMC disturbances in the magnetic components; the PN junctions are prone to rectify such signals.

11.2.4 Glass Fiber Optic Temperature Measurement

The advantages of glass fiber optic temperature measurement are that glass fiber is not heated by eddy currents and that the heat conduction of glass is low. However, the probes may be too expensive to be simply glued inside the component.

TABLE 11.1

Typical NTC Thermistor Data, Compared to the Equation (11.5). Data Used is for Thermometric 10 K Ω NTC Type JR; $R_{25} = 10$ k Ω , 5%; the Value of B in the Range 25–85°C is 3977 K+/- 0.75%

T [°C]	R/R_{25} From manufacture data	R/R_{25} Obtained by (11.5)
-20	9.6807	10.709
-10	5.5253	5.895
0	3.2640	3.390
10	1.9902	2.027
20	1.2493	1.255
25	1	1
30	0.8056	0.80251
40	0.5325	0.52785
50	0.3601	0.35631
60	0.2487	0.24626
70	0.1751	0.17391
80	0.1256	0.12525
90	0.9155	0.09186
100	0.6781	0.06849
105	0.05868	0.05949

11.2.5 Infrared Surface Temperature Measurement

This technique is quite easy to use. It is important to have surfaces with an infrared emission coefficient close to 1 (paint or enamel can be sufficient). An overestimation of the emission coefficient leads to an underestimated measured temperature. Windings should be accessible directly without insulation foil. The insulation itself gives an additional thermal resistance (insulation) because of the air, so the insulation surface temperature has an intermediate temperature, which is lower than the copper surface temperature.

11.2.6 Thermal Paint and Strips

Thermal strips and paint are quite useful, if the measurement place is visible. The thermal strips can have the problem of thermal contact on wires. Permanent or reversible grades can be used in practice.

11.2.7 Winding Resistance Measurement Method

In general, this technique is quite reliable when good low-resistance measurement equipment is used. For a copper winding, according to IEC950, the temperature rise is calculated as

$$\Delta T = \frac{(R_2 - R_1)(234,5 + T_1)}{R_1} - (T_2 - T_1) \quad (11.6)$$

where T_1 is the starting temperature at the beginning of the experiment and T_2 is the end temperature, both in [K].

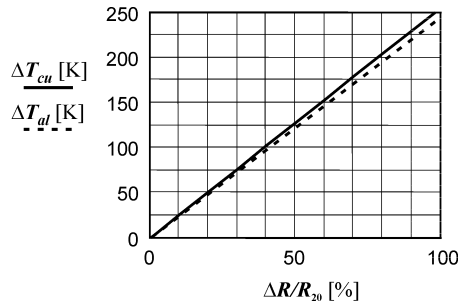


FIGURE 11.1

Average temperature rise ΔT for copper and aluminum as a function of the percentage change of the resistance ΔR . The starting temperature $T_1 = 20^\circ\text{C}$, $\Delta T = T_2 - T_1$.

The corresponding equation for aluminum conductors is

$$\Delta T = \frac{(R_2 - R_1)(225 + T_1)}{R_1} - (T_2 - T_1) \quad (11.7)$$

Figure 11.1 shows the average temperature rise as a function of the percentage change of the resistance for copper and aluminum, starting from $T_1 = 20^\circ\text{C}$, in accordance with Equations (11.6) and (11.7).

11.3 Power Losses Measurements

11.3.1 Circuit Wattmeter Measurement

In principle, the losses of power electronic components can be measured using wattmeters that have a sufficient bandwidth. The voltages in converters contain slopes up to 20 V/ns, which can reduce the accuracy of wattmeters by parasitic mass currents and by capacitive couplings. The accuracy is also limited due to the fact that two similar values, i.e., the input and the output power of a transformer, are subtracted. For example, assume 99% efficiency of a transformer. Then, even using a wattmeter with an accuracy of 0.2% results in a losses measurement accuracy of only about 40%.

A practical problem is also that the prolongation of the wires leading to a transformer is not allowed, due to the risk of damaging the circuit as the parasitic inductance increases and the semiconductors may be damaged by peak voltages or by shifted resonance frequencies. Also the number of connections can make the circuit impractical, and one needs a multiple-channel wattmeter to measure multiple-output transformers in power supplies and fluorescent lamp converters.

In some circuits a *no load* or *short circuit* test on a transformer can be performed. In that case the losses are equal to all the input power. Usually, the power factor for those tests is not very low, so reasonable wattmeter measurements can be expected.

To measure *inductor* losses, usually the leads can be prolonged without causing trouble for the circuit. However, the value of $\tan\delta$ may be so low that high-performance equipment should be used. In any case, at high frequencies and low $\tan\delta$ the measurements are not easy.

11.3.2 Oscilloscope Measurements

The wattmeter principle can also be implemented with digital oscilloscopes. However, the problem of accurate phase measurement remains. The oscilloscope channels could be calibrated to phase differences as low as 1 ns [2]. However, the necessary current and voltage transducers will introduce additional errors. One possibility to check the equipment is to measure low $\tan\delta$ capacitors down to about $\tan\delta = 0.03\%$. This $\tan\delta$ value is lower than $\tan\delta$ values achievable by inductors. The losses of the capacitor can be verified by calorimetric measurement.

11.3.1.1 Example of the Accuracy Problem in Oscilloscope Measurement

A coil of 400 VA operates at 500 kHz AC and the estimated power losses are 4 W. One wants to measure the losses with an accuracy of 0.4 W, which is 10% of the losses. The angle accuracy necessary for this accuracy is 0.001 rad. At that frequency, this value corresponds to a time accuracy of 318 picoseconds ($\frac{2\mu\text{s}}{2\pi \times 10^3} = 318\text{ps}$). That time corresponds to the delay of a less than 10 cm long transmission line (cable or leads)! The voltage and current transducers can also cause an additional part of the accuracy problem.

11.3.2 Impedance Analyzers and RLC Meters

11.3.2.1 Impedance Analyzers

For inductors, the power loss could be estimated using the expression

$$P_{\text{loss}} = \omega L \tan(\delta) I_{\text{rms}}^2 \quad (11.8)$$

where

I_{rms} is the RMS value of the inductor current.

The problem there is to have accurate measurements of the loss angle δ . Instruments that achieve high loss angle measurement accuracy combined with high frequencies are *impedance analyzers* [3]. To obtain a high accuracy measurement at low impedance, the impedance analyzers use a four-wire system. The angle error is basically an error on the voltage vector. Between 1 kHz and 1 MHz, an accuracy of 0.1% can be achieved in measuring $\tan\delta$ for impedance values between 10 Ω and 100 k Ω [4]. At frequencies higher than 1 MHz, the impedance magnitude is still good, but the angle accuracy is reduced.

The excitation voltage and current of the basic instruments (impedance analyzers) are up to 1 V, or 20 mA. If additional amplifiers and current probes are used, one can test at some actual power level, but the angle accuracy is much lower [3]. For low impedances, a four-wire measurement is advisable.

Impedance analyzers are mainly intended to give a graphical output and are useful tools to check series or parallel resonance frequencies.

11.3.2.2 RLC Meters

The RLC meters use quite similar concepts, but they test usually at discrete frequencies. The simple versions use, e.g., 1 kHz test frequency. The more sophisticated modifications have different frequencies, even beyond 1 MHz. Some RLC meters use high voltage or currents. RLC meters are mainly intended for measuring parameter deviations at given frequencies.

Low-cost RLC meters use frequencies of 1 kHz and 120 Hz. They give a first indication of the inductance and dissipation factor. However, as the frequency is low, the usual eddy current losses are not measured. Also, care should be taken in short circuit tests, as the magnetizing reactance L_m can be of the same order of magnitude as the secondary resistance R_s .

Impedance testers and RLC meters do not test at actual high power and induction levels. Their accuracy is good for linear effects such as eddy currents, but they are not accurate enough concerning core losses, as the losses are not quadratic with the induction B .

11.3.3 Q-factor Test of LC Networks

In the Q-factor test an inductor or a transformer is connected in parallel to a low loss capacitor. The frequency is set at the resonance point where current and voltage are in phase. The multiplication of the RMS current and voltage of the fundamental harmonic gives the power absorbed by the LC circuit.

$$P_{loss} = I_{LC} V_{LC} - P_{C,loss} \quad (11.9)$$

where

P_{loss} are the losses of the magnetic component

I_{LC}, V_{LC} are the RMS values of the fundamental component of the current and the voltage to the LC circuit

$P_{loss,C}$ are the losses of the capacitor.

Practically, a few problems arise in Q-factor tests:

- The losses can only be measured for sine waves.
- The resonance frequency may differ from the actually used frequency.
- The losses of the capacitor may not be well known.

- The resonance frequency may shift due to saturation of the component.
- An amplifier or an additional circuit is necessary to excite the LC circuit at the right inductance or voltage level.
- The test might be sensitive to contact and lead losses.

The inductance can also be measured by using the resonance frequency. However, the lead inductance and the parasitic inductance of the capacitors used in the test should be taken into account.

11.3.4 Power Loss Estimation by Thermal Resistance

If one knows the thermal resistance of the magnetic component and the temperature rise, one can estimate the power losses:

$$P_{\text{loss}} = \frac{\Delta T}{\mathfrak{R}_{\theta}} \quad (11.10)$$

where

ΔT is the temperature difference

\mathfrak{R}_{θ} is the thermal resistance.

The practical problems when applying this loss estimation method are the following:

1. The thermal resistance of the component is usually not known accurately, as the convection heat transfer is dependent on a lot of details.
2. The practical temperature difference is dependent on the point where it is measured and the principle of the temperature measurement.
3. The thermal resistance is dependent on the temperature difference across the component.

However, this method can be valuable for comparing different components with about the same shape and size, such as cores with different ferrite grades, in one and the same construction of a magnetic component.

11.3.5 Calorimetric Power Loss Measurement

The efficiency of power electronic converters continuously increases. Measurement methods, which tend to measure the dissipated heat directly, are among the most accurate means to measure losses. The calorimetric method is well suited for inductors and for entire power circuits. Measuring transformers may have the problem that the wires cannot be prolonged in the real circuit. Even if this is the case, a separate circuit could be built to test transformers at similar voltage and current waveforms. Instruments that

measure heat losses directly are called calorimeters. There are two kinds of calorimeters:

- Inertia calorimeters, in which the heat content and the thermal resistance are used to find the losses.
- Flow calorimeters, in which a fluid flow is used.

11.3.5.1 Inertia Calorimeter

The *inertia calorimeter* is well known and used, e.g., for material research in chemistry and physics, where samples are quite homogeneous in nature and have good thermal conductance. The total energy of a phenomenon is calculated and compensated for the heat losses through the thermal insulation. The losses in the measured component are

$$P_{\text{loss}} = \frac{\Delta T}{\mathfrak{R}_{\theta}} + \left(\sum_i M_i c_{p,i} \right) \frac{dT}{dt} \quad (11.11)$$

where

ΔT is the temperature difference inside-outside the calorimeter

\mathfrak{R}_{θ} is the thermal resistance inside-outside the calorimeter

M_i are the different masses in the system: the component (core, copper, insulation) and inner materials of the calorimeter

$c_{p,i}$ is the specific heat capacity of the different masses in the system.

The inertia calorimeter has a few drawbacks. Normally, the heat capacity of the device under test (d.u.t.) has to be known or must be low. The principle is not suited for devices with multiple masses with long internal thermal time constants.

- In a *simple closed system* the component is put in a thermally insulated box with a fan inside to homogenize the temperature [6]. The box is calibrated with a resistor as a known heat source. One has to take into account the mechanical power of the fan. After some time corresponding to the thermal time constants, the temperature difference with the environment is measured and the dissipated power can be calculated. The drawbacks of the system are the following:
 - The long settle time, as the time constant is determined by the total thermal inertia and the thermal resistance of the box.
 - The accuracy is limited by the accuracy of the thermal resistance of the box, which is dependent on the airflow in the room.
- An *improved system* uses vacuum insulation and infrared reflection. Still there is some heat drain by the wires. This system is often used to test the components at high ambient temperature,

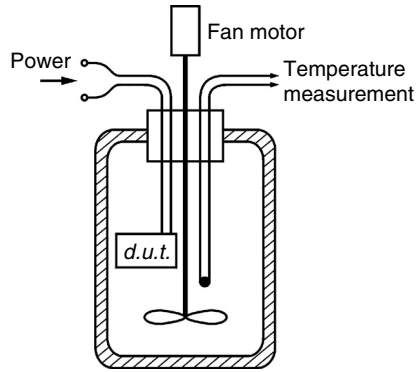


FIGURE 11.2
Inertia calorimeter principle with vacuum insulation.

such as 100°C. The system includes a vacuum-insulated, infrared-reflecting bottle, the device under test, power wires, and a fan (see Fig. 11.2).

- More *sophisticated closed systems* use copper enclosures and water jackets together with multiple temperature measurements [6].

11.3.5.2 Flow Calorimeter

11.3.5.2.1 Principle of Operation

In a flow calorimeter, the device under test is thermally insulated from the environment but cooled with a mass flow of a cooling fluid. This principle has the advantage of reducing the settling time constant of the system. Moreover, there are no fan mechanical losses inside the test chamber. At steady state, the heat loss of the device under test is the product of the mass flow of the cooling fluid, the temperature rise of the cooling fluid, and the specific heat capacity of the cooling fluid:

$$P_{\text{loss}} = m c_p \Delta T \quad (11.12)$$

where

m is the mass flow of cooling fluid (e.g., air)

c_p is the specific thermal capacity at constant temperature: for air

$c_p = 1.0090 \text{ kJ/kg} \times ^\circ\text{C}$ at 300 K; for water $c_p = 4.186 \text{ kJ/kg} \times ^\circ\text{C}$ at 289 K;

$\Delta T = T_2 - T_1$, T_1 is temperature before the device under test; T_2 is temperature after the device under test.

Very diverse implementations of this principle can be realized.

11.3.5.2.2 Accuracy of Flow Calorimeters

The accuracy of a flow calorimeter is dependent on construction, measurement details, and calibration.

1. Thermal insulation of the test room.

The losses through insulation should be low, compared to the losses of the device under test. In fact, it is sufficient if the variation of the insulation resistance is low, as the test system can be calibrated for these known losses.

2. The temperature measurement.

In practice, the temperature measurement should not be influenced by electromagnetic disturbances of the equipment under test, which may not be screened. The temperature measurements should measure the average temperature of the air. The measuring equipment should also be insensitive to the radiation heat transfer of the device under test. The temperature of the environment should be quite stable. Heat sources from outside should be avoided such as direct or indirect sunlight.

3. The settling time.

Usually a settling time of about 3 to 6 thermal time constants of d.u.t. is necessary for large variations of the dissipated power of the tested component. A typical time constant of a magnetic component is about 20 minutes, which results in about 1 to 2 hours settling time.

4. Calibration.

The final accuracy of the calorimeter is obtained by calibration with a known power by means of a resistor powered in DC. Different powers and positions in the test room have to be tested.

5. Computer modeling.

The calorimetric measurement gets more accurate if at the same time appropriate computer modeling is done.

11.3.5.2.3 *Practical Flow Calorimeter*

Here we describe a system that is based on an open air-cooled circuit, typically made for testing power electronic equipment and magnetic devices [7]. The system is sufficiently large in order to contain full converters or large components, but the same principle can be redesigned for small-scale systems as well. The temperature measurements and the heating resistor for the flow stabilization are located in a labyrinth path (see Fig. 11.3). This labyrinth structure improves the mixing of the air in order to measure average temperatures and to hide the sensors from infrared light coming from the device under test or the heating resistor. The fan is a brushless DC type, which is easy to control by the input voltage. The mass flow is stabilized by the controlled fan while maintaining a constant 5 K temperature rise between T_4 and T_3 for 200 W power of the heating resistor. At the inlet, a stack of iron sheets is used to make a thermal low pass filter to reduce the micro temperature changes, which usually are present in rooms.

Two NTC resistors in series are used for each temperature measurement to have a more uniform measurement. A circuit is made to linearize the

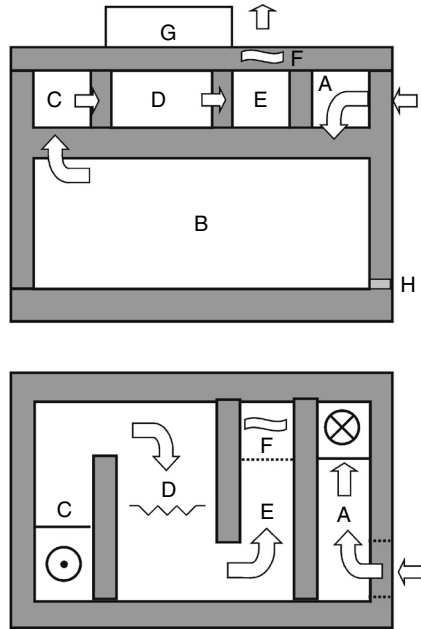


FIGURE 11.3

Front and top cross-section view of a calorimeter for loss measurements up to 600 W. The dimensions of the inner side of the test room are 704 mm × 420 mm by 312 mm high. The polyurethane insulating foam has 48 mm thickness with thermal resistance about 1.1 K/W.

a) flow calorimeter, side cross-sectional view.

A: air inlet, temperature T1

B: room for device under test

C: place for measuring the temperature T2 = T3

D: heating resistor

E: place for measuring the temperature T4

F: regulated fan

G: control circuit

H: wire feed through

b) Flow calorimeter, top view, cover removed.

measurement of the characteristic. An accurate mass flow control is obtained by heating the airflow a second time with a constant power and keeping the temperature rise constant. Significant heat conduction through wires and false inlet air must be avoided. In the arrangement there is no accuracy loss if some false inlet air (e.g., the cable feed-through point) has the same temperature as the actual air inlet.

If the heat losses are neglected and the c_p of air is assumed constant, the power losses of the device under test is

$$P_{loss} = \frac{200(T_2 - T_1)}{T_4 - T_3} \quad (11.13)$$

Tests with the proposed calorimeter show an absolute error better than 0.5% of the full power 600 W and a relative error better than 3% of the measured power.

11.3.5.2.4 Conclusions

The flow calorimetric principle is well applicable to test magnetic components at ambient temperatures, but it is not suitable for high temperature component tests. It can be used to test full converters as most of the electronic equipment is made to withstand at least 40°C. With a laboratory temperature of 25°C, a temperature rise of 15°C can be used for the tests.

11.4 Measurement of Inductances

11.4.1 Measurement of the Inductance of an Inductor

The inductance can be measured by checking the impedance for a given frequency. Accurate RLC meters measure the real and imaginary part of the impedance for a given frequency. So, they measure in fact the R - L series equivalent network. The core losses, which are conventionally represented as a resistor in parallel to the inductance L , are in that way converted in an additional series resistor, which is added to the wire DC resistance. Eddy current losses caused by normal or fringing fields are presented in the same way as an additional series resistor. If it is relevant, the variation of permeability μ depending on temperature and induction level should be taken into account. Important variations are present when the magnetic circuit contains no air gap.

11.4.2 No Load Test of Transformers

The test is similar to the test of inductors. Using a no load test of a transformer we can measure the losses in the core. Remind that non-current carrying conductors and screens are also subjected to eddy currents, which can increase the losses. In this measurement we should check whether the copper losses are negligible. We can also measure the primary and secondary self-inductances L_1 and L_2 (see Fig. 11.4).

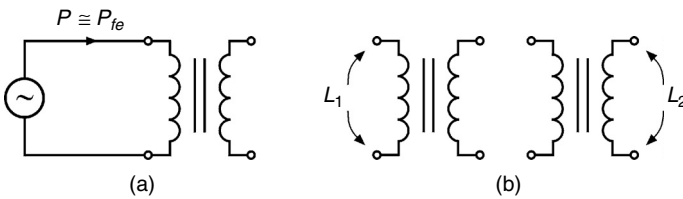


FIGURE 11.4

No load test: a) measuring core losses;

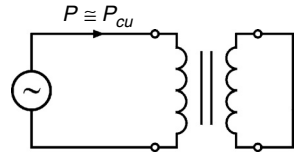
b) measuring primary and secondary self-inductances L_1 , L_2 of a transformer.

11.4.3 Short Circuit Test

In principle, the same approach as in the no load test can be applied in the short circuit test (see Fig. 11.15). We assume that the magnetizing inductance is very high ($L_{m1} \gg R_2'$) and all the losses are attributed to the ohmic resistance of the windings. In that approximated way, the measured resistive

FIGURE 11.5

Short circuit test of a transformer. Measuring ohmic losses and ohmic resistances of the windings.



part R_{meas} is the sum of the measured primary winding resistance R_1 and the transformed resistance of the secondary side R_2' :

$$R_{meas} = R_1 + R_2' = R_1 + R_2 \frac{N_1}{N_2} \quad (11.14)$$

NOTE: Here we want to warn about a measurement error, which is often made with ferrite transformers, especially those with air gap, and also with small mains frequency transformers. If the measurement frequency is low, 1 kHz or lower, it is not sure that the magnetizing reactance is much higher than the secondary resistance, especially with gapped transformers. This can seriously affect the measuring results in the classical short circuit test!

11.4.4 Measurement of the Inductances in Transformers

Here we give a procedure to check the results of the no load test for the case, when the primary and the secondary number of turns are not too different (e.g., a ratio below 5). The method can also be applied if the resistance of the windings is not low compared to magnetizing reactance. The primary and secondary windings of the transformer are put in series in two different ways, corresponding to the two possible ways of coupling (see Fig. 11.6). This gives us two measurement results, which we denote as L_a and L_b :

$$L_a = L_1 + L_2 + 2M \quad (11.15)$$

$$L_b = L_1 + L_2 - 2M \quad (11.16)$$

The inductances L_1 , L_2 , and M are defined according to the symbols used in [Chapter 1](#).

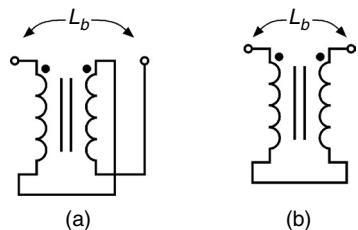


FIGURE 11.6

Measuring inductances L_a and L_b of a transformer; a) series connection, L_a ; b) inverse series connection, L_b .

We check the no load test results of L_1 and L_2 by the equation

$$L_1 + L_2 = (L_a + L_b)/2 \quad (11.17)$$

If the equality is met, then the no load test measured values of L_1 and L_2 are correct.

Using the measured values of the inductances L_a and L_b , we can find the mutual inductance M of the transformer:

$$M = \frac{L_a - L_b}{4} \quad (11.18)$$

The leakage coefficient σ and the coupling coefficient k are then found as

$$\sigma = 1 - \frac{M^2}{L_1 L_2} \quad (11.19)$$

$$k^2 = \frac{M^2}{L_1 L_2} \quad (11.20)$$

Note that σ is obtained only by measurement and no turns ratio is introduced up to now, so σ is independent of the actual or fictitious turns ratio in a transformer. If we introduce the turns ratio as N_1 and N_2 , other elements in the equivalent transformer scheme (Fig. 1.22, Chapter 1) can be calculated as

$$L_{m1} = \frac{N_1}{N_2} M \quad (11.21)$$

$$L_{m2} = \frac{N_2}{N_1} M \quad (11.22)$$

where

L_{m1} is the magnetizing inductance placed in the primary side

L_{m2} is the magnetizing inductance placed in the secondary side.

One can also substitute the magnetizing inductances in the leakage coefficient:

$$\sigma = 1 - \frac{L_{m1} L_{m2}}{L_1 L_2} \quad (11.23)$$

We can also calculate the leakage inductances $L_{\sigma 1}$ and $L_{\sigma 2}$:

$$L_{\sigma 1} = L_1 - L_{m1} \quad (11.24)$$

$$L_{\sigma 2} = L_2 - L_{m2} \quad (11.25)$$

Note that we can choose fictitious turns ratios, but σ will remain positive. For real turns ratios, $L_{\sigma 1}$ and $L_{\sigma 2}$ are positive. One can choose a fictitious turns ratio in order to make $L_{\sigma 2} = 0$, which results in an L-scheme of a transformer or $L_{\sigma 1} = 0$, which results in an inverse L-scheme.

In linear models, T, L, or inverse L schemes are equivalent, if the leakage coefficient σ has the same value. When saturation is considered, or if the real turns ratio is used, there is a preference to T-schemes. In practice, with small leakage coefficients, the L schemes are accurate enough and easy to use.

11.4.5 Measurement of Low Inductances

When the inductance becomes in the order of 1 μH or lower, special care should be taken concerning the measurement.

Although high-end impedance analyzers and RLC-meters can measure values below 1 μH , here we give an alternative method. This method might be useful for measuring leakage inductances of fly-back transformers and also for measuring the inductance of bus bars. The resistive part of the impedance is neglected here. Usually the lead inductance (the inductance of the wires) is not negligible and should be considered separately. Principally, the problem can be solved in this way:

1. A plane is chosen, which defines the physical limit of the device.
2. A current is injected perpendicular to this plane.
3. The voltage across device under test is measured with leads, which lay in this plane and are close to each other.

The approach results in a four-wire measurement (see Fig. 11.7).

A practical way to implement such a four-wire measurement is to use a sine wave generator with 50 Ω output impedance. A resistor with resistance value of 50 Ω (e.g., two 1% 100 Ω resistors in parallel) is put in series with the unknown impedance. An oscilloscope is used to measure the voltage across the unknown impedance and across the additional 50 Ω resistor. To avoid mass current problems, the voltage measurements can be done in a differential way (two probes). If some connections have to be short-circuited,

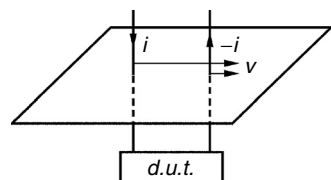


FIGURE 11.7
Four-wire measuring method.

this should be done at the limit of the component, using a copper plane. The inductance of the device under test L_{dut} is

$$L_{dut} = \frac{50}{2\pi f} \frac{V_{dut}}{V_{50\Omega}} \quad (11.26)$$

where

f is the excitation frequency, [Hz]

V_{dut} is the voltage across the device under test

$V_{50\Omega}$ is the voltage across the $50\ \Omega$ resistor.

The frequency can be 100 kHz, 1 MHz, or even 10 MHz for very small inductances, such as 10 nH. When using 159.155 kHz, 1.59155 MHz, or 15.9155 MHz, the computation is easier as it results in a round number, when the excitation frequency f is multiplied by 2π .

11.5 Core Loss Measurements

Losses in magnetic components have been studied because of their particular significance to the component design in power electronics. The main components of the losses in magnetic components are the core losses and the winding losses. Here we discuss measuring the core losses.

11.5.1 Classical Four-Wire Method

At low frequency, the copper loss of the exciting winding is an important part of the total power. The traditional solution is to use a transformer-like four-wire measurement set-up, where the current is measured at the exciting winding and an EMF (electromotive force) is sensed at the secondary winding [1,8,9]; see Fig. 11.8. The solution is still applicable at high frequency for sinusoidal wave forms, as far as the phase shift between the emf in the exciting winding and voltage at the sense winding is low. The shown parasitic capacitances of the primary C_p and of the secondary winding C_s contain the intra capacitance of the windings and the capacitance of the cables and measuring probes.

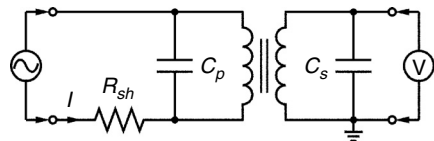


FIGURE 11.8
Transformer like material loss measurement.

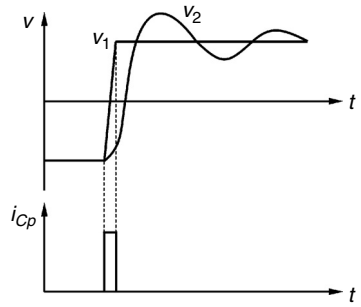


FIGURE 11.9

Sketch of the input capacitance current i_{Cp} , input voltage v_1 and sensed secondary voltage v_2 .

But if this measurement method is used in converters with wave forms having fast edges, for example square waves with variable duty ratio, then typical errors occur. Such wave forms are much common for power electronics. In these cases each voltage edge at the input causes an almost instantaneous capacitive current to flow due to the input capacitance of wires and transformer. The charge transfer is typically at half the edge voltage. In the meantime, the voltage of the sense winding does not change much. As the average charge transfer is observed at the voltage measurement side (secondary winding), the current of the input capacitance is observed as a fictitious negative power (see Fig. 11.9):

$$P_{err} \cong -\frac{1}{2}C_{in} 2f \sum_0^T (\Delta V)^2 = C_{in} f \sum_0^T (\Delta V)^2 \quad (11.27)$$

where

P_{err} is approximate power error

C_{in} is the input parasitic capacitance

f is the excitation frequency

ΔV is the voltage edge

T is the period of the excitation frequency f , $T = 1/f$ (it contains 2 voltage edges).

The power given by Equation (11.27) can result in a non-negligible contribution in the following cases: if the input connection wire is coaxial one; if some probes are connected; or if the component is immersed in oil, which increases the parasitic capacitance.

Example

At a frequency of 100 kHz, a square wave voltage with edges of 300 V and a parasitic capacitance of 100 pF results in 0.9 W error! If the measurement shunt is inductive at high frequency, which is usually the case for the charge time of the parasitic capacitance, similar errors could be present, even if one reduces the input parasitic capacitance.

Another possible cause of error in the four-wire method is the eddy current loss in exciting and sense winding. However this can be minimized using litz wire.

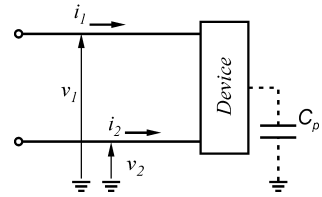


FIGURE 11.10
Two-wire method. Measuring power to a device with two feeding wires and a ground plane.

11.5.2 Two-Wire Method

11.5.2.1 Oscilloscope Based Measurement

Theoretically, the electrical power through a surface is obtained by integrating the contribution of the Poynting vector, which does express the power direction of an electromagnetic wave. This can be simplified for the power carried through a multiwire transmission line (cable), when no other power is exchanged such as by capacitive or magnetic coupling. Then, for the average power we can write

$$P_{av} = \sum v_i i_i \quad (11.28)$$

The potentials v_i and the currents i_i refer to the i -th conductor.

When there are two wires, we have the so-called two-wire method (see Fig. 11.10). In the two-wire measurement one of the two wires ($i = 2$) can be taken as reference. If the current through the capacitance of the magnetic component to earth is negligible then $i_2 = -i_1$.

At high frequency for high permeability materials, the copper losses can be kept low using an appropriate litz wire. This allows one to use a simple total power loss measurement and afterwards to subtract the copper losses. If air gaps are absent, the copper loss, including eddy current loss, can be estimated by doing a test without magnetic material. The core losses P_{fe} are

$$P_{fe} = P_{meas} - P_{cu} \quad (11.29)$$

where

- P_{meas} are the total measured losses
- P_{cu} are the measured copper losses.

To measure the total power using Equation (11.29), an oscilloscope can be used. Today oscilloscopes are capable of doing a data acquisition with phase shifts lower than 1 ns. Also multiplication of channels is a standard function.

It is important that the power measurement has a *wide bandwidth* and especially a *negligible phase shift between current and voltage* measurement. The phase shift should correspond with a time, for example, less than 10 times

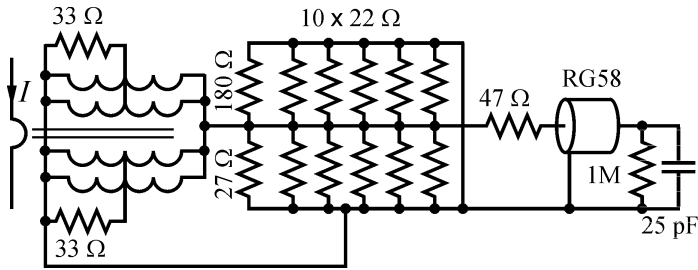


FIGURE 11.11
Electrical scheme of the current probe.

the rise time of the edges. Thus, the practical problem is to have wide band voltage and current probes and, in the same time, with a low relative phase shift between their measurements. For power measurement, it is important that the phase shift difference of voltage and current measurement is as small as possible. For example, a delay of 1 ns results already in a $\tan\delta$ difference of 0.6% at 1 MHz.

11.5.2.2 Wide Band Current Probe

Here we present a practical solution for a wide band current probe.

The actual operating frequencies for ferrites are about 20 kHz to 1 MHz. However, due to the fast voltage edges, it is good to extend the measuring characteristic of the current and voltage probes up to 50 MHz. For a wide band current probe, the use of a current transformer is preferred as mass currents to the oscilloscope (resulting in ghost signals) can be reduced. Thus, an increased accuracy is provided at equal signal levels, compared to shunt measurement.

The electrical scheme of the current probe is shown in Fig. 11.11. The high number of the resistors used is imposed for two reasons: the need for a low parasitic inductance of the equivalent resistor and the need for sufficient power dissipation ability. The input of the scope is 1 M Ω , 25 pF. The current probe was constructed using a ring core TX36/23/15-3E25. The secondary side contains two windings of 20 turns, two 0.8 mm diameter copper wires in parallel. The current transformer is loaded with a 2 Ω resistance. This results in a 0.1 V/A transfer impedance. The low resistance results in a low cut-off frequency below 150 Hz. The probe is designed to accept primary currents up to 20 A.turns RMS value.

The transmission line nature of the winding of the current probe causes the signal to be delayed by 1–2 ns.

The current probe has been tested, using a 10 V, 50 Ω generator, loaded with a 50 Ω resistor. The experimental amplitude-frequency characteristic of the probe is given in Fig. 11.12.

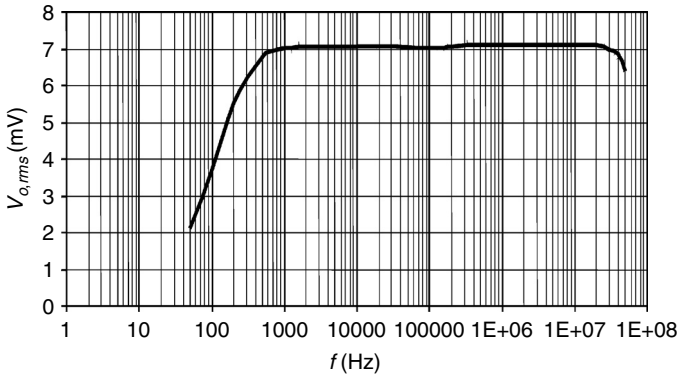


FIGURE 11.12

Amplitude-frequency characteristic of the current probe, output $V_{o,rms} = 7.071$ mV for 100 mA peak value of the measured input sine wave current.

11.5.2.3 Corresponding Voltage Probe

Here we give a practical solution for voltage probe, corresponding to the presented above wide band current probe. The electrical scheme of the voltage probe is shown in Fig. 11.13. The probe has a 1:100 ratio.

At low frequency, a high-pass characteristic is tuned to obtain a low phase shift between voltage and current measurement. In addition, the lower cut-off frequency is very low compared to the measured frequency of 100 kHz.

A small damping ($33 \Omega + 33 \Omega$) is added to give some low-pass characteristic at high frequency and to compensate the phase delay of the transmission line behavior of the current probe.

The experimental amplitude-frequency characteristic of the voltage probe is given in Fig. 11.14.

The combination of both probes was tested for a sine wave voltage. The obtained phase difference between the presented current and voltage probes is sufficient for measuring square wave forms in the range of 1 kHz to 1 MHz.

REMARK

The power measurement should be done with short wires. A first reason is that a 20–30 cm wire corresponds to 1 ns phase difference. A second reason

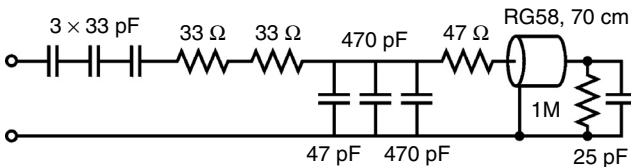


FIGURE 11.13

Electrical scheme of the voltage probe.

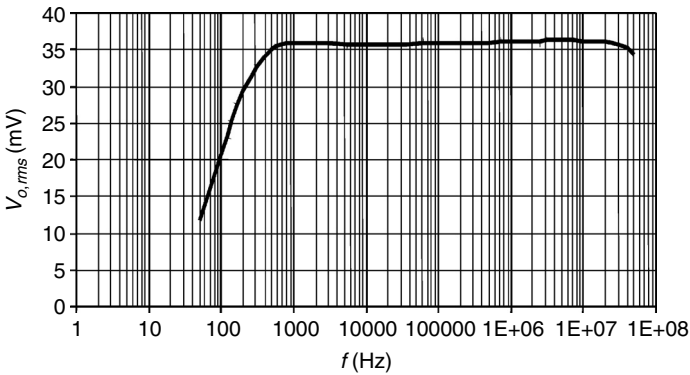


FIGURE 11.14

Amplitude-frequency characteristic of the voltage probe, output $V_{o,rms} = 35.36$ mV for 5V peak value of the measured sine voltage input.

is that an unmatched 1 m cable with some parasitic capacitance at the end acts as a quarter wavelength antenna at 50 MHz. A third reason is that the power losses of the leads are not negligible, and cannot easily be compensated due to eddy current losses in the cable.

11.5.2.4 Flux Measurement Probe

Here we present a passive integrator that can be used to estimate the flux linkage of the core (see Fig. 11.15). The integrating time constant is 100 μ s. The cut-off frequency is 845 Hz. This cut-off frequency is already low enough to result in a negligible error at 20 kHz for square waves. A high accuracy of the peak-to-peak flux measurement is required as 1% error generates about 2.5% error in the core losses. The parasitic inductance of the leads between the flux measurement place and the device under test has also to be taken into account.

11.5.3 Practical Ferrite Power Loss Measurement Set Up

A practical ferrite power loss measurement set up is shown in Fig. 11.16. A bridge converter is used to feed the measured magnetic component. The converter should have possibility of high frequency, high voltage output and

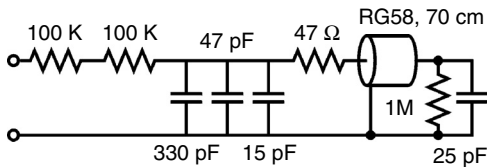


FIGURE 11.15

Electrical scheme of the flux measurement probe.

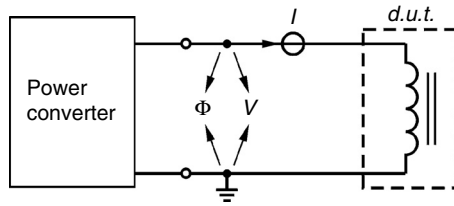


FIGURE 11.16
Practical core loss measurement set up.

regulation of the duty ratio and peak-to-peak voltage, for example presented in [10]. Also a suitable digital scope is necessary, having multiplying capability of channels.

NOTE: An exact number of periods should be displayed on the scope, triggering at the zero crossing of the current. In this way very low windowing errors are introduced.

Having measured the current I and the voltage V , we obtain the ferrite losses after subtraction of the copper losses. Using Litz wire, the copper losses are low. The order of magnitude can be estimated by doing a test without the core.

Now we have the value of the core losses, the induction B (derived by the measurement of the flux) and the excitation frequency. Thus, we can model the dependence $P_{fe} = k f^\alpha \hat{B}^\beta$, deriving optimal values of the exponents α and β and including additional dependence on dB/dt to predict more precisely losses at high voltage edges.

11.6 Measurement of Parasitic Capacitances

The parasitic capacitances in magnetic components are considered in details in [Chapter 7](#) of this book. Here we discuss the means for measuring these capacitances.

11.6.1 Measurement of Capacitance Between Windings

The capacitance between windings (inter capacitance) is very easy to measure at low frequency (1 kHz or below) with capacitance meters (CM); see [Fig. 11.17](#). In this case, the impedance of the inductance is negligible.

However, for a capacitance below 10 pF the capacitance meters are less accurate. The solution is to use a square wave generator, having frequency in the range 1 kHz–100 kHz, and to make a capacitive divider using an unknown C_{dut} in series with the known capacitance of the probe of an oscilloscope C_{sc} .

First, one has to calibrate (to measure) the capacitance of the probe C_{sc} in the same way, but using a small precise capacitance (10 pF) to be placed

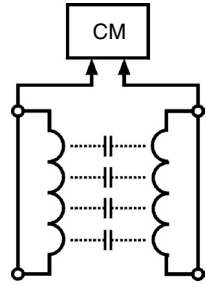


FIGURE 11.17
Measurement of the capacitance between windings by a capacitance meter (CM).

instead of the unknown one (see Fig. 11.18). Knowing the voltage of the generator V_{gen} and the voltage measured by the oscilloscope V_{sc} , the capacitance of the probe C_{sc} is

$$C_{sc} = \frac{(V_{gen} - V_{sc})C_{known}}{V_{sc}} = \frac{(V_{gen} - V_{sc})(10 \times 10^{-9})}{V_{sc}} \quad (11.30)$$

where

V_{gen} is the measured voltage of the generator

V_{sc} is the voltage measured by the oscilloscope

C_{known} is the capacitance of the known capacitor, $C_{known} = 10 \text{ pF}$ in the example (see Fig. 11.18).

Second, we connect the device under test (d.u.t.) and measure the voltage of the oscilloscope V_{sc} , as shown in Fig. 11.19. Now we can calculate the unknown capacitance of the device under test C_{dut} as

$$C_{dut} = \frac{V_{sc} C_{sc}}{V_{gen} - V_{sc}} \quad (11.31)$$

11.6.2 Measurement of the Equivalent Parallel Capacitance of a Winding

Usually the first occurring resonance frequency of a transformer is the resonance frequency resulting from the capacitance of the winding itself (the intra capacitance, as described in Chapter 7) with its inductance. In transformers, the capacitance of the high voltage winding is dominant.

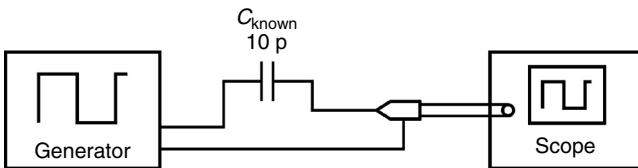


FIGURE 11.18
Calibrating the scope capacitance by a known capacitor.

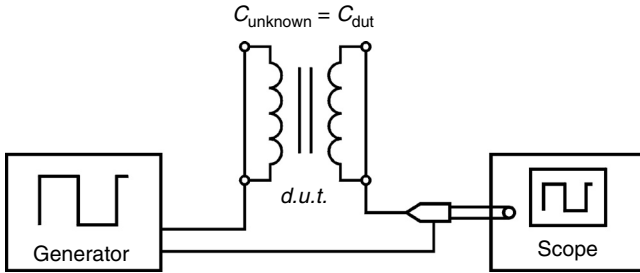


FIGURE 11.19
Accurate measurement of a small capacitance.

By the parallel resonance frequency of the winding, together with the inductance of the winding, the equivalent parallel capacitance can be derived. Also the capacitance of the probe has to be taken into account. A solution that is less sensitive to the probe capacitance is to test at the low voltage winding side or to add a winding with a low number of turns to do so. If a square wave generator is used, the edges can be recognized and a phase angle equal to zero can be easily obtained. The obtained capacitance is then the equivalent capacitance, which reflects the sum of the transformed capacitances of all the windings, as shown in Fig. 11.20. The capacitance of the high voltage winding is much higher, $N_1 < N_2$ in Fig. 11.20. The resistance, added in Fig. 11.20 (usually 10 k Ω), is necessary in order to increase the impedance of the generator, e.g., to obtain a current source in respect to the magnetic component under measurement. The sine generator in the set-up in Fig. 11.20 could be also a square generator.

NOTE: The measured capacitance is different if the secondary side is grounded or not grounded.

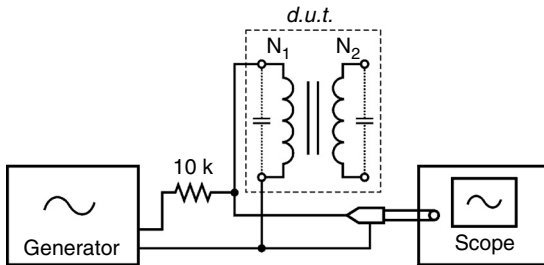


FIGURE 11.20
Measuring the resonance frequency of a magnetic component.

11.7 Combined Measuring Instruments

Component test instruments can centralize a lot of measurements, such as resistance of windings, no load inductance, short circuit inductance, $\tan\delta$, capacitance between windings, and insulation tests.

The combined measuring instruments are mainly used as an accept-reject decision device at the end of production lines and can perform this purpose very rapidly. They are very useful to check for deviating components in the production line.

NOTE: Attention should be paid when using the results from such combined measuring instruments for design purposes. The components are usually tested at low inductance levels, not corresponding to the real use, so the measured $\tan\delta$ may be different compared to the actual use, and the absolute accuracy at high frequencies (500 kHz and above) may be low, giving a wrong or even a negative $\tan\delta$ readout. Also a low inductance and a low equivalent series resistance are difficult to be measured with such instruments.

References

- [1] International Electrotechnical Commission, Switzerland, www.iec.ch
- [2] Keredec, J.-P., Validating the power loss model of a transformer by measurement: The price to pay, IEEE 37th IAS Annual meeting, October 13–18, 2002, Pittsburgh, PA, CD-ROM.
- [3] Prabhakaran, S. and Sullivan, C.R., Impedance-analyzer measurements of high-frequency power passives: Techniques for high power and low impedance, IEEE 37th IAS Annual meeting, October 13–18, 2002, Pittsburgh, PA, CD-ROM.
- [4] Data sheet of Agilent 4294A Precision Impedance Analyzer.
- [5] Hansen, P., Blaabjerg, F., Madsen, K.D., Pedersen, J.K., and Ritchie, E., An accurate method for power loss measurements in energy optimized apparatus and systems, Proceedings of EPE '99 Conference, Toulouse, France, September 1999, CD-ROM.
- [6] Patterson, D., Tricks of the trade: Simple calorimeter for accurate loss measurement, *IEEE Power Electronics Society Newsletter*, October 2000, pp.5–7.
- [7] Van den Bossche, A., Flow calorimeter for power electronic converters, Proceedings of EPE-01 Conference, Graz, Austria, August 27–29, 2001, CD-ROM.
- [8] Li, J., Abdallah, T., and Sullivan, C., Improved calculation of core loss with nonsinusoidal waveforms, IEEE, IAS 36th Annual Meeting, Chicago, September 30–October 4, 2001, pp. 2203–2210.
- [9] Brockmeyer, A., Dimensionierungswerkzeug für magnetische Bauelemente in Stromrichteranwendungen, Ph.D. thesis, University of Technology, Aachen, Germany, 1997.
- [10] Van den Bossche, A., Valchev, V., and Filchev, Todor, High-frequency high-current test platform, Proceedings of EPE-01 Conference, Graz, Austria, 2001, August 27–29, CD-ROM.

Appendix A

RMS Values of Waveforms

A.1 Definitions

The RMS (root-mean-square) values are denoted with uppercase letters without index. We use currents in the examples given here.

Physical Meaning of the RMS Value

The RMS value (often called the *effective value* or *DC-equivalent value*) of a current is an equivalent of a DC current, which has the same heat dissipation as the real current on any resistor.

RMS Value in the Frequency Domain

When a given wave form (a current in the case) comprises components with different frequency, i.e., different harmonics, then its RMS value is given by the sum:

$$I = \sqrt{\sum_{k=0..∞} I_k^2} \quad (\text{A.1})$$

where I_k is the RMS value of the k^{th} harmonic.

This sum can also be separated in the frequency domain into two components:

- The DC component: $I_{DC} = I_0$
- The AC component: $I_{AC} = \sqrt{\sum_{k=1}^{\infty} I_k^2}$

The basic (the first) harmonic is I_1 . The RMS value of the higher harmonics is

$$I_h = \sqrt{\sum_{k=2}^{\infty} I_k^2} \quad (\text{A.2})$$

Using Equation (A.2) we can write

$$I = \sqrt{I_{DC}^2 + I_{AC}^2} = \sqrt{I_{DC}^2 + I_1^2 + I_h^2} \quad (\text{A.3})$$

RMS Value in the Time Domain

The RMS value of a current, defined as $i(t)$ in the general case, is

$$I = \sqrt{\frac{1}{T} \int_{t_0}^{t_0+T} i(t)^2 \cdot dt} \quad (\text{A.4})$$

where the period of the repeating signal is T and t_0 is an arbitrary time instant.

A.2 RMS Values of Some Basic Waveforms

A.2.1 Discontinuous Waveforms

The current flows during some time interval DT and it is zero for the rest of the period T . For this case we can write

$$I = I_D \sqrt{D} \quad (\text{A.5})$$

where

D is the duty ratio

I_D is the RMS value corresponding to the nonzero part of the waveform in the frames of one period (see Fig. A.1)

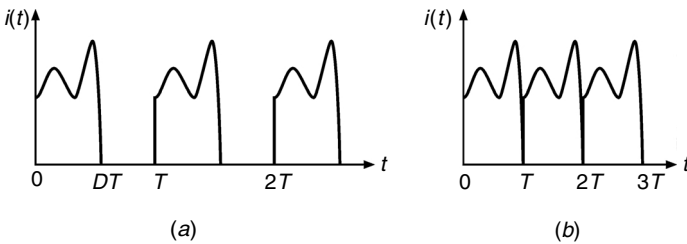


FIGURE A.1
Waveforms: (a) $D < 1$; (b) $D = 1$.

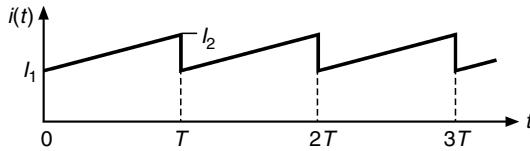


FIGURE A.2
Repeating line waveforms.

A.2.2 Repeating Line Waveforms

Repeating line wave forms are shown in Fig. A.2. The start value of the current is I_1 , the end value is I_2 , the period is T . For $0 < t < T$ the current is

$$i(t) = I_1 + \frac{t(I_2 - I_1)}{T} \quad (\text{A.6})$$

After calculating the integral corresponding to RMS value we obtain the following result:

$$I = \sqrt{\frac{1}{T} \int_0^T i(t)^2 dt} = \sqrt{\frac{I_1^2 + I_2^2 + I_1 I_2}{3}} \quad (\text{A.7})$$

We can also write this result as

$$I = \sqrt{\left(\frac{I_1 + I_2}{2}\right)^2 + \frac{1}{3}\left(\frac{I_1 - I_2}{2}\right)^2} \quad (\text{A.8})$$

Equation (A.8) describes the RMS value as a function of the average value $(I_1 + I_2)/2$ and the deviation $(I_1 - I_2)/2$. The current waveform is divided into DC current component $(I_1 + I_2)/2$ and AC current component $(I_1 - I_2)/2$. Then RMS value is calculated in a similar way to the equation (A.3).

A.2.3 Waveforms Consisting of Different Repeating Line Parts

The curve is composed from the line parts A, B, and C (see Fig. A.3), for which RMS values $I_A, I_B,$ and I_C are calculated by Equation (A.8). The RMS value of that waveform is

$$I = \sqrt{I_A^2 D_A + I_B^2 D_B + I_C^2 D_C} \quad (\text{A.9})$$

where

$D_A = T_A/T, I_A$ is the RMS value of the part with duration T_A

$D_B = T_B/T, I_B$ is the RMS value of the part with duration T_B

$D_C = T_C/T, I_C$ is the RMS value of the part with duration T_C

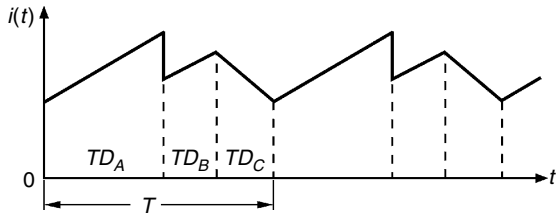


FIGURE A.3
Different repeating line parts.

Note that the current may also be discontinuous.

A.3 RMS Values of Common Waveforms

A.3.1 Sawtooth Wave, Fig. A.4.

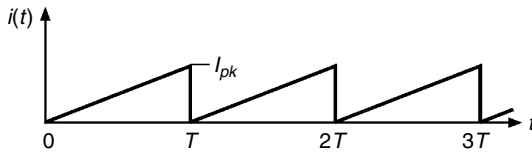


FIGURE A.4
Sawtooth wave.

$$I_{rms} = \frac{I_{pk}}{\sqrt{3}}$$

A.3.2 Clipped Sawtooth, Fig. A.5.

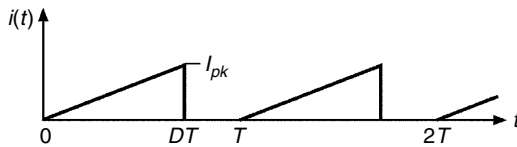


FIGURE A.5
Clipped sawtooth.

$$I_{rms} = I_{pk} \sqrt{\frac{D}{3}}$$

A.3.3 Triangular Waveform, No DC Component, Fig. A.6.

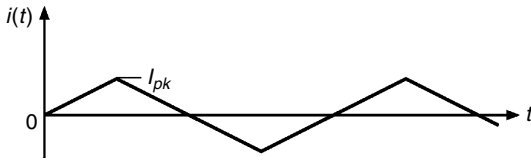


FIGURE A.6
Triangular waveform, no DC component.

$$I_{rms} = \frac{I_{pk}}{\sqrt{3}}$$

A.3.4 Triangular Waveform with DC Component, Fig. A.7.

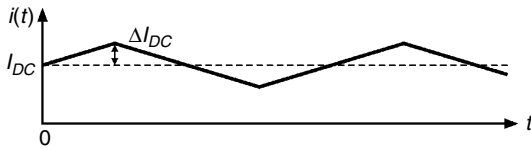


FIGURE A.7
Triangular waveform with DC component.

$$I_{rms} = I_{DC} \sqrt{1 + \frac{1}{3} \left(\frac{\Delta I_{DC}}{I_{DC}} \right)^2} = \sqrt{I_{DC}^2 + \frac{(\Delta I_{DC})^2}{3}}$$

A.3.5 Clipped Triangular Waveform, Fig. A.8.

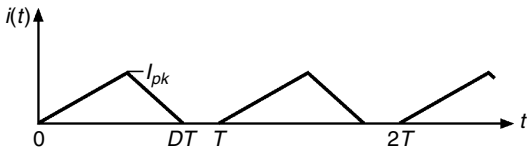


FIGURE A.8
Clipped triangular waveform.

$$I_{rms} = I_{pk} \sqrt{\frac{D}{3}}$$

A.3.6 Square Wave, Fig. A.9.

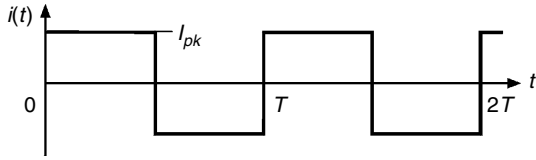


FIGURE A.9
Square wave.

$$I_{rms} = I_{pk}$$

A.3.7 Rectangular Pulse Wave, Fig. A.10.

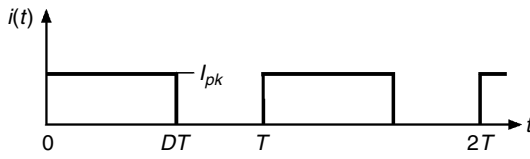


FIGURE A.10
Rectangular pulse wave.

$$I_{rms} = I_{pk} \sqrt{D}$$

A.3.8 Sine Wave, Fig. A.11.

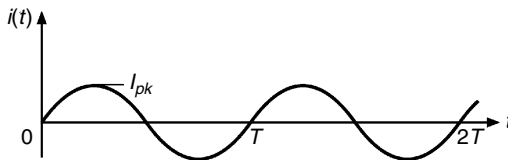


FIGURE A.11
Sine wave.

$$I_{rms} = \frac{I_{pk}}{\sqrt{2}}$$

A.3.9 Clipped Sinusoid, Full Wave, Fig. A.12.

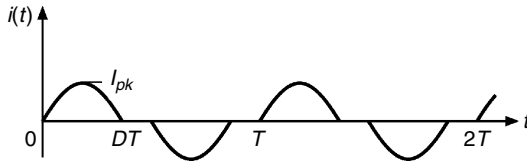


FIGURE A.12
Clipped sinusoid, full wave.

$$I_{rms} = I_{pk} \sqrt{D}$$

A.3.10 Clipped Sinusoid, Half Wave, Fig. A.13.

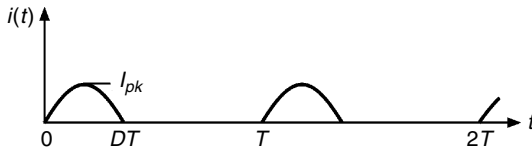


FIGURE A.13
Clipped sinusoid, half wave.

$$I_{rms} = I_{pk} \sqrt{\frac{D}{2}}$$

A.3.11 Trapezoidal Pulse Wave, Fig. A.14.

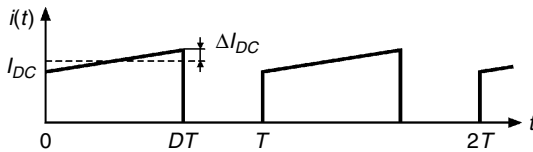


FIGURE A.14
Trapezoidal pulse wave.

$$I_{rms} = I_{DC} \sqrt{D} \sqrt{1 + \frac{1}{3} \left(\frac{\Delta I_{DC}}{I_{DC}} \right)^2}$$

Appendix B

Magnetic Core Data

A variety of ferrite cores and shapes exist. Here we give geometrical data of a selection of commonly used ferrite core shapes. In the tables we use the following abbreviations:

l_e	effective magnetic path
A_e	effective magnetic area
A_{min}	minimum magnetic area
W_a	minimum winding area
MLT	mean length per turn
MWW	minimum winding width

REMARKS

1. The parameters l_e and A_e are used to find the inductance of the core when there is no air gap, which is so called *inductance factor* A_L .
2. The parameter A_{min} is used to calculate the saturation limit.
3. The parameter effective volume V_e is used for calculating the losses in the core
4. The parameters W_a , MLT , and MWW concern the corresponding coil former.

B.1 ETD Core Data (Economic Transformer Design)

The ETD core dimensions and winding parameters are tabulated in Table B.1 and an ETD core half is shown in Fig. B.1.

B.1. ETD Core Data (Economic Transformer Design Core)

TABLE B.1

ETD Core Geometrical Dimensions and Winding Parameters

Core type, <i>a</i> [mm]	Geometrical dimensions					Effective core parameters of a set					Winding parameters		
	<i>b</i> [mm]	<i>c</i> [mm]	<i>d</i> [mm]	<i>e</i> [mm]	<i>f</i> [mm]	V_e [mm ³]	l_e [mm]	A_e [mm ²]	A_{min} [mm ²]	<i>m</i> half[g]	W_a [mm ²]	<i>MLT</i> [mm]	<i>MWW</i> [mm]
ETD29	15.8	9.8	9.8	22	11	5470	72	76	71	14	90	53	19.4
ETD34	17.3	11.1	11.1	25.6	11.8	7640	78.6	97.1	91.6	20	123	60	20.9
ETD39	19.8	12.8	12.8	29.3	14.2	11500	92.2	125	123	30	177	69	25.7
ETD44	22.3	15.2	15.2	32.5	16.1	17800	103	173	172	47	214	77	29.5
ETD49	24.7	16.7	16.7	36.1	17.1	24000	114	211	209	62	273	85	32.7
ETD54	27.6	18.9	18.9	41.2	20.2	35500	127	280	280	90	316	96	36.8
ETD59	31	21.6	21.6	44.7	22.5	51500	139	368	368	130	366	106	41.2

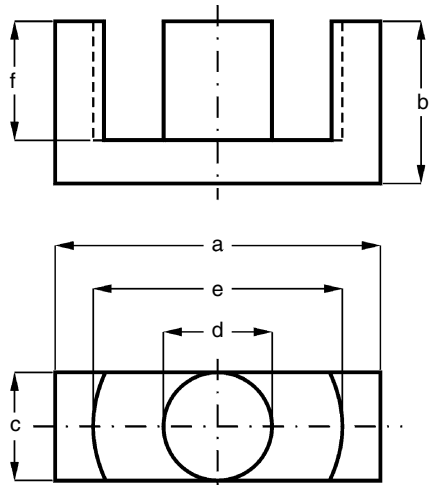


FIGURE B.1
ETD core half.

B.2. EE Core Data

The EE core dimensions and winding parameters are tabulated in Table B.2 an EE core half is shown in Fig. B.2.

TABLE B.2

EE Core Geometrical Dimensions and Winding Parameters

Core type, <i>a/b/c</i> [mm]	Geometrical dimensions			Effective core parameters of a set					Winding parameters		
	<i>d</i> [mm]	<i>e</i> [mm]	<i>f</i> [mm]	V_c [mm ³]	l_e [mm]	A_e [mm ²]	A_{min} [mm ²]	m_c half [g]	W_a [mm ²]	<i>MLT</i> [mm]	<i>MWW</i> [mm]
E5.3/2.7/2	1.4	3.8	1.9	31.4	12.7	2.5	2.3	0.08	1.76	13	2.7
E16/8/5	4.7	11.3	5.7	750	37.6	20.1		2	21.6	33	9.45
E20/10/5	5.2	12.8	6.3	1340	42.8	31.2	25.2	4	28.6	38.7	10.8
E25/13/7	7.5	17.5	8.7	2990	58.0	52.0		8	56	49	15.6
E30/15/7	7.2	19.5	9.7	4000	67.0	60	49.0	11	80	56	17.1
E34/14/9	9.3	25.5	9.8	5590	69.3	80.7		14	102	69.0	16.5
E42/21/15	12.2	29.5	14.8	17300	97.0	178	175	44	178	93	26
E42/21/20	12.2	29.5	14.8	22700	97.0	233	233	56	173	100	25.9
E47/20/16	15.6	32.4	12.1	20800	88.9	234	226	53	131	94.7	21.4
E50/21.3/14.6	14.6	34.5	12.5	20900	92.9	225	213	76	178	100	20.1
E55/28/21	17.2	37.5	18.5	44000	124	354	345	108	250	116	33.2
E60/22.3/15.6	15.6	44	13.8	27200	110	248	240	135	289	128	
E65/32/27	20	44.2	22.2	79000	147	540	530	205	394	150	39.5
E80/38/20	19.8	59.1	28.2	72300	184	392		180			

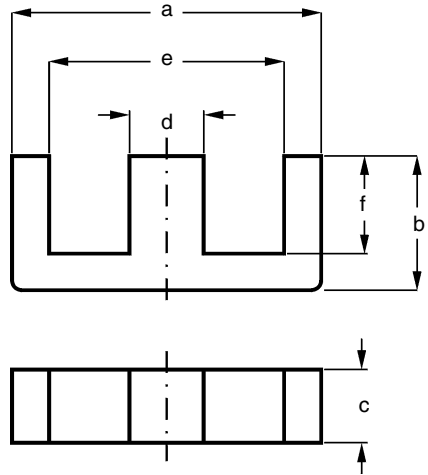


FIGURE B.2
EE core half.

B.3. Planar EE Core Data

The E planar core dimensions and winding parameters are tabulated in Table B.3. An E-core and an I-plate are shown in Fig. B.3. An E- and an I-core can be combined or 2 E-cores. The I-plates may also be used for building non-standard geometrics.

TABLE B3

EE Planar Core Geometrical Dimensions

Core type, a/b/c [mm]	Geometrical dimensions			Effective core parameters of a set of EE cores			
	<i>d</i> [mm]	<i>e</i> [mm]	<i>f</i> [mm]	V_c [mm ³]	l_c [mm]	A_c [mm ²]	m^* [g]
E14/3.5/5	3	11	2	300	20.7	14.5	1.1
E18/4/10	4	14	2	960	24.3	39.5	4.1
E22/6/16	5	16.8	3.2	2550	32.5	78.5	10.5
E32/6/20	6.35	25	3.18	5380	41.7	129	23
E38/8/25	7.6	30.2	4.45	10200	52.6	194	43
E43/10/28	8.1	34.7	5.4	13900	61.7	225	59
E58/11/38	8.1	50	6.5	24600	81.2	305	106
E64/10/50	10.2	53.6	5.1	40700	79.7	511	178

* *m* is the mass of the total E/PLT combination.

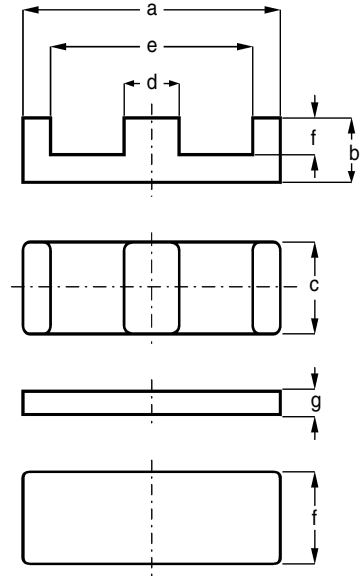


FIGURE B.3

Planar EE core half and PLT.

B.4. ER Core Data

The ER core dimensions and winding parameters are tabulated in Table B.4. An ER-core half is shown in Fig. B.4.

TABLE B.4

ER Core Geometrical Dimensions and Winding Parameters

Core type, a [mm]	Geometrical dimensions					Effective core parameters of a set					Winding parameters		
	b [mm]	c [mm]	d [mm]	e [mm]	f [mm]	V_e [mm ³]	l_e [mm]	A_e [mm ²]	A_{min} [mm ²]	m_r half [g]	W_a [mm ²]	MLT [mm]	MWW [mm]
ER9.5	2.45	5	3.5	7.5	1.6	120	14.2	8.5	7.6	0.35	2.8	18.4	2
ER11	2.45	6	4.25	8.7	1.5	174	14.7	11.9	10.3	0.5	2.8	21.6	1.85
ER14.5	2.95	6.8	4.6	11.6	1.55	333	19.0	17.6	15.4	0.9	5.1	27	1.9
ER28	14	11.4	9.9	21.75	9.75	5260	64	81.4	77	14			
ER35	20.7	11.4	11.3	26.15	14.75	9710	90.8	107	100	23			
ER40	22.4	13.4	13.3	29.6	15.45	14600	98	149	139	37			
ER48	21.2	21	18	38	14.7	25500	100	255	248	64			
ER54	18.3	17.95	17.9	40.65	11.1	23000	91.8	250	240	61			

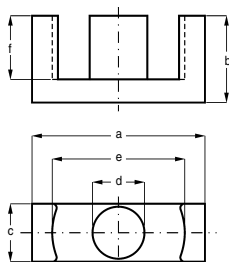


FIGURE B.4
ER core half.

B.5. UU Core Data

The U core dimensions and winding parameters are tabulated in Table B.5. An U-core half is shown in Fig. B.5.

TABLE B.5
UU Core Geometrical Dimensions and Winding Parameters

Core type, a/b/c [mm]	Geometrical dimensions		Effective core parameters				Winding parameters	
	d [mm]	e [mm]	V_e [mm ³]	l_e [mm]	A_e [mm ²]	m , half [g]	W_a [mm ²]	MLT [mm]
U10/8/3	4.35	5	309	38.3	8.07	0.9	28	30
U15/11/6	5.4	6.4	1680	52	32.3	4	38.7	46.6
U20/16/7	6.4	8.3	3800	68	56	9	73	54
U25/16/6	12.7	9.5	3380	83.6	40.3	8		
U25/20/13	8.4	11.4	9180	88.2	104	23.5	131	73
U30/25/16	10.5	14.9	17900	111	161	43	230	97
U67/27/14	38.8	12.7	35200	173	204	85		
U93/76/16	36.2	48	159000	354	448	400		

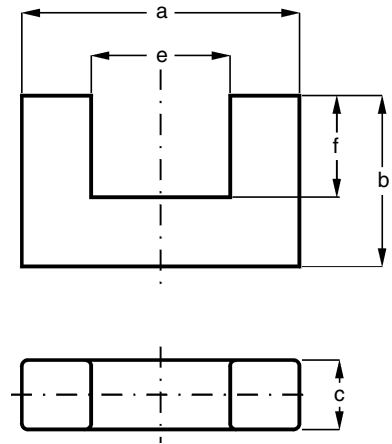


FIGURE B.5
UU Core half.

B.6. Ring Core Data (Toroid Core)

In the drawings we give not-coated cores. The ring core dimensions and winding parameters are tabulated in Table B.6. A ring core is shown in Fig. B.6.

TABLE B.6

Ring Core Geometrical Dimensions

Core type, $a/b/c$ [mm]	Effective core parameters			
	V_e [mm ³]	l_e [mm]	A_e [mm ²]	m [g]
T2.5/1.5/1	2.94	6	0.49	0.015
TC2.5/1.5/1	2.73	6	0.45	0.014
TN4/2.2/1.6	12.9	9.2	1.4	0.1
TN6/4/2	30.2	15.3	1.97	0.15
TN10/6/4	188	24.1	7.8	0.95
TN16/9.6/6.3	760	38.5	19.7	3.8
TN20/10/7	1465	43.6	33.6	7.7
TN25/15/10	2944	60.2	48.9	15
TN32/19/13	5820	76	76.5	29
TN36/23/15	8600	89.6	96	42
TL42/26/13	9860	103	95.8	53
TL58/41/18	23200	152.4	152.4	110
TX74/39/13	34300	165	208	170
T102/66/15	68200	255	267	325
T107/65/25	133000	259	514	680

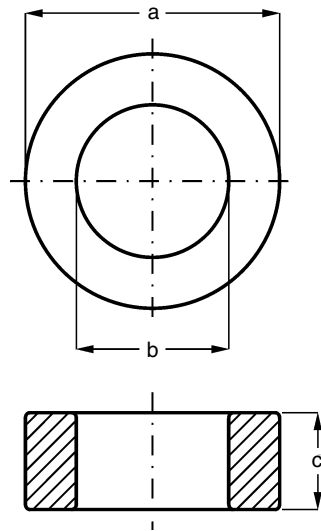


FIGURE B.6
Ring core (toroid).

B.7. P Core Data (Pot Core)

The P core dimensions and winding parameters are tabulated in Table B.7. A P-core half is shown in Fig. B.7.

TABLE B.7

Pot Core Geometrical Dimensions and Winding Parameters

Core type <i>a/b</i> [mm]	Geometrical dimensions						Effective core parameters of a set					Winding parameters		
	<i>c</i> [mm]	<i>d</i> [mm]	<i>e</i> [mm]	<i>f</i> [mm]	<i>g</i> [mm]	<i>h</i> [mm]	V_c [mm ³]	l_c [mm]	A_c [mm ²]	A_{min} [mm ²]	m , half [g]	W_a [mm ²]	MLT [mm]	MWW [mm]
P11/7	9	4.7	6.8	2.2	4.4	2.1	251	15.5	16.2	13.3	1.8	4.8	22.6	3.1
P14/8	11.6	6	9.5	2.7	5.6	3.1	495	19.8	25.1	19.8	3.2	8.65	29	4.4
P18/11	14.9	7.6	13.4	3.6	7.2	3.1	1120	25.8	43.3	36.1	6	16.8	36.7	6
P22/13	17.9	9.4	15	3.8	9.2	4.4	2000	31.5	63.4	51.3	12	26.2	44.5	7.5
P26/16	21.2	11.5	18	3.8	11	5.4	3530	37.6	93.9	76.5	20	37.1	52.6	9.3
P30/19	25	13.5	20.5	4.3	13	5.4	6190	45.2	137	115	34	53.2	62	11.1
P36/22	29.9	16.2	26.2	4.9	14.6	5.4	10700	53.2	202	172	54	72.4	74.3	12.5
P66/56	35.6	17.7	32	5.1	20.3	6.4	88300	123	717	591	550	400	130	37.9

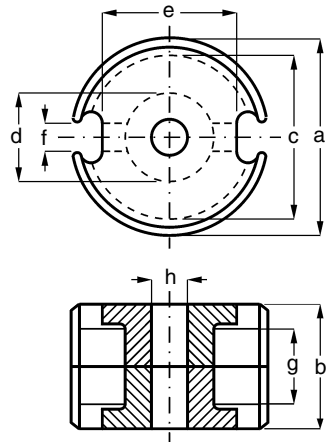


FIGURE B.7
P core.

B.8. PQ Core Data

The PQ core dimensions and winding parameters are tabulated in Table B.8. A P-core half is shown in Fig. B. 7.

TABLE B.8

PQ Core Geometrical Dimensions and Winding Parameters

Core type <i>a/b</i> [mm]	Geometrical dimensions						Effective core parameters of a set				Winding parameters		
	<i>c</i> [mm]	<i>d</i> [mm]	<i>e</i> [mm]	<i>f</i> [mm]	<i>g</i> [mm]	<i>h</i> [mm]	V_c [mm ³]	l_c [mm]	A_c [mm ²]	m_s set [g]	W_n [mm ²]	MLT [mm]	MWW [mm]
PQ20/16	14	8.8	12	10.3	7.9	4	2330	37.6	61.9	11	23.5	44	7.95
PQ20/20	14	8.8	12	14.3	7.9	4	2850	45.7	62.6	14	36	44	12
PQ26/25	19	12	15.5	16.1	10.5	6	6530	54.3	120	32	47.7	56.4	13.6
PQ32/20	22	13.5	19	11.5	11.6	5.5	9440	55.9	169	47	44.8	66.7	8.9
PQ35/35	26	14.4	23.5	25	11.8	6	16300	86.1	190	80	92.5	75.2	22.3

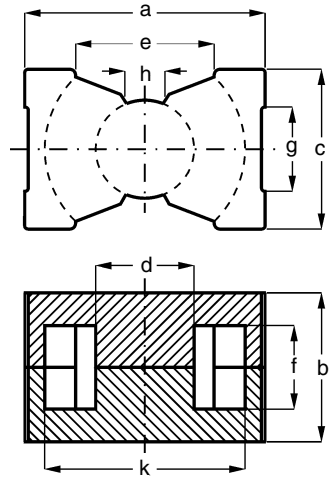


FIGURE B.8
PQ core.

B.9. RM Core Data

The RM-core dimensions and winding parameters are tabulated in Table B.9. An RM-core half is shown in Fig. B.9.

TABLE B.9

RM Core Geometrical Dimensions and Winding Parameters

Core type	Geometrical dimensions								Effective core parameters of a set					Winding parameters		
	<i>a</i> mm	<i>b</i> mm	<i>c</i> mm	<i>d</i> mm	<i>e</i> mm	<i>f</i> mm	<i>g</i> mm	<i>h</i> mm	V_c [mm ³]	l_c [mm]	A_c [mm ²]	A_{min} [mm ²]	m_r set [g]	W_a [mm ²]	MLT [mm]	MWW [mm]
RM4	11	9	4.6	10.4	3.9	9.8	>5.8	8	450	21.4	21.2	14.8	1.4	7.4	20	5.5
RM5	14.9	9.1	6.8	10.4	4.9	12.3	>6	10.2	495	19.8	25.1	19.8	3.2	9.5	25	4.8
RM8	23.2	14.3	11	16.4	8.6	19.7	>9.5	17	1850	35.5	39.5	39.5	11	30.9	42	8.6
RM10	28.5	16.2	13.5	18.6	11	24.7	>11	21.2	3470	41.7	83.2	65.3	20	44.2	52	10
RM14	42	27	19	30	15	34	>17	29	13900	70	198	168	74	111	71	18

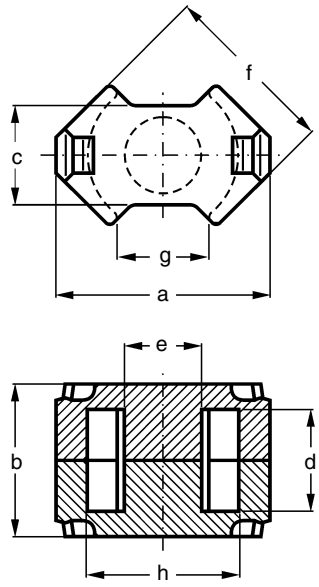


FIGURE B.9
RM core.

B.10 Other Information

Still other types of cores exist as H, DR, etc. For further information refer to specific data of the manufacturers. Relevant information about the cores and ferrite grades can be found in the corresponding sites of the world manufactures:

www.ferroxcube.com

www.mag-inc.com

www.epcos.com

www.token.com

www.samwha.com

www.ferrishield.com

www.ferrite.de

Appendix C

Copper Wires Data

C.1. Round Wire Data

Here we tabulate data about metric round wires in table C.1, about American Wire Gauge (AWG), in table C.2 and Litz wire in [table C.3](#).

TABLE C.1

Round Wire Data, Measures Table (IEC 317-0-1)

Nominal diameter [mm]	Copper Wire			Standard Enameled Wires			
	Tolerances Conductor \pm [mm]	Linear Resistance [Ω /m] at 20°C		Minimum increase [mm]		Maximum overall diameter, [mm]	
		min	max	Grade 1	Grade 2	Grade 1	Grade 2
0.020	*	48.97	59.85	**	**	0.024	0.027
0.022	*	40.47	49.47	**	**	0.027	0.030
0.025	*	31.34	38.31	**	**	0.031	0.034
0.028	*	24.99	30.54	**	**	0.034	0.038
0.032	*	19.13	23.38	**	**	0.039	0.043
0.036	*	15.16	18.42	**	**	0.044	0.049
0.040	*	12.28	14.92	**	**	0.049	0.054
0.045	*	9.705	11.79	**	**	0.055	0.061
0.050	*	7.922	9.489	**	**	0.060	0.066
0.056	*	6.316	7.565	**	**	0.067	0.074
0.063	*	5.045	5.922	**	**	0.076	0.083
0.071	0.003	3.941	4.747	0.007	0.012	0.084	0.091
0.080	0.003	3.133	3.703	0.007	0.014	0.094	0.101
0.090	0.003	2.495	2.900	0.008	0.015	0.105	0.113
0.100	0.003	2.034	2.333	0.008	0.016	0.117	0.125
0.112	0.003	1.632	1.848	0.009	0.017	0.130	0.139
0.125	0.003	1.317	1.475	0.010	0.019	0.144	0.154
0.140	0.003	1.055	1.170	0.011	0.021	0.160	0.171
0.160	0.003	0.812	0.891	0.012	0.023	0.182	0.194
0.180	0.003	0.644	0.707	0.013	0.025	0.201	0.217
0.200	0.003	0.5237	0.5657	0.014	0.027	0.226	0.239
0.224	0.003	0.4188	0.4495	0.015	0.029	0.252	0.266

(Continued)

TABLE C.1

Round Wire Data, Measures Table (IEC 317-0-1) (Continued)

Nominal diameter [mm]	Copper Wire			Standard Enameled Wires			
	Tolerances Conductor ± [mm]	Linear Resistance [Ω/m] at 20°C		Minimum increase [mm]		Maximum overall diameter, [mm]	
		min	max	Grade 1	Grade 2	Grade 1	Grade 2
0.250	0.004	0.3345	0.3628	0.017	0.032	0.281	0.297
0.280	0.004	0.2676	0.2882	0.018	0.033	0.312	0.329
0.315	0.004	0.2121	0.2270	0.019	0.035	0.349	0.367
0.355	0.004	0.1674	0.1782	0.020	0.038	0.392	0.411
0.400	0.005	0.1316	0.1407	0.021	0.040	0.439	0.459
0.450	0.005	0.1042	0.1109	0.022	0.042	0.491	0.513
0.500	0.005	0.08462	0.08959	0.024	0.045	0.544	0.566
0.560	0.006	0.06736	0.07153	0.025	0.047	0.606	0.630
0.630	0.006	0.05335	0.05638	0.027	0.050	0.679	0.704
0.710	0.007	0.04198	0.04442	0.028	0.053	0.762	0.789
0.800	0.008	0.03305	0.03500	0.030	0.056	0.855	0.884
0.900	0.009	0.02612	0.02765	0.032	0.060	0.959	0.989
1.000	0.010	0.02116	0.02240	0.034	0.063	1.062	1.094
1.120	0.011	***	***	0.034	0.065	1.184	1.217
1.250	0.013	***	***	0.035	0.067	1.316	1.349
1.400	0.014	***	***	0.036	0.069	1.468	1.502
1.600	0.016	***	***	0.038	0.071	1.670	1.706
1.800	0.018	***	***	0.039	0.073	1.872	1.909
2.000	0.020	***	***	0.040	0.075	2.074	2.112
2.240	0.022	***	***	0.041	0.077	2.316	2.355
2.500	0.025	***	***	0.042	0.079	2.578	2.618
2.800	0.028	***	***	0.043	0.081	2.880	2.922
3.150	0.032	***	***	0.045	0.084	3.233	3.276
3.550	0.036	***	***	0.046	0.086	3.635	3.679
4.000	0.040	***	***	0.047	0.089	4.088	4.133
4.500	0.045	***	***	0.049	0.092	4.591	4.637
5.000	0.050	***	***	0.050	0.094	5.093	5.141

* For these tolerances the figures are not relevant.

** For the wires with nominal diameter below 0.071 mm, the numerical value of the minimum increase of the enamel for Grade 1 is equal to 0.1 times the nominal conductor diameter.

*** Values are not fixed.

Note: The given *nominal diameters* of the wires in the Table C.1 refer to the copper diameters, as it is important for the wire resistance. Sometimes wires with the same copper diameter can have different enamel insulation thickness.

C.2. American Wire Gauge Data

TABLE C.2
American Wire Gauge Data

AWG#	Nominal cross section [mm ²]	Resistance [mΩ/m]	Nominal outer diameter* [mm]
0000	107.23	1.608	11.68
000	85.03	2.027	10.4
00	67.42	2.557	9.27
0	53.48	3.224	8.25
1	42.41	4.065	7.35
2	33.63	5.128	6.54
3	26.67	6.463	5.83
4	21.15	8.153	5.19
5	16.77	10.28	4.62
6	13.30	13.0	4.11
7	10.55	16.3	3.66
8	8.367	20.6	3.26
9	6.632	26.0	2.91
10	5.241	32.9	2.67
11	4.160	41.37	2.38
12	3.308	52.09	2.13
13	2.626	69.64	1.90
14	2.002	82.80	1.71
15	1.651	104.3	1.53
16	1.307	131.8	1.37
17	1.039	165.8	1.22
18	0.8228	209.5	1.09
19	0.6531	263.9	0.948
20	0.5188	332.3	0.874
21	0.4116	418.9	0.785
22	0.3243	531.4	0.701
23	0.2508	666.0	0.632
24	0.2047	842.1	0.566
25	0.1623	1062.0	0.505
26	0.1280	1345.0	0.452
27	0.1021	1687.6	0.409
28	0.08046	2142.7	0.366
29	0.06470	2664.3	0.330
30	0.05067	3402.2	0.294
31	0.04013	4294.6	0.267
32	0.03242	5314.9	0.241
33	0.02554	6748.6	0.236
34	0.02011	8572.8	0.191
35	0.01589	10849	0.170
36	0.01266	13608	0.152

(Continued)

TABLE C.2American Wire Gauge Data (*Continued*)

AWG#	Nominal cross section [mm²]	Resistance [mΩ/m]	Nominal outer diameter* [mm]
37	0.01026	16801	0.140
38	0.008107	21266	0.124
39	0.006207	27775	0.109
40	0.004869	35400	0.096
41	0.003972	43405	0.0893
42	0.003166	54429	0.0762
43	0.002452	70308	0.0685
44	0.00202	85072	0.0635

* The given diameter is the outer diameter of the wire including the insulation.

C.3. Litz Wire Data

TABLE C.3

Litz Wire Data (only a selection is given)

Number of strands	Nominal cross section of all conductors [mm ²]	Nominal outer diameter of Litz wire [mm]	Resistance [mΩ/m]		Welding time [s]
			min	max	
Diameter* 0.05 mm					
16	0.0314	0.327	495	652	3
25	0.0491	0.397	317	417	3
60	0.1178	0.62	132	174	5
100	0.1963	0.78	79	104	5
200	0.3926	1.12	39	52	8
420	0.8047	1.5	19	25	11
Diameter* 0.071 mm					
16	0.0633	0.44	249.1	310.3	3
25	0.099	0.54	159.4	198.6	4
60	0.2376	0.84	66.6	82.7	6
100	0.3959	1.16	39.8	49.6	8
200	0.7918	1.47	19.9	24.8	10
405	2.1033	2.097	9.9	12	19
Diameter* 0.10 mm					
16	0.1257	0.62	127.6	149.7	5
25	0.1964	0.76	81.64	95.81	5
60	0.4712	1.15	34.02	41.13	8
100	0.7854	1.47	20.41	24.68	10
200	1.5708	2.15	10.2	12.34	14
400	3.1416	2.87	5.103	6.17	19
Diameter* 0.15 mm					
50	0.88		18.3	20.1	11
150	2.66		6.3	6.7	15
200	3.53		4.7	5.0	16
300	5.30		3.1	3.6	18
400	7.07		2.3	2.5	22
Diameter* 0.20 mm					
16	0.5027	1.28	33.01	36.4	8
25	0.7854	1.55	21.13	23.28	10
60	1.885	2.3	8.8	9.99	15
100	3.14	2.9	5.28	5.99	19
550	17.29	6.75	0.93	1.03	30
Diameter* 0.28 mm					
16	0.985	1.71	16.86	18.17	10
25	1.54	2.14	10.79	11.62	12
60	3.695	3.2	4.47	4.84	16
100	6.158	4.2	2.698	2.907	20
405	24.93	8.43	0.67	0.76	60

* The given diameter is the diameter of one conductor in Litz wire.

Appendix D

Mathematical Functions

Here we give some properties of exponential and hyperbolic complex functions used in this book.

$$\sqrt{-1} = (-1)^{1/2} = j \quad (\text{D.1})$$

$$\sqrt{j} = \frac{1+j}{\sqrt{2}} = j \frac{1-j}{\sqrt{2}} = j \frac{\sqrt{2}}{1+j} \quad (\text{D.2})$$

$$e^z = e^{x+jy} = e^x (\cos(y) + j \sin(y)) \quad (\text{D.3})$$

$$\cosh(z) = \frac{e^z + e^{-z}}{2} \quad \sinh(z) = \frac{e^z - e^{-z}}{2} \quad (\text{D.4})$$

$$\lim_{z \rightarrow 0} (\cosh(z)) = 1 \quad (\text{D.5})$$

$$\lim_{z \rightarrow 0} (\sinh(z)) = 0 \quad (\text{D.6})$$

$$\lim_{z \rightarrow 0} \left(\frac{\sinh(z)}{z} \right) = 1 \quad (\text{D.7})$$

$$\tanh(z) = \frac{\sinh(z)}{\cosh(z)} \quad \coth(z) = \frac{\cosh(z)}{\sinh(z)} \quad (\text{D.8})$$

$$\lim_{z \rightarrow 0} \left(\frac{\tanh(z)}{z} \right) = 1 \quad \lim_{z \rightarrow 0} (z \coth(z)) = 1 \quad (\text{D.9})$$

$$\cosh^2(z) + \sinh^2(z) = \cosh(2z) \quad (\text{D.10})$$

$$2 \cosh(z) \sinh(z) = \sinh(2z) \quad (\text{D.11})$$

$$\tanh(z) + \coth(z) = 2 \coth(2z) \quad (\text{D.12})$$

$$a^z = a^{x+jy} = e^{x+jy+\ln(|a|)+j\arg(a)} \quad (\text{D.13})$$

$$\begin{aligned} \frac{(1+j)}{2} \sqrt{\omega_r} \coth\left(\frac{(1+j)}{2} \sqrt{\omega_r}\right) &= \frac{1}{2} \sqrt{\omega_r} \frac{\sinh(\sqrt{\omega_r}) + \sin(\sqrt{\omega_r})}{\cosh(\sqrt{\omega_r}) - \cos(\sqrt{\omega_r})} \\ &+ j \frac{1}{2} \sqrt{\omega_r} \frac{\sinh(\sqrt{\omega_r}) - \sin(\sqrt{\omega_r})}{\cosh(\sqrt{\omega_r}) - \cos(\sqrt{\omega_r})} \end{aligned} \quad (\text{D.14})$$

$$\begin{aligned} \frac{(1+j)}{2} \sqrt{\omega_r} \tanh\left(\frac{(1+j)}{2} \sqrt{\omega_r}\right) &= \frac{1}{2} \sqrt{\omega_r} \frac{\sinh(\sqrt{\omega_r}) - \sin(\sqrt{\omega_r})}{\cosh(\sqrt{\omega_r}) + \cos(\sqrt{\omega_r})} \\ &+ j \frac{1}{2} \sqrt{\omega_r} \frac{\sinh(\sqrt{\omega_r}) + \sin(\sqrt{\omega_r})}{\cosh(\sqrt{\omega_r}) + \cos(\sqrt{\omega_r})} \end{aligned} \quad (\text{D.15})$$

References

- [1] Foglier *The Handbook of Electrical Engineering*, REA staff of research and Education Association, Piscataway, NJ, 1996.
- [2] Jean Jacquelin, La dérivation fractionnaire: une relation générale entre la tension et le courant d'un dipôle., *Revue générale d'électricité, Recherche et développement*, No. 1, Janvier 1987.